ASTES

Advances in Science, Technology & Engineering Systems Journal

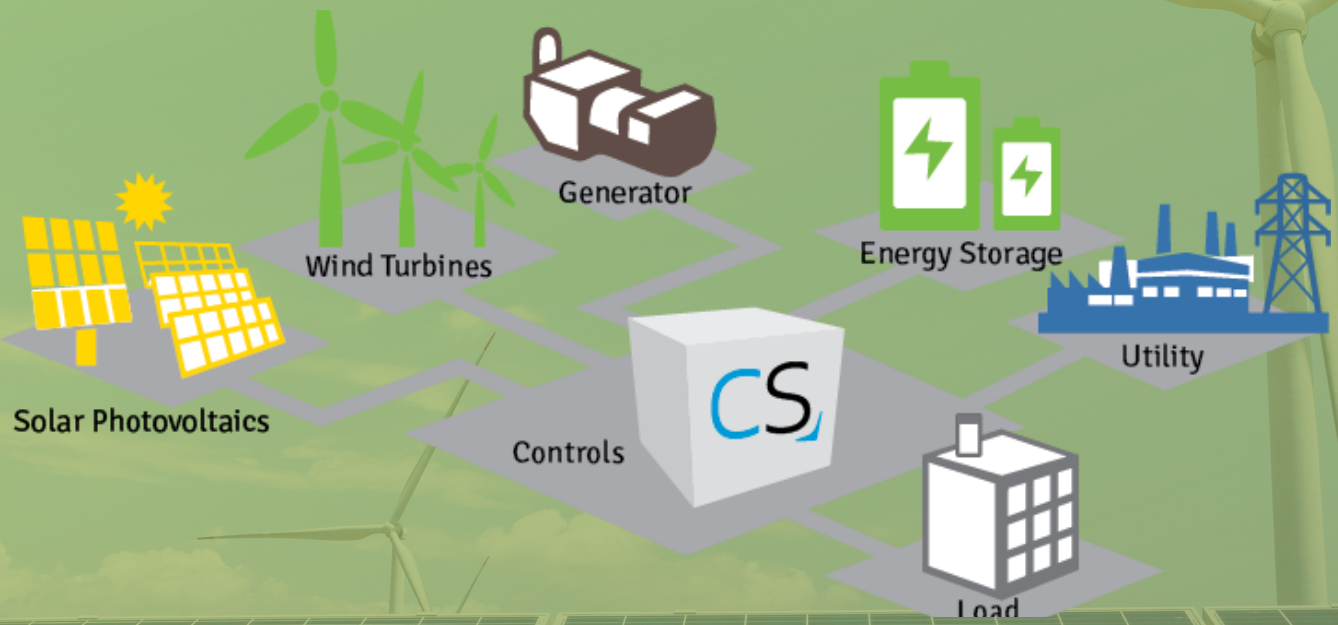

VOLUME 2-ISSUE 4|JUL-AUG 2017

www.astesj.com
ISSN: 2415-6698

Editorial

Advances in Science, Technology and Engineering Systems Journal (ASTESJ) is an online-only journal dedicated to publishing significant advances covering all aspects of technology relevant to the physical science and engineering communities. The journal regularly publishes articles covering specific topics of interest.

Current Issue features key papers related to multidisciplinary domains involving complex system stemming from numerous disciplines; this is exactly how this journal differs from other interdisciplinary and multidisciplinary engineering journals. This issue contains 26 accepted papers in Electrical domain.

Editor-in-chief
Prof. Passerini Kazmersk

ADVANCES IN SCIENCE, TECHNOLOGY AND ENGINEERING SYSTEMS JOURNAL

Volume 2 Issue 4 **July-August 2017**

CONTENTS

ASTES

Advances in Science, Technology and Engineering Systems Journal Vol. 2, No. 4, 1-7 (2017)

www.astesj.com

ASTESJ

ISSN: 2415-6698

Detection of Vandalism in Wikipedia using Metadata Features – Implementation in Simple English and Albanian sections

Arsim Susuri*, Mentor Hamiti[2], Agni Dika[2]

[1]*PhD Student, Faculty of Contemporary Sciences and Technologies, South East European University, Tetovo, Macedonia*

[2]*Proffessor, Faculty of Contemporary Sciences and Technologies, South East European University, Tetovo, Macedonia*

ARTICLE INFO

Article history:
Received: 22 February, 2017
Accepted: 20 March, 2017
Online: 27 March, 2017

Keywords:
Machine learning
Wikipedia
Vandalism
Metadata features

ABSTRACT

In this paper, we evaluate a list of classifiers in order to use them in the detection of vandalism by focusing on metadata features. Our work is focused on two low resource data sets (Simple English and Albanian) from Wikipedia. The aim of this research is to prove that this form of vandalism detection applied in one data set (language) can be extended into another data set (language). Article views data sets in Wikipedia have been used rarely for the purpose of detecting vandalism. We will show the benefits of using article views data set with features from the article revisions data set with the aim of improving the detection of vandalism. The key advantage of using metadata features is that these metadata features are language independent and simple to extract because they require minimal processing. This paper shows that application of vandalism models across low resource languages is possible, and vandalism can be detected through view patterns of articles.

1. Introduction

Vandalism is a great challenge for Wikipedia, with humans being the main cause, through various illegitimate acts leaving traces in computer systems. Our hypothesis is that vandalism can be characterized through models of article views of vandalized articles in Wikipedia and that vandalism behavior is similar across different languages. In the past, a similar research was done in [1] and [2].

This paper is an extension of work originally presented in [3], by addressing the issue of using metadata features in predicting vandalism in Wikipedia's articles across languages.

According to our hypothesis, a model developed in one language can be applied to other languages. If successful, this would drop the costs of training the classifiers separately for each language.

Applying this model of vandalism detection across different languages shows similar results. In this paper, we will explore the possibility of applying the detection of vandalism across languages through article views daily and through article editing data set. We combine these data sets in order to analyze any gains in terms of language independency of certain features.

For this purpose, we compare performances of standard classifiers for identifying vandalism in two Wikipedia data sets (Simple English and Albanian). On top of this, we compare the performances of classifiers in one language and the other one and in the combined data set.

2. Approaches

Since 2008 Wikipedia vandalism detection based on machine learning approaches has become a field of increasing research interest. In [4] authors contributed the first machine learning vandalism detection approach using textual features as well as basic metadata features with a logistic regression classifier.

In [5] authors used a Naive Bayes classifier on a bag of words edit representation and were the first to use compression models to detect vandalism in Wikipedia. In [6] authors used Dynamic Markov Compression to detect vandalism edits in Wikipedia.

In [7] author extended the approach in [4] by adding some additional textual features and multiple wordlist-based features. In [8] authors were among the first to present a vandalism

*Corresponding Author: Arsim Susuri, Faculty of Contemporary Sciences and Technologies, South East European University, Tetovo, Macedoni
Email: arsimsusuri@gmail.com

detection approach based only on spatial and temporal metadata, without the need to inspect article or revision texts.

In [9] authors, in a similar fashion, built a vandalism detection system on top of their WikiTrust reputation system [10]. In [11] authors combined natural language, spatial, temporal and reputation features used in their aforementioned works [7, 8, 9]. Besides in [11], in [12] authors were the first to introduce ex post facto data as features, for whose calculation also future revisions have to be considered. Previously, the process of the detection of vandalism required building a separate learning system for each data set, where by research is focused on each language individually, as in the case in [12]. In the learning process of transfer learning, the domains of the source task and target task are different, as explored in [13]. This work focuses specifically on learning vandalism from one article and applying the models to another article. Supporting the current trend of creating cross language vandalism classifiers, in [2] authors evaluated multiple classifiers based upon a set of language independent features that were compiled from the hourly article view counts and Wikipedia's complete edit history.

We use two data sets from Wikipedia: full history of edits in Wikipedia's Simple English and Albanian data sets[1] and article views on a daily basis[2]. For future reference, we designate data sets as "simple" for Simple English and "sq" for Albanian. The processing of these data sets is explained in the following.

2.1. Wikipedia Data sets

We use the Wikipedia History Dumps of edits dated 29.10.2015, for Simple English and Albanian. In Table 1 are summarized the number of articles and of the revisions, along with usernames. The contents of the articles, used throughout the paper, are encyclopedic and do not include re-direct articles, discussions between users, and other help-related articles.

Table 1: Statistical data of editing history – January–April 2015

Data set	Articles	Revisions	Users
Simple English	413.249	5.565.876	575.755
Albanian	172.150	1.847.827	89.843

The raw data set of article views includes MediaWiki projects, including Wikipedia. In Table 2 are shown statistical data from the raw data set, with article views as filtered data. The filtering process of raw data set is based upon the analysis period of January – April 2015. Although this period of time is relatively short, we demonstrate the viability and success in the detection of vandalism based on models created from within the data set of article views.

Table 2: Statistical data of article views – January–April 2015

Data set	Article Views
Simple English	53.866.869
Albanian	16.698.447

2.2. Revisions with vandalized content

From the main data set, each revision is transformed to a set of features, as shown in Table 3. Feature selection is based on simplicity and language independence and is similar as in [3]. For each revision, we analyze comments made about it, looking for keywords that might suggest vandalism repair.

If this type of comment is detected, we designate the previous revision as vandalism. The process of labeling revisions is incomplete and noisy. In the past, active learning has been used to solve this issue as in [14].

However, in terms of quality, automatic approach has its limitations, thus requiring the assistance of humans in specific cases of vandalism, as explained in [15]. Based on the reported period of analysis (January – April), we find that approximately 2% of revisions contain vandalism.

This is in consistency with values provided in [16], but less than values reported in [17] and in [18], which report 4-7% of revisions with vandalized content.

2.3. Article views

The raw data set is structured through article views on the hour level. We apply transformation and filtering of articles viewed on the data set, containing previous revisions. The resulting features are shown in Table 4.

In [17] authors showed that these article views are important in order to see the impact of vandalism in Wikipedia. The behavior of the vandals can be analyzed through models, as a result of vandals controlling their work and as a result of increase in curiosity from other users. In [17] authors obtained article views from Wikipedia server logs. This method offered very precise data, in terms of time, but creates a lot of data to be processed.

Many researchers use this data set. A relevant study done in [19] uses this data set in order to compare accesses in medical related information such as allergies. Access models on this data set take into account the impact of seasonal diseases. On the other hand, online users have much more access to Wikipedia than other online medical encyclopedias.

Wikipedia is a well-known on-line source of medical information. Although vandalism has not been included within this study, access models based on seasons do indicate potential vandalism targets.

To determine whether these article views appear at the moment when they were vandalized, we apply search in the edit history data set and label all article views of observed revisions as legitimate or vandalizing. We do not take into account revisions made before January 2015, or articles without any revisions made during the period January – April 2015. This way, we obtain a labeled data set in terms of revisions being vandalized or not.

The final size of data is identical to the size of the combined data set, as explained below. This labeled data set enables us to determine whether or not article view models can predict vandalism. From this final combined data set, we split the time stamp attribute in the hour attribute. With this, we enable machine learning algorithms to learn models of daily access.

2.4. The combined data set

The combined data set is a result of merging two sets of time series for each language. The data set is built by adding features

[1] https://dumps.wikimedia.org/backup-index.html

[2] https://dumps.wikimedia.org/other/pagecounts-raw/

from the revisions data set labeled in the article views data set by repeating features of revisions.

This way, for each article view, we have information about whether or not the vandalized revision is viewed and, which are the revision features. The process of merging is shown in Figure 1.

We use the split of the "hour" attribute from the time stamp of the article views data set. Based on this split, we obtain eight features in the combined data set: hour, number of requests, transferred information, anonymous edit, minimal revision, size of comment, size of article and vandalism (class label).

These features are language independent and catch metadata of the revisions used more frequently, along with models of access. In order to apply classification algorithms, we split the combined data set to the training data set (January – March) and into the testing data set (April). Statistical data of these data sets are shown in Table 6.

Table 3: Description of features in the edit history data set

Attribute	Description
Title of article	Unique identifier of the Wikipedia article.
Time stamp	Time when the revision was done.
Anonymous edit	Only if an IP address is given. Value 0 is associated with a registered user. Value 1 is associated with an anonymous user.
Minimal revision	Minimal revision has the value 1. Normal revision has the value 0. The editor can emphasize that he/she made minimal revisions in the article (re-formatting, grammar, etc.).
Size of comment	Size of comment (in bytes).
Size of article	Size of the revised article (in bytes).
Vandalism	Revision is classified as vandalism based on the analysis of comments (of the current or upcoming revisions). Value 0 is associated with legitimate revision. Value 1 is associated with vandalizing revision.

Table 4: Description of features in the article views data set

Attribute	Description
Name of the project	Name of the MediaWiki project. In our case, Wikipedia's Simple English ("simple") and Albanian ("sq").
Time stamp	Time stamp of the revision.
Title of article	Title of the Wikipedia article.
Number of requests	Number of requests at a certain hour.
Transferred information	Transfer of data (bytes) from various requests.

2.5. Performance measures

For measuring the efficiency of the classifiers, we will use Area Under Precision-Recall (AUC-PR) and Receiver Operating Characteristic (ROC), as described in [20].

AUC-PR determines the probability that the classifier correctly identifies a random positive sample (vandalism) as positive.

AUC-ROC determines the probability that a classifier correctly identifies a random sample (positive or negative). Both have values ranging from 0 to 1, where value 1 means 100% correctness in labeling all samples taken into consideration. These evaluations are implemented with a confusion matrix, based in [21], as shown in Table 5:

Table 5: Example of confusion matrix

Actual class	Classifier prediction	
	Positive	Negative
Positive	True positive (T_P)	False positive (F_P)
Negative	False negative (F_N)	False positive (F_P)

3. Detection of vandalism across languages

We use the Weka tool, which offers well known machine learning algorithms.

The following supervised machine learning algorithms have been used for this type of vandalism detection:

1. Random Forest (RF) – a supervised classification algorithm [22], which builds the model from many trained decision-making trees from the training data set sample. The default Gini's impurity criterion is used in order to ascertain the best split on the data feature.
2. Gradient Tree Boosting (GTB) – a supervised algorithm (ensemble tree) based on boosting in order to create a better classifier by optimizing the loss function. Because of the fact that for classification purposes we use two classes, we use the binomial deviation as in [23].
3. Nearest Neighbour (NN) – non parametric classification algorithm. Used in KDTree structures of Bentley [24] because of efficiency in determining separated points and in order to avoid brute force search of the Naïve Nearest Neighbour algorithm.
4. Stochastic Gradient Descent (SGD) – a stochastic approximation to the gradient descent optimization method for minimizing an objective function that is written as a sum of differentiable functions. It is one of the ways of creating linear classifiers. Easily scalable although requires adjusting many parameters. As a result of using too many parameters, the selection of the loss function impacts the performance of the classifiers. As a loss function, we use the logistic regression.

The experiment was conducted in such a way that different arrangements for the above listed classifiers are tested, although with slight differences in results. The reason for the slight differences lies in the fact that all classifiers have converged for a very large number of observations.

If we analyze the data in Table 6, we can conclude that they are not balanced which, in turn, causes problems in the performance of the classifiers used for the experiments. We solve this problem by under sampling the legitimate observations until they match the number of vandalism observations. We extend this application to other data sets.

As a result, we build a set of a balanced subset of the training and testing data. For the detection of vandalism across language, we first train the classification models for the two languages in our

data sets: Simple English and Albanian. Afterwards, these models are evaluated on the testing set for the same language, then on the testing set of the other language.

The similarities between language domains are captured by using metadata, which are language independent. The model of applying the detection of vandalism across languages enables us to generalize the editing and viewing features in Wikipedia.

Application of these models across languages has been successful in the research area of text categorization across languages [25]. In cases of applying these models in text, cultural knowledge of the relevant target language is needed as additional information for the classifiers.

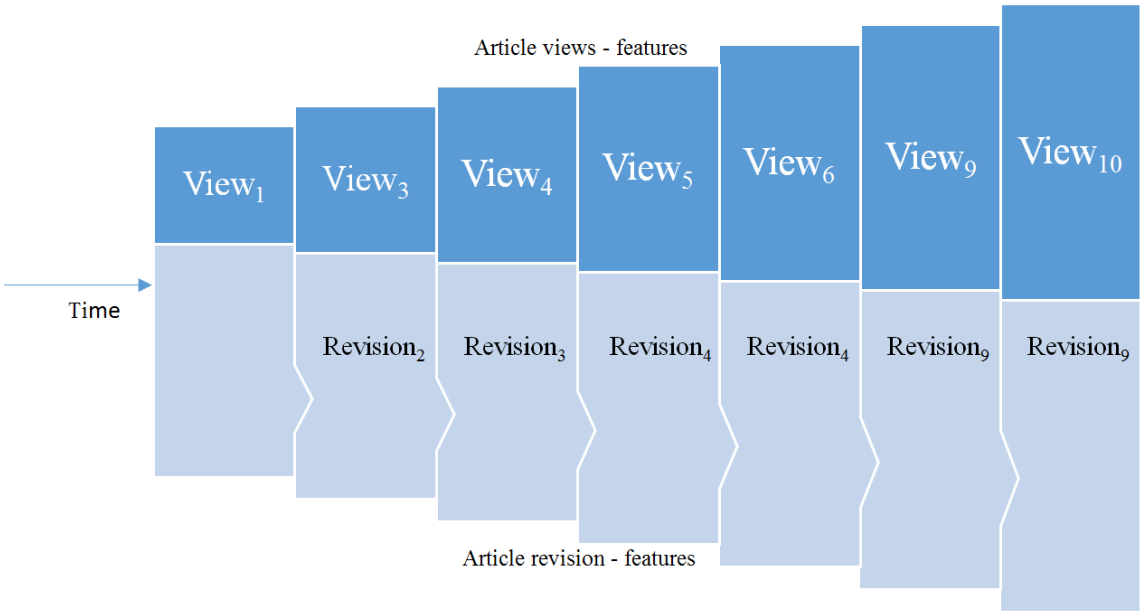

Table 6: Data sets with corresponding vandalism

Data set	Number of articles	Article views	Training set	Testing set
Simple English	413.249	53.866.869	27.543.172	9.611.483
Vandalism	(2.23%) 9.215	-	(2.14%) 589.423	(2.02%) 194.152
Albanian	172.150	16.698.447	9.943.521	5.140.374
Vandalism	(0.12%) 206	-	(0.16%) 15.909	(0.11%) 5654

The advantage of applying these vandalism detection models, built across languages, is that one model can be used for multiple languages, saving resources in developing models for each language. This is especially convenient in Wikipedia, since it contains hundreds of language sections.

This works allows the potential generalization of the concentration of vandalism research in Simple English to other low resource languages, without additional inputs.

4. Experiments and Results

The classification results are shown in Figures 2 to 7. We can see in these Figures the differences in AUC-PR and AUC-ROC values within the same language, and between the two languages used in the experiments. In the case of the designation "simple-sq," the model of the classification is trained in the English language data set and then applied in the testing data set of the Albanian language.

As far as applying classification models in the single language data sets (simple-simple, sq-sq), methods based on trees have better performances, with regards to AUC-PR and AUC-ROC values. In our case, for the revision data set, higher values have been obtained for GTB and RF, and in the case of the views data set, RF has higher values. However, in terms of time-related costs, these classifiers are the most expensive, as shown in Table 7.

Methods based on trees have higher classification results in the revision data sets.

Applying models across languages obtained lower values, proportionally, although with similar stability in comparison to the application in one language. GTB and RF classifiers have higher values in comparison to other tested classifiers.

SGD classifier has shown better results in single language data sets, and in the case when the training is based in the revision data set of the English language. Based on these results, we can conclude that the English language offers more patterns for detecting vandalism.

If we combine this fact with the fact that SGD is the fastest algorithm for training purposes (Table 7), the benefit, in terms of time costs, is much higher.

In general, the combination of the data sets does not increase the performance of the classifiers (Figures 4 and 7). There is an evident trend of an increase (although slight increase) in the performance of the classifiers of the combined data sets in comparison with the individual data sets.

Based on this, we can conclude that classifiers learn from the best models in each data set (language) but the improvements are not persistent.

Table 7: Execution time (in seconds) for the tested classifiers

Data \ Classifier		RF	GTB	NN	SGD
Training set	simple	60	150	12	6
	sq	4	12	2	1
Testing set	simple-simple	11	4	0.5	35
	sq-sq	0.5	0.5	2	0.5
	sq-simple	6	4	65	2
	simple-sq	0.5	0.5	3	0.5

The classification values in the particular language data sets of the revisions (Figures 2 and 5) are at the same level or slightly higher (up to 5%) than the actual systems. Our classification results in particular language data sets have higher AUC-PR values than AUC-ROC (Figures 2, 3, 5 and 6).

In general, the RF classifier is more appropriate for detecting vandalism across languages in terms of cost-related requirements (faster training and testing times).

If we compare AUC-PR values with AUC-ROC values of the RF classifier and GTB classifier, they are on the same level except for the training time (GTB classifier requires much more training time than RF classifier).

Another advantage of the RF classifier is the ability of scalability, which enables parallelism for vandalism detection models on full Wikipedia's sets.

The advantage of the data sets presented here is in the extraction of language independent features. These features, along with basic classifying algorithms show better performances in comparison to previous studies. The combination of editing and reading patterns shows improvement in the performance of the classifiers and enables these classifiers to use the best features from two data sets in order to predict vandalism. The RF classifier results are comparable to the results obtained in [2].

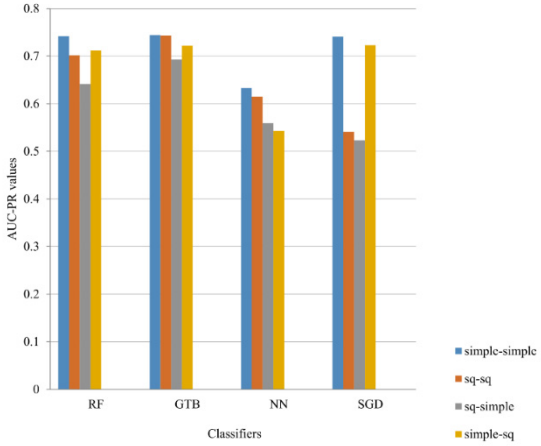

Figure 2: AUC-PR values for the article revisions data set

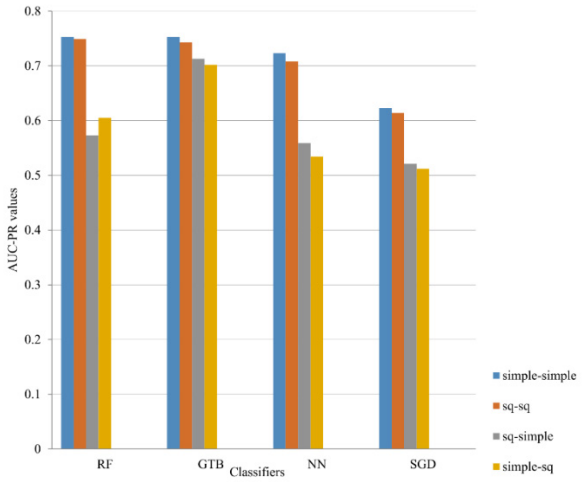

Figure 3: AUC-PR values for the article views data set

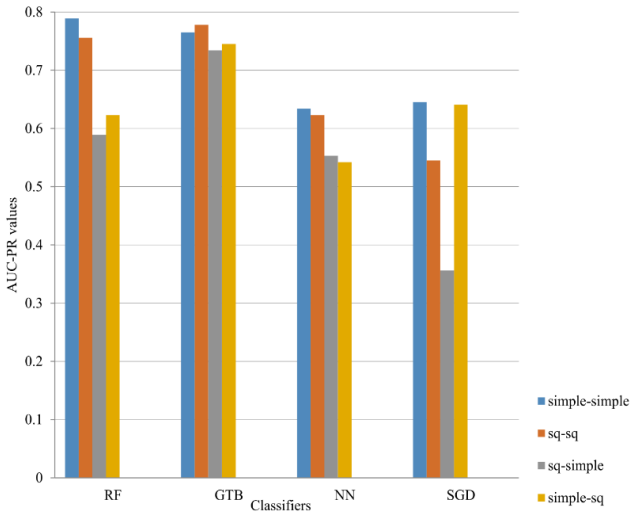

Figure 4: AUC-PR values for the combined data set

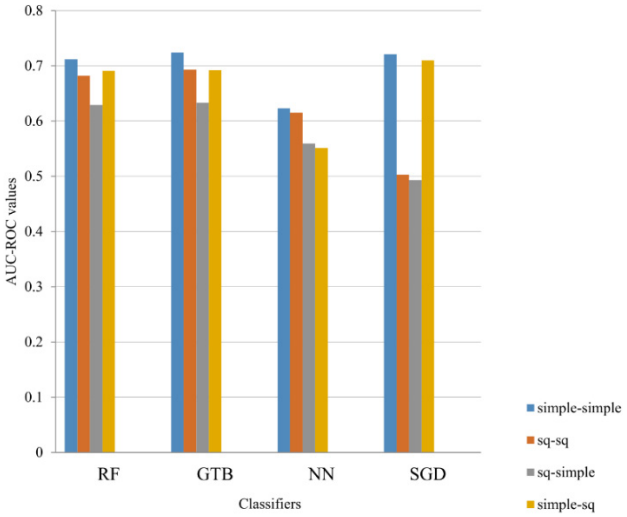

Figure 5: AUC-ROC values for the article revisions data set

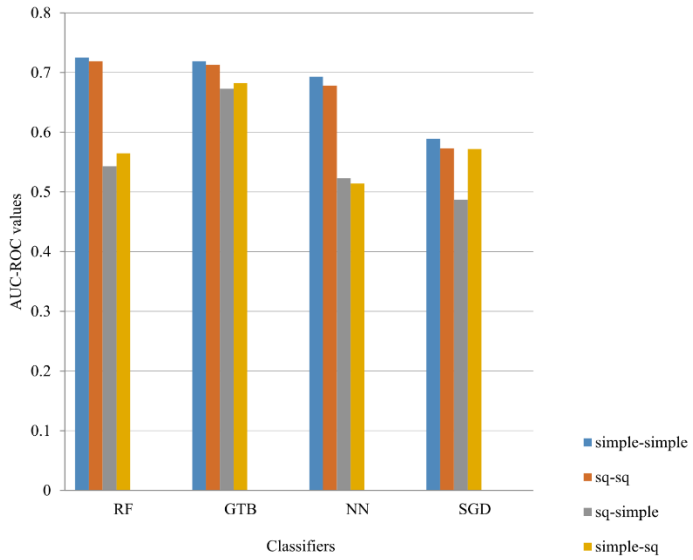

Figure 6: AUC-ROC values for the article views data set

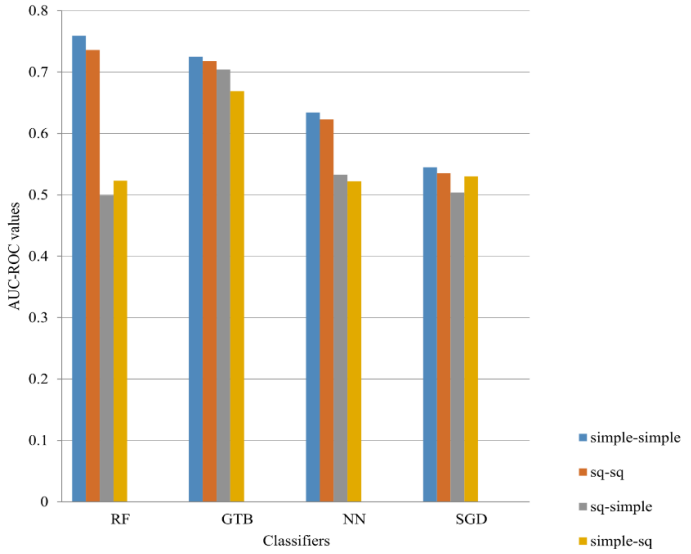

Figure 7: AUC-ROC values for the combined data set

Table 8 shows the impact of the features from the article views data set for the performance of the RF classifier. In this table, we have summarized the comparisons of the two data sets in terms of rankings of the features, based on the RF classifier. It comparatively describes the impact that each feature has on the overall performance of the RF classifier.

Although the improvements are not high, the addition of the features from the article views data set does not have a negative impact on the overall performance. The article views data set alone is not sufficient for vandalism detection and requires labeling from the revisions' data set.

However, the article views data set is a simple data set with few features that show some changes in access patterns when vandalism has occurred.

Table 8: Feature rankings of the combined data set based on the RF classifier

Features	Combined Data sets	
	simple	sq
Size of comment	0.358	0.243
Transferred bytes	0.261	0.238
Number of requests	0.196	0.354
Minimal revision	0.086	0.089
Anonymous edit	0.042	0.036
Size of article	0.041	0.024
Hour	0.017	0.017

5. Conclusions and Future Work

In this paper, we have presented data sets for the detection of vandalism and have demonstrated the application of four machine learning algorithms for the detection of vandalism within different languages and across languages. We have created three data sets from the data set of article views; full history of article edits and their combination. We have analyzed two Wikipedia editions: Simple English and Albanian.

During the experimentations, we have found out that the GTB classifier showed better performances in predicting vandalism, although in terms of time, it has higher costs.

The RF classifier has similar performances (0.2% - 0.5% difference) in comparison to the GTB classifier but with very low training costs (Table 7).

These results show that viewing and editing features of vandals are similar across languages. As a result of this fact, vandalism models of one language can be trained in one language and applied into another language. We have shown that application of the vandalism model across languages is feasible, and that view patterns can be used to detect and predict vandalism.

For future research, the inclusion of popular articles and the changes in traffic, caused by the vandalism, would be the right step to better understanding of the correlation of different data sets with regards to the impact they have on improving the vandalism detection rates.

References

[1] G. West. "Damage Detection and Mitigation in Open Collaboration Applications," Ph.D. Thesis, University of Pennsylvania, 2013.

[2] K. N. Tran, P. Christen, "Cross-language prediction of vandalism on wikipedia using article views and revisions", Pacific-Asia Conference on Knowledge Discovery and Data Mining (PAKDD), 2013.

[3] A. Susuri, M. Hamiti and A. Dika, "Machine Learning Based Detection of Vandalism in Wikipedia across Languages" in proceedings of the 5th Mediterranean Conference on Embedded Computing (MECO), Bar, Montenegro, 2016.

[4] M. Potthast, B. Stein, and R. Gerling, "Automatic vandalism detection in wikipedia" in advances in information retrieval, 663-668. Springer Berlin Heidelberg, 2008.

[5] K. Smets, B. Goethals, and B. Verdonk, "Automatic vandalism detection in wikipedia: Towards a machine learning approach" in WikiAI '08: Proceedings of the AAAI Workshop on Wikipedia and Artificial Intelligence, 2008.

[6] K. Y. Itakura and C. L. a. Clarke, "Using dynamic markov compression to detect vandalism in the Wikipedia" Proceedings of the 32nd international

ACM SIGIR conference on Research and development in information retrieval - SIGIR '09, 822, 2009.

[7] S. M. Mola-Velasco, "Wikipedia vandalism detection through machine learning: Feature review and new proposals - lab report for pan at clef 2010" in CLEF (Notebook Papers/LABs/Workshops), 2010.

[8] A. G. West, S. Kannan, and I. Lee, "Detecting wikipedia vandalism via spatio-temporal analysis of revision metadata" in Proceedings of the Third European Workshop on System Security, EUROSEC '10, 22-28, New York, NY, USA, 2010.

[9] B. T. Adler, L. De Alfaro, and I. Pye, "Detecting wikipedia vandalism using wikitrust" Notebook papers of CLEF, 2010.

[10] B. T. Adler and L. De Alfaro, "A content-driven reputation system for the Wikipedia" Proceedings of the 16th international conference on World Wide Web WWW 07, 7(Generic):261, 2007.

[11] B. T. Adler, L. De Alfaro, S. M. Mola-Velasco, Paolo Rosso, and Andrew G. West, "Wikipedia vandalism detection: Combining natural language, metadata, and reputation features" in proceedings of the 12th International Conference on Computational Linguistics and Intelligent Text Processing - Volume Part II, 277-288, Berlin, Heidelberg, 2011.

[12] A. G. West and I. Lee, "Multilingual vandalism detection using language-independent & ex post facto evidence - notebook for pan at clef 2011" in CLEF (Notebook Papers/Labs/Workshop), 2011.

[13] S. C. Chin and W. N. Street, "Divide and Transfer: an Exploration of Segmented Transfer to Detect Wikipedia Vandalism", Journal of Machine Learning Research (JMLR): Workshop and Conference Proceedings, 27, 133–144, 2012.

[14] S. C. Chin, W. N. Street, P. Srinivasan, and D. Eichmann, "Detecting Wikipedia Vandalism with Active Learning and Statistical Language Models", in Proceedings of the 4th Workshop on Information Credibility (WICOW), 2010.

[15] Q. Wu, D. Irani, C. Pu, and L. Ramaswamy, "Elusive Vandalism Detection in Wikipedia: A Text Stability-based Approach" in Proceedings of the 19th ACM International Conference on Information and Knowledge Management (CIKM), 2010.

[16] A. Kittur, B. Suh, B. A. Pendleton, and E. H. Chi, "He says, she says: conflict and coordination in Wikipedia" in Proceedings of the ACM Conference on Human Factors in Computing Systems (CHI), San Jose, CA, pages 453 - 462, 2007.

[17] R. Priedhorsky, J. Chen, S. T. K. Lam, K. Panciera, L. Terveen, and J. Riedl, "Creating, destroying, and restoring value in Wikipedia" in Proceedings of the International ACM Conference on Supporting GroupWork (GROUP), Sanibel Island, FL, pages 259 - 268, 2007.

[18] M. Potthast, "Crowdsourcing a Wikipedia Vandalism Corpus" in Proceedings of the 33rd International ACM SIGIR Conference on Research and Development in Information Retrieval (SIGIR), 2010.

[19] M. R. Laurent and T. J. Vickers, "Seeking Health Information Online: Does Wikipedia Matter?" Journal of the American Medical Informatics Association (JAMIA), 16 (2009), pages 471 - 479, 2009.

[20] J. Davis, and M. Goadrich, "The Relationship Between Precision-Recall and ROC Curves" in: ICML '06: Proceedings of the 23rd international conference on Machine learning. Pittsburgh, Pennsylvania: ACM, pp. 233–240, 2006.

[21] R. Kohavi, F. Provost, "Glossary of terms, Machine Learning" Vol. 30, No. 2/3, pages 271 -274, 1998.

[22] L. Breiman, "Random forests" Machine Learning, 45(1):5-32, October 2001.

[23] J. H. Friedman, "Greedy Function Approximation: A Gradient Boosting Machine" Annals of Statistics, 1189–1232, 2001

[24] J. L. Bentley, "Multidimensional Binary Search Trees Used for Associative Searching" Communications of the ACM, 18, pages 509 - 517, 1975.

[25] L. Rigutini, M. Maggini, and B. Liu, "An EM Based Training Algorithm for Cross-Language Text Categorization" in Proceedings of the IEEE/WIC/ACM International Conference on Web Intelligence (WI), 2005.

ASTES

Advances in Science, Technology and Engineering Systems Journal Vol. 2, No. 4, 8-13 (2017)

www.astesj.com

ASTESJ

ISSN: 2415-6698

Travelling Wave Solutions of Coupled Burger's Equations of Time-Space Fractional Order by Novel (G′/G)-Expansion Method

Rashida Hussain, Tayyiaba Rasool*, Asghar Ali

Department of Mathematics, Mirpur University of Science and Technology (MUST), Mirpur-10250 (AJK), Pakistan.

ARTICLE INFO

Article history:
Received: 09 March, 2017
Accepted: 29 March, 2017
Online: 07 April, 2017

Keywords:
Fractional complex transformation
Fractional derivatives
Fractional order coupled Burger's equations
Novel (G′/G)-expansion method

ABSTRACT

In this paper, Novel (G′/G)-expansion method is used to find new generalized exact travelling wave solutions of fractional order coupled Burger's equations in terms of trigonometric functions, rational functions and hyperbolic functions with arbitrary parameters. For the conversion of the partial differential equation to the ordinary differential equation, complex transformation method is used. Novel (G′/G)-expansion method is very effective and provides a powerful mathematical tool to solve nonlinear equations. Moreover, for the representation of these exact solutions we have plotted graphs for different values of parameters which were in travelling waveform.

1. Introduction

Fractional complex transformation as in [1] is utilized for transformation of nonlinear fractional order partial differential equations into nonlinear ordinary differential equations. The one-dimensional case of Burger's equation was introduced by a Dutch scientist J. M. Burger in 1939 see [2], its general form is given as

$$\partial_t(r) + (r.\nabla)r = s\nabla^2 r.$$

Afterward, new type of Burger's equation was presented in further research named as time-space fractional order coupled Burger's equations [3], which has the form

$$\frac{\partial^\alpha w}{\partial t^\alpha} - \frac{\partial^{2\beta} w}{\partial x^{2\beta}} + 2w\frac{\partial^\beta w}{\partial x^\beta} + c\frac{\partial^\beta (wz)}{\partial x^\beta} = 0,$$

$$\frac{\partial^\alpha z}{\partial t^\alpha} - \frac{\partial^{2\beta} z}{\partial x^{2\beta}} + 2z\frac{\partial^\beta z}{\partial x^\beta} + d\frac{\partial^\beta (wz)}{\partial x^\beta} = 0,$$

where $0 < \alpha \leq 1, 0 < \beta \leq 1, t > 0$.

An assortment of approaches occurs for nonlinear equations which gives their travelling wave and numerical solutions. Wang et al. introduced (G′/G)-expansion method [4]. This method was further reached out for coupled Burger's equations by Younas et al. [3]. In this article Novel (G′/G)-expansion method has been utilized to discover travelling wave solutions of nonlinear space and time fractional order coupled Burger's equations.

1.1. Fractional complex transformation

Fractional complex transform is the unobtrusive way for the transformation of the fractional order differential equation into integer order differential equation. This simplifies the rest of the procedure towards a solution. Presently consider

$$\delta = Lt + Mx + Ny + Oz,$$

where *L, M, N* and *O* are constants.

Let the fractional complex transformation in nonlinear fractional order coupled Burger's equations be defined as

$$\delta = \frac{Lt^\alpha}{\Gamma(\alpha+1)} + \frac{Mx^\beta}{\Gamma(\beta+1)} + \frac{Ny^\gamma}{\Gamma(\gamma+1)} + \frac{Oz^\lambda}{\Gamma(\lambda+1)}.$$

1.2. Travelling wave solution

Travelling wave solution was used for transformation of partial differential equations into ordinary differential equations. For this purpose, we consolidate two independent variables into one independent variable known as travelling wave variable *x* [5].

*Coresponding: Tayyiaba Rasool, Mirpur University of Science and Technology Mirpur AJK, Pakistan, +923418903401, tayba481@yahoo.com

Travelling wave solution of nonlinear partial differential equation

$$\partial_t w(z,t) + c\partial_z w(z,t) = 0,$$

where $z \in R,\ t > 0$, can be calculated as follows.

Applying phase plan analysis technique by presenting the travelling wave coordinates as takes after

1. Define the travelling wave variable x as $x = z - bt, z \in R$ and $b > 0$ is the propagation speed of the wave or travelling wave speed.
2. Defining the travelling wave Ansatz [6] for $w\ (z,t)$ in the following form
$$W(x) = W(z - dt) = w(z,t)$$

By the travelling wave Ansatz, we have

$$\partial_t w = -d\frac{\partial W}{\partial x} = -dW'(x),$$

$$\partial_z w = \frac{\partial W}{\partial x} = W'(x),$$

$$-bW'(x) + cW'(x) = 0, \quad x = z - bt.$$

1.3. Fractional derivatives in Caputo sense

Fractional derivative presented in the Caputo sense of $f \in C_{-1}^{n}$ [7], is defined as

$$D^{\alpha} f(r) = \frac{1}{\Gamma(n-\alpha)}\int_0^r (r-\delta)^{n-\alpha-1} f^n(\delta)d\delta.$$

By Caputo's derivative

$$D^{\alpha} L = 0,$$

where L is constant.

$$D^{\alpha}(r)^{\beta} = \frac{\Gamma(\beta+1)}{\Gamma(\beta-\alpha+1)} r^{\beta-\alpha}, \quad \beta > \alpha - 1.$$

Linear relationships of Caputo's derivative are

$$D^{\alpha}\big(f(r)g(r)\big) = \sum_{n=0}^{\infty}\binom{\alpha}{n} f^{(n)}(r) D^{\alpha-n} f(r),$$

$$D^{\alpha}\big(\theta f(r) + \varphi g(r)\big) = \theta D^{\alpha} f(r) + \varphi D^{\alpha} g(r),$$

where θ and φ are constants. This relation is likewise named as Leibnitz rule.

$$D_t^{\alpha} w(x,t) = \frac{\partial^{\alpha} w(x,t)}{\partial t^{\alpha}},$$

$$= \begin{cases} \dfrac{1}{\Gamma(n-\alpha)}\displaystyle\int_0^t (t-\delta)^{n-\alpha-1}\frac{\partial^n w(x,t)}{\partial t^n} d\delta, & n > \alpha > n-1, \\ \dfrac{\partial^n w(x,t)}{\partial t^n}, & \alpha = n. \end{cases}$$

2. Novel (G′/G)-Expansion Method

Fractional order partial differential equation of the form

$$S(w, w_x, w_t, D_t^{\alpha} w, \dots) = 0, \tag{1}$$

see [8], where $D_t^{\alpha} w$ demonstrates the modified form of Riemann-Liouville derivative presented by Jumarie [9], and S is a polynomial of unknown function $w(x,t)$ and its several nonlinear partial and fractional derivatives.

Step I: Fractional complex transformation projected by Li and He [10] was used in order to transform PDE into ODE. For required equations, complex transformation is

$$w(x,t) = w(\delta), \quad \delta = \frac{Lt^{\alpha}}{\Gamma(\alpha+1)} + \frac{Mx^{\beta}}{\Gamma(\beta+1)}, \tag{2}$$

where L and M are non-zero arbitrary constants. Complex transformation (2) converts fractional order partial differential (1) into ODE in integer order as

$$S(w, w', w'', w''', \dots) = 0, \tag{3}$$

Step II: Integrate (3) to possible extent. At that time submit the constants which are to be determined later.

Step III: Considering the solution of (3)

$$w(\delta) = \sum_{i=-m}^{m} \alpha_i \big(n + \gamma(\delta)\big)^i, \tag{4}$$

where

$$\gamma(\delta) = \frac{G'(\delta)}{G(\delta)}, \tag{5}$$

α_m and α_{-m} can't be simultaneously zero. n and α_i are constants that will be determined later. $G = G(\delta)$ satisfies the nonlinear ordinary differential equation of second order

$$GG'' = PGG' + QG^2 + R(G')^2, \tag{6}$$

where P, Q and R are genuine constants and the derivative represented by prime is with respect to δ.

By using Cole-Hopf transformation [11, 12], (6) reduces to Riccati equation

$$\gamma'(\delta) = Q + P\gamma(\delta) + (R-1)\gamma^2(\delta). \tag{7}$$

Equation (7) has twenty-five solutions [13].

Step IV: By the homogeneous balance the value of m can be calculated, where $m > 0$.

Step V: Embedding (4) together with (5) and (6) into (3), we get polynomials of the forms $\left(n + \frac{G'}{G}\right)^i$ and $\left(n + \frac{G'}{G}\right)^{-i}$. Assembling each coefficient of polynomials equivalent to zero an overdetermined set is acquired as algebraic equations comprising α_i, L, m and M.

Step VI: Values of α_i, L, m and M the constants can be obtained by solving set of the algebraic equations. Cnsequently the solutions of (6) together with the resulted values of the constants generate exact travelling wave solutions of the nonlinear (1).

3. Application of Novel (G′/G)-Expansion Method

Consider the Coupled Burger's equations of time-space fractional order form as

$$\frac{\partial^{\alpha} w}{\partial t^{\alpha}} - \frac{\partial^{2\beta} w}{\partial x^{2\beta}} + 2w\frac{\partial^{\beta} w}{\partial x^{\beta}} + c\frac{\partial^{\beta}(wz)}{\partial x^{\beta}} = 0, \quad (1)$$

$$\frac{\partial^{\alpha} z}{\partial t^{\alpha}} - \frac{\partial^{2\beta} z}{\partial x^{2\beta}} + 2z\frac{\partial^{\beta} z}{\partial x^{\beta}} + d\frac{\partial^{\beta}(wz)}{\partial x^{\beta}} = 0. \quad (2)$$

By using fractional derivatives, (1) and (2) are converted into ordinary differential equations of integer order. After integration, we get

$$k_1 + Lw - M^2 w' + Mw^2 + cM(wz) = 0, \quad (3)$$

$$k_2 + Lz - M^2 z' + Mz^2 + dM(wz) = 0, \quad (4)$$

here k_1 and k_2 are the constants of integration. By considering now the homogeneous balance of w and w' we get $m = 1$.

The trial solution $w(\delta) = \sum_{i=-m}^{m} \alpha_i \left(n + \left(\frac{G'(\delta)}{G(\delta)}\right)\right)^i$ of Novel (G′/G)-expansion method becomes

$$w(\delta) = \alpha_{-1}\left(n + \frac{G'}{G}\right)^{-1} + \alpha_0\left(n + \frac{G'}{G}\right)^{0} + \alpha_1\left(n + \frac{G'}{G}\right)^{1}. \quad (5)$$

In a similar way, the trial solution for z is

$$z(\delta) = \beta_{-1}\left(n + \frac{G'}{G}\right)^{-1} + \beta_0\left(n + \frac{G'}{G}\right)^{0} + \beta_1\left(n + \frac{G'}{G}\right)^{1}. \quad (6)$$

Using (5) and (6) into (3) also in (4), we obtain polynomials in $\left(n + \frac{G'}{G}\right)^i$ and $\left(n + \frac{G'}{G}\right)^{-i}$ on left-hand side. Now assembling each coefficient of polynomials equal to zero, we get an algebraic set of equations for $\alpha_0, \alpha_{-1}, \alpha_1, \beta_0, \beta_{-1}, \beta_1, k_1, k_2, L$ and M. After solving overdetermined set of the algebraic equations by the use of computational software Maple 18 the required solution sets are

3.1. Set 1

$$P = 0, Q = \frac{3\beta_{-1}(-1+dc)}{M(-1+d)}, R = \frac{Mc - M - \alpha_1 + dc\alpha_1}{M(c-1)},$$

$$L = 0, M = M, n = 0, k_1 = \frac{-4M\beta_{-1}^2(-1+dc)(c-1)}{(-1+d)^2},$$

$$k_2 = \frac{-4M\beta_{-1}^2(-1+dc)}{(-1+d)}, \alpha_{-1} = \frac{\beta_{-1}(c-1)}{-1+d},$$

$$\beta_1 = \frac{\alpha_1(d-1)}{c-1}, \beta_0 = 0, \beta_{-1} = \beta_{-1}, \alpha_1 = \alpha_1, \alpha_0 = 0,$$

where $M, \alpha_{-1}, \alpha_1, \beta_{-1}, \beta_1$ are arbitrary constants.

3.2. Set 2

$$P = \frac{-L\beta_{-1} + 2nL\beta_0 + 2nM{\beta_0}^2 + 2M\beta_{-1}\beta_0}{M^2\beta_{-1}}, M = M, Q = Q,$$

$$R = \frac{-L\beta_0 - M^2\beta_{-1} + {\beta_0}^2 M}{M^2\beta_{-1}}, k_1 = 0, L = L, n = n, \beta_0 = \beta_0,$$

$$k_2 = -Ln\beta_{-1} - Ln^2\beta_0 - M^2Q\beta_{-1} - M{\beta_{-1}}^2 - Mn^2{\beta_0}^2 - 2Mn\beta_{-1}\beta_0,$$

$$\alpha_{-1} = 0, \alpha_0 = 0, \alpha_1 = 0, \beta_1 = 0, \beta_{-1} = \beta_{-1},$$

where $M, Q, L, n, \beta_0, \beta_1$ are arbitrary constants.

3.3. Set 3

$$P = -\frac{\alpha_0(-1+d)}{M}, Q = Q, R = 1, L = -M\alpha_0, M = M,$$

$$k_1 = Mn\alpha_{-1}\alpha_0 - M^2Q\alpha_{-1} + M{\alpha_{-1}}^2 - M{\alpha_{-1}}^2 d - Mnd\alpha_{-1}\alpha_0,$$

$$k_2 = \frac{-M\alpha_{-1}(-2+d)(-\alpha_0 nc + MQc - 2\alpha_{-1} + d\alpha_{-1} + cd\alpha_{-1} + cdn\alpha_0)}{c^2},$$

$$\beta_{-1} = \frac{\alpha_{-1}(-2+d)}{c},$$

$$\alpha_{-1} = \alpha_{-1}, \alpha_0 = \alpha_0, \alpha_1 = 0, \beta_0 = 0,$$

$$\beta_1 = 0, \alpha_0 = \alpha_0, n = n,$$

where $Q, M, n, \alpha_0, \alpha_{-1}$ are arbitrary constants.

By using every one of these sets into (5) and (6), then consolidating with the solution $G(\delta)$ of Novel (G′/G)-expansion method, we get travelling wave solutions to Burger's equations.

Now we take *Set 1* and put it in (5) and (6) simultaneously. Then substitute all twenty-five solutions of Novel (G′/G)-expansion method into the resulted equations.

Rewriting *Set 1*, we get values of $\alpha_1, \alpha_{-1}, \beta_{-1}$ and β_1 as

$$\alpha_1 = \frac{M(R-1)(-1+c)}{-1+dc}, , \alpha_{-1} = \frac{MQ(-1+c)}{3(-1+dc)}, \alpha_0 = 0, n = 0,$$

$$\beta_1 = \frac{M(R-1)(-1+d)}{-1+dc}, \beta_{-1} = \frac{MQ(-1+d)}{3(-1+dc)}, P = 0, L = 0.$$

Putting the whole set in (5) and (6) respectively, we get

$$w(\delta) = \alpha_{-1}\left(n + \frac{G'}{G}\right)^{-1} + \alpha_0\left(n + \frac{G'}{G}\right)^{0} + \alpha_1\left(n + \frac{G'}{G}\right)^{1},$$

by putting values of $n, \alpha_{-1}, \alpha_1, \beta_{-1}$ and β_1, we get

$$w(\delta) = \frac{MQ(-1+c)}{3(-1+dc)}\left(0 + \frac{G'}{G}\right)^{-1} + 0\left(0 + \frac{G'}{G}\right)^{0} + \frac{M(R-1)(-1+c)}{-1+dc}\left(n + \frac{G'}{G}\right)^{1},$$

$$w(\delta) = \frac{MQ(-1+c)}{3(-1+dc)}\left(\frac{G'}{G}\right)^{-1} + \frac{M(R-1)(-1+c)}{-1+dc}\left(\frac{G'}{G}\right)^{1},$$

Similarly,

$$z(\delta) = \frac{MQ(-1+d)}{3(-1+dc)}\left(\frac{G'}{G}\right)^{-1} + \frac{M(R-1)(-1+d)}{-1+dc}\left(\frac{G'}{G}\right)^{1}$$

When $\rho = P^2 - 4QR + 4Q > 0$ and $(R-1)Q \neq 0$ or $(R-1)P \neq 0$ then solutions of $w(\delta)$ are

$$w^1(\delta) = \frac{MQ(c-1)}{3(dc-1)}\left\{-\frac{1}{2(R-1)}\left(P + \sqrt{\rho}tanh\left(\sqrt{\rho}\delta/2\right)\right)\right\}^{-1} + \frac{M(R-1)(c-1)}{dc-1}\left\{-\frac{1}{2(R-1)}\left(P + \sqrt{\rho}tanh\left(\sqrt{\rho}\delta/2\right)\right)\right\}^{1},$$

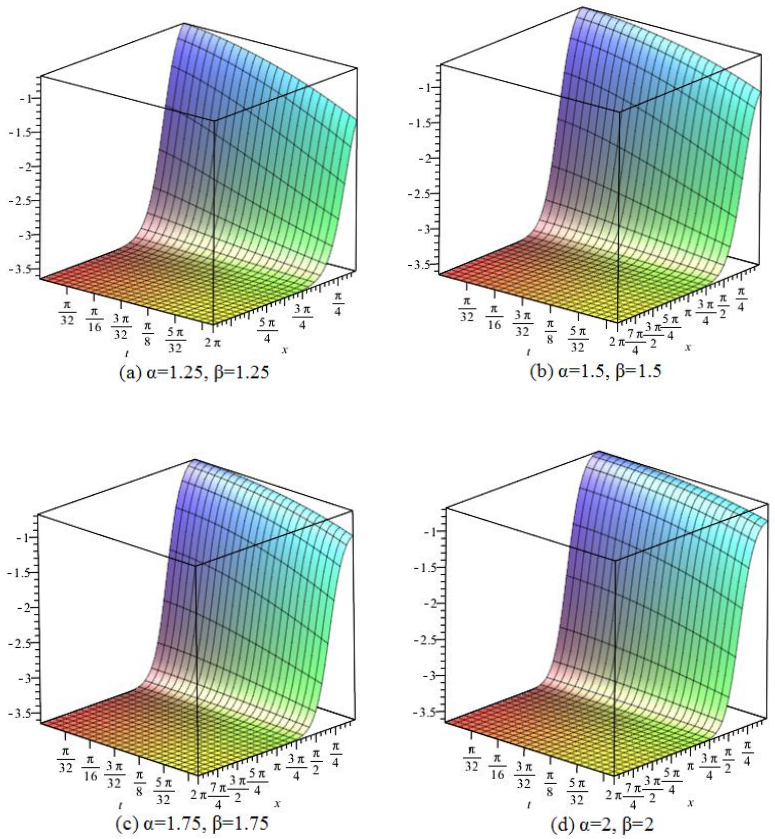

Figure 1: (a) -(d) shows singular soliton solutions of $w^1(\delta)$ for different values of parameters.

$$w^2(\delta)=\frac{MQ(c-1)}{3(dc-1)}\left\{-\frac{1}{2(R-1)}\left(P+\sqrt{\rho}coth\left(\sqrt{\rho}\delta/2\right)\right)\right\}^{-1}+\frac{M(R-1)(c-1)}{dc-1}\left\{-\frac{1}{2(R-1)}\left(P+\sqrt{\rho}coth\left(\sqrt{\rho}\delta/2\right)\right)\right\}^{1},$$

$$w^3(\delta)=\frac{MQ(c-1)}{3(dc-1)}\left\{-\frac{1}{2(R-1)}\left(P+\sqrt{\rho}\left(tanh\left(\sqrt{\rho}\delta\right)\pm isech\left(\sqrt{\rho}\delta\right)\right)\right)\right\}^{-1}+\frac{M(R-1)(c-1)}{dc-1}\left\{-\frac{1}{2(R-1)}\left(P+\sqrt{\rho}\left(tanh\left(\sqrt{\rho}\delta\right)\pm isech\left(\sqrt{\rho}\delta\right)\right)\right)\right\}^{1},$$

$$w^4(\delta)=\frac{MQ(c-1)}{3(dc-1)}\left\{-\frac{1}{2(R-1)}\left(P+\sqrt{\rho}\left(coth\left(\sqrt{\rho}\delta\right)\pm icsch\left(\sqrt{\rho}\delta\right)\right)\right)\right\}^{-1}+\frac{M(R-1)(c-1)}{dc-1}\left\{-\frac{1}{2(R-1)}\left(P+\sqrt{\rho}\left(coth\left(\sqrt{\rho}\delta\right)\pm icsch\left(\sqrt{\rho}\delta\right)\right)\right)\right\}^{1},$$

$$w^5(\delta)=\frac{MQ(c-1)}{3(dc-1)}\left\{-\frac{1}{4(R-1)}\left(2P+\sqrt{\rho}\left(tanh\left(\sqrt{\rho}\delta/4\right)+icoth\left(\sqrt{\rho}\delta/4\right)\right)\right)\right\}^{-1}+\frac{M(R-1)(c-1)}{dc-1}\left\{-\frac{1}{4(R-1)}\left(2P+\sqrt{\rho}\left(tanh\left(\sqrt{\rho}\delta/4\right)+icoth\left(\sqrt{\rho}\delta/4\right)\right)\right)\right\}^{1}.$$

There are twenty more solutions of w.

Now solutions of $z(\delta)$ when $\rho=P^2-4QR+4Q>0$ and $(R-1)Q\neq 0$ or $(R-1)P\neq 0$ are

$$z^1(\delta)=\frac{MQ(d-1)}{3(dc-1)}\left\{-\frac{1}{2(R-1)}\left(P+\sqrt{\rho}tanh\left(\sqrt{\rho}\delta/2\right)\right)\right\}^{-1}+\frac{M(R-1)(d-1)}{dc-1}\left\{-\frac{1}{2(R-1)}\left(P+\sqrt{\rho}tanh\left(\sqrt{\rho}\delta/2\right)\right)\right\}^{1},$$

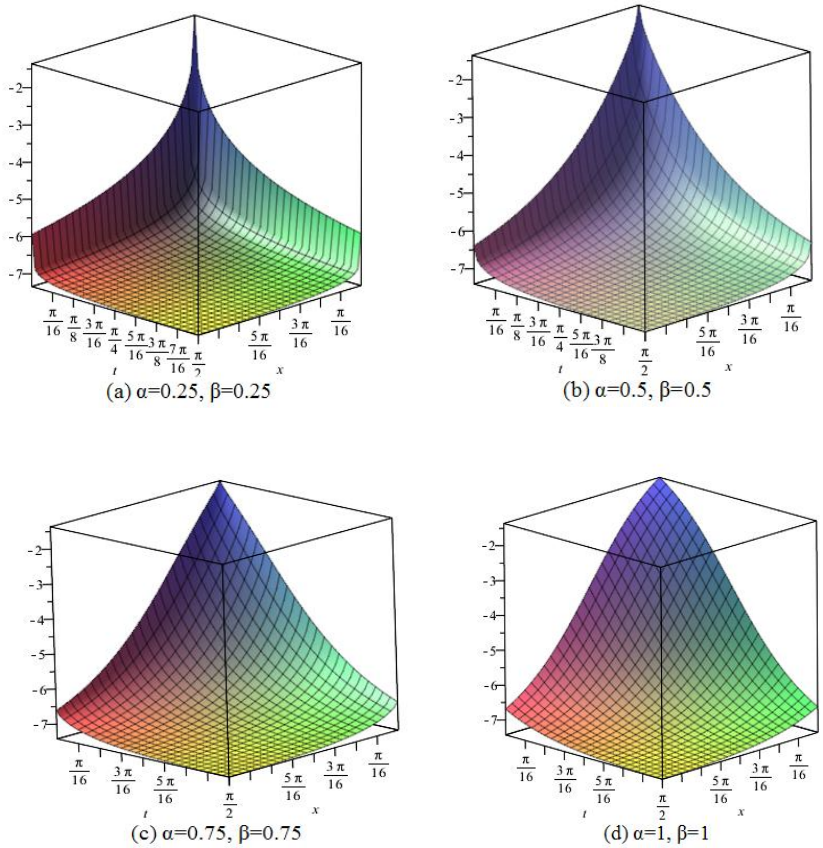

Figure 2: (a) -(d) shows singular soliton solutions of $z^1(\delta)$ for different values of parameters.

$$z^2(\delta)=\frac{MQ(d-1)}{3(dc-1)}\left\{-\frac{1}{2(R-1)}\left(P+\sqrt{\rho}coth\left(\sqrt{\rho}\delta/2\right)\right)\right\}^{-1}+\frac{M(R-1)(d-1)}{dc-1}\left\{-\frac{1}{2(R-1)}\left(P+\sqrt{\rho}coth\left(\sqrt{\rho}\delta/2\right)\right)\right\}^{1},$$

$$z^3(\delta)=\frac{MQ(d-1)}{3(dc-1)}\left\{-\frac{1}{2(R-1)}\left(P+\sqrt{\rho}\left(tanh\left(\sqrt{\rho}\delta\right)\pm isech\left(\sqrt{\rho}\delta\right)\right)\right)\right\}^{-1}+\frac{M(R-1)(d-1)}{dc-1}\left\{-\frac{1}{2(R-1)}\left(P+\sqrt{\rho}\left(tanh\left(\sqrt{\rho}\delta\right)\pm isech\left(\sqrt{\rho}\delta\right)\right)\right)\right\}^{1},$$

$$z^4(\delta)=\frac{MQ(d-1)}{3(dc-1)}\left\{-\frac{1}{2(R-1)}\left(P+\sqrt{\rho}\left(coth\left(\sqrt{\rho}\delta\right)\pm icsch\left(\sqrt{\rho}\delta\right)\right)\right)\right\}^{-1}+\frac{M(R-1)(d-1)}{dc-1}\left\{-\frac{1}{2(R-1)}\left(P+\sqrt{\rho}\left(coth\left(\sqrt{\rho}\delta\right)\pm icsch\left(\sqrt{\rho}\delta\right)\right)\right)\right\}^{1},$$

$$z^5(\delta)=\frac{MQ(d-1)}{3(dc-1)}\left\{-\frac{1}{4(R-1)}\left(2P+\sqrt{\rho}\left(tanh\left(\sqrt{\rho}\delta/4\right)+icoth\left(\sqrt{\rho}\delta/4\right)\right)\right)\right\}^{-1}+\frac{M(R-1)(d-1)}{dc-1}\left\{-\frac{1}{4(R-1)}\left(2P+\sqrt{\rho}\left(tanh\left(\sqrt{\rho}\delta/4\right)+icoth\left(\sqrt{\rho}\delta/4\right)\right)\right)\right\}^{1}.$$

There are twenty more solutions of z.

For convenience, other exact solutions are overlooked.

Conclusion

Novel (G′/G)-expansion method is an effective method for finding exact solutions of the fractional order partial differential equation. As an application, exact solutions have been all around got for time-space fractional order coupled Burger's equations. The fractional complex transformation used as a part of the exhibited work is very momentous. By utilizing this fractional transformation, fractional order partial differential equation can be converted into the integer order ordinary differential equation. Graphical portrayals insure that the required solutions are travelling wave solutions. Novel (G′/G)-expansion method is an influential mathematical tool for solving the nonlinear partial differential equations.

References

[1] J. H. He, S. K. Elagan and Z. B. Li, "Geometrical explanation of the fractional complex transform and derivative chain rule for fractional calculus," Physics Letters. A, **376(4)**: 257–259 (2012).

[2] J. M. Burgers, "Mathematical examples illustrating relations occurring in the theory of turbulent fluid motion," verhand. kon. neder. akad. wetenschappen, afd. natuurkunde, eerste sectie, **17**: 1-53 (1939).

[3] Muhammad Younis, Asim Zafar, Kalim-Ul-Haq and Muhammad Rahman, "Travelling wave solutions of fractional order coupled Burger's equations by (G′/G)-expansion method," American Journal of Computational and Applied Mathematics, **3(2)**: 81 (2013).

[4] M. L. Wang, X. Li and J. Zhang, "The (G′/G)-expansion method and travelling wave solutions of nonlinear evolution equations in Mathematical Physics," Phys. Lett. A, **372**: 417-423 (2008).

[5] Muhamad Abdel Rehim Selim Ibrahim Elshobaki, "Travelling wave solutions of reaction-diffusion equations coupled with shallow water equations," Hamburg, 9-10 (2012).

[6] A. Biswas, M. S. Ismail, "1-Soliton solution of the coupled KdV equation and Gear-Grimshaw model," Appl. Math. Comp., **216**: 36623670 (2010).

[7] Yong Chen and Hong-Li An, "Numerical solutions of coupled Burger's equations with time and space-fractional derivatives," Applied Mathematics and Computation, **200**: 87-95 (2008).

[8] Muhammad Shakeel, Qazi Mehmood Ul-Hussain, Jamshad Ahmad and Tauseef Naqvi, "Exact solutions of the time fractional BBM-Burger's equation by Novel (G′/G)-expansion method," Hindawi Publishing Corporation, Advances in Mathematical Physics, **181594**: 1-15 (2014).

[9] G. Jumarie, "Modified Riemann-Liouville Derivative and Fractional Taylor Series of Non-Differentiable Functions Further Results," Computers and Mathematics with Applications, **51**: 1369 (2006).

[10] Z. Li and J. He, "Fractional complex transform for fractional differential equations," Mathematical and Computational Applications, **15(2)**: 970-973 (2010).

[11] J. D. Cole, "On a quasi-linear parabolic equation occurring in aerodynamics," quart. appl. math., **9**: 225-236 (1951).

[12] E. Hopf, "The partial differential equation, $u_t+uu_x=u_{xx}$," comm. Pure appl. math., **3**: 201-230 (1950).

[13] S. Zhu, "The generalizing Riccati equation mapping method in nonlinear evolution equation: Application to (2+1)-dimensional Boiti-Leon-Pempinelle equation," Chaos, Solitons and Fractals, **37(5)**: 1335-1342 (2008).

ASTES

Advances in Science, Technology and Engineering Systems Journal Vol. 2, No. 4, 14-25 (2017)

www.astesj.com

ASTESJ

ISSN: 2415-6698

Evaluation of Pure Aluminium Inoculated with Varying Grain Sizes of an Agro-waste based Inoculant

Adeyemi I. Olabisi*, Thankgod E. Boye, Emagbetere Eyere

Department of Mechanical Engineering, P. M. B. 1221, Federal University of Petroleum Resources, Effurun, 330102, Nigeria

ARTICLE INFO

Article history:
Received: 01 March, 2017
Accepted: 07 April, 2017
Online: 13 April, 2017

Keywords:
Evaluation
Inoculation
Pure Aluminium
Agro-waste
Grain Size

ABSTRACT

Pure Aluminium and its alloy are widely utilized in Engineering and Industrial applications due to certain significant properties such as softness, ductility, corrosion resistance, and high electrical conductivity which it possesses. Addition of an agro-waste based grain refiner to the melt can alter the characteristics positively or negatively. Therefore, the aim of this paper is to investigate the inoculating capability of an agro-waste based inoculant and the effect of adding varying sizes of its grains on some of the properties of pure aluminium after solidification. The beneficial outcome of this investigation would enhance the economic value of the selected agro-waste and also broaden the applications of aluminium in Engineering. The assessed properties include; microstructure, micro hardness, ductility, and tensile strength. The agro-waste used as the grain refiner is pulverised cocoa bean shells (CBS). Three sets of test samples were produced using dry sand moulding process, with each melt having a specified grain size of the inoculant added to it (150, 225 and 300microns respectively). Ladle inoculation method was adopted. The cast samples after solidification were machined to obtain various shapes/sizes for the different analysis. The microstructural examination showed that the mechanical properties are dependent on the matrix as the aluminium grains became more refined with increasing grain size of the inoculant. I.e. Due to increasing grain size of the inoculant, the micro hardness increased (56, 61, 72HB) as the aluminium crystal size became finer. Meanwhile, the tensile strength (284, 251, 223N/mm^2) and ductility (1.82, 0.91, 0.45%E) decreased as grain size of the inoculant increased. The overall results showed that the used agro-waste based inoculant has the capability of refining the crystal size of pure aluminium as its grain size increases. This will make the resulting aluminium alloy applicable in areas where hardness is of superior consideration relative to tensile strength.

1. Introduction

Through innovative thinking, most of the wastes in our environment which take space, and require huge cost of disposal or pollute our ecosystem as they decompose or when burnt, can be converted for use in the industry to develop improved materials which are indigenous for enhancing cost effective production and customer satisfaction. Consequently, this work focuses on investigating the potential of cocoa beans shell which is one of the agro-waste in our environment, to be used as indigenous inoculant for improving the microstructure and mechanical properties of pure aluminium.

Pure aluminium is soft, ductile, corrosion resistant and has a high electrical conductivity. It is widely used for foil and conductor cables, but alloying it with other elements is necessary to provide the higher strength needed for other applications. Aluminium is one of the lightest engineering metals, having strength to weight ratio superior to steel. By utilizing various combinations of its advantageous properties such as strength, lightness, corrosion resistance, recyclability and formability, aluminium is being employed in an ever-increasing number of applications. This array

*Corresponding Author: Adeyemi I. Olabisi Department of Mechanical Engineering, P. M. B. 1221, Federal University of Petroleum Resources, Effurun, 330102, Nigeria
Email: adeyemi.olabisi@fupre.edu.ng

of products ranges from structural materials to thin packaging foils [1, 2].

Pure aluminium does not have a high tensile strength. However, the addition of alloying elements like manganese, silicon, copper and magnesium can increase the strength properties of aluminium and produce an alloy with properties tailored to particular applications [2].

Aluminium is well suited to cold environments. It has the advantage over steel in that its' tensile strength increases with decreasing temperature while retaining its toughness. Steel on the other hand becomes brittle at low temperatures [3].

Inoculation is defined as the addition of a certain solid particles to the molten metal in order to obtain changes in crystals distribution, more uniform microstructure, improvements in mechanical properties, and a reduction of the chilling tendency [4].

The phenomenon of crystallization following after pouring molten metal into the mould, determines the shape of the primary casting (ingot) structure, which significantly has effects on its usable properties. The crystallization of metal in the mould may result in three major structural zones [2, 5].

(a) Zone of chilled crystals (grains) formed by equiaxed grains with random crystallographic orientation, which are in the contact area between the metal and the mould.

(b) Zone of columnar crystals (grains) formed by elongated crystals, which are parallel to heat flow and are as a result of directional solidification, which proceeds when thermal gradient on solidification front has a positive value.

(c) Zone of equiaxed crystals (grains) formed by equiaxed grains with random crystallographic orientation in the central part of the casting. The equiaxed crystals have larger size than chilled crystals and are as a result of volumetric solidification, which proceeds when thermal gradient has a negative value in liquid phase.

Depending on the cooling rate, chemical composition and the intensity of convection of solidifying metal in the casting may be three, two or only one structural zone [2].

The tensile strength of wrought aluminium is not high. However, introduction of alloying elements such as silicon, copper, manganese, and magnesium can enhance the strength characteristics of aluminium and make an alloy having properties targeted at particular applications [6].

Thorough literature study revealed that the inoculant (powdered CBS) used for this work has never been used before as a grain refiner for any metal. Common aluminium melt treatment inoculants in use include MgFeSi [7], Al-Ti-C and Al-3Ti-1B [8], in situ AlN-TiN-TiB2/Al composite inoculants [9]. Addition of some special master alloys that have much particles functioning as the substrates for heterogeneous nucleation can cause the grain size of the inoculated alloys to be noticeably reduced and enhance the comprehensive properties [10 -12]. In reality, majority of the master alloys are linked to Al-based composites, in which the aluminium-based solid solution is the matrix and the inoculant particle is the secondary phase [9].

From literature search, cocoa bean shell was found to contain some already existing inoculant elements as part of its compositions. The overall content of cocoa bean shell [13] and the mineral content [14, 15] are as shown below in Table 1 and 2 respectively.

Table 1. Content of Cocoa Bean Shell Powder

Minerals	43.18%
Crude fibre	21.3%
Crude protein	17.6%
Ether extract	5.9%
Ash	9.3%
Total sugar	1.0%

Table 2. Mineral Content of Cocoa Bean Shell

Minerals	Value
Calcium	3.7g/kg
Phosphorus	4.4g/kg
Potassium	26.8g/kg
Sodium	0.2g/kg
Magnesium	4.3g/kg
Copper	39mg/kg

Therefore, the scope of this work is specifically to study the inoculating ability of the selected agro-waste and to investigate the effect of varying the grain size of the inoculant on pure aluminium. The evaluation will be limited to determining the tensile strength, ductility, micro hardness and microstructure of the resulting specimens.

2. Materials and Method

2.1 Materials/Equipment Selection

The materials selected for this research are cocoa bean shells (CBS), silica sand, water, and pure aluminium having the composition as presented in Table 3. Equipment selected include sieves of aperture 150µm, 225µm, and 300µm respectively, LCD series 2-digits and 3-digits electronic weigh balance, a 40kg capacity crucible furnace, three rectangular shaped wooden

patterns of dimension 300mm x 40 mm which were used to make a pair of cope and drag moulds, a stirrer, hack saw, Universal Testing Machine (model- UTE 100, max.capacity-30KN, Make-Fuel Instruments & Engineer's Pvt. Ltd., Maharashtra), Vickers Micro hardness tester (Make-Saroj Udyog Pvt. Ltd., Maharashtra, India), Structure reveal machine (Meji optical microscope Make ZEISS Axiovert 40 MAT, Japan), and Keller enchant. All the workshop and laboratory equipment utilized were assessed at the Federal University of Petroleum Resources, Effurun (FUPRE), and the Petroleum Training Institute (PTI), both are situated in Delta State, Nigeria.

Table 3. Composition of the chosen pure aluminium

Alloys	Al	Fe	Si	Cu	Ti	Mn
Composition	99.9	0.03	0.04	0.01	0.01	0.01

2.2 Method/Experimental Procedure

Dry sand casting method was used to produce the test samples. The agro-waste based inoculant raw material (CBS) was obtained separately (Figure 1), well sun-dried, and cleaned to remove impurities. It was then crushed, and pulverized into a fine powder and sieved using different sieves of 150, 225, and 300microns aperture respectively [16]. The samples were sand cast in the foundry workshop. The aluminium was melted using a 40 kg capacity crucible furnace pre-heated at 10°C. Three rectangular shaped wooden patterns of dimension 300mm x 40 mm were used to make a pair of cope and drag moulds. Four moulds were prepared a day before the actual casting from a mixture of dried fresh silica sand, and water. This was done to dry the mould completely in order to reduce casting defects. The four moulds were labeled as sample 1, 2, 3 and 4 respectively. A 15 Kg known quantity of pure aluminium were melted at 720°C in the crucible furnace and poured at 700°C into the pouring ladle. The first batch of the melt without addition of inoculant was poured into the mould labeled sample 1. Thereafter, a known quantity (15grams precisely) of the inoculant having grain size of 150 microns (Figure 2) was added to the melt stream and stirred manually with a stirrer in order to facilitate a homogeneous bath and poured into the second mould labeled sample 2. Also, addition of the inoculant having grain sizes of 225 (Figure 3), and 300microns (Figure 4) was done in succession and poured into the third and fourth moulds labeled sample 3, and 4 respectively. A uniform quantity (15g) of the inoculant was used for all samples produced. After, total solidification, the castings were knocked out of the moulds and thoroughly fettled and cleaned before dispatching them for evaluation.

The various test samples were cut or shaped to sizes and taken to the Petroleum training institute metallurgical/microscopic accredited laboratory for micro hardness test, tensile test and Image analyzer test respectively. As shown in the appendix, the samples were machined and measured to fit into the Universal Testing Machine as per ASTM standard. The Micro hardness of the samples was determined using Vickers Micro hardness tester, carried out under a load of 187.5 N and a dwell time of 5 seconds. Structure revealing machine was used to take micro structural images of the specimens at 40 x magnification. The etching was done using Keller enchant.

Figure 1. Raw Cocoa Bean Shells (CBS)

Figure 2. Pulverized Cocoa Bean Shells (150microns)

Figure 3. Powdered Cocoa Bean Shells (225µm)

Figure 4. Pulverized CBS (300µm)

2.2.1 Tensile Testing Procedure

As shown in Figure 5, each of the test specimens was specified to have 70mm gauge length on the tensile test specimen using the dial callipers and marker. Then the thickness and width of the specimens was re-checked using the dial callipers. The

specimen was placed on the machine grips and removed the slack by moving the lower crosshead. The load indicator was set at zero and the right side hydraulic valve was opened about halve turn. Load was applied increasingly at a slow rate. Strain value started to increase more rapidly as the load was continuously applied on the sample until it fractured. The load at failure was read from the load indicator and recorded. Using the dial callipers, the dimensions of the final gauge length, thickness and width was obtained and recorded.

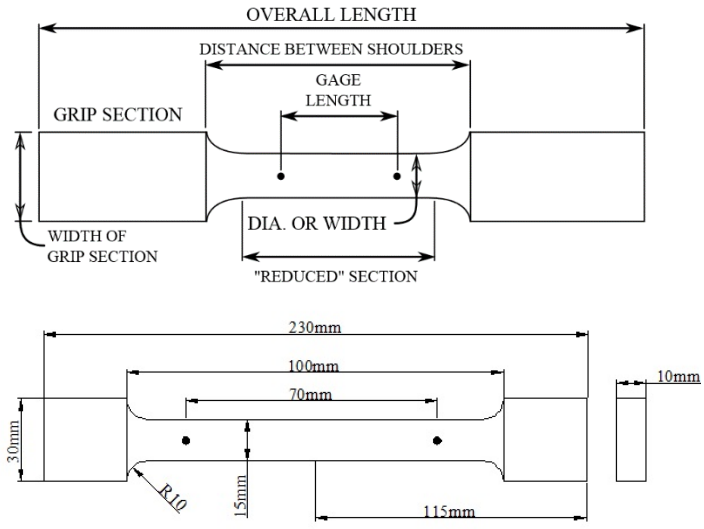

Figure 5. Tensile Test Specimen Specification

2.2.2 Microstructural Examination Procedure

The specimen was cut to a hard grip size using hack saw. As shown in the appendix, the specimens were inserted in phenolic resin in order to enable easy manual and automated grinding/polishing operations. After mounting, surface damages created by hacksaw during cutting were removed by grinding operation using emery papers of fineness number in the following increasing order: 150, 220, 320, 400, 600, 800 and 1200 respectively. During the process, water was constantly added to reduce friction on the phenolic resin surface and also air-dried with blower immediately after grinding to avoid rust. The fine scratches caused by final grinding operation were removed by mounting the specimen on a polishing machine with a mixture of manganese dioxide (MnO_2). In other to reveal the microstructural features of the polished specimen, the specimen was etched in 190ml distilled water, 5ml Nitric acid, 3ml hydrochloric acid and 2ml of hydrofluoric acid for 23seconds. After etching operation, the specimens were vigorously washed in water and blown immediately before taking them to the metallurgical microscope for inspection. The pictures resulting from inspection was magnified to 40 × 0.65 for proper understanding of the micrographs.

2.2.3 Vicker's Micro Hardness Testing Procedure

Micro hardness testing is a method of determining a material's hardness or resistance to penetration when test samples are very small or thin, or when small regions in a composite sample or plating are to be measured. During micro hardness testing, a Vicker's (DPH) diamond indenter is pressed into the mounted specimen's surface with a penetrator and a light load of up to 1000 grams. The result of applying the load with a penetrator is an indentation or permanent deformation of the material surface caused by the shape of the indenter. Accurate measurement of the resulting indentation requires the use of a special micro hardness testing microscope since the indentations are so small. The procedure is pictorially displayed in Figure 6.

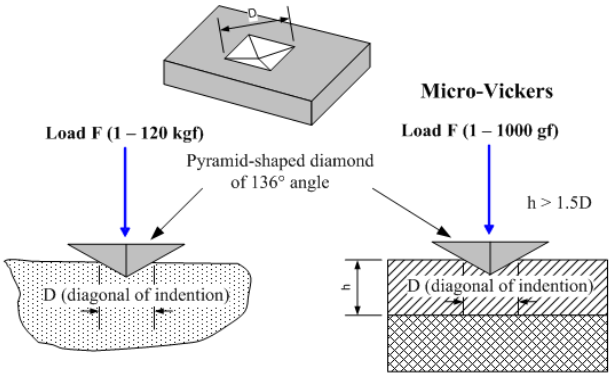

Figure 6. Vicker's Hardness Procedure

3. Results and Discussion

3.1 Tensile Testing Result

Tensile strength and ductility values are computed from the ultimate tensile testing machine.

The following equations (1) to (6) were used in calculating the tensile strength values

$$AREA = \frac{\pi D^2}{4} \quad (1)$$

$$MAX.LOAD = RL\ X\ RF \quad (2)$$

Where:

$RL = RAM\ LOAD$

$RM = RAM\ FACTOR = 6.492$

$$UTS = \frac{RL\ X\ RF}{A_O} \quad (3)$$

$$YIELD\ STRESS = \frac{UTS}{1.31} \quad (4)$$

$$YIELD\ LOAD = YS\ X\ A_O \quad (5)$$

$$\%E = \frac{L_f - L_o}{L_o}\ x\ 100 \quad (6)$$

The reading taken from the ultimate tensile testing machine is as presented in Table 4.

Table 4. Tensile Strength Test Data Obtained for all Samples

SAMPLE	L_o (mm)	L_f (mm)	D_o (mm)	D_f (in)	A_o (in^2)	RAM LOAD (RL)
Pure Al without inoculant	110	122	12.0	0.47	0.175	1300
Pure Al with 150µm inoculant	110	112	12.2	0.48	0.181	1150
Pure Al with 225µm inoculant	110	111	12.1	0.476	0.178	1000
Pure Al with 300µm inoculant	110	110.5	12.2	0.48	0.181	900

The distribution pattern of Ultimate Tensile Strength (UTS), Yield Strength (YS), and percentage Elongation (%E) of each of the specimens are calculated as follows using equations (1) to (6).

(a) Pure Al without Inoculant

$AREA = A_o = \frac{\pi D^2}{4} = 0.175\text{in}^2$

$RAM\ LOAD = RL = 1300lb$

$RAM\ FACTOR = 6.492$

$MAX.LOAD = RL\ X\ RF =$ **8439.6 *lb***

$UTS = \frac{RL\ X\ RF}{A_O} =$ **48226 psi**

$YIELD\ STRESS = \frac{UTS}{1.31} =$ **36814 *psi***

$YIELD\ LOAD = YS\ X\ A_O =$ **6442 *lb***

$\%E = \frac{L_f - L_o}{L_o}\ x\ 100 =$ **10.9%**

(b) Pure Al with 150µm inoculant

$AREA = A_o = \frac{\pi D^2}{4} = 0.181\text{in}^2$

$RAM\ LOAD = RL = 1150lb$

$RAM\ FACTOR = 6.492$

$MAX.LOAD = RL\ X\ RF =$ **7465.8 *lb***

$UTS = \frac{RL\ X\ RF}{A_O} =$ **41247.6 psi**

$YIELD\ STRESS = \frac{UTS}{1.31} =$ **31486.7 *psi***

$YIELD\ LOAD = YS\ X\ A_O =$ **5699 *lb***

$\%E = \frac{L_f - L_o}{L_o}\ x\ 100 =$ **1.82%**

(c) Pure Al with 225µm inoculant

$AREA = A_o = \frac{\pi D^2}{4} = 0.178\text{in}^2$

$RAM\ LOAD = RL = 1000lb$

$RAM\ FACTOR = 6.492$

$MAX.LOAD = RL\ X\ RF =$ **6492 *lb***

$UTS = \frac{RL\ X\ RF}{A_O} =$ **36472 psi**

$YIELD\ STRESS = \frac{UTS}{1.31} =$ **27841 *psi***

$YIELD\ LOAD = YS\ X\ A_O =$ **4956 *lb***

$\%E = \frac{L_f - L_o}{L_o}\ x\ 100 =$ **0.91%**

(d) Pure Al with 300µm inoculant

$AREA = A_o = \frac{\pi D^2}{4} = 0.181\text{in}^2$

$RAM\ LOAD = RL = 900lb$

$RAM\ FACTOR = 6.492$

$MAX.LOAD = RL\ X\ RF =$ **5842.8 *lb***

$UTS = \frac{RL\ X\ RF}{A_O} =$ **32280.7 psi**

$YIELD\ STRESS = \frac{UTS}{1.31} =$ **24641.7 *psi***

$YIELD\ LOAD = YS\ X\ A_O =$ **4460 *lb***

$\%E = \frac{L_f - L_o}{L_o}\ x\ 100 =$ **0.45%**

The above results for each specimen are converted to S. I. unit and summarized as presented below in Table 5.

Table 5. Summary of the calculated Tensile Strength and Ductility Values (converted) of each specimen.

Sample	UTS (N/mm^2)	YIELD STRESS (N/mm^2)	YIELD LOAD (N)	%E
Pure Al without inoculant	333	253	28655	10.9
Pure Al with 150µm inoculant	284	217	25350	1.82
Pure Al with 225µm inoculant	251	192	22045	0.91
Pure Al with 300µm inoculant	223	170	19839	0.45

Note in table 4 that:

D_o = Initial Diameter

D_f = Final Diameter

A_o = Initial Area

L_o = Original Length

L_f = Final Length

E = Elongation

From Table 5 above, it is shown that the tensile strength of the specimen diminishes as the grain size of the inoculant increases. This may be as a result of increased fine crystals of aluminium. Finer crystals lead to reduced tensile strength but increased compressive strength [17]. Reduced elongation (E) is also an indication of declining ductility of the metal. Ordinarily, the presence of copper in pure aluminium is to improve the strength and machinability, but other elements such as Calcium, Phosphorous, Potassium, and sodium present with it in the inoculant might have inhibited its effect on the aluminium [17].

3.2 Metallographic Test Result and Analysis

Figures 7, 8, 9 and 10 show the microstructures of the inoculated aluminium. It is obvious from the figure that the microstructure consists of two distinguished phases – a dark and a bright white phase. The rough surface was not actually from the specimen preparation but from the way the material was cast.

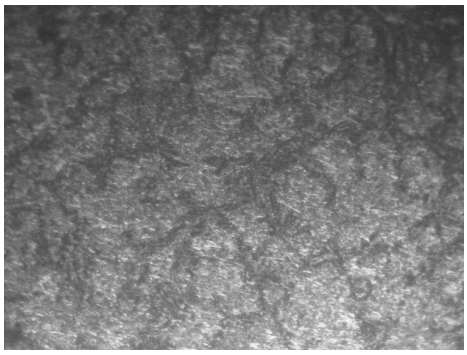

Figure 7. Pure Al sample without inoculant at × 40 Magnification

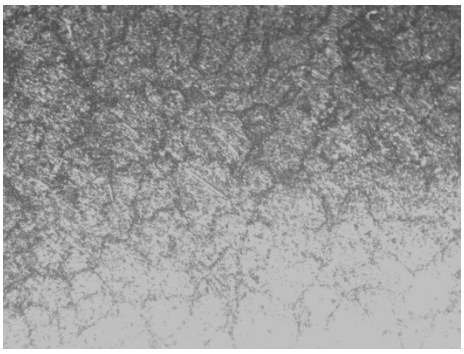

Figure 8. Pure Al sample with 150µm inoculant at × 40 Magnification

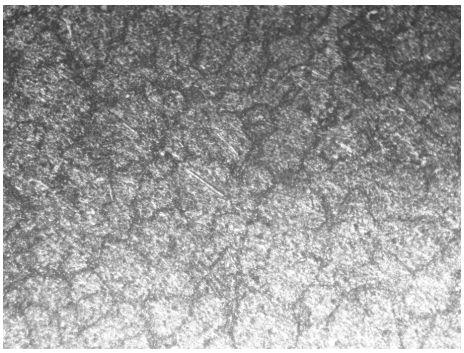

Figure 9. Pure Al sample with 225µm inoculant at × 40 Magnification

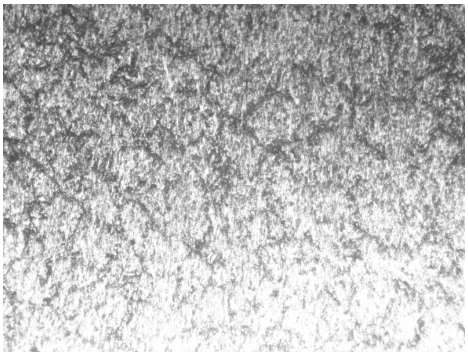

Figure 10. Pure Al sample with 300µm inoculant at × 40 Magnification

It is seen from the microstructural examination as depicted in figures 7 to 10 that addition of inoculant introduced whitish phase in the microstructure, and it became more pronounced as the grain size of the inoculant increased in the metal matrix. Also the aluminium crystals appear finer in succession. This is responsible for lower tensile strength and higher compressive strength.

3.3 Vicker's Micro Hardness Result

From the appendix (Figures 4 to 7) the results and pictures from the Vicker's hardness test are presented. It indicated that the increasing grain size of the inoculant added to the pure aluminium increases the micro hardness of the material. After conducting the Vicker's hardness test at different point on the samples, the specimen with no inoculant addition (the control sample) has an average hardness value of 29HB. While each pure Al sample with inoculant having 150µm, 225µm, and 300µm grain has an average hardness value of 56HB, 61HB, and 72HB respectively.

4. Conclusion

In this work, the effects of varying the grains size of the selected agro-waste based inoculant on some mechanical properties of pure aluminium was studied. The microstructural examination showed that the mechanical properties are dependent on the matrix as the aluminium grains became more refined with increasing grain size of the inoculant. I.e. Due to increasing grain size of the inoculant, the micro hardness increased as the aluminium crystal size became finer. Meanwhile, the tensile strength, and ductility decreased as grain size of the inoculant increased. The overall results showed that the used agro-waste based inoculant has the capability of refining the crystal size of pure aluminium as its grain size increases. This will make the resulting aluminium alloy applicable in areas where hardness is of superior consideration relative to tensile strength.

Conflict of Interest

The authors have no conflict of interest.

Acknowledgment

The authors appreciate all the personalities that contributed in one way or the other towards the breakthrough of this work.

References

[1] A. I. O. Zaid, A. I. O.,"Review of the Grain Refinement of Aluminum and its Alloys" P*roceedings of the International Symposium on Advanced Materials, ISAM*, Islamabad, Pakistan, 2001.

[2] J. Szajnar, M. Stawarz, and T. Wrobel, "Inoculation of Pure Aluminium Structure with Ti+B Addition in Impulse Magnetic Field," Journal of Achievements in Materials and Manufacturing Engineering, **14**: 64–69, 2006.

[3] ASM International, "Casting" in Metals Handbook, vol. 15 of The ASM Handbook, ASM International, Geauga County, Ohio, USA, 9th edition, 1992.

[4] O. S. I. Fayomi, A. P. I. Popoola, F. Oyawale, O. O. Ajayi, "Performance Evaluation and Multi-doped Composite Conditioned of A5-type/10%Ti-Sn Alloy: Processing and Properties". *J Fail. Anal. & Preven.* ASM International. DOI 10.1007/s11668-015-0058-x. (16): 135–141, 2016.

[5] D. VanderBoon, "Effects of Solidification Rates on Porosity Formation and Cast Microstructure in Aluminum Alloy A356. Laboratory Module 3, Grand Valley State University, 1 – 5, 2005.

[6] AZO Materials, "Aluminium – Specifications, Properties, Classifications and Applications". Retrieved from: www.azom.com/article.aspx, 2017.

[7] O. O. Ajibola, and D. T. Oloruntoba, "Effect of MgFeSi Inoculant on Properties of Cast 6061 Al Alloy for Brake Master Piston Application". Indian Journal of Materials Science. Retrieved from: http://dx.doi.org/10.1155/2015/756219, Volume 2015, Article ID 756219, 10 pages, 2015

[8] M. Bedel, L. Heyvaert, M. Založnik, H. Combeau, D. Daloz and G. Lesoult. "Process-Scale Modelling of Microstructure in Direct Chill Casting of Aluminium Alloys". *IOP Conf. Series:* Materials Science and Engineering. 012100 doi:10.1088/1757-899X/84/1/012100: **84** (2015).

[9] Qian Wang, Chunxiang Cui, Xin Wang, Lichen Zhao, Nuo Li and Shuiqing Liu, "Effect of Preparation Parameter on Microstructure and Grain Refining Behavior of In Situ AlN-TiN-TiB2/Al Composite Inoculants on Pure Aluminum". Journal of Metals, doi: 10.3390/met7020056. Retrieved from: www.mdpi.com/journal/metals **7**: 56, 2017.

[10] A. L. Greer, "Grain Refinement of Alloys by Inoculation of Melt. *Phil. Trans. R. Soc. Lond. A*, **361**: 479–495, 2003.

[11] D. Wearing, A. P. Horsfield, W. W. Xu, P. D. Lee, "Which wets TiB2 inoculant particles: Al or Al3Ti?" J. Alloy. Compd., **664**: 460–468, 2016.

[12] H. L. Zhao, Y. Song, M. Li, S. K. Guan, "Grain Refining Efficiency and Microstructure of Al-Ti-C-RE Master Alloy". J. Alloy. Compd., **508**: 206–211, 2010.

[13] B. K. G. Marcel, K. B. Andre, D. Theodore, and K. C. Seraphin, "Waste and By-products of Cocoa in Breeding Research Synthesis". International Journal of Agronomy and Agricultural Research (IJAAR), 2011.

[14] Feedipedia, "Cocoa (Theobroma Cacao) Beans and by-product. Retrieved from www.feedipedia.org, 2010.

[15] FAO, "Animal Feed Resources Information System", FAO, 1992 – 2002.

[16] Adeyemi Ibukun Olabisi., Ademoh Nuhu. Adam, Okwu Modestus Okechukwu, "Development and Assessment of Composite Brake Pad Using Pulverized Cocoa Beans Shells Filler". International Journal of Materials Science and Applications. doi: 10.11648/j.ijmsa.20160502.16. **5**(2): 66-78, 2016.

[17] R. S. Khurmi, and J. K. Gupta, "*A Text Book of Workshop Technology (Manufacturing Processes)".* S. Chand & Company Ltd. Reprinted edition:18 -18 &117–120, 2004.

Appendix

Figure 1. Mounted Microstructural Test Specimens

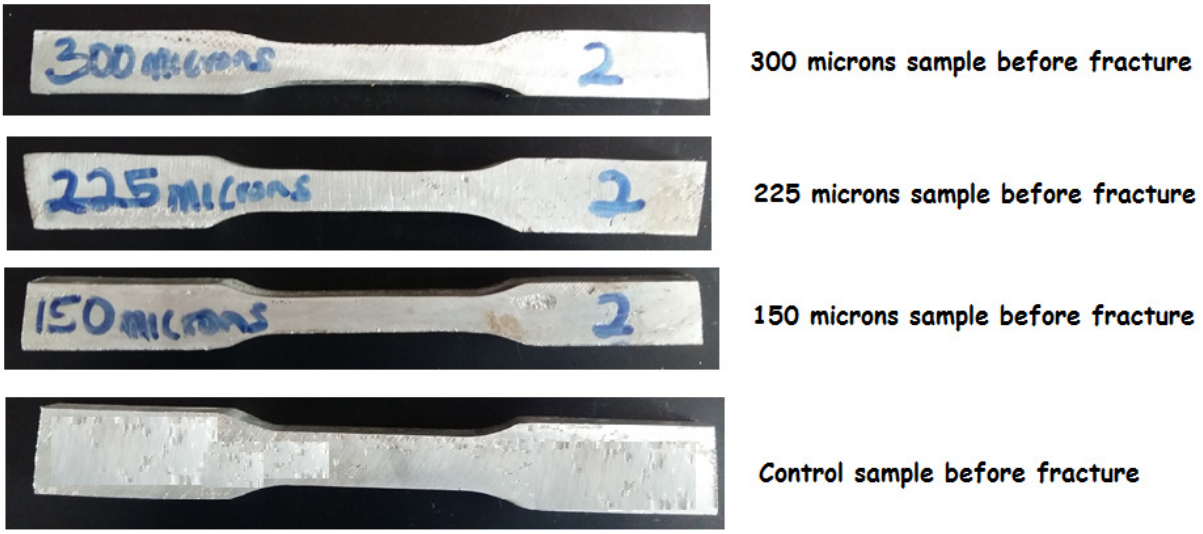

Figure 2. Tensile Strength Specimens before Fracture.

Figure 3. Tensile Strength Specimens after Fracture.

CONTROL SAMPLE VICKER HARDNESS

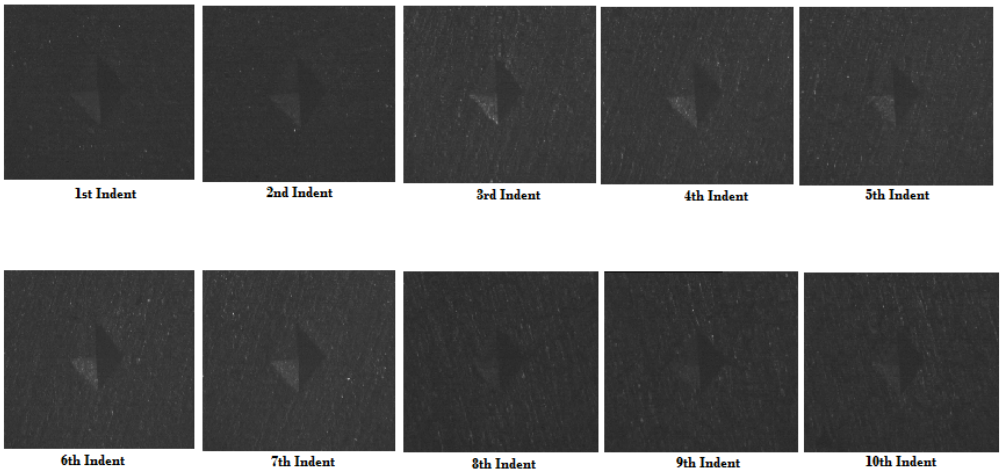

Measurement Line Duramin-5

Date :04/01/2017 Time : 03:44:33

Information : Control Sample

Limit [H] : 550.0 Case Depth : ***

X [mm]	Y [mm]	D1 [µm]	D2 [µm]	Hardness	Force	Time (s)	Lens
0.000	0.000	354.9	347.1	30.1	2000.0	5.0	10.0
0.000	0.000	361.7	335.8	30.5	2000.0	5.0	10.0
0.000	0.000	380.9	335.8	28.9	2000.0	5.0	10.0
0.000	0.000	380.9	340.3	28.5	2000.0	5.0	10.0
0.000	0.000	380.9	330.2	29.3	2000.0	5.0	10.0
0.000	0.000	374.1	330.2	29.9	2000.0	5.0	10.0
0.000	0.000	384.3	341.5	28.2	2000.0	5.0	10.0
0.000	0.000	384.3	346.0	27.8	2000.0	5.0	10.0
0.000	0.000	384.3	339.2	28.3	2000.0	5.0	10.0
0.000	0.000	378.6	339.2	28.8	2000.0	5.0	10.0

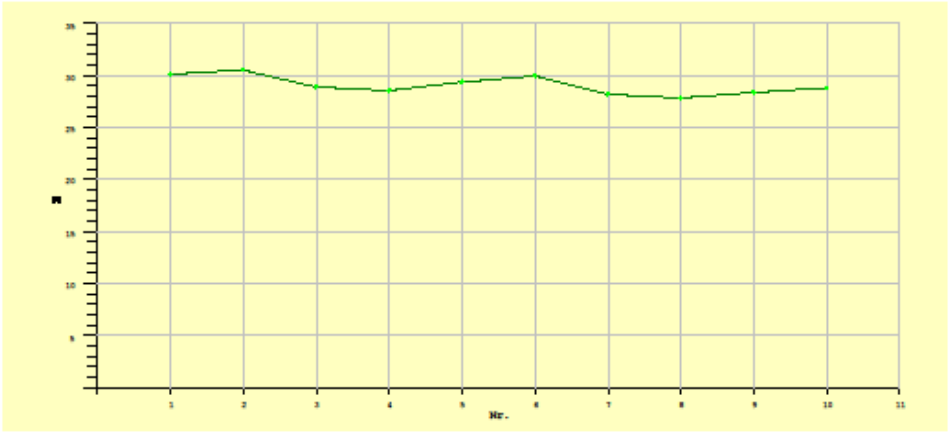

- Page 1 -

Figure 4. Vicker's Hardness Results of Non-inoculated aluminium Specimen

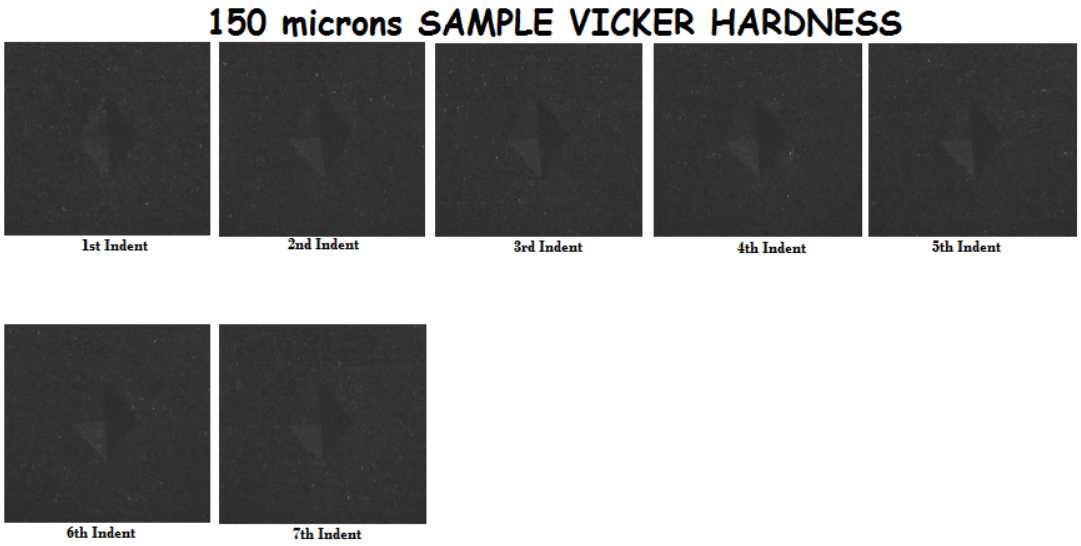

Measurement Line Duramin-5

Date :04/01/2017 Time : 01:28:50

Information : 150 microns Sample

Limit [H] : 550.0 Case Depth : ***

X [mm]	Y [mm]	D1 [µm]	D2 [µm]	Hardness	Force	Time (s)	Lens
0.000	0.000	241.9	263.4	58.1	2000.0	5.0	10.0
0.000	0.000	248.6	263.4	56.6	2000.0	5.0	10.0
0.000	0.000	249.8	263.4	56.3	2000.0	5.0	10.0
0.000	0.000	247.5	265.7	56.3	2000.0	5.0	10.0
0.000	0.000	257.7	254.4	56.6	2000.0	5.0	10.0
0.000	0.000	262.2	248.7	56.8	2000.0	5.0	10.0
0.000	0.000	253.2	261.2	56.1	2000.0	5.0	10.0

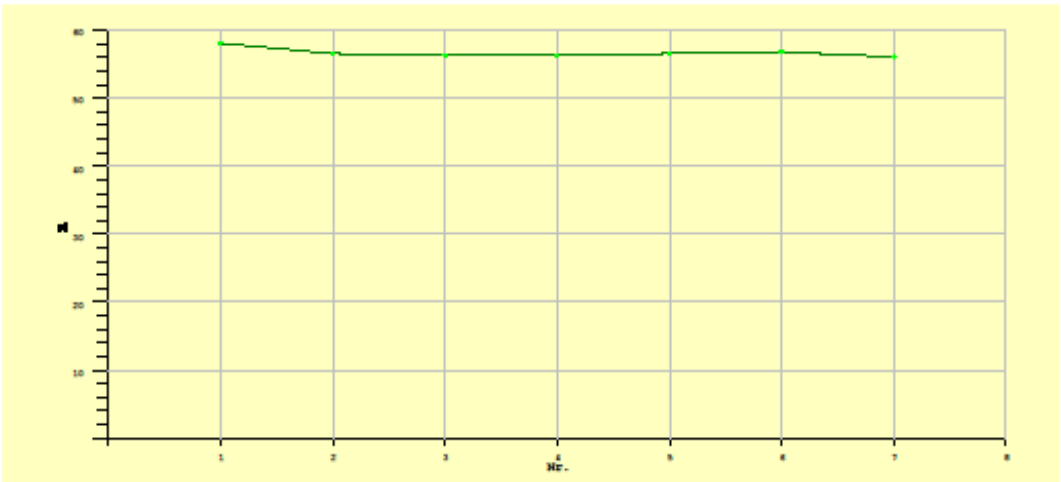

- Page 1 -

Figure 5. Vicker's Hardness Results of aluminium Specimen with 150µm grain size of the inoculant

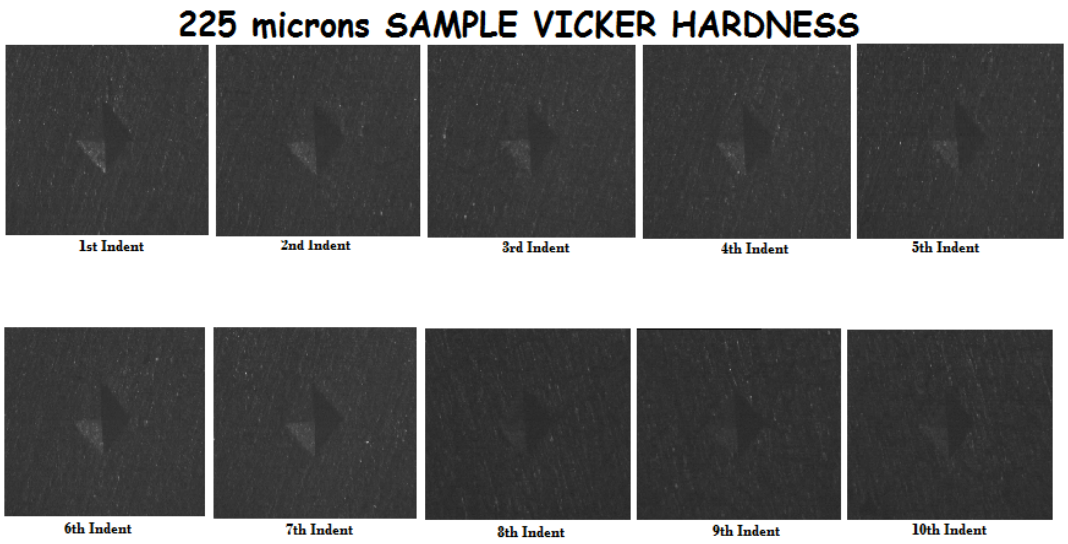

Measurement Line Duramin-5

Date :04/01/2017 Time : 02:36:59

Information : 225microns Sample

Limit [H] : 550.0 Case Depth : ***

X [mm]	Y [mm]	D1 [µm]	D2 [µm]	Hardness	Force	Time (s)	Lens
0.000	0.000	243.0	248.7	61.4	2000.0	5.0	10.0
0.000	0.000	254.3	243.1	60.0	2000.0	5.0	10.0
0.000	0.000	244.1	247.6	61.4	2000.0	5.0	10.0
0.000	0.000	243.0	245.4	62.2	2000.0	5.0	10.0
0.000	0.000	243.0	254.4	60.0	2000.0	5.0	10.0
0.000	0.000	239.6	251.0	61.6	2000.0	5.0	10.0
0.000	0.000	240.7	245.4	62.8	2000.0	5.0	10.0
0.000	0.000	241.9	246.5	62.2	2000.0	5.0	10.0
0.000	0.000	247.5	249.9	60.0	2000.0	5.0	10.0
0.000	0.000	247.5	243.1	61.6	2000.0	5.0	10.0

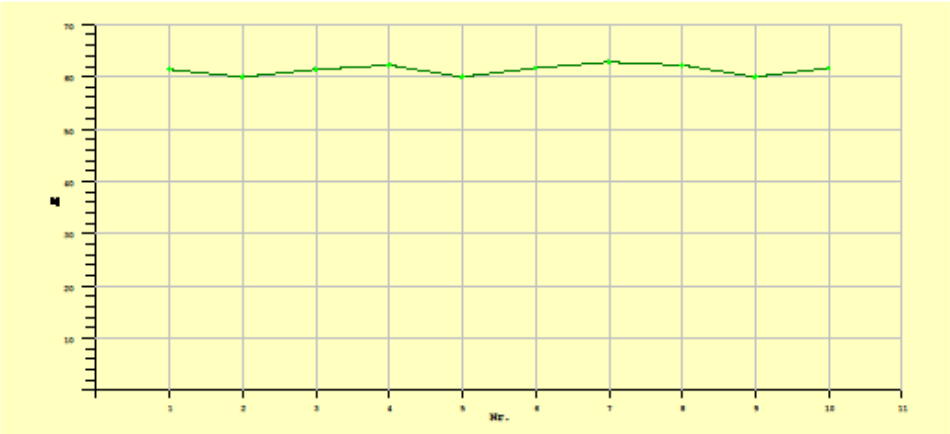

- Page 1 -

Figure 6. Vicker's Hardness Results of aluminium Specimen with 225µm grain size of the inoculant

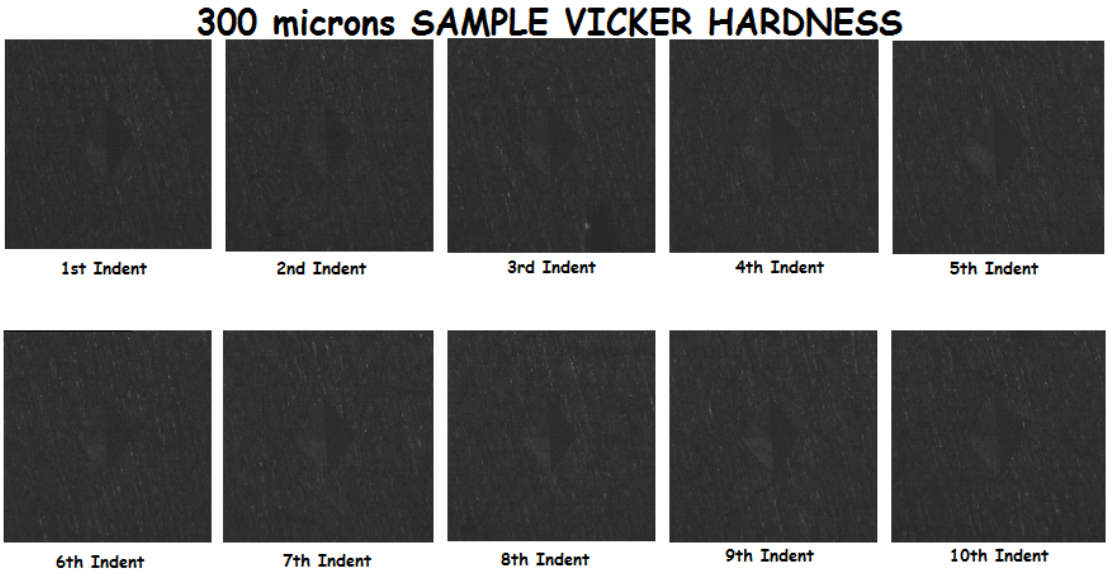

Measurement Line Duramin-5

Date :04/01/2017 Time : 22:26:15

Information : 300microns Sample

Limit [H] : 550.0 Case Depth : ***

X [mm]	Y [mm]	D1 [µm]	D2 [µm]	Hardness	Force	Time (s)	Lens
0.000	0.000	221.5	230.7	72.6	2000.0	5.0	10.0
0.000	0.000	224.9	227.3	72.6	2000.0	5.0	10.0
0.000	0.000	230.6	226.1	71.1	2000.0	5.0	10.0
0.000	0.000	220.4	226.1	74.4	2000.0	5.0	10.0
0.000	0.000	226.0	227.3	72.2	2000.0	5.0	10.0
0.000	0.000	226.0	225.0	72.9	2000.0	5.0	10.0
0.000	0.000	228.3	223.9	72.6	2000.0	5.0	10.0
0.000	0.000	226.0	223.9	73.3	2000.0	5.0	10.0
0.000	0.000	228.3	223.9	72.6	2000.0	5.0	10.0
0.000	0.000	229.4	223.9	72.2	2000.0	5.0	10.0

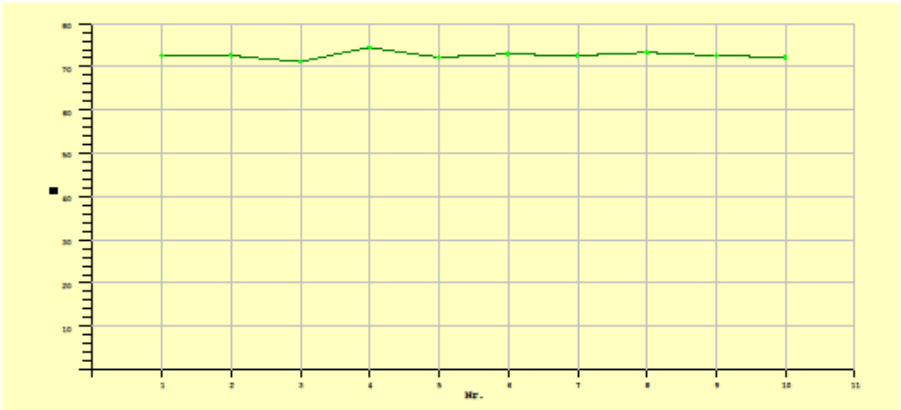

- Page 1 -

Figure 7. Vicker's Hardness Results of aluminium Specimen with 225µm grain size of the inoculant

Advances in Science, Technology and Engineering Systems Journal Vol. 2, No. 4, 26-31 (2017)

www.astesj.com

ASTESJ

ISSN: 2415-6698

Channel Inversion Schemes with Compensation Network for Two-Element Compact Array in Multi-User MIMO

Maxwell Oppong Afriyie*, Obour Agyekum Kwame Opuni-Boachie, Affum Emmanuel Ampoma

University of Electronic Science and Technology of China, Communication and Information Engineering, 611731, China

ARTICLE INFO

Article history:
Received: 01 March, 2017
Accepted: 04 April, 2017
Online: 15 April, 2017

Keywords:
Broadcasting channel
Channel Inversion
Coupling matrix
Inserted component scheme
MIMO
Multi-user
Receiving mutual impedance

ABSTRACT

In this paper, we investigate the performance of channel inversion schemes for interference cancellation with compensation network in multi-user MIMO broadcasting channel. To achieve good performance, mutual coupling between two-element compact arrays is characterized by the receiving mutual impedance method (RMIM) to formulate the compensation network-operating matrix. A prototype of two-element compensation network with an insertion loss between input and output ports better than 11 dB is fabricated. We demonstrate results to confirm that output voltages of decoupling network can effectively be removed off the coupling effect. A typical standard MIMO channel model is presented, and system performance is evaluated when coupling effects existed and after decoupling process. Bit error performance results also indicate the promising potentials of regularized channel inversion scheme with efficient decoupling scheme in massive MIMO system.

1. Introduction

The expanding interest for higher data rate, greater spectrum efficiency, larger average throughput and shorter latency by wireless systems has stimulated tremendous amount of research towards capacity enhancements of the communication links [1]. The main challenge in data transmission in broadcasting channel is interference cancellation, and channel inversion is one of the advanced technologies developed to confront the challenge. Channel Inversion (sometimes referred to as "zero-forcing (ZF) beamforming") can be viewed as a precoding strategy to undo the effects of a channel, and is one of the simplest modulation techniques for the multiuser channel [2]. This technique multiplies the vector signal to be transmitted by the inverse of the channel matrix and the result is an equalized channel to each user, and therefore, suppresses the co-channel interference [3]. It has the following advantages in the MIMO context: it is implementable with a non-iterative transmitter processing and unitary receiver processing [2], [4], and [5], therefore, no noise improvement happens at the receiver. Again, when the channel rank is restricted by the number of receiver antennas, receiver processing is not required, and the subsequent virtual channels correspond one-to-one with the receiver antennas.

Channel inversion has attracted tremendous amount of research, and is well investigated in light of the fact that it is suitable for multi-user MIMO downlink channels [6]-[11]. One noteworthy issue that should be tended to in connection to multi-user MIMO system is mutual coupling, and the development of a successful decoupling strategy to compensate the performance degradation in MIMO antennas. If mutual coupling is strong, a large portion of the power fed into one port will be coupled to the other port rather than radiating to free space; consequently diminishing the signal-to-noise ratio and restricting the channel capacity. Ref. [12] separates decoupling strategies into four classes: *1) Eigen-mode Decomposition Scheme:* Its guideline is to diagonalize the scattering matrix of a compact array using 90° and /or 180° [13]-[17]. *2) The Inserted Component Scheme*: It works on the concept of inserting a section of transmission-line between the coupled antenna ports [18]-[22]. *3) Artificial Structure Decoupling Scheme:* This method uses sub-wavelength EM structures such as electromagnetic band gap (EBG) structure [23], defected ground

*Corresponding Author: Maxwell Oppong Afriyie, University of Electronic Science and Technology of China, Communication and Information Engineering, 611731, China
Email: mmaxi12002@yahoo.com

structures (DGS) [24], and magnetic metamaterials [25], [26]. *4) Coupled Resonator Decoupling Scheme:* This method was proposed for the first time in 2014, and has the concept of decoupling pair of coupled elements using coupled resonators [12] and [27]-[30].

It is clear at this point that decoupling techniques to balance the performance degradation by coupling are widely investigated. However, its coexistence with channel inversion needs further investigation, importantly, the effects of coupling matrix on the channel coefficients, and the resulting consequences on channel inversion interference cancellation schemes that are rarely accounted for or are studied in the signal processing or communication literature. We intend to investigate the system performance of channel inversion with decoupling network scheme in multi-user MIMO system by evaluating error performance of the coupled and decoupled antenna elements at the receiving end. This paper systematically presents the measurement of receiving mutual impedance of monopole array to formulate the decoupling network operating matrix and design. For illustration, coupling matrix under coupled and compensated voltages is determined and included in the multi-user MIMO system with channel inversion interference cancellation model for the broadcasting channel.

The purpose of decoupling network however is to enhance the isolation between ports closely located within restricted space in mobile handset. It is therefore reasonable to investigate the effect of mutual coupling matrix on channel coefficients, and subsequent effects on performance of channel inversion in MIMO system after decoupling process. For reasons of clarity, the contribution of this paper is to demonstrate the impacts of mutual coupling on channel inversion after the decoupling process. We do this by fabricating a two-element decoupling network to explore the effect of coupling matrix when incorporated in the MIMO system model with channel inversion algorithm. BER performance results also indicate the promising potentials of regularized channel inversion scheme with efficient decoupling scheme in massive MIMO system

The outline of the paper is as follows: Section II presents channel inversion, coupling matrix, system and channel model. The theory of receiving mutual impedance to formulate coupling effect and to design the inserted component scheme are described in Section III. Section IV presents simulation results and discussions. Finally, we give concluding remarks in Section V.

2. System and Channel Model

In this paper, a standard MIMO channel of T transmitters and R receivers represented as a matrix H of dimension $R \times T$ is presented, where each of the entries $h_{t,r}$ is a zero-mean unit-variance complex-Gaussian fading gain. The received signal of each user can be represented as [31]

$$y_r = \sum_{t=1}^{T} h_{t,r} x_r + n_r \tag{1}$$

where x_r is the signal sent from the t^{th} antenna, and n_r defined as a standard complex-Gaussian receiver noise seen at the r^{th} user. In a vector form, the receive signal is represented as

$$y = H\left(d/\sqrt{\eta}\right) + n \tag{2}$$

where $d = [d_1, ..., d_r]^T$ and $y = [y_1, ..., y_r]^T$. The scaling factor η is introduced to restrict the transmit power to some predetermined value α

$$\|x\|^2 = \left\|d/\sqrt{\eta}\right\| = \alpha \tag{3}$$

We assume that the total transmit signal power $\alpha = 1$. The ergodic sum capacity of users with single receive antenna system in (bits/channel use) is expressed as [12], [13]

$$C_s = P \sup \log_2 | I_E + \rho H^* D H | \tag{4}$$

where P is the set of all $R \times R$ nonnegative diagonal matrices D with $tr(D) = 1$, $\rho = 1/\sigma^2$ H^* is the Hermitian transpose of H . We just consider impacts of mutual coupling and channel correlation of two-element compact array closely placed to each other due to the relatively limited space at the receiver. Hence, the channel H_o is given by [32]

$$H_o = Z_m R^{1/2} H \tag{5}$$

Z_m and $R^{1/2}$ denote the coupling matrix and spatial correlation matrix at the receiver respectively. The coupling matrix of the antenna array can be written as [33]

$$Z_m = (Z_A + Z_T)(Z^{12} + Z_T I)^{-1} \tag{6}$$

where Z_A is the antenna impedance in isolation, I is identity matrix, Z_T is the impedance of the receiver at each antenna element, chosen as the complex conjugate of Z_A and Z_{12} is the mutual impedance.

A. Plain and Regularized Channel Inversion Schemes

Recently, channel inversion has been introduced as one of transmission schemes for interference cancellation in multi-user multi input multi-output (MIMO) broadcasting channels. In the plain channel inversion (CI), data symbol is precoded with the pseudo-inverse of the channel prior to transmission; the precoded data symbol is calculated as

$$x = \left(1/\sqrt{\eta}\right) H^* (HH^*)^{-1} d \tag{7}$$

As indicated by [31], the main drawback of this approach is the high power level required to cancel the small elements of H and this arises when the channel is ill conditioned. The plain channel inversion capacity is expressed as [7]-[31]

$$C_{ci} = R \int_0^{\infty} \log\left(1 + \frac{\rho\eta}{R}\right) \frac{1}{\left(\frac{\eta}{R} + 1\right)^{R+1}} dy \tag{8}$$

$$\approx Ke^{\frac{K}{\rho}}\Psi\left(\frac{R}{\rho}\right)$$

where $\Psi(x)=\int_{x}^{\infty}\frac{e^{-t}}{t}dt$, as $R\to\infty$, $\lim_{k\to\infty}C_{ci}=\rho\log e$ bits per channel use. The regularized channel inversion (CI-R) approach is equivalent to using a minimum mean-squared error (MMSE) criterion to design the beamformer weights. This method reduces the effects of noise amplification by regularizing the inverse in the ZF filter. The precoded data symbol solution at the transmitted side is

$$x=\left(1/\sqrt{\eta}\right)H^{*}(HH^{*}+\xi\,\mathrm{I})^{-1}d \tag{9}$$

where ξ is the regularization parameter. Let the signal-to-interference noise ratio (SINR) be represented by [7]

$$SINR\approx\frac{\left(\sum_{l=1}^{R}\frac{\lambda_l}{\lambda_l+\gamma}\right)^2}{\sigma^2R^2\sum_{l=1}^{R}\frac{\lambda_l}{\left(\lambda_l+\gamma\right)^2}+R\sum_{l=1}^{R}\left(\frac{\lambda_l}{\lambda_l+\gamma}\right)^2-\left(\sum_{l=1}^{R}\frac{\lambda_l}{\lambda_l+\gamma}\right)^2} \tag{10}$$

then, the sum capacity for CI-R can be expressed as

$$C_{CI-R}\approx R\log(1+SINR) \tag{11}$$

3. Theory and Design of the Inserted Component Scheme

A. Formulation for the Mutual Coupling Effect

Mutual coupling effect between two receiving monopoles for the study is characterized by receiving mutual impedance method (RMIM) described in [34]. The two parallel monopoles operating at 2.4 GHz are placed on a metallic ground plane and connected to a $Zo=50\Omega$ load in anechoic chamber. The monopoles have length of 30 mm, radius of 2 mm and element separation of 25mm (0.2 λ at 2.4 GHz). The transmitting antenna is a horn antenna, whereas a separation of 50 mm is given between transmitting antenna and receiving monopole array. Considering the concealed impacts of the metallic ground, the scattering parameters $S_{21}^{(1)}$, $S_{21}^{(2)}$ and S_{11} are measured utilizing the procedure in [34]. If γ is complex and represents the square root of the transmitted power, the respective terminal voltages can be calculated as [35]

$$V_{21}^{(1)}=S_{21}^{(1)}\gamma\sqrt{Zo}\,,\quad V_{21}^{(2)}=S_{21}^{(2)}\gamma\sqrt{Zo}$$

and

$$V_{11}=S_{11}\gamma\sqrt{Zo} \tag{12}$$

The voltage and current relationships can be expressed as

$$V_{21}^{(1)}=V_{11}+Z_{12}I_t^{(2)} \tag{13}$$

and

$$Z_{12}=\ I_t^{(1)}=\frac{V_{21}^{(1)}}{Z_o},I_t^{(2)}=\frac{V_{21}^{(2)}}{Z_0},\text{ and }I_t=\frac{V_{11}}{Z_o} \tag{14}$$

After some manipulations, the mutual coupling between array elements is expressed as

$$Z_{12}=\left(\frac{V_{11}-V_{21}^{(1)}}{V_{21}^{(2)}}\right)Z_o\ =\left(\frac{S_{11}-S_{21}^{(1)}}{S_{21}^{(2)}}\right)Z_o \tag{15}$$

Consider a receiving antenna with array of N elements, the relationship between the uncoupled voltages $U_k(\mathrm{k}=1,2,...,N)$ and the received coupled voltages V_k can be written in a matrix notation as [36]

$$\begin{bmatrix}U_1\\U_2\\\vdots\\U_N\end{bmatrix}=\begin{bmatrix}1&-\frac{Z_{12}}{Z_L}&\cdots&-\frac{-Z_{IN}}{Z_L}\\-\frac{Z_{21}}{Z_L}&1&\cdots&-\frac{Z_{2N}}{Z_L}\\\vdots&\vdots&\ddots&\vdots\\-\frac{Z_{N1}}{Z_L}&-\frac{Z_{N2}}{Z_L}&\cdots&1\end{bmatrix}\begin{bmatrix}V_1\\V_2\\\vdots\\V_N\end{bmatrix} \tag{16}$$

where Z_t^{ki} represents the mutual impedance between the kth and the ith antenna elements and Z_L is the terminal impedance connected to the antennas.

B. Operating Matrix and Design of Compensation Network

Using (16), the operating matrix for two-element receiving array for the compensation network is expressed as

$$\begin{bmatrix}U_1\\U_2\end{bmatrix}=\begin{bmatrix}1&-\frac{Z_{12}}{Z_L}\\-\frac{Z_{21}}{Z_L}&1\end{bmatrix}\begin{bmatrix}V_1\\V_2\end{bmatrix}=\begin{bmatrix}V_1-\frac{Z_{12}}{Z_L}V_2\\V_2-\frac{Z_{21}}{Z_L}V_1\end{bmatrix} \tag{17}$$

where V_1 V_2

U_1 and U_2

Z_A, Z_B and Z_C),

each having impedance of $\sqrt{2}Z_o$, where Z_o

electrical length ϕ can be defined as $\phi = \cos^{-1}\left(\left|Z_t^{12}/Z_L\right|\right)$, whereas Ψ and θ are 90° and $\left(90^\circ + \phi\right)$ respectively.

The even-mode circuit for the power divider is shown in Fig. 1, where Y_2 and Y_3 are the input admittances of the upper and lower branches respectively. In the odd-mode shown in Fig. 2, if k^2 is the power ratio, then $-2kV_S$ and $2V_S$ are the magnitude of voltage sources at the output ports of the divider circuit. We fabricate the circuit by using the substrate FR4 with dielectric constant 4.8 at operating frequency of 2.4 GHz as shown in Fig. 3. The measured insertion losses between input and output ports of the decoupling network are shown in Fig. 4.

4. Simulation Results and Discussion

For demonstrating the performance of channel inversion schemes with decoupling network in multi-user MIMO system effectively, coupling matrix of the decoupling network under two distinct conditions is determined in an anechoic chamber. In this work, the decoupling network has been fabricated using microstrip transmission-lines, the measured insertion loss between input and output ports are better than 11 dB. The scattering parameters of the coupled monopole array are measured to determine the coupled voltages (V_1 and V_2) and coupling matrix.

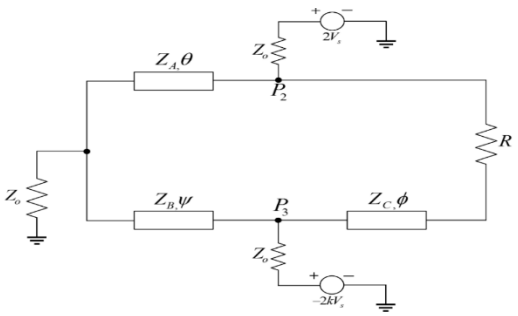

Fig. 1. Odd-mode circuit of proposed power divider.

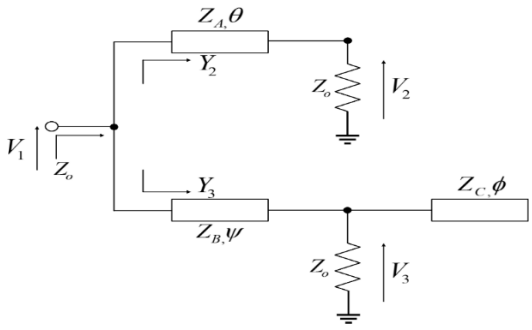

Fig. 2. Even-mode circuit of proposed power divider.

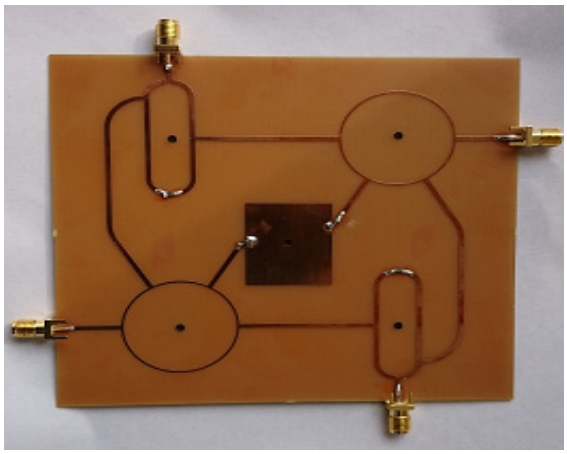

Fig.3. Photograph of the fabricated inserted compensation network.

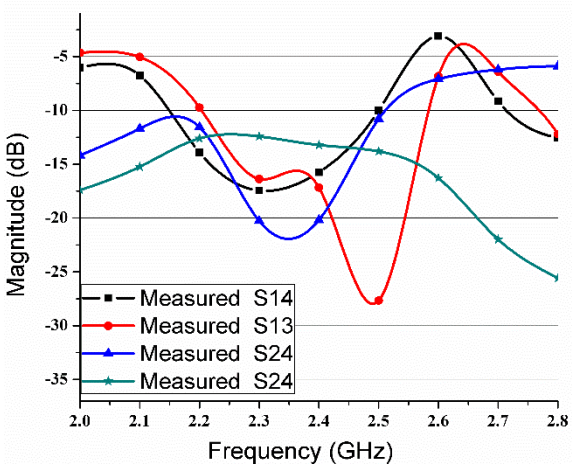

Fig.4. Measured insertion loss between input ports 1&2 and output ports 3&4

The monopole antennas in the array are connected to the decoupling network through equivalent length coaxial links and scattering parameters of the output ports of the decoupling network are measured to determine the coupling matrix for the compensated voltages (U_1 and U_2). These are incorporated into the channel inversion schemes of the multi-user MIMO broadcasting channel for performance evaluation. The BER performance of a multi-user MIMO system for plain and regularized channel inversion schemes are shown in the Fig. 5 and Fig. 6 respectively. It is clear that performance of the coupled voltages at different frequencies must incur losses to make practically identical results for the compensated voltages for the same bit error performance in both schemes due to the coupling phenomenon.

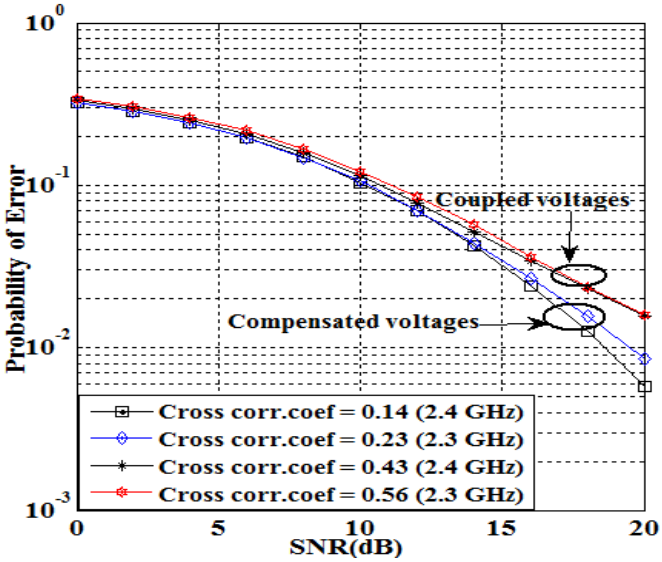

Fig.5. Bit error performance of plain channel inversion with decoupling network

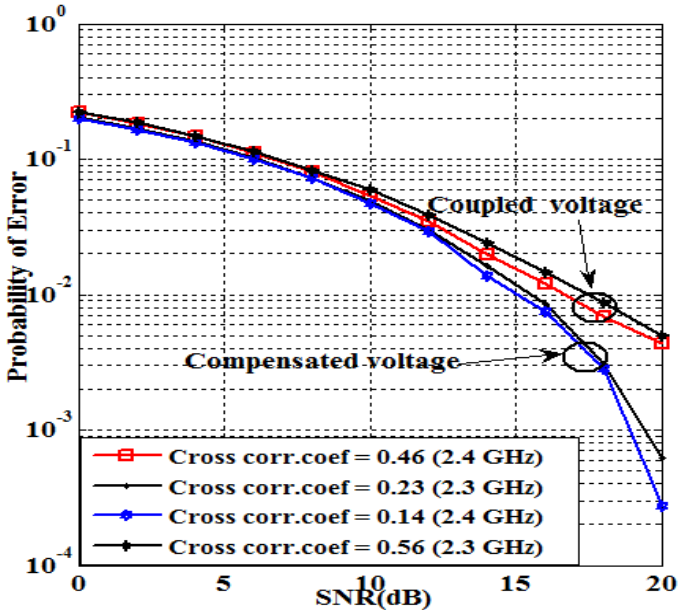

Fig.6. Bit error performance of regularized channel inversion with decoupling network

The simulation results also supports the variations of cross correlation coefficients (ρ_{12}) recorded by the procedure in [38] under both conditions. As it can be seen, the regularized scheme accomplishes better performance than plain scheme, thanks to mitigating noise enhancement. Again, in Table I, the last row defines the ratio of the voltage obtained with monopole B to the voltage obtained with monopole A. Results confirm that the ratio of the compensated voltage is very close to the uncoupled voltages, demonstrating that the compensated voltages have successfully been removed off the coupling effect. It is a known fact that channel inversion provides effective interference cancellation in multi-user broadcasting channel, however, our analysis demonstrates that an efficient decoupling network with channel inversion schemes enhance system performance and demonstrated the lesser impacts of coupling on the compensated voltages in multi-user MIMO. This is because coupling matrix can have decorrelation effect on the channel coefficient and therefore improving the error performance of multi-user MIMO system.

5. Conclusion

In this paper, we demonstrate the effect of coupling matrix on channel coefficient, and the resulting consequences on channel inversion interference cancellation schemes in multi-user MIMO system. Our results confirm that the output of the decoupling network can adequately be removed off the coupling effect. In the event that coupling affects the performance of antenna arrays, our outcomes demonstrate an opposite case. This is because the lesser impacts of coupling on the compensated voltages also translated into an improved bit error performance, indicating the promising potentials of regularized channel inversion scheme with efficient decoupling scheme in multi-user MIMO system.

TABLE I

MEASURED RECEIVING VOLTAGES

		Uncoupled Voltages (reference)	Coupled voltages	Compensated voltages
Monopole A	mag (mV)	16.64	12.4	11.55
	angle (°)	-160.64	-166.67	34.967
Monopole B	mag (mV)	16.54	15.42	12.30
	angle (°)	-139.56	-141.46	55.16
B/A	mag	0.9939	1.2199	1.065
	angle (°)	21.08	25.208	20.193

Acknowledgment

The authors are grateful to all the members of Center for RFIC and System Technology, School of Communication and Information Engineering, University of Electronic Science and Technology of China for relevant advice and discussion to this work.

References

[1] G. Caire and S. Shamai, "On the achievable throughput of a multiantenna Gaussian broadcast channel," *IEEE Trans. Inform. Theory,* vol. 43, pp. 1691-1706, July 2003.

[2] T. Haustein, C. von Helmolt, E. Jorswieck, V. Jungnickel, and V. Pohl, "Performance of MIMO systems with channel inversion," in Proc. *IEEE Vehicular Technology Conference*, VTC Spring, Birmingham, AL, pp. 35–39, May 2002.

[3] C. B. Peel, B. Hochwald, and A. L. Swindlehurst, "A Vector- Perturbation Technique for Near-Capacity Multiantenna Multiuser Communication-Part I:

Channel Inversion and Regularization," *IEEE Transactions on Communications,* vol. 53, pp. 195–202, January 2005.

[4] E. Jorswieck, G. Wunder, V. Jungnickel, and T. Haustein, "Inverse eigenvalue statistics for Rayleigh and Rician MIMO channels," in MIMO: *IEE Seminar on Communications Systems from Concept to Implementations*, pp. 1–3, Dec. 2001.

[5] V. Jungnickel, T. Haustein, E. Jorswieck, and C. von Helmolt, "A MIMO WLAN based on linear channel inversion," *IEE Seminar on in MIMO: Communications Systems from Concept to Implementations,* pp. 1–20, Dec. 2001.

[6] H. Lee, K. Lee, B. M. Hochwald, and I. Lee, "Regularized channel inversion for multiple-antenna users in multiuser MIMO downlink," in Proc. *International Conference on Communications*, Beijing, China, pp. 3501–3505, May 2008.

[7] V. Jungnickel, T. Haustein, V. Pohl, and C. von Helmolt, "Link adaptation in a multi-antenna system," *in Proc. Vehicular Technology Conference*, VTC Spring, vol. 2, pp. 862–866, Jeju, Korea, Apr. 2003.

[8] C. Masouros and E. Alsusa, "Dynamic linear precoding for the exploitation of known interference in MIMO broadcast systems," *IEEE Trans. Wireless Commun*., vol. 8, no. 3, pp. 1396–1404, Mar. 2009.

[9] P.Viswanath and D. Tse, "Sum capacity of the vector Gaussian broadcast channel and uplink downlink duality*," IEEE Trans. Inf. Theory*, vol. 49, pp. 1912–1921, Aug. 2003.

[10] S. Vishwanath, N. Jindal, and A. Goldsmith, "Duality, achievable rates, and sum capacity of Gaussian MIMO broadcast channels", *IEEE Trans. Inf. Theory*, vol. 49, pp. 2658–2668, Aug. 2003.

[11] L. Zhao, L. K. Yeung, and K.-L. Wu, "A coupled resonator decoupling network for two-element compact antenna arrays in mobile terminals, "*IEEE Trans. Antennas Propag.*, vol. 62, no. 5, pp. 2767–2776, May 2014.

[12] J. C. Coetzee and Y. Yu, "Port decoupling for small arrays by means of an eigenmode feed network," *IEEE Trans. Antennas Propag.*, vol. 6, pp. 1587–1593, Jun. 2008.

[13] S. Zuo, Y.-Z. Yin, Y. Zhang, W.-J.Wu, and J.-J. Xie, "Eigenmode decoupling for MIMO loop-antenna based on 180 coupler," *Progr. Electromagn. Res. Lett.*, vol. 26, pp. 11–20, 2011.

[14] S. K. Chaudhury, H. J. Chaloupka, and A. Ziroff, "Multiport antenna Systems for MIMO and Diversity," presented at the EUCAP, Barcelona, Spain, Apr. 2010.

[15] C. Volmer, J. Weber, R. Stephan, K. Blau, and M. A. Hein, "An eigen analysis of compact antenna arrays and its application to port decoupling," *IEEE Trans. Antennas Propag.*, vol. 56, no. 2, pp. 360–370, Feb. 2008.

[16] L. K. Yeung and Y. E. Wang, "Mode-based beamforming arrays for miniaturized platforms," *IEEE Trans. Microw. Theory Tech.*, vol. 57, no. 1, pp. 45–52, Jan. 2009.

[17] J. B. Andersen and H. H. Rasmussen, "Decoupling and descattering networks for antennas," *IEEE Trans. Antennas Propag.*, vol. 24, no. 6, pp. 841–846, Nov. 1976.

[18] S. Chang, Y.-S. Wang, and S.-J. Chung, "A decoupling technique for increasing the port isolation between strongly coupled antennas," *IEEE Trans. Antennas Propag.*, vol. 56, no. 12, pp. 3650–3658, Dec. 2008.

[19] C.-Y. Lui, Y.-S. Wang, and S.-J. Chung, "Two nearby dual-band antennas with high port isolation," presented at the *IEEE Int. Symp. Antennas Propag.*, San Diego, CA, USA, Jul. 2008.

[20] A. Diallo, C. Luxey, P. L. Thuc, R. Staraj, and G. Kossiavas, "Study and reduction of the mutual coupling between two mobile phone PIFAs operating in the DCS1800 and UMTS bands," *IEEE Trans. Antennas Propag.*, vol. 54, no. 11, pp. 3063–3073, Nov. 2006.

[21] C. Luxey, "Design of multi-antenna systems for UTMS mobile phones," in *Proc. Loughborough Antennas Propag. Conf*., pp. 57–64. Nov. 2009.

[22] F. Yang and Y. R. Samii, "Microstrip antennas integrated with electromagnetic band-gap EBG structures: A low mutual coupling design for array applications," *IEEE Trans. Antennas Propag.*, vol. 51, no. 10, pp. 2936–2946, Oct. 2003.

[23] C. Y. Chiu, C. H. Cheng, R. D. Murch, and C. R. Rowell, "Reduction of mutual coupling between closely-packed antenna element," *IEEE Trans. Antennas Propag.*, vol. 55, no. 6, pp. 1732–1738, Jun. 2007.

[24] M. M. Bait-Suwailam, M. S. Boybay, and O. M. Ramahi, "Electromagnetic coupling reduction in high-profile monopole antennas using single-negative magnetic metamaterials for MIMO applications," *IEEE Trans. Antennas Propag.*, vol. 58, no. 9, pp. 2894–2902, Sep. 2010.

[25] B. K. Lau and J. B. Andersen, "Simple and efficient decoupling of compact arrays with parasitic scatterers," *IEEE Trans. Antennas Propag.*, vol. 60, no. 2, pp. 464–472, Feb. 2012.

[26] L. Zhao, L. K. Yeung, and K.-L. Wu, "A coupled resonator decoupling network for two-element compact antenna arrays in mobile terminals," *IEEE Trans. Antennas Propag.*, vol. 62, no. 5, pp. 2767–2776, May 2014.

[27] L. Zhao and K.-L. Wu, "A broadband coupled resonator decoupling network for a three-element compact array," in *Proc. IEEE MTT-S Int. Microw. Symp.* pp. 1–3. Jun. 2013.

[28] L. Zhao, L. K. Yeung, and K. L. Wu, "A novel second-order decoupling network for two-element compact antenna arrays,"*Proc. Asia-Pacific Microwave Conf.,* 2012.

[29] K. Qian, L. Zhao, and Ke-Li Wu, "An LTCC Coupled Resonator Decoupling Network for Two Antennas" *IEEE Transactions on Antennas and Propagation,* vol. 63, No. 7, July 2015.

[30] Lin Yang, Emad Alsusa, Ulises Pineda Rico and Enrique Stevens Navarro "Linear Selective Channel Inversion Technique for Multi-user MIMO systems" IEEE 72nd Vehicular Technology Conference Fall (VTC 2010-Fall), pp. 1 - 5, 6-9 Sept., 2010

[31] Appaiah, K.; Ashikhmin, A; Marzetta, T.L "Pilot contamination reduction in multi-user TDD systems." *in Proc. IEEE International Conference on Commu*. (ICC), pp. 1-5, 2010.

[32] T. Svantesson and A. Ranheim, "Mutual coupling effects on the capacity of multi-element antenna systems," *in Proc. IEEE In Conf.: Acoustics,Speech, and Signal Processing,* vol. 4, pp. 2485-2488, Salt Lake City, UT, May 7-11, 2001.

[33] H. T. Hui, "A new definition of mutual impedance for application in dipole receiving antenna arrays," *IEEE Antennas Wireless Propagat. Lett*, vol. 3, pp. 364–367, 2004.

[34] D. M. Pozar, Microwave Engineering. Reading, MA: Addison-Wesley, 1990.

[35] Y. Yu and H.T. Hui "Design of a Mutual Coupling Compensation Network for a Small Receiving Monopole Array" *IEEE Trans. On Micro. Theory and Techniques,* vol. 59, no. 9, September 2011.

[36] K. K. Cheng and P. W. Li, "A novel power-divider design with unequal power-dividing ration and simple layout," *IEEE Trans. Microw. Theory Tech.*, vol. 57, no. 6, pp. 1589–1594, Jun. 2009.

[37] K. Jeongpyo and C. Jaehoon, "Dual band MIMO antenna using ENG zeroth order resonator for 4G system," IEEE International Worskhop on, Antenna Technology, 2009. (IWAT), pp. 1-4, 2009.

ASTES

Advances in Science, Technology and Engineering Systems Journal
Vol. 2, No. 4, 32-43 (2017)
www.astesj.com

ASTES Journal
ISSN: 2415-6698

Design of Petri Net Supervisor with 1-monitor place for a Class of Behavioral Constraints

Alexander Nuñez*,[1],Arturo Sanchez[2]

[1]*PhD Candidate, Centro de ingeniería y desarrollo industrial, CIDESI,Sistemas dinámicos y de transferencia, México*

[2]*Researcher, Unidad Guadalajara, Cinvestav, México*

ARTICLEINFO

Article history:
Received: 2 March, 2017
Accepted: 11 April, 2017
Online: 25 April, *2017*

Keywords :
Petri nets
Discrete event systems
Supervisory control theory
Ladder logic diagram
Manufacturing execution systems

ABSTRACT

This paper studies the design of supervisory controllers with a minimum number of monitor places for Manufacturing System modeled as safe Petri Nets. The proposed approach considers a class of safety specifications known as Behavioral Constraints with a restricted syntax. The set of Behavioral Constraints are represented as predicate logic formulas in normal conjunctive form. Then, each Behavioral Constraint induces a set of algebraic linear inequalities. The approach establishes an equivalence in order to minimize the number of monitor places. Thus, each Behavioral Constraint induces a single linear inequality, giving rise to a 1-monitor place Petri Net supervisor. The approach is illustrated with the design and implementation of 1-monitor place modular supervisor for an automated manufacturing prototype.

1 Introduction

The operation of manufacturing systems is increasingly challenging because of the execution of more complex tasks. In order to reduce periods for manufacturing procedures, but complying with regulatory standards to guarantee a proper operation and product quality, plenty of manufacturing features have been improved in recent years ([1]). The reconfigurability allows to change the entire procedure of an Automated Manufacturing System (AMS), but it also must minimize the use of time and resources ([2]). The safety of the operation, with all the automatic processes occurring in the AMS is a critic feature, leading to the existence of entities with the propose of guarantee safety operation, such as Supervisory Controllers (SCs). For AMS modeled as discrete event systems, Supervisory Control Theory (SCT) proposed by Wonham in [3] is a well-accepted paradigm frequently employed for designing logic controllers at the coordination and basic layers of control systems. Petri Nets provides a formal logic platform for modeling and synthesis of logic controllers as well as analysis widely used in AMS (e.g. [4] [5]). The synthesized Supervisory Controller (SC) is a Petri Net (PN) with a finite number of places, which are called monitor places. Some of the advantage of PN, more compact representations of the supervisor than their automata counterparts are usually achieved and accepts concurrency in the execution of transitions. Among several design methods considering safety specifications, the Invariant Based Control Design method [6] has been successfully employed to deal with forbidden states [7] and Behavioral Constraints [8]. However, the resulting PN may not be a minimal realization of the SC. Synthesis strategies for PN supervisor with a reduced number of monitor places have been proposed for forbidden state avoidance [9] only, not for Behavioral Constraints. This paper studies the synthesis of 1-monitor place supervisory controllers for safe PN. The proposed design approach employs the Invariant Based Control Design (IBCD) method and a class of safety specifications [10] that can be modeled as Behavioral Constraints [8]. Section 2 introduces the fundamentals of PN and SCT and the representation of Behavioral Constraints (BCs) as a set of linear inequalities. Section 3 shows the proposed technique to transform the set of Behavioral Constraint (BC) into a smaller set of linear inequalities, leading to a PN supervisor with a reduced number of monitor places using the IBCD method. Section 3 also establishes the conditions for a Supervisory Controller based on Be-

*Corresponding Author: Alexander Núñez, Pie de la cuesta 702, Querétaro, México, 554421811255 & cnunez@posgrado.cidesi.edu.mx

https://dx.doi.org/10.25046/aj020405

havioral Constraints (SCBC) to be proper. Section 4 shows the case study used in this work, an AMS, presenting its description and modeling. Then, Section 5 presents a set of BCs to be imposed in the AMS, the representation as linear inequalities and the resulting SC designed using the IBCD method, as well as its implementation as a ladder diagram.

2 Fundamentals

In this Section the basic definitions of Petri Nets and Supervisory Control Theory are introduced.

2.1 Petri Nets fundamentals

For modeling techniques, as well as structural and dynamic properties of PN the reader is refereed to [11].

Definition 1 (Petri Net) *A Petri Net is defined as the triplet (S,T,F) with S as the set of places, T as the set of transitions and $F:\{S\to T, T\to S\}$ a total relation.*

Definition 2 (Marking vector) *Let N be a PN and $S=\{s_1,s_2,\ldots,s_n\}$ its set of places. The marking vector is a mapping $M: S\to N\cup 0$ represented by $[M(s_1)\ M(s_2)\ \ldots\ M(s_n)]$.*

Definition 3 (Enabled transition) *Let N be a PN and $t\in T$ a transition of N. The transition t is said to be enabled if the marking of all input places is grater or equal than 1.*

Definition 4 (Initial marking vector) *Let N be a PN and $[M(s_1)\ M(s_2)\ \ldots\ M(s_n)]$ its marking vector. The initial marking vector is defined as the marking vector when no transition has been fired.*

Definition 5 (PN System) *Let N be a PN and M_0 its initial marking vector. A PN system is defined as a the pair (N,M_0).*

Definition 6 (Boundedness) *Let (N,M_0) be a PN system. The system is called bounded if for each place s exists a natural number b such that $M(s)\leq b$ for all reachable markings from M_0.*

If $M(s)\leq b$ holds for any place s, then the system is called b-bounded.

Definition 7 (Liveness) *Let (N,M_0) be a PN system. The PN system is called live if, for any reachable marking M and any transition t, there is a marking M' which enables t.*

Definition 8 (Safe Petri Net System) *Let (N,M_0) be a PN system. The system is called Safe if the system is 1-bounded and live.*

Even though the term Safe is defined for systems, if a PN structurally generates a Safe system is usually called Safe PN.

2.2 Supervisory Control Theory (SCT)

The automata version of SCT is developed in [3]. In this subsection, the fundamentals SCT for discrete event system modeled as PN are introduced, as seen in [6]. Moreover, the basic concepts and definitions of BC are discussed in [12] and presented in the current section.

Definition 9 (Control pattern) *Let N be a PN and T be its set of transitions.*

The control pattern Γ is defined as the set of transitions enabled in a marking M of (N,M).

Definition 10 (Transition sequence) *Let (N,M) be a PN system and T be its set of transitions.*

$\sigma = t_1 t_2 \cdots t_n$ is a transition sequence of transitions such that

- $M_{i-1} \xrightarrow{t_i} Mi$
- *t_i is enabled in M_{i-1}*

with $t_i\in T$, $\forall i=1,2,\cdots,n$.

Definition 11 (Petri Net Supervisor) *Let $L*M\leq b$ a constraint for the marking vector of a PN system (N,M) with incidence matrix D. $S: M\to\Gamma$ is a supervisor for PN system (N,M). Let C be a PN with marking M_c and set of transition T. C is the implementation of S as a PN such that*

- *Marking vector $M_c = b - L*M_0$.*
- *Incidence matrix $Dc = -L*D$*
- *Γ is the control pattern for (C, M_c).*

Definition 12 (Open loop system) *Let (N, M) be a PN system. (N, M) is also called an Open loop system.*

Definition 13 (Closed loop system) *Let (N,M) a PN system and (C, M_c) a PN implementing S, with S a supervisor. The closed loop system is defined as the synchronization of N and C.*

Definition 14 (Controllability) *Let (N,M) be a PN system and T be its set of transitions. Let $\Sigma\subset T^*$ be the set of all transitions sequences σ. Σ is called controllable if the prefix closure of Σ is invariant under the occurrence of uncontrollable transitions in N.*

Definition 15 (Admissible marking) *Let marking M_a be reachable from initial marking M_0 of a system (N,M_0) with uncontrollable transitions. M_a is an admissible marking for the constraint $L*M\leq b$ if the following conditions hold*

- *$L*M_a\leq b$*
- *For all reachable markings M_r from M_a trough the occurrence of uncontrollable transitions in (N,M) $L*M_r\leq b$*

Definition 16 (Admissible constraint) *Let (N,M) a PN system with initial marking M_0. An admissible constraint satisfies*

- *$L*M_0\leq b$*

- *All reachable markings from M_0 are admissible markings.*

Finally, the concept of safety specification is explained. A safety specification leads to the system to developed a safety property. Safety properties are often characterized as "nothing bad should happen". The mutual exclusion property, deadlock freedom are examples of safety properties [10].

2.3 Predicate representation of Behavioral Constraints

Let N be a *safe* PN with firing vector $Q=[q_1\ q_2\ \cdots\ q_l]$ and let (N,M) be a system with marking vector $M=[m_1\ m_2\ \cdots\ m_l]$.

Definition 17 *Predicate variable $A: Q \to \{True, False\}$ associated to a firing transition T_i is defined with the rule*

$$A(q_i)=\begin{cases} True\ if\ q_i=1 \\ False\ if\ q_i=0 \end{cases}$$

Definition 18 *Predicate variable $\Theta: M \to \{True, False\}$ associated to a marking place m_i is defined with the rule*

$$\Theta(m_i)=\begin{cases} True\ if\ m_i=1 \\ False\ if\ m_i=0 \end{cases}$$

Definition 19 (Behavioral Constraint (BC)) *A BC is defined with the following predicate logic syntax*

$$A(q_a)\to\Phi \tag{1}$$

with A being a predicate variable associated to firing transition T_a and Φ a formula in conjunctive normal form, composed by predicate variables associated to marking places, that is

$$\Phi=\phi_1\wedge\phi_2\wedge\ldots\phi_n \tag{2}$$

with

$$\phi_i(z_r)=\Theta(m_{r_1})\vee\Theta(m_{r_2})\vee\ldots\Theta(m_{r_l}) \tag{3}$$

with r_j as the place index in N, $j=1,2,\ldots,l$, with l the number of places associated in Eq. 3 and

$$z_r=m_{r_1}+m_{r_2}+\ldots+m_{r_l} \tag{4}$$

$$\phi(z)=\begin{cases} True\ if\ z\geq 1 \\ False\ if\ z=0 \end{cases}$$

Eqs. 1 and 2 are equivalent to

$$(A(q_a)\to\phi_1)\wedge(A(q_a)\to\phi_2)\wedge\ldots\wedge(A(q_a)\to\phi_n) \tag{5}$$

Definition 20 ($P(S\leq 0)$) *Let S be an algebraic expression formed by elements in Q and in M. The associated predicate $P: Q\times M\to\{True, False\}$ is defined with the rule $S\leq 0$.*

Proposition 21 *Let $A(q_a)$, $\Theta(m_b)$ be predicate variables and $P(q_a-m_b\leq 0)$ be their associated predicate. The following expressions are equivalent*

$$A(q_a)\to\Theta(m_b) \tag{6}$$

$$P(q_a-m_b\leq 0) \tag{7}$$

Proof. *N is a safe net, thus N is a 1-bounded net. Hence the marking vector takes only 0 and 1 values. Therefore Table 21 holds.*

q_a	m_b	$A\to\Theta$	$P(q_a-m_b\leq 0)$
0	0	T	T
0	1	T	T
1	0	F	F
1	1	T	T

Table 21 Truth table of Proposition 21

■

Using Proposition 21, BC presented in Eq. 5 can be written in an equivalent form, as shown in Lemma 22.

Lemma 22 *Let $A(q_a)$ and $\Theta(m_{k_1})$, $\Theta(m_{k_2})\ldots\Theta(m_{k_l})$ be predicate variables The BC 5 is equivalent to predicate system 8*

$$\begin{gathered} P(q_a-m_{r_{11}}+m_{r_{12}}+\ldots+m_{r_{1l}}\leq 0) \\ \vdots \\ P(q_a-m_{r_{i1}}+m_{r_{i2}}+\ldots+m_{r_{il}}\leq 0) \\ \vdots \\ P(q_a-m_{r_{n1}}+m_{r_{n2}}+\ldots+m_{r_{nl}}\leq 0) \end{gathered} \tag{8}$$

with il as the number of disjunction variables in each formula ϕ_i.

Proof. *It follows from applying Proposition 21 to BC 5.* ■

3 Supervisory Controllers design using an Equivalent representation of a set of Behavioral Constraints

Using the n inequalities induced by predicate system 8 with the IBCD method ([6]), a PN supervisor is obtained with n monitor places, each one with a bidirectional arc to transition t_a. It is presented below a procedure to design a PN SC, based on a BC as in Eq. 1 with a single monitor place.

Theorem 23 *Let $A(q_a)$ and $\Theta(m_{k_1})$, $\Theta(m_{k_2})\ldots\Theta(m_{k_l})$ be variables as in definitions 17 and 18. Let a BC for restricting the system behavior be*

$$A(q_a)\to\Theta(m_{k_1})\wedge\Theta(m_{k_2})\wedge\cdots\wedge\Theta(m_{k_n})\wedge[\Theta(m_{j_1})\vee\Theta(m_{j_2})\vee\cdots\vee\Theta(m_{j_m})] \tag{9}$$

A 1-monitor place PN supervisor can be synthesized (i. e. its incidence matrix can be calculated) with the IBCD method using linear inequality

$$m[nq_a-m_K]+[q_a-m_J]\leq 0 \tag{10}$$

with $m_K=m_{k_1}+m_{k_2}+\cdots+m_{k_n}$ and $m_J=m_{j_1}+m_{j_2}+\cdots+m_{j_m}$ and $m>0$

Proof. *See Appendix A.* ■

Corollary 24 *Let equation* $A(q_a) \rightarrow \Theta(m_{k_1}) \wedge \Theta(m_{k_2}) \wedge \cdots \wedge \Theta(m_{k_n})$ *be a BC for restricting the system behavior. A 1-monitor place PN supervisor can be synthesized (i. e. its incidence matrix can be calculated) with the IBCD method using linear inequality*

$$[nq_a - m_K] \leq 0 \tag{11}$$

with $m_K = m_{k_1} + m_{k_2} + \cdots + m_{k_n}$

3.1 Properness of a Supervisory Controller based on Behavioral Constraints

The conditions for a SCBC to be non-blocking and controllable are studied in this subsection.

Definition 25 (System Under Supervision) *Let N be a safe net and M its marking vector. Let C be the PN that implements a supervisor for N and* M_c *the marking vector of C.*

A System Under Supervision (SUS) is defined as

$$(N \| C, [M M_c]) \tag{12}$$

where N||C represents the synchronization of nets N and C with marking vector $[M\ M_c]$.

This definition complements definition 13, adding the marking vector. In the rest of the document, closed loop system will be refereed as SUS.

A supervisor is proper iff the SUS in non-blocking and controllable [3].

3.1.1 Liveness analysis

A necessary condition for non-blocking is liveness. For safe PN modeling AMS, the condition of liveness is required, as shown in this subsection. An AMS is composed by sub systems, each modeled as a live and bounded PN circuit.

Definition 26 (Partial blocking) *A system* (N, M) *is called partially blocking if there is a sub system* (N_1, M_1) *of* (N, M) *which is blocking.*

Lemma 27 *Let N be a safe PN. System*(N, M) *is live if and only if is not partially blocking.*

Proof. *As necessary condition, if a system is not partially blocking, then there is the system is live. For the sufficiency, is enough to prove that in a partially blocking system there is a transition not enabled in every reachable marking of M. Assuming a blocking system* (N_1, M_1) *with* N_1 *a sub net of N. Let t be an output transition to a place s of* N_1 *and t is not enabled in marking* M_1, *s has no tokens in* M_1. *The system is partially blocking* M_1, *hence the reachable markings from M contains element such that s has no tokens. If s has no tokens, transition t is not enabled. Therefore* (N, M) *is not live.* ■

Therefore, for safe PN, non-partial blocking is required in order to ensure a full funcionallity in the AMS. Hence by Lemma 27, liveness is required.

Now, the condition for a SCBC to be live is established. Using definition 28, of Proposition 29 and Lemma 31 are proved. Proposition 29 establishes conditions to guarantee reachability of a marking vector. Lemma 31 demonstrates if an associated marking vector is reachable, then SUS is live. Finally, Theorem 32 follows from Proposition 29 and Lemma 31, establishing condition for a SUS to be live.

Definition 28 (Marking vector associated to constraints) *Let* $A(q_a) \rightarrow \Theta(m_{k_1}) \wedge \Theta(m_{k_2}) \wedge \ldots \wedge \Theta(m_{k_n})$ *be a BC. The marking vector associated to the above constraint is defined as*

$$m_{k_j} = \begin{cases} m_{k_j} \text{ if place } k_j \text{ is not in BC} \\ 1 \text{ if place } k_j \text{ is in BC} \end{cases}$$

Proposition 29 *Let a BC of the form* $A(q_a) \rightarrow \Theta(m_{k_1}) \wedge \Theta(m_{k_2}) \wedge \ldots \Theta(m_{k_n})$ *There is not more than 1 place in the BC belonging to the same minimal S-invariant S of N if and only if the associated marking vector of the above BC*

$$R^T = \begin{bmatrix} m_1 & m_2 & \cdots & 1 & 1 & \cdots & 1 & m_{2+k_n} & \cdots & m_l \end{bmatrix}$$

with l as the number of places, is reachable.

Proof. *First the following implication is proved using its contra-positive. If the associated marking vector is reachable, then there is not more that 1 place in the BC belonging to the same minimal S-invariant. Consider S a minimal S-invariant containing 2 or more places included in the BC, and vector* $S1 = [1\ 1 \cdots 1]$ *of length m, with m as the number of places in S. The next equation is the invariance condition and guarantees that the number of tokens in an S-invariant is conservative.*

$$\begin{bmatrix} 1 & 1 & \ldots & 1 \end{bmatrix} * M_{os} = 1 \tag{13}$$

M_{os} *is the initial marking of the places in S, and for the conservativeness of the S-invariant, this value holds for any reachable marking. Let R' be a projection containing the values of R corresponding to the places in S.*

Multiplying S1 by R'

$S1 * R' \geq 2$

The above expression violates conservativeness, hence the marking is not reachable.

For the converse implication, consider that there is not more than 1 place in the BC belonging to the same minimal S-invariant S. Therefore, all places of the BC belongs to different and disjoints minimal S-invariant, this is concluded from the fact that the net N is 1-bounded and system (N, M) *is live. The last claim implies that every minimal S-invariant is marking in M, because N is a free-choice PN (see [11] Commoner Theorem). Thus, every S-invariant has a token in the initial marking, the system is live and by Lemma 27 it is not partially blocking. Hence, there is a reachable marking of the system* (N, M) *such that every place in the BC has one token simultaneously (invariants are disjoints) and the associated marking vector is reachable.* ■

Proposition 30 *Let a BC of the form* $A(q_a) \rightarrow \Theta(m_{k_1}) \wedge \Theta(m_{k_2}) \wedge \ldots \Theta(m_{k_n})$ *imposed to a system* (N, M) *and R its associated marking vector.*

The formula Φ is true if and only if the system (N,M) reaches marking R.

Proof. *By definition, vector R changes its values only in the places appearing in formula Φ. The sufficiency condition, if formula Φ is true the marking of the system is R. Assuming Φ true in some marking M_r, all Θ variables are true and, by definition, all places in the formula have one token in marking M_r. Hence, R=M_r.*

For the necessary condition consider that system (N,M) has reached marking R after some firing sequence. Using a similar argument, all places appearing in Φ have one token in R, all Θ variables are true in R, hence Φ is true in R. ■

Using previous results two useful conditions for liveness under supervision are developed.

Lemma 31 *Let a BC of the form $A(q_a) \rightarrow \Phi$ and C a PN representing a supervisor for N. If the associated marking vector of Φ is not reachable, then the SUS of C is not live.*

Proof. *If associated marking vector is not reachable, it means that the formula Φ of the BC never is true, thus transition t_a is never enabled. The system is not live.* ■

Theorem 32 *Let $A(q_a) \rightarrow \Phi$ and C a PN representing a supervisor for N.*

SUS of C is live if and only if there is a reachable marking M_r such that formula Φ is true and t_a is enabled in M_r.

Proof.

By contradiction, assume a SUS live and there is not any reachable marking such that formula $\Phi$is true and t_a is enabled. By 30, associated marking vector of the BC is not reachable, hence by 31 SUS is not live, leading to a contradiction.

Now for the sufficiency condition, assume that marking M_r is reachable and formula Φ is true and t_a is enabled in M_r. Therefore, transition t_a is enabled in SUS, hence it is enabled in systems with and without supervision. The following claim is proved in 37 from subsection 3.1.2, only transition t_a may be disabled by the supervisor. The system (N,M) is live and the SUS may only disables transition t_a. However, there is a marking M_r enabling transition t_a in the SUS, henceforth every transition is enabled in some reachable marking of SUS and by definition SUS is live. ■

3.1.2 Non-conflict analysis

If a set of BC is non-conflicting then the resulting SC is non-blocking [3]. As before, liveness is required for manufacturing systems. Hence, a set of BC is called non-conflicting if the SUS is live.

Theorem 33 *Let $A(q_1) \rightarrow \Phi_1$, $A(q_2) \rightarrow \Phi_2$, $\cdots$ $A(q_n) \rightarrow \Phi_n$ be BCs that satisfy conditions of Lemma 32. Let C be the net representing the supervisor of all the constraints.*

The set of BC is non-conflicting if and only if, every subnet of PN C generates a live subsystem.

Proof. *Necessary condition. A set of constraints is non-conflicting if the SUS is live. Assume a SUS such that there is a subnet C_1 of C generating a non-live system (C_1, M_1). Since is not live, there is a transition t_1 disabled in all reachable markings from some marking M_i. t_1 is a transition of the SUS also, therefore the SUS is not live, leading to a contradiction.*

For the sufficiency, assume that a SUS is not live. Therefore, at least a transition t of N is not enabled for all reachable markings. In the first case, t is connected to C. Then, there is a place c input to t in C with no tokens for all reachable marking. There is a transition T_1 input to c not enabled and following the same idea that t, assuming T_1 connected to C there is c_1 input to T_1 in C. Recursively until place c_n is place c (there is a finite number of places in C), there is a subnet of C with a disabled transition, hence the subnet is not live. If transition t is not connected to C, there is a transition $t^{'}$ in the same minimal S-invariant of t connected to C, and the above procedure can be followed for $t_i^{'}$. ■

Corollary 34 *Let $A(q_1) \rightarrow \Phi_1$, $A(q_2) \rightarrow \Phi_2$, $\cdots$ $A(q_n) \rightarrow \Phi_n$ be BCs that satisfy conditions of Lemma 32. Let C be the net representing the supervisor of all the constraints.*

If all the supervisory nets generated by the set of BC are disjoint then the SUS is live (i.e. the set of BCs is non-conflicting)

Proof. *If the nets are disjoint and the conditions of Lemma 32 are satisfied all the nets generate live systems, hence by Theorem 33 the set of BCs is non-conflicting.* ■

Definition 35 (Controlled Siphon) *{ [13] } Let R be a siphon in a net N with M_R as its marking vector. R is a controlled siphon if for all marking $M_R^{'}$ reachable from M_{0R}, $|M_R^{'}| \geq 1$. Otherwise, it's an uncontrolled siphon.*

That is, a controlled siphon is a siphon that never becomes unmarked.

Corollary 36 *Let $A(q_1) \rightarrow \Phi_1$, $A(q_2) \rightarrow \Phi_2$, $\cdots$ $A(q_n) \rightarrow \Phi_n$ be BCs that satisfy conditions of Lemma 32. Let C be the net representing the supervisor of all the constraints. Consider that every BC has only one variable in each respective formulae Φ_i.*

The set of BCs is non-conflicting if and only if there is not an uncontrolled siphon

Proof. *The same argument used in 33 is applied. Since all the BCs have only one variable, their corresponding nets have only one place each. The condition of a not live subnet becomes then in a subnet with no tokens, hence an uncontrolled siphon.* ■

3.1.3 Controllability analysis

This subsection shows that a SUS synthesized using the IBCD method with BC is, in fact, controllable.

Lemma 37 *Let $A(q_a) \rightarrow \Phi$ be a BC imposed to the PN N. Let C be the net representing the corresponding supervisor and let $t_b \neq t_a$*

If a transition t_b is enabled in a marking M of N, then it is enabled in marking M_c of $(N||C)$.

Proof. *Consider s_b an input place to t_b. Assume s_b as part of the constraint. The net N es safe, hence it is composed by S-invariants (i.e. state machines), thus every transition has one only input place. Hence if T_b is enabled, then s_b has a token. Obtaining the marking of*

the monitor place using the formula $m_c = -L * M$ [6] the monitor place has at least B tokens (B being the coefficient corresponding the place s_b in vector L). Calculating the incidence matrix D_c of the monitor place using $D_c = -L * D_p$, for the place s_b, the value corresponding to transition t_b is coefficient $-B$. Therefore transition t_b is enabled because the monitor place has at least B tokens, necessary to fire transition B. ■

Theorem 38 *Let $A(q_a) \rightarrow \Phi$ be a BC imposed to net N.*

Constraint is admissible (RW-controllable) if and only if transition T_a is controllable.

Proof. *By Lemma 37 no other transition of N will be disabled by the supervisor. The supervisor can disable only transition T_a. Hence the supervisor only disables controllable transitions. Therefore, any sequence of the SUS is invariant to the occurrence of uncontrollable transitions.*

■

4 AMS case study

4.1 System description and open loop model description

The AMS employed as a case study is a pneumatic punching center whose topology is illustrated in Fig. 1. The manufacturing procedure begins when a piece arrives to the storage unit (SU), then valve B (VB) opens, activating the input piston (IP). IP pushes the piece into the slot 1 (S1) of the rotatory table, while valve A (VA) retracts the IP. The motor (MR) is turned on, generating a rotation of 90 degrees clock-wise in the rotor, and the piece advances to slot 2 (S2). The piece is processed by the punching machine (PM) at slot 2, using valve E (VE) to activate the PM. Then, the motor turns 90 degrees clock-wise again, placing piece into slot 3 (S3). The piece at slot 3 is pushed by the output piston (OP), activated by valve D (VD), to a conveyor belt, and finally, valve C (VC) retracts the OP.

Each elementary component of the AMS is modeled as a two-places PN block. A place is added to the block associated to each discrete value. The set of transitions are defined as the events to change the discrete value of a component. A transition is added to the model for each event. For the initial marking, a token is added to the associated place of the initial discrete value of each component. The rest of the places remain with no tokens. Table 3 enlists the elementary components with the associated semantics of each place and transition. Fig. 2 shows the PN blocks of the AMS.

The following causal relationships complete in the open loop behavior of the AMS. Bidirectional arcs are added to the model to include the relationships in the behavior, as shown in Fig. 2.

- A piece can arrive to slot 1 only if input piston is out and there is a piece in storage (bidirectional arcs from $P2$ and $P4$ to $T5$).
- Input piston can be activate only if valve A is open, and it can be retract only if valve B is open (bidirectional arcs from $P18$ to $T4$ and from $P20$ to $T3$).
- Punching machine can be activate only if valve E is on (a bidirectional arc from $P26$ to $T11$).
- Output piston can be activate only if valve C is open, and it can be retract only if valve D is open (bidirectional arcs from $P22$ to $T14$ and from $P24$ to $T13$).

This PN is live and 1-bounded, i. e. is a safe PN. The incidence matrix d of each PN module is of the form of Eq. 14. Hence, the incidence matrix D_p of the entire system is a $28x28$ block matrix in Eq. 15. The initial marking vector m of each module is shown in Eq. 16. Hence, the initial marking vector M_o of the AMS is shown as a block vector in Eq. 17.

$$d = \begin{bmatrix} -1 & 1 \\ 1 & -1 \end{bmatrix} \tag{14}$$

$$D_p = blockdiag\{\mathbf{d}\} \tag{15}$$

$$m = \begin{bmatrix} 1 & 0 \end{bmatrix} \tag{16}$$

$$M_o^T = \left[\begin{array}{c|c|c|c|c|c|c|c|c|c|c|c|c} m & m & m & m & m & m & m & m & m & m & m & m & m \end{array}\right] \tag{17}$$

4.2 Closed loop specification modeling

The specifications to be imposed upon the AMS are described in this subsection. Four safety specifications are defined to ensure the AMS safe operation. Matching definition 19, each specification have a corresponding BC.

1. If turning on motor (T27) is enabled, then both piston (P3, P13) and punching machine (P11) are in the withdrawn position and there is a manufacturing piece in slot 1 (P6) or in slot 2 (P8). The corresponding BC is shown in Eq. 18.
2. If opening valve B to activate input piston (T19) is enabled, then there is a piece in storage (P2) and table is in load position (P15). The corresponding BC is shown in Eq. 19.
3. If opening valve D to activate output piston is enabled (T23), then there is a piece in slot 3 (P10). The corresponding BC is shown in Eq. 20.
4. If opening valve E to activate punching machine (T25) is enabled, then there is a piece in slot 2 (P8). The corresponding BC is shown in Eq. 21.

$$A(q_{27}) \rightarrow \Theta(m_3) \wedge \Theta(m_{13}) \wedge \Theta(m_{11}) \wedge [\Theta(m_6) \vee \Theta(m_8)] \tag{18}$$

$$A(q_{19}) \rightarrow \Theta(m_2) \wedge \Theta(m_{15}) \tag{19}$$

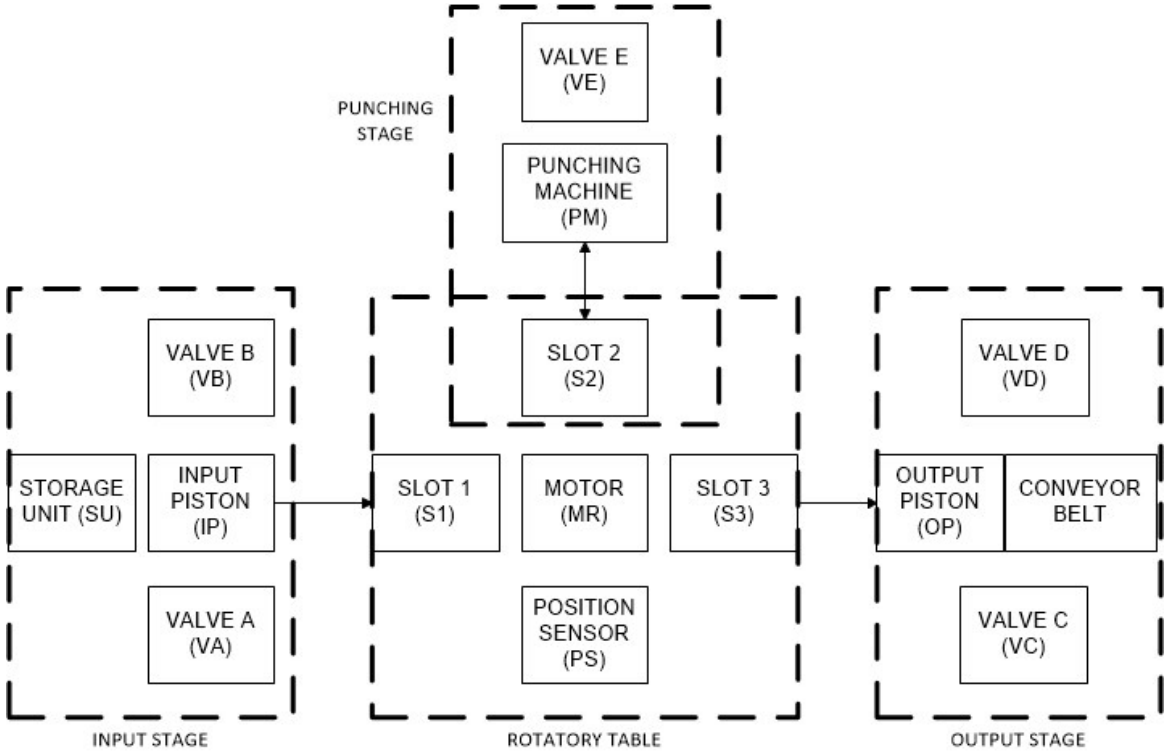

Figure 1: AMS Topology

$$A(q_{23}) \rightarrow \Theta(m_{10}) \tag{20}$$

$$A(q_{25}) \rightarrow \Theta(m_8) \tag{21}$$

Using Lemma 22, the induced system for the BCs from Eqs. 18-21 is presented in Eq. system 22 consisting of a linear system of 8 inequalities. Employing the method proposed in section 3 (Theorem 23 and corollary 24) Eqs. 18-21 are transformed into a set of 4 linear inequalities shown in Eq. system 23.

$$\begin{gathered} q_{27} - m_3 \leq 0 \\ q_{27} - m_{13} \leq 0 \\ q_{27} - m_{11} \leq 0 \\ q_{27} - m_6 - m_8 \leq 0 \\ q_{19} - m_2 \leq 0 \\ q_{19} - m_{15} \leq 0 \\ q_{23} - m_{10} \leq 0 \\ q_{25} - m_8 \leq 0 \end{gathered} \tag{22}$$

$$\begin{gathered} 7q_{27} - 2m_3 - 2m_{13} - 2m_{11} - m_6 - m_8 \leq 0 \\ 2q_{19} - m_2 - m_{15} \leq 0 \\ q_{23} - m_{10} \leq 0 \\ q_{25} - m_8 \leq 0 \end{gathered} \tag{23}$$

Using Eq. system 23 with the IBCD method, a PN supervisor is designed. The matrix L is defined in Eq. system 24. Using the equation $D_c = -L * D_p$ incidence matrix D_c of the supervisor is calculated, ans it is shown in Eq. system 25. Four self-looped arcs are added, one for each BC, connecting the monitor place with the corresponding controllable transition. The weight of each arc is the corresponding coefficient for the transition in the set of induced inequalities shown in Eq. system 23.The equation $M_{oc} = -L * M_o$ is used for calculating the initial marking vector M_{oc} of PN supervisor, shown in Eq. 26. Each monitor place is connected only to some transitions in the open loop model. Thus, each monitor place can be represented as a modular supervisor, using only the PN blocks connected to the monitor place. The resulting 4 modular PN supervisors are shown in Fig. 4.

4.3 Properness analysis

This subsection presents the analysis to show that the designed SCBC is in fact proper, i. e. the SUS is live, non-conflicting and controllable. For each BC, there are not 2 places belonging to the same PN block. Each PN block is a minimal S-invariant (see [11]).Therefore, there are not 2 places belonging to the same minimal S-invariant. Hence, by Proposition 29 the associated marking vectors for all the BCs are reachable. Now, by Proposition 30 in those markings the respective formulaes Φ are true. Since all transition of the BC are enabled in its respective associated reachable markings by Theorem 32 the SUS for every BC is live.

Now, by Theorem 33 the PN supervisor must not have any not live subnet in order to prove that the set of constraints is non-conflicting. However, the only not disjoint subnet of PN supervisor is concerned to transitions T_7 and T_8. From a quick analysis it is clear that this particular subnet is live. Hence, by 34 and Theorem 33 the SUS is live, i.e. the set of BCs is non-conflicting.

The set of constraints must be proven admissible. By Theorem 38, the set of constraints is proven admis-

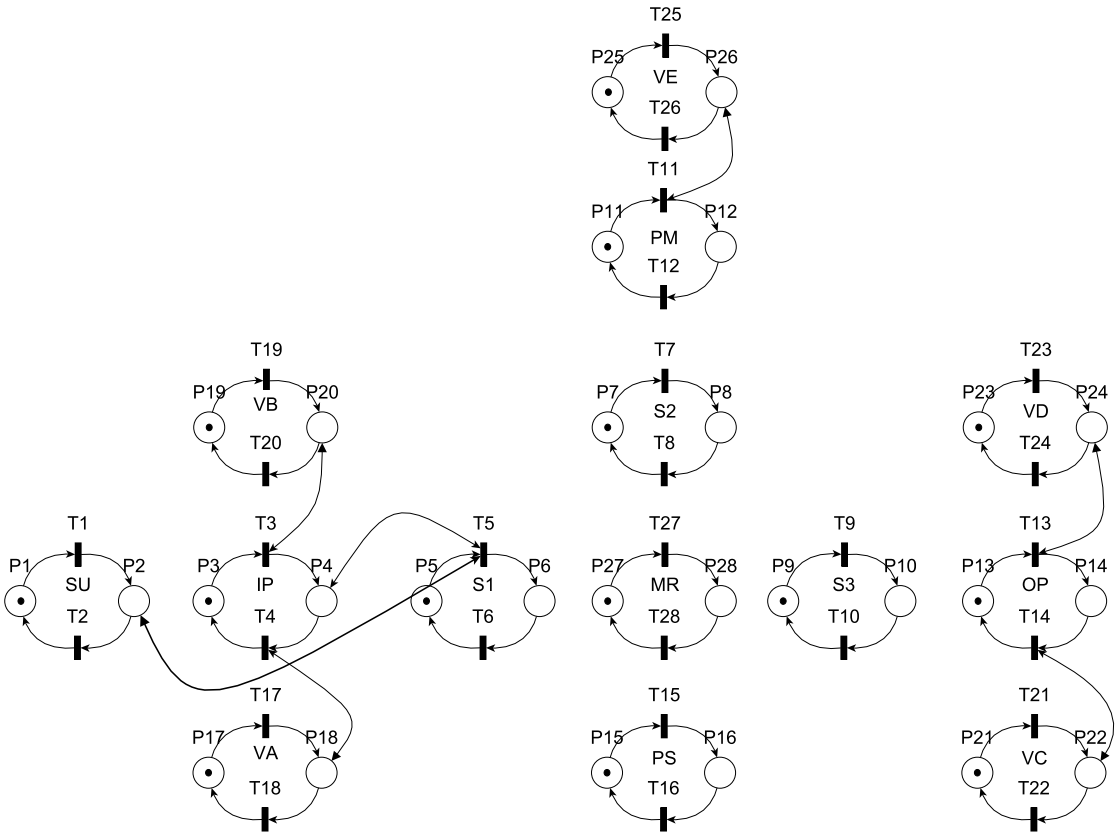

Figure 2: AMS model

sible since transitions T_{27}, T_{17}, T_{21} and T_{25} are controllable.

4.4 Ladder diagram implementation of supervisory controller

A PN can be translate into a ladder diagram for its implementation in a control device (e.g. a PLC). The general procedure for the translation of PN into ladder diagram is explained in [14]. Every place has a corresponding register in the ladder diagram. Every transition has a corresponding contact and its execution generates the change of the contact state.

The following rules are an adaptation of the translation procedure developed in [14]. Let T_a be a transition in the supervisor PN. Let P_a be an output place of T_a, connected by an arc with weight na. Let P_b be an input place of T_a, connected by an arc with weight nb.

- Each transition T_a is represented as a contact in a ladder segment.
- If P_a is 1−bounded, then it is represented by a coil with a set function. If P_a is not 1−bounded, then it is represented by an add block, adding na tokens to P_a.
- If P_b is 1−bounded, then it is represented by a coil with a reset function. Also,a normally open contact is associated to P_b in the segment.
- If P_b is not 1−bounded, then it is represented by a subtract block, subtracting nb tokens to P_b. Also, a comparison contact is associated to P_b, with the rule, greater or equal than nb.
- If $P_a = P_b$ (self-loop), then the number of tokens holds. Thus, there are not output blocks associated to P_a in the segment.

The resulting ladder diagram for the SCBC is composed by 28 segments, one for each transition of the AMS model. A part of this ladder diagram is shown in Fig. 4.4. Each segment contains the conditions to enable the corresponding transition. For example, monitor place C1 must have at least 7 tokens for enabling transition T27. The number 7 is the coefficient corresponding to transition T_{27} in the Eq. system 23. Moreover, in the Fig. 4 the weight of the bidireccional arc from monitor place C1 to transition t_{27} is 7. Monitor place C4 must have a token for enabling transition T25.

Component	Discrete Value	Place	Event	Transition	Type
Storage Unit (SU)	No piece in storage	P_1	Piece arrives to storage	T_1	uc
	Piece in storage	P_2	Piece leaves from storage	T_2	uc
Input piston (IP)	Input piston in	P_3	Activate input piston	T_3	uc
	Input piston out	P_4	Retract input piston	T_4	uc
Slot 1 (S1)	No piece in slot 1	P_5	Piece arrives to slot 1	T_5	uc
	Piece in slot 1	P_6	Piece leaves from slot 1	T_6	uc
Slot 2 (S2)	No piece in slot 2	P_7	Piece arrives to slot 2	T_7	uc
	Piece in slot 2	P_8	Piece leaves from slot 2	T_8	uc
Slot 3 (S3)	No piece in slot 3	P_9	Piece arrives to slot 3	T_9	uc
	Piece in slot 3	P_{10}	Piece leaves from slot 3	T_{10}	uc
Punching machine (PM)	Machine withdrawn	P_{11}	Activate punching machine	T_{11}	uc
	Machine active	P_{12}	Retract punching machine	T_{12}	uc
Output piston	Output piston in	P_{13}	Activate output piston	T_{13}	uc
	Output piston out	P_{14}	Retract output piston	T_{14}	uc
Position sensor of	Loading position	P_{15}	Arriving to loading position	T_{15}	uc
rotatory table (PS)	Not in loading position	P_{16}	Leaving from loading position	T_{16}	uc
Valve A (VA)	Valve A closed	P_{17}	Open valve A	T_{17}	c
retract input piston	Valve A open	P_{18}	Close valve A	T_{18}	c
Valve B (VB)	Valve B closed	P_{19}	Open valve B	T_{19}	c
activate input piston	Valve B open	P_{20}	Close valve B	T_{20}	c
Valve C (VC)	Valve C closed	P_{21}	Open valve C	T_{21}	c
retract output piston	Valve C open	P_{22}	Close valve C	T_{22}	c
Valve D (VD)	Valve D closed	P_{23}	Open valve D	T_{23}	c
activate output piston	Valve D open	P_{24}	Close valve D	T_{24}	c
Valve E (VE) activate	Valve E closed	P_{25}	Open valve E	T_{25}	c
punching machine	Valve E open	P_{26}	Close valve E	T_{26}	c
Rotatable Motor (MR)	Motor off	P_{27}	Turn on motor	T_{27}	c
	Motor on	P_{28}	Turn off motor	T_{28}	c

Figure 3: Elementary components, discrete values and events of AMS with the corresponding places and transitions assignment (uc, uncontrollable; c, controllable)

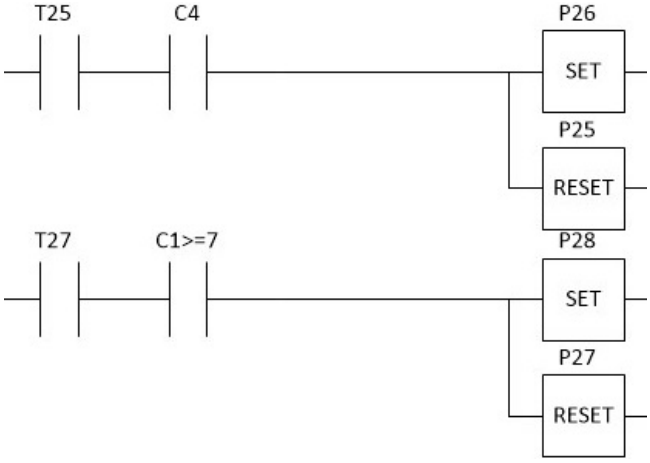

Figure 4.4 Ladder diagram

5 Conclusions

The approach presented in this work reduces the number of monitor places needed to impose a set of constraints in a AMS. In the case study, the safety specification were successfully imposed in the system behavior using 4 monitor places, showing the exact same results that using the classical approach with 8 monitor places.

The incidence matrix of a discrete event system modeled as a PN usually has a lot of zero entries. The proposed approach reduces the dimension of Matrix L of the IBCD method, avoiding unnecessary by-zero multiplications giving a computational numerical advantage.

In the context of discrete event system the state expansion leads to complicated and unreadable graphs representations, such as Finite State Machines. The use of PN gives a more compact representation of the system, but it is still possible to find very complex graphs representations when a SC is design.

It has been proposed a synthesis method for a class of BC with a restricted syntax. Giving rise to a minimal PN SC. This increases the variety that can be considered in the synthesis (i.e. forbidden states) using a solid and mathematically established procedure.

The safety specifications ensure a behavior that forbids to any unwanted situation occurs in the system. The implementation was made using techniques previously proposed. The resulting implementation is compact and is a more usable approach for manufacturing systems.

Appendix A: Proof of Theorem 23

Proposition 39 *Let x, y_1, y_2 be integer variables with*

$$L_1 = \begin{bmatrix} 0 & 0 & -2 & 0 & 0 & -1 & 0 & -1 & 0 & 0 & -2 & 0 & -2 & 0 & 0 & 0 \\ 0 & -1 & 0 & 0 & 0 & 0 & 0 & 0 & 0 & 0 & 0 & 0 & 0 & 0 & -1 & 0 \\ 0 & 0 & 0 & 0 & 0 & 0 & 0 & 0 & 0 & -1 & 0 & 0 & 0 & 0 & 0 & 0 \\ 0 & 0 & 0 & 0 & 0 & 0 & 0 & 0 & -1 & 0 & 0 & 0 & 0 & 0 & 0 & 0 \end{bmatrix} \tag{24}$$

$$L = \begin{bmatrix} L_1 \mid 0 \end{bmatrix}$$

$$D_{c1} = \begin{bmatrix} 0 & 0 & -2 & 2 & 1 & -1 & 1 & -1 & 0 & 0 & -2 & 2 & -2 & 2 & 0 & 0 \\ 1 & -1 & 0 & 0 & 0 & 0 & 0 & 0 & 0 & 0 & 0 & 0 & 0 & 0 & -1 & 1 \\ 0 & 0 & 0 & 0 & 0 & 0 & 0 & 0 & 1 & -1 & 0 & 0 & 0 & 0 & 0 & 0 \\ 0 & 0 & 0 & 0 & 0 & 0 & 1 & -1 & 0 & 0 & 0 & 0 & 0 & 0 & 0 & 0 \end{bmatrix} \tag{25}$$

$$D_c = \begin{bmatrix} D_{c1} \mid 0 \end{bmatrix}$$

$$M_{oc}^T = \begin{bmatrix} 6 & 1 & 0 & 0 \end{bmatrix} \tag{26}$$

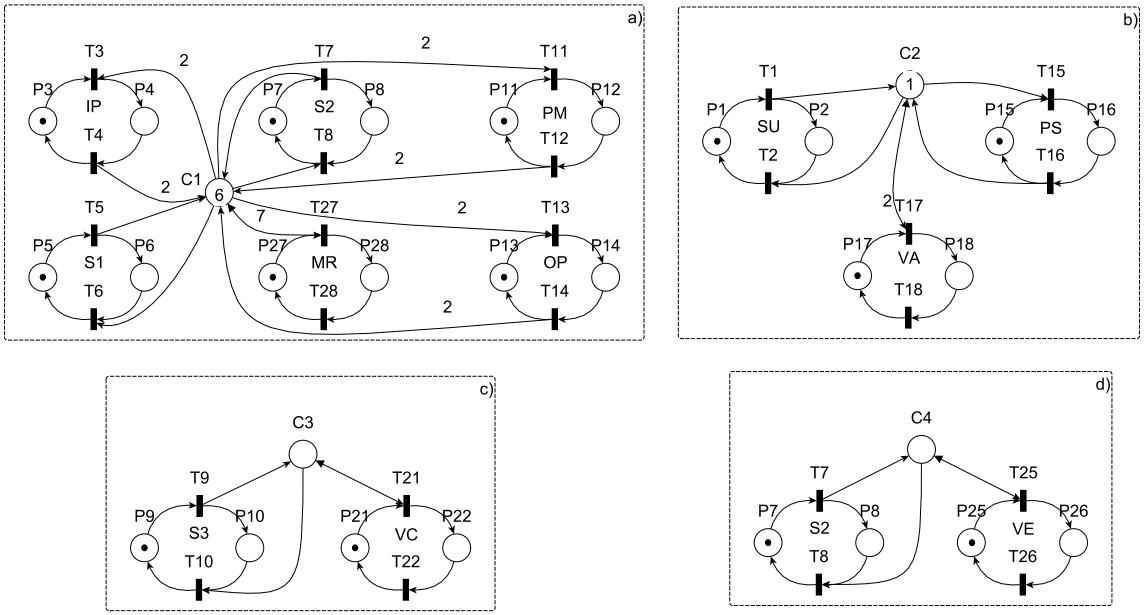

Figure 4: a) Modular supervisor for monitor place $C1$. b) Modular supervisor for monitor place $C2$. c) Modular supervisor for monitor place $C3$. d) Modular supervisor for monitor place $C4$

domain $\{0,1\}$. *The solution set for inequality*

$$(x - y_1) + (x - y_2) \leq 0 \tag{27}$$

is the same solution set for the system

$$\begin{aligned} x - y_1 &\leq 0 \\ x - y_2 &\leq 0 \end{aligned} \tag{28}$$

Proof. *The solution set of an inequalities system agrees to the intersection of each inequality solution set. Let predicate 29 be associated to system 28 and predicate 30 be associated to ineq. 27.*

$$P[(x - y_1 \leq 0)] \wedge P[(x - y_2 \leq 0)] \tag{29}$$

$$P[(x - y_1) + (x - y_2) \leq 0] \tag{30}$$

Table 39 shows that both expressions are equivalent.

Table tab:T1 Truth table for Proposition 39

x	y_1	y_2	*Eq. (29)*	*Eq. (30)*
0	0	0	T	T
0	0	1	T	T
0	1	0	T	T
0	1	1	T	T
1	0	0	F	F
1	0	1	F	F
1	1	0	F	F
1	1	1	T	T

■

Lemma 40 *Let x, $y_1, \ldots y_n$ be integer variables with domain $\{0,1\}$ and $n \geq 2$. $Y = y_1 + y_2 \cdots y_n$. Let $R = \{(x, Y) | x = \{0,1\}, Y = \{0,1,\cdots,n\}\}$ be the constrained domain. Let $\Sigma \subset R$ the solution set for the inequalities sys-*

tem

$$\begin{matrix} x-y_1 \leq 0 \\ x-y_2 \leq 0 \\ \vdots \\ x-y_n \leq 0 \end{matrix} \tag{31}$$

Then Σ is the solution set for the inequality

$$(x-y_1)+(x-y_2)+\cdots+(x-y_n) \leq 0 \tag{32}$$

or in a compact form

$$nx-Y \leq 0 \tag{33}$$

Proof. *(By mathematical induction) Let the base case be Proposition 39. The induction hypothesis of the inductive step is the Lemma statement. Therefore, it must be proved that the solution set of ineq. 34 and system 35 is the same.*

$$(x-y_1)+(x-y_2)+\cdots+(x-y_s)+(x-y_{s+1}) \leq 0 \tag{34}$$

$$\begin{matrix} x-y_1 \leq 0 \\ x-y_2 \leq 0 \\ \vdots \\ x-y_s \leq 0 \\ x-y_{s+1} \leq 0 \end{matrix} \tag{35}$$

Ineq. 34 holds if and only if

$$x-y_{s+1} \leq 0 \tag{36}$$

holds and

$$(x-y_1)+(x-y_2)+\cdots+(x-y_s) \leq 0 \tag{37}$$

also holds. This is derived from the fact that x can only take values 0 and 1. If Σ is the solution set for ineqs. 36 and 37, then σ is the solution set for 34. By induction hypothesis, if ineq. 37 holds, then system

$$\begin{matrix} x-y_1 \leq 0 \\ x-y_2 \leq 0 \\ \vdots \\ x-y_s \leq 0 \end{matrix}$$

also holds. Therefore, Σ is the set solution for system 35 and it is proven that Σ is solution for 34 and 35.

■

Lemma 41 *Let $X, y_1, y_2, \cdots, y_n, z_1, z_2, \cdots z_m$ be integer variables with domain {0,1}. Let $Y = y_1 + y_2 + \cdots y_n$, $Z = z_1 + z_2 + \cdots z_m$. Let $R = \{(X,Y,Z) | X = \{0,1\}, Y = \{0,1,\cdots n\}, Z = \{0,1,\cdots m\}\}$ be the constrained domain. Let $\Sigma \subset R$ the solution set for the inequality*

$$m(nX-Y)+(x-Z) \leq 0 \tag{38}$$

Then Σ is also the solution set for the system

$$\begin{matrix} X-y_1 \leq 0 \\ X-y_2 \leq 0 \\ \vdots \\ X-y_n \leq 0 \\ X-Z \leq 0 \end{matrix} \tag{39}$$

Proof. *The proof consists of two steps. First the inequality 38 is derived from a geometrical perspective. Then, it is proven that if Σ is solution for eq. 38, then it is also solution for system 39. By Lemma 40, the first n inequalities are equivalent to ineq. 33, therefore system 39 becomes*

$$\begin{matrix} nX-Y \leq 0 \\ X-Z \leq 0 \end{matrix} \tag{40}$$

From a geometric perspective, both inequalities in system 40 have a corresponding plane in a tree dimensional space (X,Y,Z). The solution set for each inequality is constructed with the points contained in domain R and bounded above by the corresponding plane, thus the solution set for system 39 is constructed with the points contained in domain R and bounded above for the intersection of both corresponding planes. Therefore, there is a plane such that contains the intersection of both planes and bounds above all the points contained in domain R and the solution set of system 40. The intersection of these planes is a line containing the points $(0,0,0)$ and $(1,n,1)$. In order to describe a plane equation, an orthogonal vector to the plane is required, and for its calculation a third point is obtained by convenience, $(\frac{m}{(mn+1)},1,0)$. the orthogonal vector is obtained by calculating the cross product of two vectors in the plane, for simplicity, $v_1 =< 1,n,1 >$ and $v_2 =< m, mn+1, 0 >$.

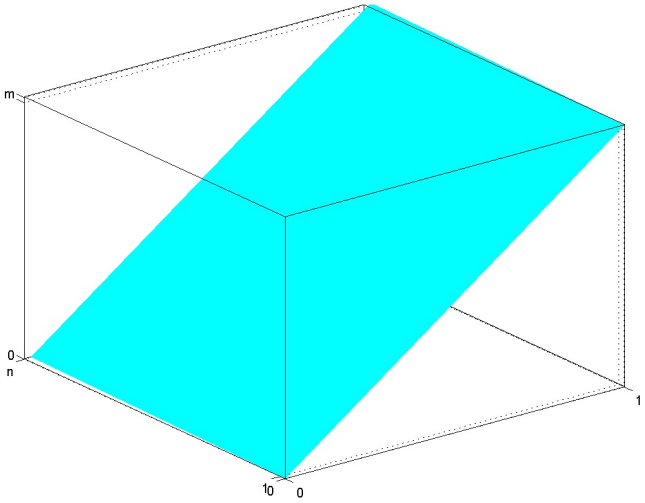

Figure 41 Solution plane

$$v_3 = \begin{vmatrix} i & j & k \\ 1 & n & 1 \\ m & (mn+1) & 0 \end{vmatrix} =< -(mn+1), m, 1 >.$$

The plane equation is $(mn+1)X - mY - Z = 0$. Thus, the solution set for $(mn+1)X - mY - Z \leq 0$ is the same of system 39. Fig. 1. shows the plane and the constrained domain R. Now it is proven that solution set Σ for ineq. 38 is the same for system 39. System 39 holds for $X = 0$. If $X \neq 0$, because of the domain constraint, then $X = 1$. If $X = 1$, 39 holds for $y_i \geq 1$ and $Z \geq 1$, then $Y \geq n$. Again because of the domain constraint, $Y = n$. Hence the set Σ that holds for expression 41 is the solution set for system 39.

$$(x=0) \vee [(Y=n) \wedge (Z \geq 1)] \tag{41}$$

$x=0$	$Y=n$	$Z\geq 1$	$(x=0)\vee[(Y=n)\wedge(Z\geq 1)]$
F	F	F	F
F	F	T	F
F	T	F	F
F	T	T	T
T	F	F	T
T	F	T	T
T	T	F	T
T	T	T	T

Table 41 Truth table of equation 41

$x=0$	$Y=n$	$Z\geq 1$	$P[(mn+1)x-mY-Z\leq 0]$
F	F	F	F
F	F	T	F
F	T	F	F
F	T	T	T
T	F	F	T
T	F	T	T
T	T	F	T
T	T	T	T

Table 41 Truth table of equation 38

The truth table of expression 41 is shown in Table 41. Using definition 20, the truth table for predicate variable for ineq. 38 $P((mn+1)x-mY-Z\leq 0)$ is showed in Table 41. It can be seen that there is a logical equivalence between expression 41 and ineq. 38 associated predicate.

■

Constraint 9 can be transformed to a system with $n+1$ inequalities, as established in Lemma 22

$$\begin{gathered} q_a - m_{k_1} \leq 0 \\ q_a - m_{k_2} \leq 0 \\ \vdots \\ q_a - m_{k_n} \leq 0 \\ q_a - [m_{j_1} + m_{j_2} + \cdots + m_{j_m}] \leq 0 \end{gathered} \tag{42}$$

By Lemma 40, the first n inequalities are equivalent to inequality

$$nq_a - [m_{k_1} + m_{k_2} + \cdots + mk_n] \leq 0 \tag{43}$$

Hence the new system

$$\begin{gathered} nq_a - m_K \leq 0 \\ q_a - m_J \leq 0 \end{gathered} \tag{44}$$

Variables q_a, m_K, m_J satisfy conditions of Lemma 41. Therefore inequality

$$m[nq_a - m_K] + [q_a - m_J] \leq 0 \tag{45}$$

shares the same solution set with system 44 and, henceforth, with system 42.

References

[1] A. Sanchez, F. Jaimes, E. Aranda-Bricaire, E. Hernandez, A. Nava, Synthesis of product driven coordination controllers for a class of discrete event manufacturing systems, Robotics and Computer-Integrated Manufacturing 26 (2010) 361 – 369.

[2] C. Yang, W. Shen, T. Lin, X. Wang, A hybrid framework for integrating multiple manufacturing clouds, The International Journal of Advanced Manufacturing Technology 86 (1) (2016) 895–911. doi:10.1007/s00170-015-8177-9. URL http://dx.doi.org/10.1007/s00170-015-8177-9

[3] W. Wonham, Supervisory Control of Discrete-Event Systems. Systems Control Group, ECE Dept, University of Toronto, http://www.control.toronto.edu/DES (2013).

[4] M. V. Iordache, P. J. Antsaklis, Concurrent program synthesis based on supervisory control, in: American Control Conference (ACC), 2010, 2010, pp. 3378 – 3383.

[5] D. Coman, A. Ionescu, M. Florescu, Manufacturing system modeling using petri nets, in: International Conference on Economic Engineering and Manufacturing Systems Brasov, November 2009, Vol. 10, 2009, pp. 207–212.

[6] J. O. Moody, P. J. Antsaklis, Supervisory Control of Discrete Event System Using Petri Nets, Kluwer Academic Publishers, 1998.

[7] A. Giua, F. DiCesare, M. Silva, Generalized mutual exclusion contraints on nets with uncontrollable transitions, in: IEEE International Conference on Systems, Man, and Cybernetics, Vol. 2, 1992, pp. 974–979.

[8] E. Yamalidou, J. Kantor, Modeling and optimal control of discrete-event chemical processes using petri nets, Computers and Chemical Engineering 15 (7) (1991) 503 – 519.

[9] A. Dideban, H. Alla, Reduction of constraints for controller synthesis based on safe petri nets, Automatica, International Federation of Automatic Control 44 (7) (2008) 1697–1706.

[10] C. Baier, J.-P. Katoen, Principles of Model Checking, The MIT Press, 2008.

[11] J. Desel, J. Esparza, Free Choice Petri Nets, Cambridge University Press, 2005.

[12] A. Núñez, A. Sanchez, Supervisory control based on behavioral constraints using a class of linear inequalities, IFAC-PapersOnLine 48 (3) (2015) 2189 – 2194. doi:http://dx.doi.org/10.1016/j.ifacol.2015.06.413. URL http://www.sciencedirect.com/science/article/pii/S2405896315006527

[13] M. V. Iordache, P. J. Antsaklis, Supervisory Control of Concurrent Systems A Petri Net Structural Aproach, Birkhäuser, 2006.

[14] G. Gelen, M. Uzam, The synthesis and {PLC} implementation of hybrid modular supervisors for real time control of an experimental manufacturing system, Journal of Manufacturing Systems 33 (4) (2014) 535 – 550. doi:http://dx.doi.org/10.1016/j.jmsy.2014.04.008. URL http://www.sciencedirect.com/science/article/pii/S0278612514000466

ASTES

Advances in Science, Technology and Engineering Systems Journal Vol. 2, No. 4, 44-50 (2017)

www.astesj.com

ASTESJ

ISSN: 2415-6698

Toward Confirming a Framework for Securing the Virtual Machine Image in Cloud Computing

Raid Khalid Hussein [1]*, Ahmed Alenezi [1, 2], Hany F.Atlam [1, 3], Mohammed Q Mohammed [4], Robert J. Walters [1], Gary B. Wills [1]

[1] *Electronic and Computer Science Dept., University of Southampton, SO17 1BJ, UK*

[2] *Dept. of Computer Science, Faculty of Computing and Information Technology, Northern Border University, 1321, Saudi Arabia*

[3] *Computer Science and Engineering Dept., Faculty of Electronic Engineering, Menoufia University, 32952, Egypt*

[4] *Dept. of Computer Science, University of Information technology and communication, Bagdad, Iraq.*

ARTICLE INFO

Article history:
Received: 04 March, 2017
Accepted: 11 April, 2017
Online: 24 April, 2017

Keywords:
Cloud Computing
Virtual Machine Image
Information Security
Virtualisation

ABSTRACT

The concept of cloud computing has arisen thanks to academic work in the fields of utility computing, distributed computing, virtualisation, and web services. By using cloud computing, which can be accessed from anywhere, newly-launched businesses can minimise their start-up costs. Among the most important notions when it comes to the construction of cloud computing is virtualisation. While this concept brings its own security risks, these risks are not necessarily related to the cloud. The main disadvantage of using cloud computing is linked to safety and security. This is because anybody which chooses to employ cloud computing will use someone else's hard disk and CPU in order to sort and store data. In cloud environments, a great deal of importance is placed on guaranteeing that the virtual machine image is safe and secure. Indeed, a previous study has put forth a framework with which to protect the virtual machine image in cloud computing. As such, the present study is primarily concerned with confirming this theoretical framework so as to ultimately secure the virtual machine image in cloud computing. This will be achieved by carrying out interviews with experts in the field of cloud security.

1 Introduction

Recent times have seen a sudden increase in the number of organisations adopting cloud computing; indeed, this growth has brought about a 21st-century computing paradigm. As a type of information technology, the cloud includes a number of internet-based commercial applications; these applications exist because of today's greater bandwidth, thus giving present-day users the chance to exploit the advantages offered by top-quality data services and application software. Being scalable in nature, cloud computing takes advantage of virtualisation to spread resources. For those who use the cloud, of particular importance is a resource base that houses numerous IT resources, the purpose of which is to distribute computing assignments that necessitate a substantial amount of processing capability. Surfers of the Web can easily ear-mark online storage space, which they can then use to safely store their data; indeed, they can also gain access to IT resources which they can employ to manage and sort their information according to their requirements. This paper builds on work which was originally presented at the IEEE International Conference on Smart Cloud 2016 [1].

Cloud computing itself gives rise to a number of security issues linked to resource scheduling, databases, virtualisation, load balancing and networks [2]. Numerous organisations are of the opinion that moving their sensitive data to central datacentres is fraught with danger. This scepticism stems from the fact that the management staff in charge of these datacentres might not be trustworthy [3]. Switching databases to a datacentre involves many security-related obstacles, e.g. access control issues, virtualisation vulnerability, integrity and confidentiality [4].

Among the most vital elements of cloud computing is virtualisation, which minimises the cost of hardware and supports techniques used for saving energy [4]. Virtualisation can be broken down into three types: application level virtualisation, operating system level virtualisation, and Virtual Machine Monitor (VMM)

* Raid Khalid Hussein, Flat 3 1 Alma road Southampton SO14 6UN, 00447466256351, Email: rkh2n14@soton.ac.uk

or hypervisor level virtualisation [5]. When one real-life machine is used to run two different virtual machines, this might affect data security, as these machines are not completely separated by the virtualisation. Moreover, the Virtual Machine Monitor, or hypervisor, has control, but not complete control, over the host and its operating system (OS) [6].

Among the most important elements of cloud computing is multi-tenancy. Indeed, while this is thought to be one of the most beneficial components of cloud computing, it nevertheless poses a threat to security, due to the fact that it spreads infrastructure resources across different customers [7]. The hardware layer of cloud computing contains no absolute separation, and thus various breaches can materialise, such as unauthorised viewing, data leakage, and theft of sensitive or confidential data [8].

Previous studies have put forth a security framework which can be used to protect the Virtual Machine (VM) image in cloud computing [1]. The present paper details exactly how the conceptual framework has been confirmed through interviews with experts in the field of cloud security. Indeed, this paper is broken down into the following sections: Section 2 summarises the concept of cloud computing, Section 3 explores concerns related to cloud security, Section 4 examines related work, Section 5 details the research methodology used, Section 6 presents the results and findings of the research, which are subsequently discussed in Section 7, and Section 8 puts forth conclusions and outlines plans for additional work in the future.

2 Cloud Computing

Recent times have witnessed the rapid development of hardware, the introduction of distributed computing, and the tremendous success of internet technologies. All of these factors have made computing resources more powerful, cheaper and more readily available than ever before [9]. Current developments in hardware and software have ushered in a new computing model called cloud computing. In the cloud, computing resources are delivered to the users as services, just like public utilities. Consumers of these resources can contract for the services based on their needs, while the services can be scaled up or down as necessary. The National Institute of Standards and Technology (NIST) defines cloud computing as "a model for enabling convenient, on-demand network access to a shared pool of configurable computing resources (e.g., networks, servers, storage, applications, and services) that can be rapidly provisioned and released with minimal management effort or service provider interaction" [10].

3 Cloud Security Issues

As concluded by the NIST, security is the primary concern when it comes to delays in adopting cloud computing [11]. This is because cloud computing has certain vulnerabilities which can potentially affect the major foundations of information security. These vulnerabilities are essentially weak points of the system that could be taken advantage of by someone attempting to infiltrate the cloud. Indeed, with the right tools, a person could gain illegal access to these resources. When talking about a threat, the basic premise is that an attacker could use unlawful means to gain access to such resources [12]. Figure 1 summarises safety and security concerns which are found in different areas of cloud computing. When it comes to virtualisation, resources can be grouped together or spread throughout numerous environments, namely Virtual Machines (VM). A VM is defined as "A way of making a physical computer function as if it were two or more computers where each non-physical or virtualized computer (machine) is provided with the same basic architecture as that of a generic physical computer.

Application level issues	Network level issues	Data Storage level issues
Authentication and access control level		Trusted level issues
Virtualisation level Issues		
VM isolation	VM rollback	VM escape
VM migration	VM sprawl	VM image sharing

Figure 1 Security issues in Cloud Computing

Virtualization technology therefore allows the installation of an operating system on hardware that does not really exist" [14]. An OS is hosted by the VM [15], with the former representing the virtualisation element which makes it possible for a guest OS to run on a host computer [13].

A very handy feature of cloud computing, multi-tenancy can be defined as "a property of a system where multiple customers, so-called tenants, transparently share the system's resources, such as services, applications, databases, or hardware, with the aim of lowering costs, while still being able to exclusively configure the system to the needs of the tenant" [16]. Multi-tenancy can be broken down into two categories: multiple instance and native multi-tenancy. With regards multiple instance tenancy, each tenant benefits from the services of a dedicated application instance from a shared OS, hardware and middleware server in a hosted environment. However, in relation to native multi-tenancy, one instance of a program can provide service to several tenants across numerous hosting resources. When looking at the Software as a Service (SaaS) model, it is clear that multi-tenancy can be linked to four varied software layers: the virtual layer, the application layer, the OS layer, and the middleware layer [17].

With regards a multi-tenancy virtualised environment, every user is assigned a VM that plays host to a guest OS. It is possible that VMs belonging to different users will have identical real-life resources as a result of resource pooling. The purpose of the VMM is to orchestrate the VMs and makes it possible for the numerous OS instances to function on the same physical hardware [18]. With regards the multi-tenancy virtualised environment, certain security elements have come into focus, such as VM isolation, which pertains to guaranteeing that VMs that function on identical physical hardware are kept apart from one another.

VMs may be transported (migrated) to various real-life hosts – a move which often occurs because of maintenance, load balancing, and fault tolerance. It is possible that a VM which has been transported may be infiltrated by an attacker and redistributed to an infected VMM or unsteady server [19]. If essential, it is possible to roll back VMs to a former state. This facility gives the user a great deal of flexibility, but also gives rise to security concerns; this is because, when it happens, the result may be a VM being exposed once more to a vulnerability that had previously been resolved [12]. In addition, it is plausible for a VM to escape

from the control of the VVM. This kind of VM can give an attacker the ability to access additional VMs in the same hardware, or disable the VMM altogether [20]. Another issue, known as VM sprawl, comes about when numerous VMs are being hosted by a system, but the majority of said VMs are serving no purpose. This situation can lead to a significant waste of the resources found within the host machine [21].

Among the most common threats to the security of the cloud is VM image sharing, simply because the image represents the initial state for new VM instances [18]. Taking into consideration both confidentiality and integrity is vital if the VM image is to be secured; this is due to the fact that, if an attacker can gain unauthorised access and is malicious, then said attacker can delete, modify, and alter administrator passwords, or formulate malicious VM instances. Another risk which certainly exists is non-compliance and running unlicensed software [5].

4 Related Work

It is certainly true that virtualisation is vital when it comes to cloud computing; however, it is also accompanied by various security concerns. Of these issues, one of the most important is VM image sharing, simply because the VM image is used to initialise new VMs. Numerous studies have focused on ways in which to secure the VM image. The Image Management System (IMS) addresses four security requirements: outdated software detection, access control, left owners' data removal, and malware protection. With this said, however, no attention is paid to privacy and integrity [22]. The Encrypted Virtual Disk Images in Cloud (EVDIC) tool looks at integrity, privacy, and access control; it does so by means of encrypting the VM image when it finishes. However, it is unable to detect outdated software or leftover owners' data removal [24]. Among other techniques to have been proposed are those used to check for software updates in the VM image [24, 25, 26]. These techniques are specifically utilised to search for software updates in the VM image, but do not take into account additional security requirements. Of these past studies, none have addressed every single security requirement necessary to safeguard the VM image in cloud computing. Hence, there is the need for a new method with which to secure all elements of the cloud-based VM image.

5 Research Methodology

This section describes the research methodology which was used to confirm the framework and identify additional requirements which are necessary in order to secure cloud computing VM images, as shown in [1]. The initial framework, shown in Figure 2, was derived from the literature review. A review by cloud security experts was carried out to explore the proposed framework and establish if any security requirements are missing.

The method used was an expert review, which is a qualitative approach. This form of research is used to gain an understanding of underlying reasons, opinions and motivations in the research area. It does not use statistical procedures or other means of quantification [27]. For this work, interviews were conducted with people who have in-depth knowledge of the subject under study [28], although the method can also use group discussions or video conferencing. This use of interviews permits the collection of valid and reliable data that are relevant to the research and its objectives [29]. The sample size requirements are based on an heuristic evaluation, which often uses between three and five experts [30].

In order to achieve the aims of the present study, interviews were carried out with a total of eight UK-based experts in the field of cloud security. The semi-structured interviews consisted of a set of questions that had been prepared in advance. The use of semi-structured interviews means that, by also employing an exploratory study, it is possible to understand the exact nature of the topic at hand [31]. All of the respondents were selected as a result of their expertise in the area under study.

Prior to commencing the interviews, every expert was required to sign a consent form after thoroughly reviewing the participant information sheet, which presented all the necessary information, including the terms and conditions of the research [32]. This study was approved by The University of Southampton Ethics Committee (reference number 22876).

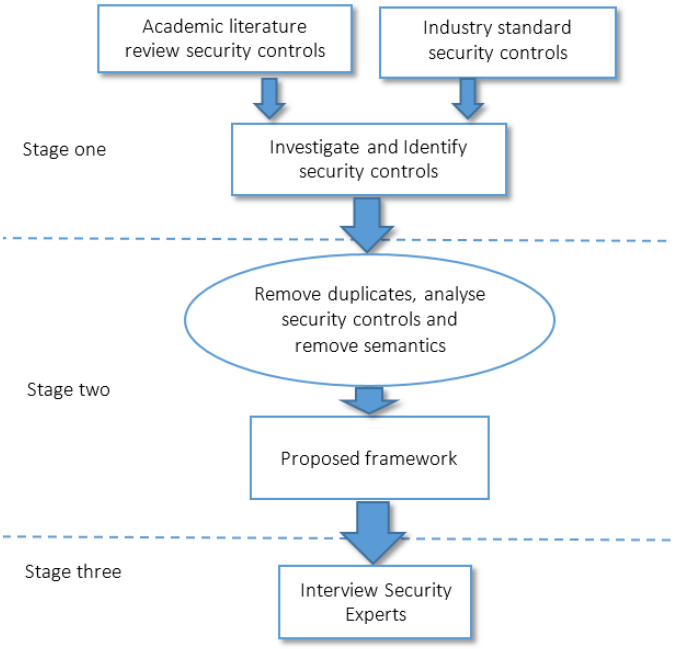

Figure 2. Framework development process to secure the VM image in cloud computing

6 Results and findings

The results are divided into two sections: Demographic Information and Qualitative Data.

6.1 Demographic Information

The data were collected from eight cloud security experts in the United Kingdom, all of whom were from different organisations.

All the interviewees had at least three years' experience dealing with cloud security and virtualisation issues, and thus all had the ability to understand and explain current security situations and trends. The interviews were conducted either face-to-face or via Skype video conferencing [34] between July and December 2016. The audio conferencing was recorded using the QuickTime recorder application. Face-to-face interviews were recorded using the Apple voice memory application. Details of the experts used in this study are presented in Table 1.

Table 1: Cloud security experts' attributes used to validate the framework

Code	Job Description	Experience (years)	Cloud involvement
A	Director of the IBM Institute of Advanced Security in Europe	17	Cloud policy
B	Cloud Systems Administrator	10	Cloud Security Architect
C	Cloud Systems Implementer	4	Cloud System Administrator
D	Cloud Security Administrator	6	Cloud System Administrator
E	Cloud Security Consultant	5	Direct advisory involvement with cloud implementation
F	Cloud Security Consultancy	4	Direct advisory involvement with cloud implementation
G	Cloud Security Consultancy	7	Cloud Security Consultant
H	Cloud Security Officer	4	Link between Cloud deployment & security policies

6.2 Qualitative Data

The purpose of the expert interviews was to review the identified security requirements and establish if there are more security requirements not included in the framework. Before interview questions were asked, each expert was given a brief background of the research area and the aim of the study. After the research had been outlined, five open-ended question were put to the experts [35]. The first question asked the cloud security experts about the importance of the identified security requirements. The experts gave an opinion about each of the requirements based on their expertise in the field. With regards the next question, the identified security requirements were defined according to the context of the study. The experts were asked to explain the security requirements in the context of securing the VM image. In the subsequent questions, they were asked whether there are more security requirements not mentioned in the framework and how they felt about the possibility of overlap or related factors. Finally, the experts were asked if they have any other methodologies or approaches to secure the VM image.

Most of the experts felt that the security requirements identified in the framework are essential when it comes to securing the VM image in cloud computing. The identified security requirements are: privacy, integrity, availability, accountability, regulatory compliance, encryption, authorisation, authentication, out-dated software detection, malware protection, left owner' data removal, auditing and trust. However, Expert B felt that regulatory compliance is irrelevant to the designed framework, while Expert D opined that privacy and trust are not necessary when it comes to securing the VM image.

Some of the experts did not agree fully with the definitions of the security requirements that are discussed in [1], and added additional details to the definitions. Most of the interviewed experts agreed with the provided definition of privacy. However, Experts B, D and E only partially agreed with this definition and added more details. Expert B was of the opinion that privacy is related to the data rather than the VM image itself. He stated that "Privacy is about saved data not the VM image. The VM image should be securely built". Moreover, Expert D believed that building a secure layer is sufficient to ensure the required security for the VM image. He said that "Privacy is the layer where you define or set policies to secure the VM image". In contrast, Expert E thought that different mechanisms, such as regulatory compliance, are required to achieve privacy. He opined that "There are other mechanisms used to ensure privacy like regulatory compliance".

The majority of the experts agreed with the provided definition of auditing. However, Experts A and C only agreed partially with this definition. Expert A believed that auditing is about keeping track of the client's access usage. He said, "Auditing is about recording the usage/access of the user to the VM image". Expert C thought that auditing is related to storing processes that are performed by the client during the access session to understand what is happening in the system. He stated that "Audit is taking a review of a system and an ongoing process to find out what is happening to something".

All the interviewed experts agreed with the provided definition of accountability and regulatory compliance. However, Expert E felt that internal compliance is essential and should be considered. He posited that "Internal compliance to reach a set of standards can also be considered". In contrast, Expert B believed that regulatory compliance indirectly affects the security of VM. He was of the opinion that keeping the operating system and anti-virus up-to-date is necessary to ensure the regulatory compliance of the VM image. He stated that "Regulatory compliance does not directly refer to VM image but, it does so indirectly as it requires Operating System and anti-virus to be to up-to-date".

Most of the experts agreed with the provided definition of encryption. However, Expert G only agreed partially with the definition. He felt that authorised devices also needed to be considered. All the interviewed experts agreed completely with the provided definitions of authentication, integrity and availability. They felt that there is no need for more details related to its definition. Most of the interviewed experts agreed with the provided definition of authorisation. However, Expert A disagreed. He felt that setting the appropriate policies is the essential element when it comes to ensuring efficient authorisation. He stated that "Administrator typically sets the policies. They define the policies for authorisation but, the process of the authorisation is automated as it is a large complicated process". Moreover, Expert G believed that authorisation is an automated process, thus meaning that the administrator is not dealing with checking users' rights. He stated that "Authorisation is usually driven out of permissions assigned to users or groups, not by administrations checking customers' right". Many of the experts agreed with the provided definition of out-dated software detection. Conversely, Expert G disagreed with this definition to some extent. He asked, "What about the software version of the virtual hardware in the VM image itself?". Expert A also disagreed with this definition. He believed that the software update should be against the versions of that particular software. Most of the experts

supported the provided definition of malware protection. With this said, however, Expert A only agreed with this definition to a certain extent, adding that malware should be detected, blocked and then removed from the VM image. Moreover, Expert E disagreed, to some extent, with this definition, but added that "It is a protective measure for detection, not a user removal. Proactive protection as well as reactive".

The majority of the experts agreed with the provided definition of left-over data removal. However, Expert A mentioned that personal data needed to be destroyed. Many of the interviewed experts supported the definition of trust. However, Expert A disagreed, to some extent, with this definition, though he mentioned that trust is all about confidence and assurance in using the VM image. He also mentioned that integrity of the VM image is important and thus the VM image should not include bugs, defects or malware.

After conducting the interviews with the cloud security experts, the security requirements were reviewed and updated based on the context for securing the VM image in cloud computing. The definitions with which the interviewed experts agreed (as shown in Figure 3), are listed below:

- Privacy: Refers to a set of policies that is used mainly for securing the data within the VM image [36], and these policies must ensure that regulatory compliance is taken into consideration.
- Auditing: Relates to recording the usage or access of authorised users to VM image resources, which helps to secure the VM image. Audit is the systematic security review of the information related to an organisation and how well it conforms to a set of criteria [37].
- Accountability: This is a measure of the amount of information an authorised customer is using during his/her session. This includes the quantity of data and time which is used to set authorisation control [38].
- Regulatory compliance: This refers to conformity to rules such as policy, law, and specifications relevant to the business while an organisation is working on the goal they wish to achieve. Regulatory compliance sometimes does not refer to the VM image itself, although it does refer to the operating system and the need for anti-virus measures to be kept up to date. Internally, it represents the set of polices specific to the organisation or the project [39].
- Encryption: A technique used to secure the shared data used by authorised users and authorised devices in a shared environment. In information systems, encryption is achieved by converting the data to a form that can only be understood by authorised people [40].
- Authentication: The process of identifying the customer as one authorised to use the cloud service. This is achieved by comparing the file of authorised users' information in the database with credentials provided by the user [41].
- Authorisation: This refers to the set of polices assigned by the administrator, while the implementation of these polices is automated [42].
- Outdated software detection: Is the comparison of software updates against the set of software versions within the VM image [18].
- Malware protection: Is a protective measure to detect, block and remove malware from the VM image. It includes proactive as well as reactive protection [26].
- Leftover owner's data removal: A technique used to promptly remove authentication details, as well as personal and private data from the VM image [22].
- Trust: Is the confidence and assurance of using the VM image, which belongs to a certain provider. In reality, it is the confidence and assurance in the provider who provides the VM image. The integrity of the VM image is important, and so the VM image should not include bugs, defects or malware [43].
- Integrity: This means that information remains unaltered while it is stored or being transmitted, and can only be modified and deleted by authorised users [44].
- Availability: Availability means that information must be available when it is needed. Systems with high availability allow access to data all the time and prevent service disruptions due to hardware failure, system upgrades, power outages, power failure, and operating system or application problems [45].

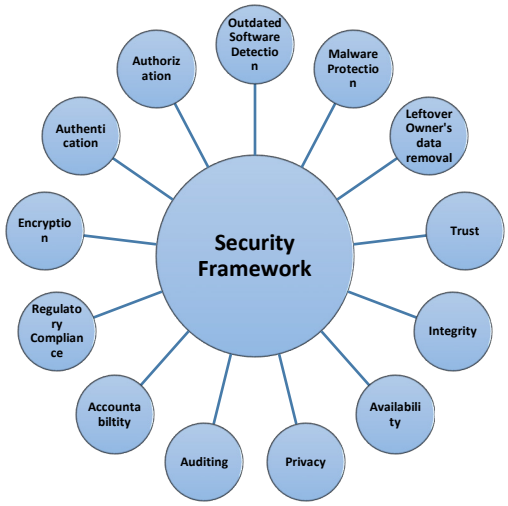

Figure 3. Security requirements agreed by security experts

All the experts agreed that the security framework designed to secure the VM image in cloud computing is comprehensive, with none of them adding more security requirements. Regarding overlaps between the security requirements and other approaches to securing the VM image, the majority of the experts did not identify overlaps between the provided security requirements. However, Expert G suggested that auditing could be substituted for accountability. Moreover, Expert D suggested that accountability is part of regulatory compliance, and so accountability can be removed.

7 Discussion

The experts reviewed the proposed framework in order to assess the importance of its factors. The majority of experts felt that the identified security requirements are important. A thematic analysis was used to examine themes within the interview results. According to the theme coding, the proposed framework factors are considered important when it comes to securing the VM image in cloud computing.

Expert B felt that regulatory compliance is not necessary to secure the VM image in cloud computing. However, regulatory compliance is one of the cloud control matrix components published by cloud security alliance [46], and for this reason regulatory compliance will be retained in the framework. Expert D argued that privacy is not important, although Mazhar et al. [18] identified privacy as an important requirement when it comes to securing the VM image in cloud computing. Therefore, privacy will also be retained in the framework. Similarly, although Expert D claimed that trust is ineffective in terms of securing the VM image in cloud computing, it is one of the cloud control matrix components published by cloud security alliance [46], and so trust is also retained in the framework. Regarding the overlap between the provided security requirements, there was no unified opinion among the experts in terms of whether there are overlaps between the proposed frameworks of the security requirements. Hence, none of the security requirements can be merged.

8 Conclusion and Future Work

As a brand-new processing paradigm, cloud computing leads to greater efficiency, minimised cost, and gives organisations round-the-clock access to a communal collection of resources and services; moreover, little is required in the way of management. In terms of elements which stand in the way of the adoption of cloud computing, security is one of the main hindrances; this is due to the fact that end-users' data are kept on the server(s) of the service provider. Discussion related to security issues has also taken into consideration the various cloud layers, with every layer accompanied by its own security problems. Of particular interest here is the virtualisation layer; indeed, the issues originating from this layer are among the most significant problems affecting the security of both the application layer and the data storage layer. As such, this study has put forth a framework focused on VM image security; the aim of this framework is to protect the VM image itself. Expert interviews were conducted in order to achieve the aims of this study; interviewees were experts in the field of cloud security. These interviews demonstrated that the theoretical security framework is sufficient to protect the VM image in cloud computing. Future work will involve questionnaires being distributed to cloud practitioners so as to further confirm the merits of the framework.

References

[1] R. K. Hussein, A. Alenezi, G. B. Wills, and R. J. Walters, "A Framework to Secure the Virtual Machine Image in Cloud Computing," 2016 IEEE Int. Conf. Smart Cloud, pp. 35–40, 2016.

[2] B. Hamlen, K., Kantarcioglu, M., Khan, L. and Thuraisingham, "Security Issues for Cloud Computing," Proc. - 9th Int. Conf. Comput. Intell. Secur. CIS 2013, pp. 150–162, 2012.

[3] M. a. AlZain, E. Pardede, B. Soh, and J. a. Thom, "Cloud computing security: From single to multi-clouds," Proc. Annu. Hawaii Int. Conf. Syst. Sci., pp. 5490–5499, 2011.

[4] T. Swathi, K. Srikanth, and S. R. Reddy, "Virtualization in Cloud Computing," Int. J. Comput. Sci. Mob. Comput., vol. 35, no. 5, pp. 540–546, 2014.

[5] C. Modi, D. Patel, B. Borisaniya, A. Patel, and M. Rajarajan, "A survey on security issues and solutions at different layers of Cloud computing," J. Supercomput., vol. 63, no. 2, pp. 561–592, 2013.

[6] S. Subashini and V. Kavitha, "A survey on security issues in service delivery models of cloud computing," J. Netw. Comput. Appl., vol. 34, no. 1, pp. 1–11, 2011.

[7] S. K. Abd, R. T. Salih, and F. Hashim, "Cloud Computing Security Risks with Authorization Access for Secure Multi-Tenancy Based on AAAS Protocol," IEEE Reg. 10 Conf. TENCON, pp. 1–5, 2015.

[8] H. Aljahdali, A. Albatli, P. Garraghan, P. Townend, L. Lau, and J. Xu, "Multi-tenancy in cloud computing," Proc. - IEEE 8th Int. Symp. Serv. Oriented Syst. Eng. SOSE 2014, pp. 344–351, 2014.

[9] Q. Zhang, L. Cheng, and R. Boutaba, "Cloud computing: State-of-the-art and research challenges," Journal of Internet Services and Applications, 2010. [Online]. Available: http://download.springer.com/static/pdf/652/art%253A10.1007%252Fs13174-010-0007 6.pdf?originUrl=http%3A%2F%2Flink.springer.com%2Farticle%2F10.1007%2Fs13174-010-0007-6&token2=exp=1455281249~acl=%2Fstatic%2Fpdf%2F652%2Fart%25253A10.1007%25252Fs13174-010-000. [Accessed: 12-Feb-2016].

[10] B. P. Rimal, E. Choi, and I. Lumb, "A taxonomy and survey of cloud computing systems," NCM 2009 - 5th Int. Jt. Conf. INC, IMS, IDC, pp. 44–51, 2009.

[11] N. Kshetri, "Privacy and security issues in cloud computing: The role of institutions and institutional evolution," Telecomm. Policy, vol. 37, no. 4–5, pp. 372–386, 2013.

[12] K. Hashizume, D. Rosado, E. Fernández-Medina, and E. Fernandez, "An analysis of security issues for cloud computing," J. Internet Serv. Appl., vol. 4, no. 5, pp. 1–13, 2013.

[13] F. Sabahi, "Virtualization-level security in cloud computing," in 2011 IEEE 3rd International Conference on Communication Software and Networks, 2011, pp. 250–254.

[14] S. Carlin, "Cloud Computing Security," Artif. Intell., vol. 3, no. March, pp. 14–16, 2011.

[15] J. Recker, "Scientific Research in Information Systems," Springer Link, 2013.

[16] J. Kabbedijk, C.-P. Bezemer, S. Jansen, and A. Zaidman, "Defining multi-tenancy: A systematic mapping study on the academic and the industrial perspective," J. Syst. Softw., vol. 100, pp. 139–148, 2015.

[17] J. Espadas, A. Molina, G. Jim??nez, M. Molina, R. Ram??rez, and D. Concha, "A tenant-based resource allocation model for scaling Software-as-a-Service applications over cloud computing infrastructures," Futur. Gener. Comput. Syst., vol. 29, no. 1, pp. 273–286, 2013.

[18] M. Ali, S. U. Khan, and A. V. Vasilakos, "Security in cloud computing: Opportunities and challenges," Inf. Sci. (Ny)., vol. 305, pp. 357–383, 2015.

[19] F. Zhang and H. Chen, "Security-Preserving Live Migration of Virtual Machines in the Cloud," J. Netw. Syst. Manag., pp. 562–587, 2012.

[20] W. A. Jansen, "Cloud hooks: Security and privacy issues in cloud computing," Proc. Annu. Hawaii Int. Conf. Syst. Sci., no. iv, p. 42, 2011.

[21] K. Sunil Rao and P. Santhi Thilagam, "Heuristics based server consolidation with residual resource defragmentation in cloud data centers," Futur. Gener. Comput. Syst., vol. 50, pp. 87–98, 2015.

[22] J. Wei, X. Zhang, G. Ammons, V. Bala, and P. Ning, "Managing security of virtual machine images in a cloud environment," Proc. 2009 ACM Work. Cloud Comput. Secur. - CCSW '09, no. Vm, p. 91, 2009.

[23] M. Kazim, R. Masood, and M. A. Shibli, "Securing the virtual machine images in Cloud computing," SIN 2013 - Proc. 6th Int. Conf. Secur. Inf. Networks, pp. 425–428, 2013.

[24] R. Schwarzkopf, M. Schmidt, C. Strack, S. Martin, and B. Freisleben, "Increasing virtual machine security in cloud environments," J. Cloud Comput. Adv. Syst. Appl., vol. 1, no. 1, p. 12, 2012.

[25] D. Jeswani, A. Verma, P. Jayachandran, and K. Bhattacharya, "ImageElves: Rapid and reliable system updates in the cloud," Proc. - Int. Conf. Distrib. Comput. Syst., no. i, pp. 390–399, 2013.

[26] K. Fan, D. Mao, Z. Lu, and J. Wu, "OPS: Offline patching scheme for the images management in a secure cloud environment," Proc. - IEEE 10th Int. Conf. Serv. Comput. SCC 2013, pp. 587–594, 2013.

[27] A. Strauss and J. Corbin, "Basics of Qualitative Research," Basics of. Qualitatice Research 2nd edition. pp. 3–14, 1990.

[28] E. C. Crn, "Qualitative Research Methods," no. May, pp. 1–8, 2005.

[29] A. Bolderston, "Conducting a research interview," J. Med. Imaging Radiat. Sci., vol. 43, pp. 66–76, 2012.

[30] H. Sharp, Y. Rogers, and J. Preece, "Interaction design: beyond human-computer interaction," Book, vol. 11, p. 773, 2007.

[31] M. Saunders, P. Lewis, and A. Thornhill, Research methods for Business Students, Fifth edit. 2009.

[32] Arlene Fink, The Survey Handbook, 2nd editio. 2003.

[33] J. G. Geer, "What Do Open-Ended Questions Measure?," Public Opin. Q., vol. 52, no. 3, pp. 365–371, 1988.

[34] V. Lo Iacono, P. Symonds, and D. H. K. Brown, "Skype as a tool for qualitative research interviews," Sociol. Res. Online, vol. 21, no. 2, 2016.

[35] U. Reja, K. L. Manfreda, V. Hlebec, and V. Vehovar, "Open-ended vs. Close-ended Questions in Web Questionnaires," Dev. Appl. Stat., vol. 19, pp. 159–177, 2003.

[36] H. J. Smith, S. J. Milberg, and S. J. Burke, "Information Privacy: Measuring Individuals' Concerns about Organizational Practices," Manag. Inf. Syst. Q., vol. 20, no. 2, pp. 167–196, 1996.

[37] C. Wang, Q. Wang, K. Ren, and W. Lou, "Privacy-preserving public auditing for data storage security in cloud computing," Proc. - IEEE INFOCOM, 2010.

[38] V. Sekar and P. Maniatis, "Verifiable resource accounting for cloud computing services," Proc. 3rd ACM Work. Cloud Comput. Secur. Work., pp. 21–26, 2011.

[39] K. Popović and Z. Hocenski, "Cloud computing security issues and challenges," no. March, pp. 344–349, 2010.

[40] J. N. Ortiz, "Functional Encryption : Definitions and Challenges Introdu ¸ c ˜ ao," vol. 2, no. subaward 641, pp. 253–273, 2014.

[41] H. Chang and E. Choi, "User Authentication in Cloud Computing\nUbiquitous Computing and Multimedia Applications," vol. 151, pp. 338–342, 2011.

[42] D. Zissis and D. Lekkas, "Addressing cloud computing security issues," Futur. Gener. Comput. Syst., vol. 28, no. 3, pp. 583–592, 2012.

[43] D. M. Rousseau, S. B. Sitkin, R. S. Burt, and C. Camerer, "Not so different after all: A cross-discipline view of trust," Acad. Manag. Rev., vol. 23, no. 3, pp. 393–404, 1998.

[44] R. Sandhu and S. Jajodia, "Integrity principles and mechanisms in database management systems," Comput. Secur., vol. 10, no. 5, pp. 413–427, 1991.

[45] Y. Cherdantseva and J. Hilton, "A Reference Model of Information Assurance & Security," 2013 Int. Conf. Availability, Reliab. Secur., pp. 546–555, 2013.

[46] Cloud Security Alliance, "Cloud Controls Matrix Working Group," 2014. [Online]. Available: https://cloudsecurityalliance.org/group/cloud-controls-matrix/.

ASTES

Advances in Science, Technology and Engineering Systems Journal Vol. 2, No. 4, 51-55 (2017)

www.astesj.com

ASTESJ

ISSN: 2415-6698

Chikungunya virus; Review of Epidemiology and Outbreak in Pakistan

Tousif Raza[*1], Habiba Ijaz[2], Naseer Ahmad[3], Muhammad Hashim Raza[4]

[1] *Rawalpindi Medical College, Rawalpindi, Pakistan, 46000*

[2]*Benazir Bhutto Hospital, Rawalpindi, Pakistan,46000*

[3] *Departments of Cardiovascular Sciences, University of Verona, Italy, 37126*

[4]*Department of Bioinformatics and Biotechnology, International Islamic University, Islamabad, Pakistan, 44000*

A R T I C L E I N F O

Article history:
Received: 16 March, 2017
Accepted: 23 April, 2017
Online: 02 May, 2017

Keywords:
Chikungunya Virus
CHIKV
Chikungunya in Pakistan

A B S T R A C T

Chikungunya virus (CHIKV) is mosquito-borne, alpha virus. It causes acute fever and acute and chronic musculoskeletal pain in humans. CHIKV has spread to 22 countries including Pakistan resulting in hundreds of thousands of death across the world. International travel stands out as one of the major risk factors for rapid global spread of the disease. CHIKV can be highly debilitating and large epidemic have severe economic consequences. Reemergence of CHIKV is serious public health concern. In the past 10 years, after decades of infrequent, specific outbreaks, the virus has caused major epidemic outbreaks in Africa, Asia, the India Ocean, and more recently the Caribbean and Americas. Chikungunya virus represents a substantial health burden to affected population, with symptoms that include severe joint and muscle pain, rashes, and fever, as well as prolonged periods of disability in some patients. Entry of virus into tissues causes infiltration of innate immune cells, monocytes, macrophages, neutrophils, natural killer cells and adaptive immune cells. Macrophages bearing the replicating virus, in turn, secrete pro-inflammatory cytokines IL-1B, TNF-a, IL-17. Together, this pro-inflammatory milieu induces osteoclastogenesis, bone loss, and erosion. Understanding the mechanisms of host immune responses is essential for the development of diagnosis, treatments and vaccines. Viral culture and isolation from blood cells of infected patients are the Gold standards for diagnosis. Early diagnosis of CHIKV is possible by nucleic acid detection techniques. Thus there is urgent need for continued research into the epidemiology, pathology, prevention and treatment of this disease. In this article, we have provided and update on Chikungunya virus with its recent epidemiology, molecular virology and antiviral therapies and vaccines.

1. Introduction

Chikungunya virus (CHIKV) is mosquito-borne, alpha virus. It causes acute fever and acute and chronic musculoskeletal pain in humans. CHIKV has spread to 22 countries including Pakistan resulting in hundreds of thousands of death across the world. International travel stands out as one of the major risk factors for rapid global spread of the disease. (1, 2) CHIKV can be highly debilitating and large epidemic have severe economic consequences. Re-emergence of Chikungunya virus is of serious public health concern. (3,4) In the past 10 years, after decades of infrequent, specific outbreaks, the virus has caused major epidemic outbreaks in Africa, Asia, the India Ocean, and more recently the Caribbean and Americas. Chikungunya virus represents a substantial health burden to affected population, with symptoms that include severe joint and muscle pain, rashes, and fever, as well as prolonged periods of disability in some patients. Entry of virus into tissues causes infiltration of innate immune cells, monocytes, macrophages, neutrophils, natural killer cells and adaptive immune cells. Macrophages bearing the replicating virus, in turn, secrete pro-inflammatory cytokines IL-1B, TNF-a, IL-17. (5) Chikungunya virus (CHIKV), an arthropod-borne virus (arbovirus) that belongs to the family Togaviridae, genus Alpha

[*]Corresponding Author: Tousif Raza, Rawalpindi Medical College, Pakistan Contact No: 00923327594005, Email: tousifraza886@gmail.com

virus.(6) Alpha viruses can be divided into New and Old World viruses. Chikungunya virus is part of the Semliki Forest SF group of Old World Alpha viruses. Chikungunya virus is a member of the arthritogenic alpha viruses, but some cases also include meningeo-encephalitis and hemorrhagic diseases too. Chikungunya and O'nyong virus have 85% similarities in their symptoms. Chikungunya virus is a small (about 60-70 nm diameter), spherical, enveloped, positive-stranded RNA virus. The chikungunya virus genome is 11,805 nucleotides long and encodes for two polyproteins. The virus consist of four nonstructural proteins and three structural proteins. (7)

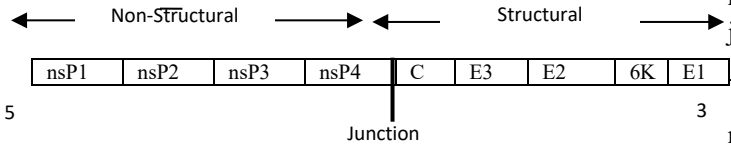

Figure 1: Chikununya virus genome structure (8)

2. Virus Replication

Virions located on the surface of the cell membrane enter the host cells by fusion and endocytosis of the viral envelope (9, 10). The uncoating of the Virions occurs in the cytoplasm. The site of mRNA transcription is in the cell cytoplasm. Replication is not restricted to a particular tissue or organs. Figure 2 shows replication as under:

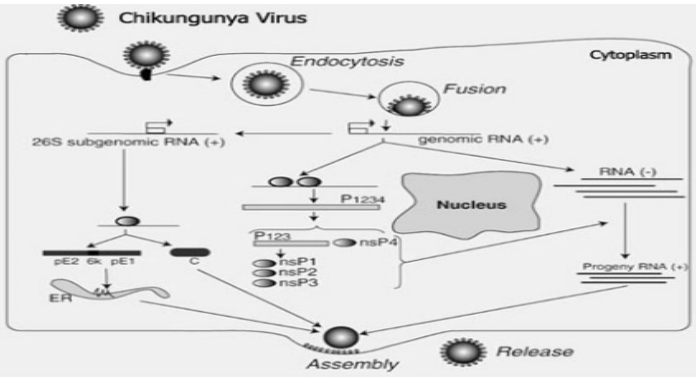

Figure 2: Replication of CHIKV (11)

3. History:

The disease was first detected in 1953 in Africa following an outbreak on the Makonde Plateau in a Swahili village in the Newalla district, Tanzania (12). The virus was isolated from the serum of febrile patient. The name chikungunya is derived from the Makonde word kungunyala, meaning "that which bends up" in reference to the stooped posture developed as a result of the arthritic symptoms of the disease. In Swahili, this means "the illness of the bended walker".

Chikungunya virus likely originated in the Central /East Africa (13), where the virus has been found to circulate in a sylvatic cycle between forest-dwelling mosquitoes and non-human primates. Currently, chikungunya fever has been identified in nearly 40 countries. Recent epidemics in Indian Ocean an Americas have led to the recognition that CHIKV is capable of moving into previously unaffected areas and causing significant levels of human suffering. (14) In 2008, chikungunya was listed as a US National institute Of Allergy and Infectious Disease (NIAID)category c priority pathogen.

4. Symptoms:

Most of people infected with Chikungunya virus will develop some symptoms are fever and very debilitating joint pain. Symptoms usually begin 3-7 days after being bitten by infected mosquito. Other symptoms may include headache, muscle pain, joint swelling, or rash. Chikungunya disease does not often results in death, but the symptoms can be severe and disabling. Most patients feel better within a week. In some people, the joint pain may persist for months. People at risk for more severe disease include newborns infected around the time of birth, older adults (>60 years), and people with medical conditions such as high blood pressure, diabetes, or heart disease. Once a person has been infected, he or she is likely to be protected from future infections

5. Diagnostic techniques:

Several methods can be used for diagnosis.

1. **Enzyme-linked immunosorbent assays (ELISA)**, Serologic tests may confirm the presence of IgM and IgG anti-chikungunya antibodies. An IgM antibody level is highest 3 to 5 weeks after the onset of illness and persists for about 2 months. Samples collected during the first week after the onset of symptoms should be tested by both serological and virological methods (RT-PCR). (15,16)
2. **Reverse transcription-polymerase chain reaction (RT-PCR)** methods are available but are of variable sensitivity. RT-PCR products from clinical samples may also be uses for genotyping of the virus, allowing comparisons with virus samples from various geographical sources. (17)
3. **Immunofluorescence assays** are sensitive and specific but lack the ability to quantify antibodies, are subjective, and require specific equipment and training. (18)
4. **Plaque reduction neutralization tests (PRNT)** are very useful because they are quite specific for alpha viruses and are gold standard for confirmation of serological test results, however it require live virus and special laboratory containment equipments. (19)
5. **Haemagglutination-inhibition test** used to diagnose disease by distinguishing chikungunya strain. Chikungunya is confirmed when symptoms such as fever and joint pain seen along with four fold Haemagglutination Inhibition antibody difference in

paired serum samples. This turns positive within 5 to 8 days of infection. (20,21)

6. **POC (**Point-Of-Care) **Assays** has been recommended to facilitate outbreak control. Rapid CHIKV IgM POC tests are now available, but little information exists regarding their performance. (22) Diagnosis of such cases require discrimination between CHIKV, Dengue and Zika Virus, this could be facilitated by use of reliable POC Assay. POC tests are highly cost-effective because they are easy to perform.

6. Vaccine Research:

A phase 2 clinical vaccine trial sponsored by the US Government in 2000, used a live, attenuated virus, developing viral resistance in 98% of those tested after 28 days and 85% still showed resistance after one year.(10) However, live chikungunya vaccines are still questionable as there could be a risk of a live vaccine possibly inducing chronic rheumatism.(23)

DNA vaccination is a technique for protecting an organism against disease by injecting it with genetically engineered DNA to produce an immunological response. Nucleic acid vaccines are still experimental. DNA vaccines have advantages over conventional vaccines as they have ability to induce a wider range of immune response types.

The recent vaccine cassette was designed based on chikungunya virus capsid and Envelop specific consensus sequences with several modifications, including codon optimization, RNA optimization, the addition of a Kozak sequence, and a substituted immunoglobin E leader sequence. These results support further study of the use of consensus CHIKV antigen in a potential vaccine cocktail.

Insecticide susceptibility status and major detoxifying enzymes activities in Aedes Albopictus (Skuse), Vector of dengue and Chikungunya in Northern part of West Bengal, India 27 Feb 2017.(10) Vector control with the use of insecticides remains the suitable method of choice to stop the transmission of these diseases.

7. Clinical Manifestations:

1. Rheumatic manifestations associated with Chikungunya virus infection:

A study of 307 patients with 32 month follow-up done on 2017 Feb 23. A Cohort of 307 patients underwent rheumatologic examinations for pain secondary to Chikungunya virus infection. The long term evaluation was conducted by telephone survey 1 and 2 years after the onset of the viral infection. At inclusion, mean age was 54 years (24-87) and 83.1% of the patients were female. Chronic joint pain was associated with synovitis in 64.2% of the patients, affecting primarily the wrists, the proximal interphalangeal joints of the fingers, and ankles.(24) Attempts to detect viral genome in joint fluid (10 patients) and synovial tissue (6 patients) using the RT-PCR technique were repeatedly unsuccessful. With a mean follow-up of 32 months, joint pain persisted in 83.1% of the patients. Functional impairment, however, was moderate, with a HAQ score of 0.44+/- 0.5.

2. Acute Respiratory Distress Syndrome,

An unusual case with all other symptoms of Chikungunya virus infection showed bilateral infiltrates involving all zones with normal cardiac size with no evidence of pleural effusion suggestive of ARDS. (25) The working diagnosis of mild ARDS as per Berlin criteria secondary to Chikungunya infection was established with baseline Acute Physiology and Chronic Health Evaluation score of 14

3. Cutaneous manifestations:

Individuals with CHIKV fever frequently present with flushed appearance involving the face and trunk, followed by a diffuse erythematous maculopapular rash of the trunk and extremities, sometimes involving the palms and soles.(26) The rash gradually fades; may evolve into petechiae, urticaria, xerosis, or hypermelanosis; or resolve with desquamation.(18, 19)

4. Neurological manifestation:

In the acute phase of illness (reported during the outbreak in Indian Ocean in 2005-2006), 23 patients presented with neurological symptoms associated with abnormal CSF tests and positive CSF immunoglobulin M (IgM) or reverse-transcriptase polymerase chain reaction(RT-PCR) for Chikungunya virus.(27) Clinical manifestations in this outbreak included altered mental status or behavior in 95%, headache in 30.4%, seizures in 26%, motor dysfunction in 4.3%, and sensorineural abnormalities in 8.7%.

8. Outbreak of Chikungunya in Pakistan:

Chikungunya virus was found as early as 1983(28). In fact, a fewer patients with chikungunya were also reported in Lahore during the 2011 dengue outbreak(29). The current outbreak(30) is said to have started on the second week of December, 2016. Different health-care authorities in Karachi estimated the total number of patients to be more than 30,000. The National Institutes of Health, Pakistan, and Armed Forces Institute of Pathology, Pakistan, have so for confirmed more than 4000 cases through qualitative RT-PCR. Ministry of Health Services, Regulation and Coordination (NHSRC) has for the first time on 26 December officially reported the outbreak to the World Health Organization (WHO).

"It is for the first time that Pakistan has officially documented the cases and has reported to WHO. The disease surfaced after some patients suffering from high fever and joint pain were taken to the facility. Pakistan undergoing substantial climate changes. The rising temperature has nurtured the outbreak of many arboviral illnesses in the region, including malaria and dengue. The deplorable sanitary conditions of most Asian countries

further adds fuel to the fire by providing excellent breeding grounds for arthropod vectors. Chikungunya is now spreading explosively in Karachi, Pakistan. Many patients develop neurological, cardiovascular, pulmonary, renal, ocular, and cutaneous sequelae following acute infection (31). Open sewers and feculent morasses, which are excellent breeding habitats for mosquitoes, can be found all throughout the city(29). There is an urgent need to get rid of the city of stagnant water bodies and to raise awareness via campaigns.

9. Prevention and Control:

The proximity of mosquito vector breeding sites to human habitation is a risk factor for chikungunya as well as for other diseases. Prevention and control relies heavily on reducing the number of natural and artificial water-filled containers habitats that support breeding of the mosquitoes. During outbreaks, clothing which minimizes skin exposure to the day-biting vectors is advised. Repellants can be applied to exposed skin, Insectide-treated mosquito nets for children, or sick or older afford good protection. Mosquito coils or other insecticide vaporizers may also reduce indoor biting.(32)

Basic precautions should be taken by people travelling to risk areas and these include use of repellents, wearing long sleeves and pants and ensuring rooms after fitted with screens to prevent mosquitoes from entering.

There is no specific antiviral drug treatment for chikungunya. It has now been shown that type1 Interferon sensing by non-myeloid cells plays a significant role in fighting against Chikungunya infection. Treatment is directed primarily at relieving the symptoms, including the joint pain using anti-pyretic, optimal analgesics and fluids. There is no commercial chikungunya vaccine.

10. Conclusion:

Chikungunya leads to (self-perceived) long term sequelae in a considerable proportion of the patients, impacting significantly on quality of life(33). Long-term chikungunya sequelae must be taken into account when dealing with this disease because of its important effects on public and individual health. Prospective large scale, long-term studies with objective assessment of signs and symptoms attributed to the disease are needed to optimally quantify and qualify these problems.

11. Recommendations:

Following recommendations can be helpful in vector control and its transmission.

1. Advocacy, social mobilization, regulatory control for public health and empowerment of communities.
2. Collaboration within the health sector and with other sectors through the optimal use of resources, planning, monitoring and decision making.
3. Integration of non-chemical and chemical vector control methods and integration with other disease control measures.
4. Evidence-based decision making guided by operational research and entomological and epidemiological surveillance and evaluation.
5. Development of adequate human resources, training and career structures at national and local level to promote capacity building and manage Integrated Vector Management (IVM).

Conflict of Interest

The authors declare no conflict of interest.

Acknowledgment

Special thanks to Prof. Shoaib Shafi and Dr. Nadeem Ikram from Benazir Bhutto Hospital, Rawalpindi for kind guidance and support. We also thank to Dr. Usman Waheed from Safe Blood Transfusion Program, Pakistan for kind guidance during review work.

References

[1] Receveur M, Ezzedine K, Pistone T, Malvy D. Chikungunya infection in a French traveller returning from the Maldives, October, 2009. Euro surveillance : bulletin Europeen sur les maladies transmissibles = European communicable disease bulletin. 2010 Feb 25;15(8):19494. PubMed PMID: 20197023. Epub 2010/03/04. eng.

[2] Heywood AE, Zwar N, Forssman BL, Seale H, Stephens N, Musto J, et al. The contribution of travellers visiting friends and relatives to notified infectious diseases in Australia: state-based enhanced surveillance. Epidemiology and infection. 2016 Aug 30:1-10. PubMed PMID: 27574034. Pubmed Central PMCID: PMC5111124. Epub 2016/08/31. eng.

[3] Weibel Galluzzo C, Kaiser L, Chappuis F. [Reemergence of Chikungunya virus]. Revue medicale suisse. 2015 May 06;11(473):1012, 4-6. PubMed PMID: 26103764. Epub 2015/06/25. Chikungunya: La reemergence. fre.

[4] Weaver SC, Forrester NL. Chikungunya: Evolutionary history and recent epidemic spread. Antiviral Res. 2015 Aug;120:32-9. PubMed PMID: 25979669. Epub 2015/05/17. eng.

[5] Mathew AJ, Ganapati A, Kabeerdoss J, Nair A, Gupta N, Chebbi P, et al. Chikungunya Infection: a Global Public Health Menace. Current allergy and asthma reports. 2017 Feb;17(2):13. PubMed PMID: 28233156. Epub 2017/02/25. eng.

[6] Lo Presti A, Cella E, Angeletti S, Ciccozzi M. Molecular epidemiology, evolution and phylogeny of Chikungunya virus: An updating review. Infection, genetics and evolution : journal of molecular epidemiology and evolutionary genetics in infectious diseases. 2016 Jul;41:270-8. PubMed PMID: 27085290. Epub 2016/04/18. eng.

[7] Weaver SCL, Marc. Chikungunya Virus and Global Spread of a Mosquito-Borne Disease. New England Journal of Medicine. 2015;372(13):1231-9. Pubmed Central PMCID: 25806915.

[8] Pietila MK, Hellstrom K, Ahola T. Alphavirus polymerase and RNA replication. Virus research. 2017 Jan 16. PubMed PMID: 28104453. Epub 2017/01/21. eng.

[9] Silva LA, Dermody TS. Chikungunya virus: epidemiology, replication, disease mechanisms, and prospective intervention strategies. The Journal of clinical investigation. 2017 Mar 01;127(3):737-49. PubMed PMID: 28248203. Pubmed Central PMCID: PMC5330729. Epub 2017/03/02. eng.

[10] JCI Silva LD. TS Chikungunya virus. The Journal of clinical investigation. 2017 01 March;127(3):737-49.

[11] Maxime Soligant BG, Stephen Higgs. Replication cycle of chikungunya: A re-emerging arbovirus. Virology. 2009;2(393):183-97. Pubmed Central PMCID: PMC2915564.

[12] Zeller H, Van Bortel W, Sudre B. Chikungunya: Its History in Africa and Asia and Its Spread to New Regions in 2013-2014. The Journal of infectious diseases. 2016 Dec 15;214(suppl 5):S436-S40. PubMed PMID: 27920169. Epub 2016/12/07. eng.

[13] Wahid B, Ali A, Rafique S, Idrees M. Global expansion of chikungunya virus: mapping the 64-year history. Int J Infect Dis. 2017 Mar 10. PubMed PMID: 28288924.

[14] Morrison CR, Plante KS, Heise MT. Chikungunya Virus: Current Perspectives on a Reemerging Virus. Microbiology spectrum. 2016 Jun;4(3). PubMed PMID: 27337473. Epub 2016/06/24. eng.

[15] Fortuna C, Remoli ME, Rizzo C, Benedetti E, Fiorentini C, Bella A, et al. Imported arboviral infections in Italy, July 2014-October 2015: a National Reference Laboratory report. BMC infectious diseases. 2017 Mar 16;17(1):216. PubMed PMID: 28302072. Pubmed Central PMCID: PMC5356298. Epub 2017/03/18. eng.

[16] Gaibani P, Landini MP, Sambri V. Diagnostic Methods for CHIKV Based on Serological Tools. Methods in molecular biology (Clifton, NJ). 2016;1426:63-73. PubMed PMID: 27233261. Epub 2016/05/29. eng.

[17] Cabral-Castro MJ, Cavalcanti MG, Peralta RH, Peralta JM. Molecular and serological techniques to detect co-circulation of DENV, ZIKV and CHIKV in suspected dengue-like syndrome patients. Journal of clinical virology : the official publication of the Pan American Society for Clinical Virology. 2016 Sep;82:108-11. PubMed PMID: 27479173. Epub 2016/08/02. eng.

[18] Moi ML, Takasaki T. Chikungunya Virus Growth and Fluorescent Labeling: Detection of Chikungunya Virus by Immunofluorescence Assay. Methods in molecular biology (Clifton, NJ). 2016;1426:143-52. PubMed PMID: 27233268. Epub 2016/05/29. eng.

[19] Cordeiro MT, Brito CA, Pena LJ, Castanha PM, Gil LH, Lopes KG, et al. Results of a Zika Virus (ZIKV) Immunoglobulin M-Specific Diagnostic Assay Are Highly Correlated With Detection of Neutralizing Anti-ZIKV Antibodies in Neonates With Congenital Disease. The Journal of infectious diseases. 2016 Dec 15;214(12):1897-904. PubMed PMID: 27923950. Epub 2016/12/08. eng.

[20] Widjaja S, Soekotjo W, Hartati S, Jennings GB, Corwin AL. Prevalence of hemagglutination-inhibition and neutralizing antibodies to arboviruses in horses of java. The Southeast Asian journal of tropical medicine and public health. 1995 Mar;26(1):109-13. PubMed PMID: 8525395. Epub 1995/03/01. eng.

[21] Adesina OA, Odelola HA. Ecological distribution of Chikungunya haemagglutination inhibition antibodies in human and domestic animals in Nigeria. Tropical and geographical medicine. 1991 Jul;43(3):271-5. PubMed PMID: 1667829. Epub 1991/07/01. eng.

[22] Burdino E, Calleri G, Caramello P, Ghisetti V. Unmet Needs for a Rapid Diagnosis of Chikungunya Virus Infection. Emerg Infect Dis. 2016 Oct;22(10):1837-9. PubMed PMID: 27347706. Pubmed Central PMCID: PMC5038423. Epub 2016/06/28. eng.

[23] Erasmus JH, Auguste AJ, Kaelber JT, Luo H, Rossi SL, Fenton K, et al. A chikungunya fever vaccine utilizing an insect-specific virus platform. Nature medicine. 2017 Feb;23(2):192-9. PubMed PMID: 27991917. Pubmed Central PMCID: PMC5296253. Epub 2016/12/20. eng.

[24] Lui NL, Leong HN, Thumboo J. Polyarthritis in four patients with chikungunya arthritis. Singapore medical journal. 2012 Apr;53(4):241-3. PubMed PMID: 22511045. Epub 2012/04/19. eng.

[25] Singh A. Acute Respiratory Distress Syndrome: An Unusual Presentation of Chikungunya Fever Viral Infection. Journal of global infectious diseases. 2017 Jan-Mar;9(1):33-4. PubMed PMID: 28250625. Pubmed Central PMCID: PMC5330044. Epub 2017/03/03. eng.

[26] Pakran J, George M, Riyaz N, Arakkal R, George S, Rajan U, et al. Purpuric macules with vesiculobullous lesions: a novel manifestation of Chikungunya. International journal of dermatology. 2011 Jan;50(1):61-9. PubMed PMID: 21182504. Epub 2010/12/25. eng.

[27] Singh A, Jain R. Neurological Manifestations of Chikungunya in Children. Indian Pediatr. 2017 Mar 15;54(3):249. PubMed PMID: 28361790.

[28] Darwish MA, Hoogstraal H, Roberts TJ, Ahmed IP, Omar F. A sero-epidemiological survey for certain arboviruses (Togaviridae) in Pakistan. Transactions of the Royal Society of Tropical Medicine and Hygiene. 1983;77(4):442-5. PubMed PMID: 6314612. Epub 1983/01/01. eng.

[29] Rahman A, Lee, H, am\nd Khan, MA. Domestic water contamination in rapidly growing megacities of Asisa: case of Karachi, Pakistan. Environ Monit Assess. 1997;44:339-60.

[30] AT Bharati M SD. Vaccine research CHIKV [Journal Article]Acta. 2017 Feb;9(1):122-23. eng.

[31] Rajapakse S, Rodrigo C, Rajapakse A. Atypical manifestations of chikungunya infection. Transactions of the Royal Society of Tropical Medicine and Hygiene. 2010 Feb;104(2):89-96. PubMed PMID: 19716149. Epub 2009/09/01. eng.

[32] Heydari N, Larsen DA, Neira M, Beltran Ayala E, Fernandez P, Adrian J, et al. Household Dengue Prevention Interventions, Expenditures, and Barriers to Aedes aegypti Control in Machala, Ecuador. International journal of environmental research and public health. 2017 Feb 16;14(2). PubMed PMID: 28212349. Pubmed Central PMCID: PMC5334750. Epub 2017/02/18. eng.

[33] Van Aalst M, Nelen CM, Goorhuis A, Stijnis C, Grobusch MP. Long-term sequelae of chikungunya virus disease: A systematic review. Travel medicine and infectious disease. 2017 Jan - Feb;15:8-22. PubMed PMID: 28163198. Epub 2017/02/07. eng.

ASTES

Advances in Science, Technology and Engineering Systems Journal
Vol. 2, No. 4, 56-58 (2016)
www.astesj.com

ASTES Journal
ISSN: 2415-6698

Matrix Encryption Scheme

Abdelhakim Chillali*

Sidi Mohamed Ben Abdellah University, Mathematics Physics and Computer Science, LSI, FP, Taza, Morocco

ARTICLEINFO

Article history:
Received: 12 April, 2017
Accepted: 04 May, 2017
Online: 14 May, 2017

Keywords:
Public key cryptography
Discrete logarithm problem
Finite field

ABSTRACT

In classical cryptography, the Hill cipher is a polygraphic substitution cipher based on linear algebra. In this work, we proposed a new problem applicable to the public key cryptography, based on the Matrices, called "Matrix discrete logarithm problem", it uses certain elements formed by matrices whose coefficients are elements in a finite field. We have constructed an abelian group and, for the cryptographic part in this unreliable group, we then perform the computation corresponding to the algebraic equations, Returning the encrypted result to a receiver. Upon receipt of the result, the receiver can retrieve the sender's clear message by performing the inverse calculation.

1 Introduction

Public key cryptographic is the fundamental technology in secure communications. It was devised by Diffie and Hellman in 1976 to secret key distribution. The mathematical problems more used are the discrete logarithm problem (DLP). In 1985 the elliptic curve discrete logarithm problem (ECDLP) was proposed independently by Koblitz and Miller. In this paper, we present the Matrix discrete logarithm problem in a new cryptographic scheme. Consider a finite field $L = \mathbb{F}_q$, where q is a power of p the characteristic of L.[1, 2, 3]
Throughout this work, we denote:
L^* multiplicative group *of* L.
Let $a, b \in L^*$ and let $x, y \in L$,

$$M_y^x = \begin{pmatrix} \frac{x}{a} - 1 & \frac{y}{b} - 1 \\ \frac{y}{b} + 1 & \frac{x}{a} + 1 \end{pmatrix}$$

$$G = \{M_y^x / det(M_y^x) = 1\}$$

$$G_q = G \mod p.$$

$$M_{y_1}^{x_1} \triangle M_{y_2}^{x_2} = M_{y_3}^{x_3}$$

where,

$$(1): \begin{cases} x_3 = \frac{b^2 x_1 x_2 + a^2 y_1 y_2}{ab^2} \\ y_3 = \frac{x_1 y_2 + x_2 y_1}{a} \end{cases}$$

$$M_k = \begin{pmatrix} \frac{k^2+1}{2k} - 1 & \frac{k^2-1}{2k} - 1 \\ \frac{k^2-1}{2k} + 1 & \frac{k^2+1}{2k} + 1 \end{pmatrix}, k \in L^*.$$

$$m = |G_q|$$

The next theorem whose proof is evident.

Theorem 1 *The set G_q with the operator $\triangle$ defined by* (1) *is a abelian group.*
The identity element is M_0^a, that if $M = M_y^x$ then $N = M_{-y}^x$ is the invertible element of M.

Remark 1 *The MDLP consists of following for two elements $M, N \in G_q$, determine the scaler $k \in \mathbb{Z}_m$ such that $M^{\triangle k} = N$. It is necessary that M be a generator of the group G_q.*

Assumption 1 *Given a group G_q and tow elements M and $N \in G_q$, there exists non polynomial time algorithm $\theta(logq)$ deciding the integer k such that $M^{\triangle k} = N$ if such a k exists.*

Assumption 2 *Given a group G_q and $\theta(logq)$ elements N_i on G_q, there exists non polynomial time algorithm $(\theta(logq))$ deciding the integers k_i, such that*

$$N_1^{\triangle k_1} \triangle N_2^{\triangle k_2} \triangle ..... \triangle N_{\theta(logq)}^{\triangle k_{\theta(logq)}} = M$$

if such k_i exist, where M is a random element on G_q.

*Abdelhakim Chillali , FP , Taza, Morocco & abdelhakim.chillali@usmba.ac.ma

https://dx.doi.org/10.25046/aj020408

2 Matrix Cryptosystem

2.1 Key distribution protocols

Let M_y^x be a generator of the group G_q.
Alice take a private key $1 < l < m$, and computes $M_{y_l}^{x_l} = M_y^{x \triangle l}$, then she transmits $M_{y_l}^{x_l}$ to Bob.
Similar, Bob takes a private key $1 < t < m$, and computes $M_{y_t}^{x_t} = M_y^{x \triangle t}$ and transmits $M_{y_t}^{x_t}$ to Alice.
In the same way Alice and Bob compute $M_{y_{tl}}^{x_{tl}} = M_{y_t}^{x_t \triangle l}$ and $M_{y_{lt}}^{x_{lt}} = M_{y_l}^{x_l \triangle t}$ respectively.

Theorem 2

$$\frac{x_{lt}}{a} + \frac{y_{lt}}{b} = \frac{x_{tl}}{a} + \frac{y_{tl}}{b} \mod p$$

The secret key is $\alpha = \frac{x_{tl}}{a} + \frac{y_{tl}}{b} \mod p$

2.2 Description of This Cryptosystem

Let $L = \mathbb{F}_q$ with $q = p^n$.
1)Space of lights: $P = G_q$.
2)Space of quantified: $C = G_q$.
3)Space of the keys: $K = L^*$.
4)Function of encryption:$\forall \alpha \in K$,

$$e_\alpha : \left| \begin{array}{ccc} P & \longrightarrow & C \\ M_y^x & \longmapsto & e_\alpha\,(M_y^x) = M_y^x \triangle M_\alpha \end{array} \right.$$

5)Function of decryption:$\forall \alpha \in K$,

$$d_\alpha : \left| \begin{array}{ccc} C & \longrightarrow & P \\ M_y^x & \longmapsto & d_\alpha(M_y^x) = M_y^x \triangle M_{-\alpha} \end{array} \right.$$

Remark 2

$$d_\alpha o e_\alpha(M_y^x) = M_y^x \triangle M_\alpha \triangle M_{-\alpha} = M_y^x$$

Remark 3 *a) Secret key :α*
b) Public keys:
1) Space of lights; P
2) Space of quantified; C
3) Space of the keys; K
4) Generator of the group P; M_y^x
5) Function of encryption; e_α
6) Function of decryption; d_α

Remark 4 *The $M_{y_l}^{x_l}$, $M_{y_t}^{x_t}$ and m are public and can known by another person, but to obtain the private key α, it is necessary to solve the Matrix problem discrete logarithm in G_q, what returns the discovery of the difficult key α.*

2.3 Numerical Example

Alice and Bob Choose the following public numbers; $p = 41$, $a = 2$, $b = 5$, and $n = 1$. They determine the group $G_{41} =< M_{31}^{26} >$, with the identity element M_0^2.

1) Exchange of the key deprived between Alice and Bob:
Alice take a private key; $l = 13 < 39$, calculation; $M_{23}^{13} = M_{31}^{26 \triangle 13}$ and send to Bob M_{23}^{13}. In turn, Bob take a private key; $t = 21 < 39$, calculation; $M_{10}^{15} = M_{31}^{26 \triangle 21}$ and send it to Alice. Alice and Bob calculate separately : $M_{18}^{13} = M_{10}^{15 \triangle 13}$ and $M_{18}^{13} = M_{23}^{13 \triangle 21}$. They determine their secret key:

$$\alpha = \frac{13}{2} + \frac{18}{5} = 6 \mod 41$$

2) Message to send:
Alice wants to send the following message

$$me = \{M_{18}^{28}, M_4^0, M_{27}^{23}, M_{36}^{34}\}$$

It encrypts it using the encryption function

M_y^x	$e_6(M_y^x)$
M_{18}^{28}	$\begin{pmatrix} 39 & 40 \\ 1 & 0 \end{pmatrix}$
M_4^0	$\begin{pmatrix} 15 & 37 \\ 39 & 17 \end{pmatrix}$
M_{27}^{23}	$\begin{pmatrix} 28 & 13 \\ 17 & 30 \end{pmatrix}$
M_{36}^{34}	$\begin{pmatrix} 28 & 25 \\ 27 & 30 \end{pmatrix}$

3) Message received:
Bob receives message crypt send by Alice

$$mr = \{\begin{pmatrix} 28 & 25 \\ 27 & 30 \end{pmatrix}, \begin{pmatrix} 28 & 13 \\ 17 & 30 \end{pmatrix}, \begin{pmatrix} 15 & 37 \\ 39 & 17 \end{pmatrix}, \begin{pmatrix} 39 & 40 \\ 1 & 0 \end{pmatrix}\}$$

It decrypts it using the decryption function

M_y^x	$d_6(M_y^x)$
$\begin{pmatrix} 39 & 40 \\ 1 & 0 \end{pmatrix}$	M_{18}^{28}
$\begin{pmatrix} 15 & 37 \\ 39 & 17 \end{pmatrix}$	M_4^0
$\begin{pmatrix} 28 & 25 \\ 27 & 30 \end{pmatrix}$	M_{36}^{34}
$\begin{pmatrix} 28 & 13 \\ 17 & 30 \end{pmatrix}$	M_{27}^{23}

3 Example for cryptography

In this example we take $p = 3$, $a = b = 1$, $n = 3$, and α root of the polynomial $X^3 + 2X + 1$. We have $P = G_{27}$, $C = G_{27}$, and $K = \mathbb{F}_{27}^*$ and $M_{\alpha^2}^{2\alpha+2}$ is a generator of the group P.

1) Exchange of the key deprived:
Alice take a private key $l = 12 < 25$, send to Bob $M_{\alpha^2}^{\alpha+1} = M_{\alpha^2}^{2\alpha+2 \triangle l}$. Bob take a private key $t = 20 < 25$, send to Alice $M_{2\alpha^2+\alpha+1}^{2\alpha^2+2} = M_{\alpha^2}^{2\alpha+2 \triangle t}$. Their secret key is

$$\beta = 2\alpha^2 + 2 + \alpha^2 + 2\alpha + 2 = 2\alpha + 1.$$

2) Message Encryption:
It is known that the encryption functions and the decryption functions are defined by:

$$e_\beta(M_y^x) = M_y^x \triangle M_{\alpha^2+2\alpha+2}^{2\alpha^2+2}$$

$$d_\beta(M_y^x) = M_y^x \triangle M_{2\alpha^2+\alpha+1}^{2\alpha^2+2}$$

Lets $x = i\alpha^2 + j\alpha + k$ and $y = l\alpha^2 + m\alpha + n$, we denote M_y^x by $ijklmn$.

Each letter is represented by a $ijklmn$ character. Often the simple The scheme a = 001000, b = 010112, ..., z = 221102 is used, but this is Not an essential feature of encryption. To encrypt a message, each letter will be decrypted by the decryption function, for a message one obtains a block of n letters (considered as an n-component vector). Consider the message 'bonjour' Which will be encrypted by the message: "crvzrng".

Table of the Symbol Encryption

M_y^x	Symbol	$e_\beta(M_y^x)$	Encrypt Symbol
001000	a	202120	h
010112	b	010220	c
010220	c	012210	d
012210	d	211110	s
012122	e	010112	b
122110	f	021210	q
122222	g	112102	m
202120	h	011101	j
202212	i	001000	a
011101	j	221102	z
011201	k	202212	i
112200	l	122110	f
112102	m	022101	w
002001	n	101212	v
020112	o	021122	r
020220	p	020112	o
021210	q	020220	p
021122	r	122222	g
211110	s	221200	y
211222	t	012122	e
101120	u	002001	n
101212	v	022201	x
022101	w	101120	u
022201	x	112200	l
221200	y	011201	k
221102	z	211222	t

4 Conclusion

Although matrix multiplication can not provide security for the encryption of a message [4, 5, 6], we have been able to construct a law of internal composition other than the law of multiplication, which allows us to create a cryptography on the matrices and which is safer for a key of reasonable length.

References

1. *A. Chillali, "Cryptography over elliptic curve of the ring $Fq[e]$, $e^4 = 0$.", World Academy of Science, Engineering and Technology., **78** , 848-850, 2011.*
2. *A. Tadmori, A. Chillali, M. Ziane, "The binary operations calculus in $E_{a,b,c}$.", International Journal of Mathematical Models and Methods in Applied Sciences., **9** , 171-175, 2015.*
3. *A. Tadmori, A. Chillali, M. Ziane, "Elliptic Curve over Ring A_4.", Applied Mathematical Sciences., **35**(9), 1721-1733, 2015.*
4. *Lester S. Hill, "Cryptography in an Algebraic Alphabet.", The American Mathematical Monthly., **36**, 1929.*
5. *Lester S. Hill, "Concerning Certain Linear Transformation Apparatus of Cryptography.", The American Mathematical Monthly., **38**(9), 1931.*
6. *Christos Koukouvinos and Dimitris E. Simos, "Encryption Schemes based on Hadamard Matrices with Circulant Cores.", Journal of Applied Mathematics and Bioinformatics., **1**(3), 17-41, 2013.*

ASTES

Advances in Science, Technology and Engineering Systems Journal Vol. 2, No. 4, 59-67 (2017)

www.astesj.com

ASTESJ

ISSN: 2415-6698

Simulation and Implementation of Sensorless Control in Multi-Motors Electric Drives with High Dynamics

Marcel Nicola*[1], Dumitru Sacerdotianu[1], Claudiu-Ionel Nicola[1], Adrian Hurezeanu[1]

[1] *Research and Development Division, National Institute ICMET Craiova, 200746, Romania*

[2]*Research and Development Division, CESI Automation Craiova, 200746, Romania*

ARTICLE INFO

Article history:
Received: 04 April, 2017
Accepted: 05 May, 2017
Online: 17 May, 2017

Keywords:
Sensorless control
Multi-motors
Electric drives

ABSTRACT

In this article we'll tackle the control of multi-motors electric drives with high dynamic, with rapid changes in torque and speed, with rigid or flexible coupling of motors, where the control strategy is FOC (Field Oriented Control) for each drives and the distributed control in local network using the CANopen protocol. In the surface mining industry, from which the electric drive application for this article is selected, the general trend is toward using asynchronous motors with short-circuit rotor, due to the advantages of this motor both in terms of design and operation. In order to achieve the variable speed, must be used the static frequency converters with sensorless control, where speed is estimated using a Model References Adaptive Control Estimator. The global control system proposed in this paper contain this type of MRAC estimator together with PI-control based, who ensures a good dynamic performance but in a lower complexity of structure such that are properly to implement in real time in a distributed control system with DSP in local network using the CANopen protocol with advantages in terms of software technology, as well as control cost and flexibility of use. Following these directions a functional application was implemented and tested in practice.

1. Introduction

This paper is an extension of work originally presented in International Conference on Applied and Theoretical Electricity (ICATE) 2016 [1].

Electric drives represent complex equipment designed to ensure optimal power supply and command of actuators during the operating processes. The development of electric drive systems was characterized in recent years by a special dynamic, linked both with technological advancements in the manufacture of semiconductor switching elements and new topologies of electric drive [2–6].

To study the behavior of the system of frequency converter plus motor prior to the actual construction of the converter, a series of numerical simulations have been carried out using MATLAB/Simulink environment. Trial and error type iterations are necessary to avoid the rough design errors, but also to identify a series of complex effects and phenomena, even if in the simulated environment, which should converge towards a positive purposefulness of the whole project. We are showing the control of electric multi-drive with high dynamic, with rapid changes in torque and speed, with rigid coupling of motors where the control strategy is FOC for each drives, sensorless control, where speed is estimated using an Estimator. Simulations were carried out in MATLAB/Simulink environment, highlighting the control structures, and the tuning parameters for a multi-drive application commonly used in surface mining industry. Sensorless control has a lot of advantages in terms of software technology, as well as control cost and flexibility of use. Therefore, the main function of the control subsystem is prediction of speed. Fortunately, achievements in control theory, such as Kalman or Luenberger estimators, have largely contributed to solving this problem. This emphasizes the importance of continuous migration of new approaches and achievements in control theory to the field of electric drives.

From point of view of control of overall system, active research area include sliding mode control [7,8], model predictive control [9–11], adaptive control, [12,13] and their references, I/O feedback linearization [14], robust control [15], artificial neural networks and fuzzy control [16,17]. In [2,8,9] a set of observers are analyzed like: super–twisting observer, an observer based on generalization

*Corresponding Author: Marcel Nicola, Research and Development Division, National Institute ICMET Craiova, 200746, Romania
Email: marcel_nicola@yahoo.com
www.astesj.com
https://dx.doi.org/10.25046/aj020409

of the phase locked–loop technique, a simple Luenberger observer, full order and reduced order adaptive system. The conclusion is that in general, these control schemes yield satisfactory results, as verified by numeric simulations and real–time experiments, making difficult to decide which sensorless control scheme performs better (in reasonable requirements of precision, like an industrial application).

From these reasons, in this article we will focus on observer, namely a MRAC-Model References Adaptive Control [12,18]. Although it doesn't have the advantage of the Kalman type estimator (which provides a good prediction even for additional uncertainty added to the measured values), this estimator has the advantage of simplicity in terms of its structure, because obviously beside the simulations which ensure a good design, it also performs the implementation of algorithms for measurement, control and prediction in a DSP, where the number of variables and performed operations must be optimized [19].

The overall control system is distributed around a local network using the CANopen protocol [20]. The multi-motor control system can drive motors with rigid or flexible coupling with rated output power between 45 kW and 75 kW, using same hardware and specifically software, but in commissioning phase, the system make an automatically dynamic identification of electrical and mechanical motor parameters. After that before each starting a static identification of motor is performed and from internal database of each DSP are selected the optimal parameters for each regulators.

We start the simulations and implementation of the functional application from this paper, with the results presented in [1,21] were the speed is measured directly with an encoder, compared with the case of sensorless control.

The functional device for driving complex multi-motor applications has the following features: driving under acceleration and braking of two (to six) engines; using the common DC bus; braking power is provided with inverter for braking energy recovery in industrial electrical network; operates in master-slave mode with vector control method; no need for various transducers: motion, position, speed, etc.

The functional model has the advantage of using a drive scheme in which independent drives will have one DC intermediate circuit properly sized. Also, a significant breakthrough in independent electrical drives is the uses of a single inverter in the network recover braking energy, while the actuators (motors) have different characteristics. Such equipment is used in applications where multiple motors are required to achieve the necessary torque or synchronous speed, such as: industrial machinery and large excavators; conveyor unit; electric traction vehicle (tram, metro); railway electric traction; cement mills, coal mills. The proposed functional model will perform and recover braking energy of each motor in the electrical network. The functional model from this paper was tested in practice for a long time period with good results.

The structure of the paper is as follows. In second section will briefly present the basics of Field Oriented Control for the induction motor and the simulations performed in sensorless control. In section 3 are presented the control strategy master-slave and the simulations in multi-motors electric drives. Section 4 show the practical implementation of the control structures from previous sections, and the experimental setup and results are presented. Finally, some conclusions will be issued and will be pointed out some ideas for continuation of work.

2. Sensorless Control of Electric Motor Drives

The technical data of each electric drive (master and slave) system, used for simulations, which includes static frequency converter designed with superior technical features providing speed regulation between zero and the rating value for induction motors with short-circuit rotor, are as follows: supply voltage: 3 x 400 Vac/50 Hz; rated output power: 45 kW; peak output: 1.5 x PN/2 minutes; operating temperature: -25°C to 45°C. The nominal parameters of each motors used in simulations are given in the below Table.

Table: Nominal parameters of motor.

Parameter	Value	Unit
Power	51136	VA
Voltage	400	Vrms
Frequency	50	Hz
Stator resistance - Rs	0.041	Ω
Rotor resistance - Rr	0.05	Ω
Leakage inductance stator - Ls	0.0008	H
Leakage inductance rotor - Lr	0.0008	H
Mutual inductance stator - Lm	0.0207	H
Rotor values - Inertia	3.1	$kg \cdot m^2$
Rotor values - Friction	0.1	N·m·s
Pole pairs - p	2	–
Snubbers resistance	10^4	Ω
Snubbers capacitance	$20*10^{-9}$	F
Diodes On-state resistance	0.001	Ω
Diodes Forward voltage	1.3	V
DC Bus Capacitance	$8400*10^{-6}$	F
Breaking chopper resistance	8	Ω
Breaking chopper frequency	4000	Hz
Breaking chopper activation voltage	750	V
Breaking chopper shutdown voltage	650	V
Machine Flux	0.73	Wb
Speed ramp (acceleration)	150	rpm/s

The model Simulink for the sensorless version is shown in Figure 1, [18]. In the following simulations, the behavior of the converter unit plus motor will be analyzed, in terms of the following quantities: stator current, rotor speed, torque and voltage in the intermediate circuit.

The classic form in s domain of a PI controller is:

$$H(s) = K_R(1 + \frac{1}{T_i s}), \quad (1)$$

where K_R is the proportional term and T_i is the integral term. For the Simulink implementation we have the equivalence [18]:

$$K_p = K_R \ , \ K_i = \frac{K_R}{T_i}, \quad (2)$$

where K_p is the proportional gain and K_i is the integral gain.

The varying parameters were: for the speed regulator Kp and Ki, for the flux controller Kp and Ki, speed ramps and the hysteresis band for the current regulator. In addition with the encoder case, the estimator which is implemented around a PI controller will also have tuning parameters Kp and Ki. The PI controllers tuning was carried out using the parameters and discrete models presented in Simulink [18]. The model Simulink is show in Figure 1, the interface for parameterization of the motor is shown in Figure 2 and the interface for the parameterization of the rectifier, inverter, intermediate filter and braking chopper is shown in Figure 3.

The chosen vector control mode is of FOC type, and the parameterization of speed regulators, flow controllers, current regulators, acceleration/braking ramp, filters and limitations is shown in Figure 4. Figure 5 show the general control diagrams of speed controllers, current and flux controllers, the transform of coordinates and calculation of the rotor position for FOC control strategy implemented in Simulink.

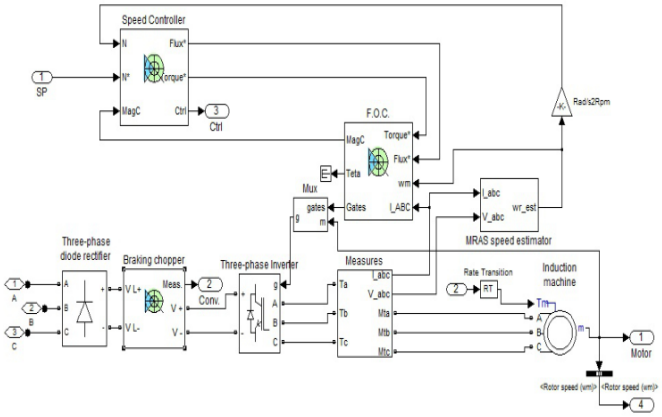

Figure 1. Simulink block diagram for sensorless model.

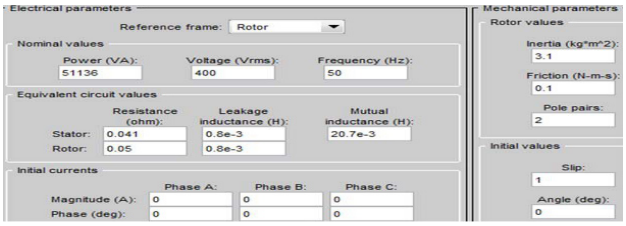

Figure 2. Interface for Parameters of motor.

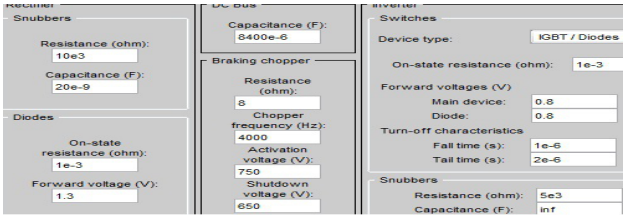

Figure 3. Interface for Parameters of Rectifier, DC Bus and Inverter.

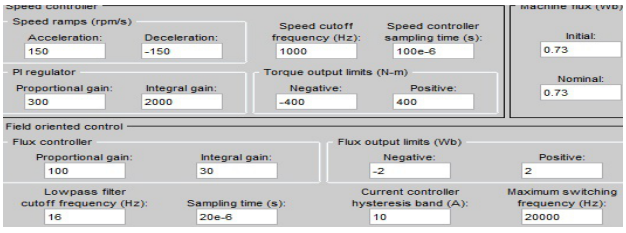

Figure 4. Interface for adjustable parameters of the controllers.

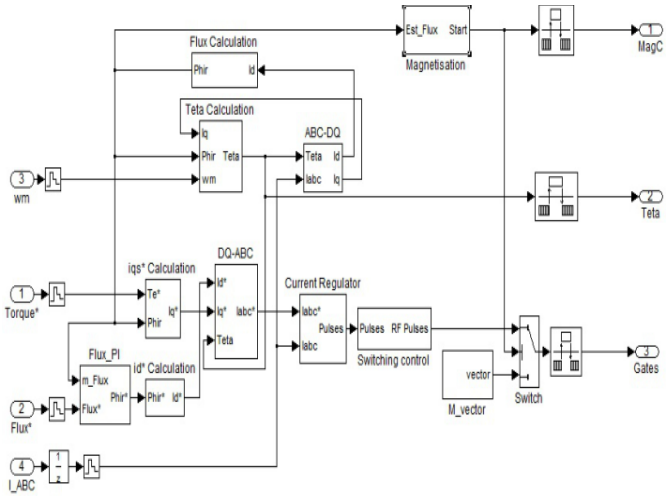

Figure 5. Field Oriented Control block diagram.

The output of speed controllers supply the electromagnetic torque (T*) and flux (Phi*) references for inner loop control. Following [18] and Figure 5 for usual electrical parameters given above we can write the equations and transfer functions for calculate the Id, Iq and the intermediate value of flux used at each iteration by de FOC strategy control in rotor reference frame.

$$I_q^* = \frac{2}{3}\cdot\frac{1}{p}\cdot\frac{L_r + L_m}{L_m}\cdot\frac{T_e}{Phi} = 0.346\cdot\frac{T_e}{Phi}\ , \tag{3}$$

$$I_d^* = \frac{Phi^*}{L_m} = \frac{Phi^*}{0.0207}\ , \tag{4}$$

$$\frac{Phi(s)}{I_d(s)} = \frac{L_m}{1+T_r} = \frac{L_m}{1+(L_r+L_m)/R_r} = \frac{0.0207}{1+0.43s}\ , \tag{5}$$

where the symbol * mean that the value is calculated and will be used to the next iteration. In this way we can write the equations for each block from Figure 5.

The type of estimator for angular speed is MRAC (see Figure 6). The equations of Blocks A and B are [12]:

$$\begin{bmatrix}\dot{\psi}_{dr}^s\\ \dot{\psi}_{qr}^s\end{bmatrix} = \frac{L_r}{L_m}\left\{\begin{bmatrix}u_{ds}^s\\ u_{qs}^s\end{bmatrix} - \begin{bmatrix}R_s+\sigma L_s s & 0\\ 0 & R_s+\sigma L_s s\end{bmatrix}\begin{bmatrix}i_{ds}^s\\ i_{qs}^s\end{bmatrix}\right\}, \tag{6}$$

$$\begin{bmatrix}\dot{\psi}_{dr}^s\\ \dot{\psi}_{qr}^s\end{bmatrix} = \begin{bmatrix}\frac{-1}{T_r} & -\omega_r\\ \omega_r & \frac{-1}{T_r}\end{bmatrix}\begin{bmatrix}\psi_{dr}^s\\ \psi_{qr}^s\end{bmatrix} + \frac{L_m}{T_r}\begin{bmatrix}i_{ds}^s\\ i_{qs}^s\end{bmatrix}, \tag{7}$$

For the speed Estimator implemented in Simulink, let note $\sigma = 1 - \frac{L_m^2}{L_r L_s}$ and starting with equations [12,13] we obtain:

$$\frac{d}{dt}\left(\Psi_{dr}^s\right) = \frac{L_r}{L_m}v_{ds}^s - \frac{L_r}{L_m}\left(R_s+\sigma L_s s\right)i_{ds}^s\ , \tag{8}$$

$$\frac{d}{dt}\left(\Psi_{qr}^{s}\right)=\frac{L_r}{L_m}v_{qs}^{s}-\frac{L_r}{L_m}\left(R_s+\sigma L_s s\right)i_{qs}^{s}, \quad (9)$$

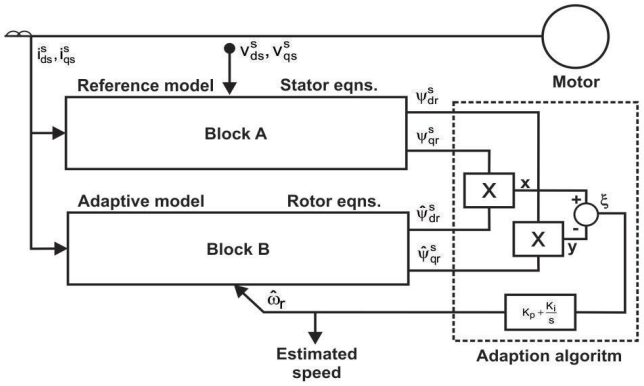

Figure 6. Speed estimator block diagram.

The encoder is thus eliminated, and the angular speed is estimated from current and voltage measurements. Using Popov hyperstability criterion, in order to achieve the overall asymptotic stability, an estimator will be achieved as follows [12]:

$$\hat{\omega}_r=\xi\left(K_p+\frac{K_i}{s}\right), \quad (10)$$

$$\xi=\hat{\Psi}_{dr}^{s}\Psi_{qr}^{s}-\Psi_{dr}^{s}\hat{\Psi}_{qr}^{s}\ . \quad (11)$$

In FOC control strategy (see Figure 1 and Figure 5) the flux and current controllers are in inner loop and the speed controller is in outer loop control. Because the speed estimator must operate faster than the outer control loops, we choose considerably lowering the tuning values for the speed regulator (so that they will be much smaller than the values of the controller from the estimator), and the optimum tuning is achieved even for an increasing dynamic of the references torque and speed like in the next set of parameters (see Figure 7):

Set of parameters no.1: Speed controller: Kp=30, Ki=20; Flux controller: Kp=100, Ki=3, hysteresis band of current controller=10A; speed estimator controller: Kp=500, Ki=5000; the speed reference is given by the sequence: [0 0.5 2 4 7 8 9]s→ [0 150 300 500 350 450 700]rpm; the torque reference is given by the sequence: [0 3 6 9 10]s→ [10 100 200 300 100]Nm.

The controllers have a good tuning even for a fluctuation of 100% in rotor resistance and for regenerative braking. Besides the good dynamic performance are achieved (stationary error, settling time, rising time, overshooting and oscillation index), due to proper tuning of the regulators PI using Ziegler-Nichols method [9] and varying the hysteresis band of current controller between 5A and 20A.

Using a quality index given by de sum of squared errors between desired speed and measured speed, after a lot of simulations the best tuning is achieved. Both in simulations and in implementation in DSP, a special attention is given to the phenomenon of saturation of component blocks. For the control loops, limiting and anti-windup components will be implemented in the PI controllers [1,18,21].

Because the influence of the tuning parameters of PI-controllers on the performance parameters is complex and somehow antagonist, trial and error type iterations are necessary when the Ziegler-Nichols method is used for tuning of each PI loop. For example increasing *Kp* and *Ki* then the stationary error and rising time are reducing but overshooting and oscillation index are rising. In practice depending on the application, the importance and the weights of the performance parameters is chosen.

In [9] are presented a set of applications where the control is predictive or PI-control based and are highlighted the advantages and disadvantages for each of them. Although the predictive control can be seen like a real time optimal control, for an induction motor with similar parameters with the above Table, in [11] is proved that dynamic performance are slightly reduced in comparison with PI-control based because of complexity of model and the controller. These can be seen like reasons for which we choose for the applications presented in this paper a PI-control based. This type of control together with MRAC estimator ensures a good dynamic performance but in a lower complexity of structure such that is properly to implement in real time in a distributed control system with DSP in local network using the CANopen protocol.

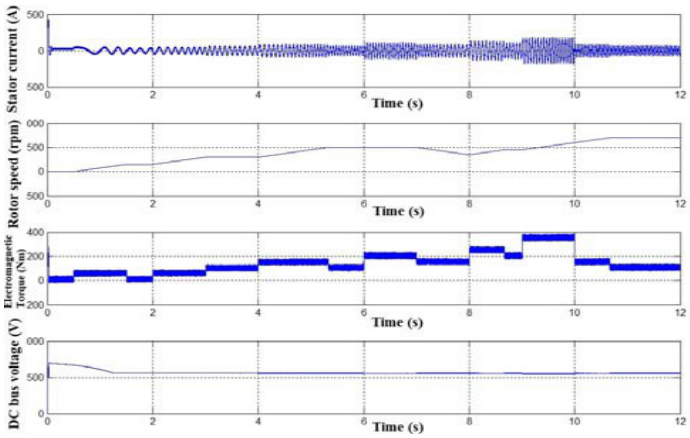

Figure 7. The simulation of sensorless model for the set no.1 of parameters of the controllers and references.

3. Multi-motors Electric Drives Control

The multi-motor applications require a synchronization of the inverters according to the type of the load and the interaction between the engines. An important feature of these applications is rigid mechanical characteristic kinematic chain as a whole. Between the electric motor and machine, there is only mechanical gear with fixed multiplication ratio. As a result, the complex drive equipment must ensure the following: equal or similar input frequency so to maintain maximum torque at each motor; frequency variation from minimum to maximum value; protection of electric motors in mechanical or electrical caused defects. In the multi-motor drives they are two essential conditions: kinematic chain and mechanical devices to be identical; mechanical characteristic of the electric motor to be more flexible. In practice, the first condition is very difficult to obtain due to operating conditions and mechanical wear, so these disadvantages should be directed to the second condition, namely the permanent and automatic adjustment of the electric motor, so it develops the needed torque at the imposed speed. The control system of the multi-motor drive includes a control system with FOC-type control

strategy for each engine. One of the control systems will be considered as master and the other one as slave.

3.1. Rigid Coupling

In the case of rigid coupling of the two motors, they must have the same speed given the fact that the load torque on each shaft can be different. The drive speed reference will be set for the master system, and the output it controls (the master engine speed) will be transmitted as a speed reference for the slave system. In actual implementation this communication is achieved as CANopen protocol. In the simulations (see Figure 8) we added a delay block to catch the effect of delays in the transmission of the reference from the master system to the slave system and the way the overall drive control system behaves. The load torques in the driving axles may be different and are considered elements of disturbance for the driving system which must provide equal speeds for the two motors.

The control systems of each engine have been presented in previously section. From single-engine simulations optimal settings will be used for the control systems. In order to increase the speed of response for the slave system for tracking the master system, the acceleration/deceleration ramp was maintained at 150rpm/s for the master system and the acceleration/deceleration ramp was increased at 1000rpm/s for the slave system. This change has given good results in simulations, and will also be implemented in the DSP's of the control systems of each engine.

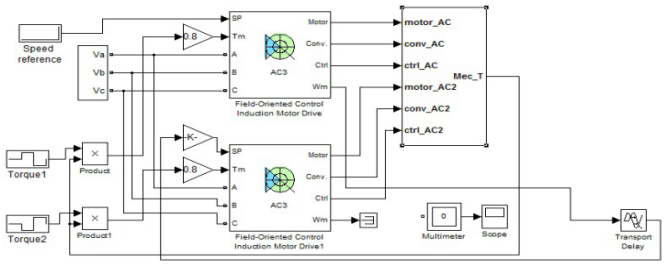

Figure 8. Simulink block diagram for multi-drives control.

Another way to increase the speed of response of the slave system was to increase the speed of response of the PI-type controllers in the slave control system by increasing the regulation parameters, but there has been no significant improvement, in addition there is the risk of overshooting in the local loops and the oscillation of the overall control loop. This alternative has not been accepted for implementation in the DSP's.

As a result of simulations, it was concluded that the overall control system has better results for delays in the transmission of the reference from the master to the slave for values up to 5ms in case of maximum 20% torque imbalance, i.e. a distribution of 60%-40% for the two motors. In practical implementation, for safety reasons, the delay will be limited to 4ms by setting the reference through the local communication network CAN between the master and the slave DSP's, using a communication method which is suitable for this time period. In practical implementation, the maximum permissible imbalance will be of 18% for the load torques, there will be a warning signal if this rating is exceeded, and the fault protection is set to a higher rating (depending on the beneficiary and the application). The quantities in question resulting from these simulations are for each master and slave subassembly: stator currents, electromagnetic torques and speeds. The voltage rating in the intermediate common DC circuit and the overall load torque in the rigid coupling shaft were achieved through simulations. We show the simulations for the next set of parameters.

Set of parameters no.1: Speed controller: Kp=30, Ki=20; Flux controller: Kp=100, Ki=3, hysteresis band of current controller=10A; speed estimator controller: Kp=500, Ki=5000; acc master=150rpm/s, acc slave=1000rpm/s, delay=4ms; the speed reference is given by the sequence: [0 0.5 2 4 7 8 9]s→ [0 150 300 500 350 450 700]rpm; the torque distribution master-slave from load torque:[50% - 50%].

Set of parameters no.2: Speed controller: Kp=30, Ki=20; Flux controller: Kp=100, Ki=3, hysteresis band of current controller=10A; speed estimator controller: Kp=500, Ki=5000; acc master=150rpm/s, acc slave=1000rpm/s, delay=4ms; the speed reference is given by the sequence: [0 9]s→ [700 900]rpm; the torque distribution master-slave from load torque:[0 3 6 9]s→ [50-50 60-40 40-60 50-50]%.

In Figure 9 at second 7, when the load torque reference decreases from 100Nm to 30Nm regenerative braking occurs and the voltage in the intermediate circuit increases. In Simulink, in order to analyze this phenomenon we have set the limits of the braking chopper between 750V (Activation Voltage) and 650V (Shutdown Voltage). For actual implementation, instead of the braking chopper, a regenerative inverter will be used.

In Figure 10 we observe that because the load torque is maximum 800 Nm, the master and slave have same speed with the reference just at low value. Between second 3 and second 6, because master has imposed 60% from load torque, the slave can follow the master but at speed less than the reference. At second 6 when the master has imposed 40% from load torque, the master can follow the speed reference, but not the slave. Starting with the second 11 when the imposed load torque is 50% for master and for slave, the speed of master and slave follow the speed reference. These simulations show that overall control system work well in limiting of saturation but evident in a practice situation from mechanical reason the protection must work immediately when the slave can't follow the master. In Figure11 because the load torque doesn't reach the saturation for same parameterization set, the slave and master follow the speed reference.

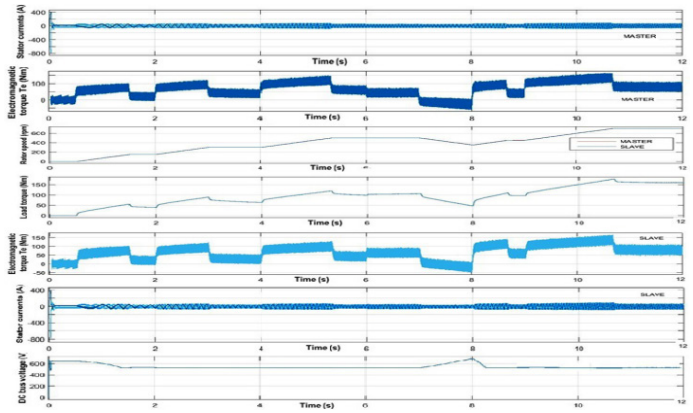

Figure 9. The simulation of master-slave drives model for the set no.1 of parameters of the controllers and references.

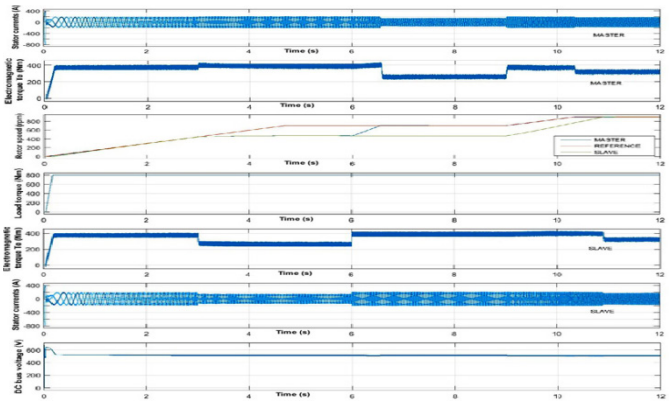

Figure 10. The simulation of master-slave drives model for the set no.2 of parameters of the controllers and references with saturation of load torque.

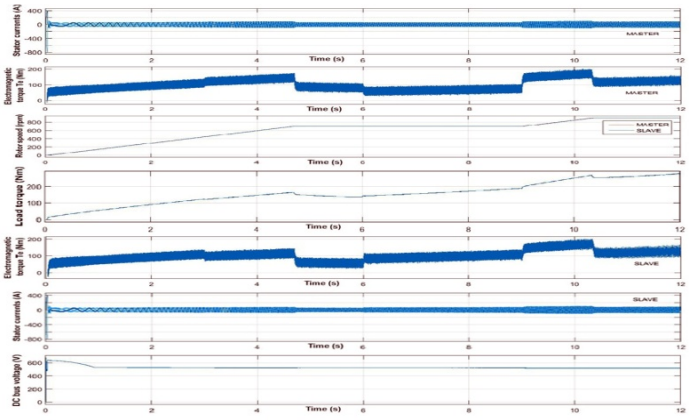

Figure 11 The simulation of master-slave drives model for the set no.2 of parameters of the controllers and references without saturation of load torque.

3.2. Flexible Coupling

In the case of flexible coupling of two or more motors, all motors must generate, as much as possible, the same torque. The load torques in the driving axles may be different and are considered elements of disturbance for the driving system which must provide equal electromagnetic torques for the two subsystems. The control system of the multi-motor drive includes a control system with FOC-type control strategy for each engine, but where the speed control loops are deactivated. One of the control systems will be considered as master and the other one as slave.

The drive motor torque reference will be set for the master system, and the output it controls (the electromagnetic torque) will be transmitted as a torque reference for the slave system. In actual implementation this communication is achieved as CANopen protocol. In the simulations (see Figure 12) we added a delay block to catch the effect of delays in the transmission of the reference from the master system to the slave system and the way the overall drive control system behaves. The control systems of each engine have been presented previously. From single-engine simulations optimal settings will be used for the control systems, except for the parameters of the speed control loop, which in this case is deactivated.

As a result of simulations, it was concluded that the overall control system has better results for delays in the transmission of the reference from the master to the slave for values up to 10ms, however in practical implementation, for safety reasons, the delay will be limited to 4ms by setting the reference through the local communication network CANopen between the master and the slave DSP's, using a communication method which is suitable for this time period.

In practical implementation, the maximum permissible imbalance for the electromagnetic torques of the master and the slave system is of 15%, there will be a warning signal if this rating is exceeded, and the fault protection is set to a higher rating (depending on the beneficiary and the application). The quantities in question resulting from these simulations are for each master and slave subassembly: stator currents, electromagnetic torques and speeds. The voltage rating in the intermediate common DC circuit and the overall load torque were achieved through simulations.

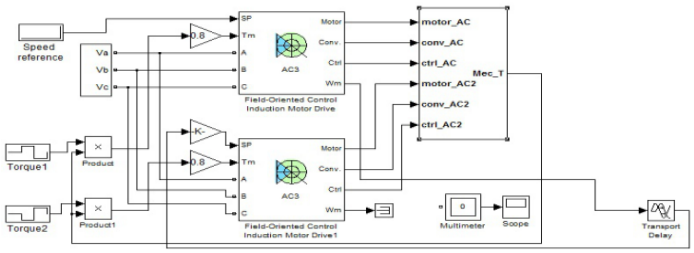

Figure 12. Simulink block diagram for multi-drives control.

We show the simulations for the next set of parameters.

Set of parameters no.1: Speed controller: Kp=30, Ki=20; Flux controller: Kp=100, Ki=3, hysteresis band of current controller=10A; speed estimator controller: Kp=500, Ki=5000; delay=10ms; the torque reference is given by the sequence: [0 0.5 1]s→ [100 200 300]Nm; the torque distribution master-slave from load torque is balanced [0 0.5 1]s→ [50 150 250]Nm.

Set of parameters no.2: Same control parameters like set no.1, delay=4ms; the torque reference is given by the sequence: [0 0.5 1 2]s→ [100 200 300 400]Nm; the torque distribution master from load [0 0.5 1 2]s→ [50 100 200 200]Nm; the torque distribution slave from load [0 0.5 1 2]s→ [20 100 100 100]Nm.

Set of parameters no.3: Same control parameters like set no.1, delay=4ms; the torque reference is given by the sequence: [0 0.5 1 2]s→ [100 200 300 400]Nm; the torque distribution master from load [0 0.5 1 2]s→ [20 100 100 100]Nm; the torque distribution slave from load [0 0.5 1 2]s→ [50 100 200 200]Nm.

In Figure 13 the overall drive performs well even for a delay of 10 ms, but with balanced distribution of torque load for the two engines. This simulation is equivalent of a linear movement for an excavator with tracks.

In Figure 14 for the sensorless type, in case of a left turn (master engine on the left) we shows that for an increased load torque in the master engine in relation to the slave engine, the equality of the electromagnetic torques is maintained between prescribed limits, but the slave engine speed is higher than the master engine speed. The behavior of the driving system for a turn to the right is similarly simulated (see Figure 15), so that for an increased load torque in the slave engine in relation to the master engine, the equality of the electromagnetic torques is maintained, but the slave engine speed is lower than the master engine speed.

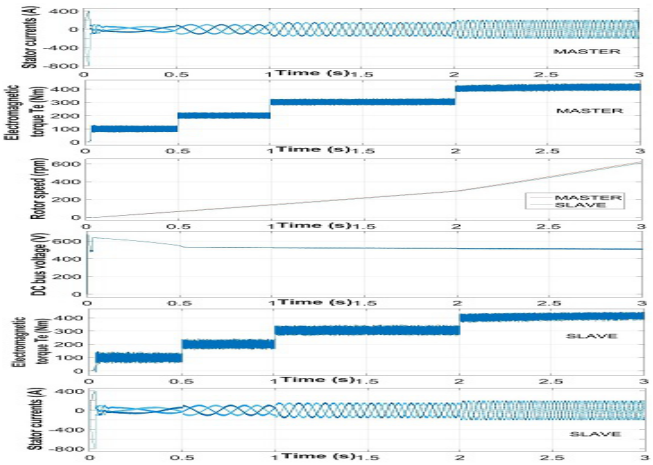

Figure 13. The simulation of master-slave drives model for the set no.1 of parameters of the controllers and references.

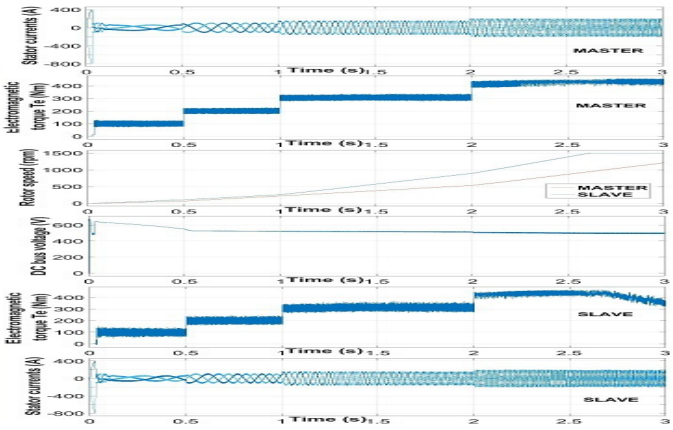

Figure 14. The simulation of master-slave drives model for the set no.2 of parameters of the controllers and references.

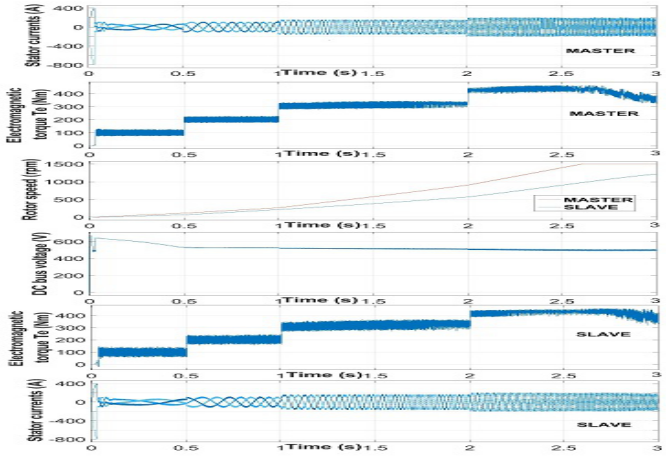

Figure 15. The simulation of master-slave drives model for the set no.3 of parameters of the controllers and references.

4. Hardware and Software Implementation

For hardware implementation of each Command and Control Unit we used the DSP dsPIC33EP810MU810 Microchip. This DSP have Harvard Architecture, 70 MIPS, Acc 40bits, PWM hardware blocks, USB, SPI and ECAN interfaces. For the three-phase diode rectifier block we used DD160N 160A / 2200V modules from Infineon and for three-phase inverter block we used LNC2W562M modules from Infineon. The current transducers are HAT 500-S from LEM with IPN = 500A, IPM= ±1500A and Ua = ±15V. The voltage transducers are LV 25-P-1000 from LEM with UPN = 10…500V and IPN = 10mA. The block diagram of hardware implementation for an application with one master and two slaves is presented in Figure 16 and contain the blocks: 1- c.c. circuit, 2-three-phase main inverter, 3- synchronization block, 4-PWM block, 5- induction motor, 6- output filter, 7- PWM block for recovery inverter, 8- three-phase recovery inverter, 9-estimation block, 10- voltage controller, 11- flux controller, 12-speed controller, 13- current controller, 14- data bus for CANopen protocol. The blocks 9 to 13 are implemented software in main DSP of each drive. An image of cabinet of hardware structure for multi-driving application is presented in Figure 17.

The software implementation is realized in MPLAB from Microchip. MPLAB is an integrated and development environment IDE, who contain editor, project manager, debugger, profiler and C/C++ optimizer. The software application supplies the following features: sensorless vectorially control of induction motors; automatically identification of electrical motor parameters; stability and fast response at fast changes of load; implementation of PWM Space Vector modulation; implementation of PI controllers and estimators; implementation of communication with PC host and local network communication with CANopen protocol. The main software blocks are: Init- make the configuration of registers and the limits of CAN converters; Clarke- implement the Clarke transformation; iClarke- implement the inverse Clarke transformation; Control- make the configuration of DSP; eCAN- make the configuration and activate the communication on CAN interface with other DSP; Ethet- make the configuration on Ethernet; Park- implement the Park transformation; iPark- implement the inverse Park transformation; Measure- implement the read and conversion of digital and analog ports; PI- make the configuration and implement the software PI controllers; Estim- implement the software estimators; SVgen-implement the software PWM Space Vector modulation; Timer-make the configuration of timers; Main- implement the main loop.

Following [19] all the software blocks that make the control of hardware structure are implemented on DSPs, for a functional application. The code for software blocks are implemented in MPLAB IDE, like a C language but optimized for DSP, where in a special format data Q15, the execution speed is increased even through the replacement of divide operations (large time consumer) by the shifting bit operations (low time consumer). When are make the implementation of the equation of speed Estimator in DSP, can appear some little errors due the data format representation instruction and the algorithm for increasing of accuracy of estimated speed value is presented in [19]. It's worth to say that the software implementation in DSP is not a trivial task and represent the last stage and the validation of the chain: theory, design, simulation and implementation.

4.1. Rigid Coupling

Similar results with those of Section III are obtained even in the case of the functional application. In Figure 18 are presented the signals recorded on the PC host for 1 minute from multi-driving application 2x45 kW rigid coupling motors. The signals presented are: master and slave speed, DC bus voltage, master and slave output current and voltage filtered.

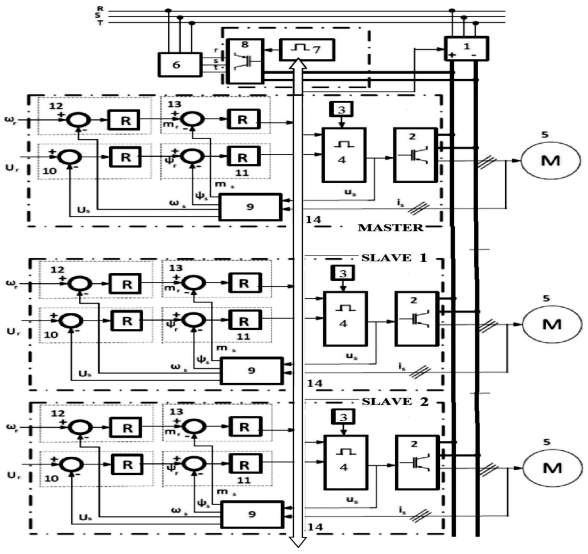

Figure 16. Hardware block diagram for electric multi-drives.

Figure 17. Picture of electric multi-drives equipment.

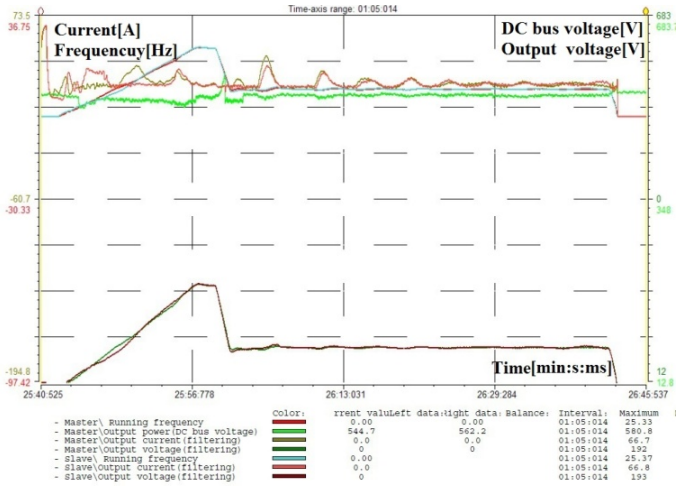

Figure 18. Signals recorded on the PC host from multi-driving application 2x45 kW rigid coupling motors.

The master and slave output speed (the red and blue line) are overlaid, indicating a very good control and stationary and dynamic performance even under acceleration and braking ramps. For each drives output voltage is directly proportional to engine speed and observe correct output voltage variation depending on engine speed. The current through motor is influenced by the functioning regime of drive motor (acceleration or braking) and by the variation of the shaft load (at constant speed). The variation of current is correct and correlated with the engine operating conditions. DC voltage value from intermediate circuit is the rectified and filtered voltage value of three-phase line voltage and is influenced by the functioning regime of drive motors (motor/generator) and the current through the motors.

4.2. Flexible Coupling

In Figure 19 are presented the signals recorded on the PC host for 7 minute from multi-driving application 3x75 kW flexible coupling motors. The signals presented are: master and slave's output current and frequency. The relationship between torque (through current) and frequency can be seen in Figure 19.

Because of the inevitable mechanical wear and tear there are differences between the master and slaves motors (gearbox wear, ground composition, mud, movement in uphill and downhill). The system tries to compensate for these differences by controlling the mediated torque for each motor. There are oscillations caused by the track movement system. Because of wear and tear these track will have the following differences: different tension, different electro-mechanical braking time, different grip.

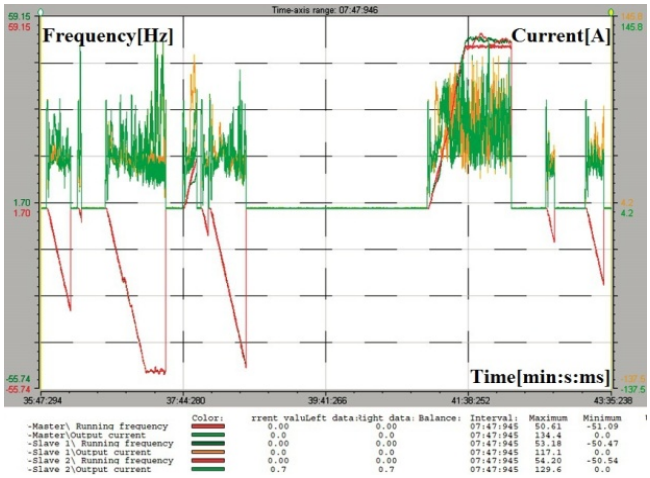

Figure 19. Signals recorded on the PC host from multi-driving application 3x75 kW flexible coupling motors.

Because of these differences when the system starts, the motors will develop completely different torque and the system is allowed to stabilize for 3 seconds, before activating the torque regulator. Only the protection features are active during the first 3 seconds, for protecting the VFDs, motors and gearboxes. In practice for the turning left or right, the upper limit frequency has been increased to 65Hz for 10 minutes so the motor from the outside trajectory can provide the necessary torque. In simulation it can be seen in Figure 14 and Figure 15 that in turn left and right the speed is maximum (1500rpm-50Hz) for motors from outside trajectory and the supplied torque is decreased.

There are a good control and stationary and dynamic performance even under acceleration and braking ramps and for front or back movement. For each drive the current through motor is influenced by the functioning regime of drive motor (acceleration or braking) and by the variation of the shaft load. The variation of currents is correct and correlated with the motors operating conditions.

5. Conclusions

It is obvious that the tuning of the controllers from the DSP will be slightly different from the one achieved through simulation, since simulations cannot identify every single mode and dynamic from practice, but the qualitative aspect will surely be maintained, and the good results achieved through simulations and the implementation of algorithms in the DSP which follow the direction of the ones in Simulink is a guarantee that the actual model will also function with good results. The system was tested in practice in surface mining, in acting of the large excavators, for a long time period with good results and proved this fact.

The results of the research consist in the implementation of the FOC sensorless control for an industrial multi-drive for applications with rigid or flexible coupling of motors, using same hardware but specifically software with rated output power between 45 kW and 75 kW.

In future approaches some interesting issues remain to be investigated, such as the digital implementation of more complex controllers for increasing the robustness and performance but optimized for DSP.

Acknowledgment

This work was carried out through the Partnerships in priority areas - PN II, developed with the support of MEN - UEFISCDI, project no. PN-II-PT-PCCA-2013-4-0157.

References

[1] M. Nicola, D. Sacerdotianu, and A. Hurezeanu, "Sensorless Control Using the Model Reference Adaptive Control Estimator in Electric Drives with High Dynamic" in International Conference on Applied and Theoretical Electricity, Craiova Romania, 2016. doi: [10.1109/ICATE.2016.7754642]

[2] C. Lascu, I. Boldea, and F. Blaabjerg, ''Super-twisting sliding mode control of torque and flux in permanent magnet synchronous machine drives" in Proc. of IEEE Ind. Electron. Conf. (IECON 2013), Viena Austria, 2013. doi: [10.1109/IECON.2013.6699635]

[3] S.B. Veeranna, U.R. Yaragatti, and A.R. Beig, "Synchronized SVPWM algorithm for overmodulation region for three-level VSI" in Proc. of IEEE Ind. Electron. Conf. (IECON 2010), Glendale USA, 2010.

[4] V. Oleschuk, G. Grandi, "Algorithms, schemes and techniques of space-vector modulation for dual-inverter systems with symmetrical multilevel phase voltage" International Review on Modelling and Simulations (IREMOS), **5(** 5), 1877-1866, 2012.

[5] V. Oleschuk, "PWM methods providing phase voltage symmetries in dual-inverter fed systems" Przeglad Electrotechniczny (Electrical Review), **89**(6), 61-65, 2013.

[6] X. M. Chen, X. L. Gong, H. X. Zhou, Z. B. Xu, Y. G. Xu, and C. J. Kang, "An Economical Rapid Control Prototyping System Design with Matlab/Simulink and TMS320F2812 DSP" in Proc. of IMECS 2010, Hong-Kong, 2010.

[7] D. Bullo, A. Ferrara, and M. Rubagotti, "Sliding mode observers for sensorless control of current-fed induction motors" in American Control Conference, San Francisco USA, 2011.

[8] S. D. Genarro, J. R. Dominguez, and M. Meza, "Sensorless High Order Sliding Mode Control of Induction Motors with Core Loss" IEEE Transactions on Industrial Electronics, **61**(6), 2678-2689, 2014. doi: [10.1109/TIE.2013.2276311]

[9] L. Wang, S. Chai, D. Yoo, L.Gan, K. and Ng, PID and predictive control of electrical drives and power converters using matlab/simulink, Wiley-IEEE Press, 2015.

[10] J. Rodriguez, P. Cortes, Predictive control of power converters and electrical drives, John Wiley & Sons, 2012.

[11] S. Ivanov, V. Ivanov, V. Rasvan, E. Bobasu, D. Popescu, and F. Stanga, "Predictive Versus Vector Control Of The Induction Motor" in 27th European Conference on Modelling and Simulation, Alesund Norway, 2013.

[12] B.K. Bose, Modern Power Electronics and AC Drives, New Jersey: Prentice Hall, 2002.

[13] G. Sieklucki, "Analysis of the transfer-function models of electric drives with controlled voltage source" Przeglad Elektrot., **7**, 250-255, 2012.

[14] C. Lascu, S. Jafarzadeh, M. S. Fadali, and F. Blaabjerg, "Direct Torque Control With Feedback Linearization for Induction Motor Drives" IEEE Transactions on Power Electronics, **32**(3), 2072-2080, 2017. doi: [10.1109/TPEL.2016.2564943]

[15] S. Legrioui, S. E. Rezgui, and H. Benalla, "Robust IM exponential reaching law sensorless control with MRAS-based online parameters identification" in IEEE 15th International Conference on Environment and Electrical Engineering, Rome Italy, 2015. doi: [10.1109/EEEIC.2015.7165265]

[16] C. Fahassa, Y. Zahraoui, M. Akherraz, and A. Bennassar, "Improvement of induction motor performance at low speeds using fuzzy logic adaptation mechanism based sensorless direct field oriented control and fuzzy logic controllers" in 5th International Conference on Multimedia Computing and Systems, Marrakech Morocco, 2016. doi: [10.1109/ICMCS.2016.7905545]

[17] G. Pavithra, G. R. P. Lakshmi, "Simulation of neuro fuzzy and ANFIS in sensorless control of BLDCM drive for high speed application" in 2015 International Conference on Computation of Power, Energy, Information and Communication, Madras India, 2015.

[18] SimPowerSystem[Online].Available:http://www.mathworks.com/products/simpower/model-examples.html.

[19] Microchip dsPIC33EP256MU810 datasheet [Online]. Available: http://www.microchip.com/wwwproducts/en/dsPIC33EP256MU810

[20] CANopen–The standardized embedded network [Online]. Available: https://www.can-cia.org/canopen/

[21] M. Nicola, D. Sacerdotianu, and A. Hurezeanu, "Simulation and Implementation of Sensorless Control Using Estimators in Electric Drives with High Dynamic" Annals of the University of Craiova, Electrical Engineering Series, **40**, 86-93, 2016.

ASTES

Advances in Science, Technology and Engineering Systems Journal Vol. 2, No. 4, 68-77 (2017)

www.astesj.com

ASTESJ

ISSN: 2415-6698

Forced Vibration Response of Double-Bay Multi-Storey Building Frames with Joints of Infinite Rigidity

Mbanusi Echefuna Cyril[*,1], Ngwu Chukwuemeka[2], Onyeka Festus[3], Onoh Felix[4]

[1]*Department of Building, Nnamdi Azikiwe University, Awka, Nigeria.*

[2]*Department of Quantity Surveying, Nnamdi Azikiwe University, Awka, Nigeria.*

[3]*Department of Civil Engineering, Michael Okpara University of Agriculture, Umudike, Nigeria.*

[4]*Department of Quantity Surveying, Enugu State University of Science and Technology, Enugu, Nigeria.*

ARTICLE INFO

Article history:
Received: 21 March 2017
Accepted: 27 April 2017
Online: 19 May, 2017

Keywords:
Amplitude of vibration
Conjugate system
Forced vibration
Lumped mass

ABSTRACT

This paper studied external-source-excited vibration response of double-bay multi-storey building frames for the effect of joint stiffening on bending moment and joint displacement. One of the frames has normal rigid joints. Three others of the frames have stiffened joints of stiffened lengths: 275mm, 425mm and 775mm respectively. Lumped mass system was the dynamic model adopted. The frames were modeled as those with flexible horizontal members, permitting rotation of joints and having multi degrees of freedom (MDOF). Classical displacement method of analysis was adopted using fixed end reactive moments which were modified to include the contributions of joint stiffening. The study revealed that stiffening of joints results in: (i) decrease in displacements at the joints; (ii) substantial reduction in deflection and significant increase of deflection ductility and energy ductility of flexural members. (iii) increase in joint moments and decrease in span moments.

1. Introduction

As skeletons constitute the load bearing components of animals with bones, so do frames constitute the major load bearing components of constructed facilities such as buildings, tricycles, towers, guyed masts, bridges, to mention only a few. Building structures [1], together with structures of other constructed facilities, are subjected not only to static, i.e. gradually applied loads or forces, but also they are subjected to time-dependent, vibration – inducing loads or forces known as dynamic loads, dynamic disturbances or dynamic excitations.

Various sources of dynamic loads or forces do exist. They can pose serious challenges to the lifespan of the constructed facility. These forms of dynamic loads [2 - 4] may be summarized as: vibrations induced by people such as to pedestrian bridges, floors with walking people, floors for sport and dance activities, floors with fixed seating and spectator galleries and high diving platforms. Machine induced vibrations could impact by way of machine foundation and supports, bell towers, structure borne sounds and ground transmitted vibrations.

In addition, there are [2, 3], wind induced vibrations that could tremendously affect buildings, towers, chimneys and masts, guyed masts, pylons, suspension and cable-stayed bridges and cantilevered roofs.

Vibrations, [2, 3, 5], induced by traffic and construction activity can deeply affect buildings, roads, railways, bridges and construction work. More vibration – induced sources were recounted in [5 - 9].

The tendency [5] of one object, applied energy, force, imposed displacement excitation source to induce another adjoining or interconnected object into vibration motion is referred to as forced vibration. In the case of building and civil Engineering structures, [5, 6], forced vibrations can be induced by any dynamic excitation source on the structure that is subjected to externally applied loads or forces.

[*]Corresponding Author: Mbanusi Echefuna Cyril, Nnamdi Azikiwe University, Awka, Nigeria | Email: cyril.mbanusi@yahoo.com

Eliminating vibrations [3, 7]. may save human lives. A good example is the vibration control of building and civil engineering structures in an earthquake scenario. Effective vibration control of building and civil engineering structures [8] lies in astuteness and acuity in structural dynamics analysis and design of structures of the constructed facility.

Stiffened joints [9] are non-deformable joints. In response to the action of external loads, they simply rotate as rigid bodies without admitting any deformation. Consequently [9] the joints are assumed to be infinitely rigid. Greater benefits of stiffened joints than there are for normal rigid joints are contained in [4, 9, 12- 14].

A typical member of a frame with flexible and stiffened segments is depicted by figure1, whereas figure 2 shows the plan of double-bay building framed structure. Figures 3 and 4 represent double-bay four-storey building frames with normal rigid and stiffened joints respectively.

Shear frame model [9] does not permit rotation of its joints but allows lateral vibration motion in its plane due to the assumed infinite rigidity of its horizontal members. Improved model, known as frames with flexible horizontal members, permits rotation of its joints [3]. Better acceptability of frames with flexible horizontal members, as a generalized dynamic model for multi-storey building structure, rather than the shear frame model, are contained in [3 - 5, 9 - 11].

This work studied forced vibration of double-bay multi-storey building frames with stiffened joints. This investigation involved four case studies. One of the frames has normal rigid joints. Three others of the frames have stiffened joints of stiffened lengths: 275mm, 425mm and 775mm respectively. Each of the frames was modeled as a structure having finite number of degrees of freedom, adopting the lumped mass element concentration at the right corner of each upper floor level, figure 5. Loading of the conjugate system is depicted in figure 6. Figure 7 presents dynamic loading for the frames.

Aim in this study is to determine the effect of joint stiffening on forced vibration of double-bay multi-storey building frames. The study sought to achieve the aim through the following objectives:

- To identify the dynamic degrees of freedom corresponding to the number of lumped masses;
- To determine the bending moment for the fundamental or conjugate system;
- To assess the complete reactions to form the identity stiffness matrix;
- To calculate the reactions at the points of imaginary supports of the conjugate system to form the load vector of the dynamic structure matrix;
- To solve the equation for forced vibration to obtain the amplitudes of forced vibration;
- To determine the bending moment values due to dynamic effect.

2. Previous Works

In [12], the author carried out dynamic analysis of tall building frames. Study in [12] revealed that it was quite insufficient to deploy any type of static analysis model to estimate the effect of dynamic loads on structures without actually carrying out dynamics analysis of such structures that may be subjected to dynamic loads. The study in [12] is related to this present work by way that both works treated dynamic analysis. They are distinct from each other in the matter of joints of infinite rigidity which was treated in this present study. Furthermore, the present work treated double-bay frames but in [12], mono-bay or single-bay frames were treated.

In [13], the author worked on the matrix analysis of frames with stiffened joints. The study in [13] established that joint stiffening enhances the structural performance of frames such as higher bending resistance and greater stability. Relatedness of work in [13] with this present study lies in the fact that both studies treated analysis of frames with stiffened joints. However, in [13], effects of static loads were determined whereas the present work determined the effects of dynamic loads. Again, the present work treated double-bay frames. In contrast, the author in [13] treated mono-bay i.e. single-bay frames.

In [9], the author investigated the stress analysis of frames with stiffened joints. The study revealed that joints of infinite rigidity bring about enhanced stability of framed structures. The common ground with the study in [9] and the present work lies in both of the studies treated joints of infinite rigidity. This very work treated dynamic analysis, whereas the author in [9] treated static analysis. This marked an uncommon ground for the two studies. Moreover, mono-bay frames were studied in [9]. The present study treated double-bay frames.

The authors in [14], studied effect of joint stiffening on the dynamic response of frames. The study in [14] revealed that stiffening of joints yielded significant decrease of dynamic bending moment values. Study in [14] is related to this present work in that both of them treated dynamic analysis of frames with stiffened joints. However, category of frames studied in [14] was mono-bay, i.e. single or one-bay, as distinct from double-bay frame treated in this present work.

Apart from distinctiveness of the present study with respective individual previous works, there exists an aspect of distinctiveness of the present study over the previous works put together. This lies in mono-bay and double-bay. The previous works studied mono-bay frames. The present work treated double-bay frames.

3. Equation of Motion

3.1. Free Vibration

At any point in time, t, in the course of a free undamped vibration of a multi degree of freedom frame the equation of motion is obtained by adding the force of inertia due to the masses in motion and the restoring forces due to the stiffness of members. Thus,

$$m_i \frac{dt^2}{d^2 X_j}(t) + K_{ij} X_i(t) = 0 \qquad (1)$$

Where, $X_i(t)$ = displacement function

m_i = mass at the i[th] floor

K_{ij} = the reaction at the i[th] floor, obtained from the bending moment diagram due to the application of unit displacement at the j[th] floor of the conjugate frame.

$$\frac{d^2xj}{dt^2}(t) = acceleration\ of\ the\ mass\ m_i$$

It is assumed that the motion of the frame is simple harmonic and so the displacement function is further defined by

$$X_i(t) = X_i \sin \omega t \tag{2}$$

Where, $x_i = amplitude\ of\ displacement\ of\ mass, m_i$

$\omega = natural\ frequency$

Performing the differentiation in Equation (1) gives:

$$m_i \frac{d^2}{dt^2}(X_i \sin \omega t) + K_{ij}X_i(t) = 0$$

$$-m_i\omega^2 X_i(t) + K_{ij}X_i(t) = 0 \tag{3}$$

Using the amplitude, equation (3) becomes

$$K_{ij}X_i - m_i\omega^2 X_i = 0$$

or

$$\left[K_{ij}X_i - m_i\omega^2\right][X_i] = 0 \tag{4}$$

Gauss reduction which is used to solve equation (4) requires, for a non-trivial solution, that the determinant of the coefficients of X equals zero i.e.

$$\left[K_{ij} - m_i\omega^2\right] = 0 \tag{5}$$

Thus, equation (5) is an eigenvalue problem whose solution yields the natural frequencies

$$\omega_1, \omega_2 \dots \dots \dots \omega_n \tag{6}$$

$where, \quad \omega_1 < \omega_2 < \cdots \omega_n$

3.2. Forced Vibration

The equation of motion for forced vibration is also time dependent and it is obtained by adding the forcing function to equation (3) and replacing the natural frequency with the forcing frequency. Thus,

$$\mathrm{m_i}\theta^2\mathrm{x_i} + \mathrm{k_{ij}}X_i(\mathrm{t}) + R_{ip}(\mathrm{t}) = 0 \tag{7}$$

Using the amplitudes, equation (7) becomes

$$[K_{ij} - \mathrm{m_i}\theta^2][X_i] + [R_{ip}] = 0 \tag{8}$$

Where, X_i = Amplitude of joint displacement due to forced vibration

θ = forcing frequency

R_{ip} = the reaction at the i[th] floor obtained from the bending moment diagram due to the application of the external load to the conjugate frame.

After obtaining the amplitude of joints displacement from the solution of equation (8) bending moment values, table 2, due to forced vibration are then determined using the relation:

$$M = \sum_{i-1}^{n} M_iX_i + M_p \tag{9}$$

Where,

M = bending moment due to forced vibration, unit = KNM

M_p = bending moment for the conjugate system due to external load, unit = KNM

Xi = amplitude of joint displacement due to forced vibration, units = mm

M_i = bending moment for the conjugate system due to unit translation at i[th] floor level.

4. Methodology

Derivation of fixed end moments due to applied loads for beams with stiffened joints can be facilitated using ideas developed by the author in [9] or making adaptations from the equations deduced by the authors in [14].

Case I: Uniformly distributed load q, on beam fixed at both ends.

$$M_A = \frac{-qL^2}{12}\left[1 + 6\left(\frac{a}{L}\right) + 6\left(\frac{a}{L}\right)^2\right] = \frac{-qL^2}{12}[1 + 6\alpha + 6\alpha^2] \tag{10}$$

$$M_B = \frac{-qL^2}{12}\left[1 + 6\left(\frac{b}{L}\right) + 6\left(\frac{b}{L}\right)^2\right] = \frac{-qL^2}{12}[1 + 6\beta + 6(\beta)^2] \tag{11}$$

Case II: Point load, P, acting within the span of the beam fixed at both ends, fixed end moment is given by:

$$M_A = \frac{-Pdc^2}{L^2}\left[1 + 2\left(\frac{a}{L}\right) + \left(\frac{a}{c}\right)\right] = \frac{-Pdc^2}{L^2}\left[1 + 2\alpha + \frac{a}{c}\right] \tag{12}$$

$$M_B = \frac{-Pdc^2}{L^2}\left[1 + 2\left(\frac{b}{L}\right) + 6\left(\frac{b}{c}\right)\right] = \frac{-Pdc^2}{L^2}\left[1 + 2\beta + \frac{a}{d}\right] \tag{13}$$

For a special case where:

c = d = L/2:

$$M_A = \frac{-PL}{8}\left[1 + 4\left(\frac{a}{L}\right)\right] = \frac{-PL}{8}[1 + 4\alpha] \tag{14}$$

$$M_B = \frac{-PL}{8}\left[1 + 4\left(\frac{b}{L}\right)\right] = \frac{-PL}{8}[1 + 4\beta] \quad (15)$$

$$M_{(1/2)} = \frac{PL}{8} \quad (16)$$

Where, with respect to figure 1,

a = length of stiffened A end of member.

b = length of stiffened B end of member.

c = distance between the point of application of the concentrated load and the end of flexible length at A side of member.

d = distance between the point of application of the concentrated load and the end of flexible length at B side of member.
α = a/L = stiffened factor at A end of member.
β = b/L = stiffened factor at B end of member.
where, α=β =a/L =b/L

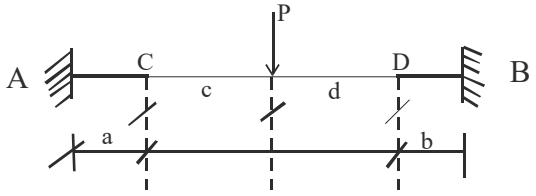

Figure 1: Flexible and stiffened segments of member.

5. Results and Discussion

5.1. Results

Table 1 contains values of bending moment, M_p, of the conjugate system due to external load.
Table 2 depicts bending moment values due to dynamic effect for forcing frequency or function, $\theta, = 5.3\sqrt{EI\ X10^{-3}}$ Rad/sec, for the frame of normal rigid joints and for the frames of stiffened joints. Table 3 presents reactions at imaginary supports due to externally applied loads for the conjugate system. Table 4 contains values of the maximum span moment due to dynamic effect for forcing frequency, $\theta, = 5.3\sqrt{EI\ X10^{-3}}$ Rad/sec for the frame of normal rigid joints and frames of stiffened joints. Table 5 contains values of amplitude of joint displacement due to forced vibration.

Figure 8 is the graph of joint moment, joint 10, due to forced vibration versus stiffening factor,α and β. Figure 9 shows the graph of the maximum span moments due to forced vibration, versus stiffening factors, α and β. Figure 10 presents the graph of joint moment, joint 11, due to forced vibration, versus stiffening factor, α and β. Figure 11 depicts the graph of joint moment, joint 12, due to forced vibration, versus stiffening factor, α and β. Figure 12 shows the graph of amplitude of joint displacement due to forced vibration versus stiffening factor, α and β.

5.2. Discussion

- With joint stiffening of double-bay frames, the bending moments due to dynamic effect are greater over the supports than they are at the mid-spans and hence the beam does not materially affect the stresses. This is more pronounced with increase in length of stiffening, tables 2 and 4. This very trend is in consonance with fundamental characteristics of the continuous beam structure.
- Values of bending moment over the supports due to dynamic effect, especially with respect to the horizontal members, are smaller for the frame with normal rigid joints than they are for the frames with stiffened joints, table 2, figures 8, 10 and 11. In figure 10, $M_{11\text{-}8}$ tends to exhibit a response that suggests closeness to effect of 'beating' on the central column joint of the first upper floor level.
- Values of bending moment at the spans due to dynamic effect are smaller for the frames with stiffened joints than they are for the frame with normal rigid joints table 4, and figure 9.
- The maximum span moments due to dynamic effect decreased progressively with increase in stiffening lengths in such a manner that between stiffening lengths of 425mm and 775mm, this trend passed through zero and migrated to negative values for the frame of stiffened length of 775mm, table 4, and figure 9. This trend suggests an optimal length of stiffening, say lo, exists at which the span moment would hit zero value. This means there must be a stiffening length versus the flexible length at which zero span moments would occur.
- This optimal stiffening length could enable optimal extension of column-free spaces in situations needing as large a column-free space as possible.
- From table 5, it would be observed that joint displacement decreased with increase in joint stiffening. This establishes that joint stiffening increases stability for double-bay building frames.
- Support moments increase with increase in stiffening factor, figures 8, 10 and 11.
- Span moments decrease with stiffening factor, figure 9.

6. Conclusion

On account of diminishing maximum span moment with joint stiffening, stiffening of joints of double-bay frame structure can be utilized to achieve large column-free spaces in building structures and structures of other relevant constructed facilities where, in the first place, large column-free spaces were functionally needed.

One of the benefits derivable from joint stiffening of double-bay frames is not reduction in end, i.e.; support moments, but in the reduction of the maximum span moments even to the barest minimum values.

Since joints stiffening of double-bay multi-storey building frames can bring about shifting or transforming of span moments from positive values, through zero, to negative values, table 4 and figure 9, then, joints of infinite rigidity: (i) substantially reduce deflection; (ii) increase deflection ductility and energy ductility of flexural members as from the instance of substantial reduction in positive span moments; (iii) yields far insignificant a deflection scenario at zero span moments; and (iv) further pushes back the

frontiers of deflection concerns for the beams when the span moments are at negative values.

Joint stiffening significantly reduces dynamic joint displacements, table 5, and figure 12, hence, enhances buckling resistance of vertical members. This leads to greater structural stability.

7. Recommendation

Where beams of double-bay multi-storey frames are of reinforced concrete, the span reinforcement due to dynamic effect should be conceived in terms of double reinforcement.

This is because span moments, depending on the stiffening lengths versus flexible lengths provided, can shift from positive value stance to the negative value stance, when operating within dynamic regime scenario.

8. Area for Further Investigation

This lies in establishment of functional relationship between stiffening lengths, flexible lengths and the overall lengths of beam spans for double-bay frames of stiffened joints so as to achieve as large a column-free space as necessary for design and construction of double-bay framed structures.

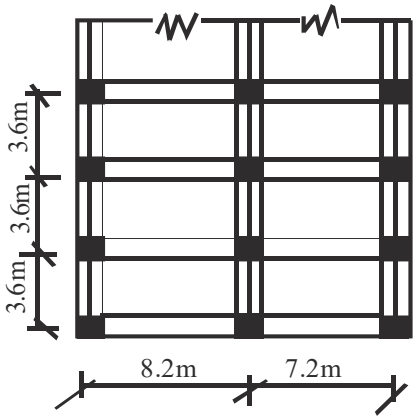

Figure 2: Plan of double-bay multi-storey building framed structure

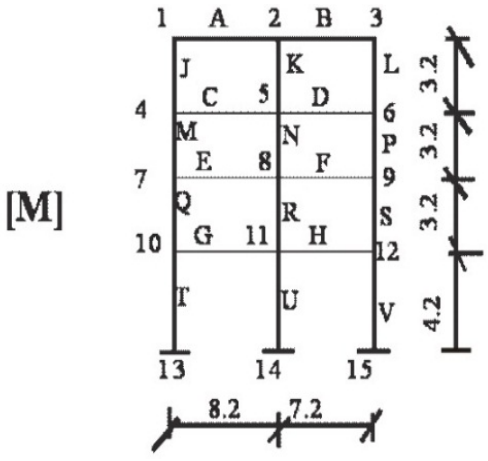

Figure 3: Double-bay four-storey normal rigid building frame

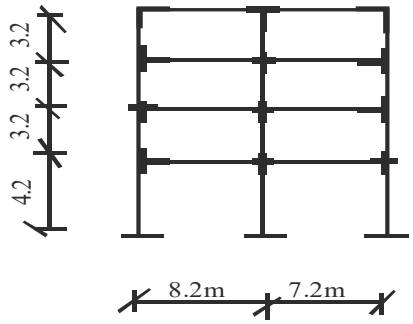

Figure 4: Double-bay four-storey building frame with stiffened joints.

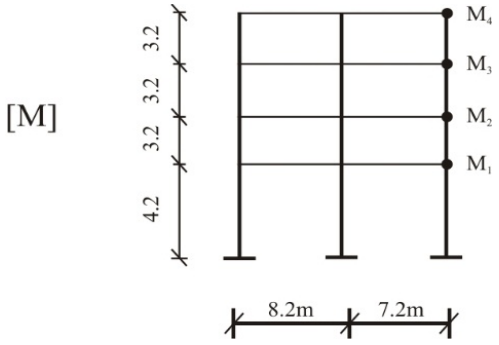

Figure 5: Dynamic model for the double-bay four-storey building frame

$q_1 = q_2 = q_3 = 45$ KN/m

$q_4 = 32$ KN/m

$P_1 = P_2 = P_3 = 15$ KN

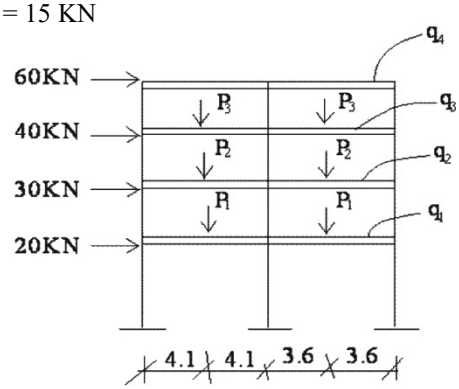

Figure 6: Loading for the conjugate system of the frames

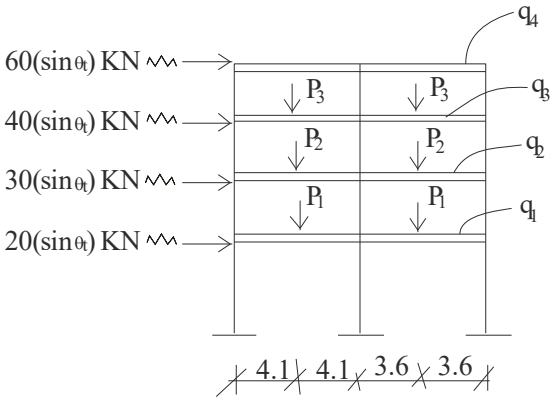

Figure 7: Dynamic loading for the frames

Table 1: Bending moment, M_p, of the conjugate system due to external load for the frames

	Normal Rigid Frame: a=b=0 (KNM)	Stiffened Frame a=b=275mm (KNM)	Stiffened Frame a=b=425mm (KNM)	Stiffened Frame a=b=775mm (KNM)
M_{1-2}	-136.62502	-172.47558	-198.63228	-263.02094
M_{1-4}	-136.62502	-172.47558	-198.63228	-263.02094
M_{2-1}	-203.58353	-246.81158	-277.60053	-340.09485
M_{2-5}	-27.00186	-31.22164	-33.75587	-35.66880
M_{2-3}	-176.58166	-215.58994	-242.84467	-304.43605
M_{3-2}	-94.13145	-123.02986	-144.95843	-205.87282
M_{3-6}	-94.13145	-123.02986	-144.95843	-205.87282
M_{4-1}	106.89054	138.2269	161.87205	226.32273
M_{4-5}	-186.96919	-231.93461	-263.83615	-343.20268
M_{4-7}	-80.07865	-93.71190	-101.96411	-116.87991
M_{5-4}	-217.48193	-260.85209	-290.78084	-362.02720
M_{5-2}	21.56789	25.48206	27.99247	32.29713
M_{5-6}	-179.20534	-217.25063	-244.03847	-308.60470
M_{5-8}	-16.70870	-18.11940	-18.74990	-21.12537
M_{6-3}	76.41084	101.80996	121.56509	178.96965
M_{6-5}	-136.44870	-175.19812	-203.70035	-276.92450
M_{6-9}	-60.03786	-73.38815	-82.13529	-97.95490
M_{7-4}	82.99792	97.43619	106.23188	120.81081
M_{7-8}	-187.0732	-231.68649	-263.43549	-343.58384
M_{7-10}	-104.00609	-134.22557	-157.20359	-222.77299
M_{8-7}	-221.03678	-265.47049	-296.16996	-369.23204
M_{8-5}	17.28348	18.81324	19.50037	21.15220
M_{8-9}	-182.67231	-221.78523	-249.32369	-314.71870
M_{8-11}	-21.08097	-24.87200	27.34590	-33.36115
M_{9-6}	61.38549	75.13015	84.14297	100.60216
M_{9-8}	-136.62009	-175.16930	-203.54165	-277.13180
M_{9-12}	-75.23460	-100.03917	-119.39868	-176.52966
M_{10-7}	122.09500	155.67195	180.58150	249.46969
M_{10-11}	-196.85976	-242.95370	-276.05115	-361.38748
M_{10-13}	-74.764.75	-87.28173	-95.46964	-112.01783
M_{13-10}	37.38238	50.16981	59.11203	80.56297
M_{11-10}	-253.18853	-305.39068	-341.49867	-427.18030
M_{11-8}	24.30368	28.33032	30.85063	36.98969
M_{11-12}	-214.20411	-261.47907	-294.72287	-373.92497
M_{11-14}	-14.68074	-15.58128	-15.92514	-16.26565
M_{14-11}	7.34037	5.68577	9.86039	11.69822
M_{12-11}	141.19614	-179.66665	-208.24449	-283.95688
M_{12-15}	-53.46003	-64.29897	-71.73173	-87.34170
M_{15-12}	26.73002	36.95925	44.41421	62.81595
M_{12-9}	87.73608	115.36768	136.51274	196.61519

Table 2: Bending moment due to dynamic effect for $\theta = 5.3\sqrt{EI\,X10^{-3}}$ Rad/Sec

	Normal rigid Frame: a=b=0 (KNM)	Stiffened Frame a=b=275mm (KNM)	Stiffened Frame a=b=425mm (KNM)	Stiffened Frame a=b=775mm (KNM)
M_{1-2}	-116.03486	-161.60428	-179.20319	-268.24866
M_{1-4}	-116.03486	-161.60428	-179.20319	-268.24866
M_{2-1}	-221.12689	-256.37968	-294.13419	-334.95391
M_{2-5}	-64.16006	-51.78553	-71.86412	-24.07263
M_{2-3}	-156.96699	-204.59211	-222.27504	-310.87573
M_{3-2}	-116.79310	-135.31369	-167.99186	-199.34768
M_{3-6}	-116.79310	-135.31369	-167.99186	-199.34768
M_{4-1}	89.74401	127.93788	147.96153	-225.19658
M_{4-5}	-160.36169	-219.65840	-234.90723	-358.59200
M_{4-7}	-70.61768	-91.72758	-86.94576	-133.39538
M_{5-4}	-241.58140	-272.22151	-318.13336	-347.25584
M_{5-2}	53.58140	44.61527	59.88292	68.63167
M_{5-6}	-151.61094	-204.06030	-211.64822	-327.02729
M_{5-8}	36.70641	-23.54337	-46.60223	88.86021
M_{6-3}	-166.23023	-189.27895	-237.62631	-257.90698
M_{6-5}	95.41714	113.39282	138.38718	178.56129
M_{6-9}	-70.81309	-75.88332	-99.23915	-79.35011
M_{7-4}	57.66173	79.53900	72.83115	126.43404
M_{7-8}	-182.90571	0243.13451	-263.50706	-378.42561
M_{7-10}	-125.24067	-163.57431	-190.67589	-252.05199
M_{8-7}	-224.25507	-254.45280	-295.44738	-334.67612
M_{8-5}	50.54224	37.28057	63.64087	6.18210
M_{8-9}	-179.11818	-234.65492	-250.33966	-358.20544
M_{8-11}	5.40211	17.47681	18.53928	29.70515
M_{9-6}	-141.05426	-161.88435	-203.16814	-233.33765
M_{9-8}	87.71443	93.09982	119.25638	92.96672
M_{9-12}	-53.33984	-68.77864	-83.91176	-140.37095
M_{10-7}	113.80187	168.01851	184.61312	262.13025
M_{10-11}	-231.775506	-277.85320	-318.29110	-419.70351
M_{10-13}	-117.97455	-109.84412	-133.67800	-157-56892
M_{13-10}	187.93779	77.63577	120.24978	152.47587
M_{11-10}	-222.66726	-273.92372	-303.25845	-372.29985
M_{11-8}	16.79523	3.45329	3.93718	17.57228
M_{11-12}	-248.46057	-297.81322	-339.60256	-421.87414
M_{11-14}	42.58854	20.43674	40.28170	52.00670
M_{14-11}	-63.86561	-42.22376	-61.54693	-76.50861
M_{12-11}	-102.54783	-139.95023	-159.45947	-263,14950
M_{12-9}	94.05616	100.17412	128.80553	225.84367
M_{12-15}	-8.49164	-39.77611	-30.65392	-37.30584
M_{15-12}	-38.32551	-5.79360	-53.02507	-12.128187

Table 3: Reactions R_{ip}, at imaginary supports due to externally applied loads for the conjugate system.

	Normal Rigid Frame: a=b=0 (KN)	Stiffened Frame a=b=275mm (KN)	Stiffened Frame a=b=425mm (KN)	Stiffened Frame a=b=775mm (KN)
R1P	-6.10088	-7.28869	-8.05812	-9.13382
R2P	4.18562	5.86440	7.14125	9.91980
R3P	-2.52118	-3.89780	-5.00249	-7.94773
R4P	2.44925	2.33683	3.38925	4.26989

Table 4: Maximum Span Moment Due to Dynamic Effect for $\theta = 5.3\sqrt{EI\ X10^{-3}}$ Rad/Sec

	Normal Rigid Frame: a=b=0 (KNM)	Stiffened Frame a=b=275mm (KNM)	Stiffened Frame a=b=425mm (KNM)	Stiffened Frame a=b=775mm (KNM)
M_{1-2}	113.88439	73.01301	46.27978	-20.60809
M_{2-3}	77.96550	45.82138	20.11064	-37.11031
M_{4-5}	119.22989	74.09292	43.86895	-32.92392
M_{5-6}	88.26692	50.51787	22.55022	-44.67972
M_{7-8}	130.41961	85.20633	54.52278	-22.55085
M_{8-9}	98.91377	60.84072	32.24611	-35.36522
M_{10-11}	138.7784	90.11540	55.22522	-30.00167
M_{10-12}	110.11582	67.31541	37.92739	-65.14092

Table 5: Amplitude of Joint Displacement Due to Forced Vibration

Stiffening factor	Joint Displacement (mm) X_1	X_1	X_3	X_4
a= b = 0 α= β = 0	4.94	5.86	6.07	8.36
a= b = 275 α= β = 0.044	3.30	4.63	5.03	6.52
a= b = 425 α= β = 0.064	2.77	3.54	4.28	5.24
a= b = 775 α= β = 0.134	1.85	2.02	3.04	4.12

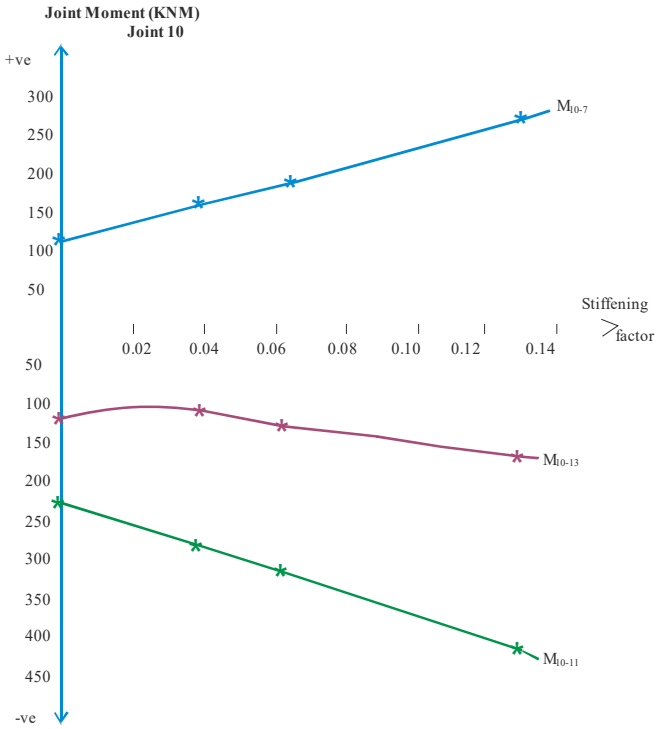

Figure 8: Graph of joint moment due to forced vibration, dynamic effect, versus stiffening factor, α and β.

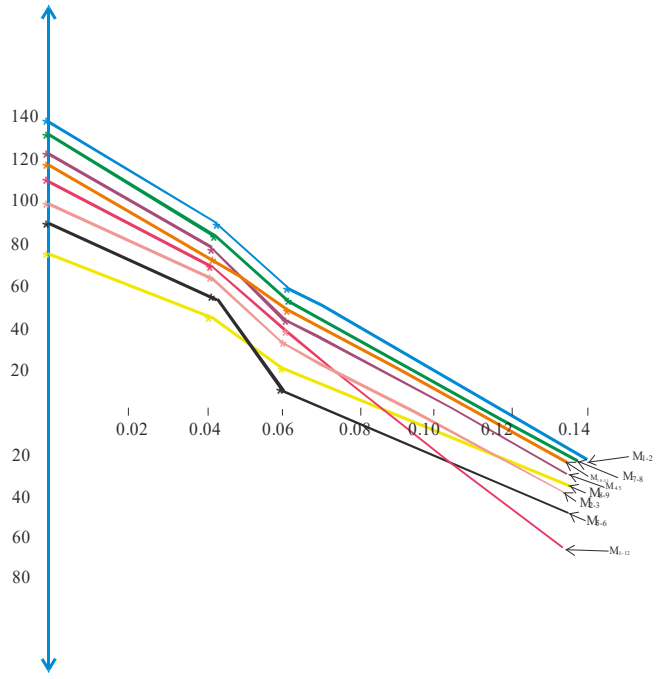

Figure 9: Graph of maximum span moments due to dynamic effect, versus stiffening factor, α and β.

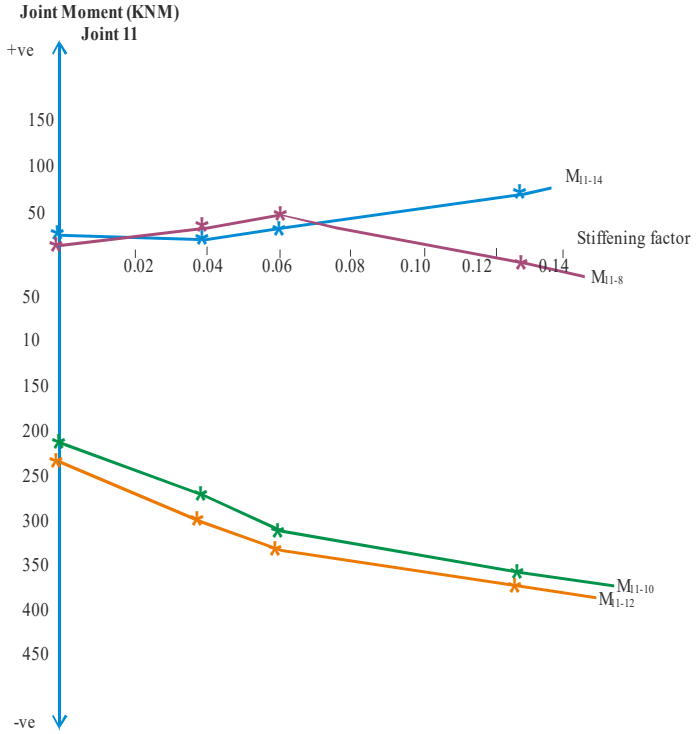

Figure 10: Graph of joint moment, joint 11, due to forced vibration, dynamic effect, versus stiffening factor, α and β.

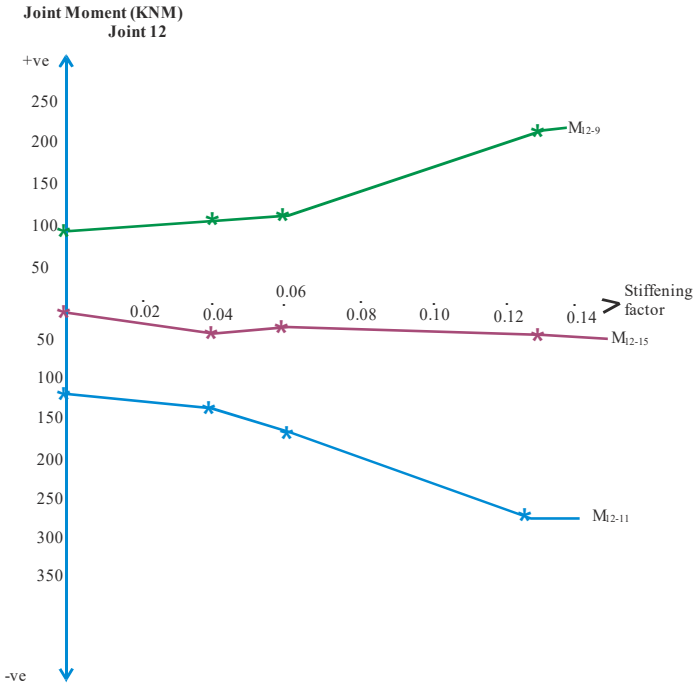

Figure 11: Graph of joint moment, joint 12, due to forced vibration, dynamic effect, versus stiffening factor, α and β.

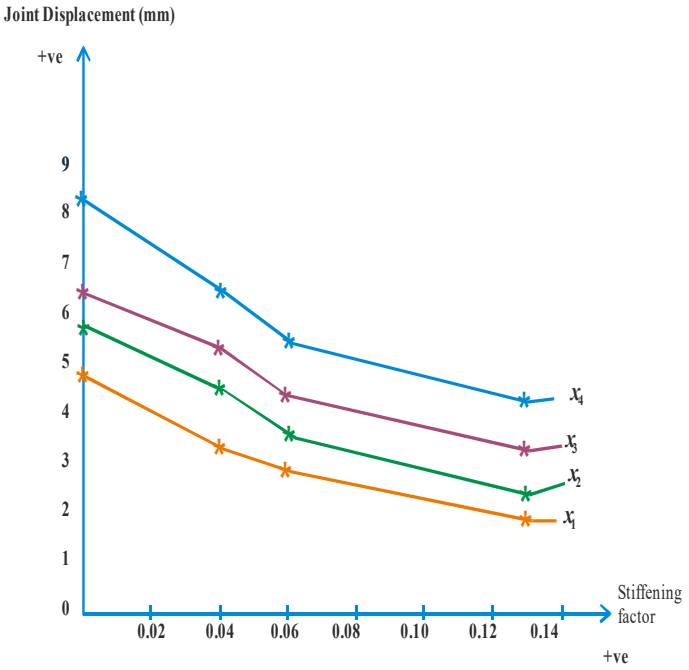

Figure 12: Graph of amplitude of joint displacement due to forced vibration, dynamic effect, versus stiffening factor, α and β.

References

[1] Bhatt, P., Programming the Matrix Analysis of Skeletal Structures, Ellis Horwood Limited, England, 1986.

[2] Bachmann, H., Ammann, W. J.,Dejschl, F., Elsenwan, J.,Floegl, I., Hirsch, G. H., Kiew, G. K., Iande, G. J., Maurenhltz, O., Natky, H. G., et al, Vibration Problems in Structures, BirkhauserVerlag, Basel, 1995.

[3] Chopra, A. K., Dynamics of Structures Theory and Application to Earthquake Engineering, Pearson, New Delhi, 2012.

[4] Mbanusi, E. C. and Obodoh, D. A., Free Vibration Response of Double-Bay Multi-Storey Building Frames with Stiffened Joints, Int'l J. of Engineering and Computer Science, Vol. 5, Issue 5, May 2016, pp. 16620 – 16638.

[5] Sundararajan, C. R., Structural Vibration Analysis, Design and Troubleshooting. http://www.training.bossintl/com/htmstructural-vibration-analysis.htm/11/1/2006.

[6] Thomson, W. T., Theory of Vibration with Application, third ed. CBS Publishers and Distributors, Delhi, 2007.

[7] Polyakor, S. V., Design of Earthquake Resistant Structures, Mir Publishers, Moscow, 1985.

[8] Hemant, B. K., Durgesh, C. R. and Sudhr, K. J., A case for use of Dynami Analysis in Designing for Earthquake Forces, Scientific Corresponding. www.iitk.ac.in/nicee/RP/2006,dynamic-analysis-current-sciencepdf,2006.

[9] Osadebe, N. N., Stress Analysis of Frames with Stiffened Joints, Proceedings on the 4th International Conference on Structural Engineering Analysis and Modeling, SEAM, Accra, 1997, pp. 136 – 145.

[10] Masur, E. F., "Discussion on Effect of Joint Rotation on Dynamics of Structures" ASCE, Mechanics Division, Vol. 88, 1962, pp. 83 – 85.

[11] David, J., Advanced Structural Mechanics, Thomas Telford, London, 2000.

[12] Anya, C. U., "Dynamic Analysis of Tall Buildings", M. Eng. Thesis, Department of Civil Engineering, University of Nigeria, Nsukka, Nigeria, 1995.

[13] Aminu, B. N. "Matrix Analysis of Multi-Storey Building Frame with Stiffened Joints", M. Eng. Dissertation, Department of Civil Engineering, Enugu State University of Science and Technology, Enugu, Nigeria, 1995.

[14] Ezeokpube, G. C. and Osadebe, N. N., "Effects of Joint Stiffening on the Dynamic Response of Frames", Nigerian J. of Technology, NIJOTECH, Vol. 29 No. 1, March, 2010, pp. 1-8.

Advances in Science, Technology and Engineering Systems Journal Vol. 2, No. 4, 78-91 (2017)

www.astesj.com

ASTESJ

ISSN: 2415-6698

The main characteristics of five distributed file systems required for big data: A comparative study

Akram Elomari*, Larbi Hassouni, Abderrahim Maizate

RITM-ESTC / CED-ENSEM, University Hassan II, ZIP Code 8012, Morocco

ARTICLE INFO

Article history:
Received: 31 March, 2017
Accepted: 13 June, 2017
Online: 26 June, 2017

Keywords:
Big Data
Data Storage
DFS
HDFS
GFS
AFS
GPFS
Blobseer
BLOB
Data Stripping
Tiered storage

ABSTRACT

These last years, the amount of data generated by information systems has exploded. It is not only the quantities of information that are now estimated in Exabyte, but also the variety of these data which is more and more structurally heterogeneous and the velocity of generation of these data which can be compared in many cases to endless flows. Now days, Big Data science offers many opportunities to analyze and explore these quantities of data. Therefore, we can collect and parse data, make many distributed operations, aggregate results, make reports and synthesis. To allow all these operations, Big Data Science relies on the use of "Distributed File Systems (DFS)" technologies to store data more efficiently. Distributed File Systems were designed to address a set of technological challenges like consistency and availability of data, scalability of environments, competitive access to data or even more the cost of their maintenance and extension. In this paper, we attempt to highlight some of these systems. Some are proprietary such as Google GFS and IBM GPFS, and others are open source such as HDFS, Blobseer and AFS. Our goal is to make a comparative analysis of the main technological bricks that often form the backbone of any DFS system.

1. Introduction

Todays, the amount of data generated during a single day may exceed the amount of information contained in all printed materials all over the world. This quantity far exceeds what scientists have imagined there are just a few decades. Internet Data Center (IDC) estimated that between 2005 and 2020, the digital universe will be multiplied by a factor of 300, this means that we will pass from 130 Exabyte to 40,000 Exabyte, which is the equivalent of 40 billion gigabytes (more than 5,200 gigabytes for each man, woman and child in 2020) [1].

Therefore, the variety and the complexity of this deluge of data, which is often unstructured, are revolutionizing the methods of data management and exploitation of the large quantity of information they convey [2,3].

Traditional data processing technologies have rapidly reached their limits and are being replaced by new systems which allow big data storage and analysis, taking on consideration what is currently known as the four V: Volume (to handle the huge amount of generated data), Velocity (to store, analyze and retrieve huge dataset as quickly as possible), Variety (to process mostly unstructured data, from multiple sources), and Value (to ask the right questions to generate maximum value) [4].

The typical schema of Big Data architecture (e.g. MapReduce) requires partitioning and distributing the processing across as many resources as possible. Otherwise many issues relative to the quantity of processed data can emerge like:

- Big data are slow to move over any network,
- Scaling up vertically (more memory, more powerful hardware) has limitations.
- A single hard drive cannot handle the size of big data.
- Failures in computing devices are inevitable

Move the “processing” into data instead of the opposite can become an obligation rather than a choice. Cloud platforms for

*Corresponding Author: Akram Elomari, RITM-ESTC / CED-ENSEM, University Hassan II, ZIP Code 8012, Morocco | Email: akramelomari@yahoo.fr

example, seem to offer countless benefits to such architecture, among the most important between those advantages is the scalability of the infrastructure that is managed by a fully outsourced service [5].

Distributed storage systems take also the same orientation.

Although the traditional systems such as centralized network-based storage systems (client-server) or the traditional distributed systems such as NFS, managed to meet the requirements of performance, reliability and safety of the data until a certain limit, they are no longer able to respond to the new requirements in terms of volume of data, high performance, and evolution capacities. And besides their constraints of cost, a variety of technical constraints are also added, such as data replication, continuity of services etc… [6,7].

In this paper, we try to discuss a set of the main characteristics of technologies used in the market and we think they are the most relevant and representative of the state of the art in the field of distributed storage. In section II, we start by explaining what Distributed File System (DFS) is. In section III, we discuss some architecture of some DFS systems while presenting the strengths and weaknesses of each of them. In section IV, we present the logic of storage as Blob. In section V, we discuss the technique of data stripping. In section VI, we discuss the issues of concurrency and some technologies used in this field. In section VII we present the tiered storage. We conclude this paper by a benchmark table of five major systems on the market: Andrew File System (AFS), Google File System (GFS), Blobseer, Hadoop Distributed File System (HDFS) and General Parallel File System (GPFS). The comparison focuses on a set of characteristics discussed and explained throughout this paper.

More specifically, our main objective in this paper is to contribute to determine the main characteristics that a Distributed File System must integrate to respond to the multiple requirements of a BIG DATA ecosystem. This study will allow us to well target the part on which we are going to conduct our research to improve the performance of a DFS.

2. What is “Distributed File system (DFS)”

A distributed file system (DFS) is a system that allows multiple users to access, through the network, a file structure residing on one or more remote machines (File Servers) using a similar semantics to that used to access the local file system. It is a client / server architecture where data is distributed across multiple storage spaces, often called nodes. These nodes consist of a single or a small number of physical storage disks.

The nodes generally consist of basic equipment, configured to just provide storage services. As such, the material can be relatively inexpensive.

The disk of each machine may be divided into several segments, and each segment is stored repeatedly (often three times) on different storage spaces, each copy of each segment is a replica.

As the material used is generally inexpensive and by large quantities, failures become inevitable. However, these systems are designed to be tolerant to failure by using the replication technique which makes the loss of one node an event "of low emergency and impact" as the data is always recoverable, often automatically, without any performance degradation.

The architecture of a distributed storage system varies depending on the technological choices driven by the use case. Nevertheless, it must generally observe some basic rules, which are required for the survival of such ecosystem and which can be summarized in the following points [8]:

- Access transparency: The remote file systems are exposed on the client machine like any local file system.
- Localization transparency: The client has no indication -by the file name- about the location of the file space neither if it is a local or remote space file.
- Concurrent access transparency: The file system state is the same for all the clients. This means that if a process is modifying a file, all other processes on the same system or remote systems that access the files see the changes in a consistent way.
- Failure Transparency: Client programs should not be affected by any loss of any node or a server.
- Heterogeneity: The File service needs to be supported by different hardware platforms and operating systems.
- Scalability: The file system should work in small environments (one to a dozen machines) as well as in large environments (hundreds or even tens of thousands of systems).
- Replication transparency: To support scalability, files must be replicated on multiple servers; transparently to clients (the system is on charge to create and maintain a designed number of replicas automatically).
- Migration transparency: any file movement in the system for management purposes should be transparent to the clients.
- Support fine-grained distribution of data: To optimize performance, the individual objects need to be located near the processes that use them.
- Tolerance for network partitioning: The file system should be tolerant to the fact that the entire network or certain segments of it may be unavailable during certain periods.

In this paper, we compare five distributed file systems: AFS, GFS, Blobseer, HDFS and GPFS. The choice to compare only those specific systems, despite of the fact that the market includes dozens of technologies, is particularly led by two reasons:

1. Our main objective is to study by focusing on the main features of the most Data File Systems required for a Big Data context. It is technically difficult to study all systems in the market in order to know their technical specifications, especially as lots of them are proprietary and closed systems. Even more, the techniques are similar in several cases and are comparable to those of the five we compare in this paper. The best known and not included in our paper because of that are: Amazon S3 File System,

OCFS (Oracle Cluster File System), GFS2 (Red Hat), VMFS (Virtual Machine File System by VMware).

2. These five systems allowed us to make a clear idea about the state of the art of this domain, thanks to the following particularities:

- AFS (Andrew File System) is a system that can be considered as a bridge between conventional systems such as NFS and advanced distributed storage systems. His big advantage is that it is available on a wide range of platforms: AIX, Mac OS X, Darwin, HP-UX, Irix, Solaris, Linux, Microsoft Windows, FreeBSD, NetBSD and OpenBSD.
- GFS (Google File System) is a proprietary system used internally by Google, which is one of the leading innovating companies. Google aims to manage huge quantities of data because of its activities.
- Blobseer is an open source initiative, particularly driven by research as it is maintained by INRIA Rennes. Blobseer choices, especially in the area of concurrency, are very interesting as discussed hereafter.
- HDFS (Hadoop Distributed File System), which is a subproject of HADOOP, a very popular Big Data system, is considered as a reference in this domain. It is therefore interesting to review its mechanisms and compare them to the other DFS systems.
- GPFS (General Parallel File System) is a system developed by IBM, a global leader in the field of Big Data. IBM commercializes this system as a product.

By choosing those five systems, we tried to make sure to have an illustration of these specific initiatives:

- Open source initiatives (BlobSeer, AFS, HDFS),
- Academic initiatives (BlobSeer)
- Big Data leader's initiatives (IBM GPFS, Google GFS)
- Business market initiatives (IBM GPS)

We think that considering these four initiatives can help to make a clear idea about the main orientations in the market of distributed storage today.

3. DFS architectures

In the following, we study the architecture of each of the five systems in order to explore the mechanisms and architectural choices of each of them and thus understand the reasons which justify these choices.

3.1. Andrew File System (AFS) architecture

A standard system that supports some characteristics of this kind of architecture is AFS.

AFS (or Open AFS currently) is a distributed file system originally developed by Carnegie Mellon University (as part of the Andrew Project. Originally named "Vice", AFS is named after Andrew Carnegie and Andrew Mellon). It is supported and developed as a product by Transarc Corporation (now IBM Pittsburgh Labs). It offers client-server architecture for federated file sharing and distribution of replicated read-only content [9].

AFS offers many improvements over traditional systems. In particular, it provides the independence of the storage from location, guarantees system scalability and transparent migration capabilities. AFS can be deployed on a wide range of heterogeneous systems, including UNIX, Linux, MacOS X and Microsoft Windows.

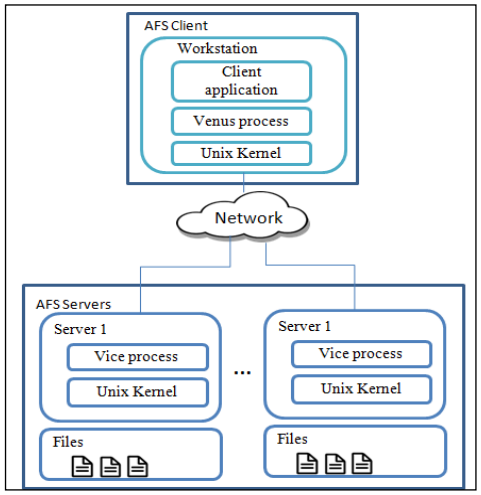

Figure 1 : AFS Design

As shown in Figure 1, the distribution of processes in AFS can be summarized as follows:

• A process called "Vice" is the backbone of the system; it is composed by a set of dedicated file servers and a complex LAN.

• A process called "Venus" runs on each client workstation; it mediates access to shared files. Venus gets the requested files from the vice process and keep them in the local cache of the client. Venus also emulates a "UNIX like" file system access semantic on the client station. "Vice" and "Venus" processes work in the back ground of the client workstation process, so the client sees a normal UNIX file system [10].

To better manage the transfer of files between servers and clients, AFS assumes the following hypothesis [11]:

- Concerned files remain unchanged for long periods;
- Those files will be updated only by their owners;
- A large local cache is enough to contain all the client files;
- Generally concerned files are of small size, less than 10 Kbytes;
- Read operations are more common than write operation;
- The sequential access is usually more common than random access;
- Most of the files are used by a single user, their owner;

- Once the file has been used, it will likely be used again in the near future.

These assumptions led AFS to adopt a fairly simple caching mechanism based on these two main elements:

- The whole content of directories and files are transferred from the server to the client (in AFS-3 by pieces of 64 kilobytes)
- Caching whole file: when the file is transferred to the client, it will be stored on the local client disk (client cache)

Using the client cache may actually be a good compromise to improve system performances, but it will only be effective if the assumptions that the AFS designers have adopted are respected. Otherwise, this massive use of the cache may compromise the data integrity.

3.2. Google File System (GFS) architecture

Another interesting approach is that adopted by GFS, which does not use cache at all.

GFS is a distributed file system developed by Google for its own applications. Google GFS system (GFS cluster) consists of a single master and multiple Chunkservers (nodes) and can be accessed by multiple clients, as shown in Figure 2 [12].

Each of these nodes is typically a Linux machine running a server process at a user level. It is possible to run both a Chunkserver and a client on the same machine if its resources allow it.

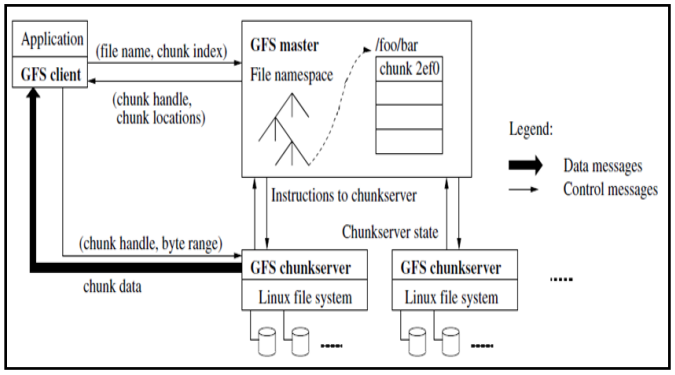

Figure 2 : GFS Design

The files to be stored are divided into pieces of fixed size called "chunks". Each "chunk" is identified by an immutable and unique “Chunk Handle” of 64 bits, assigned by the Master at its creation. The Chunkservers store chunks on local disks as Linux files, and manage to read or write a chunk using her Chunk Handle associated with a byte range.

The chunks are replicated on several Chunkservers. By default three replicas are stored, although users can designate a different number of replications if needed.

The "master" server maintains all metadata of the file system. This includes the namespace, access control information, the mapping from files to chunks and locations of existing chunks. It also controls the operations of the entire system, such as the selection and management of the master copy of a chunk (chunk lease), garbage collection (orphan chunks) and the migration of chunks between Chunkservers. The master communicates periodically with each Chunkserver to give instructions and collect its state.

The GFS client code uses the API of the file system. It communicates with the master and Chunkservers to read or write data. Clients interact with the master regarding transactions related to metadata, but all communications relating to the data themselves goes directly to Chunkservers.

Unlike AFS, neither the client nor the Chunkserver use a dedicated cache. Caches, according to Google, offer little benefit because most applications use large files or large work spaces which are too big to be cached. Not using the cache can simplify the work of the client and also the entire system by eliminating the cache coherence issues. The only exception to this rule is the metadata which can be cached on the client station. The Chunkservers does not need to use cache because the chunks are stored as local files and thus benefit from the "cache" of the Linux buffer that "cache" frequently accessed data in memory.

GFS was able to manage the failure possibility related to the cache coherence that can be noticed on AFS. But using a single master in the architecture of GFS is a real challenge; its involvement in read and write operations should absolutely be controlled so that it does not become a bottleneck. Google has tried to reduce the impact of this weak point by replicating the master on multiple copies called "shadows". These replicas are a backup of the master and better yet they can be accessed in read-only and so allowing access even when the master is down.

Google measured performance on a GFS cluster consisting of one master, two master replicas, 16 chunkservers, and 16 clients. All the machines are configured with dual 1.4 GHz processors, 2 GB of memory, two 80 GB 5400 rpm disks, and a 100 Mbps full-duplex Ethernet connection to an HP 2524 switch.

The test conditions was for 15 concurrent client accessing simultaneously N distinct files to read or write 1 GB of data

Read Average throughput: 90 MB/s

Write Average throughput: 34 MB/s

3.3. Blobseer architecture

Blobseer is a project of KerData team, INRIA Rennes, Brittany, France. The main features of Blobseer are:

- Storage of data in BLOBs,

- Data segmentation,
- Management of distributed metadata
- Control of concurrency based on a versioning mechanism.

The data stored by Blobseer is wrapped in a level of abstraction that is a long sequence of bytes called BLOB (Binary Large Object) [13].

Blobseer has focused on the problems posed by the master in GFS and HDFS, but also on competitive access to data.

The Blobseer system consists of distributed processes (Figure 3), which communicate through remote procedure calls (RPC). A physical node can run one or more processes and can play several roles at the same time.

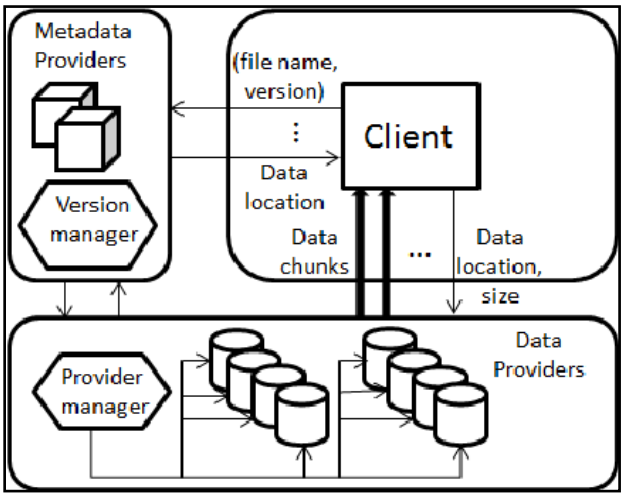

Figure 1 : Blobseer Design

The bricks of Blobseer are:

- Data providers: The data providers physically store the chunks. Each data provider is simply a local key-value store, which supports accesses to a particular chunk given a chunk ID. New data providers may dynamically join and leave the system.
- Provider manager: The provider manager keeps information about the available storage space and schedules the placement of newly generated chunks. It employs a configurable chunk distribution strategy to maximize the data distribution benefits with respect to the needs of the application. The default strategy implemented in Blobseer simply assigns new chunks to available data providers in a round-robin fashion.
- Metadata providers: The metadata providers physically store the metadata that allow identifying the chunks that make up a snapshot version of a particular BLOB. Blobseer employs a distributed metadata management organized as a Distributed Hash Table (DHT) to enhance concurrent access to metadata.
- Version manager: The version manager is in charge of assigning new snapshot version numbers to writers and to unveil these new snapshots to readers.
- The version manager is the key component of Blobseer, the only serialization point, but is designed to not involve in actual metadata and data Input/output. This approach keeps the version manager lightweight and minimizes synchronization.
- Clients: Blobseer exposes a client interface to make available its data-management service to high-level applications. When linked to Blobseer's client library, application can perform the following operations: CREATE a BLOB, READ, WRITE, and APPEND contiguous ranges of bytes on a specific BLOB.

Unlike Google GFS, Blobseer does not centralize access to metadata on a single machine, so that the risk of bottleneck situation of this type of node is eliminated. Also, this feature allows load balancing the workload across multiple nodes in parallel.

Since each BLOB can be stored as fragments over a large number of storage space providers, some additional metadata are needed to map sequences of BLOB. Although these additional metadata seem to be insignificant compared to the size of the data itself, on a large scale it represents a significant overhead. In those conditions, traditional approaches which centralize metadata management reach their limits.

Therefore, Blobseer argues for a distributed metadata management system, which brings several advantages:

- Scalability: A distributed metadata management system is potentially more scalable and open to concurrent accesses, This scalability can also cover the increase of the size of metadata.
- Data availability: Since metadata can be reproduced and distributed to multiple metadata providers, this avoids having a single centralized metadata server which then provides a single point of failure.

In addition, the implementation of the versioning mechanism via the «version manager» improves significantly the processing of concurrent access (as seen in Concurrent access paragraph).

A set of experiments was carried out on the Rennes cluster of the Grid'5000 platform [14,15]. The used nodes are interconnected through a 1 Gbps Ethernet network, each node being equipped with at least 4 GB of memory. The BlobSeer deployment consists of one version manager, one provider

manager, one node for the namespace manager. A BlobSeer chunk size of 32 MB was fixed, as previous evaluations of BlobSeer have shown this value enables the system to sustain a high-throughput for multiple concurrent data transfers. The test concerns the writing and reading of 2 GB and the Average throughput was measured:

Read Average throughput: 52 MB/s

Write Average throughput: 62 MB/s

The installation of a platform under Blobseer is of moderate difficulty. The preparation of the packages and their deployment is not very complicated but optimizations and tuning (snapshots, versioning, and concurrent accesses) require several tests.

3.4. Hadoop Distributed File System (HDFS)

A standard system that supports some characteristics of this kind of architecture is AFS. Hadoop Distributed File System (HDFS) is a distributed file system component of the Hadoop ecosystem. The Apache Hadoop software library is a framework that allows distributing the processing of large data sets across clusters of computers using simple programming models[16].

HDFS is designed to run on commodity hardware, it is highly fault-tolerant and is designed to be deployed on low-cost hardware. HDFS also provides high throughput access to application data and is suitable for applications that have large data sets. It relaxes a few POSIX requirements to enable streaming access to file system data[17].

As shown in figure 4, HDFS stores file system metadata and application data separately. Like other distributed file systems, HDFS stores metadata on a dedicated server, called the NameNode. Application data are stored on other servers called DataNodes. All servers are fully connected and communicate with each other using TCP-based protocols. The DataNodes in HDFS do not use data protection mechanisms such as RAID to make the data durable. Instead of that, the file content is replicated on multiple DataNodes for reliability. While ensuring data durability, this strategy has the added advantage that data transfer bandwidth is multiplied, and there are more opportunities for locating computation near the needed data [18].

HDFS is designed to reliably store very large files across machines in a large cluster. It stores each file as a sequence of blocks; which are the same size except the last one. The blocks of a file are replicated for fault tolerance. Files in HDFS are write-once and have strictly one writer at any time [19].

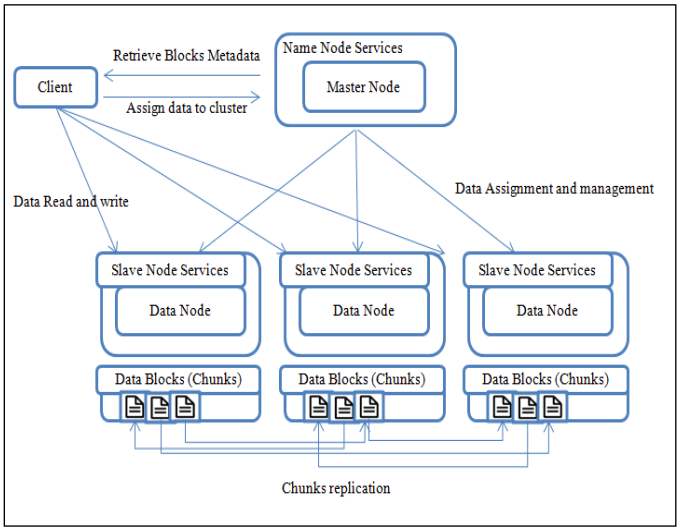

Figure 4: HDFS Design

An HDFS client wanting to read a file first contacts the NameNode for the locations of data blocks comprising the file and then reads block contents from the DataNode closest to the client. When writing data, the client requests the NameNode to nominate a suite of three DataNodes to host the block replicas. The client then writes data to the DataNodes in a pipeline fashion. The current design has a single NameNode for each cluster. The cluster can have thousands of DataNodes and tens of thousands of HDFS clients per cluster, as each DataNode may execute multiple application tasks concurrently.

Since the NameNode is unique in the cluster, saving a transaction to disk becomes a bottleneck for all other threads which have to wait until the synchronous operations initiated by one of them are complete [21]. In order to optimize this process the NameNode batches multiple transactions initiated by different clients. When one of the NameNodes threads initiates a flush-and-sync operation, all transactions batched at that time are committed together. Remaining threads only need to check that their transactions have been saved and do not need to initiate a flush-and-sync operation.

Regarding the performance, a basic test was performed on a test cluster composed by 8-nodes. The first 5 nodes of this Hadoop cluster provided both computation and storage resources (as Data Node servers). One node served as Job Tracker (Resource-Manager) and one node served as NameNode storage manager. Each node is running at 3.10 GHz CPU, 4GB RAM and a gigabit Ethernet. All nodes used Hadoop framework 2.4.0.

The test concerns the writing and reading of 10 GB of data and the average i/o rate was measured by TestDfsIO tool

“Write” Average i/o rate = 65 mb/s

“Read” Average i/o rate = 75 mb/s

The HDFS system remains simple enough to set up and manage, to add or to delete a node it needs the preparation of the post concerned and the change of some configuration files. Web interfaces make it possible to easily monitor the general condition of the nodes and even the distribution of the storage or the size of the chunks used.

Recompile the code on a particular machine can be more complicated but remains relatively simple for a system administrator.

3.5. General Parallel File System (GPFS)

A standard system that supports some characteristics of this kind of architecture is AFS. The General Parallel File System (GPFS) is a cluster developed by IBM which provides concurrent access to a single or set of file systems from multiple Storage Area Network (SAN) or network attached nodes [22].

GPFS is highly scalable and enables very high performances and availability thanks to a variety of features like data replication, policy based storage management, and multi-site operations. GPFS cluster can be deployed under AIX (Advanced IBM Unix), Linux or Windows server nodes. It can also be deployed on a mix of some or all those operating systems. In addition, multiple GPFS clusters can share data locally or across wide area network (WAN) connections [23].

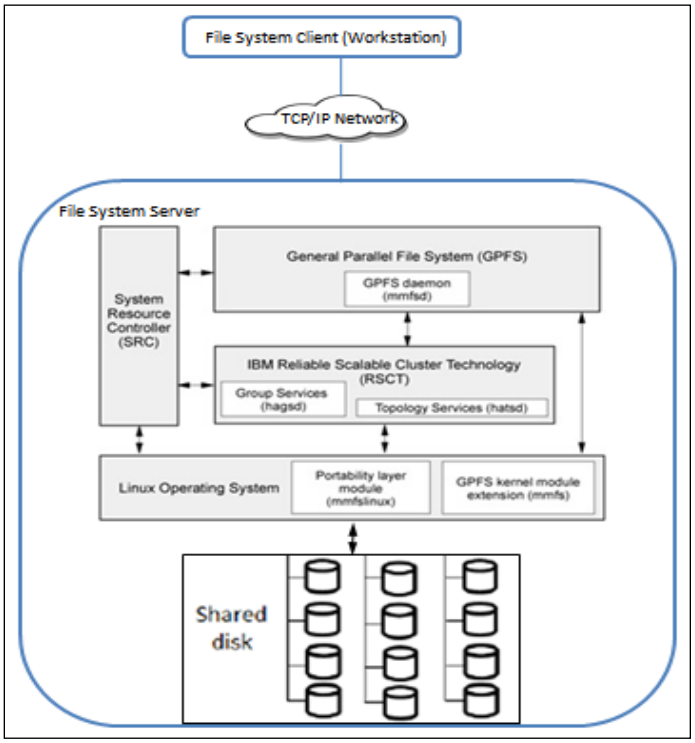

Figure 5: GPFS Design

GPFS uses the Network Shared Disk (NSD) protocol over any TCP/IP capable network fabric to transfer data to the client file system.

On the other side, GPFS server architecture is based on four modules as illustrated in Figure 5, which manage the shared disks

System resource controller (src): The main purpose of the System Resource Controller is to give to the system manager or a developer a set of commands and subroutines by which he can control and interact with the subsystems of the GPFS cluster.

GPFS daemon (mmfsd): The GPFS daemon is charged of all I/O and buffers for GPFS, this include all read/write synchronous /asynchronous operations. To grant data consistency of the system, the daemon uses a token management system. On the other hand, the Daemon manages multi threads to ensure the priority to some critical processes and protect the whole system from lagging because of some intensive routines.

The daemons running on all the nodes of one cluster keep communicating with each other to insure that any configuration changes, recovery or parallel updates of the same data structures is shared between all of them.

RSCT daemons: GPFS uses Two RSCT daemons:

- The Group Service RSCT daemon (**hagsd**) ensures a distributed coordination and synchronization with the other subsystems.

- The Topology Service RSCT daemon (**hatsd**) insures providing other subsystems with network adapter status, node connectivity information, and a reliable messaging service.

Linux Operating system : Under Linux, GPFS need to run two modules:

- Portability layer module **(mmfslinux):** This module enables communication between Linux Kernel and GPFS kernel, based on hardware platform particularity and Linux distribution specifications.

- Kernel extension **(mmfs)**: which provides mechanisms to access a file system where data is physically stored from the client operating system transparently. In fact, GPFS appear to the client like any other local file system. When any application makes a call to any file system, this call is transmitted by the client Operating system into GPFS kernel extension. The kernel extension can respond to any file system call, by using the local resources if exists, or make a request to GPFS daemon if not.

GPFS have many specific features that make it very scalable and efficient:

- A GPFS cluster can integrate and optimize the use of different disk drives with different performances;

- GPFS use data striping across disks therefore the spreading of any processing over the cluster is possible;

- Metadata management is optimized to avoid the unnecessarily access to the server;

- GPFS uses caches on the client side to increase throughput of random reads;

- GPFS allows access to files from multiple programs on read and write mode;

- GPFS improves query languages such as Pig and Jaql by providing sequential access that enables fast sorts.

On the other hand, GPFS eliminates the risk of a single point of failure because the architecture is based on the following attributes:

- Distributed metadata;

- Replication of both metadata and data;

- Minimum number of nodes (quorum);

- The recovery and reassignment of failed node is automatic;

- GPFS provides a fully POSIX semantic;

- Workload isolation;

- Enhanced Security thanks to a native encryption, stronger cryptographic keys and more robust algorithms (NIST SP800-131a);

- Provides cluster-to-cluster replication over a wide area network.

All those features make GPFS a very scalable and high available system, but it does not seem to be designed for low cost hardware platforms unlike the GFS or Blobseer for example. Nevertheless, it remains proposing interesting mechanisms for data caching or parallel access to files.

4. Data Storage as Binary Large Object (blob)

The architecture of a distributed storage system can predict and improve the accessibility of files on storage spaces. It also enables the system design scalability and resilience to the risk of failures that amplify with the quality of equipment in use. However, among the main criteria that a distributed storage system must take into consideration is how files are stored on the disks.

In fact, we are talking about applications that process large quantities of data, distributed on a very large scale. To facilitate the management of data in such conditions, one approach is to organize these data as objects of considerable size. Such objects, called Binary Large Objects (BLOBs), consist of long sequences of bytes representing unstructured data and can provide the basis for a transparent data sharing of large-scale. A BLOB can usually reach sizes of up to 1 Tera Byte.

Using BLOBs offers two main advantages:

- The Scalability: Applications which deal with data sets that grow rapidly to easily reach around terabytes or more, can evolve more easily. In fact, maintaining a small set of huge BLOBs including billions of small items in the order of a few Kbytes is much easier than directly managing billions of small files of a few kilobytes. In this case, the simple mapping between the application data and file names can be a big problem compared to the case where the data are stored in the same BLOB and that only their offsets must be maintained.
- The Transparency: A data management system based on shared BLOBs, uniquely identifiable through ids, relieves application developers of the burden of codifying explicitly management and transfer of their locations. The system thus offers an intermediate layer that masks the complicity of access to data wherever it is stored physically [24].

5. Data striping

Data striping is a well-known technique for increasing the data access performance. Each stored object is divided into small pieces that are distributed across multiple machines over the storage system. Thus, requests for access to data may be distributed over multiple machines in parallel, allowing achieving high performances. Two factors must be considered in order to maximize the benefits of access to the distributed data:

- A configurable Strategy of distribution of chunks: Distribution strategy specifies where to store the chunks to achieve a predefined goal. For example, load balancing is one of the goals that such strategy can allow. By storing the chunks on different machines, we can parallelize the concurrent access to the same object and therefore improve performances. More complex scenarios are conceivable, for example optimizing access by geographical location or by the characteristics of storage machines (place the most requested chunks on the most powerful machines ...)[25,26]
- Dynamic configuration of the size of the chunks: The performance of distributed data processing is highly dependent on how the calculation is distributed and planned on the system. Indeed, if the chunks size is too small, applications must then retrieve the data to be processed from several chunks because of increasing probability of that the size of these data requires a high number of chunks. On the other hand, the use of too large chunks will complicate simultaneous access to data because of the increasing probability that two applications require access to two different data but both stored on the same chunk. A compromise will have to be made regarding the size of chunks to enable a balance between performance and efficiency of such system.

The majority of systems that use this type of architecture, such as Google GFS, HDFS or Blobseer use a chunk size of 64 MB that seems to be the most optimized for those two criteria.

6. Concurrency

Processing concurrency is very dependent on the nature of the desired data processing and the nature of data changes. It's clear that the Haystack system which manages Facebook pictures that do not changes during their lives [27], will be different from Google GFS or IBM GPFS which are intended to manage more dynamic data.

The "lock" is a known method to solve this type of problems, which is used by many DFS including GPFS.

The General Parallel File System (GPFS) propose a parallel access mechanism using block level locking based on a very sophisticated scalable token management system. This mechanism provides data consistency while allowing concurrent access to the files by multiple application nodes. A token server manages the lock acquisition and the lock revocation, and between these too operations only the system that has the lock can modify the file.

It is clear that in case of very large file, the lock operation can cause a considerable loss of time. Fortunately, IBM has developed a sophisticated mechanism that allows locking byte ranges instead of whole files/blocks (Byte Range Locking) [28]

GFS meanwhile, offers a relaxed consistency model that supports Google highly distributed applications, but is still relatively simple to implement. Practically all Google applications mutate files by appending rather than overwriting. The mutation operations on GFS are atomic. They are treated exclusively by the "master". The namespace locks guarantee its atomicity and accuracy. The status of a file region (a region of storage space which contains a part or the entire file) after a data transfer depends on the type of mutation, the success or failure of the mutation, and the existence or not of simultaneous mutations.

Table 1 summarizes the states of a file region after a transfer. A file region is "consistent" if all clients see the same data regardless of the replicas they are reading. A region is called "defined" after a change if it is consistent and clients will see all of what this mutation wrote.

When a mutation succeeds without simultaneous write interference, the affected region is defined (and coherent by consequence): All customers will see all what the mutation wrote.

Successful simultaneous mutations leave the region undefined but consistent: all clients see the same data, but the data may not reflect what any one mutation wrote, it will be composed of mixed fragments from multiple mutations. Failed mutation makes the region inconsistent (hence also undefined): different clients may see different data at different times. GFS makes the difference subsequently between the defined regions and undefined regions.

Table 1 : File region state after mutation

	Write	Record Append
Serial success	Defined	Defined interspersed with inconsistent
Concurrent successes	Consistent but undefined	
Failure	Inconsistent	

On GFS, Data mutations may be a record write or a record append. A "record append" in GFS is different from a standard "append" in which the customer writes at the end of file. Indeed, a "record append" in GFS consists of writing a record in a block at least once even in the case of competitive changes, but at an offset that GFS itself chooses. The offset is returned to the client and marks the beginning of a defined region that contains the record.

After a sequence of successful mutations, the mutated region of the file is guaranteed to be "defined" and contains data written by the last mutation. GFS achieves this by applying chunk mutations in the same order on all replicas, but also using chunks version numbers to detect any replica that has become obsolete because it missed mutations. Obsolete replicas will never be used and will be destroyed by a garbage collector at the first opportunity.

Blobseer developed a more sophisticated technique, which theoretically gives much better results. The basic needs can be defined as following: the BLOB access interface must allow users to create a BLOB, read / write a sequence of bytes (of a known size starting from an offset) from or to the BLOB, and add a byte sequence of a certain size at the end of the BLOB.

However, given the requirements regarding competitive access to data, Blobseer developers claim that BLOB access interface should be able to:
- Manage Asynchronous operations;
- Have access to previous versions of the BLOB;
- Ensure the atomic generation of snapshots whenever the BLOB is updated.

Each of these points is covered by the following capabilities:

1. The explicit versioning: Applications that process large quantities of data must often manage the acquisition and processing of data in parallel. Versioning can be an effective solution to this situation. While the acquisition of data can lead to the generation of new snapshot of the BLOB, the data processing can continue quietly on its own snapshot that is immutable and therefore never leads to potential inconsistencies. This can be achieved by exposing data access interface based on versioning, which allows the user to directly express these workflow templates, without the need to explicitly manage synchronization.

2. Atomic snapshots generation: Snapshots can be used to protect the file system contents against any error by preserving at a point in time a version of the file system or a sub-tree of a file system called a fileset. In Blobseer, a snapshot of the blob is generated atomically each time the Blob is updated. Readers should not be able to access transiently inconsistent snapshots that are being generated. This greatly simplifies development of applications because it reduces the need for complex synchronization schemes at the application level.

The "snapshot" approach using versioning that Blobseer brings is an effective way to meet the main objectives of maximizing competitive access. Data and metadata are always created, but never overwritten. This will parallelize concurrency as much as possible, in terms of data and also metadata, in all possible combinations: simultaneous reads, simultaneous writes and concurrent reads and writes [29].

The disadvantage of such a mechanism based on snapshots, is that it can easily explode the storage space required to maintain the system. However, although each write or append generates a new version of the blob snapshot, only the differential updates from previous versions are physically stored. This eliminates unnecessary duplication of data and metadata and greatly optimizes storage space.

7. Tiered storage

Despite the high scalability of DFSs existing on the market and their ability to manage a very large number of nodes, they still dealing with managed nodes in a similar way.

Indeed, a node network in a DFS can technically be composed of several types of machines with heterogeneous storage units, managing these nodes similarly would often prevent DFS from taking advantage of the most powerful storage spaces or otherwise imposing many constraints on rudimentary storage spaces. A simple way to avoid this situation is to equip the DFS with a single type of node, therefore the management will be linear and the performance will not be impacted by the identity of the storage node. In this case the DFS is indifferent to the I/O characteristics of each node and will have to keep the same category of devices even if the technology is outdated (the case of the HDD disks), otherwise pro-actively opt for advanced technologies (the SSD for example) and undergo costs of maintenance and evolution.

Another way to address this problem is to allow DFSs to manage different device categories while equipping them with technology that enables them to intelligently manage storage policies on heterogeneous storage resources.

The "tiered storage" allows to create groups of "devices" (tiers) that have the same I / O characteristics and to manage the distribution of the storage on these groups according to the degree of solicitation of data.

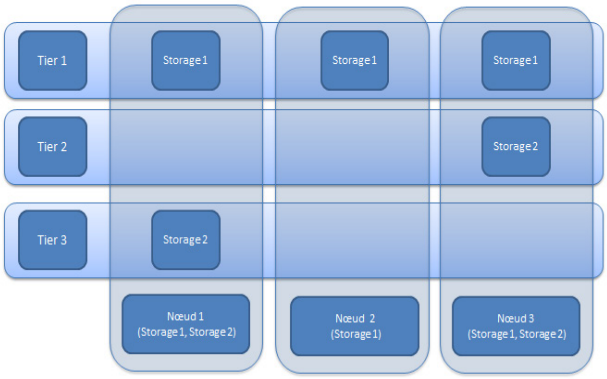

Figure 6: Tiered storage concept

Hadoop, since version 2.3.0, had introduced a major evolution that allowed the management of heterogeneous storage spaces; by using this option combined with a storage policy management API, the user can specify on which storage type this data should be stored.

Other works on Hadoop has made it possible to automate the choice of the storage space for specific data, for example based on the temperature of the data (hot data for the very demanded and cold data for those less solicited for example)[30] or even improve the architecture of HDFS as has been proposed by hatS [31] which logically groups all storage devices of the same type across the nodes into an associated “tier.” Or yet by TS-Hadoop [32] which utilizes tiered storage infrastructure, besides HDFS, to improve map reduce operations. TS-Hadoop automatically distinguish hot and cold data based on current workload, and move hot data into a specific shared disk (hcache) and cold data into HDFS respectively, so that the hot data in HCache could be processed efficiently.

The same concept is assured by other DFS like GPFS by "Spectrum Scale ILM toolkit" which allows the management of groups of storage spaces but also to automate the management of the files within these spaces. It allows to create hierarchized and optimized storage sets by grouping, in separate storage pools, discs that have close performances, similar budget characteristics or even hosted in the same physical location. Thereafter, a storage strategy tells the system what rules should be followed when storing each file.

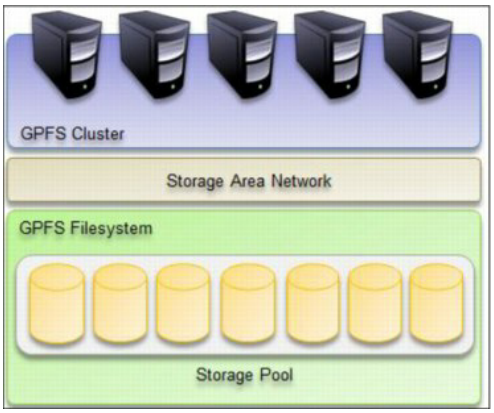

Figure 7: GPFS Storage spools as Tiered storage

The performance of a tired-storage compared to a traditional DFS can be very remarkable, allowing improvements up to 36% on the reading times on hatS for example. However, an automatic analysis must be associated to the architecture to allow automatic determination of the best storage location. This analysis can be done at the time of data storing via a specific algorithm based on the information of storage areas, or by analyzing the situation of the response time and redistribute data according to the results of the analysis (log analysis for example)

8. DFS Benchmark

As we have detailed in this article, often there is no better or worse methods for technical or technological choices to be adopted to make the best of a DFS, but rather compromises that have to be managed to meet very specific objectives.

In Table 3, we compare the implementation of some key technologies that meet the requirements listed in the paragraph "What is a Distributed File system", and that can be summarized as follows:

- Data Storage Scalability: the system can be scalable natively on the data storage capability.
- Meta Data Storage Scalability: the system can be scalable natively on the Meta data storage capability.
- Fault tolerance: the system is fault tolerant transparently to the user.
- Data Access Concurrency: how the system manages competitive access to data.
- Meta Data Access Concurrency: how the system manages competitive access to Meta data.
- Snapshots: does the system keep snapshots of files to recover from errors or crashes.
- Versioning: does the system records versions of changed files and data.
- Data Striping: does the system uses data striping over his nodes.
- Storage as Blobs: does the system store data as blobs.
- Data replication: does the system automatically replicate data.
- Supported OS: which operating systems can be used by the DFS.
- Dedicated cash: does the system support the using of dedicated cash.

Analysis of the results of Table 3 leads to the following conclusions:

- The five systems are expandable in data storage. Thus they cover one of the principal issues that lead to the emergence of Distribute File System: the capacity to extend the system to absorb more volumes, transparently to the user.

- Only Blobseer and GPFS offers the extensibility of metadata management to overcome the bottleneck problem of the master machine which manage the access to metadata; while AFS architecture does not provide metadata supporting to access to the file, GFS and HDFS has not considered necessary to extend the metadata management feature. Google considers that having a single master vastly simplifies the design of GFS and enables the master to make sophisticated chunk placement and replication decisions using global knowledge.

- Except AFS, all studied systems are natively tolerant to crash, relying essentially on multiple replications of data.
- The competitive access to the data and metadata is an important point in all big data systems. All systems use locks to enable exclusive data mutation. To minimize the slowing effect caused by locks on the whole file, GPFS manage locks on specific areas of the file (Byte range locks). Nevertheless, the most innovative method is the use of versioning and snapshots by Blobseer to allow simultaneous changes without exclusivity.

- Except AFS, all systems are using the striping of data. As discussed earlier, this technique provides a higher input/output performance by "striping" blocks of data from individual files over multiple disks, and reading and writing these blocks in parallel way.

- Blobseer seems to be the only one among the systems studied that implements the storage on blobs technique, despite the apparent advantages of such technique.

- To allow a better scalability, a DFS system must support as much operating systems as possible. However, despite that, the studied technologies remain discorded on this point. While AFS, HDFS and GPFS supports multiple platforms, GFS and Blobseer run exclusively on Linux. This can be partly explained by the popularity of AFS, HDFS and GPFS which are used in many professional contexts.

- Use of dedicated cache is also a point of discord between studied systems, GFS and Blobseer are categorical and consider that the cache has no real benefits, but rather causes many consistency problems. AFS and GPFS use dedicated cache on both client computers and servers. HDFS seems to use dedicated cache only at client level.

Table 3: Comparative table of most important characteristics of distributed file storage

	Data Scalability	Meta Data Scalability	Fault tolerance	Data access Concurrency	Meta Data access Concurrency	Snapshots	Versioning	Data Striping	Storage as Blobs	Supported OS	Dedicated cache
HDFS	YES	NO	Block Replication. Secondary Namenode.	Files have strictly one writer at any time	NO	YES	NO	YES (Data blocks of 64 MB)	NO	Linux and Windows are the supported , but BSD, Mac OS/X, and Open Solaris are known to work	YES (Client)
Blobseer	YES	YES	Chunk Replication Meta data replication	YES	YES	YES	YES	64 MB Chunks	YES	LINUX	NO
GFS by Google	YES	NO	Fast Recovery. Chunk Replication. Master Replication.	Optimized for concurrent "appends"	Master shadows on read only	YES	YES	64 MB Chunks	NO	LINUX	NO
AFS (OPEN FS)	YES	NO	NO	Byte-range file locking	NO	NO	NO	NO	NO	AIX, Mac OS X, Darwin, HP-UX, Irix, Solaris, Linux, Microsoft Windows, FreeBSD, NetBSD and OpenBSD	YES
GPFS IBM	YES	YES	Clustering features. Synchronous and asynchronous data replication.	Distributed byte range locking	Centralized management	YES	unknown	YES	NO	AIX, Red Hat, SUSE , Debian Linux distributions, Windows Server 2008	YES by AFM technology

9. Conclusion

In this paper, we made a comparative study of the main characteristics of five distributed file storage systems. Firstly, we introduced the general objective of this kind of systems and reviewed related technologies, such as architectures, Blob use, data striping and concurrent access. At the end, we provide a table (Table 3) whose each column's header is a main characteristic of a DFS system and each line's header corresponds to one of the five DFS systems compared. At the intersection of each row and column, we specify whether the characteristic is implemented by the system as well as the particularities of the implementation.

It is clear from this analysis that the major common concern of such systems is scalability. Those systems are designed to manage the amount of data that extends day after day. Centralized storage systems have many limitations and their maintenance is complicated and raises major concerns about cost. A DFS should therefore be extended with a minimum cost and effort.

Also data availability and fault tolerance remain among the major concerns of DFS. Many systems tend to use non expensive hardware for storage. Such condition will expose those systems to frequent or usual breakdowns. This issue is remedied by replication mechanisms, versioning, snapshots… that aim restoring the system state, often automatically, after a fault or total loss of any nodes.

To these mechanisms, data striping and lock mechanisms are added to manage and optimize concurrent access to the data. Systems that manage large files in large quantities need to have a developed parallel access. Locking an entire file to change a part of it can halt the access to this file for an indeterminate duration. It was therefore important to adopt solutions that will just lock the byte range concerned by the change, or even like what Blobseer implements, continue editing in a new version without blocking other clients who continue to use the current version transparently.

Working on multiples operating systems can bring big advantages to DFS. AFS is the one offering the largest variety of operating systems that can support its implementation, but as seen above AFS have some serious limitations. In perspective, we can think to improve AFS with some mechanisms of data striping and concurrency management that we think the most important features to add to this DFS.

Furthermore, saving data as BLOB combined with a mechanism of data striping and cache, which is already proposed by AFS, can ameliorate considerably the efficiency of such system and allow it to manage larger files.

Conflict of Interest

The authors declare no conflict of interest.

References

[1] John Gantz and David Reinsel, “THE DIGITAL UNIVERSE IN 2020: Big Data, Bigger Digital Shadows, and Biggest Growth in the Far East.” Tech. rep. Internet Data Center(IDC), 2012.

[2] Weili Kou, Xuejing Yang, Changxian Liang, Changbo Xie ,Shu Gan,”HDFS enabled storage and management of remote sensing data” 2nd IEEE International Conference on Computer and Communications (ICCC), Chengdu, China, 2016. https://doi.org/10.1109/CompComm.2016.7924669

[3] D. Chen , Y.Chen, B.N. Brownlow, “Real-Time or Near Real-Time Persisting Daily Healthcare Data Into HDFS and ElasticSearch Index Inside a Big Data Platform” IEEE Transactions on Industrial Informatics, 2017. https://doi.org/10.1109/TII.2016.2645606

[4] Yanish Pradhananga, Shridevi Karande, Chandraprakash Karande, “High Performance Analytics of Bigdata with Dynamic and Optimized Hadoop Cluster” International Conference on Advanced Communication Control and Computing Technologies (ICACCCT),2016. https://doi.org/10.1109/ICACCCT.2016.7831733

[5] Richard J Self, “Governance Strategies for the Cloud, Big Data and other Technologies in Education” IEEE/ACM 7th International Conference on Utility and Cloud Computing, 2014. https://doi.org/10.1109/UCC.2014.101

[6] Purva Grover, Rahul Johari, “BCD: BigData,Cloud Computing and Distributed Computing” Global Conference on Communication Technologies(GCCT), 2015. https://doi.org/10.1109/GCCT.2015.7342768

[7] T. L. S. R. Krishna, T. Ragunathan and S. K. Battula, “Improving performance of a distributed file system using a speculative semantics-based algorithm” Tsinghua Science and Technology, vol. 20, no. 6, pp. 583-593, 2015. https://doi.org/10.1109/TST.2015.7349930

[8] Paul Krzyzanowski, “Distributed File Systems Design” Rutgers University, 2012.

[9] R. Tobbicke, "Distributed file systems: focus on Andrew File System / Distributed File Service (AFS/DFS)," Proceedings Thirteenth IEEE Symposium on Mass Storage Systems. Toward Distributed Storage and Data Management Systems, Annecy, 1994. https://doi.org/10.1109/MASS.1994.373021

[10] Monali Mavani, “Comparative Analysis of Andrew Files System and Hadoop Distributed File System” LNSE (Vol.1(2): 122-125 , 2013.

[11] Stefan Leue, “Distributed Systems” tele Research Group for Computer Networks and Telecommunications Albert-Ludwigs-University of Freiburg, 2001.

[12] Sanjay Ghemawat, Howard Gobioff, and Shun-Tak Leung Google*, “The Google File System” SOSP '03 Proceedings of the nineteenth ACM symposium on Operating systems principles,2003.

[13] T. L. S. R. Krishna and T. Ragunathan, "A novel technique for improving the performance of read operations in BlobSeer Distributed File System," 2014 Conference on IT in Business, Industry and Government (CSIBIG), Indore, 2014. https://doi.org/10.1109/CSIBIG.2014.7056982

[14] D.Santhoshi, V.Teja, T.Tejaswini Singh, K.Shyam Prasad, “Supplanting HDFS with BSFS” International Journal of Advanced Research in Computer Science Volume 5, No. 4, 2014.

[15] Alexandra Carpen-Amarie, “BlobSeer as a data-storage facility for clouds :self-Adaptation, integration, evaluation.” Ph.D Thesis ENS CACHAN – BRETAGNE,2011.

[16] M. Sogodekar, S. Pandey, I. Tupkari and A. Manekar, "Big data analytics: hadoop and tools," 2016 IEEE Bombay Section Symposium (IBSS), Baramati, India, 2016. https://doi.org/10.1109/IBSS.2016.7940204

[17] K. Qu, L. Meng and Y. Yang, ”A dynamic replica strategy based on Markov model for hadoop distributed file system (HDFS)” 4th International Conference on Cloud Computing and Intelligence Systems (CCIS), Beijing, 2016. https://doi.org/10.1109/CCIS.2016.7790280

[18] Konstantin Shvachko, Hairong Kuang, Sanjay Radia, Robert Chansler Yahoo!, “The Hadoop Distributed File System” MSST '10 IEEE 26th Symposium on Mass Storage Systems and Technologies, 2010. https://doi.org/10.1109/MSST.2010.5496972

[19] C. B. VishnuVardhan and P. K. Baruah, "Improving the performance of heterogeneous Hadoop cluster," 2016 Fourth International Conference on Parallel, Distributed and Grid Computing (PDGC), Waknaghat, 2016. https://doi.org/10.1109/PDGC.2016.7913150

[20] Dhruba Borthakur, “HDFS Architecture Guide” The Apache Software Foundation, 2008.

[21] Passent M ElKafrawy, Amr M Sauber, Mohamed M Hafez, "HDFSX: Big data Distributed File System with small files support." 12th International Computer Engineering Conference (ICENCO), 2016. https://doi.org/10.1109/ICENCO.2016.7856457

[22] A. C. Azagury , R. Haas, D. Hildebrand, "GPFS-based implementation of a hyperconverged system for software defined infrastructure" IBM Journal of Research and Development, vol. 58, no. 2/3, pp. 6:1-6:12, 2014. https://doi.org/10.1147/JRD.2014.2303321

[23] Kuo-Yang Cheng, Hui-Shan Chen and Chia-Yen Liu, "Performance evaluation of Gfarm and GPFS-WAN in Data Grid environment," IET International Conference on Frontier Computing. Theory, Technologies and Applications, Taichung, 2010. https://doi.org/10.1049/cp.2010.0530

[24] Bogdan Nicolae, Gabriel Antoniu, Luc Boug_e, Diana Moise, Alexandra, Carpen-Amarie, "BlobSeer: Next Generation Data Management for Large Scale Infrastructures" Journal of Parallel and Distributed Computing, Elsevier, 2011. http://doi.org/10.1016/j.jpdc.2010.08.004

[25] Mariam Malak Fahmy,Iman Elghandour, Magdy Nagi, "CoS-HDFS: Co-Locating Geo-Distributed Spatial Data in Hadoop Distributed File System" IEEE/ACM 3rd International Conference on Big Data Computing Applications and Technologies (BDCAT), 2016 . http://doi.org/10.1145/3006299.3006314

[26] Cong Liao, Anna Squicciarini, Dan Lin. LAST-HDFS, "Location-Aware Storage Technique for Hadoop Distributed File System." IEEE 9th International Conference on Cloud Computing. 2016. https://doi.org/10.1109/CLOUD.2016.0093

[27] Doug Beaver, Sanjeev Kumar, Harry C. Li, Jason Sobel, Peter Vajgel, Facebook Inc,, "Finding a needle in Haystack: Facebook's photo storage" OSDI'10 Proceedings of the 9th USENIX conference on Operating systems design and implementation, 2010.

[28] Scott Fadden, "An Introduction to GPFS Version 3.5 Technologies that enable the management of big data" IBM Corporation, 2012.

[29] Bogdan Nicolae,Diana Moise, Gabriel Antoniu,Luc Boug´e, Matthieu Dorier, "BlobSeer: Bringing High Throughput under Heavy Concurrency to Hadoop Map-Reduce Applications" Research Report RR-7140, INRIA , 2010. https://doi.org/10.1109/IPDPS.2010.5470433

[30] Rohith Subramanyam, "HDFS Heterogeneous Storage Resource Management based on Data Temperature" International Conference on Cloud and Autonomic Computing, 2015. https://doi.org/10.1109/ICCAC.2015.33

[31] Krish K.R., Ali Anwar, Ali R. Butt. "hatS, A Heterogeneity-Aware Tiered Storage for Hadoop" 14th IEEE/ACM International Symposium on Cluster, Cloud and Grid Computing, 2014. https://doi.org/10.1109/CCGrid.2014.51

[32] Zhanye Wang, Jing Li, Tao Xu, Yu Gu, Dongsheng Wang. TS-Hadoop, "Handling Access Skew in MapReduce by Using Tiered Storage Infrastructure" International Conference on Information and Communication Technology Convergence, 2014. https://doi.org/10.1109/ICTC.2014.6983331

ASTES

Advances in Science, Technology and Engineering Systems Journal Vol. 2, No. 4, 92-98 (2017)

www.astesj.com

ASTESJ

ISSN: 2415-6698

Grid Connected Hybrid Solar and Diesel Generator Set: A Cost Optimization with HOMER

Amevi Acakpovi[*,1], Mathias B. Michael[1], Issah B. Majeed[2]

[1]*Electrical and Electronic Engineering Department, Accra Technical University, Accra, Ghana*

[2]*Electrical and Electronic Engineering Department, Takoradi Technical University, Takoradi, Ghana*

A R T I C L E I N F O

Article history:
Received: 01 April, 2017
Accepted: 14 June, 2017
Online: 26 June, 2017

Keywords:
Levelized cost
Hybrid energy supply
Diesel generator
Solar Energy
Grid connected
Emissions

A B S T R A C T

Extensive increases in electricity cost added to the numerous power outages encountered in developing countries has led to the deployment of hybrid energy supplies that mainly ensure continuity of power supply while attempting a reduction of electricity generation cost. This paper, specifically deals with the cost optimization of electricity generation from a grid connected hybrid solar and diesel generator. An electrical audit was first conducted on a selected building: the Electrical Block of Accra Technical University. The load estimate led to a total energy of 234 kWh for all electrical gadgets with the exception of the air-condition systems. The estimate was used to design the hybrid system with HOMER software that resulted in a total capacity of 115 kW and a levelized cost of electricity of 0.472 $/kWh taking into consideration no power outage in the year. Furthermore, the proposed hybrid system was made of a grid connected solar system that supplies the full load with the exception of the air-condition systems while the National Grid is used to cover the rest. In situation of power outages, the Generator Set takes over the National grid while the solar is still connected to the Grid. This mechanism was simulated and the cost of electricity in absence of the grid was estimated at 1.496 $/kWh. A general cost of electricity taking into consideration 90% ON period of the grid against 10% Off period of the grid per year, was estimated to 0.574 $/kWh. Besides, the proposed system produced savings in emission of carbon dioxide, 26.42 kg/year, sulfur dioxide, 115 kg/year and Nitrogen oxides, 56 kg/year. Finally, the system yielded a very good payback period of 10.43 years with regard to a lifetime of 25 years.

1. Introduction

Grid supply systems may be classified as On-grid or Off-grid power supplies. Large scale power also referred to as grid power or macro-grid can generate many hundreds of Megawatt, sometimes, up to the gigawatt (GW) with a centralised transmission and distribution system that can cover a country or even beyond.

On the other hand, off-grid system simply signifies power supply system that do not depend on the main grid. They are small in size as compared to main grid systems. Off-grid supplies are considered autonomous for the reason that they make use of local power generation to supply demand (IRENA, 2015) [1]. Off-grid systems include mini and micro-grids as well as standalone systems. Off-grid power supply may be deployed for a community while stand-alone systems are purposely designed for individual users or individual appliances.

Additionally, a micro-grid is a distributed energy resources comprising of demand management, storage and generation capable of operating in parallel independently from the grid. The primary purpose is to ensure local, reliable, and affordable energy security for urban and rural communities, while also providing solutions for commercial, industrial, and federal government consumers. Nayar (2010), [2] also explained that a stand-alone Micro-Grid system is an isolated small grid that include at least

[*]Corresponding Author: Amevi Acakpovi, Electrical and Electronic Engineering Department, Accra Technical University, Accra, Ghana
Email: cakpovia@gmail.com

diesel generator, inverter, batteries and uses various renewable energy sources available.

Extensive studies have been carried on microgrid hybrid systems including solar, diesel. Sopian & Othman (2005), [3] presented the performance of a hybrid solar, diesel system. The system uses the solar as a main supply and the diesel generator as an alternative supply. Storage batteries are deployed to save the excess energy produced by solar. According to (Ali et al., 2008; Sopian & Othman, 2005) [3], [4], hybrid solar-diesel generator increases the reliability of supply, reduces pollution and cost and sustains power continuously. [5] provides guidance in implementing hybrid solar systems and reported on the state of art of some PV-Diesel systems used for rural electrifications. PV/Diesel mini-grid systems have become more attractive with the rising cost of other power resources and the reducing cost of solar panels and accessories. The driving element behind this attraction for solar hybrid system is mainly cost and continuity of supply and convenience. In mountainous areas or desert where it is difficult to deploy national grid, solar is directly the preferred alternative choice as illustrated by (Yilnaz, Ozcalik, Aksu, & Karapinaar, 2015), [6] who developed a study on planning, modelling and cost analysis of a mini-grid solar PV/Diesel hybrid energy systems for houses installed in Turkey mountains. Yilmaz et al. (2015), [6] found that the cost of hybrid solar PV/diesel though higher than National grid electricity was still acceptable around 0.24 Euro/kWh. Moreover, (Alam & Bhattacharyya, 2016), [7] proposed a decentralized hybrid mini-grid system with reduced electricity cost between 0.29 and 0.31$/kWh for coastal areas using the HOMER software. Once again the main consideration was cost reduction from a former energy supply system that was solely based on solar.

Microgrid connected systems are basically made of multiple distributed generators known as DGs that connect to the grid through a transfer switch (Nguyen, Won, Ahn, & Chung, 2012; Parhizi, Lotfi, Khodaei, & Bahramirad, 2015) [8], [9]. Grid connected system have been compared in several ways to islanded microgrid system with distributed generators mainly made of renewable energies such us solar, wind etc. Othman, Gabbar, Honarmand, & Othman (2015), [10] perform a similar comparison and found that the islanded microgrid system was more robust and resistant to fault than the grid connected system. However, many studies that aimed at developing power control or energy storage systems for islanded microgrid as illustrated by (Etxeberria, Vechiu, Camblong, Vinassa, & Camblong, 2010; Pota, Hossain, Mahmud, & Gadh, 2014) [11], [12], have also realized the complexity involved and the adequacy of such systems only for remote and isolated locations. On the other hand, grid-connected system are advantageous in providing a reduced cost of electricity as the Grid electricity is always considered cheaper than locally developed power. They also provide the advantage of a continuous supply that overcomes the fluctuation of the grid by relying on the alternative supplies.

This paper is interested in grid-connected hybrid systems involving solar and generator set. This comes as a result of the growing interest in developing renewable energies for effective supply of electricity in West Africa, precisely, Ghana. In the recent past, the National grid in Ghana has been earmarked with inefficient and highly intermittent supplies that affected businesses and development in all dimensions (Aryeetey, 2005), [13]. Companies and houses therefore developed the need to be self-autonomous in power provision for their need. The obvious solution was the adoption of solar energy due to the immense availability of solar radiation in Ghana. However the cost of solar is another limiting factor reducing its deployment. Instead of solely relying on solar, it is rather used partly to supply essential but low-consuming appliances like lighting and fans.

The other alternative massively adopted in Ghana to overcome the regular interruption of electricity supply from the grid is Diesel Generator Sets. This solution was embraced as new generators have become very efficient in terms of fuel consumption and can also work with reduced level of noise. Furthermore, the cost of fuel used by the Diesel generator is relatively low as compared to other fuels.

Combining the interest of a highly available solar irradiation in Ghana to the possibility of using Diesel generator at a relatively lower fuel cost, have brought the interest in developing this hybrid solar-diesel generator that will be connected to the microgrid. Though the microgrid components include loads, DERs, master controller, smart switches, protective devices, as well as communication, control and automation systems, (Parhizi et al., 2015), [8], this paper focuses mainly on conceptual design and cost analysis of the system. The rest of the paper presents the hybrid system applied to a case study at Accra and analyses its cost benefits.

2. Methodology

A case study approach has been adopted to design the solar-diesel generator hybrid supply. The next paragraph show the framework for designing the hybrid system, the data collected on the selected location, a summary of load audit at the selected location and a design of the hybrid system using Homer.

2.1 Framework for Designing the Grid-Connected Hybrid Solar and Diesel Generator

Figure one shows the general design of the system which is made of two bus-bars connected to the PV array, the diesel generator and the grid itself. A converter playing at the same time the role of inverter and rectifier is also connected in bi-directional mode to the busbar. Finally the busbar is connected to the load in unidirectional mode to supply the required electricity.

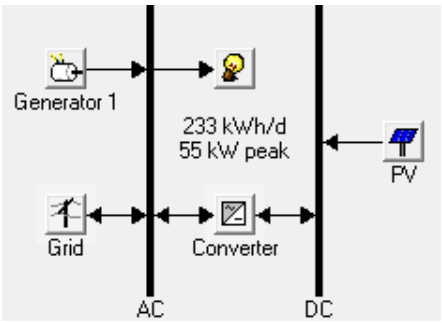

Fig.1: Proposed Model of Grid-Connected Hybrid Solar-Diesel Generator under HOMER

2.2 Selected Location and Presentation of Data

The Electrical block of Accra Technical University has been selected for this study. The geographical parameters of the location are 5.5541° N, 0.2056° W. It is a four-storey building that covers an area of 12 m x 100m, located in the premises of Accra Technical University, formerly known as Accra Polytechnic. The block contains twelve lecture rooms, a computer laboratory, two other multipurpose electrical laboratories, twenty offices for lecturers and eight washrooms. The lecture rooms are busily occupied by students and lecturers for lecturing over the day and are equipped with fans, lighting systems and socket. However the lecturer's offices have Air Conditioning Systems in addition to the fans, light and sockets.

2.3 Design of the Hybrid System using Homer

An energy audit is first established as illustrated in the table 1

APPLIANCES	QTY	RATE (KW)	TIME USAGE	TIME (Hour)	ENERGY(Kwh)
A.C(2.5HP)	1	18.630	12:00 - 14:00	2.0	37.26
FAN(60 W)	40	0.060	09:00-12:00, 13:00-15:00	5.0	12.00
LED LIGHT(40W)	13	0.040	09:00 - 21:00	10.0	5.20
FLOURESCENT BULB (15W)	73	0.015	09:00 - 21:00	10.0	10.95
FRIDGE(70W)	23	0.070	09:00 - 15:00	6.0	9.66
DESKTOP COMPUTER	45	0.250	09:00 - 15:00	6.0	67.50
LAPTOP	29	0.100	09:00 - 15:00	6.0	17.40
PRINTER (Stand-by)	25	0.075	09:00 - 15:00	6.0	11.25
PRINTER (Operation)	25	0.500		1.0	12.50
UPS	27	0.250	09:00 - 15:00	6.0	40.50
PROJECTOR	1	0.400	09:00-11:00, 13:00-15:00, 17:30-20:00	6.5	2.60
PHOTOCOPIER MACHINE (SB)	2	0.095	09:00 - 15:00	6.0	1.14
PHOTOCOPIER MACHINE (OP)	2	0.615		1.0	1.23
OUTDOOR LIGHTING	16	0.025	07:00 PM-06:00AM	12.0	4.80
TOTAL					**234**

Table 1: Energy Audit

Based on the total energy demand and the system architecture agreed upon, one must estimate the size of various components before selecting them. The sizing of the solar system is based on the determination of renewable energy window which is provided directly from the solar data obtained from NASA site. Knowing the renewable energy window and the daily load deducted from the data, the system's total AC power can be obtained from the equation (1)

$$P_{AC} = \frac{DailyLoad\left(kWh/d\right)}{R.E.Window\left(h/d\right)} \quad (1)$$

$$P_{AC} = \frac{234}{10} = 23.4kW \quad (2)$$

The AC power is converted to DC power by an inverter with an efficiency of about 90%. This implies that the DC power is obtained as shown in equation (3)

$$P_{DC} = \frac{P_{AC}}{Inv_{Eff}} \quad (3)$$

Where Inv_{Eff} stands for Inverter Efficiency

$$P_{DC} = \frac{23.4}{0.9} = 26kW \quad (4)$$

The calculated DC power is not directly used for the design but rather an Adjusted DC power due to the fact that many other factors, hardly quantifiable, contribute to the system total losses. Some of these include losses in cable, shading environment and others. In view of these, the paper proposed an adjustment factor of 30% and this has led to the determination of the adjusted DC power as follow

$$P_{DC(Adjusted)} = P_{DC} \times \eta \quad (5)$$

$$P_{DC(Adjusted)} = 26 \times 1.3 \quad (6)$$

$$P_{DC(Adjusted)} = 33.8kW \quad (7)$$

Subsequently the PV array area A can be determined as follow

$$A = \frac{P_{DC(Adjusted)}}{(1kW/m^2) \times \eta_{PV}} \quad (8)$$

Where η_{PV} is the PV system efficiency?

$$A = \frac{33.8}{1 \times 0.15} \quad (9)$$

$$A = 225.33m^2 \quad (10)$$

The next after determining the PV array's area is to estimate the solar system's capacity. The system's total energy received from the solar PV area is calculated based on equation (11) below

$$E_T = G \times A \quad (11)$$

Where G is the solar radiation from the area and E_T the total energy.

$$E_T = 5.1 \times 225.33 \quad (12)$$

$$E_T = 1149.18kWh \quad (13)$$

The system capacity can therefore be inferred with consideration to the renewable energy window as follow

$$C = \frac{E_T}{RE_{Window}} \quad (14)$$

$$C = \frac{1149.18kWh}{115} \quad (15)$$

$$C = 115kW \quad (16)$$

3. Result

This section presents the simulation results generated from the HOMER for the grid connected system followed by a scenario where power outage was simulated. The specifications of the solar panel used can be found in Appendix, Table A1.

3.1 Results from Grid Connected Systems

Table 2 and 3 show respectively the system architecture and cost summary. It can be observed that the PV array is sized with the designed capacity of 115 kW, the diesel generator is selected with a rating slightly above the solar array capacity, 150 kW so that it can fully replace the solar array in case of maintenance or breakdown.

Energy Sources	Power Ratings
PV Array	115 kW
Generator	150 kW
Grid	1000 kW
Inverter	75 kW
Rectifier	75 kW

Table 2: System's Architecture

Cost Elements	Cost ($)
Total net present cost	133.53
Levelized cost of energy	0.472
Operation cost	-7.476/yr

Table 3: Summary of cost

The estimated electrical energy produced by the different sources over a year is also presented in Table 4 and illustrated in Figure 2. It can be observed that the solar has been used as the main alternative to supply energy to the load and this is supported by the grid in case the solar energy becomes insufficient to meet the load. Because the diesel generator is meant to operate as alternative supply when the solar plant is faulty, no energy supplied by the generator can actually be observed in Figure 2.

Components	Production (kWh/yr)	Fraction
PV Array	143.216	88%
Generator	0	0%
Grid Purchase	20.033	12%
Total	163.249	100%

Table 4. Energy Production per Sources

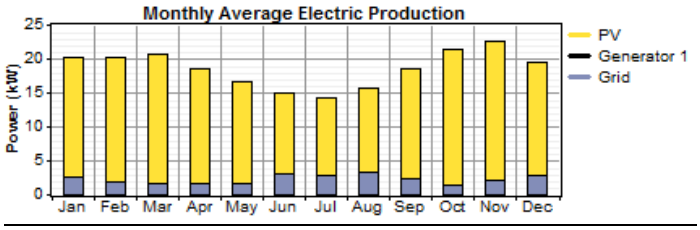

Fig.2: Energy production from various sources on a monthly basis

The load consumption as well as system results including excess electricity, unmet load and capacity shortage are respectively presented in Table 5 and 6.

Load	Consumption (kWh/yr)	Fraction
AC primary load	85,045	58 %
Grid Sales	61.837	42%
Total	146.882	100%

Table 5. Load consumption profile

Load	Consumption (kWh/yr)
Excess Electricity	2.272
Unmet load	0.00
Capacity shortage	0.00
Renewable Fraction	0.877

Table 6. Consumption parameters

Furthermore, the savings in terms of emissions are presented in Table 7.

Pollutant	Emissions (kg/yr)
Carbon dioxide	-26.420
Carbon monoxide	0
Unburned hydrocarbon	0
Particulate matter	0
Sulfur dioxide	-115
Nitrogen oxides	-56

Table 7. Emissions

3.2 Scenario of Power Outage Simulation

A power outage situation is considered in this scenario where the grid has been put off to mimic power outages, a recurrent situation encountered in developing countries. The model of the system without the grid contribution is illustrated in Figure 3

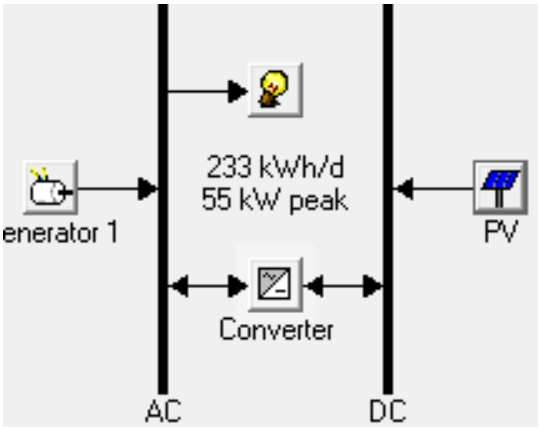

Fig.3: Model of Grid- Connected System in case of power outage

Simulation results obtained from the HOMER, show the cost summary below

Cost Elements	Cost
Total net present cost	$1,086,070.00
Levelized cost of energy	1.496$/kWh
Operation cost	$252,496.00

Table 8. Summary of cost

It can be observed that the levelized cost of electricity has significantly increased and this is justified by the fact that the supply was mainly based on the generator set (57%) that uses diesel. Similarly, it is interesting to observe that the PV system contribution was almost the same as illustrated in both Table 9 and Figure 4. This confirms the configuration of the inverter to synchronize with the Grid as well the gennerator perfectly. In other terms the cost of electricity in absebnce of the Grid would have been higher than the one shown in Table 8 if the Generator was the sole source of supply. The solar contribution which is highly significant (43%), helped to minimize the cost of electricity in power outage.

Components	Production (kWh/yr)	Fraction
PV Array	186803	43%
Generator	247247	57%
Total	434050	100%

Table 9. Energy production per sources in case of power outage

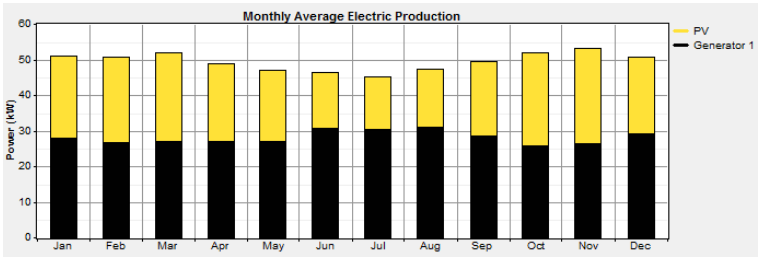

Fig.4: Energy distribution per sources in case of power outage

3.3 Estimation of Final Electricity Cost

The cost of electricity is estimated as a weighted sum of the levelized cost of electricity during ON grid and OFF grid period respectively. A rough estimate of power outages at Accra based on recent data on electricity supply shows that the power outage period in the year is about 30 to 36 days making approximately 10% of the duration of the year. The formula below applies for the calculation of the cost of electricity over a year taking into consideration the On and Off periods of the Grid.

$$Cost_{Final} = 90\% \cdot Cost_{Grid\_On} + 10\% \cdot Cost_{Grid\_Off} \quad (17)$$

$$Cost_{Final} = 0.9 \cdot 0.472 + 0.1 \cdot 1.496$$

$$Cost_{Final} = 0.574\$ / kWh$$

In summary, if the generator sets are run for 10% the period of the year, the cost of electricity will increase from 0.472($/kWh) to 0.574($/kWh)

3.4 Estimation of Payback Period

The payback period (PBP) is the amount of time that is expected before an investment will be returned in the form of income. In this case, the payback period is estimated with formula 17 as follow

$$PBP = \frac{Cost_{NPC}}{Cost_{Annual\_Net\_Cash\_Flow}} \quad (18)$$

$Cost_{NPC}$ represents the total Net Present Cost which is estimated in table 10 below.

$Cost_{Annual\_Net\_Cash\_Flow}$ represents the total Annual Net Cash Flow

As illustrated in Table 10. The $Cost_{NPC}$ takes into consideration the capital, replacement, operation and maintenance, fuel and salvage cost for the individual sources. The overall result is shown in right hand comer of the table.

Component	Capital($)	Replacement($)	O&M($)	Fuel ($)	Salvage($)	Total($)
PV	74,750	393	4,993	0	-79	80,057
Generator	13,4144	33,900	449,961	347,159	-28	857,821
Grid	0	0	-34,787	0	0	-34,787
Converter	55,250	11,079	3,329	0	-26	59,632
Other	15,000	0	233	0	0	15,233
System	158,414	1,473	-26,233	0	-124	**977,956**

Table 10: Estimation of total Net Present Cost

Furthermore $Cost_{Annual\_Net\_Cash\_Flow}$ is estimated as follow

$$Cost_{Annual\_Net\_Cash\_Flow} = Cost_{Final} \times Energy_{total} \quad (19)$$

$$Cost_{Annual\_Net\_Cash\_Flow} = 0.5744 \times 1632499$$

$$Cost_{Annual\_Net\_Cash\_Flow} = \$93{,}770.23$$

The payback period can then be deducted in reference to Equation (18) as follow

$$PBP = \frac{977956.00}{93770.23}$$

$$PBP = 10.43 \text{ Years}$$

4. Discussion and Conclusion

The results of this study confirm the multiple benefits of adopting a grid connected hybrid system as elaborated by previous studies (Ali et al., 2008), [4]. A limited list of the asserted benefits include "improved reliability and energy services, reduced emissions and pollution, continuous power supply, increased operational life, and reduced cost.

It is a fact that the reliability and energy services are automatically improved considering the fact that energy is being supplied from three different sources working in parallel, each of them having a high reliability. It is known that solar energy supply is very effective and efficient and also diesel generators are very reliable.

According to [2], electricity is mainly provided by diesel generators in Maldives, a country made of 1,192 island of which only 199 are inhabited. This again confirms the reliability of diesel generators. Our proposed system make use of a Grid connected solar system in which the solar power supplies almost all loads apart from the AC, a total of 234 kWh as indicated in Table 1. The national grid takes care of the remaining load. In case of power outage, the National grid goes off and the diesel generator in combination with the solar plant takes over the supply. This ensures a continuity of supply which increases the quality of energy service deliveries. Moreover Table 7 indicates savings in emission of carbon dioxide, 26.42 kg/year, sulfur dioxide, 115 kg/year and Nitrogen oxides, 56 kg/year.

Finally a cost analysis of the proposed hybrid system was dealt with. The levelized cost of electricity is 0.472$, equivalent to Gh₵2.04 for a continuous supply; this cost rises to 1.496 $/kWh in power outage where the load is supplied by the generator set and the solar power only. A weighted average of 0.574 $/kWh is estimated in general for the year covering both the OFF and ON time of the grid within a year.

More importantly, the unit electricity cost in Ghana for energy consumption lower than 25 kWh/month which is our case is about Gh₵8.39 for residential load and Gh₵24.2 for non-residential load [14]. Therefore this study concurs with previous studies in the direction that hybrid energy systems with renewable energy sources like solar, contribute to an obvious reduction of electricity cost. The payback period of approximately ten years and half is a very good result, considering the system's viability period of 25 years.

Appendix A

PV Module Ratings	Specifications
Module Type	YL 250P-29b
Module manufacturer	Yingli Solar
Maximum Power (Pmax)	250 Wp
Max. Power-Point Current (Imp)	8.24 V
Open-Circuit Voltage (Vmp)	30.4 V
Open-Circuit Voltage (Voc)	38.4 V
Short-Circuit Current (Isc)	8.79 A
Module Efficiency	15.30 %

Table A1. Specifications of Solar Panel

References

[1] IRENA, "Off-Grid Renewable Energy Systems: Status and Methodological Issues About IRENA," 2015.

[2] C. V Nayar, "High Renewable Energy Penetration Diesel Generator Systems," *Paths to Sustain. Energy, InTech*, pp. 1–27, 2010.

[3] K. Sopian and M. Y. Othman, "Performance of a Photovoltaic Diesel Hybrid System In Malaysia," *ISESCO Sci. Technol. Vis.*, vol. 1, pp. 37–39, 2005.

[4] B. Ali, K. Sopian, M. A. Rahman, Y. M. Othman, A. Zaharim, and A. M. Razali, "Performance of a Hybrid Photovoltaic Diesel System in a Cable Car Resort Facility," in *4th IASME/WSEAS International Conference on ENERGY, ENVIRONMENT, ECOSYSTEMS and SUSTAINABLE DEVELOPMENT (EEESD'08)*, 2008, pp. 183–187.

[5] CLUB-ER, "Rural Electrification with PV Hybrid Systems," 2013.

[6] S. Yilmaz, H. R. Ozcalik, M. Aksu, and C. Karapınar, "ScienceDirect Dynamic Simulation of a PV-Diesel-Battery Hybrid Plant for Off Grid Electricity Supply," *Energy Procedia*, vol. 75, pp. 381–387, 2015.

[7] M. Alam and S. Bhattacharyya, "Decentralized Renewable Hybrid Mini-Grids for Sustainable Electrification of the Off-Grid Coastal Areas of Bangladesh," *Energies*, vol. 9, pp. 1–16, 2016.

[8] S. Parhizi, H. Lotfi, A. Khodaei, and S. Bahramirad, "State of the art in research on microgrids: A review," *IEEE Access*, vol. 3, pp. 890–925, 2015.

[9] K.-L. Nguyen, D.-J. Won, S.-J. Ahn, and I.-Y. Chung, "Power Sharing Method for a Grid connected Microgrid with Multiple Distributed Generators," *J. Electr. Eng. Technol.*, vol. 7, no. 4, pp. 459–467, 2012.

[10] A. M. Othman, H. A. Gabbar, N. Honarmand, and A. M. Othman, "Performance Analysis of Grid Connected and Islanded Modes of AC/DC Microgrid for Residential Home Cluster," *Intell. Control Autom.*, vol. 6, pp. 249–270, 2015.

[11] H. R. Pota, M. J. Hossain, M. A. Mahmud, and R. Gadh, "Control for Microgrids with Inverter Connected Renewable Energy Resources," in *IEEE PES General Meeting*, 2014, pp. 1–5.

[12] A. Etxeberria, I. Vechiu, H. Camblong, J. M. Vinassa, and H. Camblong, "Hybrid Energy Storage Systems for renewable Energy Sources Integration in microgrids: A review," in *IPEC*, 2010, pp. 532–537.

[13] E. Aryeetey, "Guide to Electric Power in Ghana," Accra, Ghana, 2005.

[14] Electricity Company of Ghana Ltd, "Electricity Company of Ghana Limited - Current Tariff," 2016. [Online]. Available: http://www.ecgonline.info/index.php/customer-care/services/tariff. [Accessed: 22-Jan-2017].

ASTES

Advances in Science, Technology and Engineering Systems Journal Vol. 2, No. 4, 99-104 (2017)

www.astesj.com

ASTESJ

ISSN: 2415-6698

Precision Statistical Analysis of Images Based on Brightness Distribution

Muzhir Shaban Al-Ani[1], Khattab M. Ali Alheeti[*2, 3]

[1]*Department of Computer Science – College of Science and Technology, - University of Human Development – KRG – Iraq*

[2]*School of Computer Sciences and Electronic Engineering University of Essex, Colchester, United Kingdom*

[3]*University of Anbar, College of Computer Science and Information Technology, Anbar – Iraq*

ARTICLE INFO

Article history:
Received: 11 April, 2017
Accepted: 24 June, 2017
Online: 17 July, 2017

Keywords:
Image analysis
Pattern analysis
Statistical measures
Brightness distribution
Intensity Measures

ABSTRACT

Study the content of images is considered an important topic in which reasonable and accurate analysis of images are generated. Recently image analysis becomes a vital field because of huge number of images transferred via transmission media in our daily life. These crowded media with images lead to highlight in research area of image analysis. In this paper, the implemented system is passed into many steps to perform the statistical measures of standard deviation and mean values of both color and grey images. Whereas the last step of the proposed method concerns to compare the obtained results in different cases of the test phase. In this paper, the statistical parameters are implemented to characterize the content of an image and its texture. Standard deviation, mean and correlation values are used to study the intensity distribution of the tested images. Reasonable results are obtained for both standard deviation and mean value via the implementation of the system. The major issue addressed in the work is concentrated on brightness distribution via statistical measures applying different types of lighting.

1. Introduction

Color image processing can be described analogous to grayscale image processing, such as the study of algorithms and techniques for processing color information in a global three-dimensional scene and its conversion into two-dimensional image represent color in a trichromatic color model and digital color spaces [1], [2].

As with any other crime, the alteration of the image is inherent in the falsified image. Digital images are characteristics of the camera, the scene and the temporal characteristics of the pixel values. These characteristics will be different for the images taken in different configurations. These inconsistencies can be analyzed to detect the altered regions [3], [4].

Images processing play vital role in our daily life. In other words, it is the most important part in the analysis of images. The image analysis process is the extraction of meaningful information from images. In addition, image analysis can be divided into two main approaches which are: spatial domain and frequency domain approaches [5]. Statistical approach is situated within spatial domain approaches, in which can be measured many functions depending on the aim of the system [6].

The researchers are considered pattern recognition is one important part of this study in which existed many approaches that can be divided into two main categories [7]. These categories are: 1) Decision category that deals with pattern described utilised quantitative descriptors defined by length, area and texture. 2) Structural category that deals with pattern described qualitative descriptors defined by relational descriptor [8].

Brightness and intensity lead to major effect on image resolution and content. In some cases, it is not possible to compensate the incident light, so this causes big problems on the image quality. To avoid these problems, we must introduce additional step in the implemented system to show the effects raised according to incident light [9], [10].

Different statistical parameters for different aims can be applied on image processing. Image brightness and the light

[*]Corresponding Author: Khattab M. Ali Alheeti, School of Computer Sciences and Electronic Engineering University of Essex, Colchester, United Kingdom
Email: khattabheeti@yahoo.com

intensity has an important part of image quality. This approach concentrated on the statistical aspects to understand and analyze the brightness distribution of the object surface.

2. Statistical Measures

In this paper, statistical measures are employed to the different types on incident light. These statistical measures which are: standard deviation and mean values. These measures play an vital role in image processing filed including image analysis. In this research field, the standard deviation deals with the amount of variations in average. A low value indicates that data points tend to be very close to the mean, while a high standard deviation indicates that the data points are distributed over a wide range of values. In statistics and probability theory, standard deviation (σ) measures the amount of variation or dispersion from the average. A low standard deviation indicates that the data points tend to be very close to the mean. A high standard deviation indicates that the data points are spread out over a large range of values. The global mean value (μ) of an image is the average intensity of all the pixels in the image [11], [12], [13].

The standard deviation of a finite data set is given by:

$$\sigma = \sqrt{\frac{1}{N}\left[(x_1-\mu)^2 + (x_2-\mu)^2 \ldots + (x_N-\mu)^2\right]} \quad (1)$$

$$where\ the\ mean\ is \qquad \mu = \frac{1}{N}(x_1 + x_2 \ldots + x_N) \quad (2)$$

i.e.

$$\sigma = \sqrt{\frac{1}{N}\sum_{i=1}^{N}(x_i-\mu)^2} \quad (3)$$

$$\mu = \frac{1}{N}\sum_{i=1}^{N} x_i \quad (4)$$

3. Literature Review

The image analysis field is rich of literatures as well as the field of statistical measures is rich of studies. Combining of image analysis with statistical measures may empower the contribution approach. Below some of recently published papers are selected that were concentrated on both image processing and analysis with statistical measures:

Q. Al-Shayea et al., designed 3D object visualization via two dimensional images in which existed many object. This work is implemented to find the contour of the given object in each slice and then merging these contours to reconstruct the 3D objects. This approach is easy to use as well as it can be implemented on various type of images. The reconstruction process indicated a good resolution in this approach [14].

S. Greve, et al., introduced a new approach for classification of image regions. This approach is based on wavelet standard deviation descriptor. The obtained results performed for about one thousand images with region segmentation in which provided reasonable results for general application domain [15].

E. Fazal Malik et al., proposed a Content Based Image Retrieval (CBIR) algorithm which is based on the color histogram using Laplacian filter in order to reduce the noise and provides an enhanced image with more detail information. Color histogram of the filtered image is divided into bins. Mean and standard deviation are calculated for pixels in each bin to get feature vector which is used for image retrieval [16].

A. Firas Jassim, implemented a novel method that combines between median filter and simple standard deviation to get an excellent edge detector used for image processing. The visual differences between the implemented edge detector and the standard edge detectors have been shown to support the contribution in this work [17].

G. Ibrahem Raho, et al., constructed an efficient information algorithm that detects the direction of objects. This algorithm is implemented based on statistical measurements, entropy, histogram, moment and gradient. The obtained results indicate a good accuracy in object recognition. Many techniques are integrated to generate this approach which is efficient and effective approach [18].

A. Rashid et al., provided a detailed study for selecting of image processing and computer evaluate performance then compared the results and gave a better evaluation trend. For the implemented study of restoration, and elimination of noise, adding noise, then they estimated of statistical results, a certain amount of different types of noise have been added to the image, and a filtering process is carried out for the examination of the effect [19].

N. Hallil Binti Ismail et al., suggested an approach to calculate the contrast with the fixed block size independently of the spatial resolution of the input image. This approach try to resize the block size based on the spatial resolution of the input image to maintain the relationship between the block size and the image size similar to that of the sample images used in the development of the statistical model. The proposed method has been tested and demonstrated statistically to be effective in reducing inconsistency in the classification of images according to different spatial resolutions [20].

B. Büyüksaraç et al., proposed system consists of three main steps. First, we apply segmentation of the facial and hand zone using Fuzzy C-means clustering (FCM) and Threshold. FCM is a grouping technique that uses the fuzzy partition, in an iterative algorithm. After the segmentation of the face and hands, the vectors of characteristics are extracts. Then are drawn vectors of features, which are used for recognition with discrete hidden Markov model (HMM). A precision of 94.19% was obtained [21].

S. Intajag et al., proposed algorithm uses a generalized distribution of extreme values consisting of three parameters to adjust the balance of brightness and color by adjusting the location, contrast and tone granted, respectively, by the scale and shape parameters. The performance of the algorithm was evaluated using two sets of imaging data: retinal structure analysis and automated retinal image analysis. The results show that the improved histograms based on the generalized extreme value were given important characteristics to characterize the symptoms of macular degeneration [22].

X. Zhang et al., studied and demonstrated the effect of high fluorescence on the brightness of the cell images. The optical properties are very important to for enhancement and detection of biomedical applications, and disease diagnosis. The obtained results indicated that the synthesized carbon nanodots are suitable

to be used for sensitive detection [23].

T. Gao et al. designed a specific approach for real time imaging. This approach synthesized successfully and applied in living image cells. Living cells is a real time application which is one of the big challenge here. The proposed approach leading to many advantages in addition to high brightness of images. This approach provides new efficient strategies compared with other algorithms [24].

D. Oliva et al., introduced an image processing approach based on high influence of image analysis. Different techniques and thresholding and entropy are presented to perform image segmentation. Optimal strategy of thresholding is implemented by applying crow search algorithm. The obtained results, demonstrated that this approach obtains better results related to the quality and consistency [25].

The previous works concentrated in their approaches on the statistical measures as a main part of their works. In the proposed work, the statistical measures are implemented as a parameters to enhance the different types on incident light.

4. Methodology

4.1. Image Data Set Construction

The construction of image data set is required to be applied in the implemented approach. Several cases have been tried in order to access the appropriate images. Two set of images are performed via the arrangement of 20 coins; first set is built by square shape and the second set is built by circle shape. Via high resolution camera three types of light intensities are designed: normal light, sunny light and fluorescent light.

- Normal light indicated images with perfect light.
- Sunny light indicated images with sunny light.
- Fluorescent light indicated images with fluorescent light.

b. The Proposed Scheme

There are many approaches deal with the image analysis such as histogram analysis, feature extraction, image understanding, and statistical approach. This approach is concentrated on two parameters of statistical measures that are mean value and standard deviation value of image which reflect the intensities distribution in an image. The proposed approach is divided into five main steps as shown in Figure 1:

- The first step (Input color images): In this step, images are collected via high resolution camera to capture Red Green Blue (RGB) color images. The acquisition of color image with real color is an important part of the system to ensure the correct image resolution.
- The second step (Convert color image into gray image): In which color images are converted into grey scale images of eight bits. RGB images are converted into grey image with normal levels to reserve the image performance.
- The third step (Pre-processing): In this step, images are resizing and filtering to reduce noise and redundancies as possible. This is an important stage to prepare an image that is ready for the processing stage.
- The fourth step (Statistical measures): In this step, the mean, standard deviation values and correlation are calculated of grey and color images. These measurement deals with the variation of intensity of the image surface.
- The fifth step (Compare the results): In which compare the calculated results of mean and standard deviation values. This stage is realize the difference in values between various types of images.

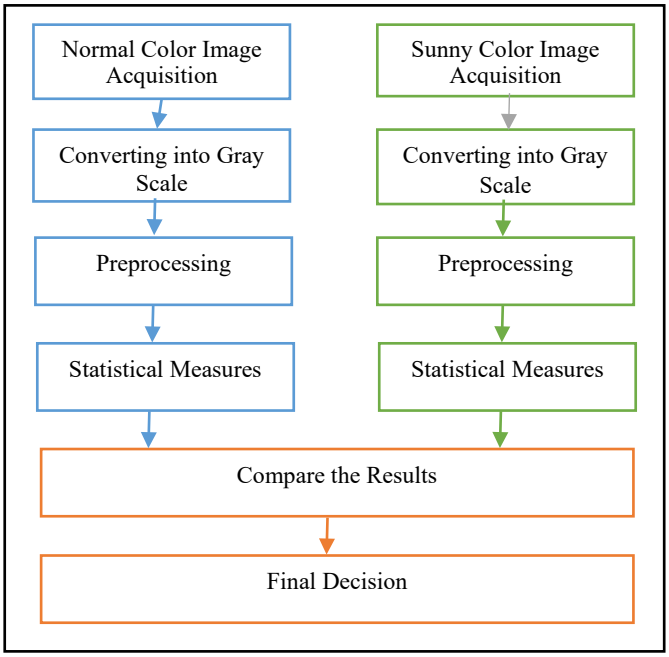

Figure 1 System Approach

5. Results and Analysis

Images are collected in three types of light intensities; normal light, sunny light and fluorescent light. Each image consists of 20 coins of money distributed in different ways as shown in Figures 2 and 3, which indicate both color and gray images of set_1 respectively. The objects in these images are arranged regularly into two forms; rectangular and circular. On one hand, Table 1 indicates that there is a similarity in standard deviation measures between images 1_1 and 1_2, images 1_3 and 1_4, images 1_5 and 1_6 because these set of images are related to the same type of lighting. On the other hand, similarities of mean values are nearly the same in all set of images. The values of mean, standard deviation and correlation are illustrated in Figure 4. The rectangular distribution of color images and gray scale image of set_1 are illustrated in figures 2 and 4. Table 2 indicates that the value of correlation approach to one when the correlation occurs with the same image and becomes approach to zero when the correlation occurs with the different image. Figures 5 and 6 indicate both color and gray images of set_2 in which objects are distributed randomly in circular form. In this case, there are no differences in the measures of standard deviation and mean values, but the difference is noted in the correlation values which are slightly larger that values obtained in images of set_1 as shown in Table 3 and 4 and demonstrated in Figure 7. This

slightly difference of measured parameters values it could be because of the difference image intensities according to the controlling source of light.

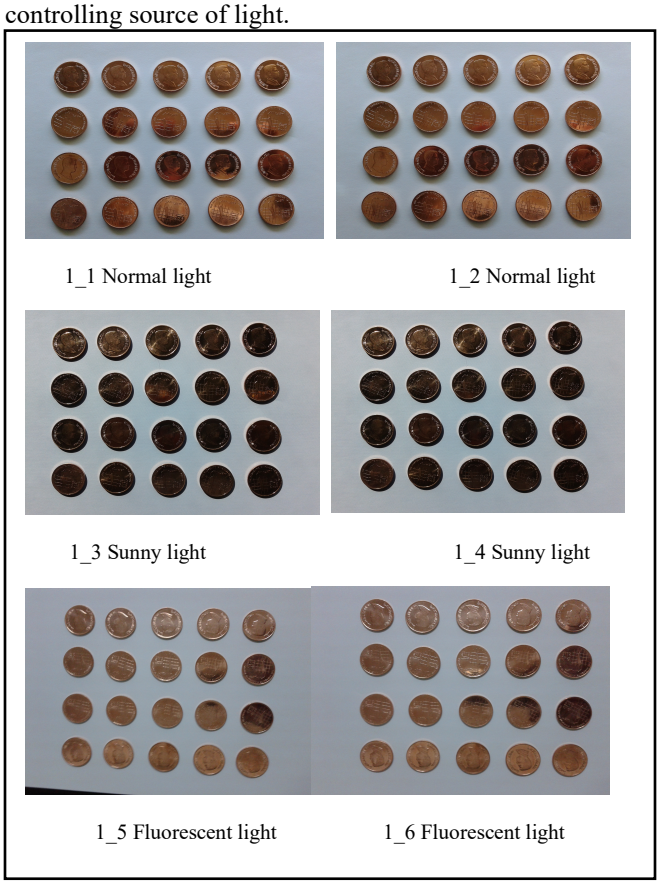

Figure 2 Original color images set_1

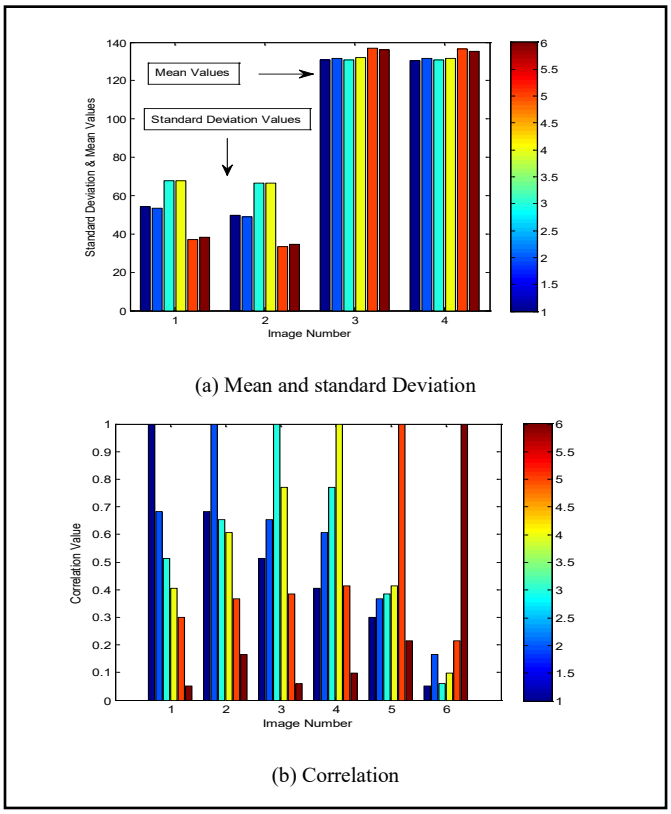

Figure 3 Gray scale images set_1

Table 1 standard deviation and mean values of set_1

Std. and mean	Im1_1	Im1_2	Im1_3	Im1_4	Im1_5	Im1_6
Std. Color	54.4339	53.4629	67.8846	67.6199	36.8979	38.3637
Std. Gray	49.8961	48.9069	66.4916	66.4916	33.2746	34.7204
Mean Color	130.8953	131.6831	130.8684	132.0300	136.8746	135.9786
Mean gray	130.3743	131.5154	130.6480	131.7335	136.3183	135.3786

Table 2 Correlation values of set_1

Corr. value	Im1_1	Im1_2	Im1_3	Im1_4	Im1_5	Im1_6
Im1_1	**1.0000**	0.6830	0.5139	0.4059	0.3009	0.0521
Im1_2	0.6830	**1.0000**	0.6540	0.6074	0.3669	0.1663
Im1_3	0.5139	0.6540	**1.0000**	0.7699	0.3843	0.0586
Im1_4	0.4059	0.6074	0.7699	**1.0000**	0.4123	0.0991
Im1_5	0.3009	0.3669	0.3843	0.4123	**1.0000**	0.2141
Im1_6	0.0521	0.1663	0.0586	0.0991	0.2141	**1.0000**

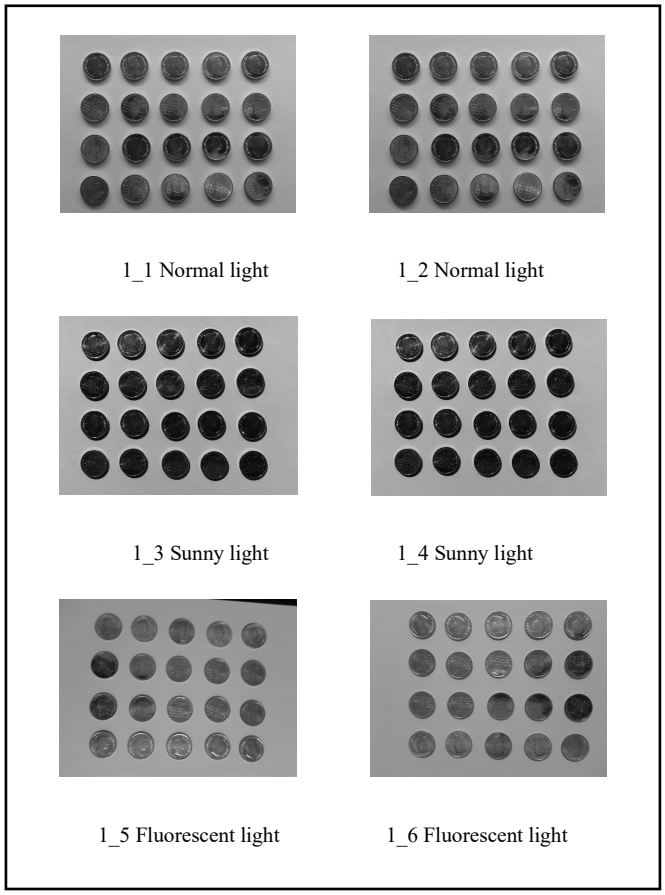

Figure 4 statistical measures of set_1

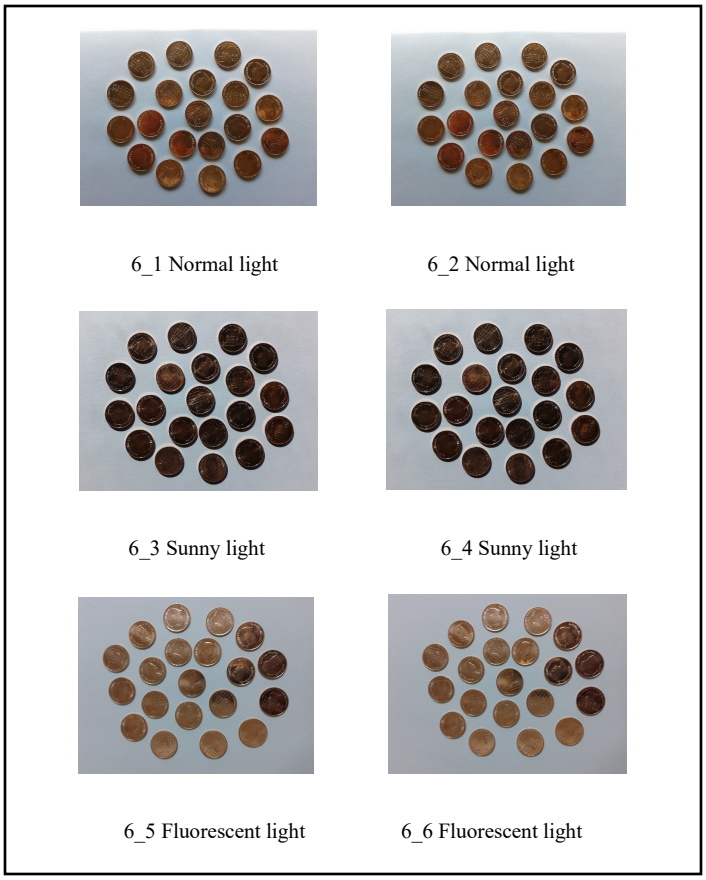

Figure 5 Original color images set_2

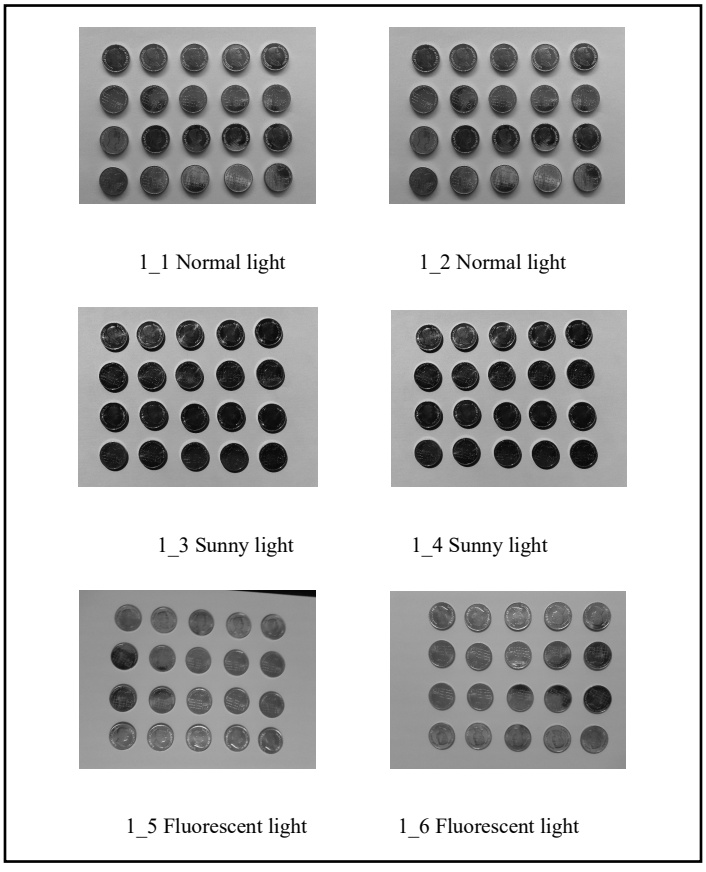

Figure 6 Gray scale images set_2

Table 3 Standard deviation and mean values of set_2

Std. and mean	Im6_1	Im6_2	Im6_3	Im6_4	Im6_5	Im6_6
Std. Color	62.1758	61.9500	73.3265	72.7418	43.9440	43.3678
Std. gray	58.4828	58.5388	72.0344	71.4614	40.0808	39.6336
Mean Color	40.8195	44.2563	135.6616	135.8909	142.6736	144.1556
Mean gray	140.7910	144.6220	135.2252	135.4476	142.7297	144.2394

Table 4 Correlation values of set_2

Corr. value	Im6_1	Im6_2	Im6_3	Im6_4	Im6_5	Im6_6
Im6_1	**1.0000**	0.8486	0.7412	0.7403	0.4854	0.4294
Im6_2	0.8486	**1.0000**	0.6233	0.6521	0.4785	0.3873
Im6_3	0.7412	0.6233	**1.0000**	0.8015	0.4485	0.4020
Im6_4	0.7403	0.6521	0.8015	**1.0000**	0.4244	0.3624
Im6_5	0.4854	0.4785	0.4485	0.4244	**1.0000**	0.6088
Im6_6	0.4294	0.3873	0.4020	0.3624	0.6088	**1.0000**

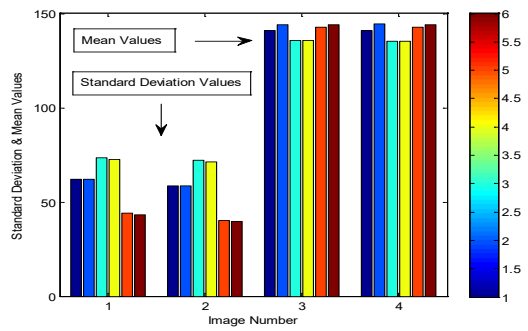

(a) Mean and standard deviation

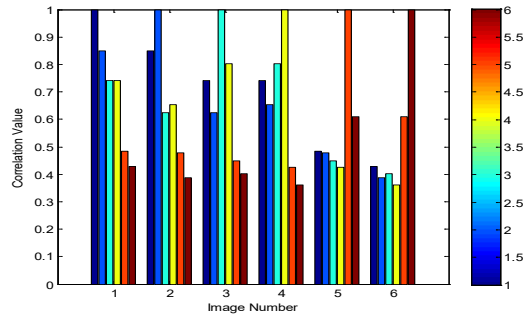

(b) Correlation

Figure 7 Statistical measures of set_2

6. Conclusions

Statistical analysis of images based on brightness distribution is implemented in this work. This simulation results show that each measure is of great importance as requirements. The selection of statistical measures is very important and should be done with caution. Using results, it is very easy to select statistics

configuration before going to an image processing complex art. Statistical analysis of images is an important topic in the image analysis field. The implemented system heavily based on statistical approach by measuring standard deviation, mean, and correlation values. Various configurations of objects are arranged in each image to detect their brightness.

The main application of this approach is to achieve the image characteristics with different types of light. In this research, emphasis has been placed on the application of statistical measurements in image analysis using images with different light parameters, regardless of the difference in the locations of shapes in the images.

Standard deviation and mean values are measured for different types of images. Various positions are designed and implemented to study and address the effect of brightness distribution via statistical measures. The obtained results indicated an adequate image surface characteristics via the application of this approach. The main finding that the use of statistical measurements have a significant impact to detect and analyze image brightness parameters, even if the difference value is small.

References

[1] M. Ravindranath Chakravarthy Bhagvati B.L. Deekshatulu, "Spectral Color Image Processing", Proceedings of the 2011 International Conference on Image Information Processing (ICIIP 2011).

[2] M. Ravindranath, Challa S. Sastry, "Compressed Sensing for Reconstruction of Reflectance Spectra from Tristimulus Values", International Conference on Information Technology for Real World Problems (VCON), India, pp. 79 - 82, 2010.

[3] T. J. de Carvalho, C. Riess, E. Angelopoulou, H. Pedrini and A. R. Rocha, "Exposing Digital Image Forgeries by Illumination Color Classification," IEEE Trans. Inf. Forensics and Security, vol. 8, no. 7, pp. 11821194, July 2013.

[4] K. Francis, S. Gholap, P.K. Bora, "Illuminant colour based image forensics using mismatch in human skin highlights," in Proc. Twentieth National Conference on Communications (NCC), pp.1-6, 2014.

[5] P. Atam Dhawan, "Medical Image Analysis", 2nd Edition, Wiley-IEEE Press, February 2011.

[6] R. Nock and F. Nielsen, "Statistical Region Merging", IEEE Transactions Pattern Analysis Machine Intelligence, vol. 26, no. 11, pp. 1452-1458, 2004.

[7] R. C. Gonzalez and R. E. Wood, "Digital Image Processing", Third Edition, Prentice Hall, Person Education International, New Jersey, 2009.

[8] R. C. Gonzalez & R. E. Woods, "Digital Image Processing Using MATLAB", Addison-Wesley, 2nd Edition 2009.

[9] B. W. Hong, S. Soatto, K. Ni, T. F. Chan. The scale of a texture and its application to segmentation. In IEEE International Conference on Computer Vision and Pattern Recognition, 2008.

[10] G. Sundaramoorthi, P. Petersen, V. S. Varadarajan, S. Soatto, "On the set of images modulo viewpoint and contrast changes", In Proceedings of the IEEE Conference on Computer Vision and Pattern Recognition, June 2009.

[11] S. Boltz, E. Debreuve, and M. Barlaud, "High-dimensional statistical distance for region-of-interest tracking: Application to combining a soft geometric constraint with radiometry", In IEEE International Conference on Computer Vision and Pattern Recognition, Minneapolis, USA, 2007.

[12] G. James, D. Witten, T. Hastie, R. Tibshirani, "An Introduction to Statistical Learning: with Applications in R", Springer, New York, Heidelberg, London, First Edition 2013.

[13] T. Hastie, R. Tibshirani, J. Friedman, "The Elements of Statistical Learning: Data Mining, Inference, and Prediction", Springer, New York, Heidelberg, London, Second Edition, 2009.

[14] Q. Al-Shayea, M. Shaban Al-Ani (2009), "Efficient 3D Object Visualization via 2D Images", International Journal of Computer Science and Network Security (IJCSNS), vol. 9, no. 11 pp. 234-239, November 2009.

[15] S. Greve, M. Grzegorzek, C. Saathoff, D. Paulus, "Classification of Image Regions Using the Wavelet Standard Deviation Descriptor", Proceedings of the International Multiconference on Computer Science and Information Technology, vol.5, pp.703–708, 2010.

[16] E. Fazal Malik and B. Bin Baharudin, "Mean and Standard Deviation Features of Color Histogram Using Laplacian Filter for Content-Based Image Retrieval", Journal of Theoretical and Applied Information Technology, Vol. 34, No.1, December 2011.

[17] A. Firas Jassim, "Semi-Optimal Edge Detector based on Simple Standard Deviation with Adjusted Thresholding", International Journal of Computer Applications, vol. 68, no.2, pp 43-48, April 2013.

[18] G. Ibrahem Raho, M. Shaban Al-Ani, Q. Al-Shayea (2014), "Object Tracking Information System Based on Statistical Measurements", International Journal of Application or Innovation in Engineering & Management (IJAIEM), vol.3, Issue 9, September 2014.

[19] A. Rashid, M. Khurrum Rahim, "Extensive Experimental Analysis of Image Statistical Measures for Image Processing Appliances", International Journal of Signal Processing, Image Processing and Pattern Recognition, vol.9, no.3, pp.49-60, 2016.

[20] N. Hallil Binti Ismail, S. Der Chen, Y. Al-Najjar, "Analysis and Improvement on Statistical Natural Measure", Journal of Theoretical and Applied Information Technology, 31st January, vol.83. no.3, 2016.

[21] B. Büyüksaraç, M. Mete Bulut, G. Bozdağı Akar, "Sign Language Recognition by Image Analysis", 978-1-5090-1679-2/16/ ©2016 IEEE Xplore.

[22] S. Intajag, S. Kansomkeat, P. Bhurayanontachai, "Histogram specification with generalized extreme value distribution to enhance retinal images", Electronics Letters, 14th, vol. 52, no. 8 pp. 596–598, April 2016.

[23] X. Zhang, J. Lu, X. Zhou, C. Guo, C. Wang, "Rapid microwave synthesis of N-doped carbon nanodots with high fluorescence brightness for cell imaging and sensitive detection of iron (III)", Optical Materials vol. 64, pp.1-8, 2017.

[24] T. Gao, H. He, R. Huang, M. Zheng, F. Fang Wang, Y. Jun Hu, F. Lei Jiang, Y. Liu, "BODIPY-based fluorescent probes for mitochondria-targeted cell imaging with superior brightness, low cytotoxicity and high photostability", Dyes and Pigments, vol. 141, pp. 530-535, June 2017.

[25] D. Oliva, S. Hinojosa, E. Cuevas, G. Pajares, O. Avalos, J. Galvez, "Cross entropy based thresholding for magnetic resonance brain images using Crow Search Algorithm", Expert Systems with Applications, vol. 79, pp. 164–180, 15 August 2017

ASTES

Advances in Science, Technology and Engineering Systems Journal Vol. 2, No. 4, 105-110 (2017)
www.astesj.com

ASTESJ
ISSN: 2415-6698

A novel algorithm for detecting human circadian rhythms using a thoracic temperature sensor

Aly Chkeir[*1], Farah Mourad-Chehade[1], Jacques Beau[4], Monique Maurice[4], Sandra Komarzynski[4], Francis Levi[3], David J. Hewson[2], Jacques Duchêne[1],

[1]*Institut Charles Delaunay UMR CNRS 6281, Rosas, University of Technology of Troyes (UTT) 10000 Troyes, France*

[2]*University of Bedfordshire, Luton, United Kingdom*

[3]*Warwick University, United Kingdom*

[4]*INSERM, University of Paris, France*

ARTICLE INFO

Article history:
Received: 07 May, 2017
Accepted: 29 June, 2017
Online: 19 July, 2017

Keywords:
Human circadian rhythm
Interpolation
Cosinor
Divergence
Temperature Sensor

ABSTRACT

Circadian rhythms undergo high perturbations due to cancer progression and worsening of metabolic diseases. This paper proposes an original method for detecting such perturbations using a novel thoracic temperature sensor. Such an infrared sensor records the skin temperature every five minutes, although some data might be missing. In this pilot study, five control subjects were evaluated over four days of recordings. In order to overcome the problem of missing data, first four different interpolation methods were compared. Using interpolation helps covering the gaps and extending the recordings frequency, subsequently prolonging sensor battery life. Afterwards, a Cosinor model was proposed to characterize circadian rhythms, and extract relevant parameters, with their confidence limits. A divergence study is then performed to detect changes in these parameters. The results are promising, supporting the enlargement of the sample size and warranting further assessment in cancer patients.

1. Introduction

Most biological processes follow circadian rhythms, with the standard period of about 24 hours. These 24-hour rhythms are driven by circadian clocks, which have been observed in plants, fungi, cyanobacteria, and humans [1, 2]. In mammals, each cell contains molecular clocks, whose coordination is ensured by the suprachiasmatic nuclei in the hypothalamus through the generation of rhythmic physiology. Such a Circadian Timing System (CTS) regulates rhythmically cellular metabolism and proliferation over the 24 hours.

The body temperature follows circadian rhythms, that are tightly related to cancer development[3] [4]. Indeed, they play an important role in the coordination of molecular circadian clocks in various peripheral organs, such as lung, liver, kidney, and intestine, and could have an effect on tumors through their regulatory effects on Heat Shock Factor (HSF), Heat Shock Proteins (HSPs), and Cold-Induced Proteins [4, 5]. Moreover, it has been demonstrated that giving chemotherapy at an accurate circadian timing improves tolerance up to fivefold and to almost doubles antitumor efficacy, compared to constant rates or wrongly timed administrations, in both rodent models and cancer patients[6] [7]. In the same way, the destruction of the suprachiasmatic nuclei suppressed any circadian rhythm in body temperature in mice, which causes a 2-3 fold acceleration of experimental cancer progression [8]. On the other hand, the temperature circadian rhythms could be disrupted by anticancer medications, and molecular clocks are impaired, as a function of dose and circadian timing in mice [9, 10]. Therefore, the circadian rhythm of body temperature is a useful biomarker of CTS function[11] [12].

The relevance of monitoring core body temperature for CTS assessment has been approved in previous works, however they all suffer from a lack of non-invasive screening tools, which has limited testing in cancer patients [13, 14]. To overcome such a problem, one could use the skin temperature, which is correlated to core temperature. However, changes in skin temperature display an opposite pattern compared to that in core body temperature, but with a similar circadian rhythm.

In our work, a non-invasive wearable sensor, Movisens® GmbH, Karlsruhe, Germany, has been used. This sensor monitors skin temperature for up to 200 hours, with the sensor able to be worn at different positions such as the hip, wrist, or chest. The temperature signals are collected at a relatively low

[*]Corresponding Author: Aly Chkeir, Institut Charles Delaunay UMR CNRS 6281, Rosas, University of Technology of Troyes (UTT) 10000 Troyes, France Email: aly.chkeir@utt.fr

sampling frequency with this sensor, that is, one point every five minutes. Using such a low frequency is possible since temperature varies slowly over time. Also, a minimal memory is required and the battery life is extended, due to reduced energy consumption for the measurement device. However, having a low signal frequency produces more difficult complications. Moreover, sensor malfunction or a subject not wearing it for a period of time causes missing data in the signals.

This paper proposes an original algorithm to analyze the circadian rhythms in skin temperature signals. It first develops an interpolation algorithm to set the signals to a higher frequency such as one sample per minute, and to fill any gap in the signals [15]. For this reason, a kernel-based machine learning algorithm is presented and compared to other classic interpolation methods. Afterwards, a rhythmometric modeling, using Cosinor models, is proposed. It aims to extract parameters such as the MESOR, the amplitude, the orthophase and the bathyphase from interpolated signals. The paper then proposes a divergence study over these features to detect changes caused by chemotherapy. Five healthy subjects' temperature signals are involved in this study, as a prerequisite for subsequent investigations involving a larger number in healthy controls and cancer patients.

2. Subjects and Methods

2.1. Subjects and materiel

In this study, three female and two male control subjects, aged 45.2 ±13.6 years, are considered. They were given a detailed description of the objectives and requirements of the study before the experiment, and they read and signed an informed consent prior to testing. The infrared Movisens (GmbH - move III) sensor was positioned on the thorax of the subjects to monitor their skin temperature for four days. It measures 5.0 x 3.6 x1.7 cm^3, and weighs 32 g. The sensor is composed of a tri-axial acceleration sensor (adxl345, Analog Devices; range: ±8 g; sampling rate: 64 Hz; resolution: 12 bit) embedded with a temperature sensor (MLX90615 high resolution 16bit ADC; resolution of 0.02°C). The recorded data is saved on a memory chip inside the sensor and transmitted to a server via GPRS. A hypoallergenic patch has been used to maintain the sensor in the upper right anterior thoracic area of the subjects.

2.2. Interpolation of temperature signals

The temperature signals have a small frequency, with occasional missing data. Let $X(k_n)_{1\leq n\leq N}$ denote the temperature samples collected for a certain subject using the sensor, with k_n in minutes. The aim of interpolation is to estimate a function $\hat{X}(.)$, that computes the temperature at any time k, and which verifies the following:

$$\hat{X}: k \to \hat{X}(k) \;\; with \;\; \hat{X}(k_n) = X(k_n) \;\; for \; 1 \leq n \leq N. \quad (1)$$

Different algorithms for interpolation such as linear, polynomial or cubic splines techniques exist in the literature [15, 16]. In the linear interpolation, temperature is represented by a straight line between any two consecutive collected measurements. Having $k \in [k_n, k_{n+1}]$, for $n \in \{1, \dots, N-1\}$,

$$\hat{X}(k) = a_n + b_n(k - k_n), \quad (2)$$

with $a_n = X(k_n)$ and $b_n = \frac{X(k_{n+1}) - X(k_n)}{k_{n+1} - k_n}$.

This technique is easy to implement, but it yields several functions, one per interval between two consecutive measurements. Moreover, it is disadvantageous for large time-intervals due to the non-specification of the linear estimation. In the polynomial interpolation, temperature is represented by a single polynomial function, which fits the measured data. By using Lagrange polynomials, one obtains the following function:

$$\hat{X}(k) = \sum_{n\in I_{N'}} \left(\prod_{\substack{j\in I_{N'} \\ j\neq n}} \frac{k - t_j}{t_n - t_j} \right) X(t_n), \quad (3)$$

where $N' \leq N$ is the degree of the obtained polynomial and $I_{N'} \subseteq \{1, \dots, N\}$. By taking N' close to N, the obtained function is specific, but with highly complex computations. Cubic splines is the most commonly used interpolation technique. It computes a set of piece-wise polynomial functions that maximize the smoothness of the whole curve. The n-th splines function defined over the interval $[k_n, k_{n+1}[$, for $n \in \{1, \dots, N\}$, is given as follows:

$$\hat{X}(k) = \alpha_n(k - k_n)^3 + \beta_n(k - k_n)^2 + \gamma_n(k - k_n) + \delta_n, \quad (4)$$

where:

$$\alpha_n = \frac{\hat{X}'(k_{n+1}) - \hat{X}'(k_n)}{6(k_{n+1} - k_n)}, \; \beta_n = \frac{\hat{X}'(k_n)}{2}, \; \delta_n = X(k_n),$$

$$\gamma_n = \frac{X(k_{n+1}) - X(k_n)}{k_{n+1} - k_n} - \frac{(k_{n+1} - k_n)\left(2\hat{X}'(k_n) - \hat{X}'(k_{n+1})\right)}{6},$$

where $\hat{X}'(.)$ is the derivative of the temperature model $\hat{X}(.)$. The values of the coefficients are then computed iteratively as shown in [2]. This technique is efficient, but proposes piece-wise functions, that need iterative computations.

TABLE I. TYPICAL REPRODUCING KERNELS

Kernel type	***General expression***
Gaussian	$\kappa(k_i, k_j) = \exp\left(-\frac{(k_i - k_j)^2}{2\sigma^2}\right)$
Polynomial	$\kappa(k_i, k_j) = (c + k_i . k_j)^q$
Exponential	$\kappa(k_i, k_j) = \exp\left(\frac{k_i . k_j}{\sigma}\right)$

This paper proposes a kernel-based regression approach that generates a single function [17, 18]. A training database is first constructed using the N collected temperature measurements $(k_n, X(k_n))_{n=1,\dots,N}$. Then a model is computed using this database, taking time as input and yielding temperature as output. This model is defined using the kernel-based ridge regression technique. The model is afterwards applied to other times, where temperature values are unknown, for interpolation. Consider a reproducing kernel κ defined from $\mathbb{R}^2$ to $\mathbb{R}$ and denote $\mathcal{H}$ its reproducing kernel Hilbert space. Some commonly used reproducing kernels are given in Table I. where the kernel parameters σ and c are positive and q is a positive integer. Then the temperature model is defined by minimizing the regularized mean quadratic error between the model's outputs and the measured data of the learning database:

$$\min_{\psi\in\mathcal{H}} \frac{1}{N} \sum_{n=1}^{N} \left(Y(k_n) - \psi(k_n)\right)^2 + \eta \|\psi\|_{\mathcal{H}}^2, \quad (5)$$

where η is a regularization parameter that controls the tradeoff between the training error and the complexity of the solution and $\|.\|_{\mathcal{H}}^2$ is the norm in the reproducing kernel Hilbert space[19]. According to the Representer theorem, that all

machine learning algorithms share, the minimization problem could be reduced to a more computation-friendly problem. Hence, the temperature model could be written as follows:

$$\psi(.) = \sum_{n=1}^{N} \alpha_n \kappa(k_n, .), \quad (6)$$

where the coefficients α_n are to be determined. Let α denote the column coefficients vector whose n-th entry is α_n. By injecting the model expression in the minimization problem, one obtains a dual optimization problem whose solution is given by:

$$\alpha = (K + \eta \mathbb{I}_N)^{-1}\mathbf{X}, \quad (7)$$

where K is a N-by-N matrix whose (i,j)-th entry is given by $\kappa(t_i, t_j)$, $\mathbb{I}_N$ is the N-by-N identity matrix and $\mathbf{X}$ is the temperature column vector, whose n-th entry is given by $X(k_n)$. Now that the model ψ is defined for each temperature signal, the temperature value at a given time n is estimated by $\hat{X}(k) = \psi(k)$.

The main advantage of the kernel-based approach remains in the fact that a single-function model is obtained, unlike the linear and cubic spline interpolations, where a piece-wise expression is obtained. In the following, and for simplicity, the notation $X(k)$ is used for the estimated signal, having a value at each minute, obtained after interpolation.

2.3. Detection of rhythmicity

The detection of rhythmicity is usually performed in the frequency domain [20]. The spectral analysis using the "Fourier transform" is a well-known study to do this [21]. In this analysis, any signal, regardless of its shape and properties, can be represented by a complex function of frequency that highlights the frequencies that make it up. By applying the inverse Fourier transform, the signal is then decomposed into an infinite sum of sine and cosine functions of infinite frequencies [22]. The signals could be deterministic such as periodic/non-periodic or random such as stationary/non-stationary. A similar analysis for periodic signals is the Fourier series analysis, which represents a function as a sum of sine and cosine functions of different frequencies.

In this paper, an algorithm based on Fourier analysis is first proposed for frequency and harmonic detection. This algorithm starts by estimating the fundamental frequency, the fundamental amplitude and phase, and the harmonic amplitudes and phases, to evaluate the *periodogram*. The term *periodogram* was introduced by Schuster in December 1934 when Fourier analysis was used to estimate periodicity in meteorological phenomena [23]. The technique was evaluated for the first time when inspecting circadian rhythms in the 1950s to measure circadian rhythms of mice after blinding [24]. The periodogram showed that periodic signals have a frequency spectrum consisting of harmonics. For instance, if the time domain repeats at ***f***, the frequency spectrum will contain a first harmonic at ***f***, a second harmonic at ***2f***, a third harmonic at ***3f***, and so forth. The first harmonic, which is the frequency at which the time domain repeats itself, is called the fundamental frequency, and has the highest amplitude. Periodograms and spectral density were originally used in chronobiology in the 1960s [25].

In order to set the periodogram, a suitable window must be applied to the signal, to reduce side-lobes. For the proposed algorithm, a normalized Hanning window has been chosen [26] since this window does not disturb the position of spectral peaks in the spectral density, although the amplitude is decreased and the peak is larger. Having the periodogram and thus the fundamental and harmonic frequencies, the temperature signal is then modeled, using the Fourier series as follows:

$$\tilde{X}(k) = M + \sum_{h=1}^{H} a_h \cos(h\omega k) + b_h \sin(h\omega k), \quad (8)$$

where ω is the angular frequency i.e. $\omega = \frac{2\pi}{\tau}$, i.e. τ is the fundamental period (duration of one cycle) and H is the number of the considered harmonics with the fundamental frequency. With respect to circadian rhythms, the rhythm persists in constant conditions with a period of around 24-hours, i.e. $\tau = 24 * 60 = 1440$ minutes. H takes values from 1 to infinity. The higher H is, the better the model $\tilde{X}(k)$ fits the observed value $X(k)$. The parameters M, a_h and b_h could be computed using the computations of Fourier series. The main advantage of this technique is that one is able to determine the exact fundamental frequency, with its following ones, by analyzing the periodogram, obtained with the Fourier transform. However, it needs the data to be equidistant and to cover more than a single cycle, otherwise the analysis would be erroneous.

One interesting method used for analyzing unequidistant and time-limited observations is the single Cosinor procedure. This study was developed to evaluate rhythmicity of un-equidistant data series[27] [28], and is frequently used in the analysis of biologic time series that have expected rhythms. Cosinor uses the least squares method to fit a sum of sine functions to a time series, as least squares procedures do not have an equidistant data limitation. Practically, it considers the Fourier series model of (8) with a precise fundamental frequency, which corresponds to 24-hours, and number of harmonics and then computes the parameters M, a_h and b_h so as to minimize the error between the signal $X(k)$ and the model $\tilde{X}(k)$. Let $e(k)$ be the residual corresponding to the value $X(k)$, that is,

$$e(k) = X(k) - \tilde{X}(k),$$

and consider the modeling error as the sum of the squared residuals (SSR) for all the data, that is,

$$SSR = \sum_k e^2(k) = \sum_k \left(X(k) - \tilde{X}(k)\right)^2 = \sum_k \left(X(k) - M - \sum_{h=1}^{H} (a_h \cos(h\omega k) + b_h \sin(h\omega k))\right)^2.$$

The parameters M, a_h and b_h are then obtained using least squares by setting the derivatives of the SSR over each parameter equal to zero. Since the temperature follows a circardian rhythm, then the fundamental frequency corresponds to 24h. Figure 1 shows an example of a Cosinor model obtained with $H = 4$. The obtained model will subsequently be used to compute significant rhythmometric parameters, as shown in the following paragraph.

Once the temperature signals are modeled, using either Fourier series or Cosinor, some features are extracted from their sinusoidal representation, as will be shown in the following paragraph.

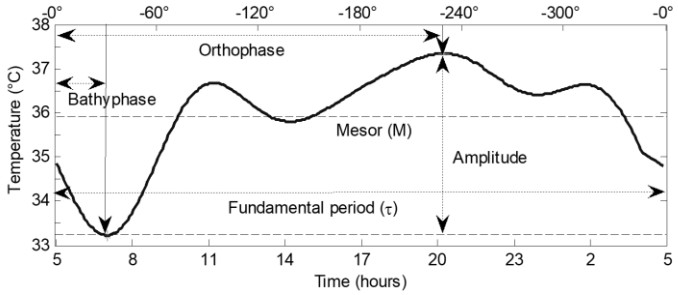

Figure 1 Circadian Rhythm Model

2.4. Features selection and divergence study

Once the temperature signal is decomposed into cumulative sine functions, using Fourier series or Cosinor, the objective here is to determine the sinusoidality of the data. This requires the extraction of some features from the models by inspecting their graph plotted against time, as shown in Figure 1. When the model is composed of more than one trigonometric function, that is, the fundamental period and some harmonics, four features could be extracted [29]:

- the MESOR (M), for "Midline Estimating Statistic Of Rhythm", that is the mean of the model,
- the amplitude (A) that is defined as the half of the difference between the maximum and the minimum of the model in one fundamental period,
- and, finally, the phases of the maximum and the minimum of the composite model including harmonic terms, which are called the orthophase Φ_O and bathyphase Φ_B respectively.

Figure 1 illustrates these features. For a control subject, these rhythmometric parameters vary slightly over time; whereas chemotherapy could produce significant modification in the circadian rhythm, which yields a divergence of one or more rhythmometric parameters. In order to detect this divergence, a sliding window algorithm is considered over the temperature signal $X(k)$ of a period of several days.

Then, for each window, the signal is modeled using the cumulative sine functions, and the four rhythmometric parameters are extracted. A statistical test, such as an exact Fisher test, Wilcoxon test or another, is then applied to check whether the values through the window diverge from their previous values. This study is motivated by the perturbation of the circadian rhythm due to chemotherapy, which induce a divergence of the statistical distributions of the extracted rhythmometric parameters.

3. Results

This section starts with the illustration of the effectiveness of the interpolation techniques. To this end, the collected temperature signals of two subjects out of the five are considered. These two have a frequency of one sample per minute over four days, whereas the remaining are measured with a rate of one sample every five minutes. An example of a skin temperature signal while wearing the IR sensor for four days, for a control pattern with an expected pattern is shown in Figure 2.

Table II. Interpolation results

Interpolation methods	*Interpolation mean error ± SD*			
	0 segment removed	*1 segment removed*	*2 segments removed*	*3 segments removed*
Linear	0.13±0.7	0.16±0.8	0.18±0.7	0.19±0.8
Cubic splines	0.15±0.7	0.17±0.8	0.19±0.8	0.25±0.9
Polynomial	0.80±1.4	0.80±1.4	0.81±1.4	0.81±1.4
Kernel-based	0.06±0.2	0.08±0.3	0.11±0.3	0.13±0.4

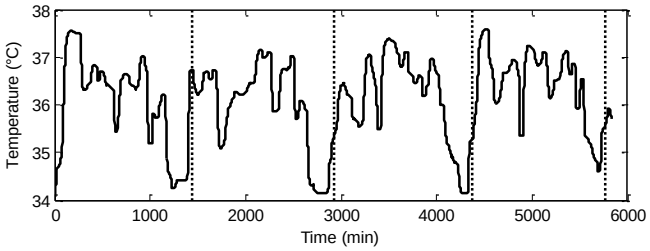

Figure 2 Skin temperature signal

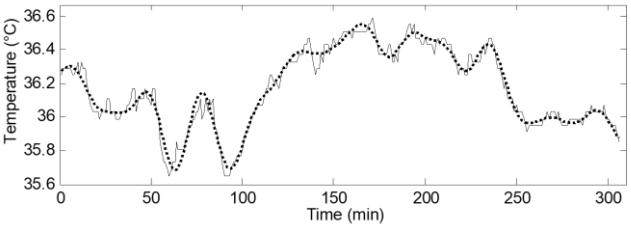

Figure 3 Kernel-based interpolation signal (dashed line) and its true measured one (straight line) for one subject over five hours, i.e. 300 minutes

In order to compare the interpolation approaches, the signals of the two subjects were divided into segments of 1440 minutes, i.e. one-day length, leading to eight segments. Then, these segments are resampled by taking one point every five minutes, leading to segments of 288 points. Thereafter, the linear, polynomial, cubic spline and kernel-based interpolation techniques were applied over these segments and the results are compared to the original observed signal. For the kernel-based interpolation, a Gaussian kernel was used, using a cross-validation algorithm to select the optimal values of the bandwidth σ and the regularization parameter η according to the learning data [17]. The mean errors for the interpolations are shown in Table II. These were computed by averaging the absolute difference between the observed and the estimated signals for the eight segments. In order to simulate the missing data, a 30-min segment was subsequently removed from the one-day length segment. This 30-min segment corresponds to six consecutive points among the 288-point segments. Then, two and three 30-min segments are removed. These segments were randomly selected within each one-day length segment. Table II shows the results for segments with no missing data (0 segment removed), one 30-min segment removed, two segments removed, and three segments removed. It is worth noting that simulations are performed 50 times and errors are averaged over all results, since the removed segments are selected randomly. The table shows that the Kernel-based algorithm yields better results with less estimation error in all cases, which is expected due its malleability and its adaptation to the curve, even under non-linear conditions.

The measured temperature signal for a typical subject for a five-hour period is shown in Figure 3. The figure also shows the interpolated signal obtained with the kernel-based interpolation.

The plot shows that the computed signal is close to the measured one, with a smooth curve produced.

Then, the objective is to illustrate the rhythmometric modeling techniques, which use the Fourier series or Cosinor. To this end, we consider the 5 temperature signals over a 4-day period, having passed the interpolation phase, i.e. the signals have no gaps, with a rate of one sample per minute. We start by applying the Fourier series, taking the fundamental period to be equal to 24 hours, i.e. 1440 minutes, followed by 3 harmonics, i.e. 12 hours, 8 hours and 6 hours. We consider that the modeling error is the average of the absolute differences between the 4-day temperature signals and their modeled ones for the 5 signals. In this case, the modeling error of the Fourier series technique with a 24-hour period is equal to 0.77. We then apply the Fourier transform to the signals to obtain their periodograms. These computations showed that the local maxima of the spectral energy are not obtained exactly at the frequencies 1/24, 1/12, 1/8 and 1/6, but very close to them.

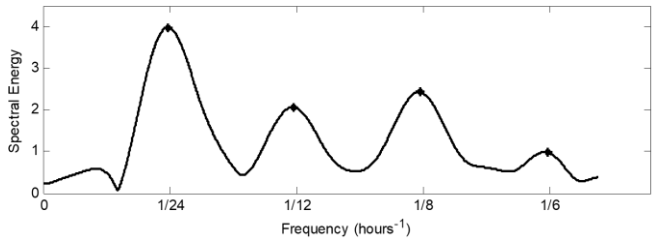

Figure 4 Periodogram generated by the Fourier analysis of the time series

Figure 4 shows a periodogram obtained for a certain subject, where the fundamental frequency is equal to 1/23.5. Let P_{max} be the fundamental period obtained by taking the maximal point of the periodogram, i.e. P_{max} is very close to 24 hours. If we take P_{max} and the following three local maxima, and perform the inverse Fourier transform, the modeling error decreases to 0.73, which was expected since this way more information is considered in the modeling. Having the fundamental period not equal to 24h is related to the fact that only four cycles (4 days) are considered, which is not enough for Fourier analysis. Afterwards, by applying Cosinor computations, while taking the fundamental period equal to 24h, and considering the following 3 harmonics, the modeling error is the least, being equal to 0.53. This shows the power of such a method with limited-duration signals.

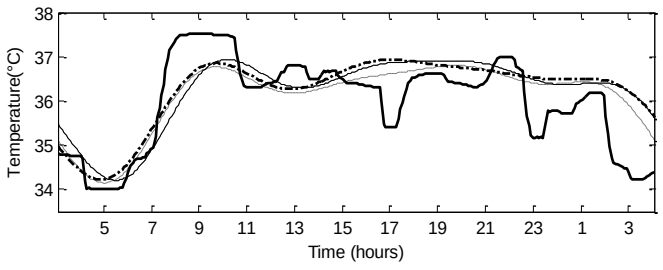

Figure 5 Temperature modeled signals using the Fourier series with a 24h period in thin dashed line, the Fourier transform with a 23.5h period in thin straight line and the Cosinor in thick dashed line, and the original signal in thick straight line.

Figure 5 shows the modeled signals in a thin dashed line for the Fourier series using a 24h period, a thin straight line for the Fourier transform using a $P_{max} = 23.5$h period and a thick dashed line for the Cosinor analysis. It also shows the original signal in thick straight line, for a one day period going from 5 a.m. till 5 am. the following day. The curves show that the obtained signals follow the original one with a small modeling error. The rhythmometric parameters, i.e. orthophase and bathyphase, are then computed. Table III shows their mean values in degrees with the standard deviations over the 5 signals. Here the parameters are extracted from the rhythmometric models obtained for the whole 4-days signals. As expected, considering the fundamental period P_{max} from the periodogram, modeling leads to a difference in the characteristics equivalent to 30 minutes, whereas both Fourier series and Cosinor lead to close values. This study shows that the Cosinor computations have promising results, to be validated with more signals later on.

Table III. Rhythmometric parameters

Mean (±SD)	*Fourier series (24h)*	*Fourier transform (P_{max})*	*Cosinor model (24h)*
Orthophase	96.9±0.6	104.1±1	97.8±0.5
Bathyphase	27.58±0.8	38.8±0.8	28.4±0.5

4. Discussion

This paper proposed a longitudinal evaluation of skin temperature measurement, collected using a thoracic sensor. The collected signals have a sampling frequency of one point every five minutes, with a length of four days for control subjects. At a first phase, we performed interpolation, using a kernel-based machine learning technique, to resample the signals to a higher frequency of one point every minute and to fill in the gaps in the measured signals. This step is crucial for the following data processing techniques. A rhythmometric study is then followed up on resampled signals, using either a Fourier representation or Cosinor. A Fourier analysis with the Fourier transform and the Fourier series is first proposed to model the signals, then a Cosinor model is constructed using Fourier analysis and least squares computations. The advantage of Cosinor remains in its robustness against un-equidistant and low-duration data, which is not the case for Fourier analysis. Rhythmometric parameters such as MESOR, amplitude, orthophase and bathyphase, are then extracted using the obtained model. For a given temperature signal of a given subject, such computations are performed for each sliding window of the signal, leading to a set of random variables that are the rhythmometric parameters. Then a divergence study is applied to detect any perturbation of the rhythm. In fact, chemotherapy can alter the circadian rhythm of the patients, therefore it is expected in that case to observe a divergence of the distributions of the rhythmometric parameters between the time span on chemotherapy and that before or after it. To detect such divergence, we can separate each parameter values into two sets (on or off chemotherapy), then apply a statistical test to detect the divergence between their distributions. This study is promising since chemotherapy-induced perturbations have been documented for over 15 anticancer drugs in experimental models, and for several drug combination protocols in cancer patients [6 14 15].

The kernel-based interpolation phase was validated using different cases of missing data in the signals, and by comparing them to well-known interpolation methods such as linear, polynomial and cubic splines. A comparison between the rhythmometric modeling techniques is then conducted, showing that Cosinor analysis leads to fewer modeling errors. Having only five signals with a 4-day duration is not enough to draw conclusions, however the results are promising for future works. Thus a larger study involving more healthy controls and

cancer patients is planned to further determine the relevance of the methodology developed here and the minimum number of harmonics. It should be possible to evaluate the effect of harmonics such as 12h, 8h, and 6h, and even to use only specific harmonics of varying frequency in order to determine the exact moment when the circadian rhythm is modified. Advanced processing such as the goodness of fit and the rhythm detection will also be applied on the signals using the F-test. Moreover, an evaluation of the IR sensor is also to be done, to verify if the observed temperature with such a sensor remains a mirror of the central temperature.

5. Acknowledgments

The authors would like to thank all clinicians, clinical research associates and technicians for their involvement in the device design and the protocol definition, set-up and monitoring. This work was supported by the Champagne-Ardenne Regional Council; PICADO project (Projet Innovant pour le Changement d'Ampleur de la Domomédecine).

References

[1] Panda, S., Hogenesch, J.B., and Kay, S.A.: 'Circadian rhythms from flies to human', Nature, 2002, 417, (6886), pp. 329-335

[2] Edgar, R.S., Green, E.W., Zhao, Y., van Ooijen, G., Olmedo, M., Qin, X., Xu, Y., Pan, M., Valekunja, U.K., Feeney, K.A., Maywood, E.S., Hastings, M.H., Baliga, N.S., Merrow, M., Millar, A.J., Johnson, C.H., Kyriacou, C.P., O/'Neill, J.S., and Reddy, A.B.: 'Peroxiredoxins are conserved markers of circadian rhythms', Nature, 2012, 485, (7399), pp. 459-464

[3] Greene, M.W.: 'Circadian rhythms and tumor growth', Cancer Letters, 2012, 318, (2), pp. 115-123

[4] Li, X.-M., Delaunay, F., Dulong, S., Claustrat, B., Zampera, S., Fujii, Y., Teboul, M., Beau, J., and Lévi, F.: 'Cancer Inhibition through Circadian Reprogramming of Tumor Transcriptome with Meal Timing', Cancer Research, 2010, 70, (8), pp. 3351-3360

[5] Reinke, H., Saini, C., Fleury-Olela, F.., Benjamin, I.J., and Schibler, U.: 'Differential display of DNA-binding proteins reveals heat-shock factor 1 as a circadian transcription factor', Genes Dev, 2008, 22, (3), pp. 331-345

[6] Levi, F., Altinok, A., Clairambault, J., and Goldbeter, A.: 'Implications of circadian clocks for the rhythmic delivery of cancer therapeutics', Philos Trans A Math Phys Eng Sci, 2008, 366, (1880), pp. 3575-3598

[7] Levi, F., Okyar, A., Dulong, S., P.F., and Clairambault, J.: 'Circadian timing in cancer treatments', Annu Rev Pharmacol Toxicol, 2010, 50, pp. 377-421

[8] Filipski, E., Li, X.M., and Levi, F.: 'Disruption of circadian coordination and malignant growth', Cancer Causes Control, 2006, 17, (4), pp. 509-514

[9] Ahowesso, C., Li, X.M., Zampera, S., Peteri-Brunback, B., Dulong, S., Beau, J., Hossard, V., Filipski, E., Delaunay, F., Claustrat, B., and Levi, F.: 'Sex and dosing-time dependencies in irinotecan-induced circadian disruption', Chronobiol Int, 2011, 28, (5), pp. 458-470

[10] Ohdo, S., Koyanagi, S., Suyama, H., Higuchi, S., and Aramaki, H.: 'Changing the dosing schedule minimizes the disruptive effects of interferon on clock function', Nat Med, 2001, 7, (3), pp. 356-360

[11] Innominato, P.F., Roche, V.P., Palesh, O.G., Ulusakarya, A., Spiegel, D., and Lévi, F.A.: 'The circadian timing system in clinical oncology', Annals of Medicine, 2014, 46, (4), pp. 191-207

[12] Scully, C.G., Karaboué, A., Liu, W.-M., Meyer, J., Innominato, P.F., Chon, K.H., Gorbach, A.M., and Lévi, F.: 'Skin surface temperature rhythms as potential circadian biomarkers for personalized chronotherapeutics in cancer patients', Interface Focus, 2011, 1, (1), pp. 48-60

[13] Ortiz-Tudela, E., Martinez-Nicolas, A., Campos, M., Rol, M.A., and Madrid, J.A.: 'A new integrated variable based on thermometry, actimetry and body position (TAP) to evaluate circadian system status in humans', PLoS Comput Biol, 2010, 6, (11), pp. e1000996

[14] Duffy, J.F., Dijk, D.-J., Klerman, E.B., and Czeisler, C.A.: 'Later endogenous circadian temperature nadir relative to an earlier wake time in older people', American Journal of Physiology - Regulatory, Integrative and Comparative Physiology, 1998, 275, (5), pp. R1478-R1487

[15] Flores-Tapia, D., Thomas, G., and Pistorius, S.: 'A comparison of interpolation methods for breast microwave radar imaging', Conf Proc IEEE Eng Med Biol Soc, 2009, 2009, pp. 2735-2738

[16] Chang, N.F., Chiang, C.Y., Chen, T.C., and Chen, L.G.: 'Cubic spline interpolation with overlapped window and data reuse for on-line Hilbert Huang transform biomedical microprocessor', Conf Proc IEEE Eng Med Biol Soc, 2011, 2011, pp. 7091-7094

[17] Mahfouz, S., Mourad-Chehade, F., Honeine, P., Farah, J., and Snoussi, H.: 'Kernel-based machine learning using radio-fingerprints for localization in wsns', Aerospace and Electronic Systems, IEEE 2015, 51, (2), pp. 1324-1336

[18] Vapnik, V.N.: 'The nature of statistical learning theory' (Springer-Verlag New York, Inc., 1995. 1995)

[19] Aronszajn, N.: 'Theory of reproducing kernels', Trans. Amer. Math. So, 1950, 68 pp. 337-404

[20] Michel Cosnard, J.D., Alain Le Breton 'Rhythms in Biology and Other Fields of Application : Deterministic and Stochastic Approache' (1983. 1983)

[21] Bloomfield, P.: 'Fourier Analysis of Time Series: An Introduction, ' (New York ;Wiley 2000, .)

[22] Fourier, J.B.J.: 'Théorie analytique de la chaleur' (1822. 1822)

[23] Bartels, J.: 'Arthur Schuster's work on periodicities', Terrestrial Magnetism and Atmospheric Electricity, 1934, 39, (4), pp. 345

[24] Halberg, F., Visscher, M.B., and Bittner, J.J.: 'Relation of visual factors to eosinophil rhythm in mice', Am J Physiol, 1954, 179, (2), pp. 229-235

[25] Panofsky, H., & Halberg, F.: 'Thermo-variance spectra; simplified computational example and other methodology. II', Exp Med Surg, 1961, 19, pp. 323-338

[26] Nuttall, A.: 'Some windows with very good sidelobe behavior', IEEE Transactions on Acoustics, Speech, and S. Processing, 1981, 29, (1), pp. 84-91

[27] Cornelissen, G.: 'Cosinor-based rhythmometry', Theoretical Biology & Medical Modelling, 2014, 11, pp. 16-16

[28] Halberg, F., Tong, Y.L., and Johnson, E.A.: 'Circadian System Phase - an aspect of temporal morphology : procedures and illustrative examples' (Springer-Verlag, 1965. 1965)

[29] Bingham, C., Arbogast, B., Guillaume, G.C., Lee, J.K., and Halberg, F.: 'Inferential statistical methods for estimating and comparing cosinor parameters', Chronobiologia, 1982, 9, (4), pp. 397-439

ASTES

Advances in Science, Technology and Engineering Systems Journal Vol. 2, No. 4, 111-114 (2017)

www.astesj.com

ASTESJ

ISSN: 2415-6698

Efficient Tensor Strategy for Recommendation

Aboagye Emelia Opoku[*, 1], Gao Jianbin[2], Qi Xia[3], Nartey Obed Tetteh[4], Opoku Mensah Eugene[5]

University of Electronic Science, Computer Science Department, China

A R T I C L E I N F O

Article history:
Received: 14 June, 2017
Accepted: 10 July, 2017
Online: 23 July, 2017

Keywords:
sentiment
Recommendation
Tensor

A B S T R A C T

The era of big data has witnessed the explosion of tensor datasets, and large scale Probabilistic Tensor Factorization (PTF) analysis is important to accommodate such increasing trend of data. Sparsity, and Cold-Start are some of the inherent problems of recommender systems in the era of big data. This paper proposes a novel Sentiment-Based Probabilistic Tensor Analysis technique senti-PTF to address the problems. The propose framework first applies a Natural Language Processing technique to perform sentiment analysis taking advantage of the huge sums of textual data generated available from the social media which are predominantly left untouched. Although some current studies do employ review texts, many of them do not consider how sentiments in reviews influence recommendation algorithm for prediction. There is therefore this big data text analytics gap whose modeling is computationally expensive. From our experiments, our novel machine learning sentiment-based tensor analysis is computationally less expensive, and addresses the cold-start problem, for optimal recommendation prediction.

1. Introduction

Recommender system as defined from the perspective of E commerce as a tool that helps users search through records of knowledge which is related to users interest and preference for a recommender system to implement its core function of identifying useful items for the user, [1, 2]. In [3] RSs is defined as a means of assisting and augmenting the social process of using recommendations of others to make choices when there is no sufficient personal knowledge or experience of the alternatives.

(RS) must predict that an item is worth recommending [4, 5]. In view of that, recommendation systems of late have become an interesting field, as they play an exquisite role in various automatic recommendation systems, and are nowadays pervasive in various domains such as recommendation of books at Amazon, music and movies recommendation at Netflix as an algorithm form tackling the information over load problem. Some of the main specific constraints or digital-age dilemmas of Recommender Systems (RSs) are; data sparsity, cold-start and issues. To overcome such problems, Matrix Factorization methods have been applied extensively by various researchers in the field. [6]-[8]. In recent times, additional sources of information are integrated into RSs. As a result, a lot of research in this field are being carried about mainly with Matrix factorization methods such as social matrix factorization (Social MF), which combines ratings with social relations [9]-[14]. Another research thread is Topic Matrix Factorization methods which combine latent factors in ratings with latent topics in item reviews [15]. In [16, 10], the authors suggested other sources of information like reviews which justify the rating of a user, and ratings which are associated with item attributes hidden in reviews producing extraordinary results but at the cost of training data and time. In this wise, we propose that, omitting such information does not aid recommendation accuracy. As a result, such problems according to research could be well taken care of through tensor decomposition as propounded by [17] and our motivation for this paper is strongly tied to these reasons. Various tensor decomposition methods have been proposed. The CANDECOMP/PARAFAC decomposition, shorted as CP decomposition, is a direct extension of low-rank matrix decomposition to tensors; and it can be regarded as a special case of Probabilistic Tensor Factorization (PTF) [18], inspired by probabilistic latent factor models [19, 20], has been proposed by various researchers as an effective tool for tackling recommendation problems [21, 22]. The era of big data has also witnessed the explosion of tensor datasets, while the large scale PTF analysis is important to accommodate the increasing datasets. A comprehensive overview can be found from the survey paper by [23]. There is therefore the need for us to solicit for tensor decomposition analysis that is able to extract hidden patterns from multi-way datasets. The core concept of senti-PTF is to capture additional sources of information occasionally neglected in

[*]Corresponding Author: Aboagye Emelia Opoku, University of Electronic Science, Computer Science Department, 86, China
Email: eoaboagye@yahoo.co.uk

various recommendation models which could efficiently improve prediction performance in RSs. The key contribution of our model is that it integrates all available data sources, that is, it provides a joint model of user, product I.D, ratings, reviews and review helpfulness.

1. Providing an effective way to exploit ratings, reviews and relations to overcome cold-start problems tightly.

2. We propose a new framework; senti-PTF which is effective in terms of prediction through error detection and solves sparsity problems.

The rest of this paper is organized as follows; Tensor

Decomposition Preliminaries are given in Section 2. In Section 3, we present the details of the experiments with datasets. In Section 4, Concluding remarks with a discussion of some future work are in the final section. Matrix Factorization and its application to personalized recommendation demonstrated the effectiveness of directly modelling all the dimensions simultaneously in a unified framework. These among other works presupposes that, tensor decomposition models performed well in terms of prediction efficiency and effectiveness compared to the various matrix factorization algorithms, in particular application to massive data processing [24]-[26]. However**,** the numerous literature concerning the subject.

1.2 Problem Statement

Regardless of the various attempt made by researchers on the subject matter; Collaborative Filtering models, they suffer from Sparsity; due to sparse rating matrix. Cold-Start; as they perform poorly on cold users and cold items for which there are no or few data. User feedback is intended to discover latent product and user dimensions. Unfortunately, traditional methods often discard review text, which makes user and product latent dimensions difficult to interpret, mainly due to the fact that, the very text that justifies a user's rating is relegated. In our opinion, ignoring rich source of information is a major shortcoming of existing works on recommender systems

1.3 Related Work

Tensor factorization methods are useful tools in recommendation systems. One prominent representative Factor-based method for recommendation systems is Probabilistic Tensor Factorization (PTF) which has been envisaged by quite a number of researchers in the recommendation system field. Tensor Factorization (BPTF) was also used to enhance prediction accuracy and recommendation using sales data by [27]. [28] also proposed the PTF model which was naturally applicable to incomplete tensors to provide both point estimate and multiple imputation for the missing entries. Tensor factorization [29] for Precision Medicine in Heart Failure with Preserved Ejection Fraction was effective. [30] in his Probabilistic polyadic factorization and its application to personalized recommendation demonstrated the effectiveness of directly modelling all the dimensions simultaneously in a unified framework. These among other works presupposes that, tensor decomposition models performed well in terms of prediction efficiency and effectiveness compared to the various matrix factorization algorithms, in particular application to massive data processing [31]-[33]. However**,** the numerous literature concerning the subject.

2.0 Proposed Sentiment-based Tensor Analysis

We propose a tensor decomposition approach to solve the sparsity, and cold-start problems of collaborative filtering algorithm making use of review sentiments and rating scores adopting Probabilistic Tensor Factorization. The main idea is to capture the latent structure of a tensor through a probabilistic factorization framework, and the latent structure is used for prediction. We jointly model ratings with review sentiments scores and model our data with probabilistic tensor factorization algorithm. In particular, CP decomposition which factorizes a tensor into a summation of rank-one tensors, where A, B and C are the latent factors. We propose probabilistic tensor factorization (PTF), which is an instance of CANDECOMP/PARAFAC (CP) tensor decomposition [34], which is a commonly used tensor model for factorization.

2. Equations

PTF's performance, we process the data into three 3rd order tensors, where each mode correspond to IDs, users and reviews, and also modelled ratings with item IDs, users and ratings respectively denoted by the tensor ABC as shown in our probabilistic model. The ratings range from 1 to 5, whiles the review sentiment were processed to 0 and 1 representing negative and positive sentiments. Tensor factorization techniques have gained popularity and have become the standard recommender approaches due to their accuracy and scalability [35]. They have probabilistic interpretation with Gaussian noise. Our model Senti-PTF combines our sentiment algorithm with probabilistic Tensor factorization framework. For Probabilistic Tensor S of size [I, J, K] where each entry is indexed as (i, j, k), and assume there is a D-dimensional latent factor A_i, B_j and C_k corresponding to each i, j and k respectively. In other words, for each dimension of the tensor, we have a latent factor matrix (A_i _D), (B_j _ D), and (C_k _D) respectively. The distribution of the unknown entry (I, j, k) given the observed tensor S is generated from Multivariate Gaussian Distribution. Given S the learning task is to model parameter theta such that the likelihood function is given by;

$$\mathrm{P}(\mathrm{S}\mid\theta)=\iiint\prod_{i=1}^{I}P(U_i\mid\mu_u,\Sigma_u)$$

$$\prod_{j=1}^{J}P(B_j\mid\mu_v,\Sigma_v)\ \prod_{k=1}^{K}P(\mathrm{t}_k\mid\mu_i,\Sigma_t)$$

$$\prod_{i=1}^{I}\prod_{j=1}^{J}\prod_{k=1}^{K}P(\mathrm{r}_{ijk}/\mathrm{A},\mathrm{B},\mathrm{C},\lambda^2)^{\delta ijk}\,d\{A,B,C\}$$

Where $\theta=\{\mu_u,\mu_v,\mu_t,\sum,\lambda^2\}$.

Given the Tensor S, the parameter θ is learned in such a way that p (S|θ) in the previous equation maximizes. Expectation Maximization is used for the posterior over latent variables P (A, B, C, S (θ)). The estimated model posterior for Finite Dimension Inference (FDI) is intractable. We therefore propose approximation inference by factorizing q(A,B,C| $\theta^{'}$) to the posterior P(A,B,C|0) more importantly;

$$q(A,B,C|\theta^{'}) = \prod_{i=1}^{I} q(u_i / M_{ui} \text{diag}(W_{ui}))$$

$$\prod_{j=1}^{J} P(V_j / M_{vj}, \text{diag(wvj)})$$

$$\prod_{k=1}^{K} P(t_k / M_{tk}, \text{diag(wtk)}),$$

where

$$\theta' = \{\text{mvi}, \text{mvj}, \text{mtk}, \text{wui}, \text{wvj}, \text{wntk}, [i]_1^I$$

$[j]_1^J, [k]_1^K\}$ are approximation variational parameters.

All approximation parameters are D-dimensional vectors and diag (w_ai) denotes a square matrix with the w_ai on the diagonal. Given q (A,B,C|$\theta^{'}$). if we apply Jensen's inequality, it produces a lower bound to the original log likelihood of the tensor S [36]

2.1 Algorithm

1: Input: S ∈ Tx,y,z, h
2: Output: S^h∈ T
3.X^h×y×z
4: Initialize x = 0
5: for H = 1,...,h
6: Sh← S (x_{one},+x;x_{two};,;)
7: end for

3. Experiments

Our experiment is designed to study the accuracy and efficiency of the senti-PTF, rat-PTF and baselines on social media review datasets which are publicly available. All the experiments are run on a Processor AMD E26110 APU with AMD Radeon R2 Graphics, 1500 Mhz, 4 Core(s), 4 Logical Processor(s) and 12GB of RAM. (a) Datasets and Parameter Settings: The real word tensor data used in our experiments are public collaborative filtering datasets; Amazon Datasets, which contains product reviews and metadata from Amazon, including 142.8 million reviews spanning May 1996 to July 2014 [37]. This dataset includes. Reviews (ratings, text, helpfulness votes), product metadata (descriptions, category information, price, brand, and image features) and links. In order to study senti-PTF's performance, we process the data into three 3rd order tensors, where each mode correspond to IDs, users and reviews, and also modelled ratings with item IDs, users and ratings respectively denoted by the tensor ABC as shown in our probabilistic model. The ratings range from 1 to 5, whiles the review sentiments were processed to 0 and 1 representing negative and positive sentiments.

3.1 Error Detection

For comparison, we implement and report the performance of senti-PTF and rat-PTF prediction. For the consistency of expression we still use "customer" and "item" to represent reviewers of automotive products. We estimate error rates on sentiments and ratings expressed, to assess the performance of our model and had the following results (figure1): The error graph shows how our algorithm; senti-PTF and rat-PTF performed. Senti-PTF performed better than rat-PTF in terms of prediction performance

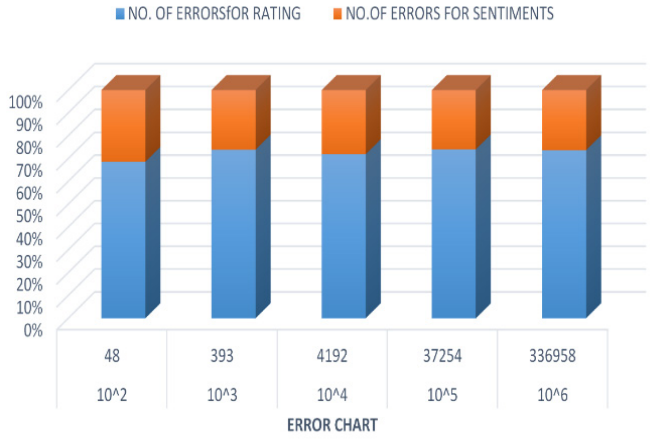

Figure 1 Error detection for senti-PTF and rat-PTF

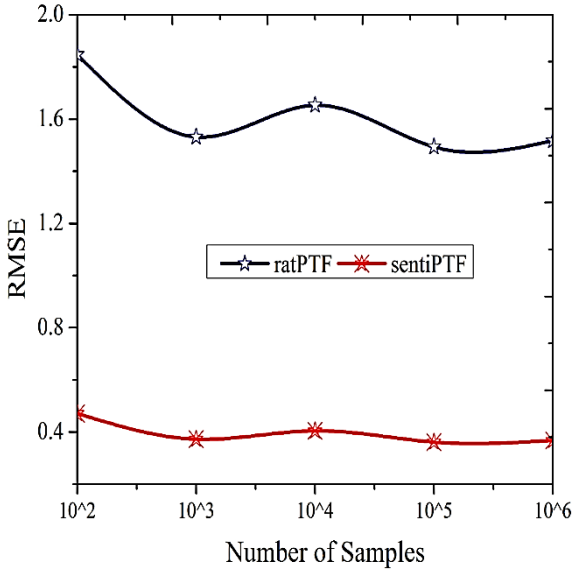

Figure 2 Root mean square error rate

4. Conclusion

A unified framework rat-PTF and senti-PTF by aligning latent factors and topics is proposed to perform Probabilistic Tensor Factorization for effective rating and sentiment prediction. In this paper, experiments on real world data sets demonstrate that our senti-PTF model outperforms the traditional CP decomposition, exploiting review sentiment beyond ratings can significantly improve recommender performance in terms of RMSE (figure2). We therefore propose Sentiment based Tensor Analysis approach

in recommendation as it solves the cold start, improves prediction efficiently and solves scalability problems of the big data era. Model integration could be envisaged in our future work [38]. Figure1 demonstrates sent-PTF achieves better performance as the tensor size increases on the Amazon datasets. The result directly sheds light on the necessity of a senti- PTF solution.

5. Conflict of Interest

We declare that, there is no conflict of interest to the publishing of this work.

Acknowledgment

This work is supported in part by the applied basic research programs of Sichuan Province (2015JY0043), the Fundamental Research Funds for the Central Universities (ZYGX2015J154, ZYGX2016J152, ZYGX2016J170), programs of international science and technology cooperation and exchange of Sichuan Province (2017HH0028), Key research and development projects of high and new technology development and industrialization of Sichuan Province(2017GZ0007)

References

[1] D. Jannach, P. Resnick, A. Tuzhilin, M. Zanker, Recommender systems|: beyond matrix completion, Communications of the ACM **59** (11) (2016) 94{102.

[2] D. Kotkov, S.Wang, J. Veijalainen, A survey of serendipity in recommender systems, Knowledge-Based Systems **111** (2016) 180{192}

[3] D. Lamprecht, M. Strohmaier, D. Helic, A method for evaluating the navigability of recommendation algorithms, Springer, 2016, pp. 247{259.

[4] B. Paudel, F. Christo_el, C. Newell, A. Bernstein, Updatable, accurate, diverse, and scalable recommendations for interactive applications, ACM Transactions on Interactive Intelligent Systems (TiiS) **7** (1) (2016) 1.

[5] R. Frey, D. W□orner, A. Ilic, Collaborative filtering on the blockchain: A secure recommender system for ecommerce.

[6] J. Wei, J. He, K. Chen, Y. Zhou, Z. Tang, Collaborative filtering and deep learning based recommendation system for cold start items, Expert Systems with Applications **69** (2017) 29{39.

[7] G.-N. Hu, X.-Y. Dai, Y. Song, S.-J. Huang, J.-J. Chen, A synthetic approach for recommendation: combining ratings, social relations, and reviews, arXiv preprint arXiv:1601.02327.

[8] G. Guo, J. Zhang, D. Thalmann, Merging Trust in collaborative filtering to alleviate data sparsity and cold start, Knowledge-Based Systems **57** (2014)57{68.

[9] Q. Yuan, L. Chen, S. Zhao, Factorization vs. regularization,Proceedings of the fifth ACM conference on Recommender systems, ACM, 2011, pp. 245{252.

[10] Y. Zhang, Grorec: a group-centric intelligent recommender system integrating social, mobile and big data technologies, IEEE Transactions on Services Computing **9** (5) (2016) 786{795.

[11] J. Tang, X. Hu, H. Gao, H. Liu, Exploiting local and global social context for recommendation, in: IJCAI, 2013, pp. 264{269.

[12] M. Bergen, S. Dutta, O. C. Walker Jr, Agency relationships in marketing: A review of the implications and applications of agency and related theories, The Journal of Marketing (1992) **1**{24.

[13] T. Chen, R. Xu, Y. He, Y. Xia, X. Wang, Learning user and product distributed representations using a sequence model for sentiment analysis, IEEE Computational Intelligence Magazine **11** (3) (2016) 34{44.

[14] C. Zheng, E. Haihong, M. Song, J. Song, Cmptf: Contextual modeling probabilistic tensor factorization for recommender systems, Neurocomputing **205** (2016) 141{151.

[15] F. Buettner, N. Pratanwanich, J. C. Marioni, O. Stegle, Scalable latentfactor models applied to single-cell rna-seq data separate biological drivers from confounding effects, bioRxiv (2016) 087775.

[16] J. Chen, X. Luo, Y. Yuan, M. Shang, Z. Ming, Z. Xiong, Performance of latent factor models with extended linear biases, Knowledge-Based Systems.

[17] G. Li, Z. Xu, L. Wang, J. Ye, I. King, M. Lyu, Simple and efficient parallelization for probabilistic temporal tensor factorization, arXiv preprint arXiv:1611.03578.

[18] A. Sapienza, A. Bessi, E. Ferrara, Non-negative tensor factorization for human behavioral pattern mining in online games, arXiv preprint arXiv: 1702.05695.

[19] C. Meneveau, I. Marusic, Turbulence in the era of big data: Recent experiences with sharing large datasets, Springer, 2017, pp. 497{507.

[20] Q. Liu, H. Jiang, Z.-H. Ling, S.Wei, Y. Hu, Probabilistic reasoning via deep learning: Neural association models, arXiv preprint arXiv:1603.07704.

[21] E. E. Papalexakis, C. Faloutsos, Unsupervised tensor mining for big data practitioners, Big Data **4** (3) (2016) 179

[22] E. E. Papalexakis, C. Faloutsos, N. D. Sidiropoulos, Tensors for data mining and data fusion: Models, applications, and scalable algorithms, ACM Transactions on Intelligent Systems and Technology (TIST) **8** (2) (2016)

[23] T.-L. Lee, Y.-C. Kuo, Computing the unique candecomp/parafac decomposition of unbalanced tensors by homotopy method, arXiv preprint arXiv: 1607.07128.

[24] W.-S. Chin, Y. Zhuang, Y.-C. Juan, C.-J. Lin, A fast parallel stochastic gradient method for matrix factorization in shared memory systems, ACM Transactions on Intelligent Systems and Technology (TIST) **6** (1) (2015) 2.

[25] P. R. Kumar, P. Varaiya, Stochastic systems: Estimation, identification, and adaptive control, SIAM, 2015. pp. 785

[26] A. Cichocki, D. Mandic, L. De Lathauwer, G. Zhou, Q. Zhao, C. Caiafa, H. A. Phan, Tensor decompositions for signal processing applications: From two-way to multiway component analysis, IEEE Signal Processing Magazine **32** (2) (2015) 145{163.

[27] B. Cyganek, S. Gruszczy_nski, Hybrid computer vision system for drivers' eye recognition and fatigue monitoring, Neurocomputing **126** (2014) 78{94.

[28] X. Yang, Y. Guo, Y. Liu, and H. Steck, "A survey of collaborative filtering based social recommender systems," *Comput. Commun.*, vol. **41**, pp. 1–10, 2014.

[29] M. Rossetti, F. Stella, and M. Zanker, "Analyzing user reviews in tourism with topic models," *Inf. Technol. Tour.*, vol. 16, no. 1, pp. 5–21, 2016.

[30] X. Amatriain, J. Basilico, Past, present, and future of recommender systems: An industry perspective, in: Proceedings of the 10th ACM Conference on Recommender Systems, ACM, 2016, pp. 211{214.

[31] H. Ma, D. Zhou, C. Liu, M. R. Lyu, I. King, Recommender systems with social regularization, in: Proceedings of the fourth ACM international conference.

[32] Q. Yuan, L. Chen, S. Zhao, Factorization vs. regularization: fusing heterogeneous social relationships in top-n recommendation, in: Proceedings of the _fth ACM conference on Recommender systems, ACM, 2011, pp.245{252}.

[33] J. McAuley, R. Pandey, J. Leskovec, Inferring networks of substitutable and complementary products, in: Proceedings of the 21th ACM SIGKDD International Conference on Knowledge Discovery and Data Mining, ACM, 2015, pp. 785{794.

[34] H. Wang, N. Wang, D.-Y. Yeung, Collaborative deep learning for recommender systems, in: Proceedings of the 21th ACM SIGKDD International Conference.

[35] A. M. Elkahky, Y. Song, and X. He, "A Multi-View Deep Learning Approach for Cross Domain User Modeling in Recommendation Systems," in *Proceedings of the 24th International Conference on World Wide Web - WWW '15*, 2015.

[36] J. McAuley, J. Leskovec, Hidden factors and hidden topics: understanding rating dimensions with review text, in: Proceedings of the 7th ACM conference on Recommender systems, ACM, 2013, pp. 165{172

[37] G. Shani, A. Gunawardana, Evaluating recommendation systems, in: Recommender systems handbook, Springer, 2011.

[38] Y. Koren and R. Bell, "Advances in collaborative filtering," in *Recommender systems handbook*, Springer, 2015, pp. 77–118.

ASTES

Advances in Science, Technology and Engineering Systems Journal
Vol. 2, No. 4, 115-120 (2017)
www.astesj.com

ASTES Journal
ISSN: 2415-6698

Solving the SAT problem using Genetic Algorithm

Arunava Bhattacharjee*, Prabal Chauhan

National Institute of Technology Durgapur, Computer Science and Engineering, 713209, India

ARTICLEINFO

Article history:
Received: 28 June, 2017
Accepted: 20 July, 2017
Online: 01 August, 2017

Keywords:
SAT
CNF
Genetic Algorithm
Crossover
Mutation
Elitism

ABSTRACT

In this paper we propose our genetic algorithm for solving the SAT problem. We introduce various crossover and mutation techniques and then make a comparative analysis between them in order to find out which techniques are the best suited for solving a SAT instance. Before the genetic algorithm is applied to an instance it is better to seek for unit and pure literals in the given formula and then try to eradicate them. This can considerably reduce the search space, and to demonstrate this we tested our algorithm on some random SAT instances. However, to analyse the various crossover and mutation techniques and also to evaluate the optimality of our algorithm we performed extensive experiments on benchmark instances of the SAT problem. We also estimated the ideal crossover length that would maximise the chances to solve a given SAT instance.

1 Introduction

A Boolean Satisfiability (abbreviated as SAT) problem involves a boolean formula F consisting of a set of boolean variables x_1,x_2,.....x_n. The formula F is in conjunctive normal form(CNF) and it is a conjunction of m clauses c_1,c_2,.....c_m. A clause is a disjunction of one or more literals, where a literal is a variable x_i or its negation. A formula F is satisfiable if there is a truth assignment to its variables satisfying every clause of the formula, otherwise the formula is unsatisfiable. The goal is to determine an assignment for every variable x satisfying all clauses.

The class k-SAT contains all SAT instances where each clause contains upto k literals. While 2-SAT is solvable in polynomial time, k-SAT is NP-complete for k>=3 . The SATs have many practical applications e.g. in planning, in circuit design, in spinglass model,in molecular biology and especially many applications and research on the 3-SAT is reported.

Some say that if we have an algorithm to solve k-SAT problem in polynomial time then cooking the food would become as easy as eating it. Speculations have been also there that a polynomial time algorithm might disapprove 2nd law of thermodynamics or can even find the god!

There are two approaches which are generally used to solve the SAT problem. The first one is local optimization or local search and the other one is genetic or evolutionary framework. The local search optimization technique is to assign some truth values to variables until we do not get a conflict[1]. After getting a conflict either the algorithm starts again or backtracks to change the value of the variable which is responsible for the conflict. So this approach uses backtracking hence time-complexity wise is not suitable (especially for large instances containing hundreds and thousands of variables). The most common algorithms in local search optimizations are GSAT(Greedy SAT)[2] and WalkSAT.

The other approach is to come up with an evolutionary algorithm[3, 4] for solving the SAT problem. They are admittedly quite fast than the traditional local search methods. However, if a given SAT instance is satisfiable but the program fails to come up with a satisfying instance within the limited time period, then it would wrongly judge the given instance as unsatisfiable. Hence it is an incomplete algorithm.

These genetic approaches involve many other factors such as crossover, mutation, parent selection and the most important factor, the fitness function. Till date we have many approaches proposed so far. For example, the SAWEA , the RFEA and RFEA2+ are based on adaptive fitness functions and use problem-specific mutation operators[5]. The FlipGA and ASAP use the MAXSAT fitness function and a local search procedure. The MAXSAT fitness value is equivalent to the number of satisfied clauses.

*Arunava Bhattacharjee, National Institute of Technology Agartala, Tripura, India, Contact: +91-9485013441 Email: bhattacharjee.arunava9@gmail.com

https://dx.doi.org/10.25046/aj020416

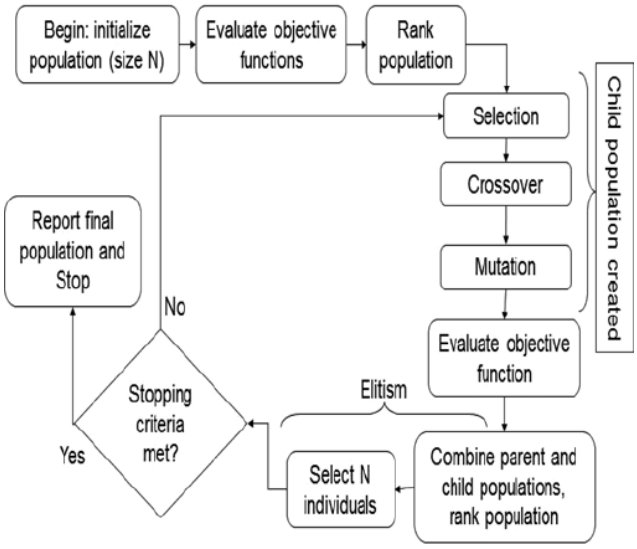

Figure 1: Basic flow chart of Genetic Algorithm design

2 Proposed Algorithm

Our algorithm combines the power of local search along with the Genetic Algorithm.

The Trivial Case:

We first check if there isnt any clause present in our formula such that all of its constituent literals are positive (negative). If this is the case, then we can immediately find a solution by assigning False (True) to all the variables.

Trivial()

- CountAllPos = No. of clauses with all constituent literals positive.
- CountAllNeg = No. of clauses with all constituent literals negative.
- If (CountAllPos == 0)
- Assign False to every variable.
- Exit.
- Else if(CountAllNeg == 0)
- Assign True to every variable.
- Exit.
- End if.
- Continue with the main algorithm.

We then eliminate all the unit literals (if present) and the pure literals (if present).

- Unit Literal Rule: If a literal appears as the single constituent of a clause in the formula, then we can safely delete all those clauses containing that literal. We also then remove the negated form of this literal from every clause in the formula where it appears.
- Pure Literal Rule: If a variable appears only in it's positive(negated) form in the whole formula, then all the clauses containing that variable can be safely deleted.

Although the benchmarks problems that we used for our experiments[6] were carefully designed not to allow this technique, however, in any random SAT instance[7] those two techniques hold good and reduce the search space to a great extent[Table 1].

Our Algorithm

1. Try the Trivial Case.
2. If solution not found yet, Eliminate Unit Literals.
3. If solution not found yet, Eliminate Pure Literals.
4. If solution not found yet, implement Genetic Algorithm.

Every chromosome in our algorithm is represented as a bit-string of length n , where n is the no of variables present in the formula.

Genetic Algorithm()

- *TOTAL_GEN* = 1
- *CURRENT_GEN* = 1
- *MAX_FITNESS* = 0
- Generate random population of size *POP_SIZE*
- Assign fitness values to every individual of the population
- For each individual a:
- If fitness(a) equals *NO_OF_CLAUSES*:
- Print Satisfiable
- Exit
- Else if fitness(a) is greater than *MAX_FITNESS*:
- *LAST_GEN* = *CURRENT_GEN*
- *MAX_FITNESS* = fitness(a)
- End if
- Sort the population by their fitness values and transfer (*ELITISM_RATE* * *POP_SIZE*) top most individuals (the ones with the higher fitness) to the next generation
- To fill up the remaining places for the new generation do the following:

- Select two fittest individuals from the current generation using Roulette-Wheel selection technique
- Apply Crossover between them. (dependent on the *CROSSOVER_RATE*)
- Apply Mutation between them. (dependent on the *MUTATION_RATE*)
- Transfer the new individuals to the next generation
- Repeat till all places for the new generation are filled
- Increment *CURRENT_GEN*
- If (*CURRENT_GEN - LAST_GEN*) > *LIMIT*:
- *TOTAL_GEN=TOTAL_GEN+CURRENT_GEN*
- If *TOTAL_GEN* > *MAX_GEN*:
- Print Not Satisfiable
- Exit
- Else goto Step 2
- End if
- Else goto Step 5
- End if

2.1 Different Parameters

Parameters used in our algorithm:

1. *MAX_GEN* : Maximum no of generations allowed for our program to run.
2. *ELITISM_RATE* : The fraction of the total no of individuals in our current generation that would be transferred to the next generation.
3. *CROSSOVER_RATE* : Determines the probability that two selected individuals would perform crossover.
4. *MUTATION_RATE* : Determines the probability that the concerned individual would undergo mutation.
5. *POP_SIZE* : The total no of individuals in any generation.
6. *LIMIT* : Specifies a threshold, if no improvement occurs for a given span of generations (specified by *LIMIT*), then a new fresh random population is generated.

The various crossover functions used:

1. Single Point Crossover : We select a pivot point (randomly) ranging between 0 to length of the chromosome and then exchange the substring from the pivot till the end of the string between the two chromosomes.
2. Two Point Crossover: We select two pivot points (randomly) ranging between 0 to length of the chromosome and then exchange the substring defined within those two points between the chromosomes.
3. Uniform Crossover: We exchange every alternate bit between the two chromosomes.
4. Greedy Crossover: This is similar to the Single Point Crossover, however we choose the pivot point in a greedy fashion.
   As a precomputation step, we first build a table of size 2*no. of variables (as we can have this many different literals possible) and store in it the no of clauses satisfied by the corresponding literal.
   So, Table[a] would store the no of clauses that the literal a would satisfy independently. We define prefix sum array 'Pre' and suffix sum array 'Suff' for a given chromosome C = $x_1x_2x_3x_4x_n$ as follows :
   Pre[i] = Table[x_1] + Table[x_2] + ...Table[x_i]
   Suff[i] = Table[x_{i+1}] + Table[x_{i+2}] +.....Table[x_n]
   Hence given a chromosome pair C1 and C2, we compute their prefix sum arrays Pre1, Pre2 and their suffix sum arrays Suff1 and Suff2 as described above.
   We choose the pivot point by the following formula,
   Pivot = index for which max(Pre1[index] + Suff2[index], Pre2[index] + Suff1[index]) is maximum for all index from [0.....length - 1] , where length is the length of the chromosome.
5. Fixed Length Crossover: We want to find out the optimal length of the crossover (the length of the substring to be swapped between the two chromosomes). So we experiment with various lengths. For a given length l, we maintain a sliding window of length l and then shift the window from left to right , and we finally swap that substring of length l (contained within that window) such that the resulting individual has the maximum fitness . We define r = Ratio of Crossover Length to Chromosome length. i.e. r = l/n. The results are displayed in Fig. 6 and Fig. 7.

The various mutation functions used:

1. Single bit flip - Flip a single bit (chosen randomly).
2. Multiple bit flip - Flip multiple bits (chosen randomly).
3. Single bit greedy - Flip a single bit which increases the fitness value for that individual.
4. Single bit max greedy - Flip that single bit which increases the fitness value for that individual to the highest as compared to flipping any other bit.

5. Multi bit greedy - Keep flipping bits (from left to right) which increases the fitness of that individual. (only a single left to right iteration).

6. FlipGA[8] - Keep flipping bits from left to right which increase the fitness of that individual. Once the right end is reached, again start from the left end until no more flipping is possible.

Mutation functions 1 and 2 are dependent on *MUTATION_RATE*. The rest aren't (due to forced mutation).

3 Experiments

POP_SIZE = 100
CROSSOVER_RATE = 0.7
MUTATION_RATE (does not matter as we used Multi bit Greedy)
LIMIT = 50
MAX_GEN = 500

The results were pleasant for instances with lesser no. of variables, however with large test cases (involving more than 80 variables) the success ratio could barely make it to 60%.

We then increased our *POP_SIZE* to 500, which improved the success rate but made our program to run extremely slow! This is because the mutation function that we were using (Multi bit greedy) was costly enough.

So we finally resorted to introduce the concept of elitism in our algorithm. We experimented with various elitism rates and found out that a 60-70 % of elitism yields best results on an average (based on runtime and success ratio).

So the final parameters for our experiments were-

1. *POP_SIZE* = 500
2. *CROSSOVER_RATE* = 1
3. *MUTATION_RATE* (does not matter as we used Multi bit Greedy)
4. *LIMIT* = 40
5. *MAX_GEN* = 200
6. *ELITISM_RATE* = 0.7

- Since we were using a high elitism rate so most of the population went on to the next generation without being mutated, so the costly mutation function needed to be used for a comparatively small part of the population, which improved the runtime.
- As we were anyway transferring 70% of the best individuals (the ones with the maximum fitness) from the current generation to the next generation, so we would like to have the remaining 30% of the new generation to be fulfilled by completely new individuals. Hence we set the *CROSSOVER_RATE* to 1 to increase the chances of getting new individuals drastically.

4 Results

As evident from Figure 2 and Figure 3 our algorithm performed quite well till test cases containing 100 variables. This had been a significant improvement over what we had achieved earlier. We also noticed that the success rate could be further increased by increasing the *MAX_GEN* (increasing the *POP_SIZE* increases the runtime drastically, so we should not increase it much), however at the cost of increased runtime.

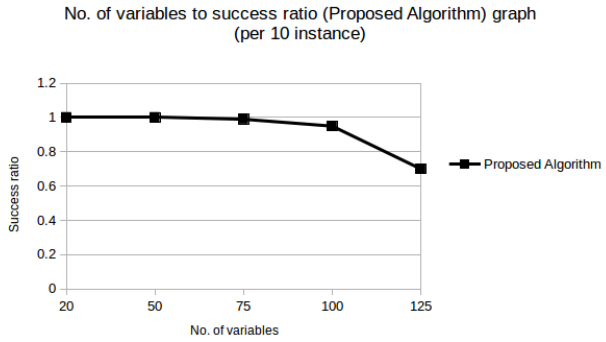

Figure 2: Success Rates

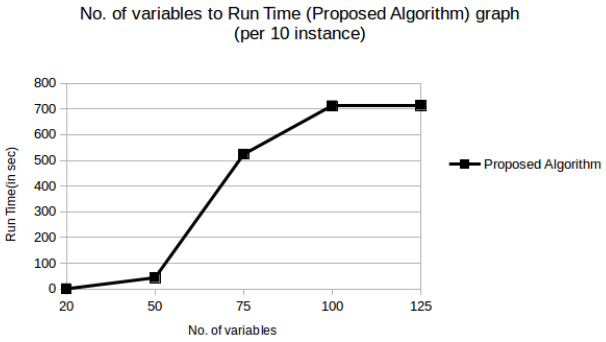

Figure 3: Run Times

Variables	Clauses	Clauses Reduced	Time(in sec)
5	20	0	0.031
50	100	10	0.054
100	200	12	0.332
25	100	0	0.069
250	1000	25	101.298
256	6336	0	107.626

Table 1: Table for Random Instances(all satisfiable)

4.1 Comparative Analysis

4.1.1 Different Crossovers

Success Rate: Clearly from Figure 4 we see that the Two point crossover performed quite well in our experiments. The Single point crossover and Greedy crossover overlap in some areas and are comparable to each other. It remains to see how they perform for instances with a very large no of variables.

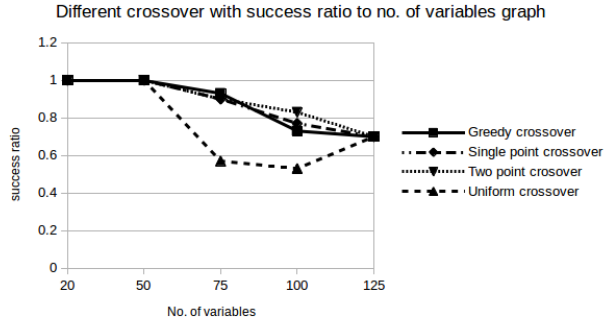

Figure 4: Success Rates of Different Crossover functions

However,a striking fact is that the uniform crossover yielded quite unsatisfactory results. We were flummoxed with its results and so to crosscheck our data we ran the program again but still the results were the same. Looks like this crossover is definitely not a choice for the Boolean Satisfiability problem.
Our implementation of uniform crossover was though, nave. It just flipped the alternating bits. It remains to see if introducing probabilistic methods to choose which bits to flip can increase the performance of this algorithm.

Runtime: Figure 5 suggests that Single point crossover and Two point crossover are the fastest (and yield good success rates as well). However, the Greedy Crossover has to perform a lot of precomputations and hence it has a larger runtime. The runtime of the Uniform Crossover doesnt really matter as it yielded a quite poor success rate.

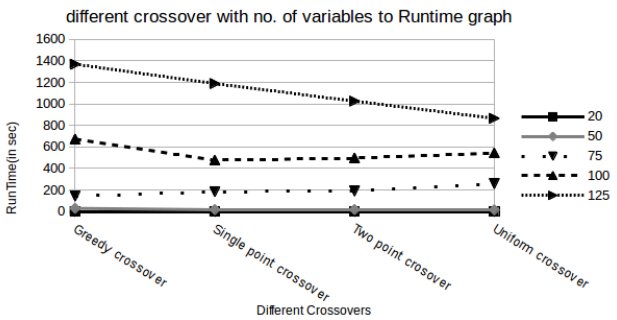

Figure 5: Run Times of Different Crossover functions

Fixed-length crossover:

We know that during the crossover phase there is an exchange of genes between the chromosomes (or namely, in our algorithm it is represented as an exchange of a substring between the two chromosomes, which themselves are represented as bit strings). What should be the ideal length of the substring to be exchanged? We tried to address this problem by conducting various experiments. We assumed that this ideal length would be a function of the no of variables present in the problem statement.

Let l be the Crossover length , i.e. the length of the substring to be exchanged between the chromosomes.

Let n be the Chromosome Length (since we represent each chromosome as a bit string of length n, where the ith bit denotes the x_i'th variable.

We defined a parameter r = Crossover Length/Chromosome Length = l/n.

We conducted experiments for crossover length ranging from 5% to 95% of the chromosome length, and the results had been overwhelming.

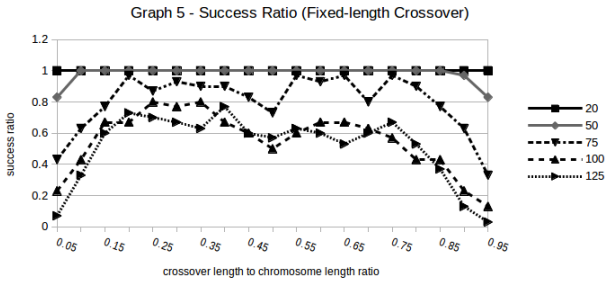

Figure 6: Success Rates for different values of r (Fixed length Crossover function)

From Figure 6, it is evident that for cases where the Crossover length was less than 20% of the Chromosome length, the success rate was pretty bad. Same was the case when the Crossover length was more than 80% of the Chromosome length.

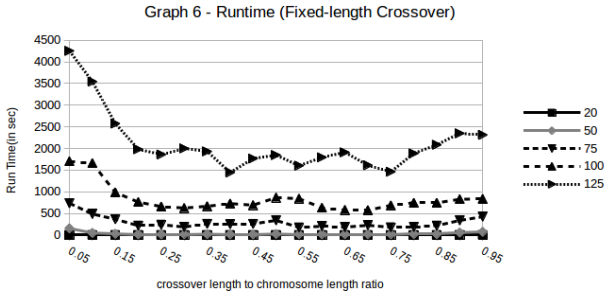

Figure 7: Run Times for different values of r (Fixed length Crossover function)

In Figure 7, we see that very small crossover lengths (< 20% of the chromosome length) have a very large runtime compared to other crossover lengths.

4.1.2 Different Mutations

Success Rate: Figure 8 shows that FlipGA dominates the success chart with around 85% of success for instances with 125 variables. The alternative Multi bit greedy too is in par with FlipGA for most of the instances except the last set of instances, where its success rate drops to 75%. But keeping these two mutation functions aside, the rest of the mutation functions perform very poorly.

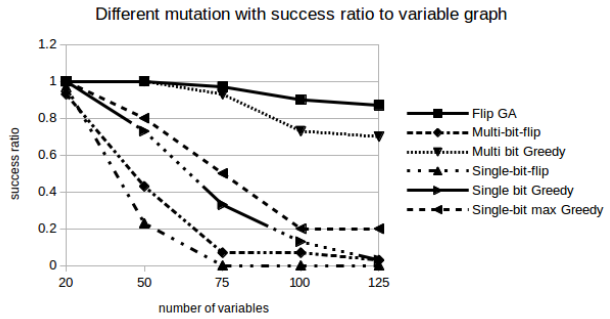

Figure 8: Success Rates for different Mutation functions

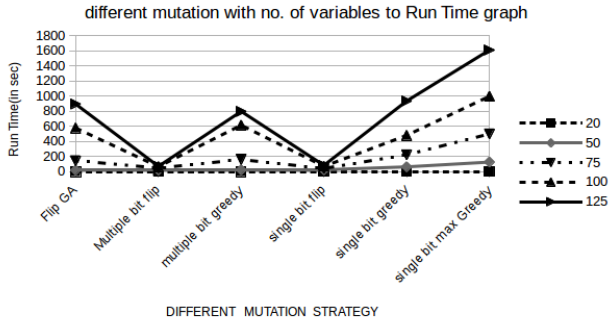

Figure 9: Run Times for different Mutation functions

Runtime: Figure 9 shows that the runtime for Multi bit greedy is slightly better then FlipGA. So its like a trade off of accuracy over runtime. Perhaps increasing the *MAX_GEN* value could improve the success ratio of Multi bit greedy without compromising the runtime to a great extent. Also, it might happen that for very large SAT instances the runtime difference betweeen these two functions might prove to be significant. The runtime of the rest mutation functions do not matter provided they have such a poor success rate.

Conflict of Interest The authors declare no conflict of interest.

Acknowledgment The authors would like to thank Dr. Pinaki Mitra, Associate Professor, Department of CSE, IIT Guwahati for his invaluable contributions and support. We also thank him for the financial support he provided for the publication of this paper.

References

[1] Peter Maandag. Solving 3-SAT (2012) http://www.cs.ru.nl/bachelorscripties/2012/Peter_Maandag___3047121___Solving_3-Sat.pdf

[2] Bart Selman, Hector Levesque, David Mitchell .A New Method for Solving Hard Satisfiability Problems(1992) www.cs.cornell.edu/selman/papers/pdf/92.aaai.g sat.pdf

[3] Istvan Borgulya. An Evolutionary framework for 3-SAT Problem (2003) hrcak.srce.hr/file/69372

[4] Stefan Harmeling. Solving Satisfiability Problems Using Genetic Algorithms (2000) https://pdfs.semanticscholar.org/70c0/6d4daabd375e818fb23cc6856fe271040095.pdf

[5] Jens Gottlieb, Elena Marchiori, Claudio Rossi. Evolutionary Algorithms for the Satisfiability Problem (2002) www.cs.ru.nl/~elenam/fsat.pdf

[6] SATLIB-Benchmark Problems http://www.cs.ubc.ca/~hoos/SATLIB/benchm.html

[7] Random instance tough SAT Generator https://toughsat.appspot.com/

[8] Elena Marchiori, Claudio Rossi. A Flipping Genetic Algorithm for Hard 3-SAT Problems (1999) https://pdfs.semanticscholar.org/e982/e6f15434df6ecfd0b59cb45b7c6875744962.pdf

ASTES

Advances in Science, Technology and Engineering Systems Journal Vol. 2, No. 4, 121-132 (2017)

www.astesj.com

ASTESJ

ISSN: 2415-6698

Pixel-Based Unsupervised Classification Approach for Information Detection on Optical Markup Recognition Sheet

Enoch Opanin Gyamfi*, Yaw Marfo Missah

Kwame Nkrumah University of Science and Technology-Kumasi, Department of Computer Science, Ghana

ARTICLE INFO

Article history:
Received: 16 June, 2017
Accepted: 28 July, 2017
Online: 20 August, 2017

Keywords:
Contrast Limited Adaptive Histogram Equalization (CLAHE)
Standard Hough Transform (SHT)
Predictive Accuracy Rate (PACC)
Precision Predictive Value (PPV)
Negative Predictive Value (NPV)

ABSTRACT

This paper proposed an Optical Markup Recognition (OMR) system to be used to detect shaded options of students after MCQ-type examinations. The designed system employed the pixel-based unsupervised classification approach with image pre-processing strategies and compared its efficiencies, in terms of speed and accuracy, with object-based supervised or unsupervised classification OMR systems. Speed and accuracy were tested using asymptotic running time and confusion matrix, respectively. The study began by involving the ideas of 50 sampled students in the design of an OMR template to be used by the proposed system. The study used six accuracy parameters to compute the effects of the three image pre-processing strategies, two-dimensional median filtering, contrast limited adaptive histogram equalisation, scanlines and standard Hough transform techniques. These strategies proved to increase the accuracy rates of the proposed system. The study finally proposed strategies to detect shaded circle bubble with its centre and block neighbouring pixels within it. These labels were stored in row-by-column one-dimensional array matrices. The study then concluded that the proposed pixel-based untrained classification OMR algorithm, is statistically fast and accurate than the object-based untrained classification OMR algorithms.

1. Introduction

Optical Mark Reading (OMR) is a novel technology in pattern recognition that can be used for several purposes, but most especially, for collecting information from Multiple Choice Questions (MCQs) paper sheets. This paper investigated into faster, timely, and inexpensive image processing strategies that could be used to extract information from scanned optical markup sheet. Currently, OMR Machines, which does this kind of processing, are high speed accurate scanners, having built-in data processing software. Some popular brands include AXIOME, SEKONIC, DARA, DATAWIN, EKEMP and Scantron. However, in Africa, more specifically in Ghana, Scantron brand-type OMR Machines are common. Their physical sizes are huge. For example, a high-volume Scantron's iNSIGHT OMR scanner takes up a space area of about 83.9×50×90.7' inches. Their prices are also very high. Again, it necessitates the use of special sheets. For instance, a large volume Scantron iNSIGHT® scanner which can process up to 15,000 custom-designed sheets per hour can be bought at a minimum price of USD 19,500. A typical custom-design OMR paper sheet is also about USD 12. These two disadvantageous features in terms of cost and size, motivates software and algorithm developers, to mimic the exact functions of these OMR Machines through software developments. Software developers thus, tend to develop low-cost, simple and accurate alternate solutions to these OMR Machines. It is with these background issues, that this paper proposed a simple and cost-effective but accurate, Graphical User Interfaced (GUI) OMR system, which used an ordinary scanner and a computer to detect information on scanned OMR sheets. Technically, the paper investigated into the viability of using pixel-based unsupervised or untrained classification approach to detect and classify patterned bubbles on OMR sheets. The performance of the algorithm, in terms of speed, accuracy and cost-effectiveness, was then tested and compared to other object-based supervised or unsupervised OMR algorithms published in literatures.

*Corresponding Author: Enoch Opanin Gyamfi, Kwame Nkrumah University of Science and Technology-Kumasi, Department of Computer Science, Ghana
Email: enochopaningyamfi@outlook.com

2. Literature Review

Three major generic development modules for recognition systems have been proposed in literatures. These were the template designing, the preprocessing and the classification modules [1, 2]. According to Addmen I.T. Solutions those recognition systems, more specifically, OMR systems, are at their utmost function when they are developed to evaluate on just a single style of sheet template layout. In this sense, the Addmen I.T. Solutions

advocated that, users of the OMR sheet template should be consulted and their perceptions need to be sought before the template design process (www.addmengroup). On their website, they again highlighted certain standard 'ISO-certified' guidelines that need to be followed when designing OMR sheet template. Preprocessing modules were proposed to prepare images by reducing data variations to a minimum so that the images are more suitable for further processing phases [3, 4]. Image preprocessing is typically the essential first step in recognition system development [5]. According to reviewed literatures, skew detection or estimation [6, 7, 8, 9], skew correction or orientation [10, 11], layout analysis [12, 13], impulse noise filtering or removal [13, 14], contrast enhancement [15], pixel perfection or sharpening [16], basic thresholding for units extraction [5], segments generation [13, 17] and Region of Interests (ROIs) [5], were most prominently used preprocessing techniques in recognition system development. The classification design module in OMR development was used to extract features from the scanned OMR sheet images using decision rules [18]. On this basis, the two procedures in decision rule classification approaches where termed as pixel-based and object-based [18]. With the pixel-based, conventional classifier generate classes for particular signatures per single pixel forming the image [18]. With the object-based, classes were generated to represent united pixels that formed objects, like shapes, on the image. They could be either supervised or unsupervised [18]. The supervised classification approach involved using methods of known informational classifiers called training sets, while the unsupervised classification methods involved studying a large number of characterized unknown pixels and distributing them into classes [18].

There were two reviewed parameters for measuring the performance efficiencies of the OMR system, which were 'Asymptotic Running Time Measurement' using graphs as adopted by the study of Stewart [19], and 'Accuracy Measurement Parameters' as given by [20, 21 and 22]. In line with the study of Stewart, using graphs to measure the asymptotic time complexity of systems, typically involved the use of the algorithm's function in the time complexity 'T(n)', calculated with the physical running time, T, and the total contiguous values of inputs 'n' received by the algorithm and tabulated during its several running times [19]. This paper also used the five accuracy parameters [20], which were the Predictive Accuracy Rate (PACC), Recall/True Positive/Sensitivity Rate (RR), Specificity/True Negative Rate (SR), Precision/Positive Predictive Value (PPV), Negative Predictive Value (NPV). The Matthews' Correlation Coefficient (MCC) was also used [21]. They were calculated as follows:

Predictive Accuracy Rate (PACC)	=	$\frac{T_p + T_n}{T_p + F_p + F_n + T_n}$ x 100%
Recall/True Positive/Sensitivity Rate (RR)	=	$\frac{T_p}{T_p + F_n}$ x 100%
Specificity/True Negative Rate (SR)	=	$\frac{T_n}{F_p + T_n}$ x 100%
Precision/Positive Predictive Value (PPV)	=	$\frac{T_p}{T_p + F_p}$ x 100%
Negative Predictive Value (NPV)	=	$\frac{T_n}{T_n + F_n}$ x 100%
Matthews Correlation Coefficient (MCC)	=	$\frac{(T_p \times T_n) - (F_p \times F_n)}{\sqrt{(T_p + F_p)(T_p + F_n)(T_n + F_p)(T_n + F_n)}}$

whereby

$\boldsymbol{False\ Positive\ (F_p)}$ $= (\lvert Total\ Positives\ (Worst\ Case)\rvert - \lvert Total\ Positive\ (Best\ Case)\rvert) + (\lvert Total\ Negative\ (Worst\ Case)\rvert - \lvert Total\ Negative\ Shaded\ (Best\ Case)\rvert)$
$\boldsymbol{False\ Negative\ (F_n)} = F_p + (\lvert Total\ Positive\ (Worst\ Case) - Total\ Positive\ (Best\ Case)\rvert)$ *or* $\boldsymbol{False\ Negative\ (F_n)} = F_p + (\lvert Total\ Negative\ (Worst\ Case) - Total\ Negative\ (Best\ Case)\rvert)$
$\boldsymbol{True\ Postive\ (T_p)} = Total\ Positive\ (Best\ Case) - F_p$ *or* $\boldsymbol{True\ Postive\ (T_p)} = Total\ Positive\ (Worst\ Case) - F_n$
$\boldsymbol{True\ Negative\ (T_n)} = Total\ Negative\ (Best\ Case) - F_n$ *or* $\boldsymbol{True\ Negative\ (T_n)} = Total\ Negative\ (Worst\ Case) - F_p$

Conferring to these equations, [23] incorporated them into their contingency confusion table. Their confusion matrix or contingency table was modified based on the definition given by Haralick [24]. The modified confusion matrix comprised of an array of probabilities whose rows and columns are both similarly categorized or designated by test and condition phases and which indicates the probability of a circle bubble being correctly identified as a member of any of the category phases as well as the probability of errors [24]. The modified confusion table of accuracy prediction is as follows:

		Condition Phase (Worst Case)		
		Condition Positive/ Shaded	Condition Negative/ Unshaded	
Testing Phase (Best Case)	Test Positive/ Shaded	True positive shaded T_p (*Correct*)	False positive shaded F_p (*Incorrect*)	Precision/Positive Predictive Value (PPV) $\frac{T_p}{T_p+F_p}$ x 100%
	Test Negative/ Unshaded	False negative unshaded F_n (*Incorrect*)	True negative unshaded T_n (*Correct*)	Negative Predictive Value (NPV) $\frac{T_n}{T_n+F_n}$ x 100
		Sensitivity/Recall Rate (RR) $\frac{T_p}{T_p+F_n}$ x 100%	Specificity Rate (SR) $\frac{T_n}{T_n+F_p}$ x 100%	

Figure 3: Modified Confusion Matrix Table for Accuracy Prediction of [24]

Studies on object-based supervised or unsupervised classification techniques in image processing were reviewed. Nine works have been done so far. However, only three [25, 26, 27], were reviewed, because, they had an extraordinary running times and predictive accuracy rates when compared to the other six. They were also easily implemented by using MATLAB®. Also, these three algorithms were current as they were designed not more than two years ago, when this research was being conducted (between 2015 to 2017). The other six algorithms [4, 28, 29, 30, 31 and 32], were proposed in earlier years (between 1999 to 2013), and they were outdated and hence unrealistic when implemented in MATLAB®

The first algorithm reviewed, the authors proposed an Optical Markup Reading strategy using Modified Multi-Connect Architecture (MMCA) technique [25]. This algorithm did not dwell on a training engine classifier. The algorithm also detected shapes instantly on the OMR sheets. Therefore, this algorithm applied the object-based unsupervised classification approach in image processing. Their strategy followed the generic conceptual procedures of any typical OMR software, whereby the software reads from a scanned or captured images, filled and unfilled small bubbles and output detected contents. However, they stored these contents in an MMCA. The MMCA functioned as an associative memory or weight matrix which was a multi-dimensional array table, that collectively stores generated shaded option labels on output (students') test paper that corresponds to a given shaded option labels on an input (examiner's) base paper [25].

The second algorithmic module reviewed, also implemented using the object-based unsupervised classification approach, identified shaded shape objects straight from scanned images without a training engine classifier [26]. Hui, Feng and Liang later characterized this algorithm as a low-cost OMR (LCOMR) technique, as the algorithm was expected to traditionally support a few number of examination sheets [33]. In their proposed methodology, scanned OMR sheets were converted from Red-Green-Blue (RGB) color type to Grayscale set, using combinations of the MATLAB® functions 'gray2ind' 'mat2gray' and 'ind2rgb' to strip hue and saturation from the image. Tanvi and Niket criticized this technique by perpetuating that the technique consumes a lot of computers' processing time and simply proposed the use of the MATLAB® function 'rgb2gray' to produce similar results [34]. The algorithm then goes on to use thresholding, skew detection for angle straightening and region of interest (ROI) techniques in getting the marked portion on the sheets. The correct answer labels are stored in an array and crossed-compared with actual answers in a database also from a master scanned answer sheets [34].

The third reviewed novel OMR algorithm used Graphical User Interfaces (GUIs) [27]. This algorithm, just like the algorithm of AL-Marakeby [32], was a supervised classification algorithm because; it involved the training of default classifiers as a single dataset. The proposed algorithm was object-based in the sense that, it detected shape object at an instance. These authors developed a GUI-based OMR in Java which aided examiner to plan and design their own OMR sheet [27]. During the OMR template design, each default attributes (size, space, position, color) of objects on the template were trained to be used in subsequent processing. This proposed system, operated under three major processes. The first process was to 'identify and find corner points of bounding box'. These corner points were used to straighten scanned images rotated more than a threshold of 11^0. The second module was to check orientation of the image's region of interest. This process calculated the direction of tilting or rotating the slanted angle of scanned images after scanning. The last module of the algorithm had to do with the 'reading of the marked fields'. In this process, the default attributes of objects on the template designed, were compared with the current attributes of the objects on the scanned templates. A rough value estimation of each attribute in the scanned images was made and a bubble could therefore be read by the algorithm as filled or unfilled when similarity was high.

2.2. Conceptual Framework of the Entire Study

The outline of the concepts backing this project is detailed in Figure 4. Different minutiae of the conceptual framework shown in Figure 4, presented an outline of concepts, assumptions and expectations of the research understudied.

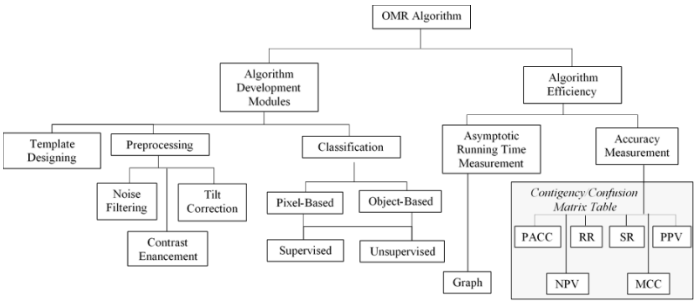

Figure 4: Conceptual Framework of the Study

3. Research Methodology

The project followed experimental research design combined with qualitative research approach. This combination aimed at forecasting the outcome of a OMR system development process through severally conducted conditional testing. An experiment was conducted on some reviewed algorithms to expose their detailed features. Following these exposed detailed features of the reviewed algorithm, they were then individually and completely developed into a software application using MATLAB®. These and other exposed features were also incorporated in developing the proposed algorithm. After that, the proposed algorithm was implemented using object-oriented code structure. Several testing and experiments were then conducted on it, to fine tune its performances until the intended outcome was achieved. The efficiency of in terms of predictive accuracy and running times of the reviewed algorithms as well as the proposed were then tested at execution. To do this, MCQ-type examinations were conducted, where students were grouped into classes, and each of the classes had a specified number of students. The number of OMR sheets filled corresponds to the number of students within a particular class. The filled OMR sheets were then scanned into folders on the primary hard disk, after which system analysis and diagnostic testing were conducted to achieve the intended outcome of the proposed method. Also, the said research design was accompanied with a qualitative research approach. The contact with qualitative data for this analysis was based on questionnaire and observation of software artifacts. Questionnaire item was used to collect data on students' perception about the layout design of the OMR sheet template to be used by the proposed system. The study was purely an interpretive study which compared the performance of several algorithms with that of the proposed algorithms, through software testing. The procedure was in such a way that, after testing all these reviewed and proposed algorithms, descriptive presentations of their inputs sizes, physical running times and accuracy rates were made. Then with appropriate statistical approaches, comparative interpretations were also conducted on each of the presentations to come out with the algorithm which had the faster and more accurate results.

3.1. Study Population, Sample and Sampling Techniques

In designing the OMR template for the proposed system, all students of the Kwame Nkrumah University of Science and Technology (KNUST) were expected to participate in this research. However, the demographic data of the population used, was limited to only the students who were in the third or fourth year of their tertiary education. These students were assumed to be very familiar and very often exposed to the current OMR sheet being used in the university, and therefore could provide impute credible data appropriate to change the layout of the OMR template to be used by the proposed OMR system. There was the need to adopt a non-probabilistic convenience sampling technique. This haphazard convenience sampling technique adopted, selected third and fourth year undergraduate students under the Computer Science Department. Using Cochran's equation [35], the sample size which was calculated at 0.85 confidence level, z-score value of 1.44, a standard deviation of 0.5, and a margin of error value being set to 0.1

$$Sample\ Size = \frac{1.44^2 \text{ x } 0.5(1-0.5)}{0.1^2} \cong 50 \quad (1)$$

Thus, in all, and through a convenient sampling technique, 50 Students were selected to respond to the questionnaire items.

4. Algorithm Implementation

The implementation of the proposed OMR algorithm was conducted in five major waves which are the template designing, document image scanning or capturing and digitization, image preprocessing stage, pixel-based unsupervised algorithm design, and lastly, presentation of the results.

4.1. Template Designing

In designing a suitable OMR sheet template for the proposed system, simple survey test questions were used. The responds from these questions posed to the students guided the subsequent design OMR sheet for the proposed system. When conducting this survey, five two-color grayscales (black and white) templates (template 1 through to template 5) were designed. The design of all these five templates followed the guidelines reviewed from the website of Addmen I.T. Solutions. Sessions of dummy MCQ-type examinations were then conducted whereby the sampled students filled the OMR template sheets. Questionnaire item was then distributed to solicit students' views as to which of the templates they preferred most

Table 1: Most Preferred OMR Template as an Alternative to the Current OMR sheet (n=50)

Variables	*f*	(%)
Template 1	1	2
Template 2	1	1
Template 3	44	88
Template 4	1	2
Template 5	3	6

From the Table 1, majority of the students (44 representing 88%), selected 'template 3' as their preferred choice. Suggestions from these students, about additional features yielded the following thematic views that were mutual among the students. They liked 'template 3' better mainly because; the instructions on that template were more adequate and clearer; the circle or oval shape of the options were more familiar; the sizes of circle shape bubbles were large and noticeable enough; the spaces between the circle bubbles were adequately evened and; the layout of contents on the template was pleasing and well-aligned

4.2. Scanning and Digitization OMR Sheet Template

The second step in our markup recognition, ensured digitization. Thus, the shaded OMR sheets were then scanned and digitized, with an EPSON® PERFECTION 2480 PHOTO scanner docked with an Automatic Document Feeder (ADF) hardware device. The output resolution of the scanner was set to as high as 300dpi. So scanned images were of high resolution quality. The scanned filled OMR sheets are then stored in a folder on a secondary storage device and the next step is to import the folder into the designed OMR software for processing

4.3. Preprocessing

After scanning and digitizing OMR sheets, they are imported into the system. Then, preprocessing phase was started. This phase of the algorithm used three techniques to enhance the image and to prepare the image to be digitally suitable for the next phase of processing. These three image preprocessing techniques used were

the pixel sharpening or perfection, noise removal or filtering and image alignment or straightening. Specifically, Contrast Limited Adaptive Histogram Equalisation (CLAHE) [36, 37] technique was used to clearly sharpen the pixels of the image. Again, Two-Dimensional Median Filtering (2D MF) [38, 39] technique was used to smoothen the pixels of the image and remove or filter speckle noise particles on scanned images. Furthermore, during image alignment or straightening was used to estimate the skew angle of the scanned document and adjust it accordingly. These techniques were necessary to address situations when examiners placed any OMR document at an improper angle relative to a given angle. Two techniques were thus, performed during the document straightening process. These techniques were the skew angle detection and skew correction relative to a suitable angle.

During the CLAHE, and the 2D MF, MATLAB® functions, adapthisteq() [36] and medfilt2() [38], were applied respectively. During skew angle detection, the algorithm began by drawing two bounding boxes around the baselines (two deep-thickened straight lines) drawn at the top and bottom portions on the OMR sheet. The bounding boxes were rectangular boxes bounding together regions of connected black pixels from the topmost or bottommost sides of the scanned images. The objective of drawing these bounding boxes was to form area around the distinct straight lines on the scanned documents that are slanted, skewed or tilted. The bounding boxes therefore formed the initial concentration area of pixels, at which skewed angles are estimated and corrected to effect the new positions of all other pixels on the digitized image. In drawing the bounding boxes, the algorithm scans through the image from the top and bottom, until it encounters two first black pixels. These first black pixels, from the top and the bottom of the document are the tip edge pixels of the two top and baselines respectively. After that, all pixels forming the tip edges of the baselines were then detected. With this, bounding rectangular boxes could then be drawn around the baselines. The algorithm adopted in drawing these bounding boxes was similar to that of [40, 41].

Next, the algorithm drew scanlines which vertically divide the area within the bounding boxes into a number of over-lapping regions called slabs. The width of each slab was 100 pixels. But if the width of the bounding box, which was divided into slabs, was not a multiple of 100 pixels, the width of that slab, which will be mostly the last slab, will then smaller than 100 pixels. The reason for choosing 100 pixels as the slab's width size was to divide the bounding box into at least 10 to 11 slabs. Through experiments with different slab widths setting the slab's width at any value between 80 to 120 pixels produced relatively similar results, but setting the slab's width below or above this range increases the overall processing time complexity of the algorithm. Thus, inside each bounding rectangular box, about 10 or 11 vertical scan lines were casted. This idea was inspired by the work of [8]. The algorithm then remembered all the hit juncture points and regression lines were drawn through these juncture points. These juncture points are the pixels at which the scanlines touched or joined the tip edge baselines. Finally, the angle slopes of the baselines were detected. These strategies are graphically illustrated in Figure 5.

The Standard Hough Transform (SHT) strategies [42] were then used to detect the actual baselines in the scanned image After the angle as well as the actual straight lines forming the baselines on the image, has also been detected, the algorithm then speculated the angle at which the pixels forming the straight line (baseline) can be mapped to correct its skewness. This part of the algorithm was inspired by the approaches of [43] as cited in [41]. All other pixels on the image were skewed correctly to lie horizontally on the scanned page. In this, correct values for pixels at a location in the skewed corrected image were calculated by weighting the true original position of the pixels with the calculated skew angle of the baseline. Some pixels are given white values, if the newly calculated location lies outside the original image. The experiments discussed here differ from those of previous investigations in that, with all these techniques combined, the algorithm could correct skewed angle up to 40^0.

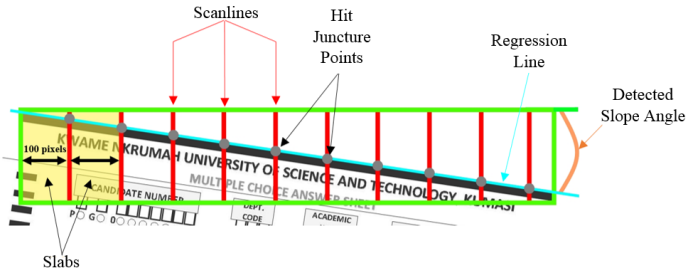

Figure 5: Skew angle detection using scanlines

4.4. The Design of the Unsupervised Pixel-Based OMR Algorithm

The circle bubble options on the custom designed OMR sheets were structurally organized, taken into consideration that, there were only two forms of grouped data to be collected. As a results, the first form of grouped data collected 'Student Details' while the second form of grouped data collected the actual 'Answers to the Multiple Choice Questions (MCQs)'. This resulted in two directional (column-wise/vertical and row-wise/horizontal) styles of shading being programmatically interpreted into software instructions and being accordingly considered using divide-and-conquer algorithm design paradigm [44]. As one sole aim of this study was to develop an untrained pixel-based classification algorithm in OMR, and to do this, locations of pixels needed to be identified on the OMR sheet. The center positions of the left most corner first circle bubble (first circle) as well as the positions of the two sequentially perpendicular (first-down) and parallel (first-right) circle bubbles, under a corresponding grouped data on the OMR Sheet, were read using MATLAB® function 'ginput ( )' or by clicking on the desired position with the 'Data Cursor' command in the MATLAB® toolbox figure.

The x-coordinate and y-coordinate VDU Cartesian values of these center pixels within the first three consecutive bubbles were stored and strategically subtracted from each other, using the 'Euclidian Metric' distance norm. All center pixels and its few surrounding neighbor pixels were now estimated with computed distance value. A thresholder pixel value of 150 was set and if the located center pixel value is less than the thresholder, then the circle bubble is classified as 'shaded' or 'dark' while, on the other hand the circle bubble is classified as 'unshaded' or 'bright' if the located center pixel value is greater than the thresholder. All shaded' or 'dark' pixels are then mapped to binary number '0'while unshaded' or 'bright' pixels are mapped to binary digit '1'. The mapped binary numbers (0s and 1s) created a results array

which is then used to compare either a vertical or horizontal 1-D array matrix. Vertical 1-D array matrices were used to store labels characters of the circle bubble options to be shaded as 'Student Details', while a horizontal 1-D array matrix was used to store labels characters of the circle bubble options to be shaded as 'Answers to Multiple Choice Questions (MCQs)'.

The next step in the algorithm carefully considered the two directional (column-wise/vertical and row-wise/horizontal) styles of shading. As with the case of the grouped data that collected personal 'Student Details', and whereby shading followed vertical or column-wise direction, extraction of results array was also made column-wisely and therefore, the comparison between column-extracted results array and vertical 1-D label array matrices, was made in a column-wise logic. For the other grouped data that collected the actual shaded 'Answers to the Multiple Choice Questions (MCQs)' and which followed the horizontal-right directional form of shading, a row-wise extraction was made from the created results array and therefore a row-wise comparison was made between the results array and the horizontal 1-D array matrix. In comparing, extracted results array were used to compare with the 1-D array matrix, after which any index position within the extracted results array that held the '0' binary number was associated with the same index position that held a consequent label character in the 1-D array matrix. The algorithm then stored the actual label character at that particular index position in a spreadsheet file.

Steps

1. ***START OMR ALGORITHM***
2. **Store in 1-D arrays, the label characters under corresponding sections on the OMR Sheet**
3. **Label all circle bubbles under corresponding sections on the OMR Sheet**
4. **Detect approximated center/middle pixel positions for first, second (first-down) and third (first-right) bubbles**

```
[x, y] ← ginput (1);
[next_x_Right, y] ← ginput (1);
[x, next_y_Down] ← ginput (1);
```

5. **Estimate the Euclidian distances between all the selected center/middle pixel of all the circle bubbles.**

```
ed_Space_x ← (next_x_right – x) + (y-y);
ed_Space_y ← (next_y_bottm – y) + (x-x);
```

6. **Apply nested loop structure for the Column-wise/Vertical directional style of shading**

```
for i←1: length of the subgroup data to be collected
    sy ← y + (i – 1) * ed_Space_y
        for j←1: length size of the 1-D array corresponding to the subgroup
            sx ← x + (j – 1) * ed_Space_x;
    end for loop
end for loop
```

7. **Declare pixel thresholder variable**

```
pixel_Thresholder ← 150; //Set pixel thresholder to classify circle bubbles
```

8. **Repeat 'Step 6' for the Row-wise/Vertical directional style of shading**
9. **//Classify pixels of Column-wise/Vertical group based on a set pixel thresholder**

```
for i←1: length of the subgroup data to be collected
    for j←1: length size of the 1-D array corresponding to the subgroup
        if ((i(next_Pixel_y, next_Pixel_x) <= pixel_Thresholder))
            c (i, j) ← 0; //Pixel Classified as Shaded
        else
            c (i, j) ← 1; //Pixel Classified as Unshaded
        end if
    end for loop
end for loop
```

10. **Repeat 'Step 9' to classify pixels of Row-wise/Vertical group as Shaded based on a set pixel thresholder**
11. **Display/Return actual bubble labels that corresponds to the shaded pixels**

```
for h=1:length (c) //Length of array storing classified binary pixels values
    shaded ← c == 0; //Counting of '0's (shaded area) in matrix 'c'
    unshaded ← c == 0; //Counting '1's (unshaded area) in matrix 'c'
        if (c (i, j) == 0) //Condition to check pixel as shaded in matrix 'c'
        student_Details ← [student_Details_Array (find (c == 0))];
    end if
    student_Details(h) ← Full_Student_Details;
end for
return Full_Student_Details
```

12. **Display/Return actual bubble labels that corresponds to the shaded pixels**

```
for i←1: length size of the 1-D array corresponding to the number of MCQs
```

```
            m ← 0; //Set initial counter for unshaded pixels
            for j=1: length size of the array for options of each single MCQ
              if (c (i, j) == 0)
                option_Shaded_MCQs ← [option_Shaded_MCQs   option_Label_MCQs]
              else
                m=m+1; //Increase counter for unshaded pixels by one
              end if
            end for loop
            if (m == 5) // Condition to check if all five bubbles are unshaded pixels
              option_Shaded_MCQs ← [option_Shaded_MCQs 'x'];
            end if
          end for loop
13.   END OMR ALGORITHM
```

5. System Implementation

A Graphical User Interface (GUI) software application was then implemented with this algorithmic flow, to use the OMR template layout preferred by the students, thus template 3. The development stages of the GUI-based OMR software application however, followed the Unified Modelling Language procedures.

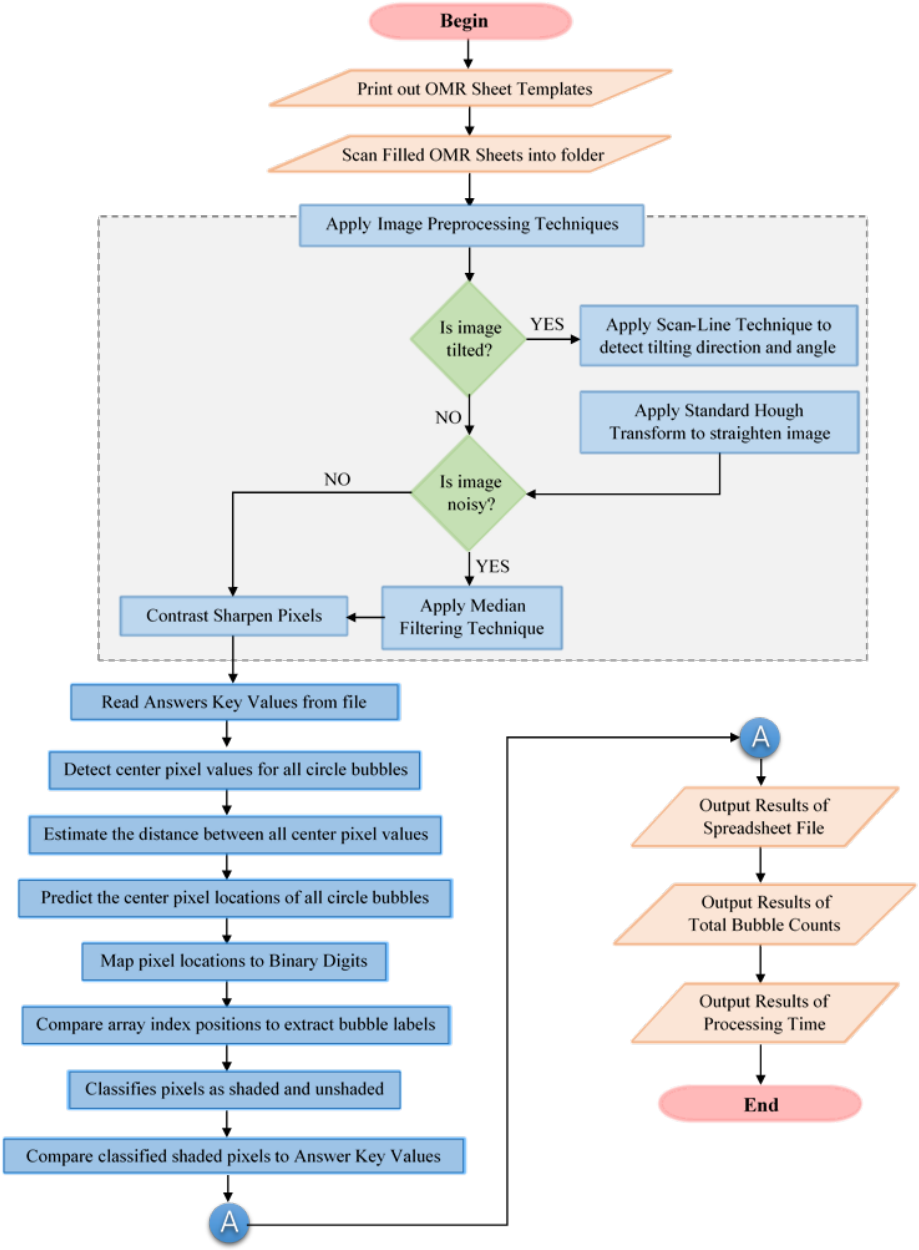

Figure 6: Flowchart of the proposed OMR System

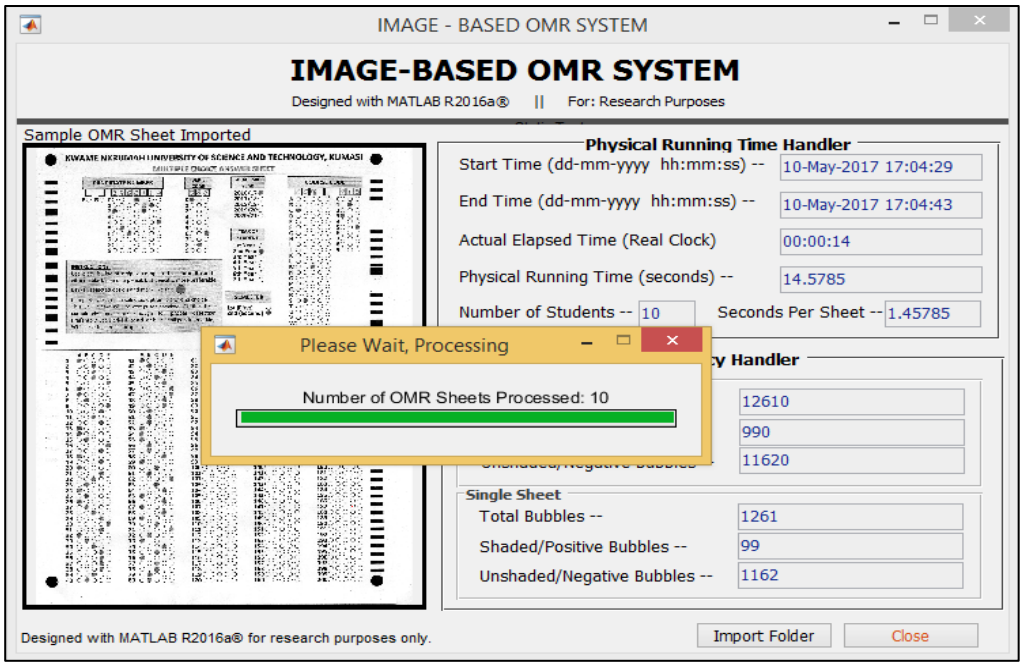

Figure 7: GUI Interface of the Image-Based OMR System (After Processing)

The Flowchart model is drawn in Figure 6. Based on the sketched flowchart unified model, a graphical user specification was developed to present shaded scores in Microsoft Excel® 2016 spreadsheet application. The Graphical User Interface (GUI) of the proposed application is shown in Figure 7.

After the proposed GUI system was developed, the dummy MCQ-type examinations were conducted to test the efficiency of the proposed OMR system, in terms of speed and efficiency. The study used two computable parameters to measure the efficiency, which were Asymptotic Running Time Measurement and Accuracy Measurement. The efficiencies of the proposed pixel-based unsupervised classification algorithm and the reviewed object-based supervised or unsupervised classification algorithms [25, 26 and 27], were then compared. Figure 7 illustrates the first physical running time comparisons between the proposed algorithm and that of [25], and then a summary of the comparisons between the proposed algorithm and the other two reviewed algorithms are presented in Table 2.

From the Figure above, the asymptotic time functions of the proposed pixel-based unsupervised (Figure 7(a)) and [25] object-based unsupervised (Figure 7(b)) classification algorithms were T(n)=38.779n0.5914 and T(n)=60.355n0.6457, respectively. Both the running time functions have positive intercept values (38.779 and 60.355) interprets that, as the number of sheets increased, the number of time taken, in seconds, to evaluate these increased in sheets, also increased. However, the positive intercept value of 38.779 construed that the proposed pixel-based unsupervised algorithm could have used 38.779 seconds to evaluate 40 OMR sheets whilst the reviewed object-based unsupervised algorithm of [25] could have been estimated to use and 60.355 seconds. Also, based on this equation, the trendlines' positive slope (gradient) values were 0.5914 for the proposed algorithm, 0.6457 for the reviewed algorithm, meaning that in any average case scenario, the proposed pixel-based unsupervised classification algorithm could have used approximately 0.5914 seconds to evaluate a single OMR sheet whilst the reviewed object-based unsupervised could have used 0.6457 seconds for the same purpose. A summary was then made on the comparative analysis of the asymptotic running time complexity functions between the proposed pixel-based unsupervised classification and the reviewed object-based unsupervised classification approaches to OMR algorithm design.

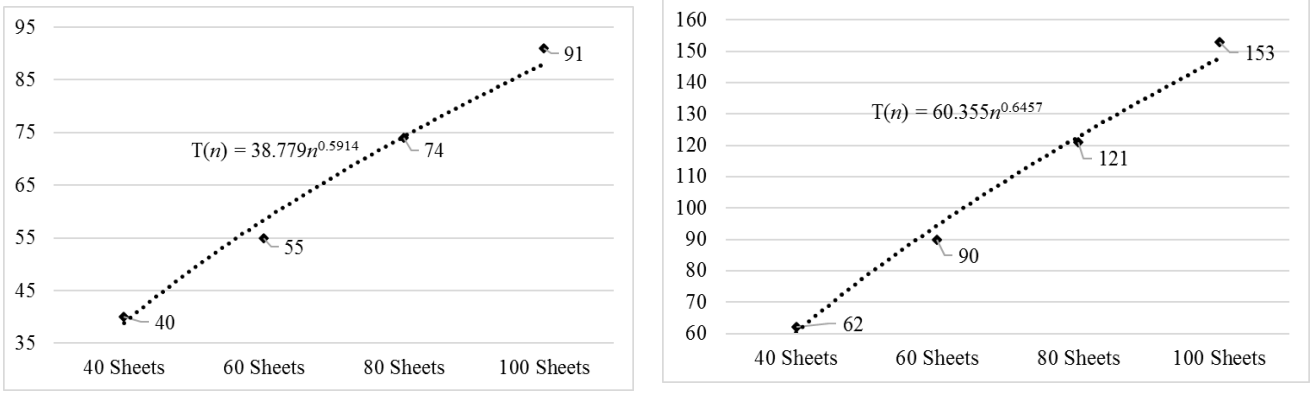

(a) (b)

Figure 8: Comparing Physical Running Times Complexity Functions between (a) the proposed algorithm and (b) [26]

Table 2: Summary of Comparisons in Asymptotic Running Time Function

Categories	Algorithm Classification Approaches			
	Pixel-Based Unsupervised	**Object-Based Unsupervised**		**Object-Based Supervised**
	Proposed from this Study	**[26]**	**[27]**	**[28]**
Asymptotic Running Time Function $T(n)= c.n^k$	$38.779n^{0.5914}$	$60.355n^{0.6457}$		
	$28.973n^{0.7616}$		$29.996n^{0.8217}$	
	$28.649n^{0.9661}$			$57.996n^{1.0004}$
Estimated Initial Running Time (in seconds) (c – '*intercept*')	28.649	60.355		
	38.779		29.996	
	28.973			57.996
	28.649 – 38.779	**29.996 – 60.355**		
Estimated Running Time Per Sheet (in seconds) (k – '*slope*')	0.5914	0.6457		
	0.7616		0.8217	
	0.9661			1.0004
	0.5914 – 0.9661	**0.6457 – 1.0004**		

Table 2 summarized the comparisons between time complexity functions of the proposed pixel-based unsupervised classification approach and the reviewed object-based supervised or unsupervised approaches. From the table, the proposed pixel-based unsupervised classification approach to OMR algorithm design yielded an initial physical running time estimates between 28.649 and 38.779 seconds whilst all the three reviewed object-based supervised or unsupervised classification approaches yielded an initial physical running time estimates between 29.996 and 60.355 seconds. Similarly, the proposed OMR algorithm was estimated to use between 0.5914 and 0.9661 to evaluate a single OMR sheet whilst the three reviewed OMR algorithm was estimated to use between 0.6457 and 1.0004 to evaluate a single OMR sheet. An indication that, the proposed algorithm used little physical time to evaluate a single or a bulky number of OMR sheets when compared to the three reviewed OMR algorithms.

Two trial test phases were used to measure the accuracy efficiency of the proposed algorithm. These phases were termed as the 'Condition Phase' and the 'Testing Phase'. In the 'Testing Phase' recordings were made on the usual physical running times of the algorithm's execution under standard and stable situations whilst in the 'Condition Phase' recordings were made on the situational physical running times of the algorithm's execution under unfavorable, hostile, unfriendly and worst case conditions, such that, the scanned OMR sheets were haphazardly folded or mishandled, tilted slightly more than the specified maximum threshold angle of 40^0 and filled with the speckled particles forming vast distortion noise levels. These amounts of information derived at the testing and condition phases were then compared and presented in a classification table or the confusion matrix table. The confusion matrix was drawn using recordings on the number of circle bubbles that are capable of being detected by the proposed algorithm when tested under both phases. This confusion matrix, as modified by [24] with the six parameters of [20] and [21], is shown in Figure 8.

In line with Figure 3, in Figure 8, the columns signified recordings derived from conditional phase while rows indicated results derived from testing phase. From Figure 8, Precision Predictive Value (PPV) was as high as 94.87%, Negative Predictive Value (NPV) was also high as 99.75%, Recall Rate (RR) was 92.50% and Specificity Rate (SR) was 99.83%. Computed results for Predictive Accuracy (PACC) rate and Matthews Correlation Coefficient (MCC) were 99.60% and 0.93, respectively. Error Rate (ER) which is calculated using the formula '(1-PACC)×100', was therefore 0.40%. The high accuracy rates for all the parameters pointed to the fact that lots of actually shaded option bubbles were accurately detected by the algorithm. Thus, the algorithm provided high reliable results when detecting correctly shaded and unshaded options on OMR sheets. Next, the accuracy level of the proposed algorithm was tested with each of the ten classes. This is presented in the second column of Table 3.

		37830		
		1200	36630	
37830	1170	1110	60	PPV=94.87%
	36660	90	36570	NPV=99.75%
		RR=92.50%	SR=99.83%	

Figure 9: Confusion Matrix Table with Numerical Recordings from the Proposed OMR System

Table 3: Accuracy Rates Comparisons between Literatures and the Proposed OMR Algorithm

Accuracy Rates	Pixel-Based Unsupervised	Object-Based Un/Supervised		
	Proposed Algorithm	[26]	[27]	[28]
PACC (%)	99.28	93.72	94.43	**97.60**
RR (%)	85.66	**85.09**	84.36	84.95
PPV (%)	92.82	77.08	76.59	**90.24**
SR (%)	99.77	-	***95.87***	-
NPV (%)	99.49	***95.94***	-	-
MCC	0.891	-	-	***0.762***

Performance accuracy raters recorded high and commendable values even when the algorithm was tested under worst case situations. It is noted from Table 3 that, in testing the accuracy of the proposed algorithm on ten different classes of diverse OMR sheets as input size, all the six accuracy rate parameters decreased in insignificant ratio, as the number of OMR sheets increased from 30 to 150 OMR sheets. For example, PACC, RR and PPV decreased from 99.60% to 98.82%, from 92.50% to 76.23% and from 94.87% to 89.91%, respectively. As shown in Table 3 the yielded average values of PACC, RR, SR, PPV, NPV and MCC were hence, 99.28%, 85.66%, 99.77%, 92.82%, 99.49% and 0.89 respectively. These accuracy rates were also compared to the accuracy rates of the reviewed object-based unsupervised or supervised classification algorithms [25, 26, and 27].

As illustrated in the Table 3, there were concrete significant gaps, in favour of the proposed OMR algorithm, between pixel-based unsupervised and the object-based unsupervised or supervised classification approaches. For example, the trainable object-based supervised algorithm proposed by [27] produced the average highest predictive accuracy rate value (PAAC=97.60%) and the Precision Predictive Value (PPV=90.24%), when compared to the other algorithms of the two authors [25] and [26]. However, these PACC and PPV values were lesser than that of the proposed pixel-based unsupervised OMR algorithm (PACC=99.28%, PPV=92.82%). The same was applicable for the computed RR, SR, NPV and the MCC accuracy parameters.

6. Key Findings of the Study

Based on the results of this study, the following are the main findings.

- The results showed that using circles (elliptical or ovals) shape as bubbles instead of the Blocks (double open squared brackets) economized space area on OMR sheet at the same time made its contents very visible to be shaded and read by the OMR system. Also, using only two grayscale (black and white) colors reduced the cost involved in printing and photocopying these sheets and required personnel with very little knowledge in computing and office duties, when implemented in real life.
- In achieving a speedy OMR system, pixel-based unsupervised classification approach was exploited in such a way that, center pixels and its few neighboring pixels rather represented circle shape options. Thus, within the algorithm, about 2 to 8 pixels centered within a circle bubble were detected and processed on, as a representative for the whole circle bubble. Current literatures used all pixels, sometimes about 250 pixels, together to form a single circle shape bubble.
- The algorithm also used throughout its processing, the row-by-column one-dimensional (1-D) array matrices either in vertical (transpose) or horizontal representations. In several literatures, array matrices were suggested to be the fasters and easiest data structures that could be implemented within any algorithm. Again, the compared literatures used associative weight memory matrices, multi-dimensional array tables and trained classifiers as their data structures. This research thus, proved these data structures to be slower
- The algorithm was designed in such a way to separately consider the two major structural groupings of circle bubbles on OMR sheet. With this effect, the algorithm utilized the divide-and-conquer algorithm designs paradigm, as segments of the algorithm were broken down to process only specific parts of the OMR sheets.
- The results showed that in achieving a more accurate level of detection on the inputted scanned OMR sheets, preprocessing techniques has to be duly considered before the algorithm goes further to classify circle bubbles using its intended pixel-based unsupervised classification method. Although, several literatures suggested numerous image preprocessing techniques, it was found out that, the three (2D median filtering technique, Contrast Limited Adaptive/Adjusted Histogram Equalization (CLAHE), and the Scan-line and Standard Hough Transform (SHT)) that were used, resulted in a high accuracy rate even when the algorithm was tested under hostile conditions.
- The results showed the output efficiencies of the proposed pixel-based unsupervised classification OMR algorithm, in terms of speed and accuracy, was better, as the number of OMR sheet inputs got large or increased. In terms of speed, the asymptotic running time complexity of the proposed pixel-based unsupervised classification algorithm was small at initial input size of OMR sheet, and increased as the number of OMR sheet increased. However, an exceptionally lesser speed was used to evaluate single OMR sheet when compared to object-based supervised or unsupervised classification algorithm. In terms of accuracy, the amount of useful and relevant information detected by the proposed pixel-based unsupervised classification algorithm were estimated be very much adequate and the amount of valueless and irrelevant information detected were predicted to be insignificant, even under very unfavorable conditions. The observed higher percentage of accuracy raters attested to this finding

7. Conclusions

The primary intention of the test results of this study was to categorize the proposed pixel-based unsupervised classification OMR algorithm as either desirable or undesirable in terms of speed and accuracy. Per the outcome of the results, the proposed OMR algorithm is concluded to be more fast and accurate when compared to the object-based unsupervised or supervised classification OMR algorithm. From a more technical perspective, the study examined the effect of three algorithm development modules, template designing, image preprocessing and content classification, on the cost, speed and accuracy of an OMR algorithm. As these algorithm development modules favoured the algorithm, the algorithm concluded to be 'good' or 'efficient'. It can be concluded that, an OMR algorithm that used the pixel-based unsupervised classification approaches and preprocessed scanned OMR sheets with noise filtering, contrast enhancement and tilt correction techniques ended up being faster and more accurate.

8. Recommendations/Future Research

8.1. Implications of this Study to Research

This study offered some important implications to research in the areas of OMR, OCR, classification approaches and image processing techniques.

- This proposed OMR system was tested in one real life application, MCQ-type examinations, but in future, researchers can extend the implementation of similar modules in this research to other real-life scenarios like the automatic attendance marking system, lotteries, consumer and community surveys, voting and product evaluation, university admission form evaluation, to mention a few.

8.2. Implications of this Study to Algorithm Developers

This study provided some implications to OMR and even OCR algorithm developers:

- Algorithm developers can investigate into how other data structures, apart from arrays, but like linked lists, stacks, queues, trees and even graphs, could be used in storing detected label characters and results and at the same time increasing its computational efficient in terms of speed and accuracy.
- Algorithm developers can research into other pixel-based supervised approaches that use training datasets as the basis of its classification.
- As the proposed OMR algorithm strictly limited itself to a single OMR sheet layout, algorithm developers could build upon this algorithm to be more scalable for classification, even using severally different or user-specified OMR sheet layouts.
- Algorithm developers can study into how pixel-based classification approaches can work best for low resolution data, as this study could not test the effects of resolution scalar features of scanned images on accuracy or speed of the algorithm
- Algorithm developers can also look into areas whereby OMR sheets could be snapshotted with a digital camera or even a smartphone camera. In this logic, and in future, further developments could be made on this proposed approach to be implemented on a mobile phone instead of on a computer.

9. References

[1] Wagenheim, M., "Grading Biology MCQ Exams at a Large State University". Retrieved from http://www.remarksoftware.com. on 24th December, 2016.

[2] Palmer, R. C. The Basics of Automatic Identification. Canadian Data systems, 21 (9), 30-33, 2009

[3] Brown, M. K., and Ganapathy, S. Preprocessing techniques for cursive script word recognition. Pattern Recognition, 16(5), 447-458, 1983

[4] Spadaccini, A., and Rizzo, V., A Multiple-Choice Test Recognition System based on the Gamera Framework. arXiv preprint arXiv:1105.3834, 2011

[5] Han, C. C., Cheng, H. L., Lin, C. L., and Fan, K. C., Personal authentication using palm-print features. Pattern recognition, 36(2), pp. 371-381, 2003

[6] Chinnasarn K. and Rangsanseri Y., "The Skew Estimation of Printed Documents", Ladkrabang Information Journal 3, pp. 14-21, 1998.

[7] Gatos, B., Papamarkos, N., and Chamzas, C., Skew detection and text line position determination in digitized documents. Pattern Recognition, 30(9), 1505-1519, 1997

[8] Chou, C. H., Chu, S. Y., and Chang, F., Estimation of skew angles for scanned documents based on piecewise covering by parallelograms. Pattern Recognition, 40(2), 443-455, 2007

[9] Yu B., and Jain A. K., A robust and fast skew detection algorithm for generic documents, Pattern Recognition 29 (10) pp. 1599–1729, 1996

[10] Yan H., Skew correction of document images using interline cross-correlation, CVGIP: Graphical Models and Image Process. 55 (6) 538–543, 1993

[11] Le D. S, Thoma G. R., Wechsler H., Automated page orientation and skew angle detection for binary document images, Pattern Recognition 27 (10) 1325–1344, 1994

[12] O'Gorman L., The document spectrum for page layout analysis, IEEE Trans. Pattern Analysis Machine Intelligence. 15 (11), pp. 1162–1173, 1993

[13] Kasturi, R., O'gorman, L., and Govindaraju, V., Document image analysis: A primer. Sadhana, 27(1), 3-22., 2002

[14] Fan, K. C., Wang, Y. K., and Lay, T. R., Marginal noise removal of document images. Pattern Recognition, 35(11), 2593-2611, 2002

[15] Celik, T., Two-dimensional histogram equalization and contrast enhancement. Pattern Recognition, 45(10), 3810-3824, 2012

[16] Pal, S. K. and Pal, A., Pattern recognition: from classical to modern approaches, World Scientific, ISBN No. 981-02-4684-6, Singapore, 2001

[17] Pornsiriprasert N. Design and development of page segmentation program for character recognition. Master's Thesis, Chulalongkorn University, 2002

[18] Pooja K, Sonam S., and Sonu A., A Survey on Image Classification Approaches and Techniques, *International Journal of Advanced Research in Computer and Communication Engineering* (2)1, 1005-1009, 2013

[19] Stewart J., Data Structures and Algorithm Analysis – Estimating Asymptotic Complexity by Experiment using Graphs, Oxford, England: Clarendon Press, 1998

[20] Bradley, A. P., The use of the area under the ROC curve in the evaluation of machine learning algorithms. Pattern recognition, 30(7), 1145-1159, 1997

[21] Désir, C., Bernard, S., Petitjean, C., and Heutte, L., One class random forests. Pattern Recognition, 46(12), 3490-3506, 2013

[22] Powers, D. M. W., "Evaluation: From Precision, Recall and F-Measure to ROC, Informedness, Markedness and Correlation". Journal of Machine Learning Technologies. Volume: 2, Issue: 1, pages: 37–63., 2011

[23] Fawcett, T., An introduction to ROC analysis. *Pattern recognition letters*, 27(8), 861-874, 2006

[24] Haralick, R. M., Glossary and index to remotely sensed image pattern recognition concepts. Pattern Recognition, 5(4), 391-403, 1973

[25] Rusul H. and Emad I. A. K., *An Image Processing Oriented Optical Mark Reader Based on Modify Multi-Connect Architecture MMCA,* International Journal of Modern Trends in Engineering and Research-IJMTER-PP 414-423, 2015

[26] Sumitra B. G., *Image Processing Based OMR Sheet Scanning.* International Journal of Advanced Research in Electronics and Communication Engineering (IJARECE), Volume 4, Issue 3, PP. 519-522, 2015.

[27] Garima K., Hemant R. R., Rana, Ishu M., Kashif O. and Narendra S., "*Implementation of OMR Technology with the Help of Ordinary Scanner"*, International Journal of Advanced Research in Computer Science and Software Engineering (IJARCSSE), Volume 3, Issue 4, pp 714-719, 2016

[28] Chinnasarn, K. and Rangsanseri, Y., *An image-processing oriented optical mark reader*. Applications of digital image processing XXII, Denver CO., 1999.
[29] TienDzung D. N., Quyet, H. M. and Phuong B. M., E*fficient and reliable camera based multiple-choice test grading system.* International Conference on Advanced Technologies for Communications, 2011.
[30] Rakesh S, Kailash A., and Ashish A., "*Cost Effective Optical Mark Reader*" International Journal of Computer Science and Artificial Intelligence, Vol. 3 Issue 2, PP. 44-49, 2013
[31] Nutchanat, S., "*Test Scoring for Non-Optical Grid Answer Sheet Based on Projection Profile Method*". International Journal of Information and Education Technology, Vol. 3, No. 2, 2013
[32] AL-Marakeby A., *Multi-Core Processors for Camera based OMR*, International Journal of Computer Applications (0975 – 8887) Volume 68– No.13, 2013.
[33] Hui D., Feng W., Liang B., "A Low-Cost OMR Solution for Educational", An International Journal of Advances in Computational Research, 2016.
[34] Tanvi S. and Niket B., "Optical Mark Recognition with Simple Scanner", An International Journal of Advances in Computational Research, 2016.
[35] Cochran, W. G., Sampling techniques (3rd ed.). New York: John Wiley and Sons, 1977
[36] Zuiderveld, K., "Contrast Limited Adaptive Histograph Equalization." Graphic Gems IV. San Diego: Academic Press Professional, pp 474–485, 1994
[37] Kim, S. J., Min, B. S., Lim, D. K., and Lee, J. H., Determining parameters in contrast limited adaptive histogram equalization. In *The 7th International Conference on Information Security and Assurance*, Vol. 21, pp. 204-207, 2013.
[38] Lim, J. S., "Two-Dimensional Signal and Image Processing.", Englewood Cliffs, NJ, Prentice Hall, pp. 469-476, 1990.
[39] Liu, Y., Noise reduction by vector median filtering. *Geophysics*, *78*(3), V79-V87, 2013.
[40] Amin A., Mari J. F., Machine recognition and correction of printed Arabic text, IEEE Trans. Man Cybernet 9 (1) 1300-1306, 1989
[41] Amin, A., Recognition of printed Arabic text based on global features and decision tree learning techniques. Pattern Recognition, 33, 1309-1323, 2000.
[42] Duda R., Hart P., Use of the Hough transformation to detect lines and curves in pictures, Communication. Association for Computing Machinery (ACM) 15 11-15, 1992
[43] Paeth A., A fast algorithm for general raster rotation, Proceedings Graphics Interface Vision Interface, Canadian Information Processing Society, pp. 77-81, 1986
[44] Chen, C., Jacobsen, H. A., and Vitenberg, R., Algorithms based on divide and conquer for topic-based publish/subscribe overlay design. *IEEE/ACM Transactions on Networking*, *24*(1), 422-436, 2016.

ASTES

Advances in Science, Technology and Engineering Systems Journal Vol. 2, No. 4, 133-138 (2017)

www.astesj.com

ASTESJ

ISSN: 2415-6698

An Efficient Authentication Method For Smart Card Verification In Online

Kanamarlapudi Venkata Srinivasa Rao[1], Ramanathan Udayakumar[*, 2], Velu Khanaa[3]

[1]*Research Scholar, Department of CSE, BIHER University, Chennai – 73, India*

[2]*Associate Professor, Department of Information Technology, BIHER University, Chennai – 73, India*

[3]*Dean-Info. BIHER University. Chennai-73, India*

ARTICLE INFO

Article history:
Received: 10 July, 2017
Accepted: 02 August, 2017
Online: 20 August, 2017

Keywords:
Zero-data
Encryption
Decryption
Smart card
Authentication
Password

ABSTRACT

The great cards are getting a charge out of a critical part inside the on-line managing wherever we have tendency to can't check the cardholder up close and personal. The phishing sites may parody the data in the middle of the customer website and along these lines the common webpage. To protect the data and managing here we have tendency to are presenting the three level confirmations. In arranged approach there are two stages i.e. Enlistment and login. All through enlistment part control the word which can figure and separated into two segments i.e. parcel one can keep inside the client or customer viewpoint, segment a couple of can keep in server perspective. Next level is to exchange the client icon which can figure and split into two shares each are keep severally. In the end zero information code will be get refreshed and it's furthermore get keep as two components. All through the login part before starting the managing the client and server ought to uncover their three-genuine data offers if each stacked data got coordinate then the client is legitimate and server isn't a phishing site.

1. Introduction

In the on-line managing the secured air is one among the key variables; to create the secured environment here we tend to are proposing three level validations. All through the enlistment section three essential true data are entered by the client. All the primary focuses are acquainted in with the procedure thus split into two offers. [1-2] Each individual share is keep in customer and server viewpoint.

In the enlistment part to attempt and do check on client, uncover a couple of offers from customer and server the client confirms the server for phishing site and server confirm the client verification? The shares keeping up in two databases are scrambled one while not knowing the mystery composing method and share two one can't get the cardboard holder and card information. [3]

The phishing sites can't be identified in conventional managing strategy, however in our philosophy though doing giving one can't enter their card data while not exchanging the correct information inside the customer viewpoint data also server should transfer the enlisted information presently the customer shares and server shares are to be stacked along for acquiring the main genuine data. Presently if the client human movement with phishing site they can't turn out the correct information.

This paper is composed as takes after. Associated take a shot at positive distinguishing proof is checked on in Section-II. In Section-III depicts Existing system, in Section-IV depicts Methodology, in Section-V manages arranged philosophies, in Section-VI Portrays Implementation and Section-VII depicts Conclusion and Future Work.

2. Related Work

Prescribe however current instruments shield against disconnected papers taking assaults, powerful assurance against on-line channel-breaking assaults needs advancements to annihilation man-in-the-center (MITM) assaults, and sensible insurance against substance control assaults needs exchange verification innovations. [4-5]

Arranged a change to Chin subject to thwart from a few shortcomings. Notwithstanding, the enhanced subject isn't exclusively still at danger of parallel session assault, however also unreliable for dynamical the client's assertion in word alteration part. thus, the present paper presents Associate in Nursing change to determine such issues. Accordingly, the arranged subject grants clients to adjust their passwords openly and immovably while not

[*]Corresponding Author: Ramanathan Udayakumar, Department of IT, BIHER, Bharath University, Chennai – 73, India | Email: rsukumar2007@gmail.com

the help of a faraway server, though furthermore giving secure common authentication. [6-8]

Propose an ultra-low memory unique mark coordinating algorithmic govern and execute it on a 32-bit positive recognizable proof. we tend to first be assessed each the amount of bearings raised and memory request of each progression of a commonplace unique mark coordinating algorithmic run the show. At that point, we have a tend to build up a memory-effective algorithmic lead for the principal memory overpowering stride arrangement by doing extra calculations inside the limitation of the day and age request. Our trial comes about demonstrate that the arranged algorithmic manage will decrease the fancied memory house by a component of sixty-two and might be ere cured in day and age on a 32-bit positive recognizable proof. [9-11]

Presents a simple and temperate client verification approach bolstered a firm mouse-operation assignment for each specimen of the mouse-operation assignment, every old all-encompassing choice and recently characterized procedural [12] choices are removed for right and fine-grained portrayal of a client's particular mouse conduct. Separate estimation and Manfred Eigen house-change systems are connected to get include components for with effectiveness speaking to the main mouse highlight space. At that point, a one-class learning algorithmic govern is used inside the separation based component Manfred Eigen house for the validation errand. The approach is assessed on a dataset of five,550 mouse-operation tests from thirty-seven subjects. escalated test comes about are encased to exhibit the effectuality of the arranged approach, that accomplishes a false-acknowledgment rate of 8.74%, a false-dismissal rate of 7.69% with a comparing verification time of 11.8 seconds. Two additional trials are giving to check the present approach [13] with option approaches inside the writing. Our dataset is out in the open offered to encourage future examination.

Propose a totally extraordinary client confirmation and key understanding topic exploitation great cards for multi-server situations with a considerable measure of less process esteem [14] and extra reasonableness. the primary merits include: (1) clients exclusively should enroll at the enlistment focus once and will utilize admissible administrations in qualified servers; (2) the subject doesn't need a check table; (3) clients will unreservedly settle on their passwords; (4) the calculation and correspondence esteem is to a great degree low; (5) servers and clients can confirm each other; (6) it creates a session enter in understanding by the client and in this way the server; (7) it's a nonce-based topic that doesn't have an overwhelming time-synchronization [15] disadvantage.

Propose a solid and sparing client validation and key understanding topic exploitation great cards. the most merits grasp the accompanying: 1) the calculation and correspondence esteem is to a great degree low; 2) there's no need for any word or check table inside the server; 3) a client will openly decide on and modify his own watchword; 4) it's a nonce-based topic that doesn't have an overwhelming time-synchronization issue; 5) servers and clients will prove each other; 6) the server will renounce a lost card and issue a swap card for a client while not dynamical his personality; 7) the security of clients might be ensured; 8) it creates a session scratch indicated by the client and in this way the server; and 9) it will stop the disconnected wordbook assault yet the key information continue amid a constructive ID is bargained. [16-18]

Arranged plans, application servers don't should keep up a confirmation table and this cherished preferred standpoint isn't tended to by past grant. In addition, the protection of clients is moreover tended to in Liao-Wang's subject [19]. amid this article, we tend to demonstrate that their plans don't appear to be secure against the server caricaturing and in this manner the pantomime assaults. At that point, we have a tendency to propose a solid client validation subject to confront up to these assaults and keep consistent merits.

Propose a totally one of a kind trilateral key trade subject exploitation great cards. the most merits of our subject include: (1) there cravings no confirmation, passwords or shared keys table inside the reliable server; (2) clients will openly settle on and adjust their own passwords; (3) the correspondence and calculation esteem is to a great degree low; (4) Two clients will prove each other by the dependable server; (5) it produces a session enter in assertion between two clients; (6) it's a nonce-based topic that doesn't have an overwhelming time synchronization disadvantage.[20-21]

3. Existing System

3.1 *Existing Authorization Procedure:*

When the client starts the dealing, they're sent to secure servers to complete the checkout method. The cardholder places Associate in Nursing order at the merchant's website by clicking the "Send Order" button on the Review Order page throughout checkout. [22-23]

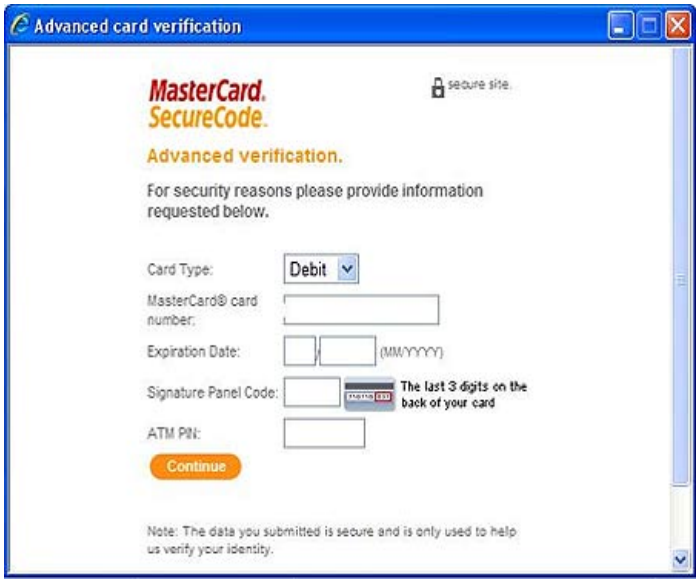

Figure 1 Existing System

(First Data Merchant Services) FDMS sends the authorization request to the issuing bank (or credit card association).

The authorization request includes:

- the credit card number

- expiration date
- the billing address (used for AVS validation)
- the CVV number (if entered)
- the amount of the order

The Issuing Bank (or Credit Card Association):

- validates the card number and expiration
- checks the amount of the order against the available credit
- checks the billing address provided against the billing address on file
- validates the CVV number (if provided)

If approved, the amount of the order is reserved from the total of available credit for the cardholder. [24-26]

The Issuing bank (or Credit Card Association) sends the authorization response to FDMS. The authorization response consists of either an approval along with Address Verification System (AVS) and Card Verification Value (CVV) response codes or a decline. Depending on the state of the authorization, the cardholder receives instructions or confirmation of the order. [27-28]

In the above process, there is no specific authentication process except password which can be easily deceived by the intruders. [29]

4. Proposed Methodology

4.1 Text substitution cipher algorithm Cryptography:

Cryptography is the system where encryption and decryption techniques are used to the network and computer for the security of the data. Encryption means the change of original information (plain text) into another form by some operations (algorithm) and decryption means the techniques of getting the original information by some operations (algorithm) from the encrypted data (cipher text).

During the registration, the user will first enter the Key value and then the password, the entered string of password is introduced into the cryptography algorithm using key value. Then obtained encrypted value is divided into two partitions evenly. First part gets stored in client and second part stored in server.

$$CT = \begin{cases} M = M + C & if\ M = 0 \\ M = M - C & if\ M > 0 \end{cases}$$

Where A=ASCII summation of Key

M=A % 2

CT= Cipher Text

Substitution algorithm

Input: Two values Password and Key value

Output: Stored two partitions, one part in Client and second part in Server.

Step-1: Accept the Password string.

Step-2: Accept the Key value from the user.

Step-3: Compute ASCII summation of Key Value C.

Step-4: For Each character in password string do the following

Step-5: Find the ASCII value of the character.

Step-6: Compute M= ASCII value Mod 2

Step-7: If M==0 then

Encrypted Character = M+C

Else

Encrypted Character = M-C

Step-8: Now repeat Step 4 to step 7 to obtain the cipher text.

Step-9: Cipher Text is introduced for length calculation L.

Step-10: Compute L/2, Part1 = 0 to L/2 and

Part 2 = L/2+1 to L.

Step-11: Individual Parts are stored in client and server respectively.

4.2 Image encryption and sharing procedure

Given Passport size photo is a shared secret image with M×N pixels. The dealer can derive shadows from M×N and generate two shared images. The new sharing process is introduced here. Given images, the secret image can be recovered with no distortion. The cover images could be reconstructed with limited distortion from specific value calculated.

4.3 Sharing procedure

The dealer chooses Odd or Even value combination from the pixel of given image. To share the secret image with the dealer converts given pixel of grayscale image into M×N pixel matrix. For instance, we assume that the chosen number is equal to odd or even and if it is odd then the corresponding pixel position is moved to share-1 and vice versa. The following algorithm illustrates the entire procedure in detail.

4.4 The algorithm

Input: One secret image

Output: Two matrices, One in share-1 and second in share-2

Step1- Take the input image and derive the M X N pixels.

Step2- Convert the given image into grayscale image. Apply the procedure to find the positions $(x_1, y_1), (x_2, y2), \ldots, (x_n, y_n)$ of the image pixels.

Step3- Use the function to calculate the odd or even characteristic of the image pixel position.

Step4- Maintain the two matrices called share-1 and share-2.

Step5- Use step3 and split the odd pixels and even pixels in the manner that, (Odd, Odd), (Odd, Even) in share-1 and (Even, Even) (Even, Odd) in share-2.

Step6- Apply pixel positions in order, for easy retrieval.

Step7- Apply pixel reversal to reverse the obtained pixels, in share-1.

Step8- Store the reversed Pixel in matrix as image called share-1.

Step9- Apply pixel reversal to reverse the obtained pixels in share-2.

Step10- Store Reversed Pixel' 'in matrix as image called share-2.

Step11- Repeat point 1 to 10 for original image (i.e. matrix of original image) to shared images conversion.

4.5 *Zero knowledge authentications*

Zero-data protocols area unit fascinating tool for the authentication verification the two stack holders here area unit Prover and supporter. The prover has got to prove himself victimization queries generated by the supporter. If the prover did not prove himself he's not attested. Zero-data protocol comprises two steps particularly Identification and Operation. Identification schemes area unit strategies by that a prover might prove his or her identity while not revealing data which will be utilized by associate degree listener to impersonate the prover. The operation done by the supporter is to verify the small print entered by the prover. Once the cardboard holder completed registration by coming into the non-public knowledge is distributed to host server. The host server successively verifies the number that is first part of authentication. For second part of authentication zero-data technique is employed.

p → v Prover to Verifier Code Passed

v → p Verifier to Prover authentication set

p → v Update zero knowledge code

5. Proposed System

In our planned system, there are a unit two phases Registration and Login part. throughout the registration part the user ought to enter the three vital authentic data and the data area unit encrypted and split into two components.

5.1 Registration Phase:

In the registration part, the system exploits three totally different authentication data,

i) User Password (with key string)

ii) Passport size image of card holder.

iii) Zero information code to be updated.

Here of these data area unit encrypted and split into two totally different components. every half goes to induce hold on within the consumer and server databases one by one. The secret is encrypted mistreatment substitution cipher formula. [30-31] Then the obtained text is split into two. The image of the user ought to get uploaded within the system. The image is shared mistreatment the formula and so odd and even pixels area unit split into two shares. eventually zero information updated code is additionally split into two components. One part of the all on top of three is get hold on in consumer and another part can get hold on in server information. [32]

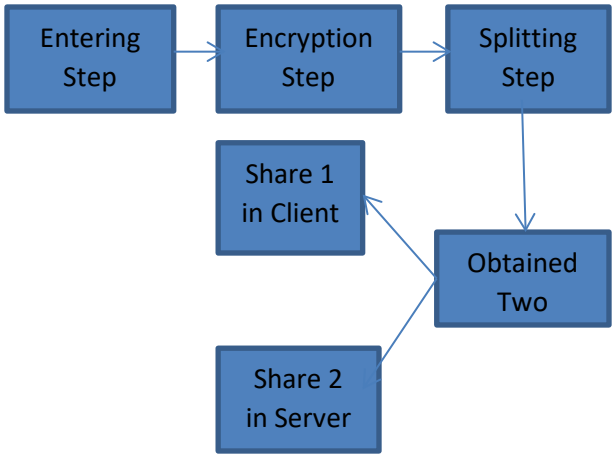

Figure 2 Registration Phase

During the coming into step input the desired details like positive identification text, user image and the zero-data code. Then within the coding step with the various algorithms mentioned higher than given inputs square measure encrypted. Then the encrypted outputs square measure spliced into two halves the two shares square measure get keep in consumer (user) and the server machine.

5.2 Login Phase:

During login section the user have to be compelled to enter Share one details of the positive identification, uploaded image and updated zero-data code, subsequently server reveal its share a pair of each of the shares square measure going stacked along and eventually apply the decipherment rule on positive identification, Image and nil data code then server verifies user positive identification and consumer verifies the image and nil data if each of them proved themselves currently consumer will enter the cardboard info for secured dealing decipherment is often done on the positive identification and image victimization the algorithms explained within the higher than section. [33]

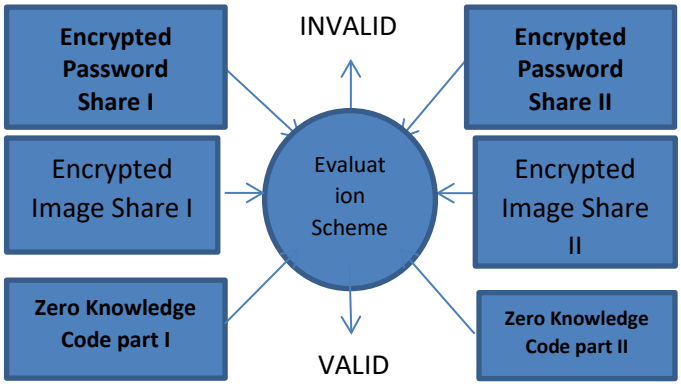

Figure 3 Login and Verification Phase

6. Implementation

In the suggested system first step is registration phase where users must upload three different information level by level. During the first level, the user must enter their password and password key as depicted in the Fig.4.

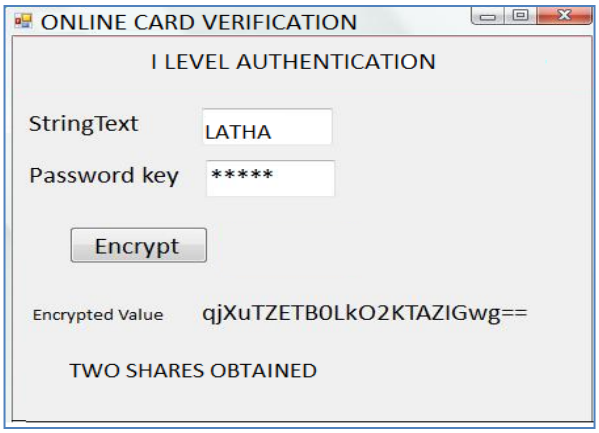

Figure 4 I Level Authentication

In the second level, they must upload their photo. Then the user can get the share that was encrypted using the respective algorithm.

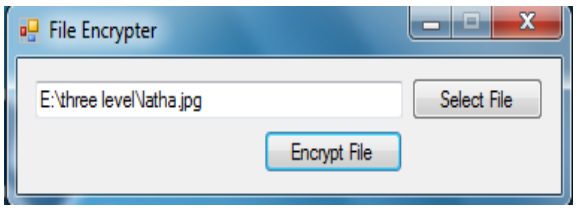

Figure 5 Image Encryption

Finally, the user must enter the zero-knowledge code which can be updated at the end of the transaction. During login phase the process has been reversed.

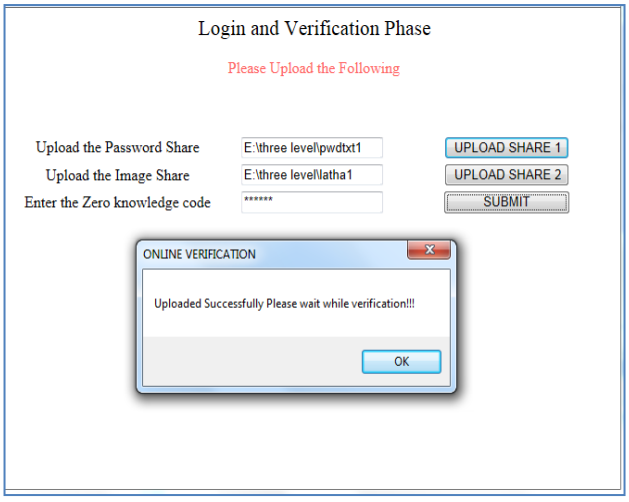

Figure 6 Login and Verification phase

After processing the three inputs the user can either precede to the transaction, else if their identity is not valid then exit from the login and it will not precede the transaction further. The validity of user will be intimated to the server and validity of server will be intimated to user.

7. Conclusion and Future Work

The arranged philosophy jam positive distinguishing proof information of client's exploitation three levels of security. to begin with level checks regardless of whether the cardboard holder could be a legitimate individual or not. On the off chance that the individual isn't substantial he can't enter revise positive recognizable proof and key for cryptography. Second level of validation is to confirm regardless of whether the server could be an honest to goodness/secure site or a phishing site, If the site could be a phishing then in that situation, the phishing site can't demonstrate the picture for that specific client to account of the established truth that the picture is produced by the stacking of two shares, one with the client and furthermore the option with the specific information of the site.

References

[1] Debanjan Das1, Megholova Mukherjee2, Neha Choudhary3, Asoke Nath Joyshree Nath"An Integrated Symmetric key Cryptography Algorithm using Generalised modified Vernam Cipher method and DJSA method: DJMNA symmetric key algorithm".

[2] Udayakumar R., Kaliyamurthie K.P., Khanaa, Thooyamani K.P., Data mining a boon: Predictive system for university topper women in academia, World Applied Sciences Journal, v-29, i-14, pp-86-90, 2014.

[3] Brintha Rajakumari S., Nalini C., An efficient data mining dataset preparation using aggregation in relational database, Indian Journal of Science and Technology, v-7, i-, pp-44-46, 2014.

[4] R. Kalaiprasath, R. Elankavi and Dr. R. Udayakumar. Cloud. Security and Compliance - A Semantic Approach in End to End Security, International Journal Of Mechanical Engineering And Technology (Ijmet), Volume 8, Issue 5, pp-987-994, May 2017.

[5] G.Megala1 A.Rajeswari2 V.Visalatchi3 Mr.B.Ganes "An Improved Secret Image Sharing Scheme with Steganography." 2011 IEEE.

[6] Udayakumar R., Thooyamani K.P., Khanaa, Deploying site-to-site VPN connectivity: MPLS Vs IPSec, World Applied Sciences Journal, v-29, i-14, pp-6-10, 2014.

[7] New Symmetric key Cryptographic algorithm using combined bit manipulation and MSA encryption algorithm: NJJSAA symmetric key algorithm Neeraj Khanna,Sayantan Chakraborty,Joyshree Nath ,A.K.Chaudhuri ,Amlan Chakrabarti ,A.K.Chaudhuri , Asoke Nath 2011 International Conference on Communication Systems and Network Technologies.

[8] Li Lu, Member, IEEE, Jinsong Han, Yunhao Liu, Lei Hu, Jinpeng Huai, Lionel M. Ni, and Jian Ma "Pseudo Trust: Zero-Knowledge Authentication in Anonymous P2Ps" Ieee Transactions on Parallel And Distributed Systems, Vol. 19, No. 10, October 2008.

[9] Ieee Sensors Journal, Vol. 11, No. 12, December 2011 3235 Zero-Knowledge Authentication Protocol Based onAlternative Mode in RFID Systems Hong Liu, and Huansheng Ning.

[10] Wen-Shenq Juang, Sian-Teng Chen, And Horng-Twu Liaw Robust And Efficient Password-Authenticated Key Agreement Using Smart Cards Ieee Transactions On Industrial Electronics, Vol. 55, No. 6, June 2008.

[11] Mrs. Hemangi Kulkarni, Aniket Yadav, Darpan Shah, Pratik Bhandari, Samuya Mahapatra "Unique ID Management" Aniket Yadav, ,Int.J.Computer Technology & Applications,Vol 3 (2), 520-524.

[12] Hamed Taherdoost, Shamsul Sahibuddin & Neda Jalaliyoon "Smart Card Security; Technology and Adoption" International Journal of Security (IJS), Volume (5): Issue (2): 2011.

[13] Udayakumar R., Thooyamani K.P., Khanaa, Random projection based data perturbation using geometric transformation, World Applied Sciences Journal, v-29, i-14, pp-19-24, 2014.

[14] Khanaa V., Mohanta K., Saravanan. T., Performance analysis of FTTH using GEPON in direct and external modulation, Indian Journal of Science and Technology, v-6, i-SUPPL.6, pp-4848-4852, 2013.

[15] Rui Wang, Shuo Chen, XiaoFeng Wang, Shaz Qadeer "How to Shop for Free Online Security Analysis of Cashier-as-a-Service Based Web Stores" 2011 IEEE Symposium on Security and Privacy.

[16] Kaliyamurthie K.P., Udayakumar R., Parameswari D., Mugunthan S.N., Highly secured online voting system over network, Indian Journal of Science and Technology, v-6, i-SUPPL.6, pp-4831-4836, 2013.

[17] "R.Kalaiprasath, R.Elankavi, Dr.R.Udayakumar, Cloud Information Accountability (Cia) Framework Ensuring Accountability Of Data In Cloud And Security In End To End Process In Cloud Terminology, International Journal Of Civil Engineering And Technology (Ijciet)Volume 8, Issue 4, Pp. 376–385, April 2017."

[18] R. Elankavi, R. Kalaiprasath, Dr.R.Udayakumar, A fast clustering algorithm for high-dimensional data, International Journal Of Civil Engineering And Technology (Ijciet), Volume 8, Issue 5, Pp. 1220–1227, May 2017.

[19] Thooyamani K.P., Khanaa V., Udayakumar R., Efficiently measuring denial of service attacks using appropriate metrics, Middle - East Journal of Scientific Research, v-20, i-12, pp-2464-2470, 2014.

[20] Thooyamani K.P., Khanaa V., Udayakumar R., Virtual instrumentation based process of agriculture by automation, Middle - East Journal of Scientific Research, v-20, i-12, pp-2604-2612, 2014.

[21] Afzel Noor "Highly Robust Biometric Smart card design" IEEE 2000.

[22] Khanaa V., Thooyamani K.P., Udayakumar R., A secure and efficient authentication system for distributed wireless sensor network, World Applied Sciences Journal, v-29, i-14, pp-304-308, 2014.

[23] Thomas Ezat A Dubbish, Robert H Slon "Examining the smart card security under the threat of Power analysis attack", IEEE transactions on computer April 2004.

[24] Kaliyamurthie K.P., Parameswari D., Udayakumar R., QOS aware privacy preserving location monitoring in wireless sensor network, Indian Journal of Science and Technology, v-6, i-SUPPL5, pp-4648-4652, 2013.

[25] Eun-Jun Yoon, Eun-Kyung Ryu, and Kee-Young Yoo "Further Improvement of an Efficient Password Based Remote User Authentication Scheme Using Smart Cards" IEEE Transactions on Consumer Electronics, Vol. 50, No. 2, MAY 2004.

[26] Brintha Rajakumari S., Nalini C., An efficient cost model for data storage with horizontal layout in the cloud, Indian Journal of Science and Technology, v-7, i-, pp-45-46, 2014.

[27] Chao Shen,Zhongmin Cai, Xiaohong Guan, *Fellow,* Youtian Du,and Roy A. axionUser Authentication through Mouse Dynamics" 2011 IEEE.

[28] Wen-Shenq Juang "Efficient Multi-server Password Authenticated Key Agreement Using Smart Cards"Manuscript received January 15, 2004.

[29] Wen-Shenq Juang, Sian-Teng Chen, and Horng-Twu Liaw "Robust and Efficient Password-Authenticated Key Agreement Using Smart Cards" 2008 IEEE.

[30] Khanna V., Mohanta K., Saravanan T., Recovery of link quality degradation in wireless mesh networks, Indian Journal of Science and Technology, v-6, i-SUPPL.6, pp-4837-4843, 2013.

[31] Ren-Chiun Wang, Wen-Shenq Juang, and Chin-Laung Lei, *Member, IEEE* "User Authentication Scheme with Privacy-Preservation for Multi-Server Environment" . IEEE COMMUNICATIONS LETTERS, VOL. 13, NO. 2, FEBRUARY 2009.

[32] Udayakumar R., Khanaa V., Saravanan T., Saritha G., Retinal image analysis using curvelet transform and multistructure elements morphology by reconstruction, Middle - East Journal of Scientific Research, v-16, i-12, pp-1781-1785, 2013.

[33] Wen-Shenq Jaung Efficient Three-Party Key Exchange Using Smart Cards Contributed Paper Manuscript received April 8, 2004.

ASTES

Advances in Science, Technology and Engineering Systems Journal Vol. 2, No. 4, 139-144 (2017)

www.astesj.com

ASTESJ

ISSN: 2415-6698

Estimation of Power System Stabilizer Parameters Using Swarm Intelligence Techniques to Improve Small Signal Stability of Power System

Hossein Soleymani[1*], Amin Hasanvand[2]

[1]*Dispatching Engineer, Qom Electricity Power Distribution Company, Qom, Iran*

[2]*Electrical Engineer, Khajeh Nasir University of Technology, Tehran, Iran*

A R T I C L E I N F O

Article history:
Received: 07 August, 2017
Accepted: 14 August, 2017
Online: 20 August, 2017

Keywords:
Power System
PSO
GA
Evolutionary Algorithms

A B S T R A C T

Interconnection of the power system utilities and grids offers a formidable dispute in front of design engineers. With the interconnections, power system has emerged as a more intricate and nonlinear system. Recent years small signal stability problems have achieved much significance along with the conventional transient constancy problems. Transient stability of the power system can be attained with high gain and fast acting Automatic Voltage Regulators (AVRs). Yet, AVRs establish negative damping in the system. Propagation of small signals is hazardous for system's health and offers a potential threat to system's oscillatory stability. These small signals have magnitude of 0.2 to 2 Hz. The professional control tactic to develop system damping is Power System Stabilizer (PSS).This paper presents application of swarm intelligence for PSS parameter estimation issue on standard IEEE 10 Generator 39 Bus power network (New England). Realization of the objective function is done with the help of interpolation investigation using MATLAB. The system performance is compared with the conventional optimization algorithms like Genetic Algorithm (GA) and Particle Swarm Optimization (PSO) based PSS controller. The strength of proposed controller is tested by examining various operating conditions. An Eigen property analysis is done on this system i.e. before installing PSS, and after the employment of GA and PSO tuned PSSs. A significant comparison is carried out with GA and PSO on the basis of convergence uniqueness and dynamic response of speed deviation curves of various generators.

1. Introduction

Recent years, power system stability and reliability have been take into account as very important issues in the context of modern power system [1]. Stressed operating conditions and competitive business enjoinments have been showing threats to power engineers for an efficient design and optimal utilization of the electrical utilities. In earlier day's system stability issue were classified as the problem related with transient stability, but, the small oscillations of magnitude 0.2-2 Hz were not major consideration. To ensure transient stability fast acting Automatic Voltage Regulators (AVRs) were employed with generators. However, later in 1960 Concordia et.al., discovered that these high gain regulators are main culprit for introducing the negative damping in the system [2].

The under damped system has an oscillatory response; hence it inculcates oscillatory instability in the power system. The oscillations of small magnitude are harmful for the stability of a power system. These oscillations can cause system collapse if not handled accurately [3]. To find a potential and cost-effective solution to this issue, initial work on Power System Stabilizer (PSS) was proposed by E. V. Larsen *et.al*. The AVR and PSS are dynamically interlinked instruments; one increases transient stability and other complement the small signal stability. To augment the system stability, design engineers should keep a bird

*Corresponding Author: Hossein Soleymani, Qepd Company, Qom, Iran, +989127499186, Email: hsb8867@gmail.com

eye's view on electromagnetic torque of the generator [4]. It has two elements; synchronizing torque, it is in phase with the variation in angle δ (load angle) and other is damping torque, which is in phase with speed deviation [5].

Design of damping controller for a poorly damped system is a formidable problem for power engineers. The damping controller is not only a potential answer for the oscillatory instability but also provides a good damping over the variety of operating conditions. The design of PSS has an ample significance to ensure the oscillatory stability. The Conventional Power System Stabilizer (CPSS) is a lead lag compensator [6]. For designing the damping controller, a designer has to find an accurate set of parameters (Gain & time constant).Proper tuning of the Lead Lag loop presents an adequate amount of damping to the system which helps the system to overcome with oscillatory instability [7].

Over the last decade many techniques were reported by the scientists to solve the PSS factor estimation problem. Some of these researches introduced techniques, to gain the robust conventional design through optimization, adaptive design with the help of expert systems (Neural Network, Fuzzy and Hybrid system), Linear Matrix Inequalities (LMI), Pole Placement and many others [8].

Recent years the enhancement in the field of damping controller design is revolutionized by the Evolutionary Algorithms. Evolutionary computations came in the picture in early 80's. Genetic Algorithm (GA), Particle Swarm Optimization (PSO), Biography Based Optimization (BBO), Bacterial Foraging Algorithm (BFA) and many more were proposed. These procedures are mathematical adaption of nature. They use nature rules to find the global optimum answer. PSS parameter estimation is a complex optimization issue [9].

The procedure towards the designing of CPSS contains following steps [10]:

1. Stability of any system depends on its initial operating conditions. In order to obtain the robust design hard operating conditions should be studied.
2. The design of the PSS should be investigated over various types of perturbations, fault locations and dissimilar system configurations. These contingencies help to ensure that design gained from the approach is robust enough [11].
3. Eigen Property analysis should be done to validate the efficacy of the design.

2. Small Signal Stability

Stability problems have already acquired prominence with every passing day. The need of the hour is to develop a robust system, which is not likely to give up in the wake of blackouts and various contingencies. IEEE/CIGRE Joint Task Force committee introduce the power system stability as follows "Small-disturbance (or small-signal) rotor angle stability is concerned with the ability of the power system to maintain synchronism under small disturbances. The disturbances are considered to be sufficiently small that linearization of system equations is permissible for purposes of analysis" [12].

Power system utilities still prefer the conventional lead-lag power system stabilizer structure. Since the PSS has engrossed the interest of researchers, extensive research has been conducted in the following fields:

- Effect of PSS on system stability
- PSS tuning methods
- Practical experience in design, installation & operation of PSS.

Figure 1 shows the conventional Delta-Omega PSS. A stabilizer is designed by suitable selection of time constants T_ω, T_1, T_2, T_3, T_4 and stabilizer gain K_{STAB}. In practical situation, a torsional filter is used for attenuating the stabilizer gain at turbine generator shaft torsional frequencies and may be neglected while designing PSS [13].

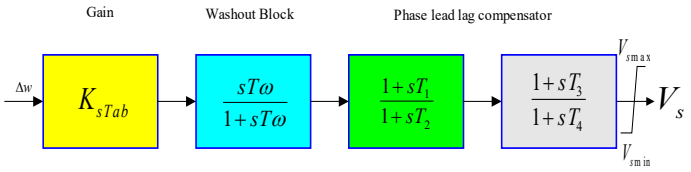

Figure 1. Power System Stabilizer transfer function model

$$\frac{V_S(s)}{\Delta\omega(s)} = K_S \left[\frac{sT\omega}{1+sT\omega}\right]\left[\frac{1+sT_1}{1+sT_2}\right]\left[\frac{1+sT_3}{1+sT_4}\right] \quad (1)$$

Where K_S is Stabilizer gain, T_ω is Washout time constant and T_1, T_2, T_3, T_4 are time constants of the lag lead networks [14].

The problem first encountered in the year 1969 reported by Concordia *et al*. was negative damping injection by turbine's speed governor loop. It could be resolved by fitting the generators with a feedback controller. This controller sensed the change in terminal power of the generator and fed it back at the AVR reference input with proper phase lead and magnitude. This generated an additional damping torque on the rotor. Hence this fact advocates the acute requirement of PSS for adequate damping in the modern power networks. Larsen and Swann [15] in 1981discussed the chronological development of damping controllers in their three-part paper. They recommended that the objective of the most appropriate stabilizer tuning criterion is to provide an adequate amount of damping to local mode of oscillations and inter area modes of oscillations. Michael J. Basler *et al*. [16] discussed power system instability and the importance of fast disturbance clearing performance. Explanation is provided regarding small signal stability, high impedance transmission lines, line loading, and high gain, fast acting excitation systems [17].

3. The Swarm Intelligent Techniques Algorithm

Swarm intelligence is a research field that models the communal behavior in swarms of insects or animals. Several algorithms ascending from these models have been anticipated to solve an extensive range of complex optimization problems. In this

work, comparative study of novel swarm algorithms like Genetic Algorithm (GA) and Particle Swarm Optimization (PSO) will be considered to estimate the parameters of PSS [18].

3.1. Particle Swarm Optimization

The particle swarm optimization (PSO) technique is a population based optimization technique first proposed by Kennedy and Eberhart in 1995 inspired by social behavior of bird flocking or fish schooling [19]. PSO as an optimization tool provides a population based search procedure in which individuals called *particles* change their position (*state*) with time [14]. In a PSO system particles fly around in a multidimensional search space; during their flight, each particle adjusts its position according to its own experience ($pbest$) and according to its neighbor's experience ($gbest$), making use of the best position encountered by itself and its neighbors.

The position of particle in an n dimensional vector can be represented mathematically as [20]:

$$X_m = (x_{m1}, x_{m2}, x_{m3}, \dots, x_{mn}) \quad (2)$$

The modification is made in current position using following equation [21]:

$$S_i^{k+1} = S_i^k + v_i^{k+1}, i = 1,2, \dots, n \quad (3)$$

Where S^k represents the current position of the particle, S^{k+1} represents the modified position of the particle and v is the velocity of each particle [22].

The velocity of each particle is n-dimensional vector given by the following equation:

$$V_m = v_{m1}, v_{m2}, \dots, v_{mn} \quad (4)$$

The velocity of each particle is updated after every iteration according to the following equation:

$$v_i^{k+1} = w_i v_i^k + c_1 rand^*(pbest_i - s_i^k) + c_2 rand^*(gbest_i - s_i^k) \quad (5)$$

Where v^k is the current velocity of the particle, v^{k+1} is the modified velocity of the particle, $pbest_i$ is the pbest of particle i, $gbest_i$ is the gbest of particle i, m is the number of members in a particle, w is the weight function for velocity of particle i and c_i is the weighing coefficients for each particle [23].

The objective function will be taken as fitness function for PSO algorithm. The best position related to the lowest value of the objective function for each particle is given as [24]:

$$Pbest_m = (pbest_{m1}, pbest_{m2}, \dots, pbest_{mn}) \quad (6)$$

And global best among all particles or best out of all *pbest* is represented as:

$$Gbest_m = (gbest_{m1}, gbest_{m2}, \dots, gbest_{mn}) \quad (7)$$

The velocity and position of particles are updated after each iteration [25].

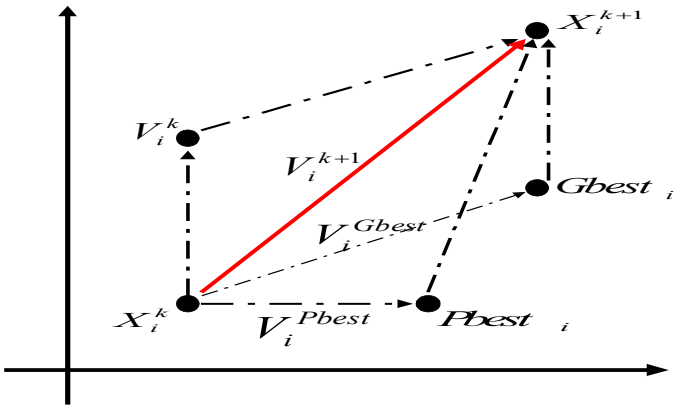

Figure 2. Concept of a searching point by PSO

Where

V_i^k is current velocity of particle *i* at iteration *k*.

V_i^{k+1} is modified velocity of particle *i*.

X_i^k is current position of particle *i* at iteration *k*.

X_i^{k+1} is modified position of particle *i*.

V_i^{Pbest} is velocity based on *Pbest*.

V_i^{Gbest} is velocity based on *Gbest*.

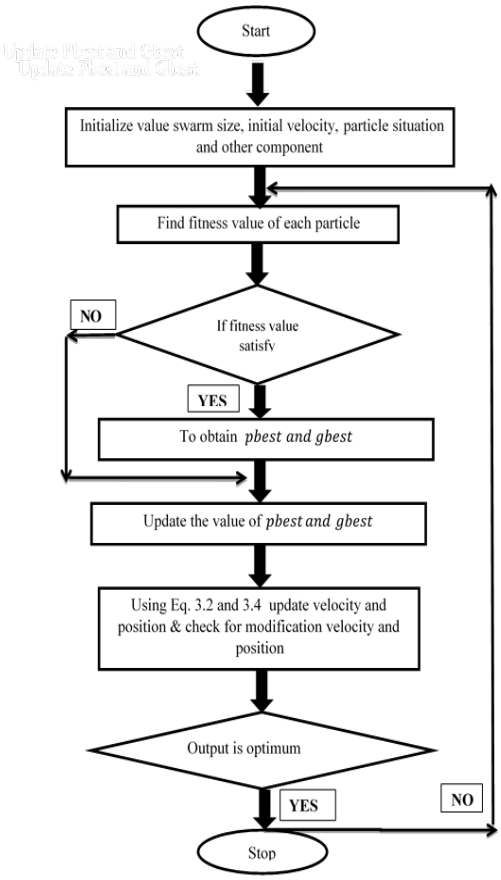

Figure 3. Flow Chart of PSO

Figure 3 shows the flow chart for the optimal allocation of PSO procedure [26].

3.2. Genetic Algorithm

A genetic algorithm (GA) is a search and optimization procedure which acts by mimicking the evolutionary principles and chromosomal processing in natural genetics. A GA begins its search with a random set of solutions usually coded in binary strings. Every solution is assigned a fitness which is directly related to the objective function of the search and optimization issue [27]. Thereafter, the population of solutions is modified to a new population by applying three operators similar to natural genetic operators- reproduction, crossover, and mutation. It works iteratively by successively applying these three operators in each generation till a termination criterion is satisfied. Over the past decade and more, GAs have been successfully applied to a wide range of problems, because of their simplicity, global perspective, and inherent parallel processing [28].

4. Mathematical Recognition of Objective Functions

To realize the polynomial in various orders MATLAB curve fitting tool is employed. Following are mathematical expressions associated with the objective functions [29].

$$f(x) = p_1(x) + p_2 + p_3(x) + p_4 + \cdots + p_{59}(x) + p_{60} \quad (8)$$

$$f(x) = p_1(x)^2 + p_2(x) + p_3 + \cdots + p_{88}(x)^2 + p_{89}(x) + p_{90} \quad (9)$$

$$f(x) = p_1(x)^3 + p_2(x)^2 + p_3(x) + p_4 + \cdots + p_{117}(x)^3 + p_{118}(x)^2 + p_{119}(x) + p_{120} \quad (10)$$

5. Simulation Outcomes and Discussion

Table 1 shows the Eigen characteristic analysis of New England System with and without PSS [30].

It is observed that when PSS is not installed with generators, system shows poor damping. Some of the poorly damped types (swing modes) are shown in the following table. The real part of the Eigen value is positive.

Although the damping controller designed through evolutionary algorithms is quite robust and proved effective in all operating contingencies yet to show the efficacy of the proposed controller extreme conditions are chosen. The performance of the controller is exhibited in terms of hard situations. For this reason, here three phase disturbances are verified and speed responses of those generators are shown which are near by the disturbance locations [31].

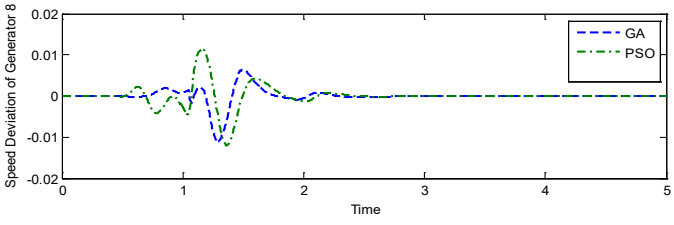

It can be observed from the responses of various generators that PSS tuned through GA gives less dynamic response as compared with PSO tuned PSS. Figures 5 to 8 are the speed deviation curves of various generators under dissimilar perturbations and disturbance locations [32].

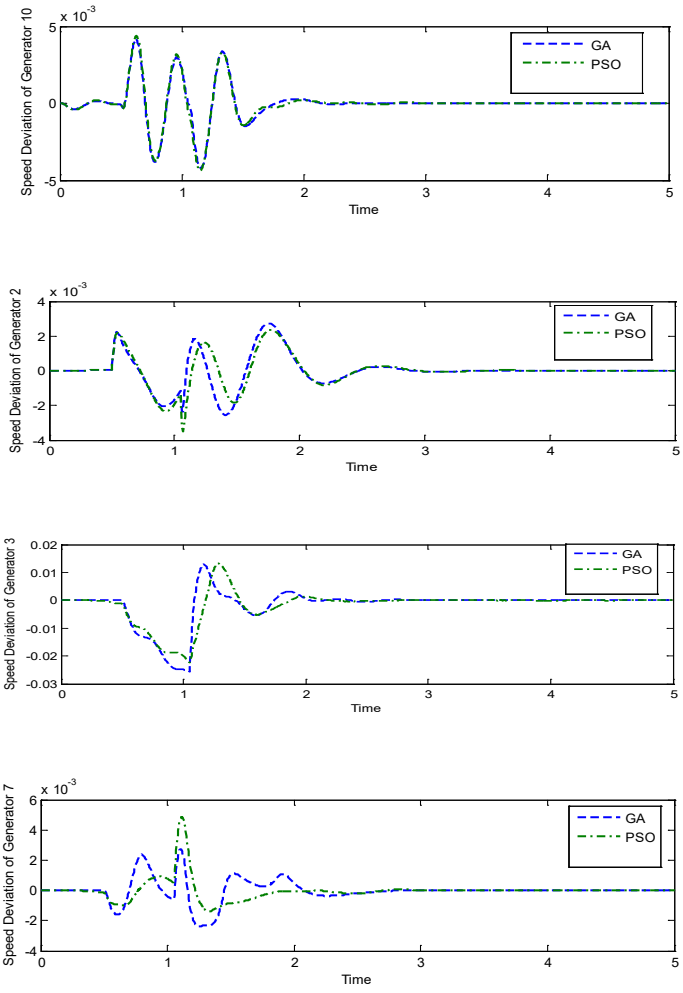

Table 1. Eigen Values and Damping Ratios With and Without PSS

Without PSS		With PSS	
Eigen Values	**Damping Ratio**	**Eigen Values**	**Damping Ratio**
0.0926-i0.2063	-0.0259	-0.1823-i0.3003	0.7595
0.0926+0.2083	-0.0259	-0.1823+i0.3003	0.7595
1.3110-i0.3730	-0.0316	-0.9979-i0.0404	0.3813
1.3110+i0.3730	-0.0316	-0.9979+i0.0404	0.3813
0.2300+i4.0882	-0.0083	-1.0262-i0.7672	0.538
0.2300-i4.0882	-0.0083	-1.0262+i0.7672	0.538
0.0501-i13.863	-0.015	-11.3849-i10.7133	0.5099
0.0501+i13.863	-0.015	-11.3849+i10.7133	0.5099
0.0033-i5.3036	-0.0014	-34.7713-i59.6870	0.4307
0.0033+i5.3036	-0.0014	-34.7713+i59.687	0.4307

The factors of all 10 PSSs gained from solving optimization issue using PSO is shown in Table 2. The convergence

characteristics of various optimization methods for variation of objective function and iteration is shown in Figure 8 [33].

Table 2. PSS factor for 10 Machine 39 Bus Using PSO [34-38]

Generator Number	K_{stab}	T_1	T_3
1	25.31	0.048	0.03
2	29.32	0.067	0.07
3	46.3	0.185	0.03
4	32.09	0.141	0.19
5	25.74	0.1	0.1
6	27.02	0.18	0.04
7	21.31	0.1	0.07
8	26.8	0.15	0.1
9	26.19	0.08	0.05
10	22.85	0.11	0.03

6. Conclusion

In this article endeavor is made to implement GA and PSO for finding the optimal parameters of Power System Stabilizer (PSS) for New England Power system. From this revision following points can be accomplished:

a. Flourishing realization of conventional speed based objective functions in four dissimilar polynomials is presented in section 4. The qualified analysis of these realizations is shown with the help of dynamic responses of speed deviation curves of the generators. It is observed that linear combination of linear, quadratic and cubic polynomial gives the finest response.

b. The consequential comparison of application of two optimization methods namely GA and PSO algorithm in PSS design problem.

References

[1] F. P. deMello and C. Concordia, "Concepts of synchronous machine stability as affected by excitation control," IEEE Trans. Power Apparat. Syst., vol. PAS-88, pp. 316–329, 1969.

[2] E. V. Larsen, and D. A. Swann, "Applying power system stabilizers, parts I, II & III," IEEE Trans. Power App. & Sys., vol. PAS-100, no. 6, pp. 3025-3046, June 1981.

[3] Michael J. Basler, Richard C. Schaefer, "Understanding power system stability", 58th Annual Conference for Protective Relay Engineers, 2005, Volume , Issue , 5-7 April 2005, pp. 46-67.

[4] BoonsermChangaroon, Suresh Chandra Srivastava and DhadbanjanThukaram, "A Neural Network Based Power System Stabilizer Suitable for On-Line Training—A Practical Case Study for EGAT System" IEEE Transaction on Energy Conversion, Volume 15, Issue 1, Mar 2000, pp. 103 - 109.

[5] A. M. Sharaf, T. T. Lie and H. B. Gooi "Neural Network Based Power System Stabilizers", Proceedings of the IEEE ANNES'93, New Zealand, June 1993. pp. 306-309.

[6] Ravi Segala, Avdhesh Sharma and M.L. Kothari, "A self-tuning power system stabilizer based on artificial neural network" Electrical power & energy systems, 2004, vol. 26, no6, pp. 423-430.

[7] DK Chaturvedi and Malik OP. Neuro fuzzy power system stabilizer. IEEE Trans Energy Convers 2008;23:887–94.

[8] Y. Zhang, G. P. Chen, 0. P. Malik, G. S. Hope, "An artificial neural network based adaptive power system stabilizer", IEEE Transactions on Energy Conversion, Vol. 8, No. 1, March 1993.

[9] A. Doi and S. Abe, "Coordinated Synthesis of Power System Stabilizers in Multi-machine Power Systems", IEEE Transactions on Power Apparatus and Systems, vol. 103, no. 6, pp. 1473-1479, 1984.

[10] Kennedy J, Eberhart R. Particle swarm optimization. In: Proceedings of IEEE international conference on neural networks, vol. IV. Perth, Australia, November 29–December 1; 1995. p. 1942–8.

[11] K. W. Wang, C. Y. Chung, C. T. Tse, and K. M. Tsang, "Multimachine Eigenvalue Sensitivities of Power System Parameters",IEEE TRANSACTIONS ON POWER SYSTEMS, VOL. 15, NO. 2, MAY 2000.

[12] C. Y. Chung, Member, IEEE, K. W. Wang, C. T. Tse, Member, IEEE, X. Y. Bian, and A. K. David, Fellow, IEEE, "Probabilistic Eigenvalue Sensitivity Analysis and PSS Design in Multimachine Systems", IEEE TRANSACTIONS ON POWER SYSTEMS, VOL. 18, NO. 4, NOVEMBER 2003.

[13] Seung-MookBaek, Student Member, IEEE, Jung-Wook Park, Member, IEEE, and Ian A. Hiskens, Fellow, IEEE, "Optimal Tuning for Linear and Nonlinear Parameters of Power System Stabilizers in Hybrid System Modeling", IEEE TRANSACTIONS ON INDUSTRY APPLICATIONS, VOL. 45, NO. 1, JANUARY/FEBRUARY 2009.

[14] Y. L. Abdel-Magid, & M. A. Abido, "Optimal multiobjective design of robust PSSs using genetic algorithms," IEEE Trans. Power Sys., vol. 18, no. 3, pp.1125-1132, August 2003.

[15] M. A. Abido, "Optimal design of PSSs using particle swarm optimization," IEEE Trans. Energy Con., vol. 17,no. 3, pp. 406-413, September 2002.

[16] M. A. Abido, "A novel approach to conventional power stabilizer design using tabu search," Int. J. Electric Power Energy Sys. vol. 21, pp. 443-454, June 1999.

[17] M. A. Abido, "Robust design of multimachine PSSs using simulated annealing," IEEE Trans. Energy Con., vol. 15,no. 3, pp. 297-304, September 2000.

[18] H. Shayeghi and S. Jalilzadeh, "Robust PSS Design Using Chaotic Optimization Algorithm for a Multimachine Power System", IEEE Trans. Energy Con.978-1-4244-3388-9/09.

[19] D.K. Sambariya and R. Prasad, "Robust tuning of power system stabilizer for small signal stability enhancement using metaheuristic bat algorithm",Electrical Power and Energy Systems 61 (2014) 229–238.

[20] Bonabeau, E., Dorigo, M., &Theraulaz, G. (1999). Swarm intelligence: From natural to artificial systems. New York, NY, USA: Oxford University Press, Inc..

[21] Kassabalidis, I., El-Sharkawi, M. A., II Marks, R. J., Arabshahi, P., & Gray, A. A. (2001). Swarm intelligence for routing in communication networks. Global Telecommunications Conference, GLOBECOM '01 (Vol. 6, pp. 3613–3617).IEEE.

[22] Kennedy, J., &Eberhart, R. (1995). Particle swarm optimization. In Proceedings of the 1995 IEEE international conference on neural networks (Vol. 4, pp. 1942–1948).

[23] Karaboga, D., &Akay, B. (2009). A comparative study of artificial bee colony algorithm. Applied Mathematics and Computation, 0096-3003, 214(1), 108–132.

[24] Passino, K. M. (2002). Bio mimicry of bacterial foraging for distributed optimization and control. IEEE Control Systems Magazine, 22(3), 52–67.

[25] Hossein, A., & Hossein-Alavi, A. (2012). Krill herd: A new bio-inspired optimization algorithm. Communications in Nonlinear Science and Numerical Simulation, 17,4831–4845.

[26] Yang, E., Barton, Nick H., Arslan, T., & Erdogan, Ahmet T. (2008). A novel shifting balance theory-based approach to optimization of an energy-constrained modulation scheme for wireless sensor networks. In Proceedings of the IEEE congress on evolutionary computation, CEC 2008, June 1–6, 2008 (pp. 2749–2756).Hong Kong, China: IEEE.

[27] Rajabioun, R. (2011). Cuckoo optimization algorithm. Applied Soft Computing, 11,5508–5518.

[28] H. Othman, and et al., "On the design of robust power system stabilizers," IEEE Proc of 28th conf on Dec. & control, pp. 1853-1857, December 1989.

[29] Y. Yu, and Q. Li, "Pole-placement power system stabilizers design of an unstable nine-machine system, IEEE Trans. Pr Sys., vol. 5, no. 2, pp.353-358, May 1990.

[30] Julio C. R. Ferraz, Member, IEEE, Nelson Martins, Fellow, IEEE and Glauco N. Taranto, Member, IEEE, "Coordinated Stabilizer Tuning in Large Power Systems Considering Multiple Operating Conditions",1-4244-1298-6/2007 IEEE.

[31] P. S. Rao and I. Sen, "Robust pole placement stabilizer design using linear matrix inequalities," IEEE Trans. Power Syst., vol. 15, no. 1, pp. 313–319,2000.

[32] IEEE Committee Report on excitation systems (1981).

[33] M. J. Gibbard,: "Robust design of fixed-parameter power system stabilizers over a wide range of operating conditions", IEEE Trans. Power Syst., Vol. 6, No.2, pp.794-800, 1991.

[34] P. Kundur, "Power system stability and control" McGraw Hill, New York, 1994.

[35] Erik Cuevas, Miguel Cienfuegos, Daniel Zaldívar, Marco Pérez-Cisneros, "A swarm optimization algorithm inspired in the behavior of the social-spider",Expert Systems with Applications 40 (2013) 6374–6384.

[36] James J.Q. Yu, Victor O.K. Li: "A Social Spider Algorithm for Global Optimization" Technical Report No. TR-2003-004, Dept. of Electrical & Electronic Engineering, the University of Hong Kong, Oct 2013.

[37] Chatterjee, S. and Laudato, M. (1997). Genetic algorithms in statistics: procedures and applications. Commun. Statist. Simula., 26 (4), 1617-1630.

[38] J. Chow, Graham Rogers. "Power system toolbox." Cherry Tree scientific Software, Available: http://www. ecse. rpi. Edu/pst/PST. Html,2000.

ASTES

Advances in Science, Technology and Engineering Systems Journal Vol. 2, No. 4, 154-164 (2017)

www.astesj.com

ASTESJ

ISSN: 2415-6698

Design and Construction of a remote control switching device for household appliances application

Mbunwe Muncho Josephine*

University of Nigeria Nsukka, Electrical Engineering, University of Nigeria Nsukka, 410001, Nigeria

ARTICLE INFO

Article history:
Received: 25 March, 2017
Accepted: 22 August, 2017
Online: 04 September, 2017

Keywords:
Remote Control
Radio Frequency
Transmitter System
Receiver System
Security System

ABSTRACT

Remote control switching device for household application is a home device used to control the switching of household appliances from a distance. It serves to make the switching of household appliances easy for the elderly, physically challenged, the young and anyone who, in any circumstance, needs comfort and security. This paper develops a remote control system using the Radio Frequency technology utilizing multiplexers, demultiplexers, encoders, decoders, and Radio Frequency module with the analysis of various technologies which can be used for the development of a remote control system. A security system is incorporated in this remote control to provide a secured usage of the system from a distance of about ten meters away. To achieve the aim of this work: a transmitter system is design and constructed which processes and sends out signal when a button is pressed; the construction of a receiver system which receives and processes the signal from the transmitter system, then turn on or turn off the appliances; and incorporate a security system which allows transmission of signal only when certain condition is met. Avoiding the use of microcontroller, this paper developed an affordable, reliable and effective remote control system for household applications.

1. Introduction

Remote controls devices are devices that sends digitally-coded pulses to control functions like power, volume, tuning, temperature set point, fan speed, just to name a few, to control different equipments. These devices are usually small wireless handheld objects with an array for various adjustable setting buttons for television channel, track number, and volume. For many devices, the remote control contains all the function controls while the controlled device itself has only a handful of essential primary controls. The earlier remote controls used ultrasonic tones [1]. Remote control has continually evolved and advanced over recent years to include Infrared (IR), Radio frequency, Bluetooth connectivity, motion sensor-enabled capabilities, voice control. IR remote control has been proved to be the most popular equipment for office application, for example, control of air conditioner, turn on or switch off light as well as the normal use of satellite receivers and Televisions [2]. In this paper, while implementing the use of various technologies incorporating security, a remote control system which uses the radio frequency technology is developed.

1.1. Background of remote control switching device

Most homes make use of many electrical and electronics appliances such as the television set, standing fan, ceiling fan, air conditioner, lighting bulbs, video players, radio, etc. All these appliances require switching to turn on and turn off these appliances traditionally. This manual switching of any home appliance is an inconvenient method for physically disabled or elderly or even for the young and busy individuals when frequent switching operation is required. Thus, an easier method of switching is developed to replace this manual switching method, using an advanced switching method for electronic home appliances.

The early wired remotes made possible for users to control appliances at a distance, but the wired remote also limited the user's mobility by either tethering or tripping the users. If the user ran the remote control's cord under the rugs and furniture, effectively anchoring the device to one location in the room, the remote thereby limits the freedom of movement for which it was designed to provide. But if the cord is left out in the open, the users might stumble over it. The wireless remote control solved all these challenges of the wired remote control and effectively takes control of the household. The use of remote to restore order to the household [3], changes life style; brings multi-function and multi-platform lives easy.

Various technologies have evolved in the past: controlled by radio waves; used to execute commands transmitted by electromagnetic waves; and also the use of battery-operated low-frequency radio transmitter remote control for consumer electronics [4]. The idea for an electronic remote control, which worked wirelessly by shining a beam of light onto a photoelectric

*Mbunwe Muncho Josephine, Department of Electrical Engineering, University of Nigeria Nsukka, +2348036675952 & mamajoesix@gmail.com

cell, came up in the United State in 1955 [3, 4]. Advancement in remote control kept going till recent days where many technologies such as infrared, radio frequency, Bluetooth, Global System for Mobile (GSM) communications control are used for remote control.

The major technology used in home remote controls is infrared (IR) light [2]. The signal between a remote control handset and the device that it controls consists of pulses of infrared light, which is invisible to the human eye, but can be seen through a digital camera, video camera or a phone camera. The transmitter in the remote control handset sends out a stream of pulses of infrared light when the user presses a button on the handset. A transmitter is often a light emitting diode (LED) which is built into the pointing end of the remote control handset. The infrared light pulses form a pattern unique to that button. The receiver in the device recognizes the pattern and causes the device to respond accordingly. Radio Frequency (RF) remote control is used to control distant objects using a variety of radio signals transmitted by the remote control device. As a complementary method to infrared remote controls, the radio remote control was used with electric garage door or gate openers, automatic barrier systems, burglar alarms (for security and also for restriction of the use of household appliances) and industrial automation systems [3]. The importance and benefit of remote control for household applications using radio frequency technology varies:

- It is not affected by line of sight.
- It penetrates most solids materials and passes through walls.
- It transmits signals to longer range, more than that of infrared technology.
- It is not sensitive to light, to weather or any environmental conditions.

This paper is confined to the use of Radio Frequency (RF) technology in switching to control household appliances which involves:

- The design and construction of a transmitter circuit that switches to send signal to the receiver circuit using the RF technology.
- The design and construction of a receiver circuit that receives signal from the transmitter circuit via RF technology then acts to switch on or off a household appliance.

2. Remote control Technologies

Years ago some remote control made use of wires, but modern remote control now works based on wireless communication. This allows information to be exchanged between two devices without the use of wire or cable [5]. There are various technologies that can be used for developing wireless remote control for household application. Each technology has its own merits and limitations. Various works have been done by different people on different remote control:

2.1. Infrared control

The dominant remote-control technology in home applications is the infrared (IR), also known as "heat". The basic premise at work in an IR remote control is the use of light to carry signals between a remote control and the device it is directing. Infrared light is in the invisible portion of the electromagnetic spectrum [2-4]. Infrared remote control for home appliances works based on technology similar to the Television remote operation. Infrared radiation is the region of the electromagnetic spectrum between microwaves and visible light. In infrared communication an LED transmits the infrared signal as bursts of non-visible light. At the receiving end a photodiode or photoreceptor detects and captures the light pulses, which are then processed to retrieve the information contained. An Infrared remote control transmitter sends out pulses of infrared light that represent specific binary codes [2]. These binary codes correspond to commands, such as Power ON or Power OFF. The receiver receives the signal and the microprocessor carries out the corresponding command [1]. The infrared receiver sits on the front of the device where can easily get the incoming signal from the remote control. In an infrared remote, when a push button is pressed, the integrated circuit detects it and sends the binary command to the LED at the front of the remote [2] as shown in Figure 1.

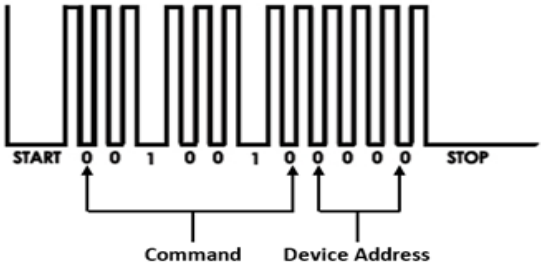

Figure 1. The remote control binary command

The LED sends out a series of light pulses that corresponds to the binary command to the receiver. In Figure 1, the 'start' indicates when the button is pressed while the 'stop' indicates when the button is released. When the infrared receiver on the appliance picks up the signal from the remote and verifies from the address code that it is supposed to carry out this command, it converts the light pulses back into the electrical signal. This signal now passes to the microprocessor, which carries out the intended command. Figure 2 shows the two circuits for an infrared control [2]: the transmitter and the receiver circuits.

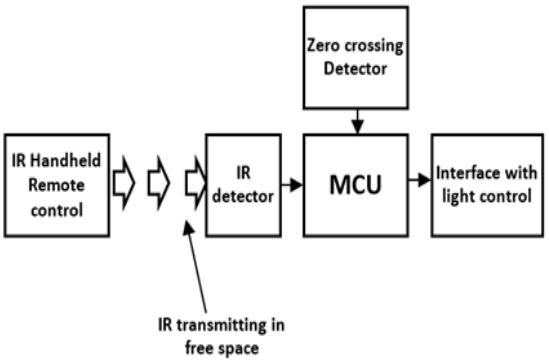

Figure 2. Block diagram of infrared control

The transmitter circuit consists of the power supply which is usually a battery supplying the required voltage for the encoder and the IR transmitter. There is the encoder which encodes the information received from the switches and then generates a modulated signal which is sent to the transmitter. This encoder

can be an Integrated Circuit (IC) 555 timer which acts as an actable multi-vibrator whose output makes the IR transmitter to be in high state and produce the infrared beam through the concave lens of the IR LED [6]. This infrared beam produced from the infrared LED travels in a straight path is then transmitted to the receiver circuit. The receiver circuit consists of the power supply, the infrared receiver, the decoder, the relay driver and the relay, and this connects the appliance controlled to the mains power supply. The power supply of the receiver circuit is usually connected from the mains through rectification as the circuitry uses DC voltage. The infrared receiver is a photo diode which is usually the IC's (TSOP 1738 or TSOP 1740), whose output is high when idle and goes low when it receives a signal [6]. The received signal is transmitted to the decoder or demodulator which demodulates the frequency of the signal and activates the relay driver which triggers the relay to be activated or deactivated. The activation and deactivation of the relay brings about a switching operation which turns on or turn off the connected appliance.

The infrared remote control has the performance of the high signal to noise ratio, strong anti-interference, reliable transmission of information, and untouchable, low power and affordable [1]. This remote is also use for industrial control, the aerospace, the security and so on. The disadvantages of using infrared includes: being limited to line of sight; the transmitters and receivers must be almost directly aligned (that is, able to see each other) to communicate [2]. It is easily blocked by materials such as people, walls, and plants and has short range; as a result, it performance drops off with longer distances. It is light and weather sensitive; direct sunlight, rain, fog, dust, pollution can affect transmission. The data rate transmission is lower than typical wired transmission [1].

2.2. Radio Frequency (RF) control

Instead of sending out light signals, an RF remote transmits radio waves that correspond to the binary command when the button is been pressed. Radio frequency (RF) is any of the electromagnetic wave frequencies that lie in the range extending from 3 kHz to 300 GHz, which include those frequencies used for communications or radar signals [7]. When a RF current is supplied to an antenna, it gives rise to an electromagnetic field that propagates through space. Any RF field has a wavelength that is inversely proportional to the frequency. A radio receiver on the controlled device receives the signal from the radio transmitter and decodes it. RF remote control system is designed for controlling the power switch of household appliances [7]. It consists of two parts: the remote controller which consists of a transmitting unit and a power amplifier which generates modulated RF signals and sends it out when a function button is pressed. The other part is placed in the household appliances section that is made up of a receiving unit and a power management block. It receives and demodulates the signal and send to the power management block [6, 7]; and relay using battery supply to boost the energy coming from the received RF signal to open or close the power switch of the electrical equipment as shown in Figure 3.

Radio remote control is used to control distant objects using a variety of radio signals transmitted by the remote control device. This type of control makes use of the radio waves for signal transmission. RF remotes tend to cost a bit more, have longer range, and is not affected by line of sight as is the case for Infrared. However, it cannot be used for very long range and any transmitter operating in the range can carry out the control.

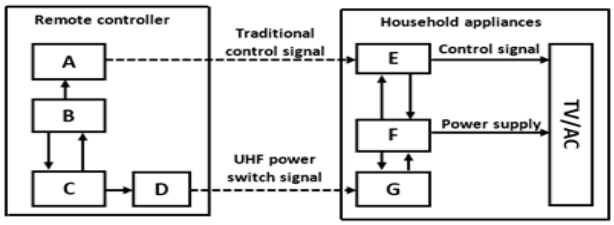

A – Traditional remote control transmit unit
B – Battery power supply
C – Remote control transmitting unit
D – Power amplifier
E - Traditional remote control receive unit
F – Power management
G - Remote control receiving unit
TV/AC – Television/Air conditioner

Figure 3. Block diagram of Radio Frequency Control

2.3. Global system for mobile communication module

The Global System for Mobile (GSM) communication module (SIM900) is a complete Quad-band GSM/GPRS device which can be embedded in circuits. The SIM900 delivers GSM/GPRS 850/900/1800/1900MHz performance for voice, SMS, Data, and Fax in a small form factor and with low power consumption [8]. It is equipped with analog audio interface, Analog to Digital (A/D) converter, Antenna pad, Serial interface which enables the interfacing of the SIM900 to micro controller.

2.3.1. Remote control using SIM900

The GSM control with the SIM900 makes use of the GSM mobile network which uses a sim card and is interfaced directly to the micro controller. This control method is used [8] to control the household appliances remotely. The medium of transmission in this control is the mobile network. With this, it will be convenient to control any device wirelessly, especially helpfully for outdoor remote control. SMS sent to the sim card in the network module is read by the micro controller. The micro controller is then programmed to carry out a switching task when it receives a preset SMS.

If the message is preset in the micro controller program, the micro controller then triggers a relay corresponding to the specified load to activate and make the circuit of that load and the mains. If a different message is sent to the GSM module as specified in the micro controller to turn off a particular load, the micro controller sends a low output to the relay to deactivate to break the circuit of the specified load and the mains. Merits of this control includes its ability to control home appliances over any range as long as there is GSM network at the receiver station and the transmitter station [7, 8]. The micro controller can also be programmed to give a feedback on successful turning on or turning of an appliance. It can control as many appliances as there are output pins of the micro controller.

Its high cost with the cost of buying the micro controller and programming of the micro controller adds to the demerits of this control method. This control method cannot be used in a remote area where there is no GSM network. Also, this control consumes user airtime when sending a control signal.

2.3.2. Dual-Tone Multi-Frequency application

Dual-tone multi-frequency (DTMF) signaling is an in-band telecommunication signaling system using the voice-frequency band over telephone lines between telephone equipment and other communications devices and switching centers. The DTMF system uses a set of eight audio frequencies transmitted in pairs to represent 16 signals, represented by the ten digits, the letters A to D, and the symbols # and * [9]. These ten digits, letter A to D and symbols # and * forms the telephone keypad. Modern telephone got rid of the letters [10]. The DTMF telephone keypad is laid out in a 4×4 matrix of push buttons in which each row represents the low frequency component and each column represents the high frequency component of the DTMF signal. Pressing a key sends a combination of the row and column frequencies [9]. For example, the key 1 produces a super imposition of tones of 697 and 1209 hertz (Hz). This is shown in Table I.

Table I. DTMF Keypad Frequencies

	1209 Hz	1336 Hz	1477 Hz	1633 Hz
697 Hz	1	2	3	A
770 Hz	4	5	6	B
852 Hz	7	8	9	C
941 Hz	*	0	#	D

2.3.3. Remote control using DTMF

This system adopts existing common telephone network to realize remote control. As long as main control terminal is in the range of GSM, it can make use of the working method of DTMF to realize the communication between transmission and reception. DTMF signals are widely used and concerned because of its low power consumption, strong anti-interference, less peripheral parts, large code capacity and easily interfaced with all kinds of sensors. DTMF receiver includes DTMF grouping filter and DTMF decoder. It is composed of a group of low audio signals and a group of low audio signals. In the GSM control using DTMF technology, a mobile phone serves as the transmitter, in the receiver section, another mobile phone serves to receive the transmitted signal which is the mobile/GSM modem as shown in the control block diagram of Figure 4.

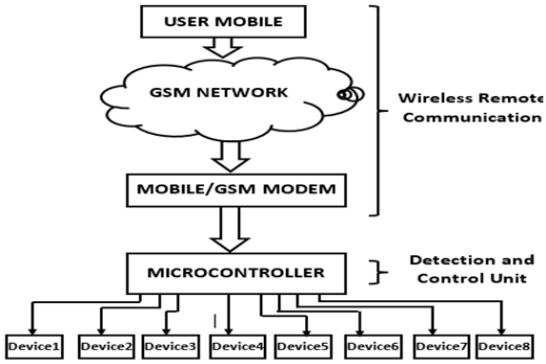

Figure 4. Remote control using DTMF

The mobile phone in the transmitter section is set to automatically answer calls, and it is interfaced to the DTMF decoder through the headset port. When the phone transmitter calls the phone receiver, it automatically answers, any key pressed on the phone transmitter sends a code according to the Table 1 above to the DTMF decoder, the DTMF decoder decodes this code and sends a 4-bit output to the micro controller, the micro controller is programmed to react to this inputs from the DTMF decoder [9]. For specific key pressed, the micro controller may be programmed to output a high to trigger the relay to activate and make the circuit of the home appliance and the mains, and for another key pressed, the micro controller is programmed to output a low to deactivate the relay and break the circuit of the home appliance and the mains.

DTMF control takes full advantages of the public switched telephone network, which makes it realize the remote control and receive the full-duplex communication [11]. The transmission distance of the control signal is not restricted as long as there is GSM network where the phone transmitter is, and there is a GSM network at the location of the receiver. The limitation of this control is that the number of home appliance it can control is limited to the keypad of a phone which is twelve in number; six keys to turn on and six keys to turn off appliances.

2.4. Descriptions of components

The various components used to achieve a Radio Frequency remote control include:

1) The HT12E (the encoder) [12], as shown in Figure 5.

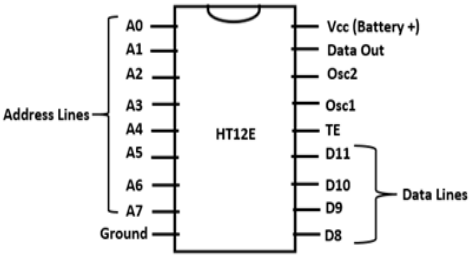

Figure 5. HT12E encoder

These IC, HT12E is of the family of encoders which is capable of encoding information which consists of N address bits and 12 – N data bits [12]. The '12' in the name means 8 address lines and 4 data lines while E letter represents 'Encoder'. The four data lines of this encoder are the four input lines. These lines are used to give input which is to be encoded. In encoding, data is being wrapped up. For instance, if a binary signal '1001' is needed at the output end, it is required to make data pins as '1001'. To make the data pin like this, 'high' or 5 volts (which digitally means '1') is fed to pins 'D0' and 'D3' while 'low' or 0 volts (ground) is fed to pins 'D1' and 'D2'. This together gives '1001' which is transmitted out from the 'Data out' pin of the HT12E. The input given to data pin is in parallel form which is being transmitted into serial form from the data output pin.

1) The HT12D (the decoder) [13], as shown in Figure 6.

The HT12D is paired with the HT12E for complete encoding and decoding of information. Like the encoder, the '12' in the name means 8 address lines and 4 data lines but the letter 'D' represents 'Decoder' [13]. Here, the data lines serve as the output pins. The encoded data which comes from the transmitter side goes into the Data in (Din) pin. The data which was in serial order

gets decoded and the output is generated at the four data line pins in same order as that on transmitter pin. For instance, if the binary of '1001' is fed into the Data in (Din), the data line pins will be "1, 0, 0, 1" for 'D8, D9, D10, D11' respectively where '1' is high (5 volts) and '0' is low (0 volts).

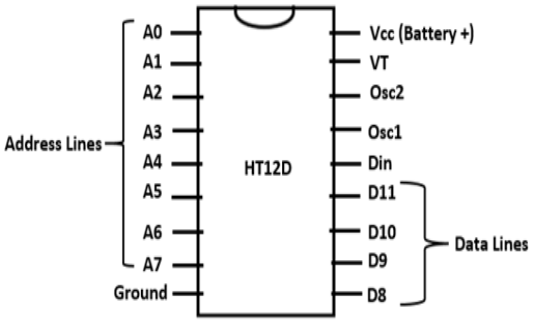

Figure 6. The HT12D paired up for complete information coding

The address line is used to direct data from the encoder to travel to a specific decoder. When using a single pair of encoder-decoder IC, the address pins are usually left unconnected. But if there is more than one decoder but only single encoder, it is necessary to give an address to the data that it might travel to specific decoder only and the data should not leak at unnecessary decoders. This is useful for the security of our data.

1) The IC‑74147

The HT12E discussed above provides only four inputs, for remote control application. This limits the number of devices that can be controlled. The 74147 in another encoder, which encodes 10 – Line Decimal information to 4 – Line Binary Coded Decimal (BCD) information [14]. This IC is a multiplexer as it allows ten (10) inputs and gives out four (4) outputs which correspond to the input of the HT12E where the outputs of 74147 is connected [13, 14]. The logic circuit is as shown in Figure 7 and the truth table is as shown in Table II.

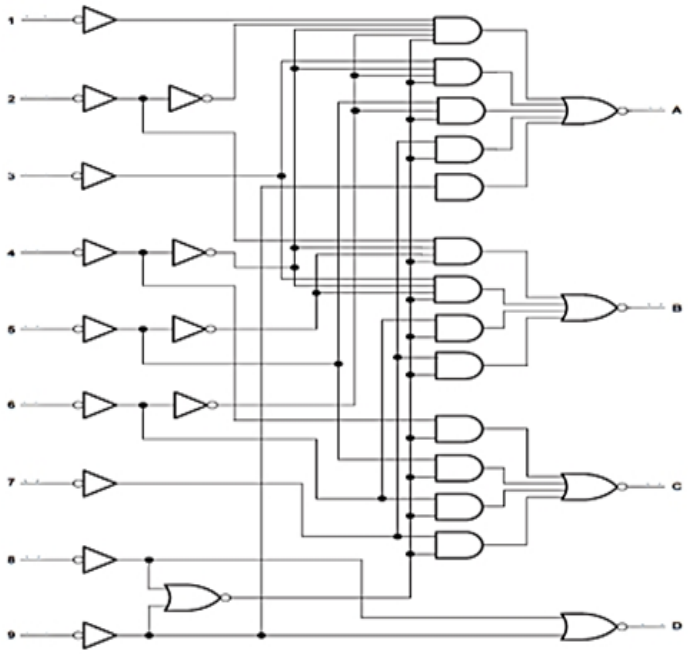

Table II. Truth table of 74147

INPUTS									OUTPUTS			
1	2	3	4	5	6	7	8	9	D	C	B	A
H	H	H	H	H	H	H	H	H	H	H	H	H
X	X	X	X	X	X	X	X	L	L	H	H	L
X	X	X	X	X	X	X	L	H	L	H	H	H
X	X	X	X	X	X	L	H	H	H	L	L	L
X	X	X	X	X	L	H	H	H	H	L	L	H
X	X	X	X	L	H	H	H	H	H	L	H	L
X	X	X	L	H	H	H	H	H	H	L	H	H
X	X	L	H	H	H	H	H	H	H	H	L	L
X	L	H	H	H	H	H	H	H	H	H	L	H
L	H	H	H	H	H	H	H	H	H	H	H	L

1) The 74138

The HT12E encodes a 4 – line BCD information which is transmitted to the HT12D which decodes the 4 – line BCD information to give 4 outputs through the four output pins. The 74138 is a 3 – Line to 8 – Line Decoders/Demultiplexers which allows 3 inputs to give out 8 outputs [15]. It only takes three of the HT12D outputs and demultiplexes it to eight outputs allowing the control of eight appliances. The internal circuitry is a logic circuit comprising of AND, OR and NOT gates as shown in Figure 8 and the truth table is as shown Table III [15].

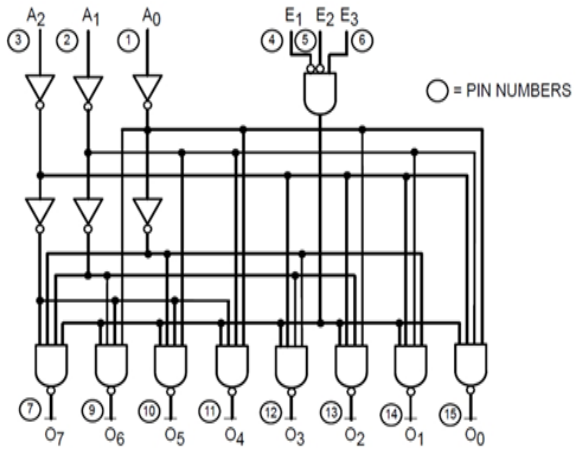

Figure 8. Logic circuit of 74138

Table III. Truth table of 74138

INPUTS			OUTPUTS							
A_0	A_1	A_2	Y0	Y1	Y2	Y3	Y4	Y5	Y6	Y7
L	L	L	L	H	H	H	H	H	H	H
H	L	L	H	L	H	H	H	H	H	H
L	H	L	H	H	L	H	H	H	H	H
H	H	L	H	H	H	L	H	H	H	H
L	L	H	H	H	H	H	L	H	H	H
H	L	H	H	H	H	H	H	L	H	H
L	H	H	H	H	H	H	H	H	L	H
H	H	H	H	H	H	H	H	H	H	L

1) The 7476

This IC is a flip flop built with two independent J-K flip-flops with individual J-K, clock, preset and clear inputs [16]. Its function table is as shown in Table IV.

Table IV. Function table of 7476

INPUTS					OUTPUTS	
$\overline{PRE}$	$\overline{CLR}$	CLK	J	K	Q	$\overline{Q}$
L	H	X	X	X	H	L
H	L	X	X	X	L	H
L	L	X	X	X	H	H
H	H	↓	L	L	Q_O	$\overline{Q}_O$
H	H	↓	H	L	H	L
H	H	↓	L	H	L	H
H	H	↓	H	H	TOGGLE	
H	H	H	X	X	Q_O	$\overline{Q}_O$

This IC can be connected in the toggle mode such that when it detects a negative edge trigger in the clock input, it toggles the state of the output from high to low or vice versa.

1) The Amplitude Shift Keying (ASK) RF Module

This RF module comprises of an RF Transmitter and an RF Receiver. The transmitter/receiver (Tx/Rx) pair operates at a frequency of 434MHz [17]. An RF transmitter receives serial data and transmits it wirelessly through RF through its antenna connected at pin 4. The transmitted data is received by an RF receiver operating at the same frequency as that of the transmitter. In this RF system, the digital data is represented as variations in the amplitude of carrier wave. This type of modulation is known as Amplitude Shift Keying (ASK). The RF transmitter and receiver are shown in the Figure 9 [17].

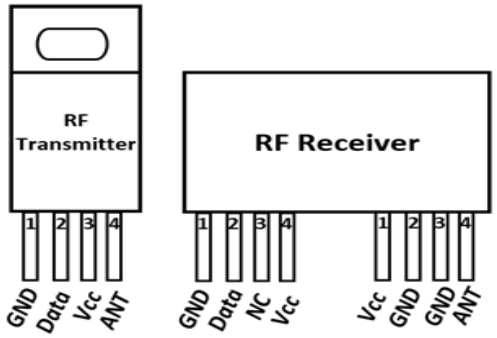

Figure 9. The RF module for transitions and receiving data

The RF transmitter transmits any data fed into the data pin (pin 2) through the antenna connected at the antenna pin (pin 4). The receiver receives any data transmitted on its frequency through the antenna connected at the antenna pin (pin 8) and puts the data out through the data pin (pin 2).

1) The IC 7805

This IC is a voltage regulator, it has three pin outs: the input voltage pin, the ground pin and the output voltage pin. When a voltage greater than 5V is applied through the input pin, and the ground pin connected to the ground of the voltage source, the output pin gives out a voltage of +5V. From the name 7805, the "78" indicates that it is a positive voltage regulator, and the "05" indicates that it is a 5V regulator. With the help of this IC, positive power supply of 5V is achieved.

3. Design and Development of the System

The design method is as follows:

- Component specifications are as shown in Table V.

Table V. Components specification

COMPONENTS	VOLTAGE (V)	CURRENT (mA)
Transformer	12	1000
Bridge rectifier	200	6000
HT12E	5	0.5
HT12D	5	0.5
7805	5	5
7812	12	5
74138	5	5
74147	5	5
7476	5	5
BC548	5	5
Relay	12	30
RF transmitter module	5	5
RF receiver module	5	5

- The system mainly comprises of two parts: the transmitter, and the receiver. The transmitter stands alone and makes use of power supply from a cell. It comprises of the input system, multiplexers and modulator. The receiver on the other hand comprises of the demodulator, demultiplexers, flip flops and control relays. The receiver section circuitry is divided into three sections: the power supply circuitry, the signal receiving circuitry and the switching circuitry.

3.1. The Transmitter circuit design

The transmitter section consists of the following components: Battery, 7805, 10µF capacitor (x2), 1KΩ resistor (x6), 74LS147, push button (x5), HT12E, ASK RF module transmitter. The transmitter section is powered by a 9volts battery. Due to the specifications of the components of the transmitter, 5 volts is required to power the ICs. This led to the voltage regulation by the use of the voltage regulator 7805, which regulates the 9 volts to 5 volts. This regulated voltage powers the whole transmitter section circuitry.

The input pins of the 74LS147 which is a multiplexer is connected to the voltage source to make the pins logic one (1 – high). These pins are connected through resistors functioning as current limiting resistors. These resistors limit the current into the

74LS147 through the following analysis. The resistors R1 to R5 are the current limiting resistors. The IC 74147 requires a current of 5mA and from the relation. The resistor calculation is shown in equations 1 and 2.

$$V = IR \Rightarrow R = \frac{V}{I} \quad (1)$$

For a current of 5mA and a voltage of 5 volts,

$$R = \frac{5}{0.005} = 1000\Omega = 1k\Omega \quad (2)$$

Therefore, resistors R1 to R5 with value of 1kΩ each limit the current into the IC 74147 to 5mA.

The input pins of the 74LS147 each is connected through a push button to the negative terminal of the battery. This is to provide logic zero (0 – low) to the IC when switched. When the button is pressed, the output pins changes as provided in the truth table of Table II. For this work, the control is for five appliances only. Pins 4, 3, 2, 1, 13 of the 74LS147 are used. When the buttons to these pins are switched independently, the output pins give logic output as analyzed in the Table VI.

Table VI. IC 74LS147 signal multiplexing function

Pin	Button pressed	Input	Output
4	B1	XXXXXXLHH	LLLH
3	B2	XXXXXLHHH	HLLH
2	B3	XXXXLHHHH	LHLH
1	B4	XXXLHHHHH	HHLH
13	B5	XXLHHHHHH	LLHH

The binary equivalent of these outputs LLLH, HLLH, LHLH, HHLH, and LLHH is 0001, 1001, 0101, 1101, and 0011 respectively. This output of 74LS147 is fed to the input of the HT12E. The HT12E is a parallel data to series data encoder; it encodes the parallel data inputs (the output of 74LS147) that it receives from 74LS147 to a series data that it sends out through the Data out pin (pin 17). The encoding function of the HT12E gives an instance input of binary 1001 as shown in the Figure 10 [18].

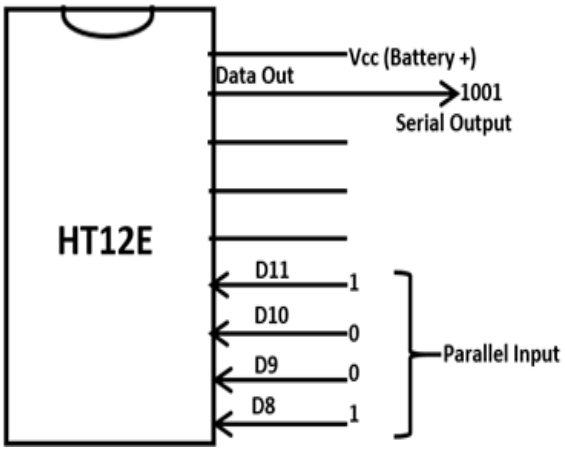

Figure 10. HT12E parallel to series encoder

The serial output of the HT12E is transmitted to the RF module. The ASK RF module operates at a frequency of 434MHz, and transmits data that it receives using the radio frequency medium through the antenna connected at the antenna pin. The velocity of the transmitted data is the velocity of free space.

$$c = 3\times10^8 \quad (3)$$

The wavelength is calculated from equation 4.

Where

$$c = f\lambda \Rightarrow \lambda = \frac{c}{f} = \frac{3\times10^8}{434\times10^8} = 0.69m = 69cm \quad (4)$$

This implies that the wavelength (λ) of the transmitted data is 69cm.

3.2. The Receiver circuit design

The receiver section has three sections that work together to receive and process the received signal and carry out a switching operation. These sections include: the power supply and the control section.

3.2.1. The power supply

The power supply comprises of the following components: 220/12V transformer, bridge rectifier, capacitors, 7805, 7812 and AC plug. The power supply provides the voltages required by the ICs for proper operation. It involves the rectification of AC voltage to DC and the regulation of this DC to a voltage as required by the ICs. The transformer steps down the AC voltage to 12 volts, the bridge rectifier carries out a full wave diode rectification to give an output voltage as analyzed from equations.

Peak value of the output voltage:

$$V_m = 12\times\sqrt{2} = 16.97V \quad (5)$$

Average value of output voltage:

$$V_{av} = \frac{2V_m}{\pi} = \frac{2\times16.97}{\pi} = 10.8V \quad (6)$$

Root mean square value of voltage:

$$V_{rms} = 12V \quad (7)$$

Ripple voltage output:

$$V_{ac} = \sqrt[2]{V_{rms}^2 - V_{av}^2} = \sqrt[2]{12^2 - 10.8^2} = 5.23V \quad (8)$$

Voltage across the ripple capacitor:

$$V_{dc} = V_{ac} + V_{av} = 5.23 + 10.8 = 16.03V \quad (9)$$

This output voltage across the capacitor is regulated by the voltage regulator 7805 to give a +5V, and the 7812 also regulates this voltage to give a +12V. This makes available three terminals for 5V, 12V and ground respectively.

3.2.2. The control section

This section carries out the control of household appliances. It is responsible for receiving the signal from the transmitter,

processing this signal and switching "ON" or "OFF" an appliance. It comprises of the following components: HT12D, 74138, 7476 (×3), resistors (1KΩ ×7), transistors (BC548 ×5), diodes (1n4001 ×5), ASK RF module receiver and relays (×5).

The ASK module receives signals transmitter at a frequency of 434MHz from the transmitter, it sends this signal out through its data pin (pin 2) to the data-in pin (pin 9) of HT12D. The ASK module operates with a voltage of 5 volts and a current of 5mA, this gave rise to a current limiting resistor connected to the voltage input of this module whose value is as calculated in equation 10.

$$R = \frac{V}{I} = \frac{5}{0.005} = 1000\Omega = 1k\Omega \quad (10)$$

The HT12D is a series to parallel data decoder which decodes the serial binary data. It receives from ASK module to parallel data and gives out this parallel data through its output pins, pins 12, 13, 14, 15. It gives out a "high" for binary one (1) and a "low" for binary zero (0) which is 5 volts and 0 volts respectively. An instance is given in the Figure 11 for when the HT12D receives a binary input of "1001" from the ASK module.

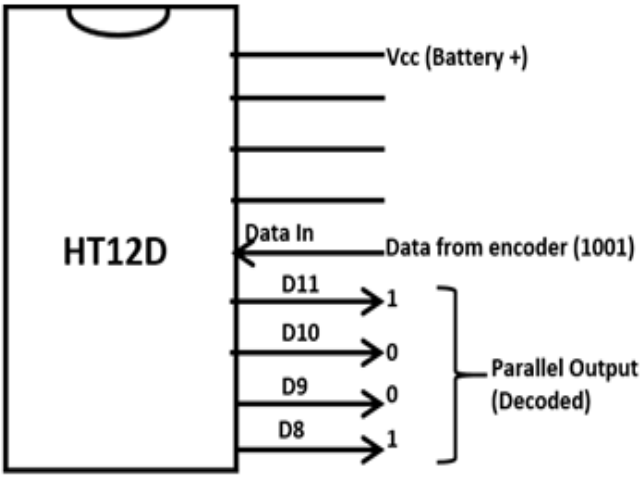

Figure 11. HT12D series to parallel to decode

The data decoded by the HT12D is a multiplexed data from the IC 74LS147 encoded by HT12E. This data decoded by HT12D, needs to be de-multiplexed. The output of this HT12D is therefore fed transmitted into the input pins of the IC, 74LS138. The 74138 is a 3 – Line to 8 – Line Decoders/De-multiplexer which allows 3 inputs to give out 8 outputs. It only takes three of the output pins of HT12D as input and de-multiplexes it according to the signal output of Table VI as shown in the Table VII.

Table VII. IC 74LS138 signal de-multiplexing function

HT12D Output	74LS138 Input	Output	Pin triggered
LLLH	LLL	LHHHHHHH	15
HLLH	HLL	HLHHHHHH	14
LHLH	LHL	HHLHHHHH	13
HHLH	HHL	HHHLHHHH	12
LLHH	LLH	HHHHLHHH	11

The Table VII shows that when button to pins 4, 3, 2, 1, 13 of the IC 74LS147 of the transmitter is pressed, pins 15, 14, 13, 12, 11 of the IC 74LS138 of the control section is triggered from "high" to "low" (5 volts to 0 volts). These output pins of the 74LS138 each is fed into a flip-flop. The IC 7476 is a flip flop built with two independent J-K flip-flops with individual J-K, clock, preset and clear inputs. With the five outputs of the 74LS138, three of the IC 7476 is required. The flip flop is configured in a toggle mode such that when the clock input receives a negative shot trigger, the output is toggled. With this configuration of the flip-flop, when a button is pressed, the output of the flip flop will be "high" (5 volts), when the same button is pressed again, the same output goes "low" (0 volts).

The outputs of the flip flops each is fed to the base of a transistor, BC548. The application of this transistor is for switching. When the output of the flip flop is high, the voltage at the base of the transistor becomes 5 volts, this biases the transistor and allows current to flow from the collector to the emitter. When the output of the flip flop is low, the voltage at the base of the transistor is 0 volts and thereby not biased, current will not flow to the emitter from the collector. A resistor is used at the base of the transistor to limit the current to the required base current (I_b) of 5mA. The value of this resistor is calculated from equation 3.10. A relay is connected at the collector of the BC548 and 12volts power supply as the relay is rated 12volts. The normally connected and the normally open terminals of the relay are connected to the switching terminals of the two-way switch which is used to achieve double control; manual and remote control. The AC life terminal is connected to the control terminal of the two-way switch, and the neutral connected to the load. The second terminal of the load is then connected to the control terminal of the relay. When the relay and the two-way switch are switched to one path, the connected load is turned on, when the relay and the two-way switch is switched to different path, the load is turned off. In this case, either of the relay or the manual switch can be used to turn on or off the connected load.

3.2.3. *The Security Design*

The security design of the system comprises of additional circuitry added to both the transmitter and the receiver sections. It makes the receiver able to receive signal from the transmitter only when a condition set in the receiver is met on the transmitter. The circuit consists of push buttons connected to the address pins of the IC HT12E for the transmitter section and also push buttons connected to the address pins of HT12D for the receiver section.

Transmission of signal from the transmitter to the receiver is only possible when the address line of the transmitted signal is the same with the address line of the receiver system. Exploring this, the push buttons in the receiver section are used to pre-set some pins as desired by the user to logic zero. The user of the transmitter must set similar pins on the transmitter section to logic zero before transmission will be possible. With this, only the user who knows the preset pins in the receiver can set the transmitter to transmit signal to the receiver.

4. The Simulation of the project

Computer aided simulation of the project was carried out using a computer software called proteus. With proteus the project circuits were implemented by selecting various components of the design and interconnecting these components as regards to the project design.

4.1. Implementation of the circuit on a temporary board

Implementation of the circuit on a temporary board is for clarification purposes and testing of components reliability and functionality. The project design was carried out on a temporary board to ensure proper connection for testing as shown in Figure 12.

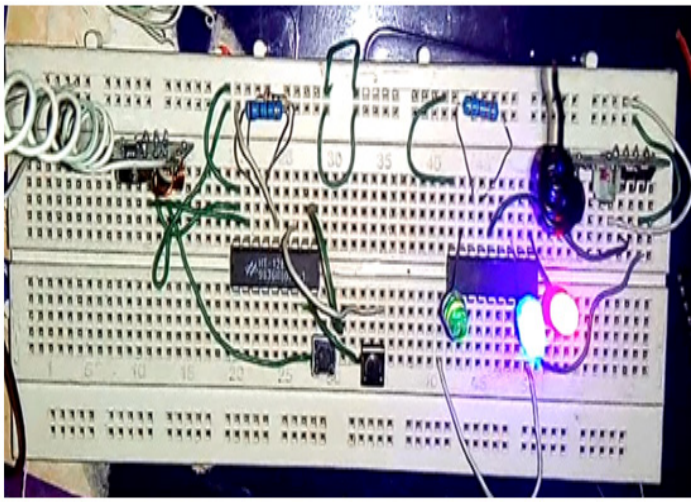

Figure 12. Implemented circuit on a temporary circuit board

On the temporary project board, signals sent through the transmitter by pressing push buttons on the board were transmitted to the receiver and the action caused the switching on and off of an LED connected at the output section of the receiver. The result from test-running the circuit on the bread board was positive.

4.2. Construction on a permanent board

Subject to the positive result from the test on a temporary project board, implementation of the circuit on a permanent circuit board was carried out. This implementation involves the soldering of the components to the board, and carrying out appropriate connections of the components. The components were arranged on the circuit board following the specification of the circuit design. The construction of the work on the permanent circuit board (Vero board) is as shown in Figure 13 to Figure 17.

4.3. Testing

The testing of the circuit design was carried out while the project was implemented on the permanent circuit board. After soldering the power supply circuit on the receiver section, this power supply was tested to ensure that it gives the expected voltage of +5V and +12V and it tested positive. At completion of the construction of the transmitter and receiver section, an LED was connected to the TE pin out of the HT12D, whenever transmission is possible between the transmitter and the receiver, this LED will be on; with this, monitoring effectiveness of signal transmission was possible. When the implementation was complete, the project was equally tested to ensure that it is working. For the range of operation, the transmitter was moved away from the receiver while transmitting signals to estimate the distance for operation. The estimated range of operation of the project was within one hundred meters (100m).

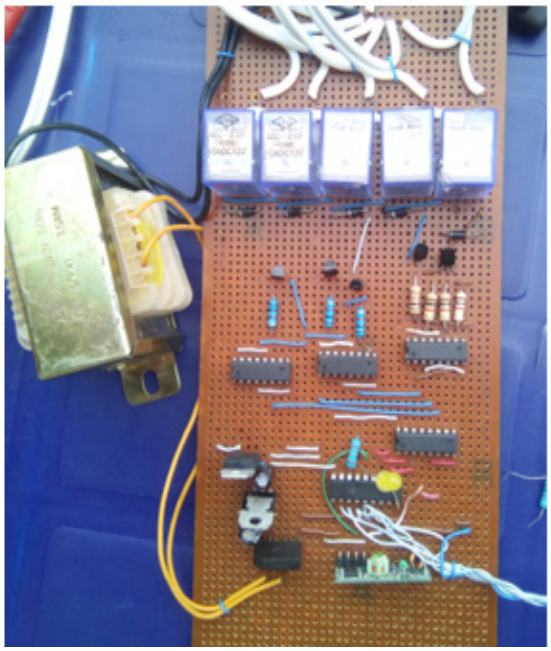

Figure 13. The receiver section showing the transformer

Figure 14. The receiver section showing two loads being controlled

Figure 15. Image showing the soldering work

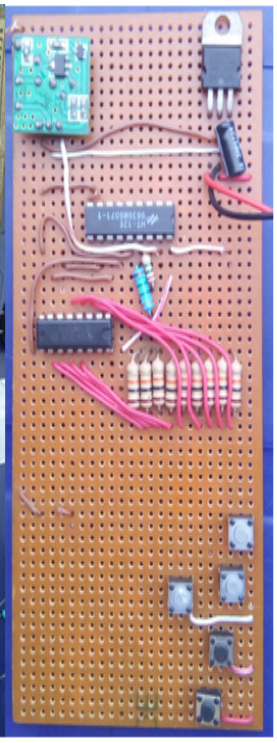

Figure 16. Image showing the transmitter section

4.4. The Engineering measurement and evaluation bill

The bill of engineering measurement and evaluation for the project is given as shown in Table VIII.

Table VIII. Bill of Engineering Measurement and Evaluation

MATERIAL	QUANTITY	COST (Naira)
HT12E and HT12E	1 each	150 each
RF MODULE	1	2000
74147 and 74138	1 each	100 each
7476	3	150
BC548	5	100
BUTTON	15	150
DIODE (1N4001)	5	50
RELAY	5	250
RESISTORS	11	220
7805, 7812, BATTERY & RECTIFIER	1 each	50 each
TRANSFORMER	1	500
CAPACITORS	2	60
Packaging	----------	700
TOTAL		4880

4.5. Analysis and Results

When the transmitter is powered, a voltage of 5volts is impressed on the pins 11, 12, 13, 1 and 2 of the IC74147. With the resistors (1 kΩ each) in series to these pins, a current of 5 mA flows through each of these pins. When the button to a pin is pressed, a zero voltage (0 volts) is impressed to the pin and no current flows through the pin of the IC. This leads to series of signal processing within the circuit as analyzed in Table IX.

Table IX. Analysis of signal transmission

Transmitter			Receiver		
Button Pressed	74147 Input	HT12E Input	HT12D Output	74138 Output	Load Triggered
B1	XXXXXXLH H	LLLH	LLLH	LHHHHHH H	Load 1
B2	XXXXXLHH H	HLLH	HLLH	HLHHHHH H	Load 2
B3	XXXXLHHH H	LHLH	LHLH	HHLHHHH H	Load 3
B4	XXXLHHHH H	HHLH	HHLH	HHHLHHH H	Load 4
B5	XXLHHHHH H	LLHH	LLHH	HHHHLHH H	Load 5

From Table IX, a button pressed in the transmitter causes a logic signal transmission from the input of 74147 to the out of 74138 which triggers a load as in the table. The analysis of voltages, resistance values in the circuits are shown in equations 1 to equation 10 and the packaged completed project of an example has been developed for controlling two lighting points and having three socket outlets for the proposed appliances: a refrigerator, water heater and an air conditioner as shown in Figure 17.

Figure 17. Image showing the project completed and packaged

Remote controls developed with the technology of Infrared can only transmit signal within line of sight. This project transmits signal through obstacles on the line of sight. Other works with similar transmitting technology of Radio Frequency can be manipulated and controlled with any device transmitting signal on the same frequency. This project has security feature which states that the receiver can only receive signal from a transmitter carrying signal with the same signal address by the receiver.

5. Conclusion

Remote control is very important in household application, it brings about comfort when controlling and operating household

appliances. It makes life easy while trying to make switching operation of appliances. In this work, the design and construction of a remote control for household application has been achieved. A transmitter system (the handheld remote), which comprises of encoder, multiplexer, RF module, push buttons, etc. has been developed which when operated, sends a signal to the receiver system. This receiver system receives and processes the signal from the transmitter, then turn ON or turns OFF an appliance. The receiver system which comprises of decoder, de-multiplexer, flip-flops, transistor, relays etc. has also been developed which when receiving signal from the transmitter processes of the signal, switches ON or switches OFF a load. Incorporating a security system, allows transmission of signal only when certain conditions are met, thereby providing security for household appliances and the aim achieved.

References

[1] A. Roy Delgado, R. Picking and V. Grout, "Remote-Controlled Home Automation Systems with Different Network Technologies", University of Wales, Wrexham, UK, 2013.

[2] Abdulaleem A. Rasheed, "Detection and study of various IR handheld remote control signals and using them for home applications", *IEEE Conference on Education and e-Learning Innovations (ICEELI)*, Sousse, 2012.

[3] C. Woodford, "How remote control and radio control work", 8 September 2015.[Online].Available:http://www.explainthatstuff.com/remotecontrol.html. [Accessed 9 April 2016].

[4] N. Neil, "Wikipedia, the free encyclopedia", 7 April 2016. [Online]. Available: https://en.wikipedia.org/wiki/Remote_control. [Accessed 9 May 2016].

[5] M. M. Ahmed, E. Ahmed and K. T. Ahmmed, "Automated Irrigation Control and Security System with WirelessMessaging", 2013 International Conference on Informatics, Electronics and Vision (ICIEV), Dhaka, 2013, pp. 15. doi: 10.1109/ICIEV.2013.6572595

[6] L. Jianjun, Li Zhishu and M. Mingyi, "A New USB Home Appliances based on PC and Infrared Remote Control Protocol", *IEEE 2010 International Conference on Computer and Communication Technologies in Agriculture Engineering*, Chengdu, 2010.

[7] L. Chen, Z. Wang, J. Chen, Li Fule, H. Wenhan, B. Xiao, C. Zhang and W. Zhihua, "A RF Remote-Control Transceiver with Zero-Standby Power Based on RFID Technology", *IEEE 2010 Asia Pacific Conference on Postgraduate Research in Microelectronics and Electronics (PrimeAsia)*, Shanghai, 2010.

[8] C. Gang, X. Tiefeng, L. Taijun, Yan Ye, X. Gaoming, "A GSM-based wireless remote controller", *IEEE 2011 International Conference on Electronics, Communications and Control (ICECC)*, Zhejiang, 2011.

[9] Md. Shariful Islam, Md. Badsha Mia, Kazi Tanvir Ahmmed, "Wireless Remote Switching System for Controlling Devices with an Algorithm based DTMF Detection", *IEEE 2014 International Conference on Electrical Engineering and Information and Communication Technology (ICEEICT)*, Dhaka, 2014.

[10] Liu Wei, Jiang Wenlong, Gao Yonghui, Ren Tao, "Remote Control of Smart Household Based on DTM", *IEEE 2010 2nd International Conference on Advanced Computer Control (ICACC)*, Shenyang, 2010.

[11] A. J. A. Mghawish, "A Practical Approach for Mobile-Based Remote Control", *European Scientific Journal of European Scientific Institute, ESI,* vol. 9, no. 18, pp. 194-201, 2013.

[12] Cornell, "HT12A/HT12E - Series of Encoders Datasheet", [Online]. Available:https://people.ece.cornell.edu/land/courses/ece4760/FinalProjects/s2008/cl457_yft2/cl457_yft2/datasheets/HT12E.pdf. [Accessed 13 May 2016].

[13] Farnell, "HT12D/HT12F 2 Series of Decoders Datasheet", [Online]. Available: www.farnell.com/datasheets/1525377.pdf. [Accessed 12 May 2016].

[14] T. Instrument, "SN74147 10-Line to 4-Line BCD Priority Encoder – Datasheet", [Online]. Available: http://www.ti.com/lit/gpn/sn74147. [Accessed 11 May 2016].

[15] T. Instruments, "74138 3-Line To 8-Line Decoders/Demultiplexers – Datasheet", [Online]. Available: www.ti.com/lit/ds/symlink/sn74ls138.pdf. [Accessed 11 May 2016].

[16] T. Instrument, "SN7476 Dual J-K Positive-Edge-Triggered Flip-Flops with Preset and Clear – Datasheet", [Online]. Available: http://www.ti.com/lit/gpn/sn7476. [Accessed 12 May 2016].

[17] WENSHING, "Wireless Hi Power Transmitter and Receiver Module – Datasheet", [Online]. Available:http://cdn.sparkfun.com/datasheets/Wireless/General/TWS-BS-3_433.92MHz_ASK_RF_Transmitter_Module_Data_Sheet.pdf. [Accessed 12 May 2016].

[18] Pingjun Wei, Xiaojing Li, Zhoufeng Liu and liangbo Zhu, "Design of Intelligent Control System of Eight-Way Wireless Remote Control Crane Based on RF Technology", *IEEE 2012 International Conference on Advanced Mechatronic Systems*, Tokyo, 2012.

ASTES

Advances in Science, Technology and Engineering Systems Journal Vol. 2, No. 4, 165-172 (2017)

www.astesj.com

ASTESJ

ISSN: 2415-6698

Finite Element Modeling for Wind Response of Aluminum Wall Cladding in Tall Building

Okafor Chinedum Vincent*, Mbanusi Echefuna Cyril, Kevin Chuks Okolie, Dominic Anosike Obodoh

Department of Building, Nnamdi Azikiwe University, Awka, Nigeria

ARTICLE INFO

Article history:
Received: 26 July, 2017
Accepted: 19 August, 2017
Online: 05 September, 2017

Keywords:
Tall building
BS6399-2:1997
Finite element analysis
Aluminum wall cladding panel

ABSTRACT

This paper analyzed wind loading responses of Aluminum Wall cladding panels in Tall Building using Ikeja Lagos State Nigeria. The wind loads were calculated according to Standard and Specification From BS6399-2:1997 Using the wind speed data of Lagos state Nigeria and finite element analysis, we predicted the responses of these Aluminum wall Cladding panels to the design wind loads being calculated. The result of the calculation from BS6399-2:1997 showed that the aluminum cladding panels located on the facade upwind was subject to positive pressure, which increases with height. Also, the cladding panels located on the leeward, as well as sidewalls, were subjected to negative pressure, which tended to be high at the top and bottom corners due to flow separation. From the result of the modeling and analysis, the researcher found out that stresses on the aluminum wall cladding panels were generally below the material yield point, showing that the high wind speed was not the reason for the collapse of aluminum cladding panels in the locality being considered. Instead, the reality lies on one or more issue on the materials construction and placement as discussed.

1. Introduction

The aerodynamics of tall buildings induced by the wind flow surrounding the building is characterized as that of a bluff body [1].The key factor affecting the aerodynamic loads on a bluff body include the approaching boundary layer wind, the characteristics of the bluff body and the condition of direct surrounding of the body such as presence of other bluff bodies [2].

Furthermore, buildings are obstructing the motion of air called wind, and as a result, the wind is exerting force on buildings [3].

Wind is composed of multitudes of eddies of varying sizes and rotational characteristics carried along in a general stream of air moving relative to the earth surface [4]. These eddies may give wind its gusty characteristic [4]. High wind speed of short duration are called gust. Large eddies whose dimensions are comparable with the structure tend to envelope the building (Figure 1) as they give well corrected pressure while small eddies result in pressure on various part of a structure that becomes practically unrelated with distance of separation[4]. Cladding on the other hand is the application of one material over another to provide skin or layer intended to control the infiltration of weather element or for aesthetic purpose. It is buildings envelop [5].

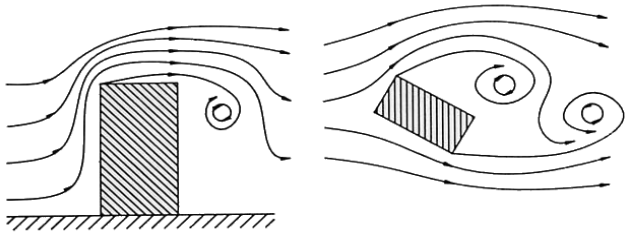

Figure 1: Generation of eddies

Today in Nigeria, many office building use aluminum cladding panel (figure 6) because it is versatile, lightweight and durable unlike other cladding materials. Aluminum cladding panels has certain recycling properties that help in creating a wide range of customized panel with metal finishes.

As is well known, the claddings and various building components are relatively small elements and their size is typically very small in relation to the entire structure [3]. So localized wind pressure variation according to BS6399-2:1997,[6] is required for their design and the analysis of the responses of the cladding panels to the design wind load is done using finite element analysis which is the subject matter of discussion in this paper.

*Okafor Chinedum Vincent, Department of Building, Nnamdi Azikiwe University, Awka, Nigeria | Email: chinedumokafor117@yahoo.com

Aim in this study is to analyze the wind loading responses of aluminum wall cladding panels of tall buildings using finite element analysis.

The study sought to achieve the aim through the following objectives to:

- Determine the magnitude of the design wind pressure on the wall cladding panels of the tall building,
- Calculate the wind speed at subsequent height of the tall building,
- Determine the static responses of the aluminum wall cladding panels to the design wind pressure, and
- Ascertain the regions on the wall cladding panel that require proper attention during the design and installation of the panel.

1. Flow phenomenon

1.1. *Positive pressure*

As shown in Figure 2, the maximum positive pressures generally occur at the windward wall and all facades will become windward for certain wind directions. The cladding panels located on that wall will become windward for same reason. The positive pressure increases as height increases which mean that the lower part of the building will be subjected to lower positive pressure and the top part of the building subjected to higher positive pressure except the top edges were the wind tends to negotiate with the edge, which results in lower positive pressure.

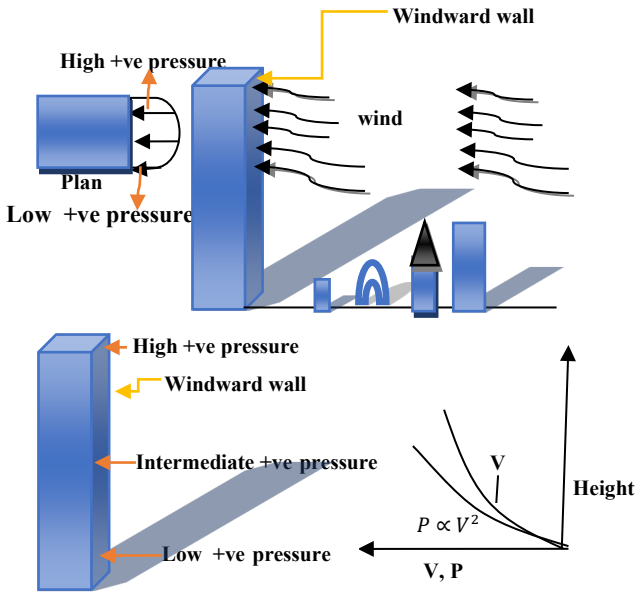

Figure 2: Pictorial representation of positive pressures acting on building facade.

1.2. *Negative pressure*

Cladding panels located at the leeward wall, as well as sidewall of the tall building, are subjected to negative pressures (suction) which are very high at the corners of the tall building due to flow separation [3]. Suction can also be very high at the top-bottom corner region due to intense flow separation. The increase of these suction or negative pressure is mainly due to the shape of the building and not associated with increase in height and speed of the wind.

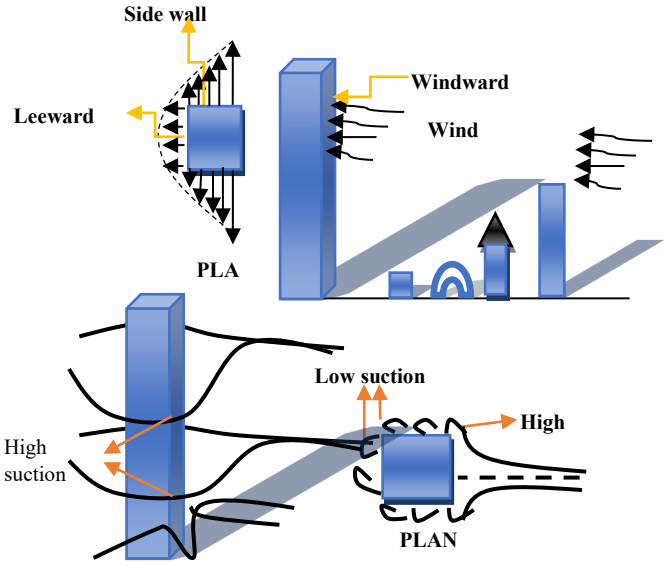

Figure 3: Pictorial representation of negative pressures acting on building facade.

2. Flow separation

Pressure gradient is one of the factors that affect flow immensely. A negative pressure gradient is termed a favorable pressure gradient because it enhances the flow of the wind while a positive pressure gradient is termed an unfavorable pressure gradient because it retards the flow.

From Figure 4 below, we have adverse pressure gradient downstream of S_2, this effect is felt more strongly in the region close to the windward wall of the tall building where the momentum is lower than in the region near the free stream. A continuous retardation of the flow brings the wall shear stress at the point S_2 on the windward wall to zero. From these point onwards, the shear stress becomes negative (S_3) and the flow reverses and a region of recirculation flow develops (figure 3).

We can see in figure 3 that the flow no longer follows the contour of the tall building. We say that the flow has separated. The point (S_2) where the shear stress is zero is called the point of separation. Depending on the flow conditions, the recirculation flow terminates and the flow may become reattached to the body. A separation bubble was also formed (figure 3).

There are various factors that can influence this reattachment one of which maybe that the pressure gradient has become more favorable due to body geometry or that the flow which was initially laminar may have undergone transition within the bubbles and may become turbulent [7]. A turbulent flow has more energy and momentum than laminar flow and this can kill separation and flow may re-attach.

3. Methodology

3.1. Research Designs

The proposed study work is mainly focused to analyze the wind loading responses of aluminum wall cladding panels of a typical tall building.

The procedure employed in order to achieve this aim is outlined below:

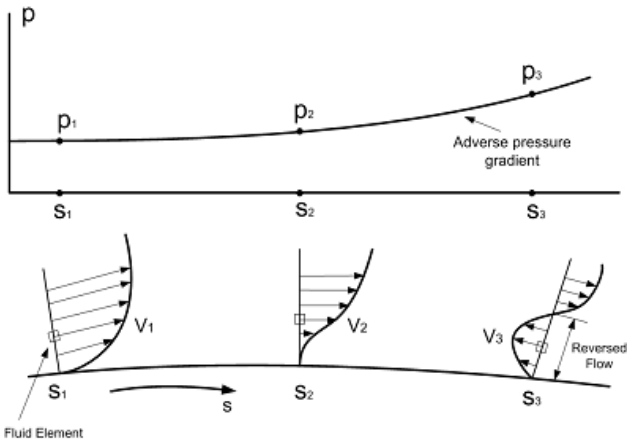

Figure 4: Pressure gradient and flow separation.

1. Getting a proper record of the wind speed distribution of the locality in consideration (Ikeja, Lagos state Nigeria).
2. Using the wind profile power law equation to determine the wind speed at subsequent heights for the 15th storey high rise building.
3. Calculating the values of the wind pressure on the Aluminum wall claddings using wind loading codes (BS6399-2-1997).
4. Analyzing the responses of the aluminum wall cladding to the wind pressure using LISA finite element analysis software.

3.2. Area of the Study

For the research work, wind speed data of Ikeja, Lagos state, Nigeria was used with reference to the wind speed map of Nigeria determined from 40years of measurement at 10m height.

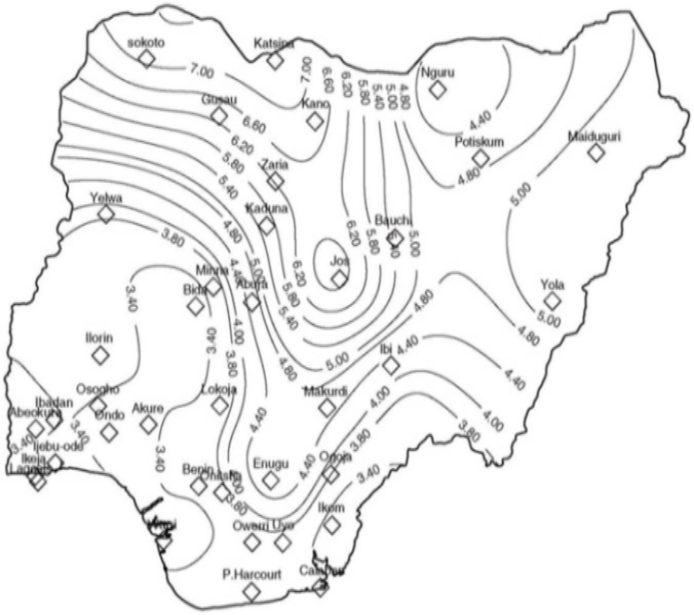

Figure 5: Nigerian wind map in m/s determined from 40 years measurements at 10m height, obtained from Nigerian metrological department, oshodi,lagos state, Nigeria(NIMET).

3.3. Case study

The building selected for this part of the case study was a 62m x 30.5m x 47.8m, 15- story typical office building (Figure 6). A 1.22m parapet was provided above the roof making total height of the building equal to 48.8m. The structural system contained reinforced concrete rigid frames in both directions as shown in Figure 6. The floor slabs were assumed to provide diaphragm action. The wall cladding panels are 120mm (width) × 2440mm(length)×4mm (thickness)

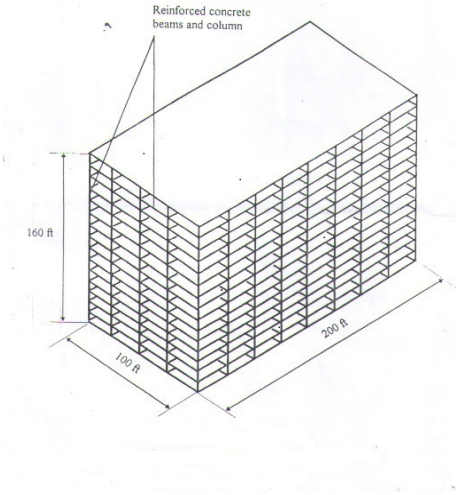

Figure 6: Structural system of the 48.8m tall building

4. Analytical procedure

From the wind speed map above it can be deduced that Lagos State (Ikeja) has a wind speed of 3.40m/s measured from a 10 meter height. Using the power law, wind speed at subsequent height can be calculated with results, as follows:

The wind profile power law relationship is:

$$\frac{u}{u_r} = (\frac{z}{z_r})^a \quad (1)$$

Where u is the wind speed (in meters per second) at height z (in meters), and u_r is the known wind speed at a reference height (z_r) . The exponent (a) is an empirically derived coefficient that varies dependent upon the stability of the atmosphere. For neutral stability conditions, is approximately 1/7, or 0.143.

In order to estimate the wind speed at a certain height (z), the relationship would be rearranged to:

$$u=u_r(\frac{z}{z_r})^a \quad (2)$$

The fundamental wind speed of the tall building 15th floor = 4.256m/s

Now, the Design wind speed can be calculated as

$$V_s= V_b\times S_a\times S_d\times S_s\times S_p \quad (3)$$

$$S_a=1+0.001\Delta_S \quad (4)$$

To determine the standard effective wind speed

$$V_e= V_s.S_b \quad (5)$$

Calculate the dynamic pressure

$$q_s=0.613V_e^2 \quad (6)$$

To calculate the external wind pressure on the windward wall of the tall building.

$$P_e=q_b.C_a.C_{pe} \quad (7)$$

Table 1: Fundamental wind speed as per wind speed power law equation

Storey	Wind Speed(m/s)
15th floor	4.256
14th floor	4.203
13th floor	4.159
12th floor	4.112
11th floor	4.061
10th floor	4.000
09th floor	3.946
08th floor	3.880
07th floor	3.807
06th floor	3.724
05th floor	3.628
04th floor	3.514
03th floor	3.372
02th floor	3.182
01st floor	2.883

According to table 5 of [6], C_{pe} for leeward wall and sidewall have negative values which accounts for the negative values of the wind pressures shown in table 3.

Where V_s is the site wind speed, V_b is the basic wind speed, V_e is standard effective wind speed, S_a is an altitude factor, Δ_S is the site altitude in meters, S_d is a direction factor, S_s is a seasonal factor, S_p is a probability factor, S_b is the roughness factor, q_s is the dynamic pressure, P_e stands for the wind pressure, C_a is the size effect factor for external pressure, C_{pe} is the external pressure coefficient for the building surface.

4.1. Finite element modeling

The static analysis of the response of the aluminum wall cladding panels to wind was carried out using LISA FINITE ELEMENT SOFTWARE.

It was done firstly, by modeling the typical aluminum cladding panel with standard size of 120mm (width) × (2440mm) lenght×4mm (thickness) fixed at each ends.

Table 2: Mechanical material properties of Aluminum wall cladding panel

Young modulus	72Gpa
Poisson ratio	0.33
Density	5.5kg/m^3
Ultimate tensile strength	110 to 180mpa
Yield strength	120mpa
Shear modulus	26Gpa
Shear strength	110mpa

The Figure above is a finite element model of a typical Alloy EN AW-3103(Al Mn1) aluminum wall cladding panel of standard size of 1200mm (width) $\times 2440mm(length) \times 4mm(thickness)$.

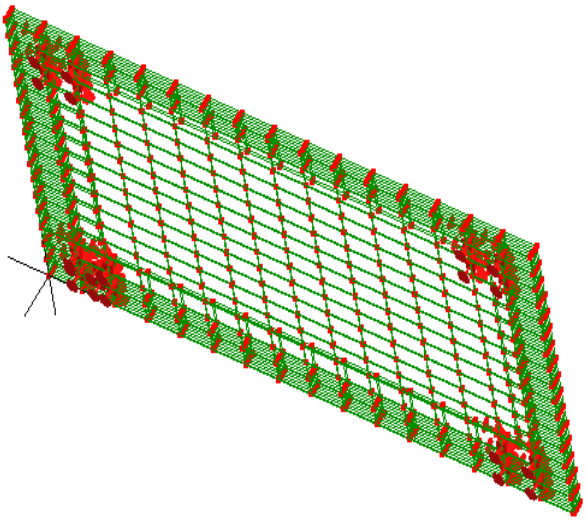

Figure 7A: Analytical model of the aluminum wall cladding panel showing nodes.

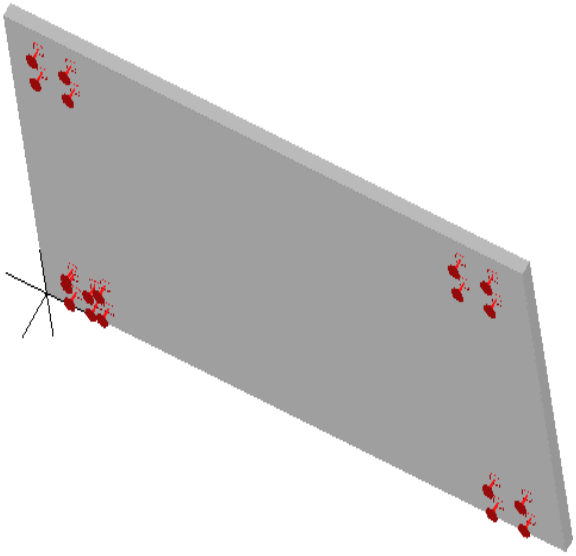

Figure 7B: Analytical model of the aluminum wall cladding showing element surface

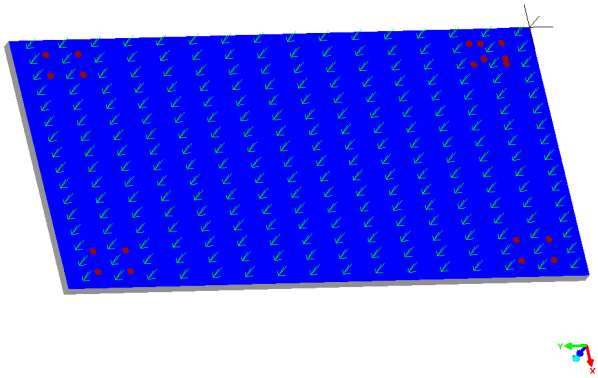

Figure 8: Analytical model of the aluminum wall cladding subjected to varying design wind pressure.

These aluminum cladding panels are fixed at the ends and subjected to wind loads calculated as per BS6399-2:1997 at different floors.

5. Result

Table 3: Design of wind pressure on the aluminum cladding panels of the tall building

Floor	H_r(m)	Pe wind-ward (Pa)	Pe lee-Ward (Pa)	Pe sidewall Zone A(Pa)	Pe sidewall Zone B(Pa)
15th floor	48.77	47.702	-28.060	-72.956	-44.896
14th floor	44.1	45.297	-26.645	-69.277	-42.632
13th floor	40.95	43.622	-25.660	-66.716	-41.056
12th floor	37.80	42.267	-24.863	-64.649	-39.784
11th floor	34.65	40.707	-23.945	-62.257	-38.312
10th floor	31.5	38.989	-22.935	-59.631	-36.696
9th floor	28.35	37.068	-21.960	-57.096	-35.136
8th floor	25.2	34.644	-20.795	-54.067	-33.272
7th floor	22.05	32.155	-19.655	-51.103	-31.448
6th floor	18.9	29.331	-18.355	-47.723	-29.368
5th floor	15.75	26.009	-16.845	-43.797	-26.952
4th floor	12.6	22.121	-15.110	-39.286	-24.176
3rd floor	9.45	17.423	-13.100	-34.055	-20.957
2nd floor	6.30	12.438	-10.365	-26.954	-16.587
1st floor	3.150	8.2740	-6.895	-17.927	-11.032

5.1. Case 1 for cladding panels located at the windward wall of the 15th floor subjected to positive wind pressure of 47.702

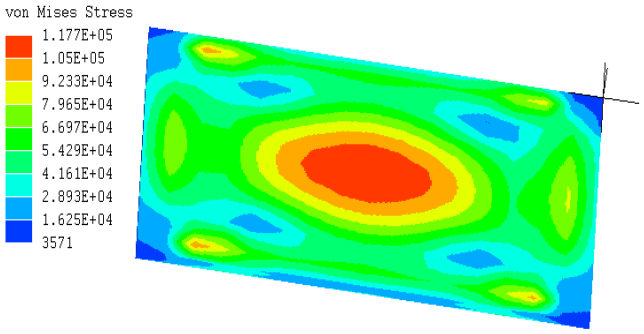

Figure 9: Von mises stress on the cladding panel

Von mises stresses of the cladding for characteristic wind pressure of 47.702N/M^2 was shown in figure 20. The largest stress occurs at the centre of the panel, and its value was 0.117Mpa. According to [8], the minimum to maximum yield tensile stress of 3013 Aluminum sheet is 120mpa. From the result shown in figure 14, the maximum von mises stress was 0.117mpa which is smaller than 120mpa.

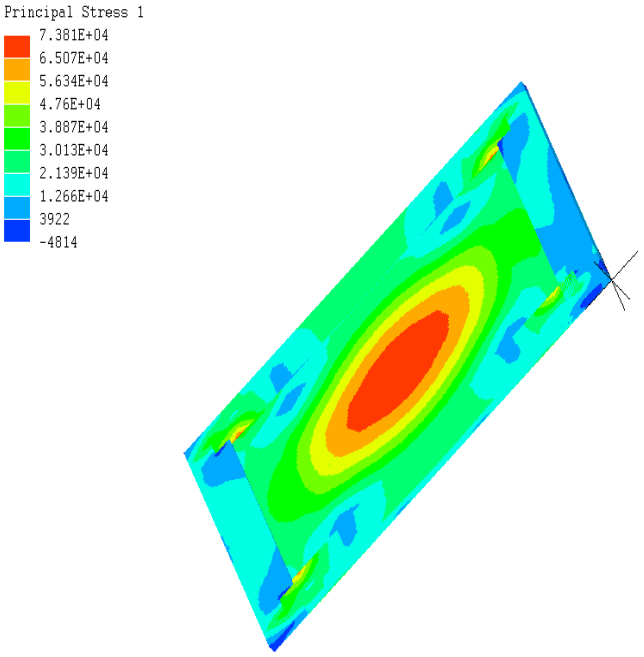

Figure 10: Principal stress 1 of the cladding panel.

According to maximum principle stress theory, failure will occur when the maximum principal stress in a system reaches the values of the maximum strength at elastic limit in simple tension test. From the image above, it can be deduced that the maximum normal stress that occurred at the major principal plane was located at the centre of the panel with value of 0.6348MPa. In [8], the ultimate tensile strength of 3103 aluminum is between 110 to 180Mpa. 0.6348MPa is less than 110MPa.

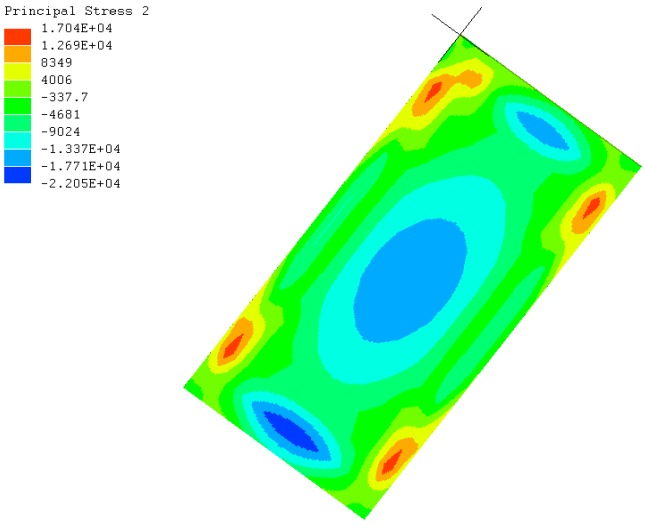

Figure 11: Principal stress 2 of the cladding panel.

The maximum normal stress that occurs at the principal plane 2 is located at the region where the fasteners are attached with maximum principal stress of 0.01704MPa. This principal stress was lower than the ultimate tensile stress of the cladding panel.

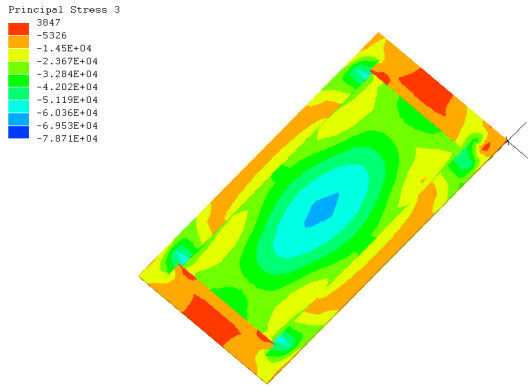

Figure 12: Principal stress 3 of the cladding panel.

The major principal stress 3 on the cladding panel is shown on the diagram above with maximum value of 0.003847Mpa.

5.2. Case 2 for cladding panels located at the 15th floor of the leeward wall while being subjected to a design wind pressure of -28.060N/M²

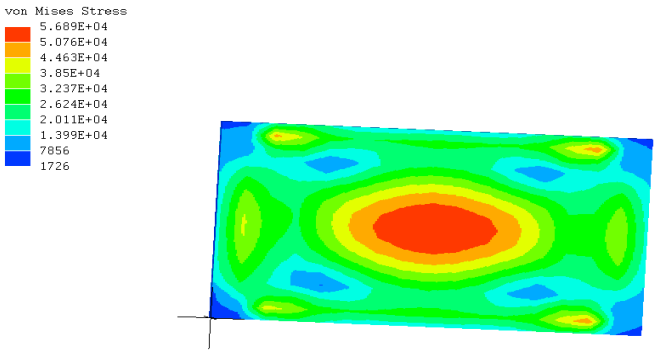

Figure 13: Von mises stress of the panel.

The largest stress was recorded at the centroid of the panel with a value of 0.05689MPa knowing that the panel was supported at the ends. This stress is less than the yield stress of 120mpa.

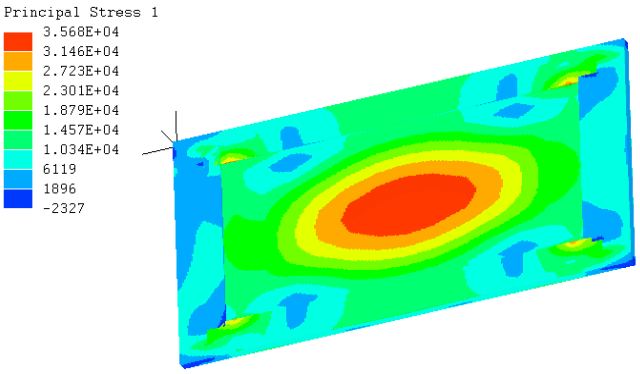

Figure 14: Principal stress 1 of the cladding panel.

From the principal stress contour diagram in Figure 14, the maximum normal stress acting on the major principal plane of the panel occurred at the center of the panel with a value of 0.03568MPa. This value was smaller than 110mpa.

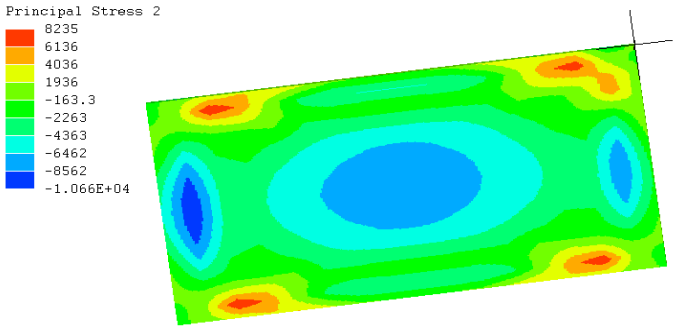

Figure 15: Principal stress 2 of the cladding panel.

According to [8], the stress limit for 3013Aluminium sheet is 110mpa. From the result shown in figure 15, Maximum principal stress=0.008235MPa, which was smaller than 110mpa.

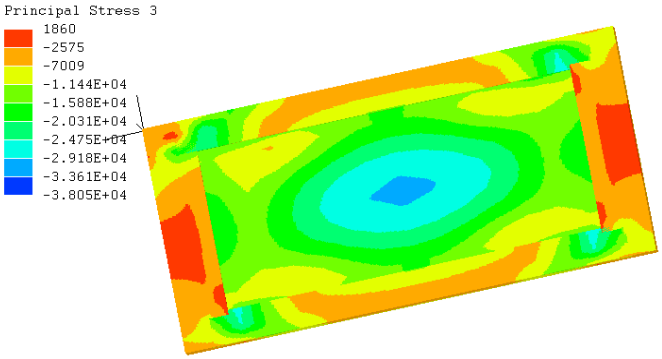

Figure 16: Principal stress 3 of the cladding panel.

From figure 16, the major principal stress =0.001860Mpa which was smaller than 110mpa.

5.3. Case 3 for cladding panels located at the zone B side wall of the 15th floor subjected to suction wind pressure of -44.896Pa.

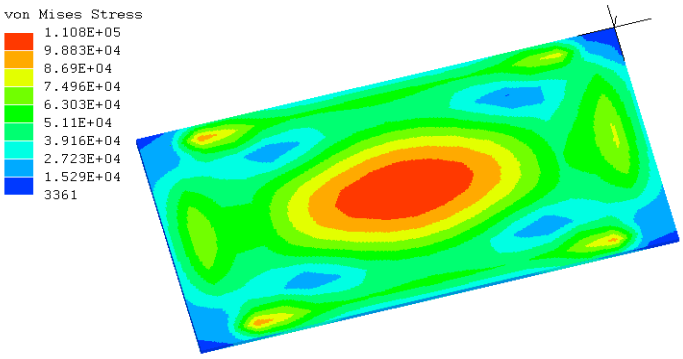

Figure 17: Von mises stress of the cladding panel

From the contour diagram in figure 17, the maximum von mises stress was located at the centre of the panel. Also because the panel was supported at the 4 sides, the wall cladding was deformed inwards from the centroids when normal pressure applied on the panel. The value of this maximum von mises stress was 0.1108MPa which was smaller than 120Mpa.

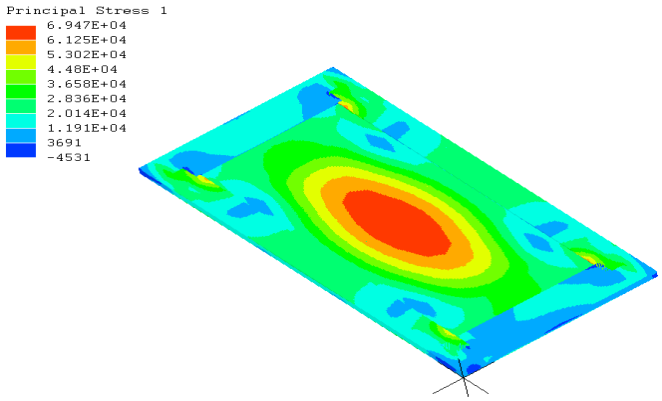

Figure 18: Principal stress 1of the cladding panel

Major Principal Stress=0.06947MPa which was lower than 110MPa.

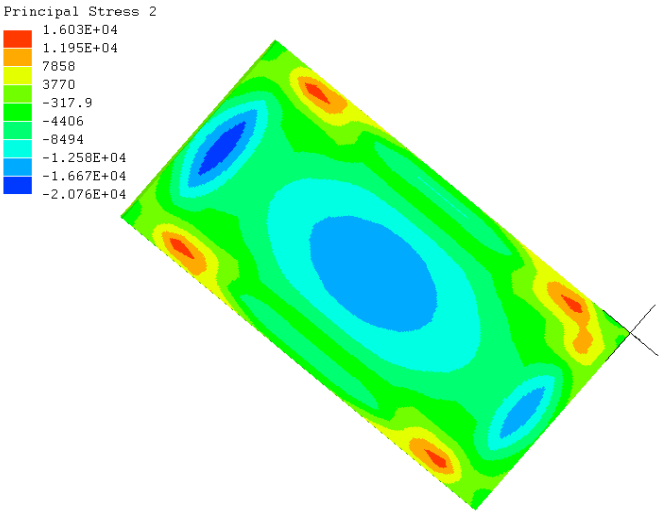

Figure 19: Principal stress 2 of the cladding panel

Major Principal stress 2=0.01603 MPa which was also lower than 110MPa.

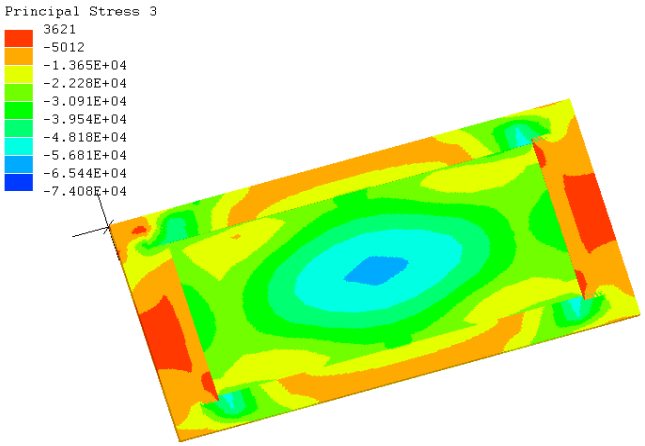

Figure 20: Principal stress 3 of the cladding panel.

Major Principal Stress=0.003621MPa which was lower than 110MPa.

5.4. *Case 4 for cladding panels located at the zone B side wall of the 15th floor subjected to suction wind pressure of -72.956Pa.*

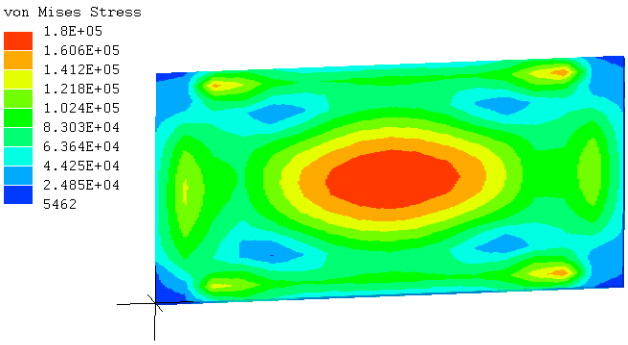

Figure 21: Von mises stresses of the cladding panel.

From the contour diagram in Figure 21, the maximum von mises stress was located at the centre of the panel. Also because the panel was supported at the 4 sides, the wall cladding was deformed inwards from the centroids when normal pressure applied on the panel. The value of this maximum von mises stress was 0.1800MPa which is smaller than 120MPa.

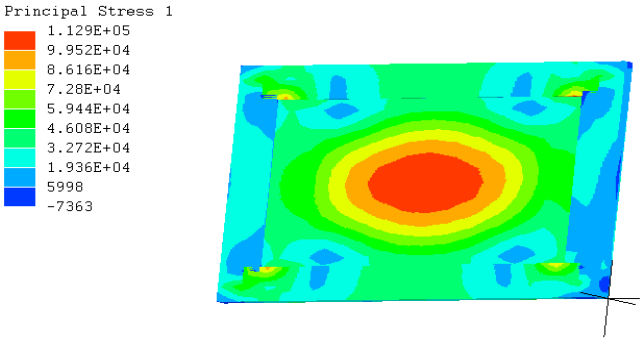

Major Principal Stress= 0.1129 MPa which was lower than 110MPa.

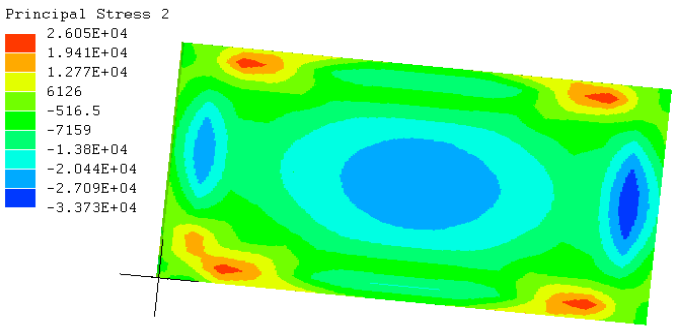

Figure 23: Principal stress 2 of the cladding panel

Major Principal Stress=0.2605 MPa which was lower than 110mpa.

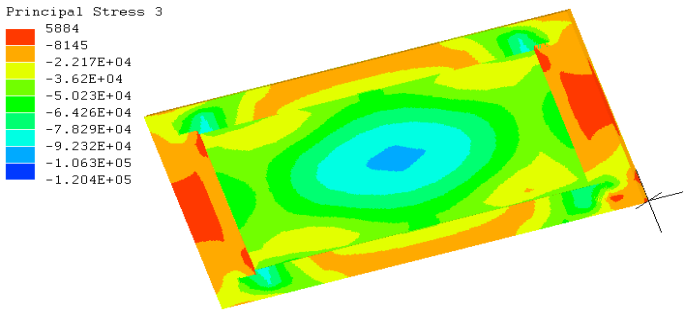

Figure 24: Principal stress 3 of the cladding panel

Major Principal Stress=0.005884 MPa which was lower than 110MPa.

6. Discussion and Conclusion

Based on the results, the writer believes that the high wind speeds were not responsible for the failure of Aluminum wall cladding panels in ikeja Lagos state in Nigeria; instead, the failures lies on one or more of the reasons explained below.

I. Poor workmanship and inadherence to installation details: The writer believes that poor workmanship and inadherence to application and installation details in the part of the cladding installer can seriously result in the incessant failure of cladding panels in the region being considered. These may include:

- **A.** Incorrect fixing of the panel to the supporting framework
- **B.** Insufficient allowance for panel movement
- **C.** End grain and onsite cuts not being sealed

II. Dark colored finish: The use of light colored paint is highly recommended for cladding. Research has clearly demonstrated that light colored paint provides much better service life for both the panel and paint used externally. Dark colored surface (especially on the north or west facing walls) heat up significantly more than light colored surface and this in turn will cause the panel to shrink and movement may lead to splitting.

As a rule of thumb, the light reflective value (LRV) of the paint should be greater than 30% or a total solar reflective value (TSR) greater than 29%. This will ensure your paint color is not too dark [9]. Heat reflective paints should be used where possible.

III. Use of lower quality aluminum cladding panels: The use of lower quality aluminum cladding panels can result to failure of cladding panels when subjected to minimal wind loads. It is recommended that the installer check the basic feature of the cladding panel before purchasing it. A durable cladding panel should have the following features.

Alloy Used- AA3103

Feature of the cladding panel before purchasing it. A durable cladding panel should have the following features.

Alloy Used- AA3103

Panel Thickness- 4mm (reference thickness)

Weight- 5.5kg/m^2

Tensile Strenght-40N/MM^2

Coating- PVDF Based fluorocarbon coating

Warranty- 10 years

7. Recommendation

Claddings are a critical and important architectural feature of a building and represent a significant portion of the overall cost of a building construction [10]. Given the ever growing complexity and variety of modern building envelopes, the evaluation of their performance, in terms of structural integrity and durability as well as comfort requirements, in the pre-construction and construction phase is essential in order to avoid undesirable and costly problems during the service life of the building.

On this premise, the researcher recommends that the following tests should be carried out before cladding installation.

- pre-construction mock ups
- Curtain wall air infiltration test
- Structural performance test

8. Areas for further study

There are still some areas in which detail study is required. One of which is:

I. Analyses of the responses of Aluminum wall cladding panels to vortex shedding in high rise building.

II. Analysis of the responses of the entire Aluminum wall cladding system to wind loading in High-rise buildings

References

[1] Roshko, “Perspectives on bluff body aerodynamics”. Journal of wind Engineering and Industrial Aerodynamics, 49, 79-100(1993)
[2] K. Bernard, “prediction of wind loads on Tall building” PhD thesis. University of western ontini, (1993).
[3] K. Suresh, wind tunnel testing for design of building façade,WFM team,2016
[4] P. Mendis, T. Ngo, N. Haritos, A. Hri, B. Samali, J. Chueng, “wind loading on tall building” journal of structural Engineering 2(2)2007,41-54(2007)
[5] Z. Ftihah, “Case Study Of Cladding” http://www.prezi.com(2014)
[6] BS 6399-2:1997. Loading for Buildings-part 2: “code of practice for wind loads”.BSI
[7] Aerospace,Mechanical&Mechatronic Engg “Separation Of Flow”. University of Sydney, (2005)
[8] BS EN 485-2:2007 “Aluminum and aluminum alloys”. Sheet, strip and plate. Mechanical properties.BSI
[9] Design pine, “Cladding Installation, design pine group,2013
[10] Team WFM, “Façade Testing Procedure,WFM team,2015

ASTES

Advances in Science, Technology and Engineering Systems Journal Vol. 2, No. 4, 173-179 (2017)

www.astesj.com

ASTESJ

ISSN: 2415-6698

Mathematical Model Based on Newton's Laws and in First Thermodynamic Law of a Gas Turbine

Ottmar Rafael Uriza Gosebruch*,1, Carlos Alexander Nuñez Martin[1], Eloy Edmundo Rodríguez Vázquez[1], Eduardo Campos Mercado[2]

[1]*Cidesi, Control Department, 76125, Mexico.*

[2]*Cinvestav, Control Department 07360, Mexico.*

ARTICLE INFO

Article history:
Received: 18 July, 2017
Accepted: 11 August, 2017
Online: 05 September, 2017

Keywords:
Control volume
Isentropic
Adiabatic
Isobaric
Isothermal

ABSTRACT

The present article explains the modeling of a Gas Turbine system; the mathematical modeling is based on fluid mechanics applying the principal energy laws such as Euler's Law, Newton's second Law and the first thermodynamic law to obtain the equations for mass, momentum and energy conservation; expressed as the continuity equation, the Navier-Stokes equation and the energy conservation using Fourier's Law. The purpose of this article is to establish a precise mathematical model to be applied in control applications, for future works, within industry applications.

1. Introduction

Nowadays, turbines have become a very important engineering development with several applications in almost all markets not only the aviation industry but also from oil and fuel industry to daily commuting applications as mass transportation.

There are several types of turbines; however this article will be centered in gas turbines. A gas turbine operates within the principle the Joule - Brayton cycle where compressed air is mixed with fuel, and afterwards burned under constant pressure conditions [Weston, 1992]. A gas turbine energy plant is an internal combustion system that converts chemical energy released from the burned fuel into heat energy, which converts to mechanical and/or electrical energy at the output of the process [1].

A simple gas turbine power plant consists of three main components: a compressor, a combustor, & a gas turbine. The resulting high pressure gas is expanded through the turbine to perform work output often used to drive a shaft connected to a mechanical arrangement in order to produce the required form of energy (mechanical/electrical).

A gas turbine, commonly called, combustion turbine, consists of an upstream rotating compressor coupled to a downstream turbine with a combustion chamber in between. The increasing usage & applications of gas turbines drive the necessity to design more complex dynamic systems. For such enterprise, the necessity, to understand turbo machinery behavior & deep knowledge on how to control them, has grown exponentially [2].

1.1. Mathematical models of Gas Turbines.

Diving into mathematical models of gas turbines; one of the mostly used is the Rowen's model which is a simplified mathematical representation of four gas turbines covering a horsepower range from 26,000 HP to 108,000 HP. The model incorporates, both, the control and fuel system characteristics as well as those relative to the turbo machinery. This model is suitable for a wide range of ambient temperatures, and the influence of axial flow compressor variable inlet guide vanes is included in the models as appropriate to the actual machinery configuration. The Rowen's Model is one of the vastly used mathematical models in turbo machinery applications as it also incorporates control system logic [3].

Other example of mathematical models is led by the Department of Mechanical and Process Engineering in the ETH based in Zurich which has been working in smart controlled gas turbines to obtain fuel efficient-reliable operation [4].

A control-oriented model is necessary for the purpose of modeling and fault detection. An oriented model defines the input-output behavior of the micro gas turbine system with reasonable precision at low computational complexity. It is designed to include explicitly all relevant transient effects and is

*Ottmar Rafael Uriza Gosebruch, Cidesi, Control Department, 76125, Mexico
Email: urisk_1@hotmail.com

represented by a set of nonlinear ordinary differential equations, which are derived from physical first principles [5].

1.2. Operation of the Gas Turbine.

The basic operation of the gas turbine is similar to the steam power plant except that air is used instead of water. Fresh atmospheric air flows through a compressor that brings it to higher pressure. Energy is then added by spraying fuel into the air and igniting it so the combustion generates a high-temperature flow. This high-temperature with high-pressure gas enters a turbine, where it expands down to the exhaust pressure, producing a shaft work output in the process.

The turbine shaft work is used to drive the compressor and other devices such as an electric generator that may be coupled to the shaft. The energy that is not used for shaft work comes out in the exhaust gases, so these have either a high temperature or a high velocity. The purpose of the gas turbine determines the design so that the most desirable energy form is maximized. Gas turbines are used to power aircraft, trains, ships, electrical generators, or even tanks [6, 7].

In an ideal gas turbine, gases undergo three thermodynamic processes: an isentropic compression, an isobaric (constant pressure) combustion and an isentropic expansion. Together, these make up the Brayton cycle. That is shown below:

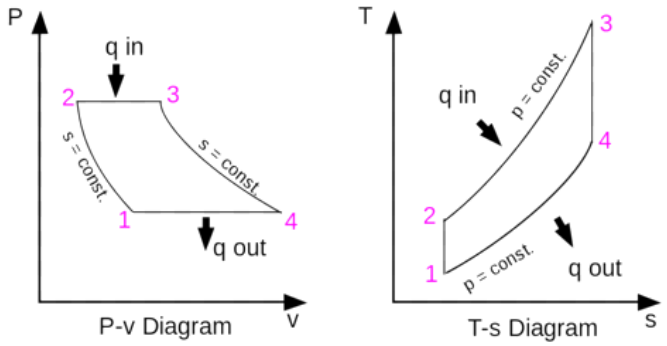

Figure 1. The Brayton cycle [8].

In a practical gas turbine, mechanical energy is irreversibly transformed into heat when gases are compressed (in either a centrifugal or axial compressor), due to internal friction and turbulence. Passage through the combustion chamber, where heat is added and the specific volume of the gases increases is accompanied by a slight loss in pressure. During expansion the stator and rotor blades of the turbine, irreversible energy transformation, once again, occurs.

2. Main variables in the system.

2.1. Main sections of a Gas Turbine.

The combustion (gas) turbines are being installed in many of today's natural-gas-fueled power plants and they are complex machines, but they basically involve three main sections.

Beginning with the air intake design; this drag air into the compressor which pressurizes it and feeds it to the combustion chamber inside the engine at speeds of hundreds of miles per hour. Then, the combustion system typically made up of a ring of fuel injectors that inject a steady stream of fuel into combustion chambers where it mixes with the air supplied. The mixture is then burned at temperatures of more than 2000 degrees F. The combustion produces a high temperature, high pressure gas stream that enters and expands through the turbine section.

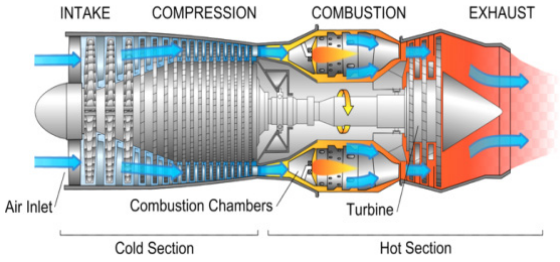

Figure 2. Main sections in a gas turbine [9].

The turbine, finally, is an intricate array of alternate stationary and rotating aerofoil-section blades. As hot combustion gas expands through the turbine, it spins the rotating blades. The rotating blades perform a dual function: they drive the compressor to draw more pressurized air into the combustion section, and they spin a generator to produce electricity [10].

2.2. Main variables from the thermodynamic process.

The main stage variables are defined based upon the independent states within the thermodynamic process during the Brayton cycle. As it is shown in the next image, there are 4 main states during the process in which all the variables involved have a different behaviour in specific points through the cycle but these does not mean that the variables will remain static throughout the entire process. Refer to figure 5 to understand the different stages within the cycle.

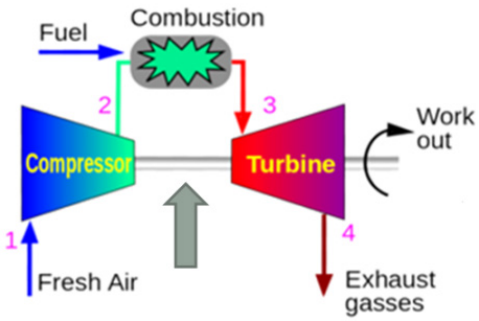

Figure 3. Main sections of a Gas Turbine [11].

The main variables in a thermodynamic process are: density, pressure, temperature and fluid velocity.

The Joule-Brayton Cycle illustrates the basic Gas Turbine stages during the transformation process of fluid energy into rotatory work; in each step there are specific conditions (isentropic compression & expansion as well as isobaric combustion and cooling) that must need to be taken into account during the mathematical modelling definition [11].

3. Mathematical model

The mathematical model was developed using the physics conservation laws such as the mass conservation, the linear momentum conservation, the ideal gases equation and the energy conservation.

3.1. Continuity equation.

The continuity equation is governed by the principle that mass is neither created nor destroyed, just transformed. This principle is one of the foundations in the study of fluids movement. This concept is defined by differential and integral equations. Consider an arbitrary control volume in a flux. By the principle of conservation of mass, the sum of the mass variation rate from inside the volume and the mass that travels to the surface of the volume is zero. Figure 6 describes the mass conservation through the control volume:

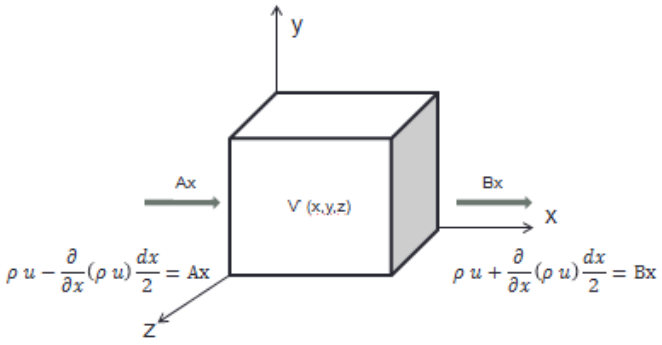

Figure 4. Control volume for the mass conservation.

Where *Ax* is the mass flux that enters the system and *Bx* is the mass flux that is leaving the system through the x axis. For the value of *Ax* and *Bx* it is necessary to use a Taylor series expansion and the equation is the next one:

$$(Ax - Bx) = \left(\rho u - \frac{\partial(\rho u)}{\partial x}\left[-\frac{\Delta x}{2}\right] - \left[\rho u - \frac{\partial(\rho u)}{\partial x}\left[\frac{\Delta x}{2}\right]\right]\right) \quad (1)$$

The change rate of the accumulated mass flow is given by the next equation:

$$\frac{\partial}{\partial t}(\rho dxdydz) = \frac{\partial \rho}{\partial t} dxdydz \quad (2)$$

Finally, by applying the same analysis in all axes and gathering the terms in equation (2), the result is the continuity equation:

$$\frac{\partial \rho}{\partial t} + \nabla(\rho, \vec{V}) = 0 \quad (3)$$

3.2. Cauchy equation.

The previous analysis using CV for the mass conservation is also used for the linear momentum conservation. It is necessary to apply the Newton's second law to a differential fluid element. This also holds that the sum of the forces on a particle is equal to the rate of change of its linear momentum.

The CV that holds the linear momentum conservation is the same that in the previous analyses:

Where *Ax* is the linear conservation that enters the system and *Bx* is the linear conservation that is leaving the system through the x axis. Also it is necessary to use a Taylor series expansion. The equation that holds this is the next one:

$$(Ax - Bx) = \left(\rho Vu - \frac{\partial(\rho Vu)}{\partial x}\left[-\frac{\Delta x}{2}\right] - \left[\rho Vu - \frac{\partial(\rho Vu)}{\partial x}\left[\frac{\Delta x}{2}\right]\right]\right) \quad (4)$$

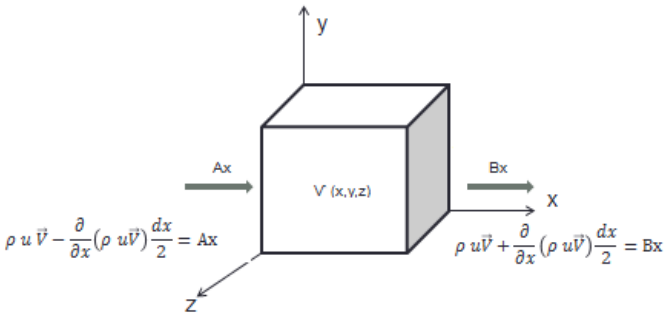

Figure 5. Control volume for the linear momentum conservation.

The change rate of the accumulated linear momentum is given by the next equation:

$$\frac{\partial}{\partial t}(\rho \vec{V})dxdydz = \left[\vec{V}\frac{\partial \rho}{\partial t} + \rho\frac{\partial \vec{V}}{\partial t}\right]dxdydz \quad (5)$$

By applying the same analysis as in the continuity equation and gathering the terms in equation (5), and equalling to the surface and body forces, the resulting is the Cauchy equation:

$$\frac{\partial \vec{V}}{\partial t} + \left[u\frac{\partial V}{\partial x} + v\frac{\partial V}{\partial y} + w\frac{\partial V}{\partial z}\right] = \frac{1}{\rho}F_B + \frac{1}{\rho}F_s \quad (6)$$

And finally for the right hand side of the equation (6), it holds that the body forces are just the gravity and the surface will be manage as an input, so [12,13,14]:

$$\frac{\partial \vec{V}}{\partial t} + \left[u\frac{\partial V}{\partial x} + v\frac{\partial V}{\partial y} + w\frac{\partial V}{\partial z}\right] = g + \frac{1}{\rho}F_s \quad (7)$$

3.3. Energy differential equation.

The first law of thermodynamics states the conservation of energy. Considering a system, that changes in the power expressed by the sum of the input energy as heat and work. The power system comprises the internal energy and kinetic energy. The next figure represents the control volume of the conservation of energy in the system:

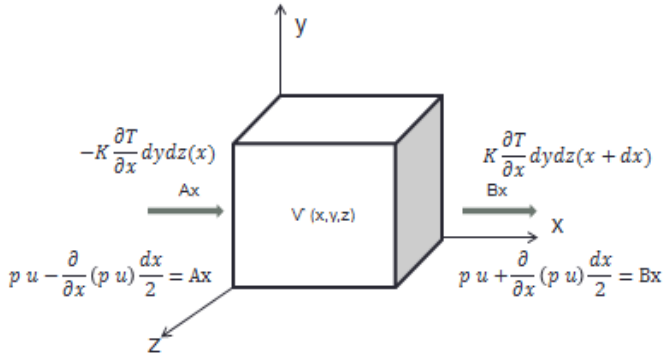

Figure 6. Control volume for the energy conservation.

Where Ax is the amount of heat and works that enters and Bx is the amount of heat and work that comes out analyzed only on the x-axis:

$$(Ax - Bx) = \left(Kdx\left[\frac{\partial T}{\partial x}[x+\Delta x] - \frac{\partial T}{\partial x}[x]\right] - \frac{\partial (pu)}{\partial x}\frac{dx}{2} - \frac{\partial (pu)}{\partial x}\frac{dx}{2}\right) \quad (8)$$

And analysing the relations in the three axes of the quantity of fluid that occupies in the element infinitesimal generates the equation.

$$\left(K\frac{\partial^2 T}{\partial x^2} + K\frac{\partial^2 T}{\partial y^2} + K\frac{\partial^2 T}{\partial z^2} - \frac{\partial (pu)}{\partial x} - \frac{\partial (pv)}{\partial y} - \frac{\partial (pw)}{\partial z}\right) dxdydz \quad (9)$$

Given the equation of the first law of thermodynamics, the material derivative of the energy of the system is expressed as follows:

$$\frac{D}{Dt}\left[\frac{\rho u^{\vec{2}} + \rho v^{\vec{2}} + \rho w^{\vec{2}}}{2} + \rho gz + \rho \tilde{u}\right] dxdydz \quad (10)$$

Equaling the equation (9) and (10) and substituting the consideration that the internal energy expressed by the next equation:

$$\tilde{u} = \int_{T_0}^{T} CpdT \quad (11)$$

The next equation is the equation that involves the temperature in the system and by adding some terms relate of the shear forces expressed everything in a vector form is the equation well known as the energy balanced equation [12,15,16]:

$$\rho Cp\left[\frac{\partial T}{\partial t} + \vec{V}\nabla T\right] + q = -K\nabla^2 T - p\nabla\vec{V} + \mu\varphi; \quad (12)$$

3.4. State differential equation of ideal gases.

The ideal gas law is the equation of state of a hypothetical ideal gas. It is a good approximation of the behavior of many gases under many conditions, although it has several limitations.

The next images represent the curve lines of the relationship between pressure (on the vertical, *y*-axis) and volume (on the horizontal, *x*-axis) for an ideal gas at different temperatures: lines that are farther away from the origin represent higher temperatures.

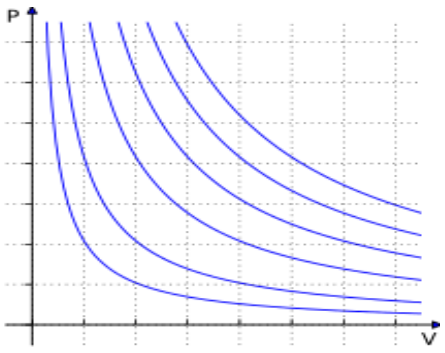

Figure 7. Graph of isotherms ideal gases [17].

The ideal gas law is often written as $PV = nRT$:

Where:

- P is the pressure of the gas,
- V is the volume of the gas,
- n is the amount of substance of gas (in moles),
- R is the ideal, or universal, gas constant, equal to the product of the Boltzmann constant and the Avogadro constant,
- T is the absolute temperature of the gas.

The state of an amount of gas is determined by its pressure, volume, and temperature. Therefore, an alternative form of the ideal gas law may be useful. The chemical amount (n) (in moles) is equal to the total mass of the gas (m) (in grams) divided by the molar mass (M) (in grams per mole):

$$n = \frac{m}{M} \quad (13)$$

By substituting the last equation in equation number (12):

$$PV = \frac{m}{M}RT \quad (14)$$

Subsequently introducing density $\rho = m/V$, we get:

$$P = \rho\frac{R}{M}T \quad (15)$$

Defining the specific gas constant $R_{\text{specific(r)}}$ as the ratio R/M [12, 17]:

$$P = \rho R_{specific} T \quad (16)$$

It is common, especially in engineering applications, to represent the specific gas constant by the symbol R. In such cases, the universal gas constant is usually given a different symbol such as R to distinguish it. As establish pressure, density and temperature as variables, it is possible to derivate in respect of time and it obtains the next equation:

$$\frac{\partial p}{\partial t} = RT\frac{\partial \rho}{\partial t} + R\rho\frac{\partial T}{\partial t} \quad (17)$$

The equation (17) is the last one in order to describe a gas turbine behaves by differential equation.

3.5. Mathematical modelling simplifications.

The next step is to express all derivate with respect of space in derivate with respect of time using the chain rule.

$$\frac{\partial \rho}{\partial t} = \frac{\partial \rho}{\partial n}V \quad (18)$$

And for the second order derivate the equation is as follow:

$$\frac{\partial^2 \vec{V}}{\partial n^2} = \frac{\frac{\partial}{\partial t}\left(\frac{\partial \vec{V}}{\partial n}\right)}{\frac{\partial n}{\partial t}} = \frac{\frac{\partial}{\partial t}\left(\frac{\frac{\partial \vec{V}}{\partial t}}{\frac{\partial n}{\partial t}}\right)}{\frac{\partial n}{\partial t}} = \frac{\frac{\partial^2 \vec{V}}{\partial t^2}\frac{\partial n}{\partial t} - \frac{\partial \vec{V}}{\partial t}\frac{\partial^2 n}{\partial t^2}}{\left(\frac{\partial n}{\partial t}\right)^3} \quad (19)$$

$$\frac{\partial^2 \vec{V}}{\partial n^2} = \frac{-\frac{\partial \vec{V}}{\partial t}\frac{\partial \vec{V}}{\partial t}}{\left(\vec{V}\right)^3} \quad (20)$$

Applying the equations (18) and (20) to equations of conservation of mass, momentum, pressure and energy:

$$\frac{\partial \rho}{\partial t} = -\frac{\rho}{2u}\frac{\partial u}{\partial t} \quad (21)$$

$$\frac{\partial u}{\partial t} = \frac{1}{2\rho}F_s \quad (22)$$

$$\frac{\partial T}{\partial t} = -\frac{K^2}{2(\rho Cp)^2 u^3}[T - T0]\frac{\partial u}{\partial t} - \frac{p}{\rho Cpu}\frac{\partial u}{\partial t} + \frac{2\mu}{\rho Cpu^2}\frac{\partial u}{\partial t}\frac{\partial u}{\partial t} \quad (23)$$

$$\frac{\partial p}{\partial t} = -RT\frac{\rho}{2u}\frac{\partial u}{\partial t} - \frac{RK^2}{2\rho Cp^2 u^3}[T - T0]\frac{\partial u}{\partial t} - \frac{Rp}{Cpu}\frac{\partial u}{\partial t} + \frac{2R\mu}{Cpu^2}\frac{\partial u}{\partial t}\frac{\partial u}{\partial t} \quad (24)$$

4. Simulations.

The simulations results are plotted in 3 different steps, the first part represents the compressor, in which the main variable to follow is density; also temperature and pressure are plotted. Then the second step is the combustor, here the main variable to follow is the temperature but also the variable of density is plotted, just remembering that the combustion is an isobaric process, in other words, the pressure doesn't suffer a significant change. Finally and control objective, the rotor; in here, it is necessary to keep a set point of velocity, because it is where all the work and main subsystems that the gas turbine will feed are connected. The next image is the Joule - Brayton cycle that represents the 3 main steps that just were described.

The first curve is the adiabatic compression; the second curve the isobaric combustion and finally the adiabatic expansion.

As explained during compression, the main variable that to be controlled is the density; Figure 11 represents the hatch that allows the amount of air to pass while opened at 90% of its capacity thus generating a density approximately of 50 Kg/m^3.

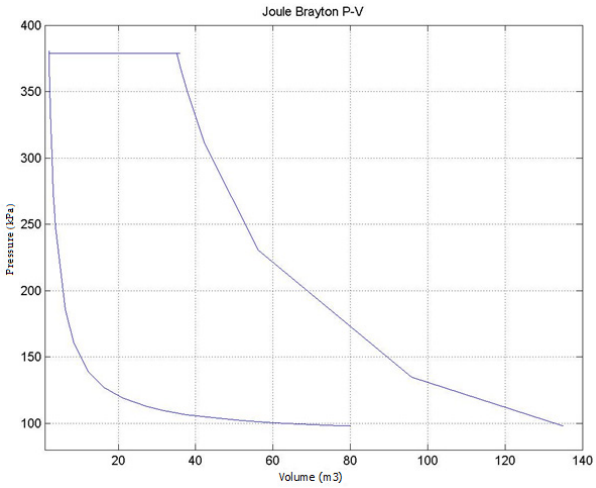

isotherms ideal gases.

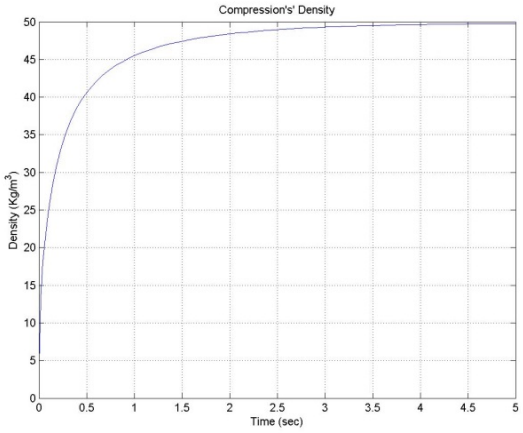

Also the pressures temperature were plotted as seen on figure 10.

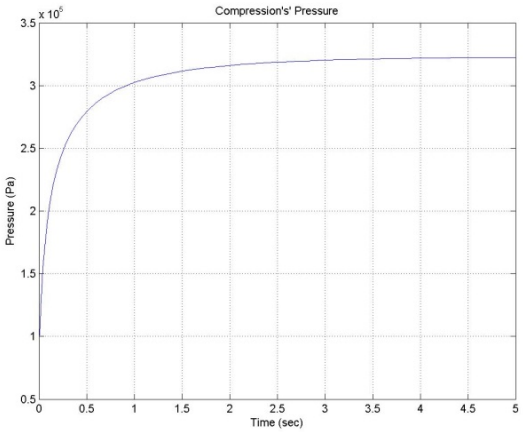

The hatch opened at *90%* of its capacity generating a pressure of *380 KPa* approximately. The systems needs a certain fluid velocity to start working, for that reason the hatch it is opened proportionally during the first *15* seconds until the fluid velocity reached a speed of *80 m/s*. Then the hatch is opened in one shot until *90%* of it capacity.

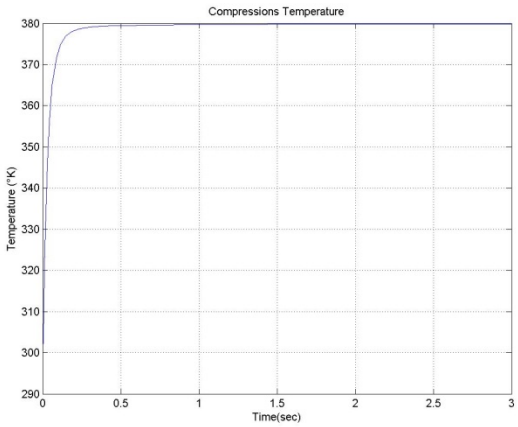

The temperature reached during compression was 380°K approximately.

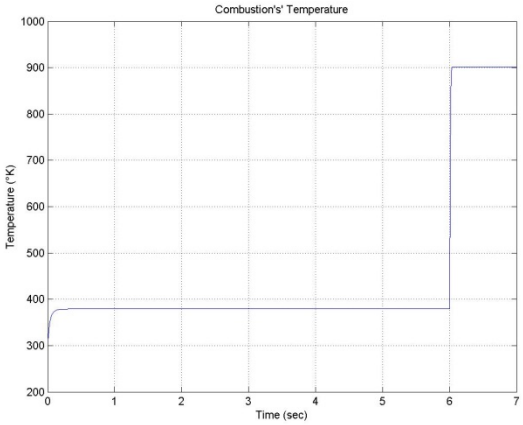

The highest temperature reached throughout all operating cycle was during combustion phase while opening the fuel hatch at *90%* of its capacity as the main variable during this stage is temperature as combustion is done ay isobaric conditions so while the pressure stayed the same, the final temperature reached was 900°K approximately.

The objective of a gas turbine control logic is to be able to vary the rotor speed as needed at the precise timing. The next image shows the rotor behaviour through the cycle;, it splits into two different phases; first during compression and finally during combustion.

The last figure shows the final rotor velocity was *650 rev / seconds* when the hatch of the air and fuel were opened at *90%.*

5. Future work

5.1. Algorithm control in the system.

Advanced controlled systems based in mathematical modeling can sustain the next development steps as it increases the deep knowledge of what is happening from a complete system vision criteria and guarantees the results that are required, as it gives complete control of the rotor's movement ,the speed that is required, the pressure inside the compressor and finally the temperature of the combustion chamber to work along with an inter-cooling system at the precise timing that is needed so the output of the cycle is within the expected range of efficiency and performance [18].

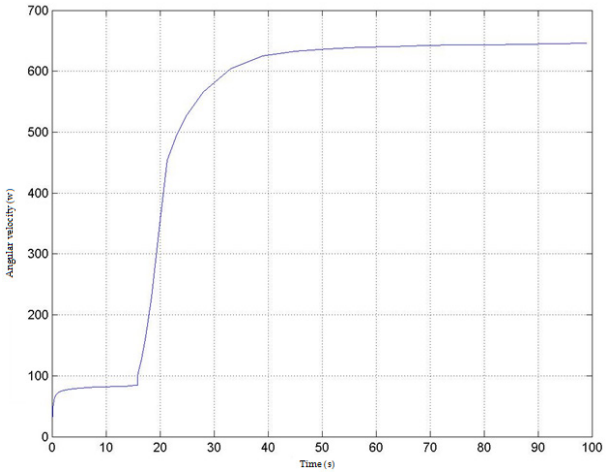

For the implementation of this idea, new combustor and blade designs will be required to allow appropriate heat exchange between cold and hot fluids, ensuring high integrity and risk mitigation of the structural components as well as health and safety conditions respectively. New manufacturing techniques for these complex geometries will be required that can enhance mass transfer during the internal cooling cycle [19].

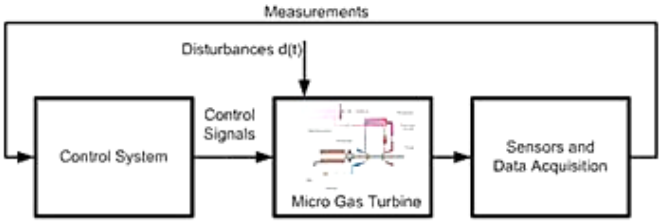

6. Conclusions

The complexity of the systems and the effective applications of gas turbines drive the need to develop highly complex mathematical models with a high accuracy in order to precisely control the turbine dynamics in order to exceed efficiency and performance balance. If correctly applied, it can be ensured that all the variables from the system cycle are going to be within the working limits conditions that the turbine would demands. The model developed is based in the three main systems particular to the turbine: compressor of the fluid, rotor shaft and combustion chamber.

Finally, advanced controlled systems based in mathematical modeling increase the reliability of what is happening in the complete system giving a holistic view and guarantee the results that are required with an optimal efficiency.

References

[1] Ekstrom, T. E. and Garrison, P. E., 1991, "Large Gas Turbines for Mechanical Drive Applications", GER-3701, GE Company, Schenectady, NY, August 1991.

[2] Rowen, W. I., 1983, "Simplified Mathematical Representations of Heavy Duty Gas Turbines", ASME Paper 83-GT-63 and ASME Journal of Engineering for Power, October 1983, Page 865.

[3] Simpson, C. Aalburg, M. B. Schmitz, R. Pannekeet, V. Michelassi, F. Larisch, "Application of Flow Control in a Novel Sector Test Rig", Journal of Turbomachinery, 136(4), 041002 , Sep 26, 2013, TURBO-12-1249.

[4] M. Sunar, S. S. Rao, "Recent Advances in Sensing and Control of Flexible Structures Via Piezoelectric Materials Technology", Applied Mechanics Reviews, Vol.52.

[5] J. Bordeneuve-Guibe, C. Vaucoret, "Robust multivariable predictive control: an application to an industrial test stand", Control Systems IEEE, Vol. 21, Issue 2.

[6] Ozsoy, A. Duyar, ; R. Kazan, R. Kilic, "Power turbine speed control of the GE T700 engine using the zero steady-state self-tuning regulator", Intelligent Engineering Systems, 1997. INES '97. Proceedings, 1997 IEEE International Conference on.

[7] Zohuri, Brahman. "Gas Turbine Working Principles", Combined Cycle Driven Efficiency for Next Generation Nuclear Power Plants, 2015.

[8] Online: https://en.wikipedia.org/wiki/Brayton_cycle.

[9] Online: http://cset.mnsu.edu/engagethermo/componentsgasturbine.html

[10] Chacartegui, R., Sánchez, D., Muñoz, A., & Sánchez, T. (2011). Real time simulation of medium size gas turbines. *Energy Conversion and Management.* Modeling of off-design multistage turbine pressures by Stodola's ellipse. *Energy Incorporated, PEPSI user's group meeting.* Richmond, Virginia: Bechtel Power Corporation.

[11] https://wn.com/gasturbine/wikipedia

[12] Dixon, S. L. (1998). *Fluid Mechanics and Thermodynamics of Turbomachinery, Fourth edition.* Woburn, MA, USA: Butterworth-Heinemann.

[13] P. Chiesa, E. Macchi, "A Thermodynamic Analysis of Different Options to Break 60% Electric Efficiency in Combined Cycle Power Plants", ASME Turbo Expo 2002: Power for Land, Sea, and Air, Vol. 1: Turbo Expo 2002, ASME, GT2002-30663, pp. 987- 1002.

[14] Online: https://www.boundless.com/physics/textbooks/boundless-physics-textbook/temperature-and-kinetic-theory-12/ideal-gas-law-104.

[15] B. Facchini, L. Innocenti, E. Carnevale, "Evaluation and Comparison of Different Blade Cooling Solutions to Improve Cooling Efficiency and Gas Turbine Performances", ASME Turbo Expo 2001: Power for Land, Sea, and Air, Vol.3: Heat Transfer; Electric Power; Industrial and Cogeneration, 2001-GT- 0571, pp. V003T02A025.

[16] G. Richards, Williams M., and Casleton K. "Novel cycles: oxy-combustion turbine cycle systems", Combined cycle systems for near-zero emission power generation, 2012.

[17] Online: https://en.wikipedia.org/wiki/Idealgas.

[18] L. Chi-Huang, T. Ching-Chih, "Adaptive Predictive Control With Recurrent Neural Network for Industrial Processes: An Application to Temperature Control of a Variable-Frequency Oil-Cooling Machine, Industrial Electronics IEEE Transactions on, 04/2008; 55(3):1366 - 1375.

[19] García Nieto, Paulino, Esperanza García-Gonzalo, Antonio Bernardo Sánchez, and Marta Menéndez Fernández. "A New Predictive Model Based on the ABC Optimized Multivariate Adaptive Regression Splines [24] Approach for Predicting the Remaining Useful Life in Aircraft Engines", Energies, 2016.

[20] D.W. Clarke, "Application of generalized predictive control to industrial processes", Control Systems Magazine IEEE, Vol. 8, Issue.

ASTES

Advances in Science, Technology and Engineering Systems Journal
Vol. 2, No. 4, 180-188 (2017)
www.astesj.com

ASTES Journal
ISSN: 2415-6698

Kalman filter Observer for SoC prediction of Lithium cells

Faten Ayadi*, Mongi Lahiani,Nabil Derbel

University of Sfax, Electrical Engineer, Sfax Engineering School, 3000, Tunisia

ARTICLEINFO

Article history:
Received: 09 August, 2017
Accepted: 29 August, 2017
Online: 23 September, 2017

Keywords:
Li Ion batteries
SoC estimation
non linear fractional model
Impedance Spectroscopy
Fractional Order Calculus
Kalman Filter

ABSTRACT

The SoC estimation of Li Ion batteries presents a difficult task for almost applications in order to ensure their higher energy density and their safety. Hence, there have been several methods to optimize the state of charge of the Lithium cells such as observer strategies which have been considered in this work. Kalman filter observer has been selected for state optimization. It has been considered to stabilize the error estimation of battery state thanks to its gain through the following non linear fractional model. The fractional model has been deduced from analysis of Impedance Spectroscopy data and it has been well defined by Fractional Order Calculus. The performance of Kalman filter has been evaluated through the simulation results. They have improved the efficiency and limits of Kalman theory to determine the actual internal state of cells.

1 Introduction

The optimization of state of charge for Lithium batteries presents the main effect on their internal states in several applications [1]. It leads to maintain the activities of applications in permanent way.
The state of charge (SoC) is meaningful parameter that is defined in case of discharge of the battery [2]. It presents the shift time of battery capacity through the following expression [3]:

$$SoC(t) = 100 * \int_{t_0}^{t} \frac{I_b(\tau)}{Q} d\tau \qquad (1)$$

with I_b: the current of the battery, Q: the nominal capacity of the battery and τ: Time of energy storage.
The SoC optimization is a difficult issue for different domains due to its dependency on some factors such as battery capacitance, temperature and internal resistance and also the problem of defining it easily [4]. Therefore, many researches have focused on the possibility to estimate the SoC of the Lithium cells through different techniques [5,6,7] such as Direct measurements [8], Book keeping estimation [9], SoC estimation based on models [10].
The most considered technique for SoC optimization is Observer techniques [11,12].
This method is based on puting the following battery model to the observer and update the optimization of the states by calculating their erros which are the set of difference data between the measured and desired state [13]. The model based methods presents among the diagnosis technology and especially fault diagnosis. They are designed for extraction parameter from impedance spectra and optimization the state of the electrochemical systems. It has been described in figure 1.

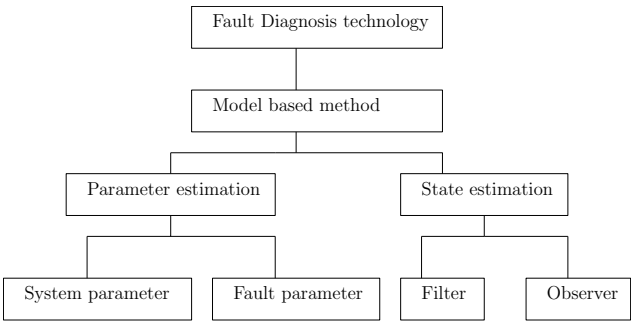

Figure 1: Properties of the model based method for fault mechanism and diagnosis

The equivalent battery models permit to make conformity between electrochemical impedance and electric impedance measured by Electrochemical Impedance Spectroscopy (EIS). They own medium mathematical complexity and they ensure good precision in field of optimization.
In general, there is a fractional order aspect of equivalent models for electrochemical systems [14, 15,

*Faten Ayadi, Sfax-Tunisia, fatenayedi65@gmail.com

https://dx.doi.org/10.25046/aj020424

16]. Moreover, the fractional models have been well defined by Fractional Order Calculus (FOC) [17]. Thanks to fractional order calculus, the several dynamic and chemical phenomena of Lithium battery have been perfectly characterized. Many researches have improved the efficiency of fractional order in electrochemical fields [18] for example: according to Ichise et al., fractional calculus has been used for analysis of electrode processes through an analog simulation of non-integer order transfer functions [19].
SoC estimation based on model for electrochemical systems requires an accurate fractional descriptor observers [20]. In addition, there are some researchers who have focused on this direction like Yan Ma and Xiuwen Zhou have considered the fractional kalman filter observer to optimize the state of charge of Li Ion batteries [21] and also Fei Zhang et al. has proposed the extended Kalman filter to ensure the stability of error estimation of SoC [22].

The objective of this research work consists on presenting new strategy for SoC estimation based on observer for Lithium cells.
Kalman Filter has been proposed to determine correctly the state of Lithium batteries. It has been more explained and described in section 4.2 . Indeed, Kalman filter has been theoritically checked and there has been improved that it is efficient method in field of prediction of State of Charge (SoC).

2 Dynamic model for Lithium battery

The Lithium battery considered in this paper is Lithium cell LiFePO4, model (SP-LFP40AHA). This part has focused on defining the dynamic phenomenon of selected Lithium battery by analysis of Impedance spectroscopy data in each frequency range.

In fact, Impedance Spectroscopy (IS) has been the most considered strategy in field of estimation of state of charge of electrochemical systems thanks to its benefits. It is direct measurement that precises a suitable circuit related to characteristics of impedance curve at the level of frequency domain [23]. The measurement of impedance has been carried out in frequency range from 0.01 Hz to 1 KHz. Futhermore, impedance spectroscopy may identify the parameters of the several components for the equivalent circuit such as diffusion coefficient and kinectic variables [24, 25, 26]. The Lithium battery is closely non linear system and there is difficulty to identify its chemical coefficients and variables. So, thanks to impedance spectroscopy, there is possibility to determine the several chemical internal reactions which then can be defined by equivalent model.

Figure 2 shows the measured impedance diagram in 50% of SoC for wide range of frequencies. The several dynamic phenomena of Lithium battery have been appeared in each frequency range.:

- Parasitic effects and electro migration in the electrolyte and connectors at high frequency part ($300Hz < f <$ 355 Hz).
- Charge transfer inside the battery and exactly in the interface between the electrode and electrolyte at mid frequency part ($354.8Hz < f <$ 3.54 Hz). It is identified by $Z_{C_{PE}}$ which is defined in next section.
- Diffusion phenomena of ionic species in low frequency ($f <$ 3.54 Hz). It is identified by Z_w which is defined in next section.

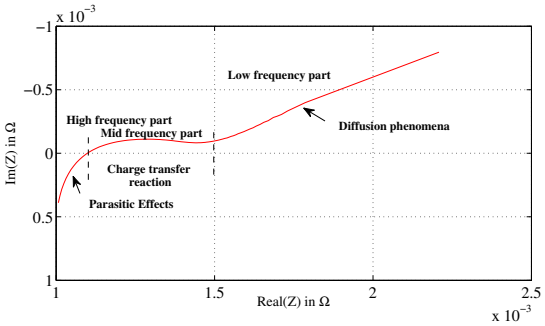

Figure 2: Measured Impedance spectra for LiFePO4, model (SP-LFP40AHA) in 50% of SoC

Hence, the topology of equivalent model for chosen Lithium cell has been presented in figure 3. Dynamic battery has been modelled by set of electrical components.

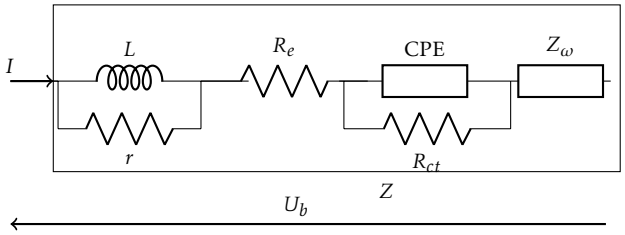

Figure 3: Topology of equivalent model for Lithium cell LiFePO4, model (SP-LFP40AHA)

With I: the Current of LiFePO4 battery, Z: Impedance of LiFePO4 battery , U_b: the terminal of LiFePO4 battery.

The several effects over frequency range have been illustrated as:

- High frequency effects have been defined by inductance L in parallel with his interne resistance r .
- Electrode effects have been presented by ohmic resistance R_e.
- Mid frequency effects have been defined by parallel circuit constant phase element CPE- transfer resistance R_{ct} .

- Low frequency effects have been identified by Warburg impedance Z_ω

Li Ion cells is non linear electrochemical system and there is difficulty to deduce its appropriate properties. So, in order to obtain the optimal values of battery model variables which have been shown in figure 3, there has been used the genetic algorithm (G.A) as fitting procedure.
The optimal values of model have been determined through mechanism of evolutionnary algorithm which is described in figure 4.

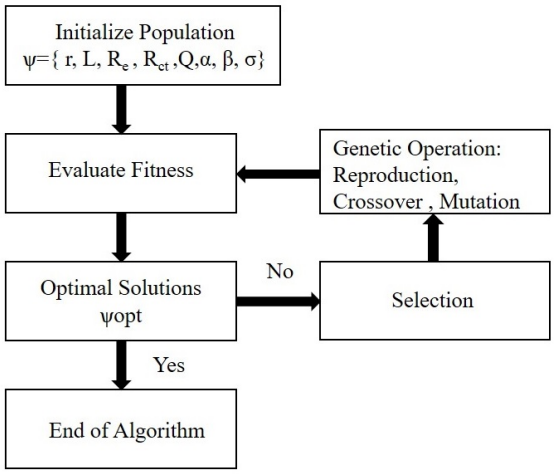

Figure 4: Mechanism of Genetic Algorithm

The dynamic model for LiFePo4 has been described in figure 5 and its structure is based on hysterisis phenomenon which is presented by open circuit voltage OCV and from impedance spectroscopy analysis.

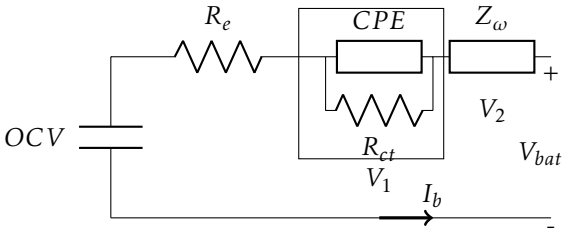

Figure 5: Dynamic Model topology for Lithium cell

The inductance element L hasn't been involved in the battery model because the Lithium ion cells are less applied in high frequencies range.

2.1 Parameters of battery model

There are different parameters related to equivalent model such as:

- The double layer capacitance CPE models the imperfect capacitors that appear in experimental spectra. It is defined by its fractionnary impedance through the following expression [24]:

$$Z_{C_{PE}} = \frac{1}{Q(j\omega)^{\beta}} \tag{2}$$

with : $Q > 0$, $0 \leq \beta \leq 1$

- Z_ω is fractionnary impedance for warburg element. Its main characteristic consists in its straight line with constant slope at the level of Nyquist diagram in low frequency values. The impedance Z_ω can be written as in semi infinite diffusion [25]:

$$Z_\omega(j\omega) = \frac{\alpha\sqrt{2}}{(j\omega)^{\sigma}} \tag{3}$$

with : α : the diffusion parameter and $\sigma = 0.5$.

- OCV: Open Circuit Voltage and it is considered as crucial variable that expresses many criterias of performance for the battery. The open circuit voltage is used for SoC estimation [26].

A non linear relationship between OCV and SoC has been illustrated in the litterature. In fact, some recent works have proposed some approximations for this relationship in order to facilitate its calculation.

Among these approximations, the relation between OCV and SoC is considered as [27]:

$$\begin{aligned} OCV(z) = K_0 + K_1\frac{1}{e^{\lambda_1(z-\Theta_1)}} + K_2\frac{1}{e^{\lambda_2(z-\Theta_2)}} \\ + K_3\frac{1}{e^{\lambda_3(z-1)}} + K_4\frac{1}{e^{\lambda_4 z}} + K_5 z \end{aligned} \tag{4}$$

with z is the state of charge of the battery, $K_{i=1...5}$ are the linear parameters and $\lambda_{i=1..4}$, $\Theta_{i=1..2}$ are the non linear parameters.

Table 1 presents each values of the following coefficient K_i in order to fit the measured curve OCV. This set of values has been determined by Genetic Algorithm and it has been considered as optimal results by the process.

Table 1: Values of coefficient K_i

K_0	K_1	K_2	K_3	K_4	K_5
2.67	2.7	2.85	2.93	3.1	3.4

This approximation relationship has been plotted in figure 6.

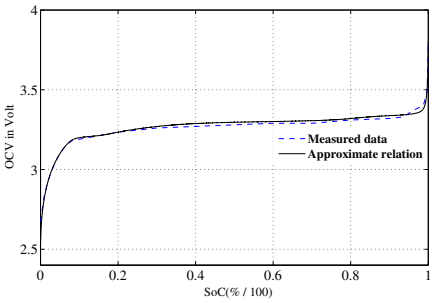

Figure 6: Diagram of OCV over SoC range

The objectif of battery model is defining the several electrochemical reactions which own the fractional criterias. They are expressed by Fractional Order Calculus (FOC).

3 Non Linear fractional model

The dynamic model which has been shown in figure 5 is considered as non linear fractional model. The fractional order calculus is a tool for defining the fractional models. The fractional aspect in general presents among the characteristics of electrochemical systems. They have been developed and evaluated through fractional order calculus in some researches [28]. Besides, by recent works, the FOC has been defined as mathematic operator using differentiation with integration to non integer order ${}_aD_t^q$ where q: the order, a and t : the bounds of the operation. It is applied in science fields like bioengeneering [29], electronics [30, 31] and control theory [32]. In addition, almost engineer applications have focused on FOC startegies which are based generally on describing the aspects of dynamic systems by condensed expressions and considering non local characteristics such as thermal diffusion phenomenon [33] and botanical electrical impedances [34].

Fractional order calculus is denoted as [35]:

$$ {}_aD_t^q = \begin{cases} \frac{d^q}{dt^q} & if \quad q > 0 \\ 1 & if \quad q = 1 \\ \int_0^t d\tau^{-q} & if \quad q < 0 \end{cases} \tag{5} $$

with ${}_aD_t^q$ is initialized q^{th} order differintegration.

At the level of this work, FOC is fractional differentiation and according to Grunwald-Leitnikov, it can be written as [36, 37]:

$$ D^q x(t) = \lim_{\triangle T \to 0} \frac{1}{T^q} \sum_{i=0}^{\frac{t}{\triangle T}} (-1)^i \binom{q}{i} x(t - i\triangle T) \tag{6} $$

with $\triangle T$: the sampling time, q: the order Grunwald-Leitnikov fractional derivative of $x(t)$.

$$ \binom{q}{i} = \frac{\Gamma(q+1)}{\Gamma(i+1)\Gamma(q-i+1)} \tag{7} $$

where $\Gamma(q)$ is the generalization of factorial function [38]. It is expressed as:

$$ \Gamma(q) = \int_0^\infty y^{q-1} e^{-y} dy \tag{8} $$

In this part, the constant phase element CPE and the warburg element Z_ω have been considered as fractional elements [39].

In fact, the fractional element is defined as [39]:

$$ Z_{fractional} = \frac{1}{Y(jw)^\delta} \tag{9} $$

where: Y is the coefficient; $-1 \leq \delta \leq 1$: the arbitrary order of the fractional element which can be an integer or a fraction. It is characterized by straight vertical line in Nyquist plot for low frequency domain.

For CPE, its fractional model is given as [20]:

$$ Z_{C_{pe}} = \frac{1}{C_1(j\omega)^\beta} \tag{10} $$

For Z_ω, its fractional model is given as [20]:

$$ Z_{warburg} = \frac{1}{W(j\omega)^\sigma} \tag{11} $$

where: W is the coefficient and β, σ are the arbitrary orders of the fractional elements: $0 \leq \sigma \leq 1$ and $0 \leq \beta \leq 1$.

In this work, the double layer capacitance CPE has treated as perfect capacitor C_1 and then its following equation is given as:

$$ Z_{C_{pe}} = \frac{1}{C_1(j\omega)} \tag{12} $$

Among the effectiveness of FOC for electrochemical systems, it defines precisely the chemical phenomenon of Lithium batteries. It has been improved in figure 7 for measured impedance spectrum in 50% of SoC of Lithium batteries.

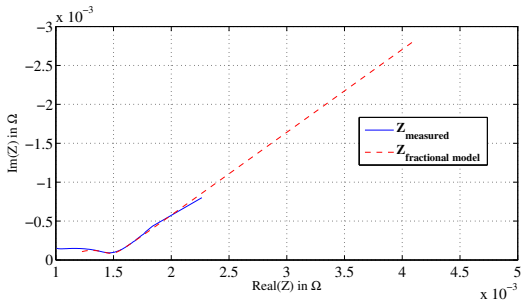

Figure 7: Measured Impedance vs Impedance model presented by FOC

The dynamic behavior of the battery which has been presented by FOC has been given as:

- For diffusion phenomenon: It has been defined by $Z_{warburg}$.
- For charge transfer phenomenon: It has been defined by capacitor C_1 in parallels with resistor R.

According to figure 7, the diffusion phenomena has been obvisiouly well defined by FOC. The straight line of $Z_{warburg}$ is similar to line with constant slope of Z_{ω}.

Thanks to FOC, the equivalent circuit of the battery can be deduced and hence the chemical reactions can be identified through many parameters related to different circuit components.

3.1 Fractional battery model

The equations of the fractional model from figure 4 has been expressed as in the following form:

$$D^{\beta} V_1 = \frac{I_b}{C_1} - \frac{V_1}{R_{ct} C_1} \tag{13}$$

where V_1: the voltage at the level of $R_{ct}C_1$ parallel circuit.

$$D^{\sigma} V_2 = \frac{I_b}{W} \tag{14}$$

where V_2: the voltage at the level of warburg element.

$$D^{1} z = \frac{I_b}{C_n} \tag{15}$$

where C_n : the capacity of the Li Ion battery .

The voltage of Lithium battery V_{bat} is the sum of open voltage and voltages at the level of the electrode resistance R_e , the RC parallel circuit and warburg element.

It can be written as:

$$V_{bat} = OCV(z) + R_e I_b + V_1 + V_2 \tag{16}$$

3.2 State space for Lithium battery model

Through the different equations (13)-(16), the state space for Lithium cell can be given as:

$$\begin{aligned} D^{q} x(t) &= Ax(t) + Bu(t) \\ y &= Cx(t) + Du(t) \end{aligned} \tag{17}$$

where: $x(t)$: the vector of the following states;

$$x = \begin{pmatrix} z & V_1 & V_2 \end{pmatrix}^T$$

A, B, C, D: The matrices with:

$$A = \begin{pmatrix} 0 & 0 & 0 \\ \frac{-1}{R_{ct}C_1} & 0 & 0 \\ 0 & 0 & 0 \end{pmatrix}, \; B = \begin{pmatrix} \frac{1}{C_n} \\ \frac{1}{C_1} \\ \frac{1}{W} \end{pmatrix}, \; C = \begin{pmatrix} K_5 & 1 & 1 \end{pmatrix},$$

$D = R_e$, $q = \begin{pmatrix} 1 & \beta & \sigma \end{pmatrix}$, $y = V_{bat}$: Output of state space.

$u(t)$: Input of state space with $u = I_b$ (The current of the battery).

4 SoC optimization using fractional observer

The observers have been considered as an alternating tool for some problems which exist in practice like: the high cost of installation of the devices and long time of measurements of the missing variables. The main role of observers is determining the unknown variables related to the state vector and reducing the use of expensive sensors [40]. This area has been attractive by many researches [41,42] and many kind of observer strategies have been evolved especially for several classes of chemical systems to estimate their internal states [43, 44]. In addition, the use of observers becomes a challenge in front of many requirements of accuracy and suitable estimation performances. For the recent workers, there was set of types of observers which have been cited in electrochemical fields [45].

The design of observers owns an appropriate methodolgy. It has been firstly based on linear forms with presence of noises [46]. Then, there has been a developpement at the level of their forms due to the complexity of the systems. Hence, non linear observers have been widely considered [47]. They have based on mathematical models and they are evaluated by observer's equations. Indeed, the gain and the optimization of error dynamics are the main properties for model based observers.

Figure 8 presents the procedure of observer design.

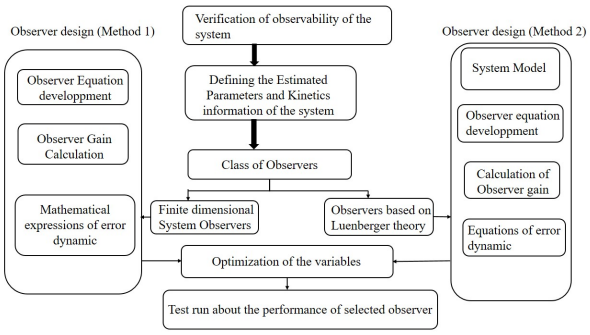

Figure 8: Procedure of observer design

Moreover, the observer is among elements of control theory and it estimates in real time the state of given system from measurements of its inputs and outputs. Its principle has been described in figure 9.

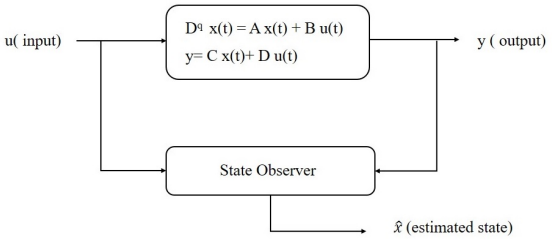

Figure 9: Reconstruction of state space involving the state observer

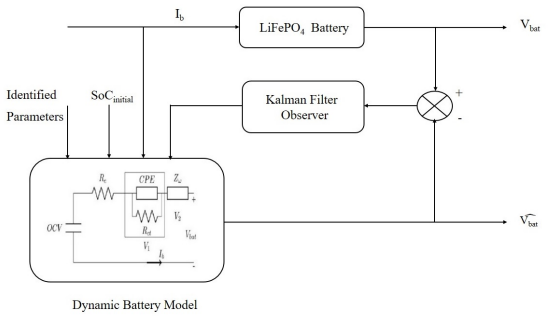

Figure 10: Battery model based on SoC estimation through the feedback method Kalman filter observer

4.1 Observability of non linear fractional model

The observability is criteria for control approach. It is based on defining the behavior of internal states of the system by knowledge of its measured outputs [48]. The observability condition is main part for observer designing and especially it depends on the formulation of the given system where there is choice of type of observability. Futhermore, there is two kinds of observability conditions: observability matrix and observability Gramian. In this work, the observability Gramian [49] has been considered to detect the aspect of given system.

The state space (17) for non linear fractional system has been firstly evaluated for its observability and then it has been put into the state observer. It is effectively observable at time t if there is $\theta < t$ where the state at time t can be finded by knowing its outputs over the interval $[\theta\ t]$ [50].

The observability Gramian matrix W(θ, t) is defined as [51]:

$$W(\theta,t) = \int_{\theta}^{t} E_{\gamma}(A^T(t-\tau)^{\gamma})C^T C E_{\gamma}(A(t-\tau)^{\gamma})d\tau \quad (18)$$

where E_{γ} is Mittag-Leffler function which is expressed as follows [52]:

$$E_{\gamma}(x) = \sum_{k=0}^{\infty} \frac{A^k}{\Gamma(1+\gamma k)} \quad (19)$$

with $\gamma > 0$

According to the battery model, the observability matrix W(θ, t) is expressed as:

$$\mathrm{W}(\theta,\ t)=\begin{pmatrix} 6.100 & 5.8965 & 5.9512 \\ 5.75 & 5.9512 & 6.110 \\ 5.9512 & 6.12 & 7.110 \end{pmatrix}$$

This matrix is invertible and thus its inverse $W^{-1}(\theta,t)$ exists.

Futhermore, the non linear fractional model is observable and there is possibility to estimate its internal state from knowledge of its external outputs. Hence, this model would be synthetized through an observer by following method which has been shown in figure 10 :

As described in figure 10, SoC estimation is ensured by feedback method Kalman Filter which has been explained in next sections.

4.2 Fractional Kalman filter (FKF) observer design

Model battery variables are not available directly to measure them. Hence, they need an accurate optimal tool to determine them which is fractional kalman filter (FKF).

Kalman filter is an estimator algorithm based on the informations about the given model and input, output signals in presence of noise [53]. Its operation can be done in real time using the actual input measurements and the previously calculated states. Kalman filter doesn't need past informations during its run where it tries to find the minimum mean square error optimization states of the actual Lithium states.

The objectif of fractional Kalman filter is getting an appropriate optimization results by reducing the cost function in the following steps [54]:

$$arg\min_{x}[(\hat{x_k}-x)\hat{P_k}^{-1}(\hat{x_k}-x)^T + (y_k+Cx)R_k{}^{-1}(y_k+Cx)^T] \quad (20)$$

with $\hat{x_k}$ is the state vector prediction and $\hat{P_k}$ is the error covariance of state estimation.

The FKF is recursive algorithm and the form of state space (17) has been expressed as discrete form from stochastic theory:

$$\begin{aligned} For\ k \geq 1 : x(k+1) &= [\triangle^q TA + diag(q)I]x(k) \\ &- \sum_{i=2}^{N+1}(-1)^i \binom{q}{i} x(k+1-i) + \triangle^q TBu(k) \\ &+ w(k) \\ y(k) &= Cx(k) + Du(k) + v(k) \end{aligned} \quad (21)$$

with $\binom{q}{i} = \gamma_i = C_q{}^i = \frac{q!}{i!(q-i)!}$

$w(k)$: Stochastic disturbance; $v(k)$: Output noise.

Fractional Kalman filter owns two main steps where the state estimate is evaluated through several equations presented in figure 11:

- Prediction step: permits to compute and update the state estimate and error covariance through mathematical relation between the priori estimation $(\hat{x_k}^-, \hat{P_k}^-)$ and the posterior estimation $(\hat{x_k}^+, \hat{P_k}^+)$.

- Correction step: updates the measurements of state estimate and error covariance.

The formulation of FKF designed for state optimization [20, 55, 56] has been summarized in figure 11:

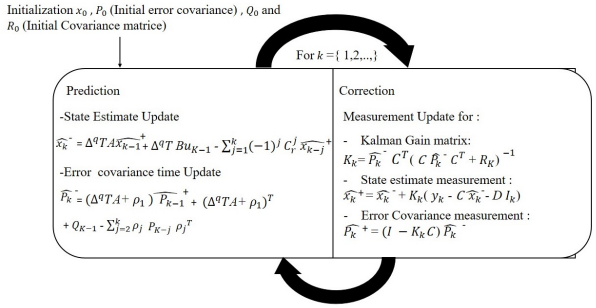

Figure 11: Fractional Kalman Filter for state optimization

5 Simulation results and analysis

The performance of fractional Kalman filter has been evaluated for SoC estimation of the battery by Logiciel Matlab Simulink and the run time of simulation is about 1000 secondes.

The several simulation results have been performed through set of conditions:

- The fractional model of Lithium battery is observable
- The initial SoC value has been considered as 0.88.
- Presence of stochastic disturbance and output noise $w(k)$ and $v(k)$.

5.1 Analysis of error for SoC estimation

Figure 12 shows the SoC optimization by proposed observer Kalman filter and its error estimation.

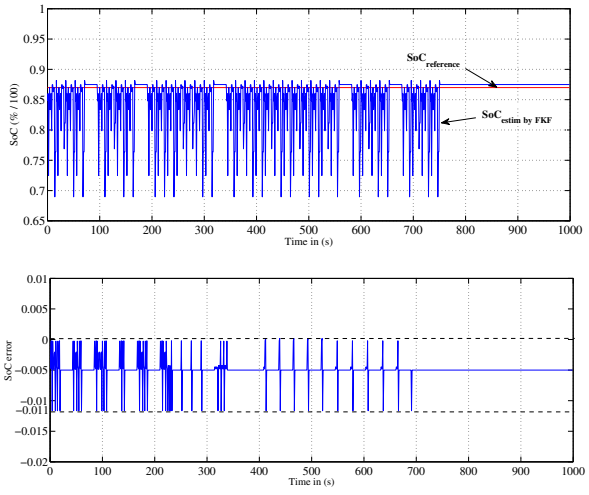

Figure 12: SOC estimation and its error by Fractional Kalman filter observer

According to figure 11, Kalman filter well optimize the SoC of the battery . It provides good state of charge estimation error thanks to its accuracy for parameter estimation. Hence, the stability between the model and the observer has been perfectly ensured by Kalman filter.

Besides, the dispersion of error of SoC estimation for fractional kalman filter is not totally concentrated at zero error. It is more dispersed and tends to -0.005 due to the problem of choice of initial parameters. This explains that the optimal values of SoC are not exactly equal to real SoC values.

5.2 Analysis of rise time for SoC estimation

The rise time of proposed estimation method may explain about its speed responses and improves its dynamic performance.

The desired state of charge by Kalman filter observer converges slowly to real state. Thus, it isn't considered for real time applications.

Kalman filter owns limits for convergence of the variables. It takes a long period to reach to real values of the following state of charge (SoC) due to its slowly operations. According to figure 11, the estimated state has been firstly fluctuated in narrow range and then it has been converged to real SoC. Hence, Kalman Filter observer is very slow method and it owns long rise time for SoC estimation.

So, Kalman filter doesn't operate perfectly in term of estimation rise time and it yields to get bad quality of state optimization for electrochemical systems.
It has high time consumption due to the long time of calculation of the covariances (P_k, Q_k, R_k).

5.3 Discussion

The dynamic performance of Kalman filter has been synthetized through simulation results. Kalman filter observer can estimate the state of charge of Lithium battery despite of its limits.

In fact, it has high time consumption which depends on two reasons:

- The first reason: It is related to calculation of feedback coefficients. For Kalman filter, its gain is determined through the equations related to prediction and correction steps.
- The second reason: There is long time of calculation of complex covariances which makeS a big time consumption for Kalman filter.

Besides, Kalman filter has high estimation rise time due to its slow responses for SoC prediction of Lithium batteries.

In order to get better the state estimation for batteries, the extension form of these proposed techniques can be considered.

6 Conclusion and Outlook

A new strategy for SoC estimation has been described in this work which has based on state observer. Its main principle is using the equivalent fractional model of Lithium battery and determining from it the state of charge through observer methods. The battery model has been defined from impedance spectroscopy analysis. Each chemical property of the battery has been modelled through set of electrical components. The selected technique for state optimization is Fractional Kalman filter. Its operation for SoC estimation has been explained. The performance of this method and several aspects of SoC estimation (Rise time and time consumption) have been evaluated theoretically and there has been improved that Kalman filter observer has benefits and limits to predict the internal state of the batteries due to its long rise time and time consumption.

Future goals of this work is overcoming the limits of Kalman filter by considering its extension form or a robust and fast observer tool for SoC estimation which is Proportional Integral Observer (PIO). It well defines through its operations the actual states of electrochemical systems.

7 References

1. Garcia-Valle, Rodrigo, Peas Lopes, Joo A, Electric Vehicle Integration into Modern Power Networks, Springer-Verlag New York 2013.
2. P. Christopher Manning, Eli White, Douglas Nelson, Abhijit Khare, Development of a Plug-In Hybrid Electric Vehicle Control Strategy Employing Software-In-the-Loop Techniques, SAE 2013 World Congress & Exhibition.
3. Akram Eddahech, Olivier Briat, Jean-Michel Vinassa, Real-time SOC and SOH estimation for EV Li-ion cell using online parameters identification, Energy Conversion Congress and Exposition (ECCE), 2012 IEEE.
4. John Chiasson, Baskar Vairamohan, Estimating the State of Charge of a Battery, IEEE transactions on control systems technology, vol. 13, no.3, May 2005.
5. Languang Lu, Xuebing Han, Jianqiu Li, Jianfeng Hua, Minggao Ouyang, A review on the key issues for lithium-ion battery management in electric vehicles, Journal of Power Sources: Volume 226, 15 March 2013, Pages 272 - 288.
6. Nalin A. Chaturvedi, Reinhardt Klein, Jake Christensen, Jasim Ahmed, Aleksandar Kojic, Algorithms for Advanced Battery-Management Systems, IEEE Control Systems (Volume: 30, Issue: 3, June 2010).
7. Nicolas Watrin, Benjamin Blunier, A.Miraoui, Review of adaptive systems for lithium batteries State-of-Charge and State-of-Health estimation, Transportation Electrification Conference and Expo (ITEC), 2012 IEEE.
8. Li Ran, Wu Junfeng, Wang Haiying, Li Gechen, Prediction of state of charge of Lithium-ion rechargeable battery with electrochemical impedance spectroscopy theory, Industrial Electronics and Applications (ICIEA), 2010, the 5th IEEE Conference on.
9. Valer Pop , Henk Jan Bergveld, Dmitry Danilov, Paul P. L. Regtien, Peter H. L. Notten, Battery Management Systems: Accurate State-of-Charge Indication for Battery-Powered Applications, Springer Netherlands, Volume: 9, 2008.
10. Dorin V. Cadar, Dorin M. Petreu, Cristian A. Orian, A method of determining a lithium-ion battery's state of charge , Design and Technology of Electronics Packages, (SIITME) 2009. 15th International Symposium for.
11. Kong Soon Ng, Chin-Sien Moo, Yi-Ping Chen, Yao-Ching Hsieh, Enhanced coulomb counting method for estimating state-of-charge and state-of-health of lithium-ion batteries, Applied Energy, Volume 86, Issue 9, September 2009, Pages 1506 -1511.
12. Xiaosong Hu, Fengchun Sun, Fuzzy Clustering Based Multimodel Support Vector Regression State of Charge Estimator for Lithium-ion Battery of Electric Vehicle, Intelligent Human-Machine Systems and Cybernetics, 2009. IHMSC '09. International Conference on.
13. Valer Pop , Henk Jan Bergveld, Dmitry Danilov, Paul P. L. Regtien, Peter H. L. Notten, Battery Management Systems: State of-the-Art of battery, State-of-Charge determination , Springer Netherlands, pp 11-45, 2008.
14. Fengchun Sun, Xiaosong Hu, Yuan Zou, Siguang Li, Adaptive unscented Kalman filtering for state of charge estimation of a lithium-ion battery for electric vehicles , Energy, Volume 36, Issue 5, May 2011, Pages 3531 - 3540.
15. Jonghoon Kim, B. H. Cho, State-of-Charge Estimation and State-of-Health Prediction of a Li-Ion Degraded Battery Based on an EKF Combined With a Per-Unit System , IEEE transactions on vehicular technology, vol. 60, no. 9, November 2011.
16. Bharath Pattipati, Chaitanya Sankavaram , Krishna Pattipati, System Identification and Estimation Framework for Pivotal Automotive Battery Management System Characteristics , IEEE Transactions on Systems, Man, and Cybernetics, Part C (Applications and Reviews), Volume: 41, Issue: 6, Nov. 2011.
17. Yulan Zhao, Haitao Yun, Shude Liu, Huirong Jiao, Chengzhen Wang, State-of-charge Estimation for Lithium-ion Batteries Using a Multi-state Closed-loop Observer, Journal of Power Electronics, Vol. 14, No. 5, pp.1038-1046, September 2014 .
18. Lokenath Debnath, Recent applications of fractional calculus to science and engineering, Journal of Power Electronics, Vol. 14, No. 5, pp.1038-1046, September 2014.

19. M.Ichise, Y.Nagayanagi and T.Kojima , An analog simulation of non-integer order transfer functions for analysis of electrode processes, Journal of Electroanalytical Chemistry and Interfacial Electrochemistry Volume 33, Issue 2, December 1971, Pages 253 -265.
20. Jun Xu, Chunting Chris Mi, Binggang Cao, Junyi Cao, A new method to estimate the state of charge of lithium-ion batteries based on the battery impedance model, Journal of Power Sources, Volume 233, 1 July 2013, Pages 277 - 284.
21. Yan Ma, Xiuwen Zhou, Bingsi Li and Hong Chen, Fractional modeling and SOC estimation of lithium-ion battery , IEEE/CAA Journal of Automatica Sinica, Volume: 3, Issue: 3, July 10 2016.
22. Fei Zhang, Guangjun Liu and Lijin Fang, A battery State of Charge estimation method with extended Kalman filter , Advanced Intelligent Mechatronics, AIM 2008. IEEE/ASME International Conference on.
23. S.M.M. Alavi, C.R. Birkl, D.A. Howey, Time-domain fitting of battery electrochemical impedance models , Journal of Power Sources, Volume 288, 15 August 2015, Pages 345352.
24. Baojin Wang, Zhiyuan Liu, Shengbo Eben Li, Huei Peng, State-of-Charge Estimation for Lithium-Ion Batteries Based on a Nonlinear Fractional Model, IEEE Transactions on Control Systems Technology, May 2016.
25. Dominik Sierociuk, ANDRZEJ DZIELINSKI, Fractional Kalman Filter algorithm for the states, parameters and order of fractional system estimation, Int. J. Appl. Math. Comput. Sci., 2006, Vol. 16, No. 1, 129 -140.
26. Tarek Raissi, Mohamed Aoun, Robust state estimation for fractional systems, Conservatoire National des Arts et Metiers - Paris, France, National Engineering School of Gabes, Tunisia, Rome, September 14 - 16, 2016.
27. J.C. Trigeassou, N. Maamri, J. Sabatier, A. Oustaloup, A Lyapunov approach to the stability of fractional differential equations, Signal Processing Volume 91, Issue 3, March 2011, Pages 437 - 445.
28. S. Buller, M. Thele , R.W.A.A. De Doncker, E. Karden, Impedance-based simulation models of supercapacitors and Li-ion batteries for power electronic applications, IEEE Transactions on Industry Applications, Volume: 41, Issue: 3, May-June 2005.
29. Autolab Application Note EIS04, Electrochemical Impedance Spectroscopy (EIS) Part 4 Equivalent Circuit Models, 1 July 2011.
30. Li Ran, Wu Junfeng, Wang Haiying, Li Gechen, Prediction of state of charge of Lithium-ion rechargeable battery with electrochemical impedance spectroscopy theory, Industrial Electronics and Applications (ICIEA), 2010, the 5th IEEE Conference on.
31. Domenico Di Domenico, Yann Creff, Eric Prada, Pascal Duchene, Julien Bernard, Valrie Sauvant-Moynot, A Review of Approaches for the Design of Li-Ion BMS Estimation Functions, Oil & Gas Science and Technology Rev. IFP Energies nouvelles, Vol. 68 (2013), No. 1, pp. 127-135.
32. J.-P. Diard, B. Le Gorrec, C. Montella, ELECTRICAL CIRCUITS CONTAINING CPEs, Bio-Logic, March 29, 2013.
33. J.-P. Diard, B. Le Gorrec, C. Montella, DIFFUSION IMPEDANCES, Bio-Logic, August 7, 2012.
34. JLei Pei, Rengui Lu , Chunbo Zhu, Relaxation model of the open-circuit voltage for state-of-charge estimation in lithium-ion batteries, IET Electrical Systems in Transportation Volume: 3, Issue: 4, December 2013.
35. Fei Feng, Rengui Lu , Guo Wei, Chunbo Zhu, Online Estimation of Model Parameters and State of Charge of LiFePO4 Batteries Using a Novel Open-Circuit Voltage at Various Ambient Temperatures, Energies, April 2015.
36. I. Sadli, M. Urbain, M. Hinaje, J.-P. Martin, S. Ral, and B. Davat, Online Estimation of Model Parameters and State of Charge of LiFePO4 Batteries Using a Novel Open-Circuit Voltage at Various Ambient Temperatures, Energy Conversion and Management 51, 2010, 2993-2999.
37. Laurent Sommacal ,Pierre Melchior, Jean-Marie Cabelguen, Alain Oustaloup, Auke Jan Ijspeert, FRACTIONAL MULTIMODELS OF THE GASTROCNEMIUS FROG MUSCLE, IFAC Proceedings Volumes, Volume 39, Issue 11, January 2006, Pages 254-259.
38. B. T. Krishna, K. V. V. S. Reddy, Active and Passive Realization of Fractance Device of Order 1/2, Hindawi Publishing Corporation Active and Passive Electronic Components Volume 2008, Article ID 369421, 5 pages.
39. Yifei Pu, Xiao Yuan, Ke Liao, Jiliu Zhou, Ni Zhang, Xiaoxian Pu, Yi Zeng, A recursive two-circuits series analog fractance circuit for any order fractional calculus, ICO20: Optical Information Processing, China, August 21, 2005.
40. Gary W. Bohannan, Analog Fractional Order Controller in Temperature and Motor Control Applications, Journal of Vibration and Control 14(9-10):1487-1498, September 2008.
41. J.-D. Gabano, T. Poinot, Fractional modelling and identification of thermal systems, Signal Processing Volume 91, Issue 3, March 2011, Pages 531 - 541.
42. Isabel S. Jesus, J.A. Tenreiro Machado, J. Boaventura Cunha, FRACTIONAL ELECTRICAL DYNAMICS IN FRUITS AND VEGETABLES, IFAC Proceedings Volumes, Volume 39, Issue 11, January 2006, Pages 308-313.
43. Ivo Petras, YangQuan Chen, Fractional-order circuit elements with memory, Carpathian Control Conference (ICCC),2012, 13th International.
44. Ivo Petras, Fractional-Order Nonlinear Systems Modeling, Analysis and Simulation, ISBN 978-3-642-18100-9, Springer Heidelberg Dordrecht London New York, 2011.
45. Concepcin A. Monje, YangQuan Chen, Blas M. Vinagre, Dingy Xue, Vicente Feliu, Fractional-order Systems and Controls Fundamentals and Applications, ISBN: 978-1-84996-334-3, Book Advances in Industrial Control 2010.
46. Dochain D, Couenne F, Jallut C, Enthalpy based modelling and design of asymptoticobservers for chemical reactors, "International Journal of Control" - Vol. 82, no. 8, p. 1389-1403 (2009).
47. Aguilar-Garnica E, Garcia-Sandoval JP, Gonzalez-Figueredo C, A robust monitoring tool for distributed parameter plug flow reactors, Computers & Chemical Engineering Volume 35, Issue 3, 8 March 2011, Pages 510-518.
48. Lpez-Negrete R, Biegler LT, A moving horizon estimator for processes with multi-rate measurements: a nonlinear programming sensitivity approach, Journal of Process Control Volume 22, Issue 4, April 2012, Pages 677-688.
49. del-Muro-Cuellar B, Velasco-Villa M, Jimnez-Ramrez O, Fernndez-Anaya G, lvarez-Ramrez J, Observer-based smith prediction scheme for unstable plus time delay processes, Ind. Eng. Chem. Res. 2007, 46, 4906-4913.
50. B.S. Bhangu, P. Bentley, D.A. Stone, C.M. Bingham, Observer techniques for estimating the state-of-charge and state-of-health of VRLABs for hybrid electric vehicles, Vehicle Power and Propulsion, 2005, IEEE Conference.
51. Kravaris C, Hahn J, Chu Y, Advances and selected recent developments in state and parameter estimation, Computers & Chemical Engineering, Volume 51, 5 April 2013, Pages 111-123.
52. K. Balachandran, V. Govindaraj, M. Rivero, J. A. Tenreiro Machado and J. J. Trujillo , Observability of Nonlinear Fractional Dynamical Systems, Hindawi Publishing Corporation Abstract and Applied Analysis, Volume 2013, Article ID 346041, 7 pages.
53. Lee S, Observer for discrete-time Lipschitz non-linear systems with delayed output, IET Control Theory & Applications, Volume: 5, Issue: 1, January 6, 2011 .
54. Dong Y, Yang Y, Observer design for a class of multi-input multi-output nonlinear systems, International Journal of Systems Science Volume 42, 2011 - Issue 4.
55. Katsuhiko Ogata, Modern Control Engineering Fifth Edition, ISBN-13: 978-0136156734, Pearson, September 4, 2009.
56. Tsakalis K, Stability, controllability and observability, 2013.

ASTES

Advances in Science, Technology and Engineering Systems Journal Vol. 2, No. 4, 189-196 (2017)

www.astesj.com

ASTESJ

ISSN: 2415-6698

Big Data Analytics for Healthcare Organization, BDA Process, Benefits and Challenges of BDA: A Review

Siva Sankara Reddy Donthi Reddy*, [1], Udaya Kumar Ramanadham[2]

[1]*Department of Computer Science & Engineering, BIHER, Bharath University, Chennai, Tamilanadu, India*

[2]*Department of Information Technology, BIHER, Bharath University, Chennai, Tamilanadu, India*

ARTICLE INFO

Article history:
Received: 10 July, 2017
Accepted:05 September, 2017
Online: 09 October, 2017

Keywords:
Big Data
Big Data Analytics
Healthcare
BDA process
BDA Advantages

ABSTRACT

Day by day, data grows exponentially large using advanced technology and it requires effective analytical techniques to analyze the unknown and useful facts, patterns, associations and new trends which will provide new way for giving treatment to diseases and to provide good quality healthcare at low cost for everyone. This paper describes uncover valuable insights, various lifestyle choices, some social determinants, clinical and financial factors that it may effect the overall health of an individual. It also presents how to analyze the facts by using big data analytics to improve the healthcare in the world and also describes the various steps involved in Big Data Analytics process and discusses its advantages and challenges which show impact on healthcare organization.

1. Introduction

In the digital world, data are generated as large sets from various sources. The fast transition from conventional to digital technologies has contributed to the growth of big data. It provides evolutionary breakthroughs in many fields with collection of large datasets. Big Data is generated everyday by diverse segments of industries like business, finance, manufacturing, healthcare, education, research and development etc. In general, it refers to the collection of large and complex datasets which are difficult to store and process using traditional database management tools or data processing applications. So there is need of developing and using an effective, innovative tools and technologies offered by Big Data. Data can be of structured, unstructured and semi-structured type. Different variety of data include the text, audio, video, log files, sensor data etc. in petabytes and beyond. As the data is too big from various sources in different form, it is characterized as 5 V's. The 5 V's of Big Data are: Volume, Variety, Velocity, Veracity and Value [1].Volume represent the size of the data - how large the data is. The size of the data can be represented in terabytes and petabytes. Variety represents the data which appears in different forms. Velocity represents the motion of the data and the analysis of streaming of the data. Veracity represents the availability and accountability of various sizes of data. Value represents the high quality of data. The Big Data helps more to healthcare in the world [9].The healthcare organization has generated large amount of data till date, which is scaled in petabytes or exabytes. According to [3], with such fast and rapid growth of data, U.S. healthcare alone will soon reach the zettabyte (1021 gigabytes) scale. The main goal of healthcare industry is to analyse this big volume of data for unknown and useful facts, patterns, associations and trends with the help of machine learning algorithms, which can give new innovative techniques for treatment of various diseases. The aim is to provide high quality healthcare at lower cost to all. This can be a beneficial one for the entire world. Big Data sources are showed in the following Figure 1.

2. Characteristics of Big Data:

The 5 V's of Big Data relevant to Healthcare are:

i) **Volume:** As described earlier, healthcare industry produces the variety of data with more growth rate. According to EMC report and the research firm IDC, the healthcare data increases with 48 per cent annually. In 2013 year, the healthcare data was 153 Exabyte's and it may increase to 2,314 Exabyte's by 2020.[1-2]

ii) **Variety:** In the past, the healthcare organization was generating clinical data of patients with similar symptoms, storing and analysing it to derive the most effective course of treatment for the admitted patient. Now the healthcare industry is focusing on complete healthcare, by providing an effective treatment through analysis of a patient's data from various other sources also. This refers to the variety. Generally, the varied health care data falls into one of the three categories - i.e. structured, semi structured and unstructured. Generally the following data is collected:

*Corresponding Author: Udaya Kumar Ramanadham, Professor, Department of Information Technology, BIHER, Bharath University, Chennai, Tamilanadu, India, Contact No: (+91) 9789994242, E-Mail: rsukumar2007@gmail.com

clinical data from Clinical Decision Support systems (CDSS) (physician's notes, genomic data, behavioural data, data in Electronic Health Records (EHR), Electronic Medical Records (EMR)), machine generated sensor data, data from wearable devices, Medical Image data (from CT scan, MRI, X Ray's etc.), medical claim related data, hospital's administrative data, national health register data, medicine and surgical instruments expiry date identification based on RFID data[3-6], social media data like Twitter data, Facebook data, web pages, blogs and various articles.[7]

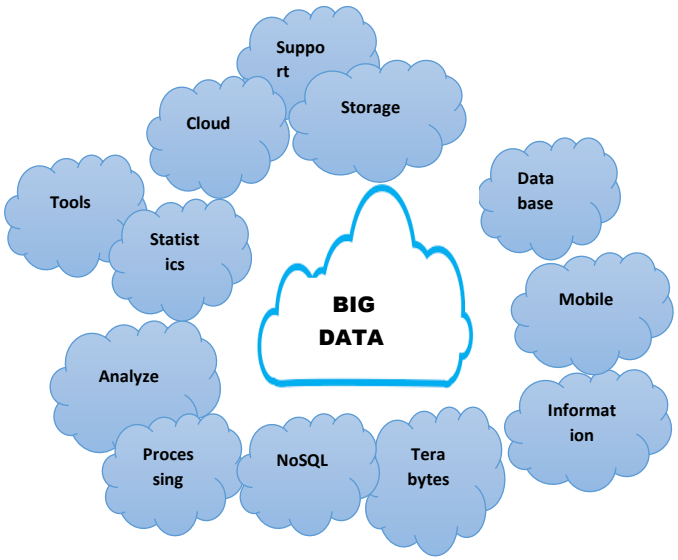

Figure 1: Big Data Sources

iii) Velocity: It refers to the frequency and speed at which data is generated, captured and shared. More data is generated by consumers as well as businesses with in shorter cycles, from hours, minutes, and seconds down to milliseconds. The wearable devices and sensor devices collect real time physiological data of patients rapidly. This new data which is being generated every second is posed a complex and critical challenge for data analysts. Social media data is also added to velocity as the users views, posting data, feeding data scale up in seconds to enormous amount in case of epidemics/national disasters.

iv) Veracity: It refers to trustworthiness of data. Data is accumulated in real-time and at a rapid pace, or velocity. The continuous flow of new data presents new challenges. Just as the volume and variety of data that is collected and stored has changed, so is the velocity at which speed it is generated and that is necessary for accessing, analyzing, and comparing as well as taking decisions based on the output. Most healthcare data has been traditionally static—paper files, x-ray films, and scripts. Velocity represents regular monitoring, such as more daily diabetic glucose measurements (or more continuous control by insulin pumps), blood pressure readings, and EKGs. Meanwhile, in many medical situations, constant real-time data (trauma monitoring for blood pressure, operating room monitors for anesthesia, bedside heart monitors, etc.) can mean the difference between life and death.[8-9]

v) Value: It refers to the quality of data. The data of EMR's and EHR's are recognized as high value data normally. But it is too difficult to certify the value of data from social media. So, the effective analytical methods are needed for the high value data to lead for better quality, effective healthcare solutions and innovations.

The following Figure 2 depicts the 5 V's of Big Data in Healthcare.

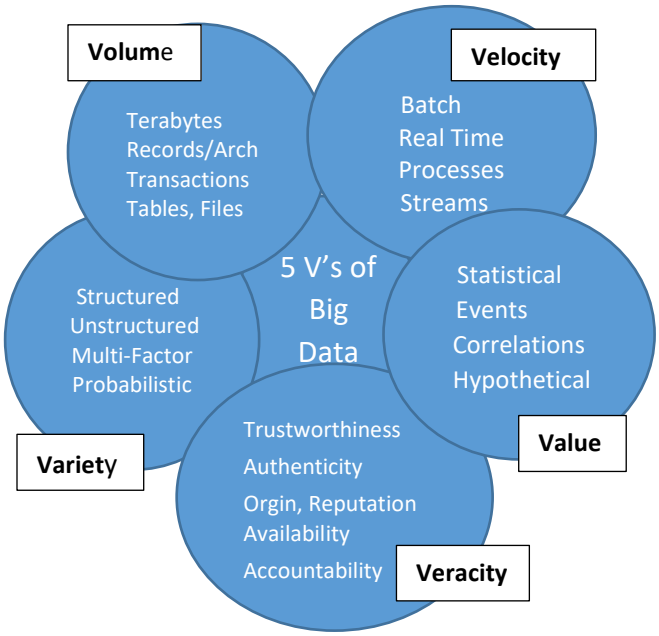

Figure 2: Five V's of Big Data in Healthcare

3. Literature Survey:

By increasing digitization of healthcare information, it is needed to improve the quality of healthcare, results, and reducing the costs. The advanced tools and technologies are used in health care organizations to generate valuable insights of digital healthcare information. The organizations must analyse patient information to more accurately measure the risk and for better outcomes. At the same time, many organizations are working to increase data transparency for producing latest insightful knowledge.

To exchange health information between various providers and payers, some integrated delivery networks can be formed. The pharmaceutical companies are tied up to protect patients' privacy while making data available to qualified researchers outside the organization.

Kiyana Zolfaghar et al. [17] has presented prediction model to give possible solutions for congestive heart failure incidents using Mahout Framework. The raw data is pre-processed and converted to encoded format which will be given as input to the Mahout framework, using random forest algorithm.

Joseph M. Woodside [18] has presented, inefficient vendors can be identified, and who is poor in the member's lifestyle

decisions and compliance with preventative care programs. For individuals, intensives can be given, such as cash, gift cards which are considered as one of the recommended changes in the health care system.

Existing analytical techniques can be applied to the vast amount of existing patient related health and medical data to reach a deeper understanding of results, which can be applied at the point of care. Ideally, these data would inform each physician and their patients during the decision-making process and used to identify the appropriate treatment option for that particular patient.

4. BDA Initiatives for Healthcare Industry in the World

Most of the countries have initiated the number of big data initiatives around the world. Some of the initiatives are described as follows:

New Zealand's Ministry of Health has collaborated with New Zealand Society to Study about Diabetes. These have used SAS. [10]

Data analysis for providing a Virtual Diabetes Register which combines and filters the health information to determine accurately that how many people are diagnosed with the diabetic condition and predicting who can develop diabetes in the future.[12]

McKinley Children's Centre of California provides child welfare services in Los Angeles country. The organization serves for more than 700 children annually, which provides the services such as residential care, foster care and adoptions, special education, and mental health services. The center has launched an innovative big data analytics for initiating the staff identifying the variables that impact each child's success and identifying the right combination of programs to improve outcomes. [13]

The Data Science Institute of Columbia University, New York has collaborated with the New York City Department of Health and Mental Hygiene (NYC DOHMH) for working a project that focuses on the detection of disease outbreaks in New York City restaurants. The main goal of this project is to identify and analyze the unprecedented volumes of user-contributed opinions and comments on social media sites such as Twitter, Face book and Yelp, which host massive amounts of content by users about their real-life experiences and opinions about restaurants. It will help to extract reliable indicators of otherwise-unreported disease outbreaks associated with the restaurants. The NYC DOHMH analyses these indicators, as they are produced, to decide when additional action is required to be taken. This project is developing non-traditional information extraction technology over redundant, noisy, and often ungrammatical text-- for a public health task of high importance to society at large. [14]

WellPoint, Inc. is an Indiana polis-based health Benefit Company wanted to reduce the waste of resources (money) by improving the utilization management (UM) process, which governs the pre-approval of healthcare insurance coverage for many medical procedures. Its goals were to accelerate processing of physicians' treatment requests, save members' time and improve efficiencies in the approval process, while continuing to base UM decisions on medical evidence and clinical practice guidelines(for ensuring consistency in process).It was a very big challenge considering the volume of data that is analyzed in making UM decisions. WellPoint was teamed the IBM on a new method to UM: using the cognitive system IBM Watson to provide approval guidelines for nursing staff, based on clinical and patient data. WellPoint trained Watson with 25,000 historical cases. The system uses hypothesis generation and evidence-based learning to generate confidence-scored recommendations that help nurses make decisions about UM. The new system provides responses to all requests in seconds, as opposed to 72 hours for urgent pre-authorization and three to five days for elective procedures with the previous UM process. Encouraged with success of the system, today 15,835 healthcare provider offices use it. [15]

Seattle Children's Hospital and Regional Medical Centre is using big data analytics as part of its Clinical Standard Work (CSW) program, which defines patient populations and recommends an ideal protocol for each population, allowing ensuring that every patient at the hospital receives the same standard of care. The CSW program gets the enormous data from enterprise data warehouse (EDW) which currently integrates data from 10 sources across the hospital, including electronic medical records (EMRs) and billing systems. With the help of CSW program, the doctors and nurses get complete information based on thousands of data points of each patient, they get answers to complex queries about potential treatments and procedures, and identify pathways of care for patients with particular needs, regardless of provider. Clinicians can also evaluate treatment protocols for determining the resources which need to be allocated by hospital. [16]

Seton Healthcare Family, based on Texas, Austin. It has used the IBM Content and Predictive Analytics for Healthcare solutions. The system gives an integrated view of relevant clinical and operational information to drive more informed decision making. By teaming unstructured content (History and Physical, Discharge Summaries, Echocardiogram Reports, and Consult Notes) with predictive analytics, Seton is able to identify patients likely for re-admission and introduce early interventions to reduce cost, mortality rates, and improved patient quality of life.

Doctors at UCLA with the help of IBM Watson Foundations have recently started using data streaming technology in order to make more informed decisions about brain functions and abnormalities. Using IBM Watson foundations, physicians are able to gather data from sensors to analyze brain functions in real time. As a result of the use of this technology, patient care can be substantially improved, and doctors have more time to serve for more patients.

The U.K.'s National Health Service uses cloud analytics software to pluck numerical and text data on health-care facilities from spread sheets and databases and presents it in plain English on its website, NHS Choices. This endeavor is helpful to its citizens, as they can make better choice about their care based on information of about 50,000 health care facilities. The software uses natural language generation techniques and to examine through structured data and automatically present it in story form.

US State of North Carolina processes about 88 million claims totaling about $12 billion annually from 66,000 providers who treat the state's two million Medicaid patients., The State's

Department of health and human services in collaboration with IBM used big data analytics to help identify suspicious billing patterns by healthcare providers. Using three years' worth of North Carolina Medicaid claims data, IBM data mining software, which featured special algorithms and modeling capabilities, was applied to detect common fraud and abuse schemes. Almost 90% reduction in fraud was achieved.

Informatics for Integrating Biology and the Bedside (i2b2) is an NIH-funded National Centre for Biomedical Computing based at Partners HealthCare System. The i2b2 Centre developed a scalable informatics framework that will enable clinical researchers to use existing clinical data for discovery research and, when combined with IRB-approved genomic data, facilitate the design of targeted therapies for individual patients with diseases having genetic origins.

The Human Connective project which led by Washington University, University of Minnesota, and Oxford University is working to map the human brain by making a comprehensive connectivity diagram. It will produce invaluable information about brain connectivity, its relationship to behavior, and the contributions of genetic and environmental factors to individual differences in brain circuitry and behavior. This will help to figure reasons why certain people have certain brain disorders, help the physicians to easily diagnose and in certain cases prevention of mental or physical illness. Over a 3-year span (2012-2015), the Human Connectome Project (HCP) has scanned 1,200 healthy adult people and the generated data is made publicly accessible quarter wise.

In January 2015, President Obama announced a new biomedical research project that is “Precision Medicine” which will use the power of big data to help for the development of specialized drugs to cure the diseases like cancer and diabetes. The program shall collect genetic data of one million Americans so scientists could develop drugs and treatments tailored to the characteristics of individual patients.

5. Big Data Analytics Process Steps:

There are different steps in Big Data Analytics process.

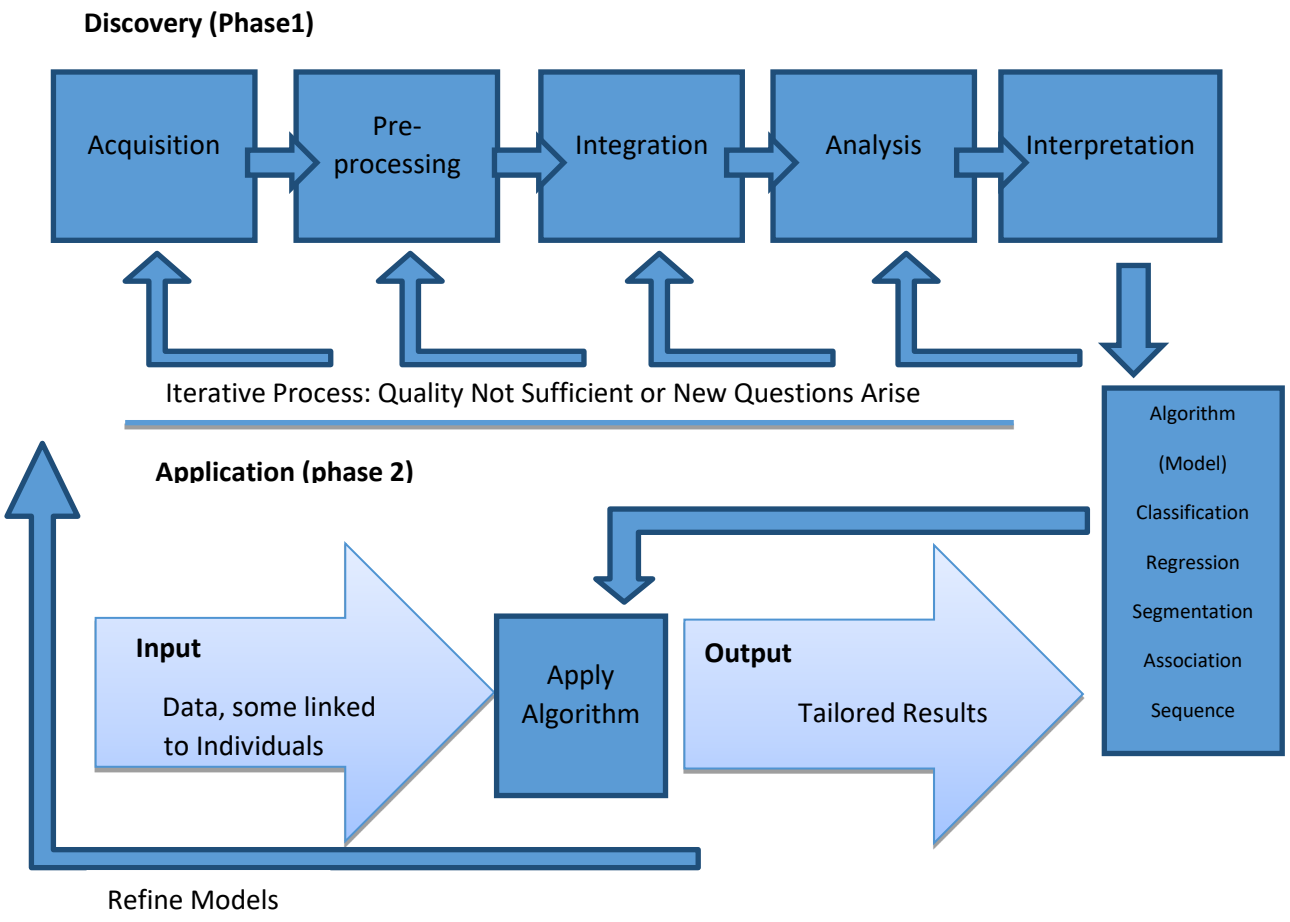

Figure3 Functional Architecture of Big Data Analytics Process

ii) **Cleaning of Data:** Generally, the healthcare data is seen as flaws like many patients don't share their data completely like data about their dietary habits, weight and lifestyle. In this type of cases the empty fields need to be filled appropriately. Another example, the gender can be either at most one of two values i.e. male or female. In case any other value or no value is present then such entries need to updated and handled accordingly. The data from sensors, prescriptions, medical image data and social media data need to be expressed in a structured and suitable form for performing effective analysis.[2]

iii) **Integration of Data:** The BDA process makes use of data where accumulated across various platforms. This data may be varied in metadata (the number of fields, type, and format). The total data can be grouped correctly and consistently into a dataset which can be effectively used for data analysis purpose. This is a very challenging task, considering the big volume and variety of big data.

iv) **Querying, Analysis and Interpretation of Data:** After cleaning of data and integration, the next step is to query the data. A query can be simple one like what is mortality rate in a particular area? Or complex query like how many patients with diabetes would be likely to develop heart related problems in next 6 years? Based upon the complexity of the query, the data analyst can choose appropriate platform and analytic tool.

The following Figure 3 depicts the functional architecture of Big Data Analytics process steps.

5.1 Technology Support for Big Data Analytics in Health Care:

There are large number of open source and proprietary platforms and tools available in the market. Some of them are Hadoop, Map Reduce, Storm, Grid Grain. Big Data Databases like Cassanadra, HBase, Mongo DB, Couch DB, Orient DB, Terrastore, Hive etc. Data Mining tools like RapidMiner, Mahout, Orange, Weka, Rattle, and KEEL etc. File Systems like HDFS and Gluster. Programming Languages like Pig/PigLatin, R, and ECL. Big Data Search Tools like Lucene, Solr etc. Data Aggregation and Transfer Tools like Sqoop, Flume, and Chukwa. Other tools like Oozie, Zookeeper, Avro, and Terracotta. Some open source platforms are also available like Lumify, IKANOW [11].

The criteria for platform evaluation may be varied for different organizations. Generally the ease of use, availability, the capability to handle voluminous data, support for visualization, high quality assurance, cost, security can be some of the variables to decide upon the platform and tool to be used. Some of the platforms and tools are mentioned the following Table

Table 1 Platforms & Tools for Big Data Analytics in Healthcare

Platforms &Tools	Description
The Hadoop Distributed File System (HDFS)	HDFS enables the underlying storage for the Hadoop cluster. It divides the data into smaller parts and distributes it across the various servers/nodes.
MapReduce	MapReduce provides the interface for the distribution of sub-tasks and the gathering of outputs. When tasks are executed, MapReduce tracks the processing of each server/node.
PIG and PIG Latin	Pig programming language is configured to assimilate all types of data (structured/unstructured, etc.). It is comprised of two key modules: the language itself, called PigLatin, and the runtime version in which the PigLatin code is executed.
Hive	Hive is a runtime Hadoop support architecture that leverages Structure Query Language (SQL) with the Hadoop platform. It permits SQL programmers to develop Hive Query Language (HQL) statements akin to typical SQL statements.
Jaql	Jaql is a functional, declarative query language designed to process large datasets. To facilitate parallel processing, Jaql converts "'high-level' queries into 'low-level' queries" consisting of MapReduce tasks.
Zookeeper	Zookeeper allows a centralized infrastructure with various Services, providing synchronization across a cluster of servers. Big Data analysis applications utilize these services to coordinate parallel processing across big clusters.
HBase	HBase is a column-oriented database management system that sits on top of HDFS. It uses a non-SQL approach.
Cassandra	Cassandra is also a distributed database system. It is designated as a top-level project modeled to handle big data distributed across many utility servers. It also provides reliable service with no particular point of failure (http://en.wikipedia.org/wiki/Apache_Cassandra) and it is a NoSQL system.

Oozie	Oozie, an open source project, streamlines the workflow and coordination among the tasks.
Lucene	The Lucene project is used widely for text analytics/searches and has been incorporated into several open source projects. Its scope includes full text indexing and library search for use within a Java application.
Avro	Avro facilitates data serialization services. Versioning and version control are additional useful features.
Mahout	Mahout is yet another Apache project whose goal is to generate free applications of distributed and scalable machine learning algorithms that support big data analytics on the Hadoop platform.

6. Big Data Analytics Benefits in Healthcare

The massive amount of data provides the opportunities for researchers in the Healthcare field to use tools and techniques for opening the hidden answers. Big Data Analytics tools and techniques can be applied in effective way on large sets of data then the following benefits will be given:

i) Individuals/Patients: Generally, when treatment is given to a patient, then the historical data can be considered such as a set of similar patients about the symptoms, drugs used outcome/response of different patients. With the help of BDA, the specific treatment is given for a patient based on his genomic data, location, weather, lifestyle, medical history, response to certain medicines, allergies, family history etc. When the genome data is fully explored for some kind of relation and it can be established between the DNA and a particular disease. Then the specific line of treatment can be constructed for every individual. The patients will benefit in the following ways:

- Correct and effective treatment can be applied.
- Health related issues will be known in better way.
- Preventive steps can be taken in time.
- Continuous health monitoring at patients location using wearable wireless devices.
- Designing specialized treatment for patient.
- Life expectancy and quality will be found in advance.

ii) Hospitals: By using effective BDA techniques on the data availability, the hospitals can get following benefits:

- Predict the patients staying and readmission information.
- New healthcare plans will be developed to prevent hospitalization.
- Various questions can be answered by analyzing the data using BDA tools and techniques regarding disease treatment.
- The hospital management can take and manage administrative decisions in the better way.

iii) Insurance Companies: The government is reimbursed the large amount of expenditure for giving medical claims for patients. We can analyze, identify, predict and minimize the possible frauds related to medical claims by using BDA. [3]

iv) Pharmaceutical Companies: By using BDA techniques effectively, the R&D can help pharmaceutical companies to produce drugs that may be most effective for treating a specific disease with in the shorter period.

v) Government: The BDA can help in improving the public health surveillance and speed up the response to disease outbreaks. The government can use demographic data, historical data of disease outbreak, weather data, data from social media over disease keywords like cholera, flu etc. BDA can analyze this massive data to predict epidemics, finding correlation between the weather and likely occurrence of disease. Therefore preventive measures can be taken to avoid the same. [3]

7. Big Data Analytics - Challenges:

The advantages of big data are more for healthcare, but there are number of challenges which can be broken up.

i) Unstructured and Provenance of Data: The BDA process can collect data from different sources. Most of the data is unstructured data like medical prescriptions, blogs, tweets, status updates, and comments. It is necessary to generate right metadata for this unstructured data and transform it into a structured format. The image and video data should be structured for semantic content and search. By using data analysis process, the provenance of data along with its metadata should be carried out so it is easy to track the processing steps when error generates [3]. Some intelligent processing techniques should be proposed to deal the data input from sensors and wearable devices. This will help to filter/derive the meaningful data, which can then be stored on permanent storage. Therefore it will save space.

ii) Missing or Incomplete Data: Some patients may hide their personal information about his/her life style at the time of filling forms or oral interviews by doctors. Some fields may be empty at the time of storing the data in digital format. Sometimes it may happen that some of the fields produce wrong results. If analysis is done on the empty or wrong fields of data, then it may or may not get processed. In both the cases they produce wrong results. If we leave some records as empty then the analysis may not on cumulative data. If we take wrong value fields then the analysis is incorrect and unreliable. This type of issues will be addressed.

iii) Quality of Data: When we consider data from social media, then we need to ensure that data whether it is a valid data or not. So it is great challenge to determine the validation and quality of data.

iv) Technical Challenges: There are different technical challenges.

- Data aggregation with different database management systems is also a great challenge in BDA. By dividing certain standard database design practices meant for a

specific domain like healthcare, financial sector etc., it can be made easier [3]. We are required more technological standards and protocols for different database management systems to integrate seamlessly.

- The traditional algorithms can be scaled up to handle the big volume of data in data mining processes or analysis. The processors speed has come to a point beyond which it's hard to increase in parallelogram process. So the trend can be moved towards multi-core processors. In such a scenarios, we need statistical algorithms which can be parallelized otherwise the computing performance will decrease when they handle complex big volume data.[9] The interactive response time is another big problem while apart from this scaling complex query processing techniques to terabytes. [3]
- An analysis is more useful if a non-technical person is able to understand and interpret it. The large volume and variety of data is too hard to represent it visually in a more understandable and easy way. A user should be able to perform the repeated analysis with the different set of assumptions, data sets and parameters. It will help the user to better understand the analysis process and verify whether the system works in a required way or not.
- We need careful evaluation process to use the best platform and tool for market floods.

v) **Data Security:** Data Security is another major challenge as more and more data is digitized. Most of the people are not willing to share their personal data with a fear of security breach. If there is assurance for data security, then the problem can be managed. There should be strict government policies and norms for what data can be shared and what not. Apart from this, strong technological hardware and software level security precautions and measures should be implemented to prevent the hacking and interpreting malicious code.

vi) **Lack of Experts:** There is a more shortage of qualified and experienced data scientists in the world. So it is necessary to create an expertise in the field of data science to turn the promises of big data into reality.

8. Innovative Ideas and Solutions:

The following are some possible new innovative ideas and solutions of Big Data in Healthcare industry.

- **Clinical Decision Support:** BDA technologies predict outcomes or recommend alternative treatments to clinicians and patients at the point of care by understanding, analyzing, categorizing and learning from them.
- **Personalized Care:** By predicting and analyzing disease symptoms in advance personalized care is taken (e.g., genomic DNA sequence for cancer care) in real time to highlight best practice treatments to patients. These solutions may offer early detection and diagnosis before a patient develops disease symptoms.
- **Public And Population Health:** BDA solutions that can help in searching and identifying patient population via social media data to predict flu outbreaks based on consumers' search, social content and query activity. BDA solutions can also help clinicians and epidemiologists performing analyses across patient populations and care venues to help identify disease trends.
- **Clinical Operations:** BDA can produce accurate solutions for clinical operations without waiting for longer time to take fast decisions.
- **Policy, Financial and Administrative:** BDA has supported the decision makers to integrate and analyze data related to key performance indicators on policy and financial aspects.

9. Conclusion and Future Work

Big Data Analytics in healthcare is evolving into a promising field for giving new insights from huge data sets and improving results while reducing costs. Its strength is high; however there are more challenges to overcome. Big Data Analytics has the potential to transform the way healthcare providers from traditional ways to more suitable and right tools and technologies to gain insight from their clinical and other data repositories and make constructive decisions. In the future we'll see the rapid, widespread implementation and use of big data analytics across the healthcare organizations and the healthcare industry. To that end, the challenges must be discussed and see the overcoming measures. As big data analytics become more important, more attention will be required, due to some issues such as guaranteeing privacy, safeguarding security, establishing standards and governance, and continually improving the tools and technologies. Big data analytics and applications in healthcare are at an initial stage of development, but rapid advancements of Big Data platforms and tools can accelerate their maturing process.

Conflict of Interest

The authors declare no conflict of interest.

Acknowledgment

I would like to thank to all people who help me prepare this paper completely. I would also thank to my guide who help me and get proper suggestions. I would like to thank to all website and journal papers which I have referred to create my review paper successfully.

The authors would like to thank all reviewers and Prof. Passerini Kazmerski, Editor for his valuable comments on the manuscript.

References

[1] Jasleen Kaur Bains, "Big Data Analytics in Healthcare- Its Benefits, Phases and Challenges" , International Journal of Advanced Research in Computer Science and Software Engineering, Volume 6, Issue 4, April 2016,Available online at: www.ijarcsse.com

[2] Wullianallur Raghupathi and Viju Raghupathi, "Big *data analytics in healthcare: promise and potential*", *Health Information Science and Systems* 2014, **2**:3, Available: http://www.hissjournal.com/content/2/1/3

[3] VivekWadhwa,"*The rise of big data brings tremendous possibilities and frightening perils*",April2014.Available:http://www.washingtonpost.com/blogs/innovations/wp/2014/04/18/therise-of-big-data-brings-remendous-possibilities-and-frightening-perils/

[4] D. Agrawal et. al, "*Challenges and Opportunities with Big Data*", Big Data WhitePaper-Computing Research Association, Feb-2012, Available: http://cra.org/ccc/docs/init/bigdatawhitepaper.pdf

[5] Nambiar, R. ; Cisco Syst., Inc., San Jose, CA, USA ; Bhardwaj, R. ; Sethi, A. ; Vargheese, R.,"*A look at challenges and opportunities of Big Data*

analytics in healthcare", IEEEConference 2013, Available: http://ieeexplore.ieee.org/xpl/login.jsp?tp=&arnumber=6691753&url=http%3A%2F%2Fieeexplore.ieee.org%2Fxpls%2Fabs_all.jsp%3Farnumber%3D6691753

[6] Ahmed E. Youssef," *A Framework for Secure Healthcare Systems Based on Big Data Analytics in Mobile Cloud Computing Environments*", The International Journal of AmbientSystem and Applications 06-2014, Available: http://airccse.org/journal/ijasa/papers/2214asa01.pdf

[7] J. Archenaa, E.A. Mary Anita," *A Survey of Big Data Analytics in Healthcare and Government*", Procedia Computer Science, Elsevier, Volume 50, 2015, Pages 408–413,Big Data,Cloud and Computing Challenges, Available: http://www.sciencedirect.com/science/article/pii/S1877050915005220

[8] Matthew Herland, Taghi M Khoshgoftaar and RandallWald, "*A review of data mining using bigdata in health informatics*", Herland et al. Journal of Big Data 2014, Springer, 1:2 Available: http://www.journalofbigdata.com/content/1/1/2

[9] MH Kuo, T Sahama, AW Kushniruk, EM Borycki, DK Grunwell, ―"*Health big data analytics: current perspectives, challenges and potential solutions*", International Journal of Big Data Intelligence ,Vol. 1, Issue 1, pp.114-126.

[10] Bernard Marr, "*How Big Data Is Changing Healthcare*", Available: http://www.forbes.com/sites/bernardmarr/2015/04/21/how-big-data-is-changing-healthcare/

[11] "Improve Healthcare Win $3,000,000", Available: http://www.heritagehealthprize.com/c/hhp

[12] Cynthia Harvey, "50 Top Open Source Tools for Big Data", Available: http://www.datamation.com/data-center/50-top-open-source-tools-for-big-data-1.html

[13] "Big Data Provides True Picture of Diabetic Population", Available: http://www.sas.com/en_us/news/sascom/2014q1/nz-ministry-of-health.html http://www-01.ibm.com/common/ssi/cgi-bin/ssialias?subtype=AB&infotype=PM&appname=SWGE_YT_YT_USEN&htmlfid=YTC03753USEN&attachment=YTC03753USEN.PDF

[14] Health Analytics, Available: http://datascience.columbia.edu/health-analytics

[15] http://www.ibm.com/smarterplanet/us/en/ibmwatson/assets/pdfs/WellPoint_Case_Study_IMC14792.pdf

[16] Linda L. Briggs, *"BigData means better care at Seattle's Children Hospital*", Available: http://tdwi.org/articles/2013/08/13/big-data-analytics-smarter-care.aspx

[17] Kiyana Zolfaghar, Naren Meadem, Ankur teredesai, Senjuti Basu Roy, Si-Chi Chin."Big Data Solutions for Predicting Risk-of-Readmission for Congestive Heart Failure Patients".2013 IEEE International Conference on Big Data, 978-1-4799-1293-3/13. http://dx.doi.org/10.1109/bigdata.2013.6691760

[18] Joseph M. Woodside. Virtual Health Management, 2014 11th International Conference on Information Technology New Generations 978-1-4799-3187-3/14. http://dx.doi.org/10.1109/itng.2014.124

ASTES

Advances in Science, Technology and Engineering Systems Journal Vol. 2, No. 4, 197-203(2017)

www.astesj.com

ASTESJ

ISSN: 2415-6698

Application of Computational Fluid Dynamics Model in High-Rise Building Wind Analysis-A Case Study

Okafor Chinedum Vincent*,1

[1]*Department of Building, Nnamdi Azikiwe University, Awka, Nigeria*

ARTICLE INFO

Article history:
Received: 19 September, 2017
Accepted: 13 October, 2017
Online: 31 October, 2017

Keywords:
BS6399-2:1997
CFD
Wind tunnel testing

ABSTRACT

Over the years, wind loading codes has been a crucial tool in determining design wind loads on buildings. Due to the limitations of these codes especially in height, wind tunnel testing is recommended as the best approach in predicting wind flow around buildings but carrying out wind tunnel testing in the preliminary as well as final design stage of a project has proven uneconomical and incurs additional cost to the client. In response to this, CFD which is a virtual form of wind tunnel testing was developed. From immersive researches and experiments carried out by previous researchers, best practice guidelines have been given on the use of CFD in predicting wind flow around buildings. This paper compares the results of a case study application of computational fluid dynamics simulation in determining the wind loads on the facade of a typical 48.8m high-rise building to the predictions given in British wind Standards BS6399-2:1997, using wind speed data of Lagos state Nigeria. From the results, it was shown that the latter can offer considerable saving and highlight problem areas overlooked by the British code of practice (BS6399-2:1997).

1. Introduction

Wind induced pressure is a major design consideration for analyzing the response of facade to wind loads. However, there are often several discrepancies between the existing guidelines available for determining wind loadings and the corresponding pressure obtained from computational fluid dynamics.

A facade can constitute up to 25% of the total building costs with the average cost of a facade in the region of £400 per m^2 possibly reading £500 per m^2 for a high specification bespoke façade [1].The aerodynamics of high-rise building induced by the wind flow surrounding the building is characterized as that of a bluff body [2]. The key factor affecting the aerodynamics loads on a bluff body includes the bluff body and the conditions of direct surrounding of the body such as the presence of other bluff body [3].

There are three methods of determining the wind induce loads on a building, which are the use of

- Wind loading codes
- Wind tunnel testing
- Computational fluid dynamics

Most wind loading codes have their own limitations in providing necessary guidelines for the wind design of buildings such as height limitation, shielding factor and complicated geometry of the building.[4],suggested that most major wind codes can only analyze wind loads and acceleration of tall buildings with square or rectangular cross section and maximum aspect ratio of six. In order to calculate wind loadings on structures with height and geometry different from that stipulated in the wind loading codes, major standards recommend the use of wind tunnel testing[5].

Wind tunnel testing is regarded as the best practice in determining wind loads on a structure. However, according to [6], the cost of wind tunnel tests is comparatively high and conducting wind tunnel tests at the preliminary design stage is uneconomical. The shape of the building normally changes few times during the preliminary stage and this will add to the testing cost. Also, wind tunnel testing enables more flexibility in mimicking the surroundings of buildings to reality as compared to the design standards, measurements are only recorded at limited locations on the model and it may suffer from incompatible similarity requirement due to reduced scale setup [7].

*Corresponding Author: Okafor Chinedum Vincent, Nnamdi Azkiwe University, Awka,Nigeria. Email: chinedumokafor117@yahoo.com

Computational fluid dynamics on the other hand is a computer based mathematical modeling tool capable of dealing with flow problems and predicting physical fluid flow and heat transfer [8]. A number of best practice guidelines have been published that classify proper computational conditions for the resolution of wind around building[9].These best practice guidelines provide valuable information on how computational fluid dynamics should be used in order to avoid or at least reduce user error caused by the incorrect use of CFD. Some of these best practice guidelines includes "best practice guidelines for the CFD simulation of flows in urban environment"[10], "Recommendations on the use of CFD in wind engineering"[11], "Aij guidelines for practical applications of CFD to pedestrian wind environment around buildings"[12], "The best practice guidelines"[13]. CFD can be adopted in wind design as it is able to model the actual surrounding in full scale as compared to reduced scale when it is done in wind tunnel experiments [14].

The aim of this study is to compare the results obtained from a CFD simulation of a typical high-rise building to the prediction given by the British wind design standards [15]

The study sought to achieve this aim through the following objectives:

- Determining the wind speeds at subsequent height of the high-rise building using wind profile logarithm law
- Calculating the magnitude of design wind pressure on the facade of the high-rise building using BS6399-2:1997 and CFD
- Comparing the results obtained from BS6399-2:1997 to the results gotten from CFD simulation.

2. Methodology

2.1. Case study

The structural system of the symmetrical building is illustrated in Figure1. This building is assumed to be situated in Lagos state, Nigeria and the shape and dimension are modified to suit the analysis. It is a 62m x 30.5m x 47.8m, 15- story typical office building (Figure 1). A 1.22m parapet was provided above the last floor making total height of the building equal to 48.8m. The structural system contained reinforced concrete rigid frames in both directions as shown in Figure 1. The floor slabs were assumed to provide diaphragm action.

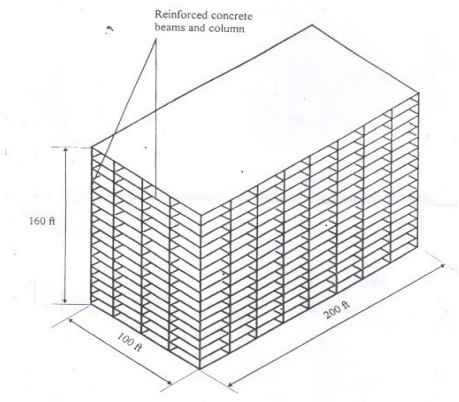

Figure 1:Structural system of the 48.8m tall building

2.2. Area of the study

Wind speed data of Ikeja, Lagos state, Nigeria was used with reference to the wind speed map of Nigeria determined from40years of measurement at 10m height.

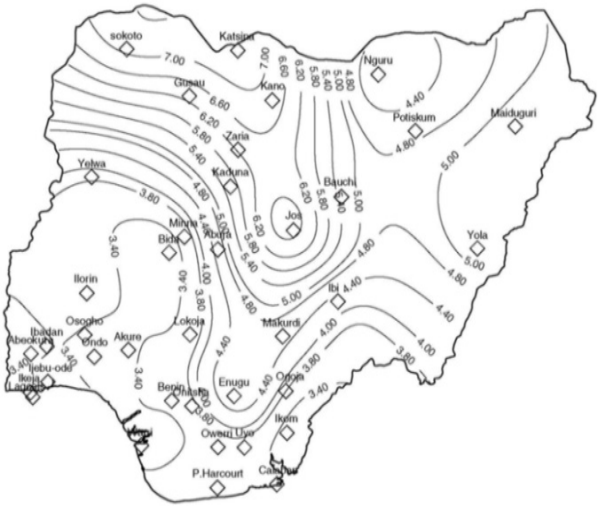

Figure 2: Nigerian wind map in m/s determined from 40 years measurements at 10m height, obtained from Nigerian metrological department, oshodi, lagos state, Nigeria (NIMET).

3. Analytical Procedure

From the wind speed map above it can be deduced that Lagos State (Ikeja) has a wind speed of 3.40m/s measured from a 10 meter height. Using [16], wind speed at subsequent height can be calculated with results, as follows:

The logarithm wind profile relationship is

$$u_z = \frac{u_x}{k}\left[\ln\left(\frac{z}{z_0}\right)\right] \quad (1)$$

Where u_z =wind speed at height, z is the building height,u_x is the friction velocity=0.3027m/s, k is the von Karman constant=0.41 and z_0 is the roughness length=0.1m

Table 1: Wind speed as per log profile law

Storey height	Floor Height(m)	Wind velocity(m/s)
15th floor	48.77	4.569
14th floor	44.10	4.507
13th floor	40.95	4.440
12th floor	37.80	4.382
11th floor	34.65	4.317
10th floor	31.50	4.247
9th floor	28.35	4.169
8th floor	25.20	4.082
7th floor	22.05	3.984
6th floor	18.90	3.870
5th floor	15.75	3.735
4th floor	12.60	3.571
3rd floor	9.450	3.358
2nd floor	6.300	3.059
1st floor	3.150	2.547

The fundamental wind speed of the tall building 15th floor = 4.569m/s

Now, the Design wind speed as per [15] can be calculated as

$$V_s = V_b \times S_a \times S_d \times S_s \times S_p \quad (2)$$

$$S_a = 1 + 0.001\Delta_S \quad (3)$$

To determine the standard effective wind speed

$$V_e = V_s . S_b \quad (4)$$

Calculate the dynamic pressure

$$q_s = 0.613 V_e^2 \quad (5)$$

To calculate the external wind pressure on the windward, leeward and sidewall of the high-rise building.

$$P_e = q_b . C_a . C_{pe} \quad (6)$$

According to table 7, 8 and 9 of [15], C_{pe} for leeward wall and sidewall have negative values which accounts for the negative values of their wind pressures.

Where $V_s$is the site wind speed, V_b is the basic wind speed,V_e is standard effective wind speed, S_a is an altitude factor, Δ_S is the site altitude in meters,S_d is a direction factor,S_s is aseasonal factor,S_p is a probability factor,S_b is the roughness factor,q_s is the dynamic pressure, P_e stands for the wind pressure,C_a is the size effect factor for external pressure,C_{pe} is the external pressure coefficient for the building surface.

4. CFD Analysis Procedure

4.1. Computational Domain

Generally, the size of the entire computational domain depends on the targeted area and the boundary condition [9].

A key part of the modeling is the choice of the domain size and the positioning of the (single) high-rise building within that domain. Recent CFD studies have used [11] as a starting point in determining the domain size. The recommendation from [11] are as follows: the inlet, the lateral and top boundary are 5H away from the building where H is the building height, blockage ratio should exceed 3%[12] and the outlet should be positioned at least 15H behind the building.

The computational domain used for the study was given According to recommendations by [11], the inlet, the lateral and the top boundary away from the high-rise building model was 5H. while outflow boundary is 15H, leading to a blockage ratio of 1.8%. Where H represents the height of the building.

It is important to choose proper boundary condition since these decide to a large extent the solution in the computational domain [10]. Data generation used to describe the boundary conditions of the CFD study are presented in section 4-5, based on full scale measurements where relevant.

The governing equation for all fluid flow is the Navier Stokes Equation (7), (8), (9), (10)

$$\mathrm{DivU}=0 \quad (7)$$

$$\frac{\partial \mathrm{u}}{\partial \mathrm{t}} + \mathrm{div}(\mathbf{U}\mathrm{u}) = \frac{-\partial \mathrm{p}}{\mathrm{p}\,\partial \mathrm{x}} + \mathbf{v}\mathrm{divgrade}\mathbf{U} \quad (8)$$

$$\frac{\partial \mathrm{v}}{\partial \mathrm{t}} + \mathrm{div}(\mathbf{V}\mathrm{u}) = \frac{-\partial \mathrm{p}}{\mathrm{p}\,\partial y} + \mathbf{v}\mathrm{divgrade}\mathbf{V} \quad (9)$$

$$\frac{\partial \mathrm{w}}{\partial \mathrm{t}} + \mathrm{div}(\mathbf{W}\mathrm{u}) = \frac{-\partial \mathrm{p}}{\mathrm{p}\,\partial z} + \mathbf{v}\mathrm{divgrade}\mathbf{W} \quad (10)$$

The 2nd part of the equation is the viscous term, the 3rd part is the pressure gradient and the 4th part is the convective term

In order to describe the turbulent flow, the instantaneous term in equation (7), (8), (9),(10) is decomposed into its mean and fluctuating part as follows

$$U = U + u^i \quad (11)$$

$$V = V + v^i \quad (12)$$

$$W = W + w^i \quad (13)$$

$$P = P + p^i \quad (14)$$

Substituting equation (11), (12), (13), (14) into equation (7), (8), (9), (10), results to a time averaged solution to the Navier Stokes Equation for an incompressible fluid flow:

$$\frac{\partial u}{\partial t} + div(Uu) = \frac{-\partial p}{p\partial x} + \mu divgrade U + \left[-\frac{\partial u^{i^2}}{\partial x} - \frac{\partial v^{i^2}}{\partial y} - \frac{\partial w^{i^2}}{\partial z}\right] \quad (15)$$

$$\frac{\partial v}{\partial t} + div(Vu) = \frac{-\partial p}{p\partial y} + \mu divgrade V + [-\frac{\partial u^i v^i}{\partial x} - \frac{\partial v^{i^2}}{\partial y} - \frac{\partial v^i w^i}{\partial z}] \quad (16)$$

$$\frac{\partial w}{\partial t} + div(Wu) = \frac{-\partial p}{p\partial z} + \mu divgrade W + [-\frac{\partial u^i w^i}{\partial x} - \frac{\partial v^i w^i}{\partial y} + \frac{\partial w^{i^2}}{\partial z}] \quad (17)$$

Where U, V, W are velocity vectors, P is pressure, $[-\frac{\partial u^{i^2}}{\partial x} - \frac{\partial v^{i^2}}{\partial y} - \frac{\partial w^{i^2}}{\partial z}]$, $[-\frac{\partial u^i v^i}{\partial x} - \frac{\partial v^{i^2}}{\partial y} - \frac{\partial v^i w^i}{\partial z}]$, $[-\frac{\partial u^i w^i}{\partial x} - \frac{\partial v^i w^i}{\partial y} + \frac{\partial w^{i^2}}{\partial z}]$ from equation (15), (16) and (17) are referred to as Reynolds stresses because they are fluctuating component from the convective term of equation (8), (9) and (10)

Turbulence model is used to model the Reynolds stresses in order to close the RANS equation of fluid flow. It is an unfortunate fact that no single turbulence model is universally accepted as being superior for all classes of problem. The choice of turbulence model will depend on consideration such as the physics encompassed in the flow, the established practice for a specific class of problem and the level of accuracy required.

For this case study, RNG K-εmodel by [17] was used for the modeling of turbulence because of its superior responsiveness to the effect of streamline curvature, vortices and rotations. Using this model, results into two addition equation ("k" and "ε")

4.2. RNG Kε Turbulence quatity transport equation:

$$\text{For K} = \frac{\partial}{\partial_t}(\rho k) + \frac{\partial}{\partial_{xi}}(\rho k u_i) = \frac{\partial}{x_j}\left(a_k . u_{eff} . \frac{\partial_k}{\partial_{xj}}\right) - \rho_e + \mathrm{P}_k \quad (18)$$

$$\text{For } \varepsilon = \frac{\partial}{\partial_t}(\rho\varepsilon) + \frac{\partial}{\partial_{xi}}(\rho\varepsilon u_i) = \frac{\partial}{\partial x_j}[(u + \frac{u_t}{\partial_\epsilon})\frac{\partial_\epsilon}{\partial_{xj}} - C_{1\varepsilon}\frac{\varepsilon}{\kappa}P_\kappa - \mathrm{C}^*_{2e}\rho\frac{\varepsilon^2}{\kappa} \quad (19)$$

Where $\mathrm{C}^*_{2e} = C_{2\varepsilon} + \frac{C_\mu \eta^3 (1 - \eta/\eta_0)}{1+\beta\eta^3}$, $\eta = \frac{S\kappa}{\varepsilon}$ and $S = (2S_{ij}Sij)^{1/2}$. k is the turbulence kinetic energy of the flow,ε is the disspitation energy, $C_{1\varepsilon}$ =1.42, $C_{2\varepsilon}$ =1.68, C_μ = 0.0845, $\eta_0 = 4.38$, $\beta = 0.012, \sigma_\varepsilon = 0.17194, \sigma_k = 0.1794$.

4.3. Inflow Boundary

At the inflow boundary layer, the mean velocity profile is usually obtained from the log profile corresponding to the upwind terrain via the roughness length Z_0.

For steady RANS simulation, the mean velocity profile and turbulence quantity are obtained based on the formula suggested by [18], in which the vertical profile for $u_{(z)}, k_{(z)}, \varepsilon_{(z)}$ stands for velocity, turbulence kinetic energy and dissipation energy respectively in the atmospheric boundary layer assuming a constant shear stress with height as follows:

$$u_z = \frac{u^*_{ABL}}{\kappa} \ln\left(\frac{Z+Z_0}{Z}\right) \quad (20)$$

$$k_{(z)} = \frac{u^{*2}_{ABL}}{\sqrt{C_\mu}} \quad (21)$$

$$\varepsilon_{(z)} = \frac{u^{*3}_{ABL}}{\kappa(z+z_0)} \quad (22)$$

4.4. Outflow Boundary

At the downwind boundary, an outflow boundary was used with constant static pressure and boundary condition for k and ε set to those of inlet. Backflow was not observed because the outlet boundary was sufficiently far away from the building.

4.5. Wall Boundary

According to [19], within the computational domain, generally three different regions can be distinguished.

- The central region of the domain where the actual obstacle (building) are modeled explicitly with their geometrical shapes.
- The upstream and downstream region where the actual obstacles are modeled implicitly, i.e. their geometry is not included in the domain but their effect on the flow can be modeled in terms of roughness e.g., by means of wall functions applied to the bottom of the domain.

On the ground, a rough wall was specified to model the effect of the ground roughness. According to [19],

$$k_{s_{ABL}=30y_0} \quad (23)$$

Where y_0 is aerodynamic roughness length=0.1m, roughness constant(c_s) =0.5. No slip boundary type was specified for the wall velocity

4.6. Top Boundary

As also specified by [18], specific attention is needed for the boundary condition at the top of the domain, along the length of the top boundary, the values from the inlet profile of u, k, ε at this height are imposed. ($u = 4.569, k = 0.300\, m^2/s^2$, $\varepsilon = 0.001317\, m^2/s^3$). According to [19], the application of this particular type of top boundary condition is important because other top boundary condition (symmetry, slip, wall, etc) can themselves cause stream wise gradient in addition to those caused by wall function.

5. Solver Setting

SIM-FLOW commercial CFD code was used to perform the simulation. The 3D steady RANS equation was solved. The simple algorithm was used for pressure-velocity coupling, pressure interpolation was second order and second- order discritizaton scheme were used for both the convective terms and the viscous terms of the governing equation for fluid flow.

6. Results and Discussions

The turbulent nature of wind is a key parameter for high rise buildings and needs to be analyzed accurately in pre-construction and post-construction stages of the building.A body can be considered as an aerodynamic bluff when flow streamlines do not follow the surface of the body similar to the case of streamlined body but detach from it bearing regions of separated flow and wide trailing wake [6].

It is very important to understand flow patterns around buildings in order to validate the model results in wind simulation. As shown in figure 3 and 4, wind flows around the typical high-rise building with the boundary layer wind velocity profile. The CFD simulation was able to display regions of flow separation as well as wake of the bluff body. When wind flows around bluff bodies and comes across regions of adverse pressure gradients (positive pressure gradients), the flow separates and depending on the geometry of the bluff body forms series of recirculation flows at the downstream (leeward wall) usually referred to as wake as can be seen in figure 3 and 4 below. This wake accounts for the lower negative pressure (suction) experienced along that region.

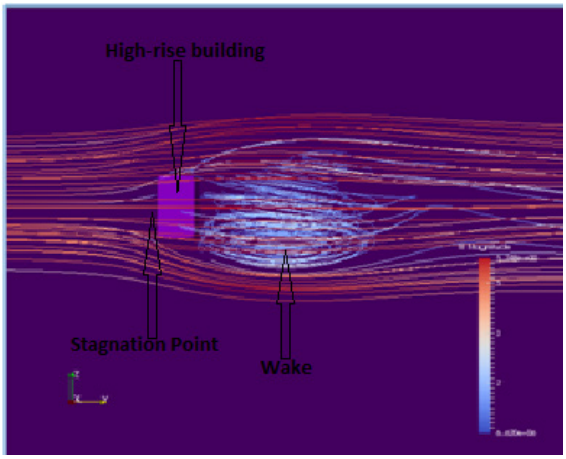

Figure 3: Plan view showing flow separation and wake around the high-rise building

The average wind pressure obtained in CFD was compared to the design wind pressure prediction of [15].the author found out considerable disparity in regards to the wind pressure distribution. [15], assumes higher positive wind pressure at the top of the high-rise building with a value of 0.043kpa in cognizance to the ideology that pressure increases as velocity with height. Whereas, the CFD analysis shows that pressure distribution do not constantly follow that ideology. According to the CFD analysis, a value of 0.013kpa was calculated as the maximum pressure at the windward wall located in the 6th floor as shown in table 2 but as

we go higher up to the 10th floor, this value is seen to decrease down to 0.012Kpa at the 11th floor as can be seen in table 2.

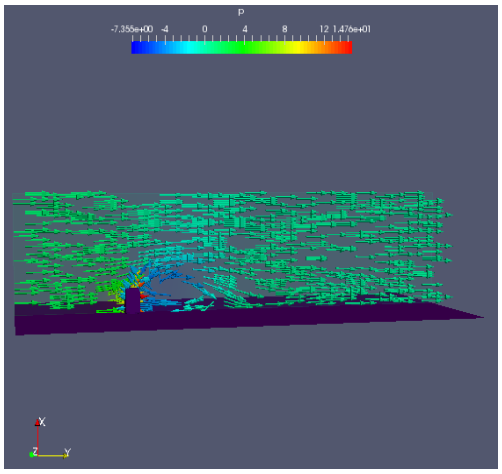

Figure 4: symmetrical view of wind around the high-rise building

Table 2: windward pressure via CFD analysis

Floor	Height(m)	Wind P (kpa)
15th	48.768	-0.0256
14th	44.8	0.0798
13th	40.98	0.0100
12th	37.8	0.0112
11th	34.65	0.0122
10th	31.5	0.0130
9th	28.35	0.0135
8th	25.2	0.0136
7th	22.05	0.0134
6th	18.9	0.0130
5th	15.75	0.0124
4th	12.6	0.0119
3rd	9.45	0.0113
2nd	6.30	0.0109
1st	3.150	0.0108

Table 3: windward pressure via BS6399-2:1997

Floor	Height(m)	Wind P (kpa)
15th	48.768	0.04304
14th	44.8	0.04172
13th	40.98	0.04075
12th	37.8	0.03972
11th	34.65	0.03860
10th	31.5	0.03740
9th	28.35	0.03584
8th	25.2	0.03394
7th	22.05	0.03178
6th	18.9	0.02933
5th	15.75	0.02643
4th	12.6	0.02292
3rd	9.45	0.01844
2nd	6.30	0.01382
1st	3.150	0.009584

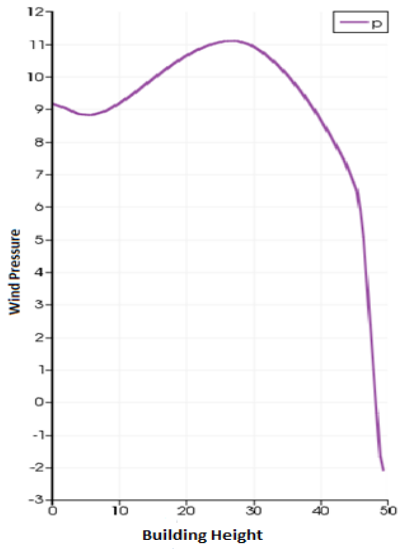

Figure 5: windward pressure as per CFD analysis

Pressure coefficient is a dimensionless number which describes the relative pressure throughout a flow field in fluid dynamics. Wind pressure coefficients are generally estimated by assuming an incompressible fluid scenario and using the equation given below;

$$C_P = {P - P_{ref}}/{0.5\rho_a v_{ref}^2} \quad (24)$$

Where c_p is the pressure coefficient, P is pressure at location of interest, P_{ref} static pressure, ρ_a is air density, v_{ref} is the velocity at reference location.

Table 4: pressure and Cp value at windward wall via CFD analysis

Floor	Height(m)	Pressure(Kp)	Pressure(c_p)
1st	3.150	0.0108	0.8
2nd	6.300	0.0109	0.8
3rd	9.450	0.0113	0.8
4th	12.60	0.0119	0.9
5th	15.70	0.0124	0.9
6th	18.70	0.0130	1.0
7th	22.05	0.0134	1.0
8th	25.20	0.0136	1.0
9th	28.35	0.0135	1.0
10th	31.50	0.0130	1.0
11th	34.65	0.0122	0.9
12th	37.80	0.0112	0.8
13th	40.95	0.0100	0.7
14th	44.80	0.0798	0.6
15th	48.77	-0.0257	-0.2

The maximum pressure coefficient on the windward, leeward and sidewall of the high-rise building according to the CFD analysis are 1.0,-0.48 and -0.61 respectively. The c_p of 1.0 observed at the windward wall of the high-rise building signifies stagnation point. Stagnation points are the point on the high-rise building where the local velocity (u_{mag} is 0).

Table 5: Pressure and Cp value at leeward wall via CFD analysis

Floor	Height(m)	Pressure(Kp)	Pressure (c_p)
1st	3.150	-0.065	-0.50
2nd	6.300	-0.063	-0.49
3rd	9.450	-0.062	-0.48
4th	12.60	-0.061	-0.48
5th	15.70	-0.061	-0.48
6th	18.70	-0.016	-0.48
7th	22.05	-0.063	-0.49
8th	25.20`	-0.064	-0.50
9th	28.35	-0.066	-0.51
10th	31.50	-0.068	-0.52
11th	34.65	-0.069	-0.54
12th	37.80	-0.071	-0.55
13th	40.95	-0.072	-0.57
14th	44.80	-0.076	-0.59
15th	48.77	-0.081	-0.63

Table 6: Pressure and Cp value for sidewall via CFD analysis

Floor	Height(m)	Pressure(Kp)	Pressure (c_p)
1st	3.150	-0.088	-0.68
2nd	6.300	-0.089	-0.69
3rd	9.450	-0.091	-0.71
4th	12.60	-0.092	-0.72
5th	15.70	-0.092	-0.72
6th	18.70	-0.093	-0.72
7th	22.05	-0.094	-0.73
8th	25.20	-0.096	-0.75
9th	28.35	-0.097	-0.76
10th	31.50	-0.097	-0.76
11th	34.65	-0.096	-0.75
12th	37.80	-0.096	-0.75
13th	40.95	-0.095	-0.74
14th	44.80	-0.091	-0.71
15th	48.77	-0.079	-0.61

Table 7: Pressure and c_p value for windward wall as per BS6399-2:1997

Floor	Height(m)	Pressure(Kp)	Pressure (c_p)
1st	3.150	0.0096	0.600
2nd	6.300	0.0138	0.600
3rd	9.450	0.0184	0.665
4th	12.60	0.0229	0.732
5th	15.70	0.0264	0.772
6th	18.70	0.0293	0.799
7th	22.05	0.0318	0.818
8th	25.20	0.0339	0.833
9th	28.35	0.0358	0.844
10th	31.50	0.0374	0.850
11th	34.65	0.0386	0.850
12th	37.80	0.0397	0.850
13th	40.95	0.0407	0.850
14th	44.80	0.0417	0.850
15th	48.77	0.0430	0.850

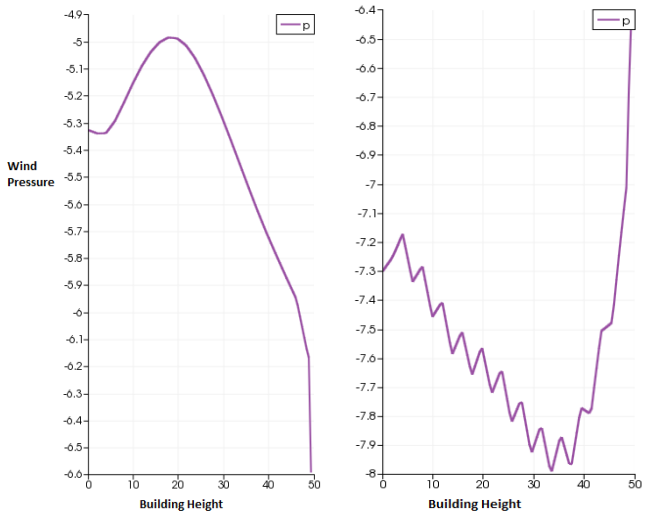

Figure 6: maximum pressures on leeward and side wall

Table 7: Pressure and c_p value for Leeward wall as per BS6399-2:1997

Floor	Height(m)	Pressure(Kp)	Pressure (c_p)
1st	3.150	-0.0080	-0.5
2nd	6.300	-0.0115	-0.5
3rd	9.450	-0.0139	-0.5
4th	12.60	-0.0157	-0.5
5th	15.70	-0.0171	-0.5
6th	18.70	-0.0184	-0.5
7th	22.05	-0.0194	-0.5
8th	25.20	-0.0204	-0.5
9th	28.35	-0.0212	-0.5
10th	31.50	-0.0220	-0.5
11th	34.65	-0.0227	-0.5
12th	37.80	-0.0234	-0.5
13th	40.95	-0.0240	-0.5
14th	44.80	-0.0245	-0.5
15th	48.77	-0.0253	-0.5

Table 8: Pressure and c_p values for Sidewall A as per BS6399-2:1997

Floor	Height(m)	Pressure(Kp)	Pressure (c_p)
1st	3.150	-0.0216	-1.3
2nd	6.300	-0.0307	-1.3
3rd	9.450	-0.0370	-1.3
4th	12.60	-0.0417	-1.3
5th	15.70	-0.0455	-1.3
6th	18.70	-0.0487	-1.3
7th	22.05	-0.0516	-1.3
8th	25.20	-0.0540	-1.3
9th	28.35	-0.0562	-1.3
10th	31.50	-0.0582	-1.3
11th	34.65	-0.0599	-1.3
12th	37.80	-0.0617	-1.3
13th	40.95	-0.0632	-1.3
14th	44.80	-0.0646	-1.3
15th	48.77	-0.0666	-1.3

Table 9: Pressure and c_p value for Sidewall B as per BS6399-2:1997

Floor	Height(m)	Pressure(Kp)	Pressure (c_p)
1st	3.150	-0.0133	-0.8
2nd	6.300	-0.0189	-0.8
3rd	9.450	-0.0227	-0.8
4th	12.60	-0.0257	-0.8
5th	15.70	-0.0280	-0.8
6th	18.70	-0.0299	-0.8
7th	22.05	-0.0317	-0.8
8th	25.20	-0.0332	-0.8
9th	28.35	-0.0346	-0.8
10th	31.50	-0.0358	-0.8
11th	34.65	-0.0369	-0.8
12th	37.80	-0.0379	-0.8
13th	40.95	-0.0389	-0.8
14th	44.80	-0.0398	-0.8
15th	48.77	-0.0410	-0.8

According to Bernoulli's equation, static pressure is at its maximum value at stagnation point. This static pressure is called stagnation pressure. As can be seen in table 4, from the 30th -50th floor where c_p is 1.0 recorded the highest wind pressure on the windward wall.

Whereas, [15], prescribed the pressure coefficient of 0.85,-0.5, and -1.3 as maximum c_p value at the windward, leeward and sidewall of the high-rise building respectively.

7. Conclusion

The wind pressure at different levels of the high-rise building obtained from CFD simulation for the 48.767m high-rise building were compared to the predictions given by [15]. More so, the limitations of the three methods in calculating wind loads on high-rise buildings (BS6399-2:1997, wind tunnel testing and CFD) were discussed.

The researcher also statedthat with strict adherence to the CFD best practice guidelines for wind around buildings stipulated in [10], [12], [13], CFD can serve as an alternative approach to the costly and time-consuming wind tunnel testing in predicting with considerable accuracy wind behavior around high-rise buildings both in the preliminary as well as final design stage of a project constructions. Also, result of the CFD analysis showed that the wind pressures obtained are usually lower than those predicted by [15] which can result in greater economy in the structural framing.

However, more experimental work is required to validate the CFD analysis. This work will take place at Nnamdi Azikiwe University awka, Nigeria.

References

[1] M.Overend, K.Zammit; "wind loading on cladding and glazed facades"internatonal symposium onthe application of architectural glass, ISSAG 2006.http//www.Isaag.com

[2] Roshka, "perspectives on the bluff body aerodynamics" Journal of wind engineering and industrial aerodynamics, 41, 79-100(1993)

[3] K.bernard, "prediction of wind loads on tall building" PHD thesis University of western Ontini, (1993).

[4] K.Nguyen "A study of aerodynamic wind loads on tall building using wind tunnel tests and numerical simulation" PHD thesis University of Melbourne,(2009)

[5] D.Kwon& A. Kareem, "Comparative study of major international wind codes and standards for wind effects on tall buildings" Engineering structures, vol.51, pp.23-35(2013)

[6] D.Mohotti,P.Mendis,T.Ngo, "Application of computational fluid dynamics(CFD) in predicting the wind loads on tall buildings-A case study".ACMSM23,Byron Bay Australia,(2014).

[7] H.Montezeri, B.Blocken, "CFD Simulation of wind induced pressure coefficients in buildings with and without Balconies". Validation and sensitivity analysis. Building and Environment, 60,137-147(2013).

[8] H.Versteeg, W.Malalasekera. "An introduction to computational fluid dynamcs: The finite volume method" England: Pearson education ltd, (1995).

[9] D.kim. "The application of CFD to building analysis and design: A combined approach of an immersive case study and wind tunnel testing". PHD thesis, Virginia polytechnic institute and state university.USA, (2014).

[10] J.Franke, A.Hellsten, H.Schlunzen, B.Carrissimo,(2007) "best practice guidelines for the CFD simulation of flows n urban environment". COST 732: quality assurance and improvement of micro scale meteorological models. Cost office Brussel, ISBN 3-00-018312-4

[11] J.Franke,C.Hirsch,A.Jensen,H.Krus,M.Schatzmann,P.Westbury,S.Miles,J. Wisse,N.Wright,(2004) "Recommendations on the use of CFD in wind engineering", COST ActionC14:Impact of Wind and storm on city life and Built Environment,vonkarmanInstute for Fluid Dynamics.

[12] Y.Tominaga,A.Mochida,R.Yoshie,H.Kataoka,T.Nozu,M.Yoshikara,T.Shira sawa,(2008).Aij guidelines around buildings .Journal of wind engineering and industrial Aerodynamics,96(10-11),1749-1761.ISSN 0167-6105,http://dx.doi.org/10.1016/j.jweia.2008.02.058

[13] M.Casey, T.Wintergersk, "Best practice guidelines, ERCOFTAC special interest group on quality and trust in industrial CFD.ERCOFTAC, Brussels,(2000).

[14] E.Vafaeihosseini, A.Saghels, R.Kumar, "Computational fluid dynamics approach for wind analysis of high-rise buildings: Report: 111T/TR/2013/1,center for earthquake engineering, international institute of information technology,Hyderabad,India.

[15] BS6399-2:1997.Loading for buildings-part 2: code of practice for wind loads BSI

[16] Online Available: http://en.m.wikipedia.org/wiki/log_wind_profile.

[17] V.Yakhot,S.Orszag,S.Thangam,T.Gatski,C.Speziale,(1992) "Development of turbulence model for shear flows by a double expansion technique" physics of fluids A,Vol.4,No.7,pp1510-1520

[18] P.Richards,R.Hosey, "Appropriate boundary conditions for computational wind engineering model using the K-e model", J.wind eng.ind.aerod, 46-47,145-153,(1993)

[19] B.Blocken, T.Stathopoulos, J.Carmeliet, "CFD simulation of the atmospheric boundary layer: wall function problems"atmos.enviro, 41(2), 228-252,(2007).

ASTES

Advances in Science, Technology and Engineering Systems Journal Vol. 2, No. 4, 204-208 (2017)

www.astesj.com

ASTESJ

ISSN: 2415-6698

A Review of Anti- Podal Vivaldi Antenna Operating in Cellular Mobile Communications

Asim Alkhaibari

University of Umm Al-qura, Mecca, Saudi Arabia

ARTICLE INFO

Article history:
Received: 26 October, 2017
Accepted: 22 November, 2017
Online: 10 December, 2017

Keywords:
Ultra Wideband
Worldwide interoperability for-microwave access
Long term evolution
Antipodal Vivaldi antenna
Long Term Evolution Advanced
Wireless-fidelity
Worldwide Interoperability for-Microwave access
Global system for mobile
Voltage Standing Wave Ratio
Return Loss
Perfect Electric Conductor
Computer Simulation Technology

ABSTRACT

The antenna proposed is a new geomantic structure of Ultra-Wideband (UWB) Anti- Podal Vivaldi antenna (AVA). It remarkably offers an attractive performance over the bands of cellular networks. However, its benefits are not limited only in particular applications, whereas radar imaging, mining detection, the biomedical science in the heating of brain cancer tumor and treatment, and the wireless communication are considered as the main applications suitable for utilization. Therefore, the focus on this paper is to spot the light illuminating into the cellular communications network Systems. On the other hands, several characteristics of Vivaldi antenna have been provided such as the gain, return loss, Voltage Standing Wave Ratio (VSWR), current distribution and E- fields. Finally, the results illustrate the capability and feasibility of the designed antenna.

1. Introduction

Vivaldi antenna has been classified from the most attractive antennas in the fabrication, design and applications[1, 2, 3]. This is simply because of a wide range of numerous benefits emerged in the industrial developments. To begin with, it is a small size of antenna and the dimensions can be controlled from several parameters to operate over a wider bandwidth [2, 4]. The antenna also can be capable in optimization from the physical structure change side as well as the parameter change by using CST Simulation. Thus, it helps the end users an alternative solution in the industrial projects. An example of its valuable applications is that it can contribute in cellular networks Generations [1] as its compatibility in the technical performance and physical structure are a place of commercial utilization. It can also offer several applications in UWB communication systems [2]. Moreover, the gain obtained from the design provides with an indoor coverage area suitable in the required cellular networks generations with end fire characteristics and a strong radiation directivity [5]. For instance, the commercial buildings consist of several floors and offices that need a unique coverage and independent wireless network access. Therefore, the technical specifications results in a customer satisfaction, if the operators exploit this kind of antenna in the business. On the other hands, several numerous steps have been applied to the physical structure of antenna for the sake of characteristics improvement such as adding slots or notches on the patch layer [6]. Thus, Vivaldi antenna confidentially will be able to deal with more directive gain and higher data rates in the wireless networks [1, 6] as Bluetooth, wireless cellular networks supporting the military demands, Wireless Fidelity (WIFI), Worldwide Interoperability for Microwave Access (WIMAX), Global System for Mobile (GSM), Universal Mobile for Telecommunications System (UMTS), Long Term Evolution (LTE), Long Term Evolution – Advanced (LTE-A) without any issues from the antenna side. AVA applications, however, are not limited to the industrial applications, but also expanded to the medical applications such as in treating brain and neck cancers [7].

*Correponding Author: Asim Alkhaibari, asem1983@hotmail.com

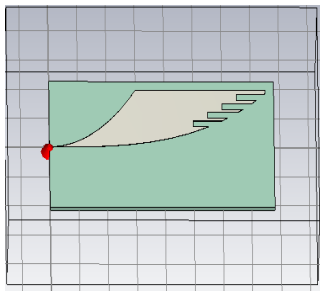

Figure 1: AVA geometric structure of proposed antenna

2. Antenna Geometry and Structure of Design

AVA is a planner antenna with UWB and linear polarizations [1, 4, 7]. The proposed antenna in this paper is illustrated in figure 1 showing a new shape. The power radiation, formation and creation of pattern radiations are a playground of technology in which particular operating frequencies offer different behavior better than others. Several sources can be used to feed the antenna and satisfy the matching and the transition requirements, whereby determining maximum bandwidth along with the operational frequencies. The designed antenna consists of a specific substrate material RF- 4 (Free Loss) and constant parameters as Epsilon (4.3) and Mute (1) with an overall dimension which is: 78mm x43mmx1.6mm. It is fed directly by discrete port. In addition, it has two exponential tapered layers as conductors with .07mm thickness and its material is made from Perfect Electric Conductor (PEC). The first one is stacked on the top of substrate fed via discrete port and the another one is printed on the bottom of substrate as a mirror with increased aperture acting as a ground plane. The parallel lines of the printed curves on the top are called stripline, where it has a balanced and fixed impedance allowing to transition process deliver more radiated power to the radiation curves, which defines the maximum wavelength between the inner curve edges acting as a horn antenna. The antenna, however, is notched with parallel slots for the sake of improving the performance such as the current distributions, radiation pattern, directivity, the gain and reducing return loss.

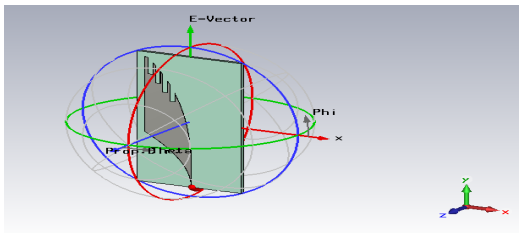

Figure 2: AVA angle and direction of radiation pattern

The formulas shown "(1)" and "(2)" describe how the layers are designed [1] on the substrate as follow:

$$Y_{outer} = A1 \times e^{b1 \times outer^2} + X1 \qquad (1)$$

$$Y_{inner} = A2 \times e^{b2 \times inner^3} + X2 \qquad (2)$$

A1=98.6, A2=100, b1=200$\times e^{-6}$, b2=400$\times e^{-9}$, inner=75mm, outer=30mm, Height=1.6mm, C1=-99.5mm, C2=-101mm, where:

- A1 and A2 represent as the scaling factor which is considered from the most important parameters to fix the geometric structure of antenna, so any poor adjustment of this factor causes a geometric change of the antenna and distortion issue as a consequence of the characteristics degradation.
- The outer and inner values act such as the counter of antenna heights
- b1 and b2 refer to the exponential opening rate.
- X1 and X2 refer to the displacement as an offset.

The dimension of antenna was designed and optimized in order to operate from the lower frequencies around 1GHz based on this formula:

$$F(GHz) = C/(2 * L(mm) \times \sqrt{\epsilon_r}) \qquad (3)$$

Where, C is the speed of light, ϵ_r is the permittivity of substrate material and L is the maximum aperture length of antenna.

However, the designed antenna consists from three parts so the first one is the radiator curves representing the exponential curves inside the antenna, the second part is the directivity curves which are the outer curves and the last part is the matching line of antenna connecting to the source. Consequently, the methodology adopted of this designed antenna is that the microwave frequencies propagate directly towards the flare edges with a proper characteristic of radiation patterns different from each operating frequency and fixed over a graded physical structure at the edge, so that it forms a range of wider bandwidth as and the outer curves are responsible in controlling the antenna beam and the radiation patterns, whether it provides with a wider range of coverage and suitable gain or not, whereas the parallel lines are responsible for matching the impedance and allowing the signals to pass over the graded inner curve as a results of electromagnetic frequencies.

3. Results and Discussions

AVA with a new shape modeled has been designed using CST. The performance illustrates its capability to be strongly utilized in a closed area such as indoor coverage solutions and in a shorter distance such as in Bluetooth and WIFI wireless networks or any kind of cellular networks wireless communications in handing calls or data like handover. The Return loss (S11) as shown in figure. 3 clarifies a positive impression which is less than -10dB with optimum performance over UWB starting from 1GHz to 10GHz. Moreover, the gain showed a significant increase over all UMTS and GSM between 1-2 GHz, then it slightly decreased with an acceptable level from 2-5GHz, which is the area offered of WIFI, WIMAX and Bluetooth technologies as shown in the figure 4. In addition, there was a steady state of VSWR over the bandwidth, which proves the compatibility of the antenna, about 1.5:1 as illustrated in the figure 5.

The Electric field radiation and the radiation patterns at 1GHz, 2GHz, 2.4GHz, 2.6GHz, and 5GHz respectively are presented in figure. 6 and figure.7. It demonstrates that each frequency has specific characteristics in coverage, whether it is wider or more directional at particular beam-width measured in degrees. The more wider coverage with suitable gain, the best it works in close or indoor coverage solutions such as commercial buildings, rooms, offices. However, the carrier frequencies that have a very narrow beam-width can be resolved by adding a new antenna to get a reasonable coverage and radio frequency scattered or diffracted from the edges of closed buildings.

On comparisons with electric fields radiations modeling, the structured antenna as shown in figures 6 (a,b,c,d and e) illustrates that it has a higher current distribution at1GHz rather than the others frequencies as this phenomenon is referred to electromagnetic fields penetration impact in the materials, media with surroundings reducing radio frequencies propagation and the nature of electromagnetic spectrum wavelength. Thus, the higher frequencies are susceptible of modular interactions with some particular materials as a result of energy absorption dependent on the type of material.

On the other hands, the figure 7 (a,b,c,d and e) provides the distribution of radiation pattern prediction of the geometric model at several frequencies. Indeed, the radiation pattern is considered one of the most important factors in determining the coverage prediction at any place. In comparison, it seems that 1GHz and 5GHz showed a wider coverage, whereas the lowest coverage were at 2.4GHz and 2.6 GHz.

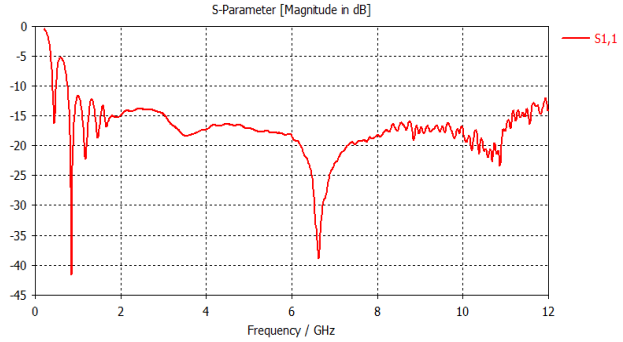

Figure 3: Return loss over frequency

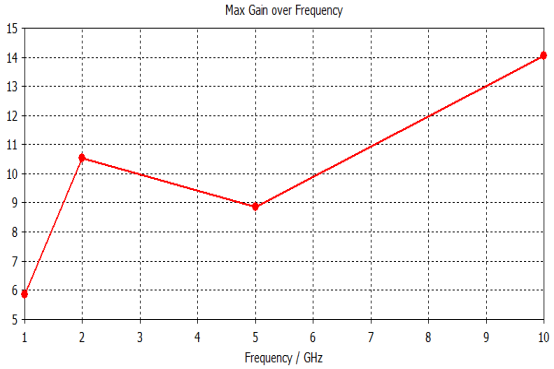

Figure 4: Antenna gain over frequency

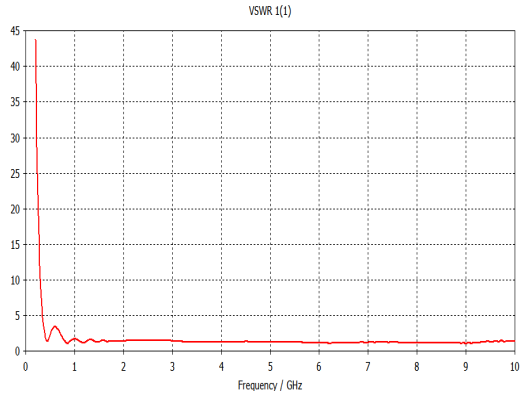

Figure 5: VSWR of AVA over frequency

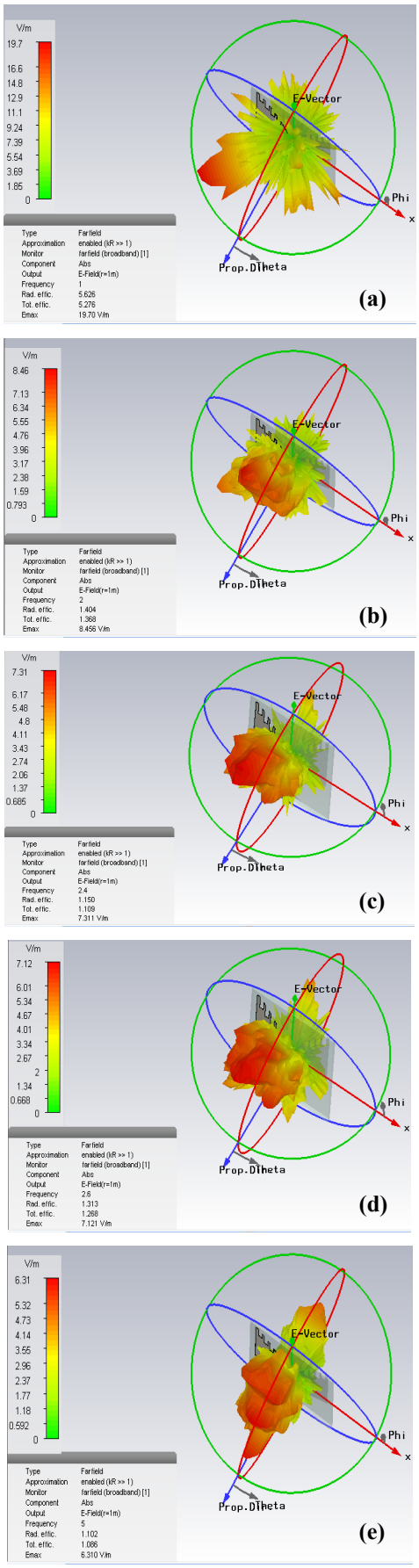

At (a) 1GHz (b) 2GHz (c) 2.4GHz (d) 2.6GHz (e) 5GHz
Figure 6: Electric Field Radiation

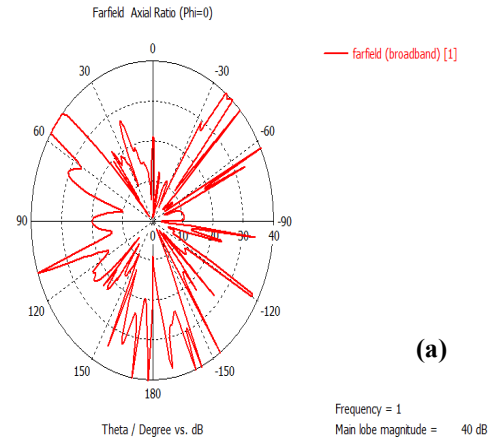

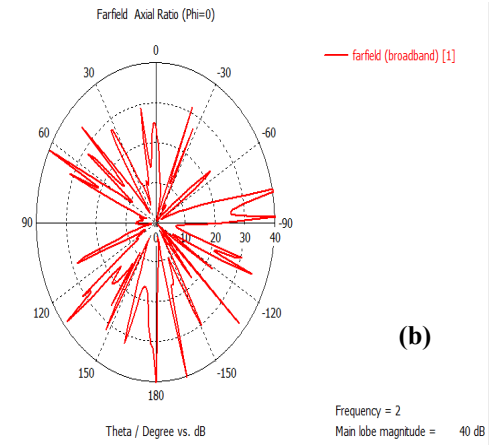

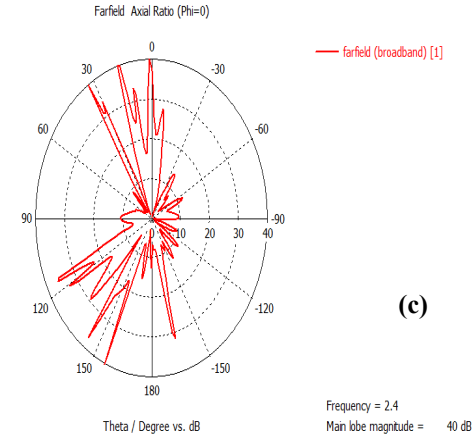

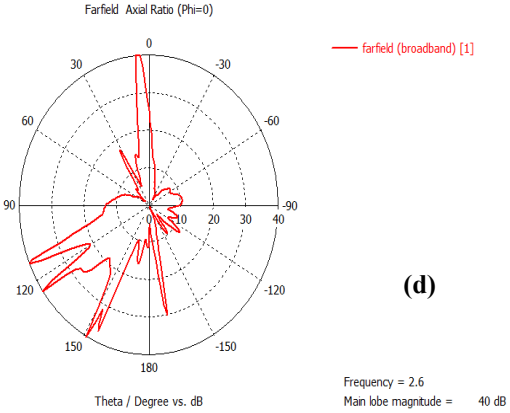

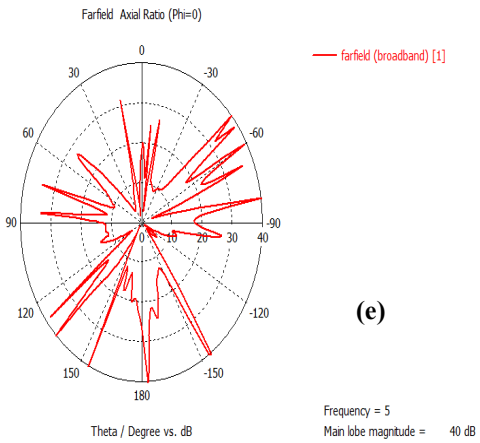

At (a) 1GHz (b) 2GHz (c) 2.4GHz(d) 2.6GHz (e) 5GHz

Figure 7: Directivity Pattern

4. Conclusion

AVA has a new shape model with a higher range of UWB from 1GHz to10 GHz. The antenna characteristics depict the performance such as the radiation pattern, the main lobe ,side lobe and electric fields. The linear improvements of gain illustrated the ability of antenna in indoor coverage solutions, where the cellular networks operators and providers for service strongly focus on this factor. Commercially, it can be utilized, designed and distributed on the walls and ceiling to produce a solution of indoor coverage issue in the present time. Moreover, the gain lineally increased between 5-10GHz is not limited to cellular networks technology, but also exploited in different applications such as UWB communications and X- band radar systems. However, the major drawback of this work is that AVA was not fabricated. Secondly, it needs further investigation for the gain reduction from 2GHz to 5GHz about 1.5dB. The reason, perhaps, due to data collection errors in simulation, since the gain should be increased linearly over the frequency when it increases. Otherwise, it may refer to the total losses contributed on the antenna structure at a specific band, although the comparisons between simulation and fabrication results lead to the facts on behind these minor issues. Overall, the abnormality of gain should not impact negatively on the essential innovation of antenna shape.

5. Acknowledgement

I am so grateful to University of Umm Al- Qural for tremendous assistance to keep me continued in both contribution and development in scientific research.

6. References

[1] G. Vinci and R. Weigel, "Multiband Planar Vival Antenna for Mobile Communication and Industrial Applications," *2010 International Conference on Electromagnetics in Advanced Applications*, Sydney, NSW, 2010, pp. 93-96.

[2] L. Yang, H. Guo, X. Liu, H. Du and G. Ji, "An antipodal Vivaldi antenna for ultra-wideband system," *2010 IEEE International Conference on Ultra-Wideband*, Nanjing, 2010, pp. 1-4.

[3] J. Bai, S. Shi and D. W. Prather, "Modified Compact Antipodal Vivaldi Antenna for 4–50-GHz UWB Application," in *IEEE Transactions on Microwave Theory and Techniques*, vol. 59, no. 4, pp. 1051-1057, April 2011.

[4] Fisher, James. "Design and Performance Analysis of a 1-40GHz Ultra-Wideband Antipodal Vivaldi Antenna." *Proceeding of the German Radar Symposium GRS 2000*. 2000.

[5] G. Teni, N. Zhang, J. Qiu, and P. Zhang, "Research on a novel miniaturized antipodal Vivaldi antenna with improved radiation," *IEEE Antennas and wireless propagation letters,* vol. 12, pp. 417-420, 2013.

[6] K. Aravinda Reddy, S. Natarajamani and S. K. Behera, "Antipodal Vivaldi antenna UWB antenna with 5.5GHz band- notch characteristics," *2012 International Conference on Computing, Electronics and Electrical Technologies (ICCEET)*, Kumaracoil, 2012, pp. 821-824.

[7] Alsulaiman, Khaled A., et al. "Design of Ultra Wideband Balanced Antipodal Vivaldi Antenna for Hyperthermia Treatment." *PIERS Proceedings*. 2013.